Advances in Isotope Geochemistry

Pete Burnard *Editor*

The Noble Gases as Geochemical Tracers

Springer

Advances in Isotope Geochemistry

Series Editor

Jochen Hoefs

For further volumes:
http://www.springer.com/series/8152

Pete Burnard
Editor

The Noble Gases as Geochemical Tracers

Springer

Editor
Pete Burnard
Centre National de la Recherche
Scientifique
Centre de Recherches Pétrographiques
et Géochemiques
Vandoeuvre-lès-Nancy
France

ISBN 978-3-642-28835-7 ISBN 978-3-642-28836-4 (eBook)
DOI 10.1007/978-3-642-28836-4
Springer Heidelberg New York Dordrecht London

Library of Congress Control Number: 2012952675

Printed on acid-free paper

Springer is part of Springer Science+Business Media (www.springer.com)

Preface

This book represents a landmark in the application of noble gases to the Earth sciences. When you turn to the pages within you will see that this unique set of tracers has now made the transition from the domain of a few specialist laboratories to become a standard part of the geochemists' toolkit in tackling an array of both fundamental and applied science problems. Although noble gases are used extensively as a dating tool in geological and environmental systems and are also extensively studied in cosmochemistry, each of which could fill a book alone, this volume specifically focuses on how noble gases are used as tracers in terrestrial systems. This is very much a nuts and bolts 'how-to-do-it' book and as such is complementary to recent reviews that take a more theoretical and process-oriented approach. This refreshing approach provides essential reading for understanding the advantages, state-of-the-art analyses, and current limits, of these tracers in the context of the different terrestrial tracer applications, some of which are very recent. This is a 'must' first port of call for those just starting in the field and will also be a critical resource for those in the field who have been around a little longer and who, like me, always have room to learn and apply new best practice.

It does not seem so long ago when, as a graduate student, I was (and remain) in awe of the scientists who firmly established the field of noble gas geochemistry; sitting in meetings with excitement as big egos challenged each other, with no quarter given, on the origins and evolution of the Earth and its atmosphere; and the slight clamminess of my hands when I realised that I would have to defend my own work and ideas in this arena. Some comfort and a degree of disbelief occurred when I realised how little then we actually knew about the very structure of the deep Earth; and how few observations these early but fundamental models were based on. When applying the noble gases to more practical matters I still pull out the 1961 paper by Zartmann, Wasserburg and Reynolds, with the understated title of 'Helium, argon and carbon in some natural gases' that describe the fundamental principles behind how we use noble gas isotopes today to understand multiphase crustal fluid systems. Despite arriving a little later to the field, the sense of potential for noble gases to contribute in a major and fundamental way to our basic understanding of Earth formation and evolution as well as their ability to interrogate and quantify the processes controlling so many natural systems provided a buzz then that still remains today.

Fifty one years after Zartmann et al., this book captures the same sense of excitement, but with half a century of additional community experience improving sample collection, analysis and data interpretation of this tracer suite. Central to many chapters in the book are the array of techniques that we use to release the noble gases from solid samples. While they might sound like extracts from a medieval torture chamber handbook, with samples releasing their noble gas information through being crushed, heated, melted or ablated, the exceptional care and exactitude that reduces blanks and maximises signal for each application are detailed here. Where samples are collected as free water, gas or oil, whether from the depths of the ocean or from commercial oil and gas boreholes, the system and component features required to collect, store and preserve robust samples are presented in the respective chapters. Each sample type also presents its own challenge in preparation before analysis: removal of water, gas or oil from the vacuum system; cryo-separation of the noble gases; low blanks; fast sample throughput—all before the mass spectrometry. It is nevertheless the improvements in mass spectrometry that form the foundation of the subject expansion and the reason that noble gases are now a must-have tool in any Earth or Environmental Science research institute of repute. Electronics stability, source sensitivity, multiplier and amplification technology, software control and data handling, magnet stability and speed, mass resolution, multi-collection. Without these advances, achieving the analytical reproducibility and precision needed for each application and unlocking the detail of the processes controlling the natural systems reviewed here would have been an impossibility.

The noble gases as tracers are still making a significant contribution to a breadth of science problems that would surely amaze the early subject pioneers. Their chemical inertness, sensitivity to radiogenic noble gas input, fluid mixing and physical processing allow the identification and quantification of the physical environment to be tractable in a way not possible by any other technique. There is not a single tracer set in our geochemistry armoury that is quite so powerful or broadly useful — but perhaps I am writing with a small bias.

In showing how to win the data from the different natural systems, this volume provides an excellent review of precisely how noble gases are used across the application landscape. The chapters in this volume have been arranged logically from the history of their discovery and early uses to the basics of sample preparation and mass spectrometry and detail the noble gases in the terrestrial atmosphere that form the basis for most laboratory standards. These introductory chapters are followed by global environmental applications that include reconstruction of the past atmosphere and environment from ice cores, aquifers and lakes, reconstruction of ocean circulation and nutrient input from ocean waters and sediment flux. Chapters review how noble gases are applied to identifying hydrocarbon reserves and, perhaps slightly ironically, also in assessing the safety of burying the carbon dioxide produced by combustion of oil and natural gas for Man's energy needs. The book starts to

conclude with chapters that show how modern and ancient hydrothermal systems can be understood. The greatest of science challenges tackled by noble gases is left to the last chapter on tracing the evolution of the terrestrial mantle, which arguably provided the experience and expertise that spun out many of the other applications detailed. The description of how the study of noble gases in mantle materials have revolutionised our understanding of the nature and origin of volatiles in the Earth and how the Earth's mantle has evolved through time is certainly a contribution, from many, to the basic understanding of our planet that the noble gas community can be proud of.

Prof. Chris Ballentine
The University of Manchester

Contents

The Noble Gases as Geochemical Tracers: History and Background

Pete Burnard, Laurent Zimmermann and Yuji Sano

Abstract

This chapter describes the discovery of the noble gases and the development of the first instrumentation used for noble gas isotopic analysis before outlining in very general terms how noble gases are analysed in most modern laboratories. Most modern mass spectrometers use electron impact sources and magnetic sector mass filters with detection by faraday cups and electron multipliers. Some of the performance characteristics typical of these instruments are described (sensitivity, mass discrimination). Extraction of noble gases from geological samples is for the most part achieved by phase separation, by thermal extraction (furnace) or by crushing *in vacuo*. The extracted gases need to be purified and separated by a combination of chemical and physical methods. The principles behind different approaches to calibrating the mass spectrometers are discussed.

1 Introduction

Occupying the last column of the Periodic Table and therefore characterized by a filled outer valence shell, the noble gases do not form chemical compounds at conditions relevant to natural processes on Earth: while Kr and Xe do have an extensive chemistry (Grochala 2007), this is typically only with highly electronegative elements such as F and O, which in natural terrestrial systems are already bound to more reactive elements than the noble gases. The noble gases and their isotopes are able to provide unique constraints on certain geological processes owing to their inert behavior and because numerous nuclear reactions are recorded in the noble gas isotopic compositions. While many of these applications are related to constraining the duration of geologic events (thermochronology, absolute dating, surface exposure dating etc.), this volume aims to describe sampling strategies, analytical methodologies and data interpretation for the use of noble gases as *tracers* in the Earth Sciences: tracers of geological fluids, of mantle circulation, of seawater

P. Burnard (✉) · L. Zimmermann
Centre de Recherches Pétrographiques et Géochimiques, BP 20Vandoeuvre-lès-Nancy Cedex, France
e-mail: peteb@crpg.cnrs-nancy.fr

Y. Sano
Center for Advanced Marine Research, Ocean Research Institute, The University of Tokyo, Nakano, Tokyo 164–8639, Japan

P. Burnard (ed.), *The Noble Gases as Geochemical Tracers*, Advances in Isotope Geochemistry,
DOI: 10.1007/978-3-642-28836-4_1,

circulation, of dust falling from space, of hydrocarbon reserves, of past climate change and of potential future CO_2 storage in crustal reservoirs.

1.1 History

The discovery of the noble gases was initially by inference rather than isolation. Helium was first identified as an element simply from its absorption spectrum in the solar chromosphere (by Lockyer in 1868; it would be another 27 years before it was actually isolated as an element). Similarly, the presence of an unknown gas of low density (which later turned out to be Ar) in the atmosphere was proposed by Rayleigh in 1895 because nitrogen from distilled air had a different density to chemically produced nitrogen. This observation lead to more refined distillation experiments by Ramsay (1898) which positively identified Ar as an element and also led to the isolation of Kr, Ne and Xe (for which Ramsey and Rayleigh would receive Noble Prizes).

The discovery that an alpha particle produced by decay of U was in fact a helium nucleus (by accumulating α particles in an evacuated tube by recoil through a thin window) allowed Rutherford and Strutt to make the first radiometric age measurements in 1905: by heating various U-bearing minerals and weighing the He that was produced, they were able to constrain the age of the earth to be greater than 400 Ma. Rutherford and Strutt were well aware of the problem of potential He loss from minerals on geological timescales and so correctly considered the 400 Ma estimate to be a minimum estimate; but even so, this was a major advance as previous estimates considered that the maximum age of the Earth was of the order 20 Ma. However, as a result of the He loss problem the U+Th/He radio chronometer was largely ignored until the beginning of the 1990s when a better understanding of the kinetics of He loss in certain U bearing minerals ushered in the possibility of quantitative U+Th/He thermochronometry (Farley 2002).

Noble gases were central to understanding the structure of the atom, and the first isotopic separation—using the first mass spectrometer—was made by JJ Thomson and F.W. Aston in 1913 to separate ^{20}Ne from ^{22}Ne. This development opened the floodgates for research into isotopes, and 10 years later multiple isotopes of all the noble gases except for ^{3}He had been identified (despite a hiatus forced by the First World War), for the most part by Dempster at the University of Chicago: Dempster's 1918 mass spectrometer (Dempster 1918) laid down the blueprint for the magnetic field filters used in mass spectrometers to this day. Helium-3 was only identified in 1939 by cyclotron mass spectrometry at Lawrence Berkely Nat. Labs, CA, by Alvarez and Cornog (1939), who used the 60-in. cyclotron as a mass spectrograph to show that ^{3}He is a stable isotopic constituent of natural helium. The $^{3}He^{2+}$ ions were detected using the nuclear reaction ^{28}Si(^{3}He, p)^{30}P(β)^{30}Si and the radio-activity of ^{30}P quantified by a Geiger counter. The activity of pure atmospheric helium was 12 times higher than that of tank helium derived from a natural gas well. They concluded that the ^{3}He/^{4}He ratio of air helium is about 10 times greater than that of natural gas helium.

The advances in mass spectrometry resulting from the Manhattan Project (1942–1946) opened up opportunities in geo-and cosmochemistry in the post war years. At the forefront of mass spec development during the Manhattan project, Nier, now in Minnesota, returned to the geochronology and geochemistry he started in the pre-war years as a grad student at Harvard. Seminal papers on K-Ar dating (Aldrich and Nier 1948a) and on the He isotopic composition of the atmosphere (Daunt et al. 1947) resulted from the impressive 15 cm radius, 60° mass spectrometers and electron impact ion sources that Nier built at that time. These machines were capable of separating ^{3}He + from HD^{+} to HHH^{+} interferences. Nier and his co-workers discovered large variations in ^{3}He/^{4}He ratios of natural materials: Aldrich and Nier presciently stated in their 1948 paper (Aldrich and Nier 1948b) that "The present study can hardly be regarded as more than a preliminary exploration of a new and fascinating field of investigation. It is apparent that a far more comprehensive and systematic study will be required to definitely establish the natural source of ^{3}He and ^{4}He."

Noble gas mass spectrometers owe significantly to Nier's legacy; indeed, many modern mass specs still employ a *Nier-type* ion source (see Sect. 2). Further advances in noble gas mass spectroscopy in the 65 years or so since Nier's inventions have been gradual rather than leaps in performance. Two exceptions are Reynold's (at Berkeley) development of static (i.e. isolated from pumps) mass spectrometry in 1956 (Reynolds 1956) thereby significantly increasing sensitivity, and the development of a new electron impact source by Baur and Signer in the late 1970s (Baur 1980) which is characterized by better pressure linearity.

Clarke et al. (1969) measured the $^3He/^4He$ ratios of deep Pacific water by using a 10-in radius, low volume, and static vacuum mass spectrometer, with an electron multiplier for ion detection, reducing samples sizes by three orders of magnitude compared to Aldrich and Nier (1948a). Two examples of Clarke mass spectrometers remain operational to this day (Scripps Institution of Oceanography and Woods Hole Institution of Oceanography [e.g. Jenkins (1987), Lupton et al. (1990)]. In 1976, Takaoka and co-workers developed a noble gas mass spectrometer to measure all noble gas isotopes, which was commercialized in 1982 as the VG MM-3000 (Hooker et al. 1985). At the same time Sano et al. (1982) used a 6-inch static mass spectrometer (6-60-SGA, Nuclide Co.) for terrestrial He isotope measurements, reporting an atmospheric $^3He/^4He$ ratio of $(1.43 \pm 0.03) \times 10^{-6}$, which agreed well with the critical value of $(1.399 \pm 0.013) \times 10^{-6}$ determined by Mamyrin et al. (1970) (see below).

In the ex-Soviet Union, Mamyrin et al. (1969) independently developed the "Reflectron" time of flight mass spectrometer with $m/\Delta M \sim 2{,}000$ and even more sensitive than the latest magnetic sector mass spectrometers. Until the mid-1980s, there were only seven laboratories in the world routinely measuring terrestrial He isotopes: Ontario, St. Petersburg, Boston, San Diego, Tokyo, Osaka and Cambridge.

In 1986, the VG-5400, a successor of the MM-3000 was introduced and soon after the MAP-215–50 became available. These machines have since produced the majority of terrestrial noble gas analyses in many laboratories around the world (e.g. Sano and Wakita 1985). However, further development in noble gas mass spectrometry ceased for almost 20 years following the success of the VG-5400 and MAP-215 instruments.

In 2004 two brand-new multicollector noble gas mass spectrometers (HELIX-SFT, GV instruments and Noblesse, Nu Instruments) were announced, with the possibility of precisely measuring the atmospheric $^3He/^4He$ ratio on samples size of 1×10^{-7} ccSTP, three order of magnitude smaller than the original Clarke-type instrument. Figure 1 shows the technical progress

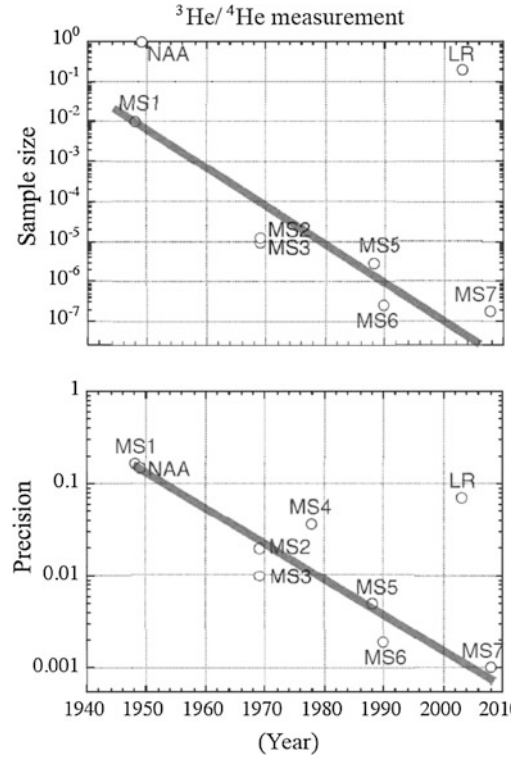

Fig. 1 Technical advances in helium isotope measurements with time. *Top* and *bottom* show the decrease in sample size required to measure He isotopes and the improvement in analytical precision, respectively. *MS1*: Aldrich and Nier (1948b); *MS2*: Clarke et al. (1969); *MS3*: Mamyrin et al. (1969); *MS4*: Nagao et al. (1981); *MS5*: Sano and Wakita (1988); *MS6*: Lupton et al. (1990); *MS7*: Sano et al. (2008); NAA: Coon (1949); LR: Wang et al. (2003)

Table 1 Common interferences found in the region of the noble gases

Species	Mass/Charge	Noble gas	Resolution required[a]	Comment
$^{1}H^{2}D^{+}$	3.0215	^{3}He	509	Present in all mass spectrometers
$^{3}H^{+}$	3.0161	^{3}He	150 000	
$^{1}H^{1}H^{1}H^{+}$	3.0238	^{3}He	384	Present in all mass spectrometers
$12C^{+++}$	4.0000	^{4}He	1,538	
$^{1}H_{2}{}^{18}O^{+}$	20.015	^{20}Ne	894	
$^{1}H^{19}F^{+}$	20.006	^{20}Ne	1,406	
$^{40}Ar^{++}$	19.981	^{20}Ne	1,778	Liquid N_2 trap during Ne analysis
$^{20}NeH^{+}$	21.000	^{21}Ne	3,276	
$^{12}C_{3}{}^{1}H_{6}{}^{++}$	21.023	^{21}Ne	709	
$^{63}Cu^{+++}$	20.976	^{21}Ne	1,202	
$CO_{2}{}^{++}$	21.995	^{22}Ne	6,232	Liquid N_2 + getters during Ne analysis
^{66}Zn +++	21.975	^{22}Ne	1,405	
$^{12}C_{3}{}^{+}$	36.000	^{36}Ar	1,109	
$^{1}H^{35}Cl^{+}$	35.977	^{36}Ar	3,947	
$^{1}H^{37}Cl^{+}$	37.974	^{38}Ar	3,458	
$^{12}C_{3}{}^{1}H_{2}{}^{+}$	38.016	^{38}Ar	699	
$^{12}C_{3}{}^{1}H_{4}{}^{+}$	40.031	^{40}Ar	580	
$^{12}C_{6}{}^{1}H_{6-12}{}^{+}$	78–86	Kr isotopes	~600	
$^{12}C_{10}{}^{1}H_{4-16}{}^{+}$	124–136	Xe isotopes	~550	Common pump oil or grease fragments

Sensitivity of the mass spectrometer 1: common interferences found in the region of the noble gases. [a] Mass resolution is expressed as mass/peak width; the quoted resolutions are the resolutions necessary to separate the interference from the neighboring noble gas isotope

of helium isotope measurements with time. Taking into account only mass spectrometry (MS1–MS6) developments, the sample size required for helium isotope analysis as well as the precision of the analyses have improved on an approximately logarithmic scale with time since their invention. Recently, high sensitivity (sample sizes of 10^{-7} ccSTP) and high precision (estimated error of 0.1 % at 1 σ) helium isotope measurements have been reported by Sano et al. (2008).

With the advent of high resolution, multicollector noble gas mass spectrometry, the precision and sensitivity for the remaining noble gases—which all have more than two isotopes—have also increased. It is important to note that all noble gases have at least one (and usually more) non-abundant isotopes requiring multicollection using secondary electron multipliers (SEM) and sometimes requiring multiple SEMs. Multiple SEM machines are considerably more complex to construct and operate than faraday-only multicollector mass spectrometers.

One of the major issues for Ne isotope analyses are the isobaric interferences on $^{20}Ne^{+}$ by $^{40}Ar^{+}$ and $H_{2}^{18}O^{+}$ and on $^{22}Ne^{+}$ by $CO_{2}{}^{++}$ (see Table 1), requiring high resolving power mass filters in order to cleanly separate the signals. This is now possible for $^{20}Ne^{+}$ on both Nu and GV (now Thermo fisher) mass spectrometers, producing data with $^{20}Ne/^{22}Ne$ and $^{21}Ne/^{22}Ne$ uncertainties that have decreased by factor 2–5 compared to single collector data (Colin et al. 2011; Marrocchi et al. 2009; Parai et al. 2009).

Multicollection also provides major advantages for the analysis of Kr and Xe isotopes, as both noble gases have numerous isotopes (6 and 9 stable isotopes, respectively) and their atoms have short half lives in the mass spectrometer due to their high ionization cross-sections compared to the lighter noble gases. These multicollector (>2 collector) machines have been routinely producing data for 2 or 3 years at the time of writing (Holland and Ballentine 2006; Holland et al. 2009); from this early work it is

clear that the precision of noble gas analyses that is now possible will open up new opportunities and directions in the isotope geochemistry of the noble gases.

Obviously, improvements in materials, vacuum techniques, multiple collectors and ion optics have contributed to the high standards expected of commercial mass spectrometers today, but the for the most part modern mass spectrometers closely resemble those of Nier and Reynolds (indeed, some are still operational with excellent data still produced by glass 'Reynolds' machines).

Some individual labs have made technical advances that have very specific applications. Wang et al. (2003) reported that a sensitive laser spectroscopic method could be been applied to the quantitative determination of ^{3}He/^{4}He for ratios in the range 10^{-7}–10^{-5}. Resonant absorption of 1,083 nm laser light photons by metastable ^{3}He atoms in a discharge cell was measured by frequency modulation saturation spectroscopy while the abundance of ^{4}He was measured by a direct absorption technique. Even though the results on three different samples extracted from the atmosphere and commercial helium gas were in good agreement with values obtained by mass spectrometry, a large amount of sample helium, about 0.2 ccSTP was required for analysis. This is far beyond the terrestrial helium sample size for practical use. Resonance Ionization Mass Spectrometry has also been developed in some noble gas laboratories which increases precision and reduces detection limits for Xe and Kr isotope determination (Crowther et al. 2008; Gilmour et al. 1994; Iwata et al. 2010; Mamyrin et al. 1969; Strashnov et al. 2011; Thonnard 1995). The turbo compressor source developed by H. Baur of ETH increases the partial pressure of (noble) gases in the source by using a molecular drag pump within the mass spectrometer volume, thereby increasing sensitivity for He and Ne by a factor ~100 (Baur 1999).

1.2 Conventions

Quantities of noble gases are reported either in moles of gas or as cm^3 Standard Temperature and Pressure (STP); it should be noted that although STP is usually defined as 273.15 K and 101.325 kPa (=1 bar), some definitions use 100.000 kPa (McNaught and Wilkinson 1997). Use of moles should be encouraged. As a consequence, noble gas concentrations are usually expressed as moles (or cm^3 STP) per gram of rock or fluid. Sometimes, although rarely, these are converted to percent or ppm of the noble gas by weight, as is common for other elements in many branches of geochemistry. However, performing the simple conversion demonstrates how 'rare' the noble gases are: a typical olivine crystal might contain ~10^{-13} mol ^{4}He g^{-1}, or about 0.5 ppt ^{4}He. The abundances of ^{3}He or the rare isotopes of Xe are typically >10^6 times lower.

There is no single convention for reporting isotope ratios. Most commonly, the actual ratio is reported; this is practical where isotopic variations are relatively large. Where small isotopic variations are involved, the 'delta' notation is commonly used where:

$$\delta_{iX} = \left[\frac{\left({}^{i}X/_{r}X \right)_{sample}}{\left({}^{i}X/_{r}X \right)_{standard}} - 1 \right] \times 1000$$

where ${}^{i}X$ is the 'anomalous' isotope and ${}^{r}X$ is the reference isotope. For all systems with the exception of He, it is usual to place a non-radiogenic isotope as the denominator. Thus, δ^{40}Ar would refer to the permil variations in the ^{40}Ar/^{36}Ar ratio.

Because the non-radiogenic He isotope (^{3}He) is the least abundant isotope, historically He isotope ratios have been reported as ^{3}He/^{4}He ratios (i.e. radiogenic isotope as the denominator). Furthermore, it is common to report ^{3}He/^{4}He ratios normalized to the atmospheric ^{3}He/^{4}He ratio, Ra. Thus, a sample with a ^{3}He/^{4}He ratio of 1 Ra would have real ratio of 1.39×10^{-6} (see Chap. 2). However, when plotting He isotopes against other isotope ratios (which are ubiquitously quoted with the more traditional non-radiogenic/radiogenic notation), this often leads to unnecessarily complex, inverse relationships. In these instances, it is preferable to use ^{4}He/^{3}He (not normalized to Ra).

Relative noble gas abundances are frequently expressed normalized to ^{36}Ar and the ratio normalized to that of air, commonly known as the F-value notation:

$$F(i) = \frac{\left(i/^{36}Ar\right)_{sample}}{\left(i/^{36}Ar\right)_{air}}$$

Thus F(^{80}Kr) = 2 corresponds to a ^{80}Kr/^{36}Ar ratio twice the ratio of air.

2 Noble Gas Mass Spectrometry

2.1 Principles

As with all mass spectrometers, noble gas mass spectrometers consist of an ion source, a mass filter and collector(s). The "standard" configuration which accounts for >95 % of operational mass spectrometers at the time of writing consists of an electron impact source, a magnetic sector filter and detection using a combination of Faraday cups and secondary electron multipliers (SEMs). The magnetic field is measured by one or more Hall probes. Magnet control and data collection are usually done via proprietary software; on the modern generation of mass spectrometers (post 2002), control of source and multiplier voltages are also performed via a software interface.

The most common "non-standard" mass spectrometer solution involves ionisation using resonant lasers and a time of flight mass filter with detection by microchannel plates (Gilmour et al. 1994; Lavielle et al. 2006). Alternatively, atom trap or penning trap noble gas mass spectrometers also exist (Lu and Mueller 2010; Neidherr et al. 2009). These configurations are adapted to specific analytical problems and are not "off the shelf" solutions, therefore will not be dealt with here: the reader is instead referred to the publications above.

Most, but not all, noble gas mass spectrometers are operated in "static" mode, that is to say all the gas available is admitted into the mass spectrometer with the pumps isolated (Reynolds 1956) (by contrast, "dynamic" mode is where the sample gas is slowly bled into the mass spectrometer while simultaneously pumping the spectrometer). "Static" mode considerably increases mass spectrometer sensitivity with the disadvantage that the signal changes over time as the gas is gradually consumed by ionisation. Usually this is accounted for by performing an extrapolation to the instant the gas was diluted into the mass spectrometer (Fig. 2). An additional consequence of operating in "static" mode is that very low mass spectrometer backgrounds are required because, as soon as the pumps are isolated, background levels in the spectrometer envelope will begin to rise. This is countered by including one or more getters in the isolated volume and by rigorous vacuum techniques: noble gas mass spectrometers are exposed to air very infrequently (usually several years between ventings) and are thoroughly baked at temperatures up to 350 °C after being at atmospheric pressure.

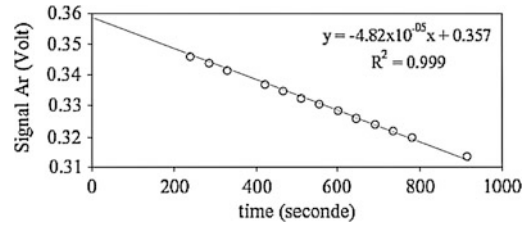

Fig. 2 Signal of ^{40}Ar versus time in a VG5400 mass spectrometer (200 μA trap current). ≈200 s are necessary to dilute the gas into the mass spectrometer and to determine field positions for each argon isotope. The signals were extrapolated to the instant the gas was diluted into the mass spectrometer (t = 0) in order to account for consumption by ionisation of the gas during measurement

2.1.1 Electron Bombardment Sources

While magnet and collector configurations are relatively straightforward and have much in common with non-noble gas mass spectrometers, good mass spectroscopic analyses require a thorough understanding of how a noble gas source functions. All commercial noble gas mass spectrometers past and present use either modified Nier-type sources (Fig. 3) or Baur-Signer sources, both of which depend on a filament to create an electron beam which then ionize gas

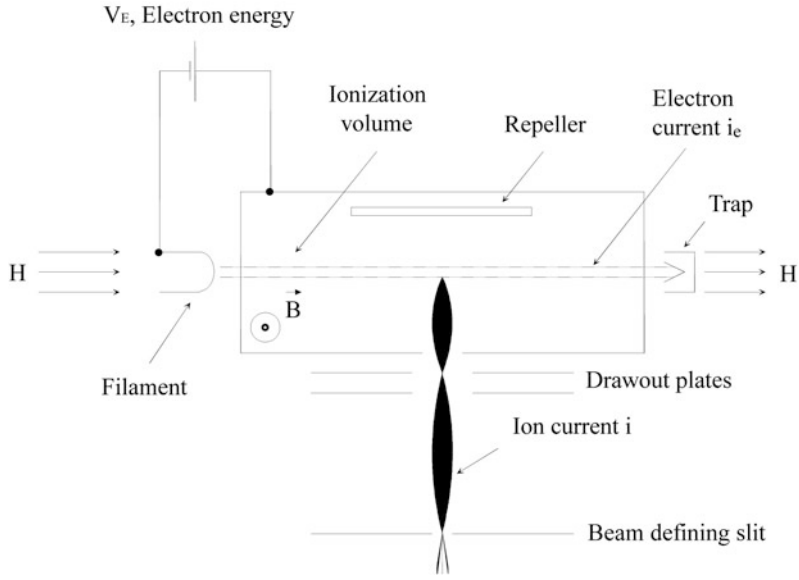

Fig. 3 Schematic of a Nier-type source. A tungsten filament operating at a current of around 2.5 A emits a beam of electrons which passes through the ionisation volume and is measured by the trap. The electron current received by the trap, H, is usually of the order 10–800 μA; the filament current is regulated in order that H is kept constant. A magnetic field (B) in the source increases the electron path length and thus increases sensitivity. The ions are extracted by adjusting the voltages on the repeller and draw out plates

molecules in an ionization chamber by electron bombardment (where an energetic electron colliding with a neutral gas atom or molecule dislodges an electron from the neutral species, thereby creating a positive ion). An ion repeller behind the electron beam and a series of lenses extract the ions from the source and focus these into a well-collimated ion beam.

The ionisation chamber of Nier-type sources are placed within a magnetic field (usually created by small external permanent magnets) which increases the path length of the electrons in the ionisation region, thereby increasing the sensitivity of the source but with the disadvantage that this induces mass discrimination effects in the source itself. Baur-Signer sources have no magnetic field within the source relying instead on a circular filament to provide a focussed, conical electron beam. These sources therefore have considerably less mass discrimination but also typically have lower sensitivity than Nier-type sources. The efficiency of the source increases with mass (Fig. 4) for a given source setting.

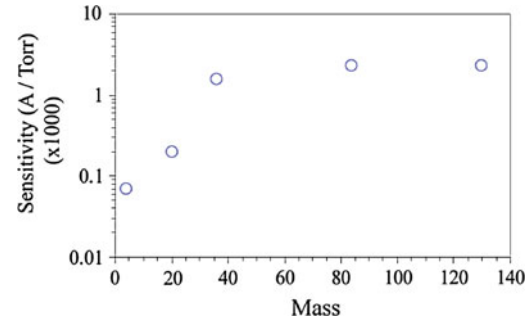

Fig. 4 Sensitivity vs. mass of gas analysed (^{4}He, ^{20}Ne, ^{36}Ar, ^{84}Kr and ^{130}Xe). For the same source settings, sensitivity increases with the mass of the gas analysed and depends only on the effective ionisation cross section of the target atom (Botter and Bouchoux 1995)

The intensity of the electron beam is monitored within the source (the "trap current", usually between 10 and 800 μA) and the filament current controlled so as to keep electron beam intensity constant. Intensity of the electron beam has a strong effect on both sensitivity and mass discrimination (see Sect. 2.1.2 below) of the mass spectrometer (Fig. 5), therefore it is

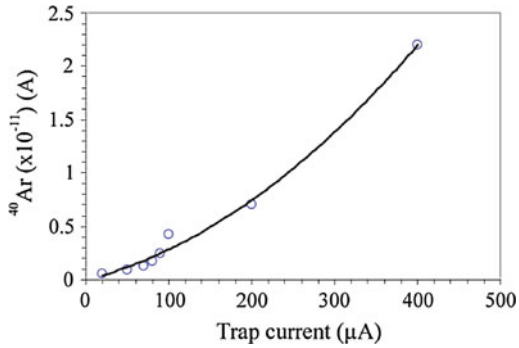

Fig. 5 ^{40}Ar signal as a function of trap current, VG5400. A constant pressure of argon was introduced in the mass spectrometer for each measurement. For all other source settings kept constant, the signal increases approximately linearly with the trap current

important to ensure the electron beam intensity does not fluctuate.

2.1.2 Pressure Dependent Effects

The response of a noble gas ion source depends on the pressure within the source itself (Burnard and Farley 2000); as a result, the sensitivity of the mass spectrometer is not linear with pressure, and mass discrimination also depends on the quantity of gas being analyzed (i.e. the pressure in the source). These effects are considerably less important for Bauer-Signer type sources than for modified Nier-type sources (see Figs. 6 and 7). As a result, it is important that pure noble gases are admitted into the mass spectrometer preferably one noble gas at a time, and that samples and standards are similar in purity, pressure and composition (see Sect. 2.2.3). It is thought that these pressure dependent effects result from the distribution of space charges within the ionization volume (Burnard and Farley 2000; Baur 1980). Space charges result from passing an electron beam through the insulated ionization volume. At small ion currents (low source pressures), the ion chamber is essentially well isolated and large space charge potentials can exist. However, increasing the density of ions in the source (high source pressures), these space charges can be redistributed by the ions themselves. Hence the pressure-dependent effects are more significant at high electron beams (high trap currents; Fig. 6). Pressure dependent effects are most significant for He and can be >5 % for typical sample sizes for Nier-type sources (Sano et al. 2008): mass discrimination will be greater for He than for the remaining noble gases due to the large mass difference between the two He isotopes, and, in addition, He requires higher electron beam currents (higher trap currents) than the heavier noble gases in order to compensate for the lower He ionization efficiency (Fig. 4), and increasing trap current is a convenient way of increasing He sensitivity.

2.1.3 Isobaric interferences

Despite thorough baking and the presence of getters in the mass spectrometer, there are frequently background atoms or molecules in the region of the noble gas peaks. Common interferences that are known in noble gas mass spectrometers are given in Table 1 (an exhaustive list is not possible, particularly at high masses where many different molecules may exist).

2.2 Extraction and Purification

In general, the noble gases are present in low to very low concentrations in geological materials (fluids and rocks); in certain circumstances, radiogenic noble gases such as ^{4}He or ^{40}Ar may comprise up to a few percent of a fluid or mineral (e.g. air contains nearly 1 % ^{40}Ar by volume) but more usually these are present at ppm concentrations or lower. The less abundant noble gases may be present at only a few thousand atoms per gram. There are two obvious consequences of this observation: (1) relatively large bulk samples are required compared to many other geochemical analyses and (2) it is necessary to extract and separate the noble gases from their host phase(s) for analysis. Extraction of noble gases depends on the nature of the major phase (fluid, solid) and on the scientific objectives (bulk or micro sampling). Analysis by mass spectrometry typically requires samples of a single, pure noble gas, therefore purification and separation of the noble gases is required following extraction. Most modern

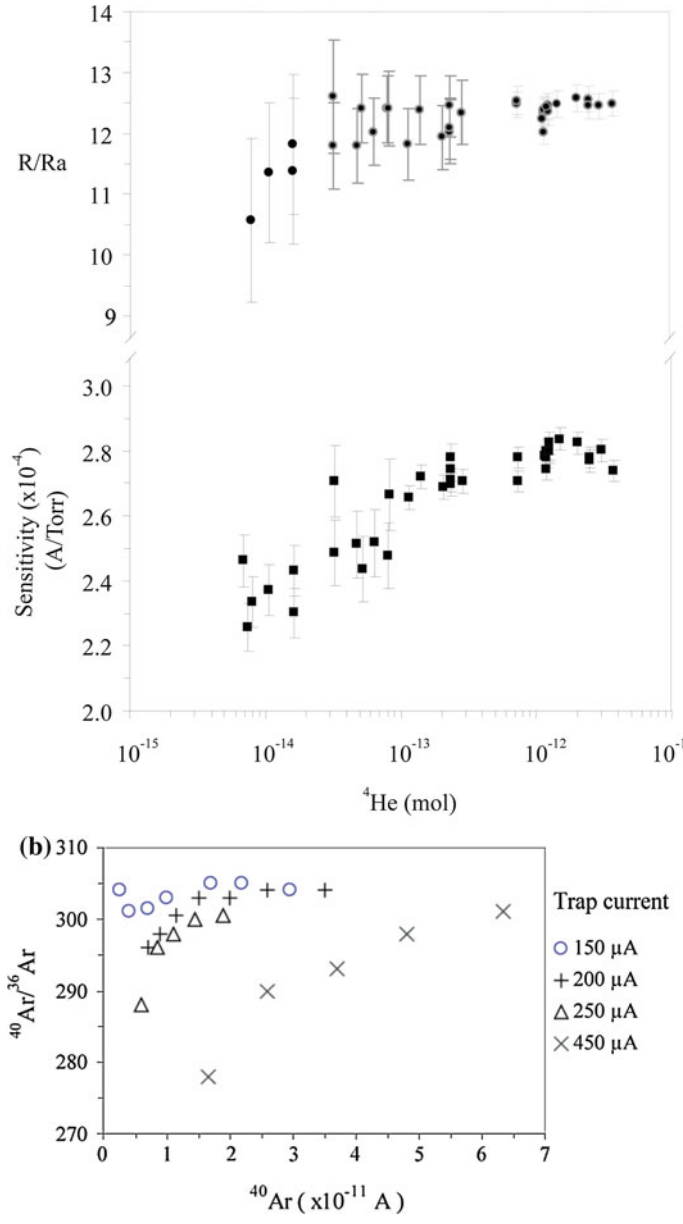

Fig. 6 Non-linearity of a Nier-type source. **a** He isotope discrimination and He sensitivity as a function of pressure ($\equiv^4$He mol) for constant source settings (trap current = 400 µA). **b** ^{40}Ar/ ^{36}Ar discrimination as a function of trap current and pressure ($\equiv^{40}$Ar signal). Coulié (2001) similarly observes an increase in mass discrimination for Ar, up to 8 %, as a function of the trap current

extraction-purification systems are made of steel as most types of glass are permeable to He.

2.2.1 Extraction: Fluid Samples

The noble gases are in general poorly soluble in both aqueous and hydrocarbon liquids, hence, under vacuum, they will preferentially partition into the head space above a liquid. Extraction of noble gases from liquids makes use of this property: the sample is equilibrated with a volume under static vacuum (i.e. a volume isolated from all pumps), and the noble gases (along with any other insoluble gases such as CH_4 or CO_2) exsolve from the liquid into the headspace (Fig. 8). As the equilibration time may be long (>30 min for the heavy noble gases), samples may be heated and/or stirred to accelerate degassing. Further details on preparation of petroleum samples are available in (Pinti and Marty 1995) and Chap. 9 of this

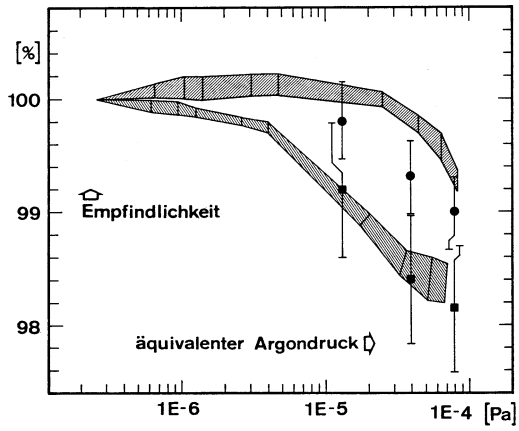

Fig. 7 Non-linearity of Ar sensitivity of a baur-signer source (from Baur 1980). Measured (*shaded areas*) and simulated (*data points*) relative Ar-sensitivity of a GSVII (GS98) Baur-Signer ion source versus equivalent Ar pressure (equivalent Ar pressures were obtained by measuring the ion current of ^{40}Ar during stepwise admission of known amounts of He to the static mass spectrometer; the measured ^{4}He ion current was multiplied by $\sqrt{(^{4}He/^{40}Ar)}$ to get an equivalent ^{40}Ar ion current and a corresponding equivalent Ar pressure that would cause the same space charge). The measurements were performed with two different α-slit settings, 0.063 rad for the upper curve and circular symbols, 0.038 rad for the lower curve and square symbols. The maximum sensitivities (=100 %) for the two slits are 1.1 and 1.0 mA $torr^{-1}$ respectively. The measurements were made at 2.5×10^{-4}. A total filament emission and 100 eV electron energy

volume, and of water samples in (Beyerle et al. 2000) and Chaps. 5 and 6 of this volume.

Fluid samples are commonly collected in copper pinch-off tubes where a length of annealed, refrigeration grade Cu tubing is placed between two clamps (Fig. 9). The tube is connected to the fluid source (gas, water or petroleum) and once satisfactorily filled with the fluid (i.e. no air remains in the tube, sometimes requiring extensive flushing of the Cu tube), the clamps are tightened creating a cold-weld seal trapping the fluid between the clamps. In order to extract the fluid from the sample, the end of the Cu tube is connected to the vacuum system (usually via the expansion chamber), the clamp closest to the extraction system is removed and the tube gently opened using pliers or a small vice.

2.2.2 Extraction: Solid Samples

Noble gases may be sited either within a mineral's lattice (for example, in situ production of the radiogenic noble gases or dissolved components) or within a liquid or a melt inclusion trapped in the mineral in question. Solutions exist which favour preferential extraction of noble gases from either site. Heating the sample using a furnace or a long-wavelength laser (CO_2 or Nd-YAG) will release gases from the mineral lattice either by diffusion or by melting the sample, but this will also release any inclusion-hosted gases within the sample. Fluids can be released from fluid inclusions by crushing the sample under vacuum; some targeted applications also use short wavelength lasers to open vesicles or fluid inclusions (Burnard et al. 1998; Raquin et al. 2008), although the quantities of the less abundant noble gases in individual inclusions are generally insufficient for analysis.

Most furnaces for noble gas extraction are double vacuum systems, where the sample is placed in an interior tube which is heated by an external resistance element, itself located in a second, evacuated tube (otherwise the resistance element would be rapidly consumed by atmospheric oxygen) (Fig. 10). Temperatures of 2,150 °C have been reported using this type of furnace (Turner et al. 1990), although more commonly maximum temperatures are of the order 1,600–1,800 °C.

It is also possible to place the resistance element within the same vacuum as the sample (i.e. no double vacuum system) with the advantage that less refractory metal is required (reducing fabrication and running costs). However, having the heating element in the same volume as the sample considerably degrades vacuum quality, requiring more rigorous purification of the noble gases after extraction.

Induction furnaces can also be used to heat samples for noble gas analyses; a radiofrequency alternating current in a solenoid coil external to the vacuum system induces a current in a metal crucible (usually of Ta or Mo) within the vacuum chamber, thereby heating the crucible to temperatures up to 1,800 °C. While induction

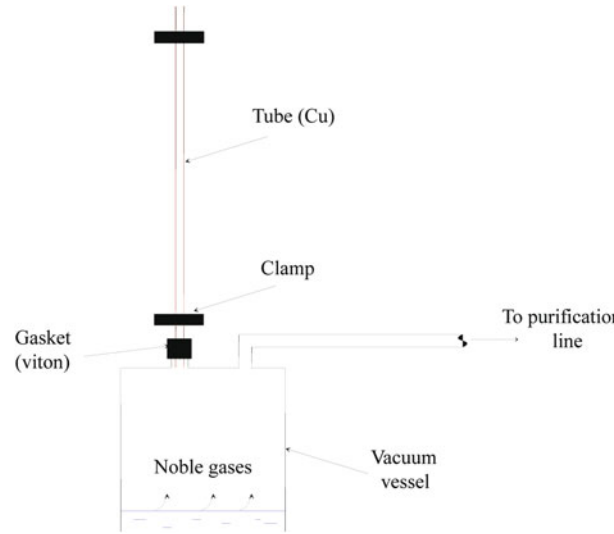

Fig. 8 Schematic diagram of an expansion device for extracting noble gases from liquid samples. The tube is connected to the expansion vessel via a viton gasket; once a good vacuum has been obtained, the lower clamp is opened, transferring the water from the tube into the vacuum vessel. Being insoluble, the noble gases preferentially partition into the headspace above the liquid, ready for purification and analysis

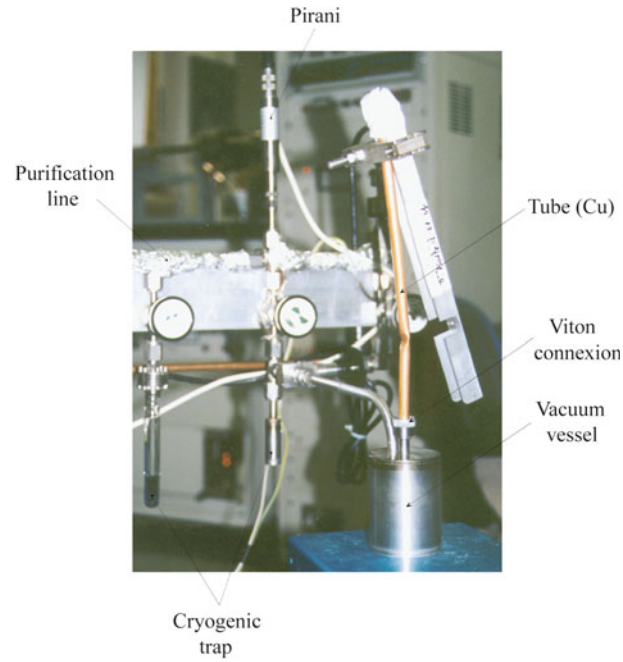

Fig. 9 A copper pinch-off tube in place for analysis

furnaces are efficient and reliable, the vacuum envelope cannot be made of a conducting material: usually this is made of glass which, in turn, results in high He blanks.

Although largely used for U + Th/He thermochronology, diode (808 nm) or Nd-YAG (1,064 nm) lasers can be used instead of resistance elements in order to heat small (10s of mg) samples. In these systems, the sample is placed within a laser cell with a suitable window that transmits the laser wavelength and yet withstands the UHV conditions required for noble gas analyses (sapphire is commonly used) (Foeken et al. 2006; House et al. 2000). Addition

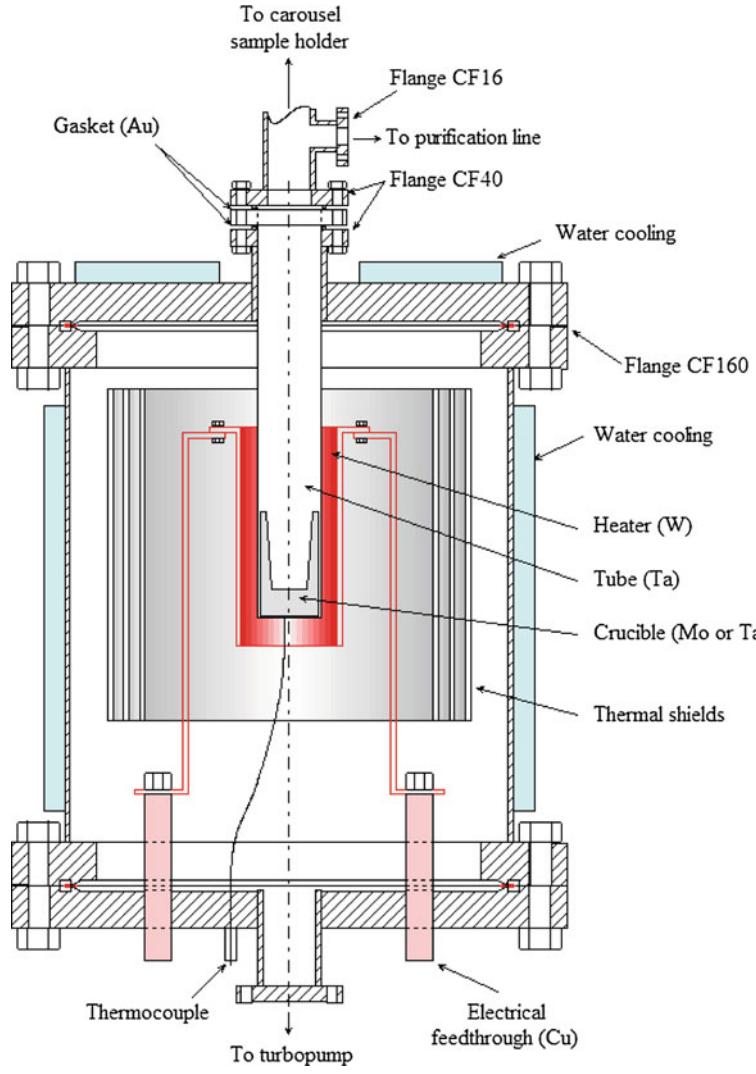

Fig. 10 Schematic diagram of a classical double-vacuum high temperature furnace

of a flux which couples well with the laser wavelength may permit larger sample volumes to be melted [e.g. up to 150 mg quartz according to Foeken et al. (2006)].

Crusher devices aim to reduce the sample grainsize under vacuum thus rupturing vesicle and (fluid) inclusions in the samples (Scarsi 2000). It is important therefore to start with grains that are considerably larger than the inclusions/vesicles in the sample. All crushers are "home-made" and as a result there are many different designs. Two broad types of crusher can be identified, those that crush by repeated "hammering" under vacuum, and those that crush the sample principally by application of pressure to the sample. The former (Fig. 11) typically place a soft-iron piston in a vertical tube above the sample and then use external electromagnets to raise and drop the piston on the sample. Repeated (up to several hundred) strokes can be used to completely pulverise the sample. Pressure-type crushers have a mortar connected via a bellows to an external device which applies pressure to the samples (Burnard et al. 2003). The pressure is created either by a hydraulic press or by screw threads [common

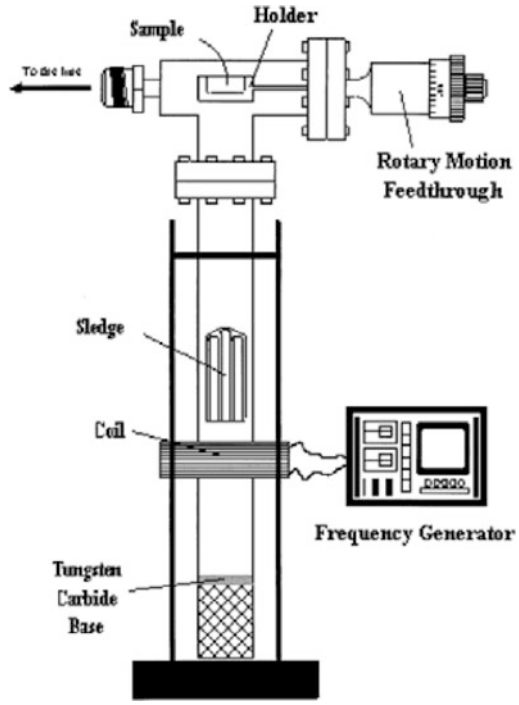

Fig. 11 Schematic view of a Piston type crusher from (Scarsi 2000). The sample is placed in the holder at the top of the tube. When ready (i.e. when blanks are acceptable), the holder is rotated and the sample falls to the base of the tube (slots cut in the piston or "sledge" permit the sample to pass to the bottom of the tube) and the piston actuated by means of the external electromagnet induced in the coils around the tube

examples use a modified valve assembly to transfer the movement onto the sample (Stuart et al. 1994)].

2.2.3 Purification

It is necessary to purify the extracted gases in order to admit pure (or as pure as possible) noble gases into the mass spectrometer. Purification usually takes advantage of the non-reactivity of the noble gases, chemically removing active species from the extracted gases. "Getters" are active metal surfaces which combine with the reactive gases either by adsorption or more commonly by chemi-sorption. Common metals are Ti or Zr based alloys (Ag is also known), either in the form of a sponge or deposited onto a high surface area substrate. Usually the getter is "activated" at high temperature (up to 900 °C), which creates the active metal surface. "Flash getters" evaporate a layer of the metal onto the interior of the vessel. Getters are usually more efficient for most gases when held at moderate temperature (e.g. c. 500 °C for Ti sponge) but they will also consume active gases at room temperature. The precise purification cycles vary considerably from laboratory to laboratory and/or depending on the nature of the sample (e.g. the quantity of active gases to be removed) but will commonly use both hot and cold getters. Although in theory the noble gases are not affected by getters, there is some evidence that in fact Xe can be irreversibly adsorbed on some getter materials (D Pinti pers comm.).

2.2.4 Cryoseparation

In order to separate mixtures of (purified) noble gases released from the sample into single noble gas aliquots suitable for analysis, the noble gas mixture is commonly reversibly adsorbed onto a substrate at low temperature (Reynolds et al. 1978). The substrate is usually activated charcoal or sintered metal; plain metal stainless tube can also be used (Lott 2001). Raising the temperature will sequentially release the noble gases in order of mass; the exact temperatures depend on the installation and substrate but common values (temperatures in Kelvin) for activated charcoal are He: 20; Ne: 50; Ar: 140; Kr: 180; Xe: 280. For condensing Ar, Kr and Xe on activated charcoal, the trap can be cooled with an external liquid nitrogen bath ($T = 77$ K) but in order to condense He and Ne temperatures lower than liquid nitrogen are required [c. 15 K for He and c. 40 K for Ne (Reynolds et al. 1978)] a refrigerator that cools to below c. 20 K is required. The most common solutions use a Gifford McMahon cooler where a compressed He expansion cycle cools a cryogenic trap containing activated charcoal or similar adsorbent. Numerous commercial propositions exist.

2.3 Calibrating Noble Gas Mass Spectrometers

The response of the mass spectrometer has to be calibrated against standards of known isotopic composition and/or known quantity of noble gas. While some mineral standards are beginning to appear, most calibrations are performed relative to a gas standard where a bottle contains a pre-determined pressure of gas of known isotopic composition. An aliquot of this gas (trapped between two valves) is expanded into the mass spectrometer (after purification and/or cryogenic separation as necessary). For Ne, Ar, Kr and Xe, the gas used is almost always air (at reduced pressure); the composition of the atmosphere is assumed to be known and constant (see Chap. 2 of this volume). Some laboratories also use air for He calibration; however, given the low abundance of He in the atmosphere, relatively large volumes of air are required with attendant difficulties purifying the He. Various laboratories have fabricated their own He standards for example by extracting the He from He-rich rocks (MORB glasses), by purifying He-rich volcanic gases (most commonly from "Murdering Mudpots", Yellowstone National Park, USA, or Reunion Island) or by mixing known quantities of ^{3}He and ^{4}He. The best known of the latter is the HeSJ standard (Matsuda et al. 2002) which has been distributed to several noble gas labs worldwide. However, it should be noted that all the "home-made" He standards are nevertheless ultimately calibrated against atmospheric He which is also assumed to have a constant concentration and composition.

References

Aldrich LT, Nier AO (1948a) Argon 40 in potassium minerals. Phys Rev 74(8):876–877

Aldrich LT, Nier AO (1948b) The occurence of He-3 in natural sources of helium. Phys Rev 74(11):1590–1594

Alvarez LW, Cornog R (1939) He-3 in helium[4]. Phys Rev 56(4):379

Baur H (1980) Numerische simulation und praktische erprobung einer rotationssymmetrischen ionenquelle für gasmassenspektrometer. No. 6596. In, vol. ETH, Zürich

Baur H (1999) A noble-gas mass spectrometer compressor source with two orders of magnitude improvement in sensitivity. EOS 80:F1118

Beyerle U, Aeschbach-Hertig W, Imboden DM, Baur H, Graf T, Kipfer R (2000) A mass, spectrometric system for the analysis of noble gases and tritium from water samples. Environ Sci Technol 34(10):2042–2050

Botter R, Bouchoux G (1995) Spectrométrie de masse. Techniques de l'ingenieur, Analyse et caracterisation 4:2615

Burnard PG, Farley KA (2000) Calibration of pressure-dependent sensitivity and discrimination in Nier-type noble gas ion sources. Geochem Geophys Geosyst 1:2000GC000038

Burnard PG, Farley KA, Turner G (1998) Multiple fluid pulses in a samoan harzburgite. Chem Geol 148:99–114

Burnard PG, Harrison DW, Turner G, Nesbitt R (2003) Degassing and contamination of noble gases in Mid-Atlantic Ridge basalts. Geochem Geophys Geosyst 4(1). doi:10.1029/2002GC000326

Clarke WB, Beg MA, Craig H (1969) Excess 3He in the sea: evidence for terrestrial primordial He. Earth Planet Sci Lett 6:213–220

Colin A, Burnard P, Graham DW, Marrocchi Y (2011) Plume-ridge interaction along the Galapagos Spreading Center: discerning between gas loss and source effects using neon isotopic compositions and 4He-40Ar-CO2 relative abundances. Geochim Cosmochim Acta (75):1145–1160. doi:10.1016/j.gca.2010.11.018

Coon JH (1949). He-3 isotopic abundance. Phy Rev 75(9):1355–1357

Coulie E (2001) Chronologie Ar/Ar et K/Ar de la dislocation du plateau éthiopien et de la déchirure continentale dans la corne d'afrique depuis 30 Ma. In, vol. Université de Paris XI, Orsay

Crowther SA, Mohapatra RK, Turner G, Blagburn DJ, Kehm K, Gilmour JD (2008) Characteristics and applications of RELAX, an ultrasensitive resonance ionization mass spectrometer for xenon. J Anal At Spectrom 23(7):938–947

Daunt JG, Probst RE, Johnston HL, Aldrich LT, Nier AO (1947) A new method of separation of the isotopes He3 and He4. Phys Rev 72(6):502–503

Dempster AJ (1918) A new method of positive ray analysis. Phys Rev 11(4):316–325

Farley KA (2002) (U-Th)/He dating: techniques, calibrations, and applications. Rev Mineral Geochem 47

Foeken JPT, Stuart FM, Dobson KJ, Persano C, Vilbert D (2006) A diode laser system for heating minerals for (U-Th)/He chronometry. Geochem Geophys Geosyst 7(4)

Gilmour JD, Lyon IC, Johnston WA, Turner G (1994) RELAX: an ultrasensitive, resonance ionization mass spectrometer for xenon. Rev Sci Instrum 65(3):617–625

Grochala W (2007) Atypical compounds of gases, which have been called 'noble'. Chem Soc Rev 36(10):1632–1655

Holland G, Ballentine CJ (2006) Seawater subduction controls the heavy noble gas composition of the mantle. Nature 441(7090):186–191

Holland G, Cassidy M, Ballentine CJ (2009) Meteorite Kr in earth's mantle suggests a late accretionary source for the atmosphere. Science 326(5959):1522–1525

Hooker PJ, Bertrami R, Lombardi S, O'Nions RK, Oxburgh ER (1985) Helium-3 anomalies and crust-mantle interaction in Italy. Geochim Cosmochim Acta 49(12):2505–2513

House MA, Farley KA, Stockli D (2000) Helium chronometry of apatite and titanite using Nd-YAG laser heating. Earth Planet Sci Lett 183(3–4):365–368

Iwata Y, Ito C, Harano H, Aoyama T (2010) Improvement of the resonance ionization mass spectrometer performance for precise isotope analysis of krypton and xenon at the ppt level in argon. Int J Mass Spectrom 296(1–3):15–20

Jenkins WJ (1987) H-3 and HE-3 in the beta triangle—observations of gyre ventilation and Oxygen Utilization rates. J Phys Oceanogr 17(6):763–783

Lavielle B, Gilabert E, Thomas B, Lavastre V (2006) New RIS-TOF facility for measuring very small Kr and Xe gas samples. Geochim Cosmochim Acta 70(18):A344–A344

Lord Rayleigh; Ramsay W (1895) VI. Argon: a new constituent of the atmosphere. Philosop Trans Royal Soc London A 186:187-241

Lott DE (2001) Improvements in noble gas separation methodology: a nude cryogenic trap. Geochem Geophys Geosyst 2:2001GC000202

Lu ZT, Mueller P (2010) Atom trap trace analysis of rare noble gas isotopes. Adv At Mol Opt Phy 58:173–205

Lupton JE, Johnson HPe, Embley RWe (1990) Water column hydrothermal plumes on the Juan de Fuca Ridge, special section; axial seamount; an active ridge axis volcano on the central juan de Fuca ridge. J Geophys Res B: Solid Earth Planet 95(8):12,829–812,842

Mamyrin BA, Anufriyev GS, Kamenskiy IL, Tolstikhin IN (1970) Determination of the isotopic composition of atmospheric helium. Geochem Int 7:498–505

Mamyrin BA, Tolstikh In, Anufriye Gs, Kamenski Il (1969) Isotopic analysis of terrestrial helium on a magnetic resonance mass spectrometer. Geochem Int Ussr 6(3):517

Marrocchi Y, Burnard PG, Hamilton D, Colin A, Pujol M, Zimmermann L, Marty B (2009) Neon isotopic measurements using high-resolution, multicollector noble gas mass spectrometer: HELIX-MC. Geochem Geophys Geosyst 10:art no. Q04015

Matsuda J, Matsumoto T, Sumino H, Nagao K, Yamamoto J, Miura Y, Kaneoka I, Takahata N, Sano Y (2002) The 3He/4He ratio of new internal He standard of japan (HESJ). Geochem J 36(2):191–195

McNaught AD, Wilkinson A (1997) IUPAC Compendium of Chemical Terminology, 2nd edn. Blackwell Science, Cambridge

Nagao K, Takaoka N, Matsubayashi O (1981) Rare gas isotopic compositions in natural gases of Japan. Earth Planet Sci Lett 53(2):175–188

Neidherr D, Cakirli RB, Audi G, Beck D, Blaum K, Bohm C, Breitenfeldt M, Casten RF, George S, Herfurth F, Herlert A, Kellerbauer A, Kowalska M, Lunney D, Minaya-Ramirez E, Naimi S, Rosenbusch M, Schwarz S, Schweikhard L (2009) High-precision Penning-trap mass measurements of heavy xenon isotopes for nuclear structure studies. Phys Rev C: Nucl Phys 80(4)

Parai R, Mukhopadhyay S, Lassiter JC (2009) New constraints on the HIMU mantle from neon and helium isotopic compositions of basalts from the Cook-Austral Islands. Earth Planet Sci Lett 277(1–2):253–261

Pinti DL, Marty B (1995) Noble gases in crude oils from the Paris Basin, France: implications for the origin of fluids and constraints on oil-water-gas interactions. Geochim Cosmochim Acta 59(16):3389–3404

Ramsay W, Travers MW (1898) On a new constituent of atmospheric air. Proc Royal Soc London 63 (1): 405–408

Raquin A, Moreira MA, Guillon F (2008) He, Ne and Ar systematics in single vesicles: mantle isotopic ratios and origin of the air component in basaltic glasses. Earth Planet Sci Lett 274(1–2):142–150

Reynolds JH (1956) High sensitivity mass spectrometer for noble gas analysis. Rev Sci Instrum 27(11): 928–934

Reynolds JH, Jeffery PM, McCrory GA, Varga PM (1978) Improved charcoal trap for rare gas mass spectrometry. Rev Sci Instrum 49(4):547–548

Sano Y, Wakita H (1988) Precise measurement of helium isotopes in terrestrial gases. Bull Chem Soc Japan 61:1153–1157

Sano Y, Tokutake T, Takahata N (2008) Accurate measurement of atmospheric helium isotopes. Anal Sci 24(4):521–525

Sano Y, Tominaga T, Nakamura Y, Wakita H (1982) He-3/He-4 ratios of methane-rich natural gases in japan. Geochem J 16(5):237–245

Sano Y, Wakita H (1985) Geographical distribution of (super 3) He/(super 4) He ratios in Japan; implications for arc tectonics and incipient magmatism. J Geophys Res B 90(10):8729–8741

Scarsi P (2000) Fractional extraction of helium by crushing of olivine and clinopyroxene phenocrysts: effects on the $^{3}He/^{4}He$ measured ratio. Geochim Cosmochim Acta 64(21):3751–3762

Strashnov I, Blagburn DJ, Gilmour JD (2011) A resonance ionization time of flight mass spectrometer with a cryogenic sample concentrator for isotopic analysis of krypton from extraterrestrial samples. J Anal At Spectrom 26(9):1763–1772

Stuart FM, Turner G, Taylor R (1994) He-Ar isotope systematics of fluid inclusions: resolving mantle and crustal contributions to hydrothermal fluids. In: Matsuda J (ed) Noble gas geochemistry and cosmochemistry. Terra Scientific, Tokyo, pp 261–277

Thonnard N (1995) Resonance ionization of heavy noble-gases—the potential of krypton and xenon measurements from single presolar grains. Meteoritics 30(5):588

Turner G, Burgess R, Bannon M (1990) Volatile-rich mantle fluids inferred from inclusions in diamond and mantle xenoliths. Nature 344:653–655

Wang LB, Mueller P, Holt RJ, Lu ZT, O'Connor TP, Sano Y, Sturchio NC (2003) Laser spectroscopic measurement of helium isotope ratios. Geophys Res Lett 30(11):1592

Noble Gases in the Atmosphere

Yuji Sano, Bernard Marty and Pete Burnard

Abstract

The atmosphere is the primary terrestrial reservoir of the heavy noble gases (Ne, Ar, Kr, Xe) and precise knowledge of the isotopic composition of atmospheric noble gases is important for many—if not all—fields of noble gas geochemistry. Air noble gases, including helium, are very commonly used as a running laboratory standard for calibrating instrumental discrimination and sensitivity (see Chap. 1), hence any potential temporal or spatial heterogeneities in the atmospheric noble gas composition could have consequences for the reliability and comparability of noble gas data. Metrological measurements such as the determination of Avogadro's constant and the gas constant also depend on accurate determination of the isotopic composition (and isotopic masses) of atmospheric noble gases. However, absolute isotopic measurements are not straightforward and this section reviews both how absolute isotopic determinations have been made and assesses the temporal and spatial variability of the atmosphere at the present and in the recent (<2 Ka) past.

1 Determination of the Present-Day Atmospheric Noble Gas Compositions

1.1 Absolute Determinations of the Atmospheric $^{3}He/^{4}He$

The terrestrial air contains He with a concentration of 5.24 ppm by volume (Gluckauf 1946; Gluckauf and Paneth 1946), considerably lower than would be predicted from solid Earth degassing of radiogenic ^{4}He, because He escapes from the high temperature exosphere to inter-planetary space as a result of its light mass (Kockarts and

Y. Sano (✉)
Division of Ocean-Earth System Science, Atmosphere and Ocean Research Institute, The University of Tokyo, Kashiwano-ha, Chiba 277-8564, Japan
e-mail: ysano@aori.u-tokyo.ac.jp

B. Marty · P. Burnard
Centre de Recherches Pétrographiques et Géochimiques, BP 20 Vandoeuvre-lès-Nancy Cedex, France

P. Burnard (ed.), *The Noble Gases as Geochemical Tracers*, Advances in Isotope Geochemistry,
DOI: 10.1007/978-3-642-28836-4_2,

Nicolet 1962) Helium is nevertheless supplied to the atmosphere by the solid Earth through volcanic activity (Craig et al. 1975), fault movements, erosion and groundwater circulation (Sano et al. 1998). The helium content and isotopic composition of the atmosphere are therefore the result of a balance between degassing from the mantle and crust, and escape of He isotopes to space. Since the residence time of He in the atmosphere is approximately 10^6 years (Torgersen 1989) and is significantly longer than the mixing time in the atmosphere of a few years (Tans et al. 1989), the air $^3He/^4He$ ratio is believed to be constant on a global scale (Lupton 1983). On this basis most laboratories engaged in helium isotope measurements use atmospheric helium as a natural isotopic standard (Lupton and Graham 1991). The $^3He/^4He$ ratios of terrestrial samples are usually expressed as a unit of Ra where Ra is the atmospheric $^3He/^4He$ ratio.

Aldrich and Nier (1948) were the first to measure the atmospheric $^3He/^4He$ ratio although their measurements were not calibrated against an absolute standard (i.e. pure ^3He and ^4He were not available); Coon (1949) also reported $^3He/^4He$ ratios of atmospheric and natural gases using neutron activation analysis where ^3He was detected by counting ionization pulses arising from the disintegration products of the reaction $^3He(n,p)^3H$ induced by thermal neutrons. Their measured atmospheric $^3He/^4He$ ratio was $(1.3 \pm 0.2) \times 10^{-6}$, which agreed well with the value of $(1.2 \pm 0.2) \times 10^{-6}$, reported by (Aldrich and Nier 1948).

There are only three absolute $^3He/^4He$ measurements of atmospheric helium in the literature. In 1970, Mamyrin et al. (1970) reported that the atmospheric $^3He/^4He$ ratio in St. Petersburg, Russia, was $(1.399 \pm 0.013) \times 10^{-6}$ (1σ) and that air helium ratio did not vary with latitude, longitude, and altitude (up to 10 km) within the error margins of the individual measurements of about $2 \sim 3$ %. Clarke et al. (1976) re-determined the atmospheric $^3He/^4He$ ratio in Ontario, Canada. The value of $(1.384 \pm 0.006) \times 10^{-6}$ (1σ) was somewhat lower but in agreement, within error, of the St Petersburg value. The average of the two measurements, 1.39×10^{-6} was accepted as the air $^3He/^4He$ ratio until the end of 1980s when Sano et al. (1988) determined an atmospheric $^3He/^4He$ ratio of $(1.343 \pm 0.013) \times 10^{-6}$ (1σ) at Ueno Pak, central Tokyo, Japan. This value was apparently lower than the previous data. Either experimental artifacts and/or natural phenomenon accounted for the difference. The International Union of Pure and Applied Chemists (IUPAC) committee currently uses Sano et al's value $(1.343 \pm 0.013) \times 10^{-6}$). In 1990, Davidson and Emerson (1990) measured the absolute ^3He content of air by mass spectrometry. When combined with an earlier measurement of the atmospheric ^4He abundance (Holland and Emerson 1987), this provides an additional estimate of the atmospheric $^3He/^4He$ ratio of $(1.393 \pm 0.014) \times 10^{-6}$ (1σ). The average of the above determinations taking into their weighted errors is $(1.382 \pm 0.005) \times 10^{-6}$ (1σ) and this is likely the best estimate of atmospheric helium isotopic composition (Ra) for the period 1970–1990.

It should also be noted that Matsuda et al. (2002) have prepared an artificial mixture of ^3He and ^4He to be used as an internal standard for precise measurements of mantle-derived samples and for cosmogenic dating. Since He is depleted in air and the isotopic composition is low compared with mantle-derived or cosmogenic samples, a large volume of air is needed to obtain an adequate ^3He signal in the mass spectrometer, creating purification difficulties. It is in any case preferable to have the composition of the standard as close as possible as the samples. As a result, an artificial standard with a high $^3He/^4He$ ratio was required. The standard prepared for the purpose is called the "He Standard of Japan" (HESJ) and the recommended ratio is 20.63 ± 0.10 Ra (1σ) calculated by the weighted mean of six independent determinations relative to air in four noble gas laboratories.

1.2 Absolute Measurements of Atmospheric Ar Isotope Ratios

Of all the noble gases, accurate determination of the atmospheric Ar isotopic composition is

probably the most important; not only is Ar the most abundant atmospheric noble gas but is certainly the most measured noble gas. For example, the K–Ar and Ar–Ar methods for dating rocks and minerals depend on knowledge of the atmospheric $^{40}Ar/^{36}Ar$ and $^{40}Ar/^{38}Ar$ ratios for mass discrimination corrections (Turrin et al. 2010) and for correcting for atmospheric contamination.

The atmospheric Ar isotope ratio was originally reported in a seminal paper by Nier (1950a) and has more recently been revisited by two independent studies. Absolute isotope determinations consist of creating reference gases with known isotopic ratios by mixing known quantities of the pure (or as near-pure as possible) isotopes. The reference gases are then used in order to characterize instrumental mass fractionation (IMF) in the mass spectrometer. Once the IMF is well known then the unknown (atmospheric Ar) can be measured and corrected for the mass spectrometer fractionation in order to estimate the true isotope composition.

Nier (1950a) mixed isotopically pure ^{40}Ar and ^{36}Ar produced by selective thermal diffusion; the respective quantities were determined volumetrically. The discrimination of two different mass spectrometers (MS1 and MS2) were constrained using four mixtures with different $^{40}Ar/^{36}Ar$ ratios; this mass discrimination was measured at 1.6 ± 0.3 per mil per mass unit for the MS1 mass spectrometer (the more accurate of the two mass spectrometers). Nier measured values of 295.5 ± 0.5 (1σ) and 0.1,880 ± 0.0003 for $^{40}Ar/^{36}Ar$ and $^{38}Ar/^{36}Ar$ respectively on laboratory air (dried over hot lithium metal); commercially available gas (Air Reduction Sales Corporation) was also analyzed but found to be fractionated (depleted in ^{36}Ar and ^{38}Ar relative to air).

The isotopic composition of air was re-investigated in 2006 by Lee et al. (2006) who used considerably more precise gravimetric methods to constrain the masses of the isotopic mixtures, and used multicollection mass spectrometry (a MAT271 gas source mass spectrometer) to better constrain the discrimination and isotopic ratios. Lee et al. proposed $(^{40}Ar/^{36}Ar)_{air} = 298.6 \pm 0.3$ (1σ) and $(^{38}Ar/^{36}Ar)_{air} = 0.1885$. Most recently, Valkiers et al. (2008) using a similar methodology to Lee et al. (gravimetric mixtures but starting with different gases) confirmed the redetermined $^{40}Ar/^{36}Ar$ value (obtaining a value of 298.7 ± 0.1) but disagreed for the $(^{38}Ar/^{36}Ar)_{air}$ measurement, finding a value of 0.1898 ± 0.0001.

Without constraining the IMF, Mark et al. (2011) recently measured $^{40}Ar/^{36}Ar$ and $^{38}Ar/^{36}Ar$ on different air aliquots reasoning that since IMF results in mass-dependent fractionation, then the true atmospheric isotopic composition should lie on the mass fractionation line (the slope defined by $\sqrt{(40-36)/(38-36)}$) passing through the raw (non-IMF corrected) mass spectrometer data. Assuming that this hypothesis is correct, it would appear to confirm that the Lee et al. (2006) measurements are the best estimate of modern air (Fig. 1).

It is important to note that commercial processing of air can fractionate Ar isotopes: Valkiers et al. (2008) observed a spread in $^{40}Ar/^{36}Ar$ of ~ 1 % in commercial sources of Ar produced by distilling air. However, Mark et al. (2011) found no difference between commercial Ar (produced by distilling air) and locally sampled air. Similar variations have been observed for Ne isotopes (Pavese et al. 2005). Mass fractionation for distilled gases depends in fact on the distillation process itself and may vary from tank to tank.

1.3 Absolute Measurements of Ne, Kr and Xe Isotopic Compositions

Nier (1950b) determined the isotopic compositions of Ne, Kr and Xe in the atmosphere using the same mass spectrometer (MS1) as that used for the air Ar isotope measurements see above). Mass discrimination was estimated either by using the $^{36}Ar^{++}/^{40}Ar^{++}$ ratio (for Ne) or assuming that the mass discrimination in the spectrometer for Ar (which was accurately determined using synthetic mixtures of ^{36}Ar, ^{38}Ar and ^{40}Ar) applied to all the heavy noble gases: individual isotopes were not available for the other noble gases, preventing direct determination of mass discrimination for each

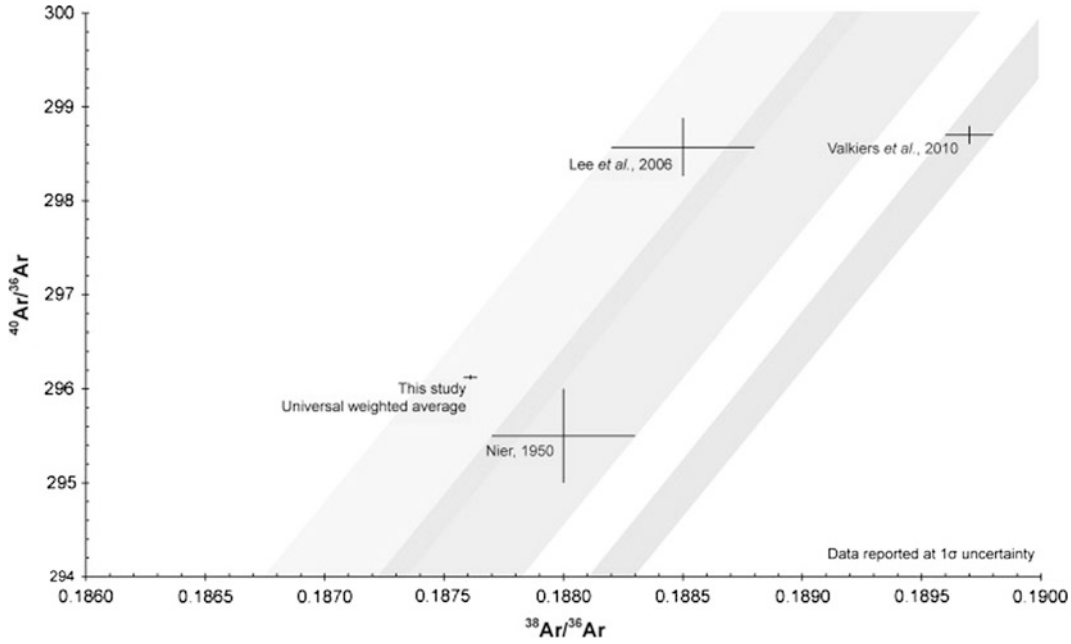

Fig. 1 Estimates of atmospheric Ar isotope ratios (modified after Mark et al. 2011). Lee et al. (2006) and Valkiers et al. (2008) refined the original Nier $^{40}Ar/^{36}Ar$ ratio but were unable to agree on an atmospheric $^{38}Ar/^{36}Ar$ value. Mark et al. measured atmospheric Ar without constraining fractionation, therefore Mark et al's value (the value shown is the average of 180 measurements with the reported standard error) should fall all on the mass fractionation line passing through the true value. The slanted grey bars indicate the mass fractionation line (and associated uncertainty) passing through the three (Nier, Lee and Valkiers) absolute measurements. Mark et al's data are consistent with the Lee et al. estimate of the atmospheric Ar

element. The Ne isotopic composition of air was re-determined by (Eberhard et al. 1965) and was found to be essentially identical to Nier's measurement.

The Ne, Kr and Xe isotopic measurements by Nier in the late 1940s (Nier 1950b) have not changed since, although the errors have been reduced by modern redeterminations (Table 1): the fact that these values are still valid over 60 years after their determination are testament to a highly skilled analyst.

Subsequent absolute determinations of the Ne, Kr and Xe isotopic compositions have been made by the Institute for Reference Materials and Measurements (IRMM) group, Geel, Belgium (Aregbe et al. 1997, 1998, 1996b; Valkiers et al. 1998); these measurements are currently used by IUPAC (Laeter et al. 2003) as the best estimates for atmospheric Kr and Xe isotopic composition. The IRMM approach is to prepare synthetic volumetric or gravimetric mixtures of gases from single isotope gases in order to calibrate instrumental mass fractionation in the MAT271 mass spectrometer used for the determinations (e.g. near-pure ^{86}Kr was added to atmospheric Kr to create known variable isotope ratios). Potential diffusive fractionation of Kr and Xe isotopes during sample inlet were monitored and corrected for (and found to deviate from ideal gas behavior by only a few ppm). Bottles of Kr and Xe were prepared from purified air (by the Messer Greisheim company) which were then calibrated and certified as primary isotope gas standards by IRMM (IRMM-2030 for Kr and IRMM-2000 for Xe), with traceable and certified isotopic compositions (Aregbe et al. 1996b).

Concerning the atmospheric Ne isotope compositions IUPAC refers to a 1984 paper by (Bottomley et al. 1984) and not the IRMM study (Valkiers et al. 2008). Table 1 provides both the IUPAC preferred values and the more recent

Table 1 IUPAC approved noble gas isotopic compositions of the atmosphere (Laeter et al. 2003)

Element	Dry air abundance, ppmv[a]	Isotope	IUPAC	Alternative	Comments
Helium	5.24	^{3}He	0.000 001 34(3)	0.000 001 382 (5)	IUPAC = Sano et al.; Alternative = average (see text)
		^{4}He	0.999 998 66(3)	0.999 998 62(36)	
Neon	18.18	^{20}Ne	0.9048(3)	0.90472(14)	Essentially the values determined by Nier although a reference is given to Bottomley (Bottomley et al. 1984). Alternative calibration from Valkiers et al. (1994)
		^{21}Ne	0.0027(1)	0.00266(26)	
		^{22}Ne	0.0925(3)	0.09262(26)	
Argon	9,340	^{36}Ar	0.003 365(30)	0.003 336(4)	IUPAC considers Nier's values most reliable due to uncertainties on ^{38}Ar; Lee et al. (2006) chosen as alternate because of confirmation by Mark (Mark et al. 2011)
		^{38}Ar	0.000 632(5)	0.000 629(1)	
		^{40}Ar	0.996 003(30)	.996 035(4)	
Krypton	1.14	^{78}Kr	0.003 55(3)		(Aregbe et al. 1996b)
		^{80}Kr	0.022 86(10)		
		^{82}Kr	0.115 93(31)		
		^{83}Kr	0.115 00(19)		
		^{84}Kr	0.569 87(15)		
		^{86}Kr	0.172 79(41)		
Xenon	0.09	^{124}Xe	0.000 952(3)		IUPAC data from (Valkiers et al. 1998)
		^{126}Xe	0.000 890(2)		
		^{128}Xe	0.019 102(8)		
		^{129}Xe	0.264 006(82)		
		^{130}Xe	0.040 710(13)		
		^{131}Xe	0.212 324(30)		
		^{132}Xe	0.269 086(33)		
		^{134}Xe	0.104 357(21)		
		^{136}Xe	0.088 573(44)		

[a] *ppmv* parts per million by volume fraction $\approx$ parts per million by mole fraction

IRMM determinations, which differ from IUPAC only in the measurement uncertainty.

Thus it appears that the atmospheric compositions of Ne, Ar, Kr and Xe have been well calibrated and for Ar, Kr and Xe there are reference materials available for laboratories interested in making SI-traceable determinations. Nevertheless, all the measurements were made on commercially produced gases (made by distilling air) supplied by Messer which could have systematic offsets relative to air; this has been established for the case of neon (Pavese et al. 2005). It should be noted that most laboratories normalize their analyses to the quoted atmospheric values and essentially report only relative isotope ratio variations, therefore the potential errors in reported data (which are only relative isotope shifts and not absolute measurements) are relatively minor.

2 Heterogeneity of the Modern Atmosphere

2.1 Possible Temporal Variation of Atmospheric Helium Isotopes

Oliver et al. (1984) carefully measured and reported the He concentration in the Earth's lower atmosphere. The value of 5.222 $\pm$ 0.017 ppm by volume (1σ) agrees well with the certificated number of 5.239 $\pm$ 0.004 ppm (1σ)

determined by (Gluckauf 1946). Although the He contents are identical, Oliver et al. (1984) suggested that (3–12) $\times$ 10^{16} ccSTP of He had been released into the atmosphere from natural gas production between 1939 and 1981. This anthropogenic He should have increased the 1981 inventory of atmospheric He by 0.1–0.6 % compared to (Gluckauf's 1946) determination, even though the excess was not detectable in their measurements. Stimulated by this work, Sano et al. (1989) measured the ^{3}He/^{4}He ratios of 20 air samples at several different sampling sites and dates. There was a possible change of the atmospheric helium isotope ratio from 1.362 $\times$ 10^{-6} in December 1977 to 1.339 $\times$ 10^{-6} in September 1988, or a decrease in ^{3}He/^{4}He of about 0.74 ‰/year. Although this change could be attributed to local/non-global effects or experimental artifacts, the observations are also consistent with a significant anthropogenic release of crustal He with low ^{3}He/^{4}He ratio ($\sim$3 $\times$ 10^{-8}). Lupton and Graham (1991) countered that this estimated rate of decrease in ^{3}He/^{4}He was not statistically different from a zero time rate of change (TROC). They also reported California marine air data which showed a TROC of (+0.09 $\pm$ 0.43) ‰/year (2σ), i.e. that there was no evidence that the atmospheric He isotope ratio is changing with time. Sano et al. (1991) re-evaluated the original Sano et al. data and reported a non-zero TROC of ($-$0.81 $\pm$ 0.62) ‰/year (2σ). Taking into account the TROC of three independent determinations (Davidson and Emerson 1990; Mamyrin et al.1970; Sano et al. 1989) as well as that of Lupton and Graham, the conclusion of Sano et al. (1991) was that the average TROC based on laboratory measurements of contemporary air was ($-$0.245 $\pm$ 0.055) ‰/year (2σ).

Hoffman and Nier (1993) reported an absolute helium isotopic ratio which was measured by a double focusing mass spectrometer in November 1956. Their value of (1.371 $\pm$ 0.019) $\times$ 10^{-6} (2σ), when combined with the previously reported results above, effectively extending the integration time to a 32 year period, gave a regression line corresponding to a TROC of ($-$0.3 $\pm$ 8.7) ‰/year (2σ). Sano (1998) reported a TROC of ($-$0.9 $\pm$ 1.6) ‰/year (2σ) based on the comparison between GEOSECS Pacific Expedition ^{3}He/^{4}He data (Site 263 and 251) which was calibrated against California marine air collected in 1973 (Lupton and Graham 1991) and South Pacific deep seawater values (SA-7 and SA-6 of Sano et al. (1995)) against air from Chiba, Japan in August 1992.

Pierson-Wickman et al. (2001) measured the isotopic composition of He trapped in historical metallurgical slag from France and the United Arab Emirates in an attempt to investigate variations in the atmospheric ^{3}He/^{4}He ratio with time. Iron is manufactured through the oxydo-reduction of Fe-ore reduced over charcoal with air being pulsed and circulated through the furnaces. The best results in terms of sample reproducibility was obtained for blast furnaces that appeared during the Middle Age in which the temperatures reached 1,600 °C and the mass of circulated air was comparable to the mass of processed Fe-ore, assuring efficient ventilation and therefore noble gas exchange with air. Air was trapped in 0.1–1 mm size vesicles contained in the slag matrix having a composition of forsterite therefore with negligible helium diffusivity at environmental temperatures. Pierson-Wickman et al. found that the He isotopic composition of air trapped in vesicles from industrial slags from the Middle Age and from the beginning of the 20th century was 30 $\pm$ 12 ‰ (at 95 % conf. level) higher than Today. They considered various natural sources and sinks of He isotopes in the period concerned and concluded that these could account for this significant change in atmospheric ^{3}He/^{4}He. Thus they concluded that crustal helium rich in radiogenic ^{4}He has been released to the atmosphere due to industrial activities (mostly mining and hydrocarbon exploitation), and that the inferred fluxes from anthropogenic activity were consistent with the observed variation. They suggested a TROC of ($-$0.14 $\pm$ 0.07) ‰/year (2σ).

Lupton and Evans (2004) compared the ^{3}He/^{4}He ratio of samples of Pacific marine air collected over the 30 year period from 1973 to 2003 against a secondary geothermal gas standard and also against a running air standard. They concluded that the rate of change of air ^{3}He/^{4}He

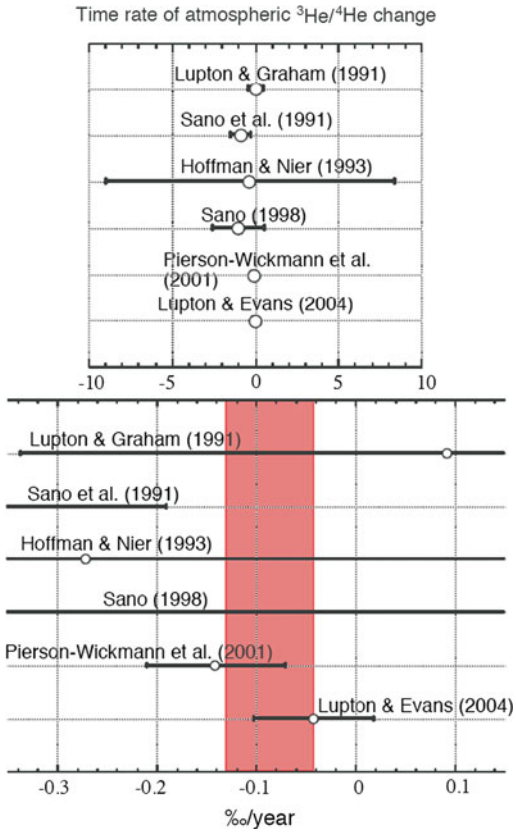

Fig. 2 A compilation of the time rate of atmospheric ^{3}He/^{4}He changes in the literature. *Top* and *bottom* show the change (‰/year) on large and small scales, respectively

over the past 30 years fell between –0.10 and +0.02 ‰/year, which is a TROC of (−0.042 ± 0.061) ‰/year. Figure 2 shows the compilation of the time rate of atmospheric ^{3}He/^{4}He change in the literature. When we take into account all TROCs, the weighted mean of the various estimates is (−0.086 ± 0.045) ‰/year (2σ). This value is apparently distinct from the zero rate of change, even though it corresponds to only 2.6 ‰ change in the atmospheric ^{3}He/^{4}He ratio over the past 3 decades, which is below the detection limit of most laboratories in the world.

Very recently Matsuda et al. (2010) reported that the ^{3}He/^{4}He ratios in some old Chinese porcelain were significantly higher than the present-day air value. They claimed that porcelain can be used as a paleo-atmosphere time capsule over historical times. Taking into account their data, the average ^{3}He/^{4}He ratio is 1.516 ± 0.043 × 10^{-6} (1σ, assuming that present Ra = 1.382 × 10^{-6} from Table 1) at 1400AD and 1.447 ± 0.030 × 10^{-6} (1σ) at 1700AD. They took an average of both data, 1.476 ± 0.025 × 10^{-6} (1σ) as a pre-1700AD atmospheric value (i.e. before the Industrial Revolution) and suggested a TROC of (−0.34 ± 0.18) ‰/year (2σ) under the assumption that the air ^{3}He/^{4}He ratio decreased linearly during the 200 years since the middle of the 18th century to 1970AD. This TROC is significantly larger than the average TROC of (−0.086 ± 0.045) ‰/year (2σ) as calculated in the above discussion.

Sano et al. (2010) have reexamined the ^{3}He/^{4}He ratios of air presumed to be trapped in historical metallurgical slag derived from Japan. They observed that it is difficult to use the Ra unit when discussing a possible temporal variation of the air ^{3}He/^{4}He ratio (because this is Ra itself!) but instead expressed the data relative to the He Standard of Japan (HESJ; see above). The mean ^{3}He/^{4}He ratio of gases extracted from metallurgical slag found at refineries in operation between AD1603 and 1907 in Japan was (5,106 ± 108) × 10^{-5} R_{HESJ} (2σ) and was consistent with the reported value of (5,077 ± 59) ;× 10^{-5} R_{HESJ} in historical slags from France and United Arab Emirates (Pierson-Wickmann et al. 2001). These values are about 40 ‰ higher than that of average modern air (4,901 ± 4) × 10^{-5} R_{HESJ} from AD 2006 to 2008 (this value is obtained by the average of air samples with various locations as discussed below).

2.2 Anthropogenic Sources of Atmospheric Helium

All slag ^{3}He/^{4}He data as well as porcelain are plotted against the year together with the modern air value in Fig. 3 (top panel). When we assume all data are correct, the simple linear regression taking into account the weight of each experimental error yields a slope of –(0.41 ± 0.11) × 10^{-5} R_{HESJ}/year (2σ), which is equivalent to a TROC of (−0.084 ± 0.022) ‰/year (2σ). Since the uncertainty in the composition of the modern

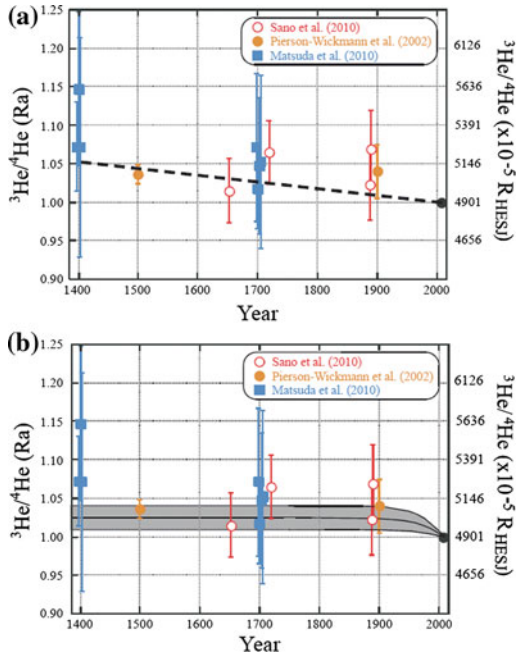

Fig. 3 Secular variation of atmospheric ^{3}He/^{4}He ratio estimated from historical metallurgical slag and old Chinese porcelain. A *dotted line* in the *top* shows a simple linear regression taking into account of weighted errors. The curve in the *bottom* shows a simulation of the ^{3}He/^{4}He change based on fossil fuel consumption (see text). The gray area in the lower panel is obtained by the uncertainty of ±65 % based on the He/C values of natural gas and petroleum

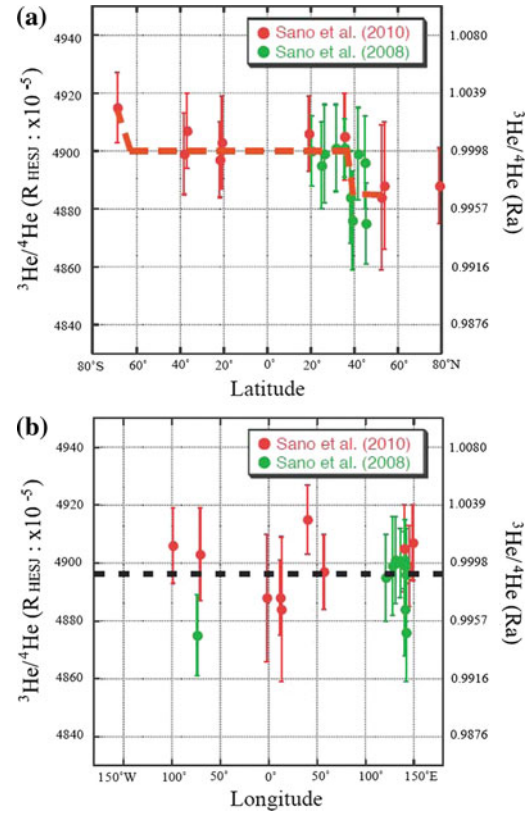

Fig. 4 The changes of atmospheric ^{3}He/^{4}He ratio with latitude (**a**), and longitude (**b**). The ^{3}He/^{4}He ratios appear to increase from north to south but they are constant from east to west

surface air, (4,901 ± 4) × 10^{-5} R_{HESJ}, is significantly smaller than that of slag and porcelain samples, the regression line should be forced to pass through the point of the air value in Fig. 4a. The resulting TROC is identical to the weighted mean of data, (−0.086 ± 0.045) ‰/year in Fig. 2.

It is possible that the decrease of the air ^{3}He/^{4}He ratio is due to a natural perturbation of the steady-state atmosphere resulting from the geomagnetic reversal at 0.79–0.76 Ma (Izett and Obradovich 1994) which probably severely depleted air helium at that time and the atmosphere is now slowly returning to equilibrium (Kockarts 1973; Sano et al. 1989). Pierson-Wickmann et al. (2001) suggested that degassing of the solid Earth could have been increased by a factor of 10 since the last deglaciation (15,000 years ago) due to recirculation of groundwater in previously frozen areas which accumulated radiogenic He while frozen, then release this during melting. Similarly, melting of glaciers that might have accumulated crustal ^{4}He could increase the rate of ^{4}He release to the atmosphere during post-glacial times. Therefore the TROC of −0.086 ‰/year may be attributable to natural processes.

In addition to natural processes, anthropogenic He sources to a non-steady-state atmosphere should be taken into account (Oliver et al. 1984). Possible sources and sinks of atmospheric He (from (Sano et al. 2010)) were estimated and are listed in Table 2. Commercial production of He gas for cryogenic purposes, welding and space missions was 7.6 × 10^9 mol/year in 2006 (US Geological Survey 2009, http://minerals.usgs.gov/minerals/pubs/commodity/helium). This value is

Table 2 Possible sources and sinks of atmospheric helium

	^{4}He (mol/year)
Total inventory[a]	9.3×10^{14}
Source	
Natural flux	
Degassing of solid Earth[a]	6.1×10^8
Recirculation of groundwater[b]	6×10^9
Fossil fuel flux (in 2006)	
Grade-A Helium production[c]	7.6×10^9
Natural gas	1.3×10^{11}
Petroleum	2.1×10^{11}
Total	3.4×10^{11}
Sinks	
Escape (thermal and non-thermal)[a]	8.3×10^8

[a] Ozima and Podosek (1983)
[b] Pierson-Wickmann et al. (2001)
[c] U.S. Geological Survey (2009)

ten times greater than the natural crustal degassing rate of 6.1×10^8 mol/year (Ozima and Podosek 1983), clearly indicating that there are likely anthropogenic sources of He in the atmosphere.

A further major source of crustal He can be attributed to fossil fuel exploitation (Pierson-Wickmann et al. 2001; Sano et al. 1989). Consumption of natural gas, petroleum and coal have been well documented by the Carbon Dioxide Information Center (http://cdiac.ornl.gov). It is reasonable to assume that the rate of consumption of fossil fuel is similar to that of production on a global scale. However, the He content of fossil fuel is known to be highly variable and difficult to constrain. Based on ~3,000 analyses of natural gas samples containing less than 8 % He in the U.S.A., (Zartman et al. 1961) reported that the He abundance showed a log-normal distribution with a mean concentration of 0.217 volume %. The mean He content in natural gas from outside the U.S.A. is not well documented, but might be 0.1 % (Oliver et al. 1984). The He/total C molar ratio of crude oil in the Paris basin, France was 800 ppm (Pinti and Marty 1995). On the other hand, there is no available datum in coal samples. We assume the He/C ratio of 7×10^{-11} for coal (an average U content = 2 ppm for coal, Th/U = 4 (Swaine and Goodarzi 1997) and an average age of coal of 360 Ma). Thus ^{4}He from coal is probably negligible.

It is then possible to calculate the anthropogenic release of crustal He due to fossil fuel production (see Table 2), resulting in a total fossil fuel flux of 3.4×10^{11} mol He/year in 2006, which is 3 orders of magnitude larger than the natural flux. On the other hand, the monotonous decrease of atmospheric ^{3}He/^{4}He ratio (the trend in Fig. 3a), i.e. a TROC of −0.084 ‰/year implies a He input to the atmosphere at 8×10^{10} mol/year based on the simple mass balance calculation where crustal He has a ^{3}He/^{4}He ratio of 3×10^{-8} (Mamyrin and Tolstikhin 1984). Thus the He flux estimated from the global fossil fuel production statistics is about 4 times higher than the TROC calculation.

From the He content in natural gas and petroleum as stated above, it is possible to simulate the secular variation of the atmospheric ^{3}He/^{4}He ratio (based on the fossil fuel consumption per year from AD 1751 to 2006 supplied by the Carbon Dioxide Information Analysis Center (http://cdiac.ornl.gov)). Little change is expected between AD 1400 and 1751 because of minimal consumption and/or production of fossil fuel compared to after the Industrial Revolution. The solid black curve in Fig. 3b shows the calculated change in atmospheric ^{3}He/^{4}He ratio together with observed slag and porcelain data. All data except for the Chinese porcelain in 1400AD (2nd crushing of POR2 in Matsuda et al. (2010)) are consistent with the calculated ^{3}He/^{4}He change within the error margins resulting from uncertainties in He/C ratios, suggesting that the simulation is valid. However, the simulation predicts an average decrease at 0.32 ‰/year for the last 10 years, significantly higher than the TROC value of -0.086 ± 0.045 ‰/year obtained by measuring contemporary air (Fig. 2). In reality, the true TROC is probably located between the monotonic decrease in the atmospheric ^{3}He/^{4}He ratio (dotted line in Fig. 3a) and the recent catastrophic

decrease (a solid curve in Fig. 3b). Even so, taking the largest variation of 0.32 ‰/year, this is still below the detection capabilities of most laboratories. Thus atmospheric He is still suitable as a laboratory standard.

2.3 Possible Spatial Variation of Atmospheric Helium Isotopes

Changes of the atmospheric $^3He/^4He$ ratio with latitude and longitude were assessed by the pioneering work of (Mamyrin et al. 1970). They reported that the spatial variation with both location and altitude (up to 10 km) was within the error margin of individual measurements of about 3 %. More recently Sano et al. (2010) measured the $^3He/^4He$ ratios of 21 surface air samples collected around the world with a precision of 2–4 ‰ (2σ) using a newly developed analytical system (Sano et al. 2008). Even though the data available are not sufficient to cover the entire planet, the sites cover high, low and mid-latitudes (ranging from Svalbard, Norway, to far Showa base, Antarctica). The atmospheric $^3He/^4He$ ratios generally increase from north to south (Fig. 4a), but they do not change significantly from east to west (Fig. 4b). The result is attributable to the fact that mixing of long-lived tracers between northern and southern hemispheres is a much slower process than east to west transport (Jacob 1999; Muller and Brasseur 1995).

By fitting the atmospheric 3He/4He ratios variation with latitude by eye (dotted curve in Fig. 4a), one obtains an apparently constant $^3He/^4He$ ratio from 38°S to 38°N, with high values in Antarctica and low values at high latitudes in the northern hemisphere (from 38°N to 46°N). When we take the uniform $^3He/^4He$ ratio in mid-latitudes, the average becomes $(4{,}901 \pm 4) \times 10^{-5}$ R_{HESJ}, which could be adopted as a representative value of the present atmosphere (see Sect. 2.2.4). This would result in a $^3He/^4He$ ratio in HESJ of 20.404 ± 0.017 (2σ) in Ra units. There is a relatively high $^3He/^4He$ ratio in Antarctica but not in the Arctic. The major source of atmospheric ^3He is auroral precipitation into the upper atmosphere in polar regions (Johnson and Axford 1969). Therefore, these higher $^3He/^4He$ ratios may be attributable to the auroral effect, but the apparently lower ratio in the Arctic needs to be investigated further.

The average $^3He/^4He$ ratio of air samples at high latitudes from 38°N to 46°N is $(4{,}886 \pm 7) \times 10^{-5}$ R_{HESJ} (2σ), 0.31 ± 0.14 % lower than the average value of $(4{,}901 \pm 4) \times 10^{-5}$ R_{HESJ}, although there is a possibility of experimental artifacts in Sano et al. (2010). The atmospheric volume at high latitudes (38°N ~ 46°N) is calculated to be about 5.2 % of the global atmosphere, assuming that the volume is proportional to surface area. The He inventory of the region is estimated to be 4.8×10^{13} mol, (5.2 % of the total inventory of 9.3×10^{14} mol (Ozima and Podosek 1983)). In order to make the regional atmospheric $^3He/^4He$ ratio 0.31 ± 0.14 % lower than the mid-latitude helium, a local input of crustal He of $(1.5 \pm 0.7) \times 10^{11}$ mol is required. This amount is significantly smaller than a single year of anthropogenic He (5.9×10^{11} mol/year). Because atmospheric circulation and mixing homogenize the atmosphere (Jacob 1999), the released anthropogenic He could rapidly dissipate, causing the air $^3He/^4He$ to be higher than expected. Note that the 0.31 ± 0.14 % anomaly is below the detection limit of most noble gas laboratories in the world.

2.4 Anthropogenic Kr and Xe

Fission of nuclear fuel produces Xe and Kr that are isotopically distinct from that of the atmosphere, the precise isotopic pattern depending on the fuel characteristics and subsequent operation of the nuclear pile. Weiss et al. (1986) demonstrated that the atmospheric ^{85}Kr ($t_{1/2} = 10.73$ years) budget is dominated by ^{85}Kr produced during fission. Aregbe et al (1996a) modeled the stable Kr and Xe isotopes expected from mixtures between air and Kr and Xe produced by two different nuclear pathways: from civil nuclear energy production in a Pressurized Water Reactor (PWR) and from plutonium enrichment. However, the lower fission yields and higher atmospheric abundance of Kr means

that stable Kr isotopes are not particularly suited to tracing nuclear atmospheric inputs. Normalising to ^{132}Xe, Agrebe et al considered that the most sensitive Xe isotopes for tracing fission produced Xe are ^{136}Xe/^{132}Xe and ^{129}Xe/^{132}Xe with production ratios greater and lower than atmosphere respectively (however, it would seem more logical to the authors of this chapter to normalize to ^{130}Xe as this is nearly completely shielded); Pu-enrichement and UOX (PWR) produce characteristically different Xe isotope patterns. Aregbe et al (1996a) compared the calculated isotope anomalies generated by 1 g of fission Xe variably diluted by air Xe with the (impressive) measuring capacity of the MAT 271 mass spectrometer at IRMM, Belgium to detect Xe isotope anomalies (about 0.02 per mil for both ^{129}Xe/^{132}Xe and ^{136}Xe/^{132}Xe). They concluded that 1 g of fission Xe diluted in 10^8 m^3 of air ($\sim 10^8$ kg air) would be detectable, and at 1 g fission Xe in 10^6 m^3 of air it would be possible to distinguish between uranium processed for civil or weapons purposes. Thus Xe isotopes have the possibility for identifying nuclear activity if air samples are available close to the reactor. Nevertheless, anthropogenic Xe is highly unlikely to have affected the isotopic composition of atmospheric Xe, given an atmospheric mass of the order 5×10^{18} kg and an annual global U production of the order 50×10^6 kg (2009 data: source: World Uranium Mining". World Nuclear Association.), approximately 1,000 years of U extraction would be required in order to create a measurable excess in the global ^{136}Xe/^{132}Xe.

2.5 Temporal Variation of Atmospheric Argon Isotopes

Apart from helium, argon is the only other noble gas for which temporal variations have been reported. Argon has three natural stable isotopes, ^{36}Ar, ^{38}Ar and ^{40}Ar with well measured relative abundances (see Table 1). While the first two are primordial, that is, have been trapped from one or several cosmochemical reservoirs when the Earth formed. There was virtually no ^{40}Ar at that time and this isotope was produced in the silicate Earth (mantle and crust) by the decay of radioactive ^{40}K. Thus ^{40}Ar accumulated in the atmosphere due to magmatic and tectonic degassing of the mantle and crust. Determining the degassing rate of radiogenic ^{40}Ar through time is important for a number of geoscientific problems such as the growth regime of the continental crust, the potassium content of the silicate reservoirs, variations in mantle convection rate and global tectonics. Consequently, there have been several attempts to determine the rate of ^{40}Ar degassing from measurements of the Ar isotope composition of ancient atmosphere presumably preserved in sedimentary rocks and ice of known ages. The first unambiguous result was obtained for the Devonian Rhynie chert by (Cadogan 1977) and later confirmed by further analysis of the same unit by other groups. Cadogan (1977) measured a ^{40}Ar/^{36}Ar ratio of 293.0 ± 1.6 (renormalized to the new value of the modern ^{40}Ar/^{36}Ar ratio of 298.6, Lee et al.) for argon trapped in this 396 Ma-old chert. Assuming that this value represents the Ar isotope composition of air at that time and from its difference relative to the present-day ^{40}Ar/^{36}Ar value, it is straightforward to compute a ^{40}Ar flux from the solid Earth of 6×10^7 mol/year for the last 400 Ma. It is interesting to compare this flux with that from the mantle. The flux of ^{3}He from the mantle was initially estimated at 1,000 mol/year Craig et al. (1975) but has been scaled down to about 500 mol/year by (Bianchi et al. 2010). With a mantle ^{4}He/^{40}Ar ratio of 2 ± 1 (Moreira et al. 1998) and a mid-ocean ridge ^{3}He/^{4}He value of 8 ± 1 Ra (Graham 2002), one finds that the contemporaneous flux of ^{40}Ar from the mantle is within the range $(1.2–8.6) \times 10^7$ mol/year. The flux value obtained from the Rhynie chert is within this range, but the large uncertainty on these numbers prevents one to derive conclusions on the importance of other ^{40}Ar sources such as the continental crust. A more positive approach to these estimates is to consider that there is a surprisingly good match despite the fact that these flux values address drastically different periods of time.

Recently, a novel approach to quantify the flux of ^{40}Ar from the solid Earth to the atmosphere has been developed by (Bender et al. 2008) using the record of air trapped in deep ice cores from Antarctica. Air trapped in ice is,

however, gravitationally fractionated and direct measurements of ice-trapped noble gas isotope ratios are not representative of ancient atmospheric compositions. Additionally, the ice record extends to less than one Ma and the expected Ar isotope variations are much lower than the precision attained by most current noble gas mass spectrometers. In order to circumvent these problems, Bender et al. first developed high precision analysis of argon isotopes by adapting stable isotope mass spectrometry (dynamic mass spectrometry, i.e. with pumps open and a variable leak inlet) since the amount of sample was large by noble gas standards. They achieved an amazing precision of 0.024 ‰ (2σ) on Ar isotope ratio measurements. Second, they made use of the fact that Ar has 3 isotopes and the ratio between two of them, ^{36}Ar and ^{38}Ar, can be safely assumed to be constant through time, at least during the last Ma, since they are not significantly produced or destroyed by nuclear reactions. Diffusion is a mass-dependent process and, in the case of Ar, can be corrected for by measuring the relative proportions of the 3 isotopes of argon trapped in ice and assuming a mass-dependent law for isotopic fractionation. They found a rate of change of the Ar isotope ratio of air (^{40}Ar/^{38}Ar in their case) of 0.066 ± 0.014 ‰/Ma, which yields a ^{40}Ar outgassing flux of $11 \pm 1 \times 10^7$ mol/year, in fact not very different from Cadogan (1977)'s value of 6×10^7 mol/year averaged over the last 400 Ma. Bender et al. concluded that their flux could be well accounted for by the sum of degassing fluxes from the mantle and the continental crust. Additionally, they proposed that their method provides a new way to date old ice, especially when other age records have been erased, although uncertainties are large ($\pm$180 Kyr).

3 Future Directions

The future of studying variations in atmospheric noble gas compositions relies on developing instrumentation in order to better measure the small differences involved and (particularly for addressing the temporal evolution of atmospheric noble gases) identifying suitable samples.

Considerable advances have been made in the last ten years and multicollector noble gas mass spectrometers are now commercially available. Although commercially available noble gas mass spectrometers are typically used in 'static' (pumps closed) mode, data from Mark et al. (2011) show that high precision noble gas isotope ratio measurements are possible on small gas quantities (of the order $\pm$0.5 per mil on the ^{40}Ar/^{36}Ar ratio with 2×10^{-12} mol Ar). These mass spectrometers can be relatively easily adapted for 'dynamic' (pumps open) measurements, resulting in the precisions available using adapted stable isotope machines (of the order 0.05 per mil for Ar (Bender et al. 2008; Lee et al. 2006)). Dynamic mass spectrometry has the ability to improve precision relative to static mass spectrometers, at the cost of requiring much (10^3) larger samples and of inducing mass fractionation during inlet of the gas into the mass spectrometer. Large sample sizes are difficult to handle, particularly for He and Ne which are difficult to separate by distillation, instead requiring chemical purification of large volumes of air. Instrumental mass fractionation resulting from the inlet leak is furthermore a major problem for measurement of He isotopes in air, because, with only 2 isotopes, it is difficult to quantify the magnitude of this fractionation during analysis.

Identification of suitable archives for noble gas (particularly He) isotope analysis is critical in order to determine temporal changes in noble gas compositions. For the present-day atmosphere, air sampled since 1976 at Cape Grim, Tasmania, under the auspices of the CSIRO, constitutes an archive of choice.

Suitable natural archives need to be able to preserve atmospheric noble gases without significant in situ production or destruction of isotopes, and without isotopic fractionation or, at least with the possibility of correcting for such fractionation with accuracy. Thus the nature of suitable archives depends on the targeted time interval. For the last couple of 1,000 years, only changes in the He isotopic composition are

expected to be detectable with modern mass spectrometry systems. Helium has, however a high diffusivity in many of the materials of interest, including glass and organics. Greater predicted variations in $^3He/^4He$ are offset by higher precision of Ar isotope measurements and ability to correct for mass discrimination.

For the last millenium, some success has been achieved using industrial slags and porcelain, and there are certainly other possibilities such as for example manufactured metal tools, munitions, scientific instruments etc.

For variations over the last Myr the ice record has proven to be exploitable for Ar isotopes and although this may be possible also for He isotopes, this poses a considerably greater challenge as (a) helium may diffuse through ice over these timescales; (b) helium has only 2 isotopes and correction for significant isotope fractionation will be model-dependent and (c) the low abundance of He in the atmosphere and atmosphere-equilibrated liquids require large sample sizes.

For the 10^8–10^9 years time intervals, the sedimentary record seems to be the only way to get ancient air but in many cases the noble gas record is likely to have been altered by isotope exchange and in situ production. So far only one sedimentary unit (the Devonian Rhynie chert) seems to have preserved an ancient atmospheric noble gas record. There is little doubt that other time capsules exist and should be investigated such as amber, evaporites, chert, and barite. Recently, Pujol et al. (2009) claimed that noble gases trapped in Archean barite were representative of the Archean atmosphere. In particular, they found that the stable isotope composition of xenon was intermediate between that of the modern atmosphere and that of primitive meteorites, suggesting time-dependent evolution for such composition.

With the advent of modern noble gas mass spectrometry and of novel analytical techniques, there is no doubt that we are opening a new chapter in the field of noble gas geochemistry with precise studies of the atmospheric evolution in space and time.

References

Aldrich LT, Nier AO (1948) The occurence of He-3 in natural sources of helium. Phys Rev 74(11):1590–1594

Aregbe Y, Mayer K, Valkiers S, DeBievre P (1996a) Release of anthropogenic xenon to the atmosphere: a large-scale isotope dilution. Int J Mass Spectrom Ion Processes 154(1–2):89–97

Aregbe Y, Valkiers S, Mayer K, DeBievre P (1996b) Comparative isotopic measurements on xenon and krypton. Int J Mass Spectrom Ion Processes 153(1):L1–L5

Aregbe Y, Mayer K, Valkiers S, DeBievre P (1997) Detection of reprocessing activities through stable isotope measurements of atmospheric noble gases. Fresenius J Anal Chem 358(4):533–535

Aregbe Y, Valkiers S, Mayer K, De Bievre P, Wessel RM, Alink A (1998) Measuring amount ratios of gas isotopes by two primary methods. Metrologia 35(1):7–16

Bender ML, Barnett B, Dreyfus G, Jouzel J, Porcelli D (2008) The contemporary degassing rate of Ar-40 from the solid Earth. Proc Nat Acad Sci USA 105(24):8232–8237

Bianchi D, Sarmiento JL, Gnanadesikan A, Key RM, Schlosser P, Newton R (2010) Low helium flux from the mantle inferred from simulations of oceanic helium isotope data. Earth Planet Sci Lett 297(3–4):379–386

Bottomley DJ, Ross JD, Clarke WB (1984) Helium and neon isotope geochemistry of some ground waters from the Canadian Precambrian shield. Geochim Cosmochim Acta 48(10):1973–1985

Cadogan PH (1977) Paleoatmospheric argon in Rhynie Chert. Nature 268(5615):38–41

Clarke WB, Jenkins WJ, Top Z (1976) Determination of tritium by mass-spectrometric measurement of He-3. Int J Appl Radiat Isot 27(9):515–522

Coon JH (1949) He-3 isotopic abundance. Phys Rev 75(9):1355–1357

Craig H, Clark WB, Beg MA (1975) Excess ^3He in deep sea-water on the East Pacific rise. Earth Planet Sci Lett 26:125–132

Davidson TA, DE Emerson (1990) Direct determination of the He-3 content of atmospheric air by mass-spectrometry. J Geophys Res [Atmos] 95(D4):3565–3569

Eberhard P, Eugster O, Marti K (1965) A redetermination of isotopic composition of atmospheric neon. Zeitschrift Fur Naturforschung Part a-Astrophysik Physik Und Physikalische Chemie A 20(4):623

Gluckauf E (1946) A micro-analysis of the helium and neon contents of air. Proc R Soc Lond A Math Phys Sci 185(1000):98–119

Gluckauf E, Paneth FA (1946) The helium content of atmospheric air. Proc R Soc Lond A Math Phys Sci 185(1000):89–98

Graham DW (2002) Noble gas isotope geochemistry of mid-ocean ridge and ocean island basalts; characterization of mantle source reservoirs. Rev Mineral Geochem 47:247–317

Hoffman JH, Nier AO (1993) Atmospheric helium isotopic ratio. Geophys Res Lett 20(2):121–123

Holland PW, Emerson DE (1987) A determination of the He-4 content of near-surface atmospheric air within the continental United-States. J Geophy Res Solid Earth Planet 92(B12):12557–12566

Izett GA, Obradovich JD (1994) AR-40/AR-39 age constraints for the jaramillo normal subchron and the matuyama-brunhes geomagnetic boundary. J Geophy Res Solid Earth 99(B2):2925–2934

Jacob DJ (1999) Introduction to atmospheric chemistry. Princeton University Press, Princeton, p 266

Johnson HE, Axford WI (1969) Production and loss of He-3 in Earths atmosphere. J Geophys Res 74(9):2433

Kockarts G (1973) Helium in terrestrial atmosphere. Space Sci Rev 14(6):723–757

Kockarts G, Nicolet M (1962) Le problem aeronomique de l'helium et de l'hydrogene neutres. Ann Geophys 18:269–290

Laeter JRD, Böhlke JK, Bièvre PD, Hidaka H, Peiser HS, Rosman KJR, Taylor PDP (2003) Atomic weights of the elements: review 2000 (IUPAC Technical Report). Pure Appl. Chem. 75(6):683–800

Lee JY, Marti K, Severinghaus JP, Kawamura K, Yoo HS, Lee JB, Kim JS (2006) A redetermination of the isotopic abundances of atmospheric Ar. Geochim Cosmochim Acta 70(17):4507–4512

Lupton JE (1983) Terrestrial inert-gases—isotope tracer studies and clues to primordial components in the mantle. Annu Rev Earth Planet Sci 11:371–414

Lupton J, Evans L (2004) The atmospheric helium isotope ratio: is it changing? Geophys Res Lett 31(13):

Lupton J, Graham D (1991) A ten-year decrease in the atmospheric helium isotope ratio possibly caused by human activity—comment. Geophys Res Lett 18(3):482–485

Mamyrin BA, Tolstikhin I (1984) Helium isotopes in nature. Elsevier, Amsterdam, p 267

Mamyrin BA, Anufriyev GS, Kamenskiy IL, Tolstikhin IN (1970) Determination of the isotopic composition of atmospheric helium. Geochem Int 7:498–505

Mark DF, Stuart FM, de Podesta M (2011) New high-precision measurements of the isotopic composition of atmospheric argon. Geochim Cosmochim Acta 75(23):7494–7501

Matsuda J, Matsumoto T, Sumino H, Nagao K, Yamamoto J, Miura Y, Kaneoka I, Takahata N, Sano Y (2002) The $^{3}He/^{4}He$ ratio of new internal He standard of Japan (HESJ). Geochem J 36(2):191–195

Matsuda J-i, Matsumoto T, Suzuki A (2010) Helium in old porcelain: the historical variation of the He isotopic composition in air. Geochem J 44(6):E5–E9

Moreira M, Kunz J, Allègre C (1998) Rare gas systematics in popping rock: isotopic and elemental compositions in the upper mantle. Science 279:1178–1181

Muller JF, Brasseur G (1995) Images—a 3-dimensional chemical-transport model of the global troposphere. J Geophys Res [Atmos] 100(D8):16445–16490

Nier AO (1950a) A redetermination of the relative abundances of the isotopes of carbon, nitrogen, oxygen, argon, and potassium. Phys Rev 77(6):789–793

Nier AO (1950b) A redetermination of the relative abundances of the isotopes of neon, krypton, rubidium, xenon, and mercury. Phys Rev 79(3):450–454

Oliver BM, Bradley JG, Farrar H (1984) Helium concentration in the Earths lower atmosphere. Geochim Cosmochim Acta 48(9):1759–1767

Ozima M, Podosek FA (1983) Noble gas geochemistry. Cambridge University Press, Cambridge, p 367

Pavese F, Fellmuth B, Head DI, Hermier Y, Hill KD, Valkiers S (2005) Evidence of a systematic deviation of the isotopic composition of neon from commercial sources compared with its isotopic composition in air. Anal Chem 77(15):5076–5080

Pierson-Wickmann AC, Marty B, Ploquin A (2001) Helium trapped in historical slags: a search for temporal variation of the He isotopic composition of air. Earth Planet Sci Lett 194(1–2):165–175

Pinti DL, Marty B (1995) Noble gases in crude oils from the Paris Basin, France: implications for the origin of fluids and constraints on oil-water-gas interactions. Geochim Cosmochim Acta 59(16):3389–3404

Pujol M, Marty B, Burnard P, Philippot P (2009) Xenon in Archean barite: Weak decay of 130Ba, mass-dependent isotopic fractionation and implication for barite formation. Geochimica Cosmochimica Acta 73:6834–6846

Sano Y (1998) Time rate of atmospheric $^{3}He/^{4}He$ change: constraints from South Pacific deep seawater. J Sci Hiroshima Univ Ser C 11:113–118

Sano Y, Wakita H, Xu S (1988) Atmospheric helium isotope ratio. Geochem J 22(4):177–181

Sano Y, Wakita H, Makide Y, Tominaga T (1989) A ten-year decrease in the atmospheric helium isotope ratio possibly caused by human activity. Geophys Res Lett 16(12):1371–1374

Sano Y, Wakita H, Makide Y, Tominaga T (1991) A ten-year decrease in the atmospheric helium isotope ratio possibly caused by human activity—reply. Geophys Res Lett 18(3):486–488

Sano Y, Takahata N, Gamo T (1995) Helium isotopes in South Pacific deep seawater. Geochem J 29(6):377–384

Sano Y, Takahata N, Igarashi G, Koizumi N, Sturchio NC (1998) Helium degassing related to the Kobe earthquake. Chem Geol 150(1–2):171–179

Sano Y, Tokutake T, Takahata N (2008) Accurate measurement of atmospheric helium isotopes. Anal Sci 24(4):521–525

Sano Y, Furukawa Y, Takahata N (2010) Atmospheric helium isotope ratio: possible temporal and spatial variations. Geochim Cosmochim Acta 74(17):4893–4901

Swaine DJ, Goodarzi F (1997) Environmental aspects of trace elements in coal. Kluwer Academic Publishers, Dordrecht, p 312

Turrin BD, Swisher CC, III, Deino AL (2010) Mass discrimination monitoring and intercalibration of dual collectors in noble gas mass spectrometer systems. Geochem Geophys Geosyst 11, Q0AA09. doi:10.1029/2009GC003013

Tans PP, Conway TJ, Nakazawa T (1989) Latitudinal distribution of the sources and sinks of atmospheric carbon-dioxide derived from surface observations and an atmospheric transport model. J Geophys Res [Atmos] 94(D4):5151–5172

Torgersen T (1989) Terrestrial helium degassing fluxes and the atmospheric helium budget; implications with respect to the degassing processes of continental crust. Chem Geol (Isot Geosci Sect) 79(1):1–14

Valkiers S, Schaefer F, De Bievre P (1994) Near-absolute gas (isotope) mass spectrometry: isotope abundance (and atomic weight) determinations of neon, krypton, xenon and argon. Elsevier, Amsterdam, pp 965–968

Valkiers S, Aregbe Y, Taylor PDP, De Bievre P (1998) A primary xenon isotopic gas standard with SI traceable values for isotopic composition and molar mass. Int J Mass Spectrom 173(1–2):55–63

Valkiers S, Varlam M, Berglund M, Taylor P, Gonfiantini R, De Bievre P (2008) Absolute measurements of isotope amount ratios on gases part II. Application of the measurement models developed on real gases. Int J Mass Spectrom 269(1–2):71–77

Weiss W, Stockburger H, Sartorius H, Rozanski K, Heras C, Ostlund HG (1986) Mesoscale transport of Kr-85 originating from European sources. Nucl Instrum Meth phys Res., Sect B 17(5–6):571–574

Zartman RE, Wasserburg GJ, Reynolds al e JH (1961) Helium, argon and carbon in some natural gases. J Geophys Res 66:277–306

Noble Gases in Ice Cores: Indicators of the Earth's Climate History

Gisela Winckler and Jeffrey P. Severinghaus

Abstract

Polar ice cores constitute excellent archives of past environmental conditions and provide us with glimpses into the Earth's climatic history over hundreds of thousands of years. For the past two decades, noble gases, used as conservative tracers, have played a substantial role in extracting information from these archives. Noble gas analysis can be performed on two types of ice core samples. First, atmospheric air, trapped in bubbles in polar ice, can be extracted and analyzed for its noble gas composition. Variations in the isotopic and elemental composition of noble gases trapped in air bubbles can be used to infer ancient environmental conditions at the surface of the ice sheets, adding to understanding of the controls on Earth's climate. For example, thermal fractionation allows for the creation of a 'gas isotope thermometer' in ice cores. Second, particles that were deposited on the surface snow and incorporated in the ice matrix can be analyzed for their noble gas isotope composition. These analyses reveal information about the input and origin of both terrestrial aerosols and extraterrestrial dust. The conservative nature of noble gases, ensuring that such fingerprints are preserved over long periods of time, and the exceptionally good dating of polar ice cores make noble gas analysis of ice cores a versatile tool to study a wide spectrum of geochemical and paleoclimatic processes: from constraints on the magnitude of temperature changes during abrupt climate transitions in the Earth's history, to determining the rate of Argon-40

G. Winckler (✉)
Lamont-Doherty Earth Observatory, Columbia University, Palisades, NY, USA
e-mail: winckler@ldeo.columbia.edu

G. Winckler
Department of Earth and Environmental Sciences, Columbia University, New York, NY, USA

J. P. Severinghaus
Scripps Institution of Oceanography, University of California, San Diego, CA, USA

P. Burnard (ed.), *The Noble Gases as Geochemical Tracers*, Advances in Isotope Geochemistry,
DOI: 10.1007/978-3-642-28836-4_3,

degassing from the solid Earth over its history, or quantifying variations in the accretion of extraterrestrial dust on the Earth's surface. Below, we present case studies to review some of the applications of noble gas analysis in the polar ice archive, both in trapped air bubbles and in particles incorporated in the ice matrix.

1 Introduction

Polar ice cores are arguably the most powerful tool for reconstructing the timing and extent of changes in earth's environment over the past 800,000 years. Because ice cores represent continuous and well-datable archives, they have dramatically advanced our understanding of how the earth's climate has changed in the past.

Ice cores collected from Greenland have revolutionized our notion of climate variability during the past 123,000 years (e.g., Dahl-Jensen et al. 2002; Grootes et al. 1993; Johnsen et al. 1997; NGRIP Project Members 2004), and have been instrumental in characterizing climate transitions from glacial to warm conditions as well as identifying and understanding past abrupt climate change (e.g., Alley et al. 2009; Severinghaus and Brook 1999).

Antarctic ice core records extend even further into the past; the longest ice core drilled in East Antarctica represents an archive going back to ~800,000 years before present, covering the past eight glacial cycles since the Mid-Pleistocene Climate Transition (EPICA Community Members 2004). The information extracted from these ice core records can provide insight into a variety of climate forcing mechanisms and provide a basis for assessing the range of natural variability of climate, and for testing regional and global climate models under a wide range of conditions.

Perhaps most importantly, polar ice cores contain remnants of ancient atmospheric air. Snow accumulating on a polar ice sheet gradually compacts under its own weight to form a layer of recrystallized and porous snow called firn, which then further compacts to form ice. In the upper part of the firn layer, the entrapped air can still mix with the atmosphere. At the base of the firn layer, at about 50–100 m, as the firn becomes impermeable ice however, the air gets occluded in bubbles in the ice and preserved over long periods of time (Schwander 1989).

Air trapped in bubbles in polar ice has been used for a variety of paleoenvironmental studies, primarily to document the variability in the composition of past atmospheres. Analyses of the trapped air bubbles have proven to be particularly useful for reconstructing the variability of greenhouse gases, such as CO_2 and CH_4, over the earth's history (e.g., Loulergue et al. 2008; Luethi et al. 2008; Petit et al. 1999).

In addition, these air bubbles contain gases such as noble gases and nitrogen, whose atmospheric concentrations and isotopic ratios have—in contrast to the greenhouse gases CO_2 and CH_4—stayed unchanged on the 100,000 year to 1 Myr time scale spanned by ice cores (Allegre et al. 1987). Variations in the isotopic ratios of these gases in the trapped air bubbles, caused by either physical processes such as thermal or gravitational fractionation within the firn or by large-scale redistribution between the atmosphere and ocean, can be used to infer climate-related processes.

An example for this is the thermal diffusion-based noble gas thermometer. Transient temperature gradients, such as a sudden cooling or warming, fractionate the air within the firn by thermal diffusion (Leuenberger et al. 1999; Severinghaus et al. 1998). The resulting gas-isotope anomalies are then locked into and preserved in the air bubbles in the ice; precise measurements of these noble gas isotope anomalies in the trapped air bubbles allow to infer the underlying transient temperature change and, thus, allow unprecedented insights into the magnitude and abruptness of past climate change (Severinghaus and Brook 1999).

Analyses of the heavy noble gas isotopes, krypton and xenon, in the air bubbles trapped in ice cores can be used to reconstruct past mean ocean temperature. This method takes advantage of the strong temperature dependence of the solubility of krypton and xenon in water (Weiss and Kyser 1978), analogous to paleotemperature reconstructions from groundwater (Aeschbach-Hertig and Solomon 2013). As the total inventory of krypton and xenon in the atmosphere and ocean is conserved through time, variations in mean ocean temperature modulate their atmospheric abundances. Krypton and xenon, measured in ice core air, allow us to reconstruct their paleoatmospheric histories, which can then be interpreted to reflect the magnitude and timing of variations in the mean ocean temperature in the past (Headly and Severinghaus 2007).

Noble gas analysis of gas bubbles trapped in ice cores is not limited to heavy noble gases but also includes helium isotopes. Unlike the other atmospheric noble gases, helium enters the ice not only at the firn/ice transition, but also at the ice/bedrock interface. Due to its small molecular diameter, helium can readily diffuse through the ice, complicating its interpretation in the archive. Despite this caveat, analysis of helium isotopes in polar ice cores allows reconstruction of processes acting at the base of the ice sheet (e.g., Craig and Scarsi 1997; Jean-Baptiste et al. 2001a), including assessing the stratigraphic integrity of the basal ice, but—given the focus of this chapter on climate-related processes—will not be described here in detail.

In addition to trapped ancient air, polar ice cores also contain small amounts of impurities that can be important indicators of past climate and environmental conditions. Examples of such impurities are mineral dust particles from deserts that are transported thousands of kilometers in the atmosphere and deposited on the ice, ash particles from volcanic eruptions, sea salt aerosols and cosmic dust particles.

In the late 1990s, Brook pioneered the development of helium isotope analysis of particles trapped in the ice (Brook et al. 2000). Helium isotope analysis allows the relative proportions of particles of cosmic, as well as of terrestrial origin to be identified. Interplanetary dust particles (IDPs), the fine fraction of extraterrestrial matter reaching the earth that is derived from cometary and asteroid debris, is highly enriched in ^{3}He, whereas terrestrial dust is dominated by radiogenic helium (^{4}He).

When combined with snow accumulation rates—a parameter typically well known in ice cores—we can determine extraterrestrial ^{3}He fluxes and reconstruct the variability of the flux of interplanetary dust particles (IDPs) to the earth (Brook et al. 2009, 2000; Winckler and Fischer 2006). On the other hand, the ^{4}He signal measured in the particles from the ice can be used to identify terrestrial dust and—by combining it with complementary terrigenous proxies—provides information about the provenance of the mineral dust deposited on the ice.

Noble gas analyses in air bubbles trapped in the ice and in the particulate matter, respectively, represent two modern analytical techniques that are motivated by a spectrum of different objectives. In this chapter we review both techniques by presenting specific climate-related case studies and discuss their impact, limitations and future potential.

2 Background: Ice Cores in Greenland and Antarctica

The fundamental idea of using ice cores to study past climate was conceived in the 1950s by the Danish scientist, Willi Dansgaard. Several deep ice cores (Fig. 1) have been retrieved from the Greenland ice sheet, among them the GRIP, GISP-2 and North GRIP cores which reach back up to 123,000 years (NGRIP Project Members 2004). The newest deep drilling project in Greenland, the North Greenland Eemian Ice Drilling (NEEM), commenced in 2007 with the goal of retrieving an undisturbed record of the full Eemian interglacial period 115,000–130,000 year ago.

The longest ice cores, however, have been drilled in Antarctica (Fig. 1). In the 1970s, ice core drilling at the Russian station 'Vostok' began, and more than 25 years later, a more than 3,500 m long ice core was drilled above Lake

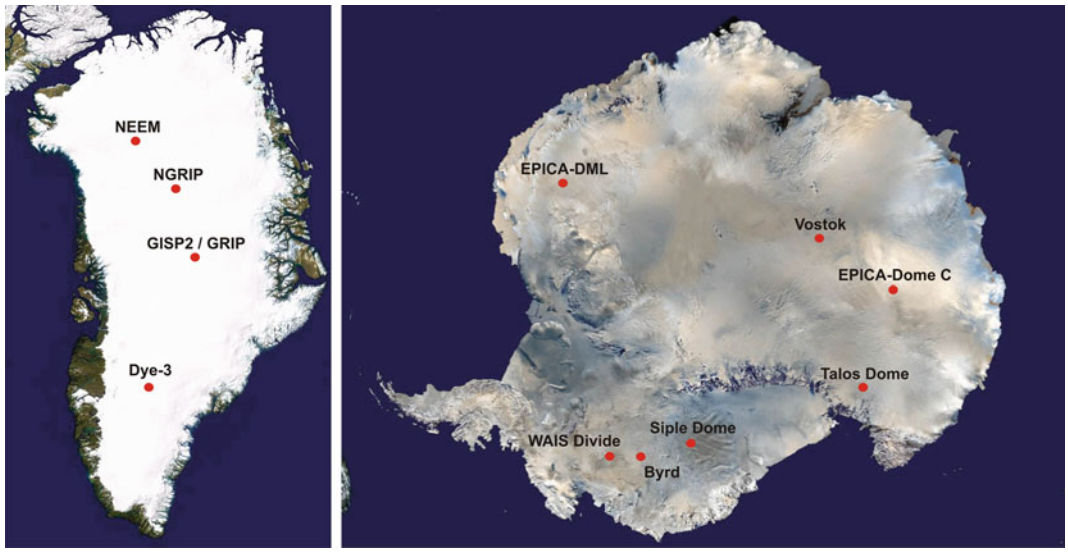

Fig. 1 Map of both polar regions indicating selected ice core drilling sites in Greenland (NEEM, NGRIP, GRIP/GISP2; and Dye 3) and in Antarctica (EPICA DML, Dronning Maud Land; Vostok; EPICA Dome C, Siple Dome; Talos Dome, Byrd and WAIS) where noble gas measurements have been performed

Vostok (78.5°S, 107°E, 3,488 m above sea level) reaching back about 400,000 years. Recently as part of the EPICA (European Project for Ice coring in Antarctica) project, a deep drill core at Dome C (EDC, 75°S, 123°E, 2,882 m above sea level) reached a record-holding 800,000 year. Another EPICA core was drilled in Dronning Maud Land (EDML, 75°S, 0°E, 3,233 m above sea level), which covers about 160,000 year and—due to its higher snow accumulation rate—allows for reconstruction of higher resolution atmospheric and climate records than previous ice cores from the East Antarctic plateau. The latest major ice coring project in Antarctica is the West Antarctic Ice Sheet Divide ice core (WAIS Divide, 79.5°S, 112°W, 1,766 m above sea level). The WAIS Divide ice core, recently completed at a length of 3,400 m, provides the first Southern Hemisphere climate and greenhouse gas records of comparable time resolution and duration to the Greenland ice cores, which will enable detailed comparison of environmental conditions between the northern and southern hemispheres.

Noble gases in trapped air bubbles have been measured in Greenland at the GISP-2 ice core (Headly and Severinghaus 2007; Kobashi et al. 2008a, b, 2009; Severinghaus and Brook 1999; Severinghaus et al. 1998), at GRIP (Landais et al. 2004b) and North Grip (Landais et al. 2004a, 2006). In Antarctica, noble gases have been measured at the Siple Dome ice core in West Antarctica (Severinghaus et al. 2003) as well as in firn air from Siple Dome (Severinghaus and Battle 2006) and at Vostok (Bender et al. 2008; Caillon et al. 2001, 2003) and Dome C (Bender et al. 2008; Dreyfus et al. 2010) in East Antarctica.

Helium isotopes in particles from ice have been measured at GISP-2 in Greenland (Brook et al. 2000) and at Vostok (Brook et al. 2009, 2000) and EDML in Antarctica (Winckler and Fischer 2006).

3 Analytical Techniques

3.1 Preparation of Ice Samples for Noble Gas Analysis

Ice cores capture a record of air bubbles as well as particulates (e.g., mineral dust, volcanic particles, and comic dust). The two types of

analyses—air bubbles and particulates—require different preparation and extraction methods.

3.1.1 Noble Gases in Trapped Air Bubbles

Typically, ice samples are taken from the inner portion of the ice core to minimize possible adverse effects of gas loss due to temperature fluctuations during core retrieval and handling. The air trapped in the bubbles is released using a designated vacuum extraction line. The early extraction method was based on a melt-refreeze technique (for details see Severinghaus et al. 1998); subsequent noble gas analyses were done using a 'wet extraction' technique (e.g., Severinghaus et al. 2003), partially based on the extraction method developed by Sowers et al. (1989). Briefly, the ice samples are placed in pre-chilled stainless steel extraction vessels containing a glass-covered magnetic stirrer. After evacuation, the vessels are warmed to room temperature releasing the trapped gas by melting. Gases are then transferred through a water trap to a collection vessel, kept at 10 K, effectively using the water vapor as carrier gas. The wet extraction method has subsequently been optimized for combined argon and nitrogen isotope measurements (Kobashi et al. 2008b) as well as for the Kr/N_2 method (Headly and Severinghaus 2007) to ensure quantitative extraction of the heavy noble gases. The extracted gas is then exposed to a hot getter to absorb N_2, O_2 and other reactive gases. A detailed overview of different gas extraction techniques can be found in Landais (2011).

3.1.2 Noble Gases in Particles from Ice Cores

The samples for the pioneering helium isotope analyses of particulate matter in ice were derived from melting subsections from the GISP-2 and Vostok ice core (Brook et al. 2000). This technique is the most direct analysis of particulates in ice cores and has been used in a subsequent study by Brook et al. (2009).

As access to ice core samples is limited and relatively large samples of ice (on the order of kilograms) are required, an alternative technique has been developed. This approach samples the excess water stream of continuous flow chemical melt-water analysis (CFA), a routine analysis in modern ice core research (Kaufmann et al. 2008). Briefly, for CFA the ice core (typically a 3×3 cm cross section) is melted on a specially designed melt head, where only the innermost section of the ice core is used for the analysis to prevent contamination. Then, the melt is directly led to a continuous flow analysis system. After the CFA, the excess water (which used to be discarded) is saved and stored in polyethylene (PE) containers.

For both techniques, directly melting the ice or using the excess water stream, the water is subsequently filtered and the particulate dust (extraterrestrial and terrigenous dust) is collected on 0.45 μm silver filters (manufactured by Osmotics–Poretics).

Each filter is then wrapped in aluminum foil. Aluminum foil balls (including the silver filter) are melted in a classical double-vacuum high temperature furnace, as shown in Fig. 10 in Burnard et al. (2013), to extract the helium. During extraction the furnace is kept exposed to a liquid nitrogen cooled charcoal trap in order to remove CO_2, H_2O and organic compounds. Further purification is performed by exposure to a getter. The gas is then collected on a cryogenically cooled charcoal trap held at $\sim$13 K and helium is separated from neon by heating the trap to 45 K. Abundance and isotopic analyses are measured using static noble gas mass spectrometry (e.g., Winckler et al. 2005; Kurz et al. 1996). Helium isotopes remain the only noble gas system measured in the particles from ice cores.

3.2 Mass Spectrometry

Two different mass spectrometric techniques are used for analyzing noble gases in trapped atmospheric air bubbles or particulates trapped in the ice, respectively.

3.2.1 Noble Gas Mass Spectrometry of Trapped Air

Isotopic ratios of noble gases in trapped air bubbles are analyzed on a multi-collector

isotope ratio mass spectrometer (Severinghaus et al. 2003, 1998). This type of mass spectrometer (e.g., Finnigan MAT 252) differs from traditional static mass spectrometers typically used to measure noble gases (e.g., Burnard et al. 2013) in that it is a dynamic-inlet instrument that uses far more sample (on the order of 1 cm^3 STP). The mass spectrometric analysis follows conventional procedures of dynamic isotope ratio mass spectrometry, with modifications designed to minimize any fractionating effects, such as thermal diffusion during volume splitting steps.

Precision is attained by bleeding sample and standard gases through two capillaries that are alternately fed into the mass spectrometer or into a waste line at high vacuum, with rapid switching between sample and standard minimizing the effect of instrument drift (McKinney et al. 1950). Mass spectrometric results must be corrected for pressure differences between sample and standards, and for the sensitivity of isotopic measurements to the elemental ratios (the so-called ''chemical slope''). The overall precision for measuring the $^{40}Ar/^{36}Ar$ ratio obtained for duplicate analyses of a 100 g ice sample is 0.012 ‰ (1 standard error of the mean, Severinghaus et al. 2003).

3.2.2 Noble Gas Analysis of Particles

Noble gases in particulates trapped in the ice are measured with a sector-field mass spectrometer and analyzed in a static mode [i.e., 'standard' configuration, as described in Burnard et al. (2013)].

4 The Noble Gas Record from Trapped Air Bubbles in Ice Cores

4.1 Paleothermometry from Thermal Diffusion: Estimate of Abrupt Temperature Change Magnitude

Quantitative estimates of temperature change in the past are instrumental to understanding the mechanism of climate change, yet classical temperature proxies suffer from numerous drawbacks. In ice cores, the oxygen isotopes of ice are affected by processes other than temperature and have been shown to underestimate the Greenland temperature changes between the last glacial period and the present by up to a factor of two. A persistent problem with many proxies is that they require an assumption that the present observed sensitivity of the proxy to temperature was also the sensitivity back through time—for example the assumption that the "spatial slope" and the "temporal slope" in temperature reconstructions from water isotopes are equal (e.g., Jouzel et al. 1997)—which is an often untested or controversial assumption. Here noble gases offer an advantage because their sensitivities are fundamental physical laws, which do not change with time. One such application of noble gases is the thermal-diffusion based gas thermometer in ice cores, which was developed over the past two decades.

Atmospheric gases are steadily trapped in bubbles in glacial ice by compaction of the 50–100 m thick layer of snow (typically called firn) on top of a polar ice sheet. Analysis of these air bubbles in ice cores drilled from the polar ice caps has yielded a cornucopia of useful information on past changes in greenhouse gas content of the atmosphere. In addition, gases whose atmospheric ratios are constant on relevant timescales ($\sim$100,000–1,000,000 year), such as the isotopes of noble gases and N_2, can reveal the impact of fractionation processes occurring within the firn. These processes include thermal diffusion (the separation of gases in a temperature gradient), and gravitational fractionation (the settling of heavier species towards the bottom in a gravitational field).

Thermal diffusion was first predicted theoretically in 1917 with the solution to the Boltzmann equation by Sydney Chapman and David Enskog, and was experimentally verified shortly thereafter (Chapman and Dootson 1917). Thermal diffusion is not to be confused with the diffusion of heat, but is rather the transport of mass by a temperature gradient, with the heavier molecules generally moving toward colder

regions. A temperature gradient exists in the firn for several centuries following a change in surface temperature due to the fact that firn is an excellent thermal insulator and the heat capacity of the ice sheet is large. This temperature gradient fractionates the air within the firn by thermal diffusion, due to the fact that the atmosphere represents a virtually infinite reservoir that cannot change. A key point is that gases diffuse about 10 times faster in firn than heat, which allows the gas composition to approach near-equilibrium with the temperature at any one depth (Severinghaus and Brook 1999; Severinghaus et al. 1998).

As the bubbles are continually closing and trapping the fractionated air at the base of the firn, an ice core contains the equivalent of a tape recording of the firn air composition over time. The noble gas isotopes record an abrupt step-function warming as a sudden positive spike in the heavy isotope followed by a gradual decay over several centuries as the firn becomes isothermal once again. The amplitude of the spike is proportional to the magnitude of the abrupt surface warming. Abrupt cooling is likewise recorded as a negative spike. Laboratory measurements of air equilibrated in a carefully controlled, known temperature gradient are used to calibrate the method, as theoretical predictions are not sufficiently accurate (Grachev and Severinghaus 2003a, b).

A complication is that gravitational fractionation also occurs in the firn, due to the settling of heavy gas species to the bottom of the stagnant column of air (Craig et al. 1988; Schwander 1989; Sowers et al. 1989). To isolate the signal due to temperature change, it is necessary to measure two different isotope pairs that have differing sensitivity to temperature, such as $^{15}N/^{14}N$ of N_2 and $^{40}Ar/^{36}Ar$ (Fig. 2). When scaled by the mass difference so that their gravitational effects are equal, their difference, known as $\delta^{15}N_{excess}$, is nominally a function of temperature only (Severinghaus and Brook 1999).

$$\delta^{15}N_{excess} = \delta^{15}N_{meas} - \delta^{40}Ar_{meas}/4 \quad (1)$$

The temperature difference between the top and bottom of the firn layer is denoted ΔT.

$$\begin{aligned}\Delta T &= \delta^{15}N_{excess} / \left(\Omega^{15} - \Omega^{40}/4\right) \\ &= \delta^{15}N_{excess} / 0.0047\,‰\,K^{-1}\end{aligned} \quad (2)$$

where Ω^{15} and Ω^{40} are thermal diffusion sensitivities of the argon and nitrogen isotope pairs.

In practice, a time-dependent numerical model of heat transport in the firn is generally used to interpret the data, because heat diffusion and advection does warm or cool the base of the firn slightly on the gas diffusion timescale and thus reduces the amplitude of the thermal diffusion signal by about 10 % depending on the firn thickness. The thermal diffusion tool is insensitive to gradual temperature changes, of order 1 K/century or less, because the firn becomes thermally equilibrated on these timescales. Diffusion of gas occurs on a timescale of a decade or so, preventing the air bubbles from recording higher frequencies than this, so this tool is only sensitive to decadal-to-centennial scale temperature variations. Fortunately, this happens to be a timescale of interest in paleoclimate research due to the wide interest in the Dansgaard/Oeschger events of the last glacial period, recorded in Greenland ice cores (Fig. 3).

4.2 Paleothermometry from Solubility: A Time Series of Mean Ocean Temperature

A persistent mystery in paleoclimate research has been the cause of the observed rise in atmospheric carbon dioxide at the ends of glacial periods. Understanding this puzzle is important because future climate depends in part on the natural feedback response of the earth system to human perturbation. A massive body of circumstantial evidence points to the deep ocean as the key reservoir for carbon dioxide variations, but basic quantitative information such as the temperature of the deep ocean over time is still lacking. A major reason is that the classical proxy for ocean temperature, the oxygen isotope ratio of benthic foraminifera, is also affected by the oxygen isotope ratio of the water. This

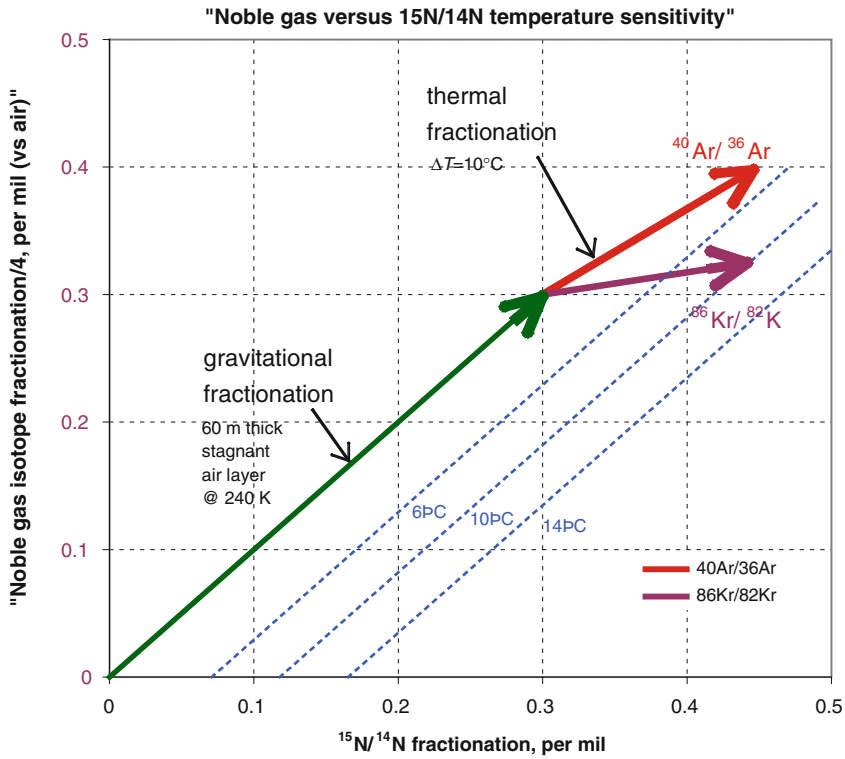

Fig. 2 Schematic of the basis for the thermal diffusion paleotemperature change indicator in trapped gases from ice cores. Thermal fractionation causes heavy isotopes to migrate toward colder regions, but the response is weaker for the noble gas pairs $^{86}Kr/^{82}Kr$ and $^{40}Ar/^{36}Ar$ than for $^{15}N/^{14}N$ of N_2 on a per-mass-unit-difference basis. Gravitational fractionation also affects gases in polar firn, with the same response for all gas pairs on a per-mass-unit-difference basis. Measurement of both a noble gas pair and $^{15}N/^{14}N$ thus permits the separation of gravitational and thermal effects (Severinghaus et al. 1998). The coloured arrows show the nominal effect of an abrupt 10 °C surface warming on the gas at the *bottom* of a 60 m thick firn column initially at 240 K. Isotherms for the ^{15}N-^{86}Kr system are shown in *blue*

fundamental ambiguity has been overcome for certain unique times such as the last glacial maximum, by directly measuring the water isotopic ratio, but a highly-resolved time series of deep ocean temperature still eludes us. Such a time series would place constraints on proposed mechanisms of carbon dioxide variation. Ice cores have the unique property that they trap samples of the atmosphere in a highly resolved time series, so a deep ocean temperature proxy contained within an ice core would be the ideal means to test these hypotheses. A further benefit of this would be that there is no relative age uncertainty between two proxies measured in the same core.

The heavy noble gases krypton and xenon are highly soluble in liquid water, and their solubility has a strong temperature dependence (Fig. 4), a principle that is also used in groundwater paleothermometry (see Aeschbach-Hertig and Solomon 2013). This fact is the basis for the mean ocean temperature paleoindicator based on measured krypton and xenon in trapped air bubbles from ice cores (Headly and Severinghaus 2007).

Because the total number of krypton, xenon, and N_2 molecules in the ocean–atmosphere system is essentially constant, a warming ocean will outgas and must cause an increase in the atmospheric inventory. The solubility of N_2 is low, and its temperature dependence is weak, making it respond much less than the noble gases. Thus the krypton/N_2 and xenon/N_2 ratios

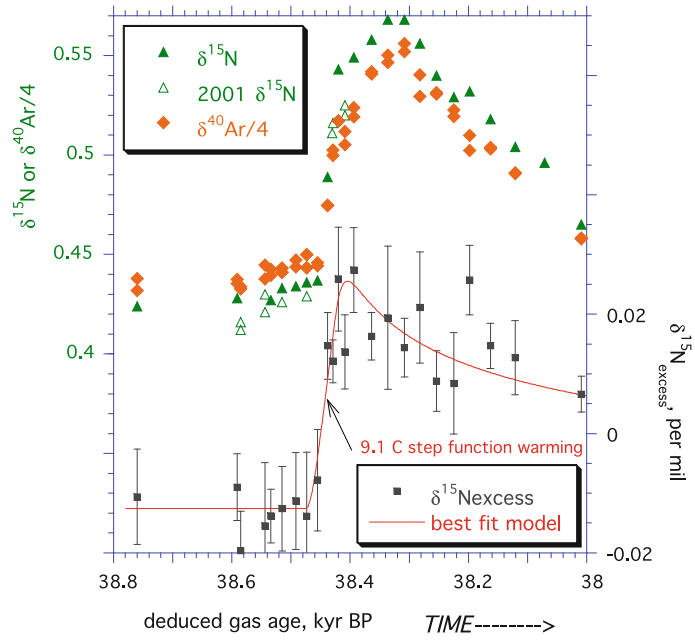

Fig. 3 Noble gas isotopic ratios in the Greenland (GISP2) summit ice core, across an abrupt warming event known as Dansgaard-Oeschger event 8 (Orsi et al. 2009). A heat transfer model forced by step function in surface temperature finds a best fit solution of 9 ± 3 °C for the warming amplitude, although considerable scatter in the data suggests some experimental artifacts. This approach also yields an estimate of the gravitational fractionation signal, which is related to the change in firn thickness. The method gives ~6 m of firn thickening, which is reasonable for this event considering that accumulation rate doubled abruptly along with the temperature change

in trapped air should record mean ocean temperature, albeit slightly weighted toward the cold end of the temperature distribution due to the nonlinearity of the solubility (Fig. 4). This nonlinearity is captured in a model that is used to interpret measured atmospheric change in terms of ocean temperature change.

Argon would be a natural choice for the less-soluble gas to which Kr and Xe are compared, however firn air studies show that the atmospheric Ar/N_2 ratio is not well retained in glacial ice due to preferential exclusion of argon from overpressured bubbles during the air entrapment process at the base of the firn. In contrast, these studies show that the atmospheric Kr/N_2 and Xe/N_2 ratios are well preserved during this process (Severinghaus and Battle 2006).

A key assumption that must be made is that the inventory of N_2 in the ocean–atmosphere system is sufficiently constant on 100,000 year timescales that its atmospheric abundance only responds significantly to solubility, despite the fact that biological denitrification and nitrogen fixation are sources and sinks of N_2. Support for this assumption is provided by the fact that the total denitrifiable pool of N amounts to less than 0.01 % of the atmospheric inventory. Bubble injection causes a ~1 % supersaturation of dissolved N_2 in the ocean (Hamme and Emerson 2004), but because only ~0.6 % of total N_2 resides in the ocean, even the extreme case of eliminating this supersaturation would cause only a 0.06 per mil fractional increase in atmospheric N_2. For comparison, the experimental error of the Kr measurement is 0.2 per mil, and that of Xe is 0.4 per mil. There is also no reason to expect that bubble injection would be reduced in a glacial climate.

To gain insight into the expected signal in atmospheric Kr/N_2 and Xe/N_2 ratios from mean ocean temperature change, it is helpful to first consider a simple isothermal box model of the

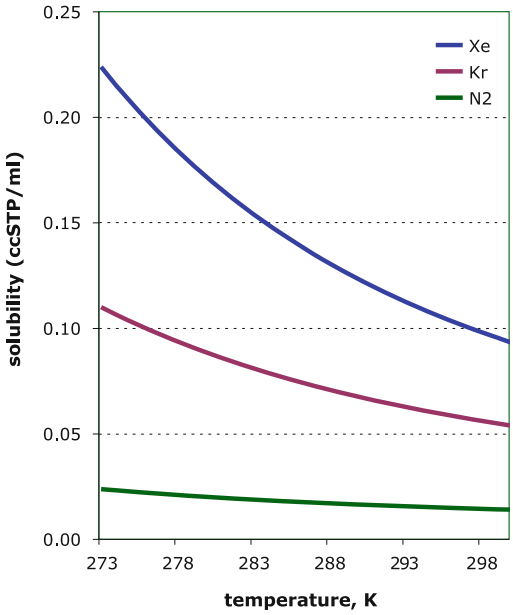

Fig. 4 Equilibrium solubility of xenon, krypton, and N_2 in seawater of salinity 35 psu, expressed as the Bunsen coefficient, in ccSTP of gas per ml of seawater (Hamme and Emerson 2004; Weiss 1970; Weiss and Kyser 1978; Wood and Caputi 1966). The equation for xenon has been corrected per (Hamme and Emerson 2004), and the underlying equations for solubility are available on the website http://web.uvic.ca/~rhamme/download.html

ocean in gas-solubility equilibrium with an overlying atmosphere. Ocean temperature T is the only variable changed; salinity, ocean volume, and sea surface atmospheric pressure are held constant. Mass conservation requires that the total number of Kr atoms in the ocean–atmosphere system before and after the temperature change must be equal (the 'superscript indicates the state after the change).

$$Kr_a + Kr_o = Kr'_a + Kr'_o \tag{3}$$

The inventory of krypton in the ocean Kr_o may be represented by the temperature-dependent Bunsen solubility coefficient $\beta(T)$ times the surface partial pressure of krypton pKr and volume of the ocean V_o (the Bunsen coefficient, in cm^3STP/cm^3STP water, describes the volume of pure gas at 1 atmosphere that will dissolve in a volume of water at equilibrium, see Fig. 4). The atmospheric inventory may likewise be simply represented as the surface partial pressure of krypton times the volume V_a that the atmosphere would have if it were at standard temperature and pressure.

$$Kr_o = \beta_{Kr}(T) p_{Kr} V_o$$

$$Kr_a = p_{Kr} V_a \tag{4}$$

$$Kr'_o = \beta_{Kr}(T') p_{Kr'} V_o$$

$$Kr'_a = p_{Kr'} V_a \tag{5}$$

Substituting (4–5) into (3), and repeating the analogous steps for N_2, then solving for the observed atmospheric quantity $\delta Kr/N_2$ yields

$$\delta Kr/N_2 + 1 = \frac{\frac{p_{Kr'}}{p_{N'_2}}}{\frac{p_{Kr}}{p_{N_2}}} = \frac{\frac{V_a}{V_o} + \beta_{Kr}(T)}{\frac{V_a}{V_o} + \beta_{N_2}(T)} \Big/ \frac{\frac{V_a}{V_o} + \beta_{Kr}(T')}{\frac{V_a}{V_o} + \beta_{N_2}(T')} \tag{6}$$

The actual mean ocean temperature is +3.5 °C presently. For illustration, let us consider the effect of cooling the model ocean from 3.0 to 0 °C. Taking V_o as $1.37 \cdot 10^{18}$ m^3 and V_a as $1.77 \cdot 10^{20}$ mol air $\cdot$ 0.02241 m^3STP $mol^{-1} = 3.97 \cdot 10^{18}$ m^3STP, the ratio V_a/V_o is 2.90 m^3STP m^{-3} (another way of saying this is that the atmosphere is effectively about 3 times bigger in volume than the ocean). Inserting the respective Bunsen coefficients, one obtains a $\delta Kr/N_2$ value of −2.1 ‰. The corresponding xenon value is −5.4 ‰. At current measurement precision, these values correspond to a signal-to-noise ratio of about 10.

A more detailed and realistic model gives a smaller change of −1.5 ‰ for krypton, largely due to the smaller volume and increased salinity of the glacial ocean (Headly and Severinghaus 2007). For comparison, preliminary measurements on ice cores using this method do show a colder glacial ocean, as expected, with a mean temperature about 3 ± 1° colder than present (Headly and Severinghaus 2007). The uncertainty quoted here is larger than the formal experimental uncertainty due to possible

systematic error in the large corrections that must be made for gravitational and thermal fractionation.

Corrections to measured values of $\delta Kr/N_2$ and $\delta Xe/N_2$ in ice core samples must be made to recover the true atmospheric values due to the physical processes occurring in the firn layer, which include gravitational settling, thermal diffusion, turbulent convection, and slow downward advection due to snow accumulation and bubble closure. Isotopic ratios ($^{15}N/^{14}N$ of N_2 and $^{86}Kr/^{82}Kr$) are measured in the same ice sample in order to make these corrections, with appropriate scalings, based on the assumption that these values do not change in the atmosphere. Convection and advection create disequilibrium, making the actual gravitational settling somewhat less than theoretically predicted (Severinghaus et al. 2010). Disequilibrium is more pronounced for slower-diffusing gases (such as xenon) than fast-diffusing gases (such as N_2) and thus must be considered carefully. A firn gas transport model incorporating all four processes with realistic estimates of past convection and snow accumulation is used to develop empirical scaling relationships between the isotopic ratios and the values to be corrected (Severinghaus et al. 2010).

Although this proxy is still under development, it is anticipated that the uncertainties will be substantially reduced as multiple records from different ice cores are compared. Because the atmosphere is well-mixed, all records should agree, providing a critical test of method reliability. Future work also includes testing the degree to which this proxy is representative of the deep ocean. Taking all waters colder than 4 °C as a working definition of the deep ocean, more than 80 % of the ocean volume lies in the deep ocean. The greater solubility at cold temperatures and the nonlinearity of the solubility-temperature relationship also contribute to dominance of the variation in this proxy by the deep ocean. Thus it seems likely that this proxy will be effectively a very good deep ocean thermometer but this needs to be quantitatively explored.

4.3 Triple Argon Isotope Composition in Trapped Air: Constraining the Outgassing Rate of ^{40}Ar from Earth's Interior

Understanding the origin of volatiles on Earth's surface is one of the fundamental problems of earth science. The volatile budget of the atmosphere and the degassing history of the earth are related to a range of fundamental processes of geodynamics, including heat production in the earth' interior and mantle mixing (e.g., Zhang and Zindler 1989; Porcelli and Wasserburg 1995).

The atmospheric concentrations of most noble gas isotopes, including the argon isotopes ^{36}Ar and ^{38}Ar, are constant on timescales of 100,000 year to millions of years (e. g., Porcelli and Wasserburg 1995; Allegre et al. 1987; Zhang and Zindler 1989). The ^{40}Ar concentration of the atmosphere, by contrast, is not constant, because ^{40}Ar is produced from radioactive decay of ^{40}K in the earth' interior and outgassed to the atmosphere. Therefore, the $^{40}Ar/^{38}Ar$ ratio of the atmosphere will increase monotonically with time.

Analyses of the isotope composition of argon in trapped air from deep Antarctic ice cores can be used to reconstruct the evolution of the paleoatmospheric $^{40}Ar/^{38}Ar$ ratio. In order to accurately reconstruct the paleoatmospheric $^{40}Ar/^{38}Ar$ ratio, one has to correct for gravitational fractionation in the firn, described in Sect. 4.1 (Craig and Wiens 1996; Schwander 1989; Sowers et al. 1989). This effect is more than an order of magnitude larger than the increase in the $^{40}Ar/^{38}Ar$ ratio of the atmosphere but it can be corrected by scaling to the gravitational fractionation of $^{38}Ar/^{36}Ar$ ratio, which is otherwise constant. Because the fractionation scales with mass difference (1.002, the ratio of the mass difference between ^{40}Ar and ^{38}Ar, and ^{38}Ar

and ^{36}Ar, respectively), the paleoatmospheric ^{40}Ar/^{38}Ar ratio can be calculated as follows

$$\delta^{40/38}Ar_{paleoatmosphere} = \delta^{40/38}Ar_{sample} - 1.002 \cdot \delta^{38/36}Ar_{sample} \quad (7)$$

Bender et al. (2008) reconstructed the paleoatmospheric ^{40}Ar/^{38}Ar history for the last ~780,000 year by analyzing samples from the Vostok and Epica Dome C ice cores (Fig. 5). The ^{40}Ar outgassing rate can be determined from the slope of the regression to be ($1.1 \pm 0.1 \cdot 10^8$ mol year^{-1}), consistent with simple models summing the outgassing from the continental crust and the upper mantle (Albarede 1998; Zhang and Zindler 1989).

Besides the significance of constraining the ^{40}Ar outgassing rate to understand the present and past geodynamics of the earth, the knowledge of the rate has important implications for ice core research itself. Tripe isotope composition of argon in trapped air allows ice samples of unknown age to be dated by dating the trapped air. Although current uncertainties of this method are fairly large [on the order of 180,000 year or 11 % of the age whichever is greater, Bender et al. (2008)], this independent dating technique could be of particular interest for dating old ice bodies of unknown age such as the rock glaciers in Mullins Valley or for future deep ice core drilling projects in Antarctica in search of very old ice.

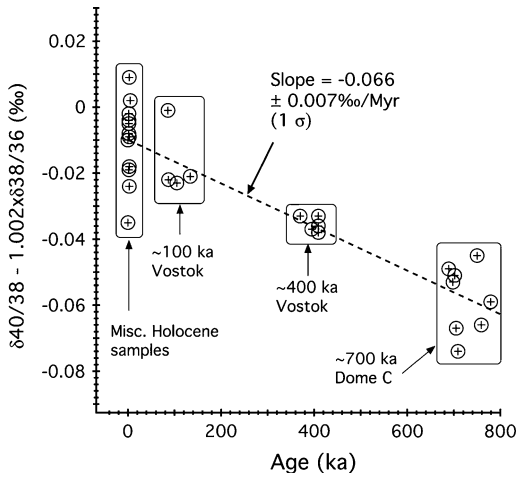

Fig. 5 Paleoatmospheric ^{40}Ar/^{38}Ar ratio, reconstructed from trapped air from the Vostok Ice core and Epica Dome C ice core, vs time. Figure from Bender et al. (2008). The results imply a contemporary rate of increase in the ^{40}Ar/^{38}Ar ratio of 0.066 ± 0.007/Myr, and a ^{40}Ar outgassing rate of (1.1 ± 0.1) · 10^8 mol yr^{-1}

5 The Noble Gas Record from Particulate Matter in Ice Cores

5.1 Reconstructions of the Flux of Interplanetary Dust from Ice Cores

Based on its specific helium isotope signatures, most notably high ^{3}He concentrations and ^{3}He/^{4}He ratios, extraterrestrial ^{3}He has been identified in a variety of climate archives: Quaternary sediments (e.g., Marcantonio et al. 1996; Takayanagi and Ozima 1987), sediments spanning the Cenozoic (Farley 1995), sedimentary rocks as old as 480 Ma (Patterson et al. 1998), loess deposits (Du et al. 2007) and, most recently, in polar ice cores. Tracing the extraterrestrial flux provides insights into a variety of questions, among them the variability of the extraterrestrial input and its relation to astronomical events, such as break-up of asteroids and comet showers, the potential impact of extraterrestrial dust on the earth' climate, and the potential use of the extraterrestrial ^{3}He signal as 'constant flux proxy' to constrain mass accumulation rates (for details, see McGee and Mukhopadhyay (2013).

Particles filtered from ice core samples represent a binary combination of a terrestrial and extraterrestrial dust component. Helium isotope analyses are uniquely suited to deconvolve the contributions from these two dust components because the helium isotopic composition of these two mixing components varies by about a factor of 10^4. Applying a simple two-component mixing model (e.g., Marcantonio et al. 1995; Patterson and Farley 1998), the fraction of extraterrestrial helium is

$$\left[{}^3\mathrm{He}_{\mathrm{ET}}\right] = \left[{}^3\mathrm{He}_{\mathrm{meas}}\right]\left(\frac{1-\frac{{}^3\mathrm{He}/{}^4\mathrm{He}_{\mathrm{TERR}}}{{}^3\mathrm{He}/{}^4\mathrm{He}_{\mathrm{meas}}}}{1-\frac{{}^3\mathrm{He}/{}^4\mathrm{He}_{\mathrm{TERR}}}{{}^3\mathrm{He}/{}^4\mathrm{He}_{\mathrm{IDP}}}}\right) \quad (8)$$

where $^3\mathrm{He}_{\mathrm{ET}}$ and $^3\mathrm{He}_{\mathrm{meas}}$ are the extraterrestrial and the measured ^{3}He concentration, respectively, and $^3\mathrm{He}/^4\mathrm{He}_{\mathrm{TERR}}$ and $^3\mathrm{He}/^4\mathrm{He}_{\mathrm{IDP}}$ denote the ratios assumed for the terrigenous ($\sim$0.01 R_a, where R_a is the helium isotope ratio of atmospheric air, 1.384 10^{-6}) and extraterrestrial endmembers ($\sim$200 R_a), respectively.

Extraterrestrial ^{3}He is delivered to the earth surface by cosmic dust [for more details, see McGee and Mukhopadhyay (2013)]. The interplanetary dust particles (IDPs) consist of a combination of asteroid and comet debris (Dohnanyi 1976) and acquire their characteristic helium signature from implantation of solar wind (e.g., Nier and Schlutter 1990). However, most IDPs $>$ 35 μm suffer severe heating during entry into the earth's atmosphere and loose their helium signal (Farley et al. 1997; Fraundorf et al. 1982). The atmosphere effectively acts as a filter, allowing only fine IDP, corresponding to about 0.5 % of the total IDP mass flux, to retain their helium signal. Thus, extraterrestrial ^{3}He data from ice cores (and other climate archives) offer a view of cosmic fluxes that is distinct from and complementary to that provided by other common extraterrestrial tracers, such as iridium or osmium, which trace the total extraterrestrial mass flux (Peucker-Ehrenbrink 1996).

^{3}He/^{4}He isotope ratios measured in particles from ice cores are typically relatively high. ^{3}He/^{4}He ratios from Greenland ice core range between 7 and 48 R_a (Brook et al. 2000); helium isotope ratios measured in particles from Antarctic ice cores are even higher than in Greenland and can be as high as 200 Ra (Brook et al. 2009, 2000; Winckler and Fischer 2006) because they are less diluted with terrestrial dust.

The high ^{3}He/^{4}He ratios measured in the particles are close to that of the extraterrestrial end-member, indicating that nearly all the ^{3}He in the ice is of extraterrestrial origin. According to Eq. (8), at least 99.8 % of the total ^{3}He is of extraterrestrial origin in all ice samples analyzed. This result is robust with respect to variations in the exact isotopic ^{3}He/^{4}He composition of both endmembers.

Ice cores offer the advantage compared to other terrestrial and marine climate archives that accumulation rates are well known. By multiplying the ^{3}He concentration with the snow accumulation rates, the flux of extraterrestrial ^{3}He can be determined

$$f_{He_{ET}} = \left[{}^3He_{ET}\right] \cdot AR_{ice} \quad (9)$$

where ^{3}He is the extraterrestrial ^{3}He concentration and AR_{ice} is the snow accumulation rate of the ice.

Figure 6 shows the reconstructed extraterrestrial ^{3}He fluxes from three different ice cores, GISP2 in Greenland (Brook et al. 2000) and Vostok (Brook et al. 2000) and EDML (Winckler and Fischer 2006) in Antarctica, covering the past 100,000 years. The studies from GISP 2 and Vostok directly used ice core samples, while the record from EDML was reconstructed with the excess water method (see Sect. 3.1.2).

Late Holocene samples from Vostok as well as from GISP 2 are replicates from the same or immediately adjacent depth levels in the ice core. The deeper samples from Vostok as well as the record from EDML represent time series. The range of ^{3}He fluxes for the replicate samples from Vostok and GISP 2, respectively, is relatively large and is thought to reflect the statistical effect of sampling a small number of IDPs in a given ice sample (Farley et al. 1997). The number of IDPs in a sample is proportional to the sample size and inversely proportional to the accumulation rate, known as the area-time product. Because ice cores tend to have relatively large accumulation rates, resulting area-time products are small. Even though large ice samples, of the order of hundreds of grams to several kilograms, are analyzed, this does not fully compensate for the effect of the high accumulation rates. The observed reproducibility between replicates or variability between adjacent samples is for all ice core studies equal to or better than the expected statistical distribution of ^{3}He data based on an atmospheric

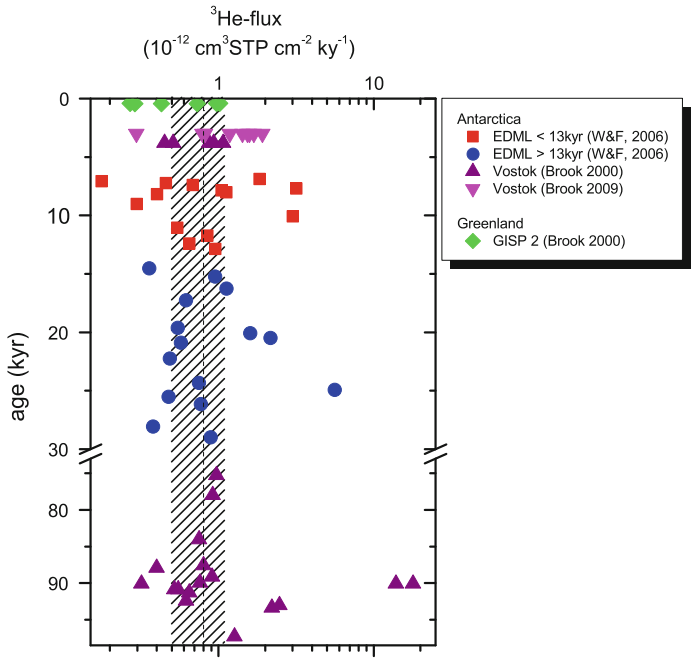

Fig. 6 Compilation of all ^{3}He flux data from polar ice cores vs age. Data are from EPICA DML (Winckler and Fischer 2006), Vostok (Brook et al. 2000, 2009) and GISP-2 (Brook et al. 2000). Please note the break on the age-axis, as no data are available between 30 and 75 kyr. High values may reflect rare large, ^{3}He-rich IDPs or short-term variability in the dynamics of IDP production, transport or accretion. The solid line and the shaded area represent an estimate of the extraterrestrial ^{3}He flux based on marine sediment [(8 ± 3) 10^{-13} cm^3 ^{3}He cm^{-2} kyr^{-1}, McGee and Mukhopadhyay 2013]

entry model [Farley et al. 1997, for details see McGee and Mukhopadhyay (2013)].

The over-all temporal and spatial variability of the reconstructed ^{3}He fluxes, as reflected by the three studies covering different time periods (Fig. 6), is in the same range as the scatter between replicate samples. This is particularly noteworthy because the three ice cores represent very different polar settings in Greenland and Antarctica, respectively, for example widely varying snow accumulation rates between 1 g cm^{-2} yr^{-1} in marine isotope stage (MIS) 5 ice from Vostok and 22 g cm^{-2} yr^{-1} at GISP2.

Perhaps most importantly we do not observe any significant change in the ^{3}He flux from interglacial (MIS 5, Vostok) to glacial (MIS 2 at EDML) to interglacial (Holocene at Vostok, GISP2 and EDML) conditions. The median extraterrestrial ^{3}He flux of all data is (8.10 ± 3.15) 10^{-13} cm^3 ^{3}He cm^{-2} kyr^{-1}. This flux is in good agreement with the best estimates of the extraterrestrial ^{3}He flux from mostly low-latitude marine sediments, (8 ± 3) 10^{-13} cm^3 ^{3}He cm^{-2} kyr^{-1} (McGee and Mukhopadhyay 2013; dashed line in Fig. 6). The consistency between the ice core based ^{3}He flux with the estimate from marine sediment cores supports a spatially and temporarily uniform deposition of IDPs on Earth.

The finding of a quasi-constant flux of extraterrestrial dust to Earth allows us to test a recent, stunning climate forcing hypothesis: Muller and MacDonald (1995, 1997) suggested that the 100,000 year climate cycles of the Quaternary are driven by fluctuations in the extraterrestrial dust accretion due to variability in the inclination of the earth (Muller and MacDonald 1995, 1997). The lack of variability in the ^{3}He flux on glacial-interglacial timescales over the past 100,000 yr is inconsistent with this hypothesis (Winckler and Fischer 2006; Brook et al. 2009) and rules out the input of

interplanetary dust as a driver of the late Pleistocene 100,000 year glacial cycles.

5.2 Reconstructions of Terrestrial Dust and Its Provenance

In addition to tracking cosmic dust, helium isotopes measured in particles from ice cores provide a record of atmospherically transported mineral aerosols (dust). Mineral dust is thought to have significant effects on the earth' radiation budget, both directly by influencing the radiative balance of the atmosphere (e.g., Arimoto 2001; Harrison et al. 2001) as well as indirectly by supplying micronutrients to the ocean (e.g., Martin 1990), thereby influencing the biological productivity of the surface ocean and, potentially, the biological uptake of CO_2 by the ocean (e.g., Bopp et al. 2003; Falkowski et al. 1998; Moore et al. 2002; Watson et al. 2000).

Polar ice cores provide an unambiguous record of dust fluxes; in particular, they show that dust deposition from the atmosphere to the polar ice sheets was about 20 times greater during glacial periods (e.g., EPICA Community Members 2004; Lambert et al. 2008; Petit et al. 1999). These dust flux records, based on major ions (non-sea salt Ca), coulter counter or laser measurements, show almost perfect agreement between individual sites across Antarctica or Greenland, to the extent that these records can be used to synchronize age scales. However, much less is known about the geographical origin of the terrestrial dust emitted and even less regarding the processes leading to increased dust mobilization.

The mineralogy, chemistry and isotopic composition of particulate dust in ice can in principle be used to identify the source areas from which the aeolian material is derived. In the past, the most successful approach has been based on radiogenic isotopes, such as neodymium, strontium and lead, and matching the observed isotopic composition of the particulate matter in the ice core with the isotopic fingerprint of potential source areas (e.g., Basile et al. 1997; Grousset et al. 1992).

The prevailing view until now has been that the source of dust to Antarctica is Southern South America, based largely on characterization of dust recovered from glacial sections of ice cores (Basile et al. 1997; Delmonte et al. 2004; Grousset et al. 1992).

Characterizing the provenance of interglacial dust has been analytically challenging due to the extremely low dust levels during interglacial periods. Recent radiogenic isotope analyses of interglacial dust samples, from the Holocene and MIS 5e, indicate that dust deposited in Antarctica during interglacial time periods may be derived from a mixture of dust sources rather than a single source. Potential sources include different regions within southern South America and other sources like Australia (Delmonte et al. 2007; Revel-Rolland et al. 2006) or possibly the Puna-Altiplano area (Delmonte et al. 2008). However, no definite conclusions have yet been drawn due to the limited data set and overlap of potential source areas (PSAs) in Sr–Nd space.

Helium isotopes measured in the EDML core in Antarctica provide a record of the dust flux and dust provenance and represent a new provenance tool that can potentially be helpful in answering this question. The ^{4}He signal in ice cores is typically dominated by the terrigenous component while the ^{3}He signal is mostly of extraterrestrial origin. Terrigenous ^{4}He has successfully been used to reconstruct dust fluxes to late Pleistocene marine sediments (Patterson et al. 1999; Winckler et al. 2008, 2005) and to modern corals (Mukhopadhyay and Kreycik 2008). Within the terrigenous fraction, resistant trace phases, such as zircons and apatite, are rich in U and Th and have consequently high concentrations of ^{4}He. Volcanic material, in contrast, has very low ^{4}He concentrations, typically 3 orders of magnitude lower than in continentally derived material (Patterson et al. 1999). Because terrigenous ^{4}He is produced from alpha-decays of U and Th within the rock matrix, it is expected to increase with the formation age of the source rock (disregarding variable helium retention characteristics of different rock types). Consequently, when paired

with another relatively constant terrigenous proxy [X] (such as Ca or ^{232}Th), the $^{4}He_{terr}$/[X] ratio is to a first order a function of the rock formation age. Conceptually, geochemical fingerprints of ^{4}He/[X] in ice core samples can then be matched up with distinct ^{4}He/[X] ratios between potential dust source areas, thus allowing tracing the provenance of the dust deposited.

Terrigenous ^{4}He can be calculated from the same data presented in the Sect. 5.1 using a simple two-component mixing model (Patterson et al. 1999)

$$\frac{^{4}He_{terr}}{^{4}He_{meas}} = \frac{(^{3}He/^{4}He)_{meas} - (^{3}He/^{4}He)_{ET}}{(^{3}He/^{4}He)_{terr} - (^{3}He/^{4}He)_{ET}}$$

where *terr* and *ET* denote the terrigenous and extraterrestrial component, respectively. Terrigenous ^{4}He-fluxes, calculated by multiplying the terrigenous ^{4}He concentration with the ice accumulation rate, are generally greater during the last glacial period than during the Holocene. However, the decrease from glacial to interglacial values is only by a factor of 2, in sharp contrast to the interglacial/glacial decrease of a factor of about 20 that is commonly observed from particulate dust flux measurements (EPICA Community Members 2004; Fischer et al. 2007; Petit et al. 1999).

A likely explanation is that the ^{4}He concentrations of the glacial dust source is smaller than that of the interglacial dust. This is supported by the isotope mixing diagram with nss Ca^{2+} as terrestrial dust reference (Fig. 7). Glacial and interglacial samples lie on well-defined mixing lines. While both mixing lines are anchored in the same extraterrestrial endmember (intercept with the ^{4}He/^{3}He-axis), their slopes are significantly different, indicating distinct terrestrial end-members. Glacial ice shows much lower ^{4}He/nssCa^{2+} ratios than interglacial ice.

Thus, the last glacial to Holocene shift in ^{4}He/nssCa^{2+}—together with the moderate decrease of the ^{4}He-flux—points to a glacial to interglacial shift in terrestrial dust sources.

There are two scenarios that could potentially explain this shift:

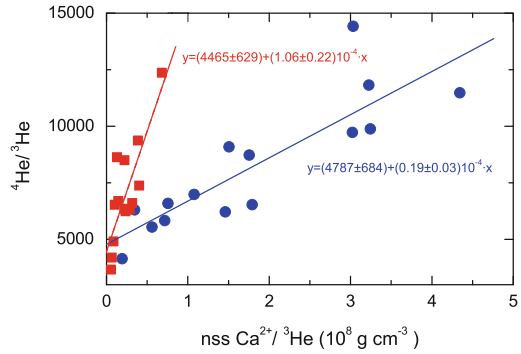

Fig. 7 Isotope mixing diagram with non sea salt Ca^{2+} (nss Ca^{2+}) as terrestrial dust reference species. Glacial (*blue symbols*) and interglacial (*red symbols*) ice samples fall along two well-defined mixing lines with matching y-intercepts (^{4}He/ ^{3}He ratio of the extraterrestrial endmember) and distinct slopes suggesting a glacial-interglacial change in terrestrial dust source distribution (Winckler and Fischer 2006)

a. Taken at face value, the ^{4}He fluxes and ^{4}He/nssCa^{2+} ratios (Fig. 7) observed across Termination 1 appear to imply a younger (and therefore less radiogenic) source of dust in glacial times, compared to interglacials. Southern South America represents a relatively young orogenic environment. Australia or South Africa, in contrast, are part of the Precambrian shield and are expected to show higher radiogenic ^{4}He concentrations.
b. Alternatively, the glacial/interglacial shift in the ^{4}He/nssCa ratio could reflect a change in the dominant dust source within South America. A possible scenario could be a change from fresh glacial outwash material, during glacial periods, with little chemical weathering to a loess/dessert dust source, during interglacials, which has been exposed to chemical weathering for a longer time. Calcium is known to be an element which is highly susceptible to chemical weathering (e.g., Taylor and McLennan 1985). The main carrier for ^{4}He is zircon (Patterson et al. 1999) which is resistant to chemical weathering. Therefore, He is expected to be retained better than calcium, and accordingly the interglacial dust is likely to show higher ^{4}He/Ca.

Comprehensive characterization of the helium isotopic composition and ^{4}He/Ca ratios of all potential source areas, including different regions in South America, Australia and possibly local Antarctic dust sources, is needed to differentiate between the two scenarios. Such work is currently in progress.

6 Summary and Future Work

Analyses of noble gases of air bubbles, trapped in ice cores, have provided important insights into the environmental record of the earth and underlying mechanisms of climate change. Additionally, helium isotope measurements of particles trapped in the ice core provide a record of the influx of extraterrestrial dust to the earth and of varying terrestrial dust input. Noble gas studies in ice core research are still a relatively new field and several lines of future research offer promising avenues of research:

- To what extent can future records of Kr/N_2 and Xe/N_2 ratios from different ice cores reduce the uncertainty in the deep ocean paleo temperature estimate? Because the atmosphere is well-mixed, records from different ice cores should agree, providing a critical test of method reliability. If successful, a precise time series of the deep ocean temperature will provide a key parameter for global climate models.
- How old is the oldest ice in Antarctica? In addition to argon isotopes (Sect. 4.3), the long-lived krypton isotope ^{81}Kr, with a half-life of 229 kyr, represents a promising tracer for dating old ice ranging from 200 kyr to 1.5 Myr. Recent breakthroughs in the atom trap trace analysis (ATTA) technique for measuring krypton isotopes (Jiang et al. 2012), combining both significant reduction in sample size and much improved counting efficiency, may pave the way for radiometric dating of old ice, complementing Ar-based dating methods.
- How did the extraterrestrial ^{3}He input vary over the Late Pleistocene? Limited availability of larger ice samples from traditional ice coring projects has so far hampered our ability to accurately determine the extraterrestrial ^{3}He flux. However, horizontal ice core sites from Greenland and Antarctica (e.g., Taylor Glacier), replicate coring and sampling excess water from CFA—together with analyzing different grain size fractions—may be helpful in providing sufficient ice for more precise ^{3}He flux estimates.
- What is the origin of dust deposited in Antarctica? A major investigation of the ^{4}He/Ca fingerprint of source areas in the Southern hemisphere is underway and will provide the background information needed to constrain the dust sources and, by doing so, help to increase our understanding of the role of dust in climate.

The case studies presented in this chapter illustrate the wide spectrum of noble gas applications in ice core research. The range of applications is even wider, but, given our focus on climate-related studies, we have not covered further noble gas studies, such as the use of helium isotopes in ice to (a) constrain basal ice dynamics from radiogenic ^{4}He diffusion from the bedrock (Craig and Scarsi 1997) or (b) to determine the accretion of lake ice in the Vostok record (Jean-Baptiste et al. 2001b) as well as the search for missing xenon in polar ice sheets (Bernatowicz et al. 1985). The potential for future advances of noble gas analyses in ice core research is very large, as a result of the drilling of new ice cores in unexplored regions and new ice cores reaching further back in time, exploration of re-exposed old ice at ice margins and blue ice areas, increases in the range of chemical and isotopic proxies measured and increasing temporal resolution of the analyses.

References

Aeschbach-Hertig W, Solomon K (2013) Groundwater circulation and palaeotemperatures by noble gas geochemistry. In: Burnard P (ed) The noble gases as geochemical tracers, advances in isotope geochemistry. Springer, Berlin doi:10.1007/978-3-642-28836-4

Albarede F (1998) Time-dependent model of U-Th-He and K-Ar evolution and the layering of mantle

convection. Chem Geol 145(3–4):413–429. doi: 10.1016/S0009-2541(97)00152-6

Allegre CJ, Staudacher T, Sarda P (1987) Rare gas systematics—formation of the atmosphere, evolution and structure of the Earth's mantle. Earth Planet Sci Lett 81:127–150

Alley RB, Marotzke J, Nordhaus WD, Overpeck JT, Peteet DM, Pielke RA Jr, Pierrehumbert RT, Rhines PB, Stocker TF, Talley LD, Wallace JM (2009) Abrupt climate change. Science 292:2005–2010. doi: 10.1126/science.1081056

Arimoto R (2001) Eolian dust and climate: relationships to sources, tropospheric chemistry, transport and deposition. Earth Sci Rev 54:29–42

Basile I, Grousset FE, Revel M, Petit J-R, Biscaye PE, Barkov NI (1997) Patagonian origin of glacial dust deposited in East Antarctica (Vostok and Dome C) during glacial stages 2, 4 and 6. Earth Planet Sci Lett 146:573–589

Bender ML, Barnett B, Dreyfus G, Jouzel J, Porcelli D (2008) The contemporary degassing rate of ^{40}Ar from the solid earth. Proc Nat Acad Sci 105(24):8232–8237. doi:10.1073/pnas.0711679105

Bernatowicz TJ, Kennedy BM, Podosek FA (1985) Xe in glacial ice and the atmospheric inventory of noble gases. Geochim Cosmochim Acta 49:2561–2564

Bopp L, Kohfeld KE, Le Quere C, Aumont O (2003) Dust impact on marine biota and atmospheric CO_2 during glacial periods. Paleoceanography 18(2)

Brook EJ, Kurz MD, Curtice J, Cowburn S (2000) Accretion of interplanetary dust in polar ice. Geophys Res Lett 27(19):3145–3148

Brook EJ, Kurz MD, Curtice J (2009) Flux and size fractionation of ^{3}He in interplanetary dust from antarctic ice core samples. Earth Planet Sci Lett 286:565–569. doi:10.1016/j.epsl.2009.07.024

Burnard P, Zimmermann L, Sano Y (2013) The noble gases as geochemical tracers: history and background information. In: Burnard P (ed) The noble gases as geochemical tracers, advances in isotope geochemistry. Springer, Berlin doi:10.1007/978-3-642-28836-4

Caillon N, Severinghaus JP, Barnola J-M, Chappellaz J, Jouzel J, Parrenin F (2001) Estimation of temperature change and of gas age ice age difference, 108 kyr BP, at Vostok, Antarctica. J Geohysical Res Atmos 106(D23):31893–31901 doi:10.1029/2001JD900145

Caillon N, Severinghaus JP, Jouzel J, Barnola J-M, Kang JC, Lipenkov VY (2003) Timing of atmospheric CO_2 and Antarctic temperature change across termination III. Science 299(5613):1728–1731. doi:10.1126/science.1078758

Chapman S, Dootson FW (1917) A note on thermal diffusion. Phil Mag 33(193–98):248–253

Craig H, Scarsi P (1997) Helium isotope stratigraphy in the GISP2 ice core. Eos 78

Craig H, Wiens RC (1996) Gravitational enrichment of ^{84}Kr/^{36}Ar ratios in polar ice caps: a measure of firn thickness and accumulation temperature. Science 271:1708–1710

Craig H, Horibe Y, Sowers T (1988) Gravitational separation of gases and isotopes in polar ice caps. Science 242(4886):1675–1678

Dahl-Jensen D, Gundestrup NS, Miller H, Watanabe O, Johnsen SJ, Steffensen JP, Clausen HB, Svensson A, Larsen LB (2002) The NorthGRIP deep drilling program. Ann Glaciol 35:1–4

Delmonte B, Basile-Doelsch I, Petit J-R, Maggi V, Revel-Rolland M, Michard A, Jagoutz E, Grousset F (2004) Comparing the Epica and Vostok dust records during the last 220,000 years: stratigraphical correlation and provenance in glacial periods. Earth Sci Rev 66:63–87

Delmonte B, Petit J-R, Basile-Doelsch I, Jagoutz E, Maggi V (2007) Late quaternary interglacials in East Antarctica from ice-core dust records. In: Sirocko F, Litt T, Clausen M (eds) The climate of past interglacials. Amsterdam, pp 53–73

Delmonte B, Delmas RJ, Petit J-R (2008) Comment on ''dust provenance in Antarctic ice during glacial periods: from where in southern South America?'' by D. M. Gaiero. Geophys Res Lett 35:L08707. doi: 10.1029/2007GL032075

Dohnanyi JS (1976) Sources of interplanetray dust: asteroids. In: Elsasser H, Fechtig H (eds) Interplanetary dust and zodiacal light, vol 48. Springer, Berlin, pp 187–206. doi: 10.1007/978-3-642-28836-4

Dreyfus G, Jouzel J, Bender ML, Landais A, Masson-Delmotte V, Leuenberger MC (2010) Firn processes and δ^{15}N: potential for a gas-phase climate proxy. Quat Sci Rev 29(1–2):28–42

Du X, Wang Y, Ren J, Ye X, Lu H (2007) Helium isotope investigation on magnetic reversal boundaries of loess-paleosol sequence at Luochuan, central Chinese Loess Plateau. Chin Sci Bull 52:2407–2412

EPICA_community_members (2004) Eight glacial cycles from an Antarctic ice core. Nature 429(6992):623–628

Falkowski PG, Barber RT, Smetacek V (1998) Biogeochemical controls and feedbacks on ocean primary production. Science 281:200–206

Farley KA (1995) Cenozoic variations in the flux of interplanetary dust recorded by ^{3}He in a deep-sea sediment. Nature 376:153–156

Farley KA, Love SG, Patterson DB (1997) Atmospheric entry heating and helium retentivity of interplanetary dust particles. Geochim Cosmochim Acta 61:2309–2316

Fischer H, Siggaard-Andersen M-L, Ruth U, Roethlisberger R, Wolff E (2007) Glacial/interglacial changes in mineral dust and sea salt records in polar ice cores: sources, transport, deposition. Rev Geophys 45:2005 RG000192

Fraundorf P, Lyons T, Schubert P (1982) The survival of solar flare tracks in interplanetary dust silicates on deceleration in the Earth's atmosphere. J Geophys Res 87:409–412

Grachev AM, Severinghaus JP (2003a) Determining the thermal diffusion factor for ^{40}Ar/^{36}Ar in air to aid

paleoreconstruction of abrupt climate change. J Phys Chem A 107:4636–4642

Grachev AM, Severinghaus JP (2003b) Laboratory determination of thermal diffusion constants for $^{29}N_2/^{28}N_2$ in air at temperatures from −60 to 0 °C for reconstruction of magnitudes of abrupt climate changes using the ice core fossil-air paleothermometer. Geochim Cosmochim Acta 67:345–360

Grootes PM, Stuiver M, White JWC, Johnsen SJ, Jouzel J (1993) Comparison of oxygen isotope records from the GISP2 and GRIP Greenland ice cores. Nature 366:552–554

Grousset FE, Biscaye PE, Revel M, Petit J-R, Pye K, Joussaume S, Jouzel J (1992) Antarctic (Dome C) ice-core dust at 18 k.y. B.P.: isotopic constraints on origins. Earth Planet Sci Lett 111:175–182

Hamme RC, Emerson SR (2004) The solubility of neon, nitrogen and argon in destilled water and seawater. Deep-Sea Res 51(11):1517–1528. doi:10.1016/j.dsr.2004.06.009

Harrison SP, Kohfeld KE, Roelandt C, Claquin T (2001) The role of dust in climate changes today, at the last glacial maximum and in the future. Earth Sci Rev 54:43–80

Headly MA, Severinghaus JP (2007) A method to measure Kr/N_2 ratios in air bubbles trapped in ice cores and its application in reconstructing past mean ocean temperature. J Geophys Res 112:D19105. doi:10.1029/2006JD008317

Jean-Baptiste P, Petit JR, Lipenkov VY, Raynaud D, Barkov NI (2001a) Constraints on hydrothermal processes and water exchange in lake Vostok from helium isotopes. Nature 411:460–462

Jean-Baptiste P, Petit JR, Lipenkov VY, Raynaud D, Barkov NI (2001b) Constraints on hydrothermal processes and water exchange on lake Vostok from helium isotopes. Nature 411:460–462

Jiang W, Bailey K, Lu Z-T, Mueller P, O'Connor TP, Cheng C-F, Hu S-M, Purtschert R, Sturchio NC, Sun YR, Williams WD, Yang G-M (2012, in press) An atom counter for measuring ^{81}Kr and ^{85}Kr in environmental samples. Geochim Cosmochim Acta

Johnsen SJ, Clausen HB, Dansgaard W, Gundestrup NS, Hammer CU, Andersen U, Andersen KK, Hvidberg CS, DahlJensen D, Steffensen JP, Shoji H, Sveinbjornsdottir AE, White JWC, Jouzel J, Fisher D (1997) The delta O-18 record along the greenland ice core project deep ice core and the problem of possible eemian climate instability. J Geophys Res 102(C12):26397–26410 doi:10.1029/97JC00167

Jouzel J, Alley RB, Cuffey KM, Dansgaard W, Grootes PM, Hoffmann G, Johnsen SJ, Koster RD, Peel D, Shuman CA, Stievenard M, Stuiver M, White J (1997) Validity of the temperature reconstructions from water isotopes in ice cores. J Geohysical Res 102:26471–26487

Kaufmann PR, Federer U, Hutterli MA, Bigler M, Schuepbach S, Ruth U, Schmitt J, Stocker TF (2008) An improved continuous flow analysis system for high-resolution field measurements on ice cores. Environ Sci Technol 42:8044–8050

Kobashi T, Severinghaus JP, Barnola J-M (2008a) 4 ± 1.5 °C abrupt warming 11,270 yr ago identified from trapped air in Greenland ice. Earth Planet Sci Lett 268:397–407. doi:10.1016/j.epsl.2008.01.032

Kobashi T, Severinghaus JP, Kawamura K (2008b) Argon and nitrogen isotopes of trapped air in the GISP2 ice core during the holocene epoch (0–11,500 B.P.): methodology and implications for gas loss processes. Geochim Cosmochim Acta 72:4675–4686. doi:10.1016/j.gca.2008.07.006

Kobashi T, Severinghaus JP, Barnola J-M, Kawamura K, Carter T, Nakaegawa T (2009) Persistent multi-decadal Greenland temperature fluctuation through the last millenium. Clim Change. doi:10.1007/s10584-009-9689-9

Kurz MD, Kenna T, Lassiter J, Depaolo D (1996) Helium isotopic evolution of mauna kea volcano; first results from the 1-km drill core. J Geophys Res 101:11781–11791

Lambert F, Delmonte B, Petit JR, Bigler M, Kaufmann PR, Hutterli MA, Stocker TF, Ruth U, Steffensen JP, Maggi V (2008) Dust-climate coupling over the past 800,000 years from the EPICA Dome C ice core. Nature 452(7187):616–619

Landais A (2011) Stable isotopes of N and Ar as tracers to retrieve past air temperature from air trapped in ice cores. In: Barkaran M (ed) Handbook of environmental isotope geochemistry, advances in isotope geochemistry. Springer, Berlin. doi 10.1007/978-3-642-10637-8_40

Landais A, Barnola J-M, Masson-Delmotte V, Jouzel J, Chappellaz J, Caillon N, Huber C, Leuenberger MC, Johnsen SJ (2004a) A continuous record of temperature evolution over a sequence of dansgaard-oeschger events during marine isotopic stage 4 (76–62 kyr BP). Geophys Res Lett 31:L22211. doi:10.1029/2004GL021193

Landais A, Caillon N, Goujon C, Grachev AM, Barnola J-M, Chappellaz J, Jouzel J, Masson-Delmotte V, Leuenberger MC (2004b) Quantification of rapid temperature change during DO event 12 and phasing with methane inferred from air isotopic measurements. Earth Planet Sci Lett 225(1–2):221–232. doi:10.1016/j.epsl.2004.06.009

Landais A, Masson-Delmotte V, Jouzel J, Raynaud D, Johnsen SJ, Huber C, Leuenberger MC, Schwander J, Minster B (2006) The glacial interception as recorded in the NorthGRIP Greenland ice core: timing, structure and associated abrupt temperature change. Clim Dyn 26:273–284. doi:10.1007/s00382-005-0063-y

Leuenberger MC, Lang C, Schwander J (1999) Delta 15 N measurements as a calibration too for the paleothermometer and gas-ice differences: a case study for the 8,200 B.P. event on GRIP ice. J Geophys Res 104:22163–22170

Loulergue L, Schilt A, Spahni R, Masson-Delmotte V, Blunier T, Lemieux B, Barnola J-M, Raynaud D, Stocker TF, Chappellaz J (2008) Orbital and

millennial-scale features of atmospheric CH_4 over the past 800,000 years. Nature 453:383–386. doi:10.1038/nature06950

Luethi D, Le Floch M, Bereiter B, Blunier T, Barnola J-M, Siegenthaler U, Raynaud D, Jouzel J, Fischer H, Kawamura K, Stocker TF (2008) High-resolution carbon dioxide concentration record 650,000–800,000 years before present. Nature 453:379–382. doi:10.1038/nature06949

Marcantonio F, Kumar N, Stute M, Anderson RF, Seidl MA, Schlosser P, Mix A (1995) A comparative study of accumulation rates derived by He and Th isotope analysis of marine sediments. Earth Planet Sci Lett 133:549–555

Marcantonio F, Anderson RF, Stute M, Kumar N, Schlosser P, Mix A (1996) Extraterrestrial ^{3}He as a tracer of marine sediment transport and accumulation. Nature 383:705–707

Martin JH (1990) Glacial-interglacial CO_2 change: the iron hypothesis. Paleoceanography 5:1–13

McGee D, Mukhopadhyay S (2013) Extraterrestrial He in sediments: From recorder of asteroid collisions to timekeeper of global environmental changes. In: Burnard P (ed) The noble gases as geochemical tracers, advances in isotope geochemistry. Springer, Berlin doi:10.1007/978-3-642-28836-4

McKinney CR, McCrea JM, Epstein S, Allen HA, Urey HC (1950) Improvements in mass-spectrometers for the measurement of small differences in isotope abundance ratios. Rev Sci Instrum 21:724–730

Moore JK, doney SC, Glover DM, Fung I (2002) Iron cycling and nutrient-limitation patterns in surface waters of the world ocean. Deep-Sea Res 49:463–507

Mukhopadhyay S, Kreycik P (2008) Dust generation and drought paterns in Africa from helium-4 in a modern cape verde coral. Geophys Res Lett 35. 10.1029/2008GL035722

Muller RA, MacDonald GJ (1995) Glacial cycles and orbital inclination. Nature 377:107–108

Muller RA, MacDonald GJ (1997) Glacial cycling and astronomical forcing. Science 277:215–218

NGRIP_Project_members (2004) High-resolution record of Northern Hemisphere climate extending into the last interglacial period. Nature 431:147–151

Nier AO, Schlutter DJ (1990) Helium and neon in stratospheric particles. Meteoritics 25:263–267

Orsi AJ, B., Cornuelle B, Severinghaus JP (2009) Magnitude and temporal evolution of interstadial 8 abrupt temperature change inferred from δ15 N and δ40Ar in GISP2 Ice using a new least-squares inversion. AGU chapman conference on abrupt climate change

Patterson DB, Farley KA (1998) Extraterrestrial ^{3}He in seafloor sediments: evidence for correlated 100kyr periodicity in the accretion rate of interplanetary dust, orbital parameters, and quaternary climate. Geochim Cosmochim Acta 62:3669–3682

Patterson DB, Farley KA, Schmitz B (1998) Preservation of extraterrestrial ^{3}He in 480-Ma-old marine limestones. Earth Planet Sci Lett 163:315–325

Patterson DB, Farley KA, Norman MD (1999) ^{4}He as a tracer of continental dust: a 1.9 million year record of aeolian flux to the west equatorial Pacific Ocean. Geochim Cosmochim Acta 63(5):615–625

Petit JR, Jouzel J, Raynaud D, Barkov NI, Barnola JM, Basile I, Bender ML, Chappellaz J, Davis ME, Delaygue G, Delmotte M, Kotlyakov VM, Legrand M, Lipenkov VY, Lorius C, Pepin L, Ritz C, Saltzman E, Stievenard M (1999) Climate and atmospheric history of the past 420,000 years from the Vostok ice core, Antarctica. Nature 399:429–436

Peucker-Ehrenbrink B (1996) Accretion of extraterrestrial matter during the last 80 million years and its effect on the marine osmium isotope record. Geochim Cosmochim Acta 60:3187–3196

Porcelli D, Wasserburg GJ (1995) Mass transfer of helium, argon, and xenon through a steady-state upper mantle. Geochim Cosmochim Acta 59(23):4921–4937. doi:10.1016/0016-7037(95)00336-3

Revel-Rolland M, De Deckker P, Delmonte B, Hesse PP, Magee JW, Basile-Doelsch I, Grousset F, Bosch D (2006) Eastern Australia: a possible source of dust in East Antarctica interglacial ice. Earth Planet Sci Lett 249:1–13

Schwander J (1989) The transformation of snow to ice and the occlusion of gases. In: Oeschger H, Langway CC Jr (eds) The environmental record in glaciers and ice sheets. Wiley, New York, pp 53–67

Severinghaus JP, Battle M (2006) Fractionation of gases in polar ice during bubble close-off: new constraints from firn air Ne, Kr, and Xe observations. Earth Planet Sci Lett 244:474–500

Severinghaus JP, Brook EJ (1999) Abrupt climate change at the end of the last glacial period inferred from trapped air in polar ice. Science 286:930–934

Severinghaus JP, Sowers T, Brook EJ, Alley RB, Bender ML (1998) Timing of abrupt climate change at the end of the younger Dryas interval from thermally fractionated gases in polar ice. Nature 391:141–146

Severinghaus JP, Grachev AM, Luz B, Caillon N (2003) A method for precise measurement of argon 40/36 and krypton/argon ratios in trapped air in polar ice with applications to past firn thickness and abrupt climate change in Greenland and at Siple Dome, Antarctica. Geochim Cosmochim Acta 67:325–343

Severinghaus JP, Albert MR, Courville ZR, Fahnestock MA, Kawamura K, Montzka SA, Muhle J, Scambos TA, Shields E, Shuman CA, Suwa M, Tans P, Weiss RF (2010) Deep air convection in the firn at a zero-accumulation site, central Antarctica. Earth Planet Sci Lett 293(3–4):359–367. doi:10.1016/j.epsl.2010.03.003

Sowers T, Bender ML, Raynaud D (1989) Elemental and isotopic composition of occluded O-2 and N-2 in polar ice. J Geophys Res: Atmos 94(D4):5137–5150. doi:10.1029/JD094iD04p05137

Takayanagi M, Ozima M (1987) Temporal variation of ^{3}He/^{4}He ratio recorded in deep-sea sediment cores. J Geophys Res 92:12531–12538

Taylor SR, McLennan SM (1985) The continental crust: its composition and evolution. Blackwell, Oxford

Watson AJ, Bakker DCE, Ridgwell AJ, Boyd PW, Law CS (2000) Effect of iron supply on southern ocean CO_2 uptake and implications for glacial atmospheric CO_2. Nature 407(6805):730–733

Weiss RF (1970) The solubility of nitrogen, oxygen and argon in water and seawater. Deep-Sea Res 17:721–735

Weiss RF, Kyser TK (1978) Solubility of krypton in water and seawater. J Chem Eng Data 23:69–72

Winckler G, Fischer H (2006) 30,000 years of cosmic dust in Antarctic ice. Science 313:491. doi:10.1126/science.1127469

Winckler G, Anderson RF, Schlosser P (2005) Equatorial Pacific productivity and dust flux during the mid-pleistocene climate transition. Paleoceanography 20(4):PA4025, 4010. 1029/2005PA001177 doi:10.1029/2005PA001177

Winckler G, Anderson RF, Fleisher MQ, McGee D, Mahowald NM (2008) Covariant glacial-interglacial dust fluxes in the equatorial Pacific and Antarctica. Science 320:93–96. doi:10.1126/science.1150595

Wood D, Caputi R (1966) Solubilities of Kr and Xe in fresh and seawater. In: Tech Rep USNRDL-TR-988, vol. U.S. Nav. Radiol. Def. Lab, San Francisco, California

Zhang YX, Zindler A (1989) Noble gas constraints on the evolution of the earth's atmosphere. J Geophys Res: Solid Earth 94(B10):13719–13737. doi:10.1029/JB094IB10p13719

Noble Gases in Seawater as Tracers for Physical and Biogeochemical Ocean Processes

Rachel H. R. Stanley and William J. Jenkins

Abstract

Noble gases are biologically and chemically inert, making them excellent tracers for physical processes. There are 5 stable noble gases: He, Ne, Ar, Kr, and Xe, with a range of physicochemical properties; the diffusivities of the noble gases in seawater differ by approximately a factor of 5 and the solubilities of the noble gases in seawater differ by approximately a factor of 10. This broad range in physicochemical characteristics leads to differing response to physical forcing. Thus, measurements of multiple noble gases made concurrently allow quantification of many physical processes. In seawater studies, noble gas measurements have been used to investigate air-sea gas exchange, allowing explicit separation of the bubble component from the diffusive gas exchange component, and to study equilibration during deep water formation. Argon has been used to quantify diapycnal mixing and the heavier noble gases could be useful in such studies as well. Helium, Ne, and Ar have yielded insights on ocean-cryospheric processes such as sea ice formation and basal melting of glaciers. The isotope ^{3}He has been used extensively in studies of ocean circulation, and also for quantifying ocean-lithospheric interactions. Additionally, noble gases can be combined with biologically active gases, such as O_2 or N_2, in order to quantify rates of biological production and denitrification.

1 Introduction

Dissolved noble gases are ideal in situ tracers for physical processes in the ocean because they are biologically and chemically inert and thus respond solely to physical forcing. Additionally, there are five stable noble gases with a range of solubilities and molecular diffusivities in seawater (Fig. 1). The diffusivities in seawater of the noble gases differ by a factor of seven with helium being the most diffusive (Jahne et al. 1987). The solubilities differ by more than an order of magnitude, with xenon being the most soluble (Smith and Kennedy 1983; Wood and Caputi 1966). The solubilities of the heavier noble gases (Ar, Kr, and Xe) have a strong, non-linear dependence on

R. H. R. Stanley (✉) · W. J. Jenkins
Woods Hole Oceanographic Institution, Woods Hole, MA 02543, USA
e-mail: rstanley@whoi.edu

P. Burnard (ed.), *The Noble Gases as Geochemical Tracers*, Advances in Isotope Geochemistry,
DOI: 10.1007/978-3-642-28836-4_4,

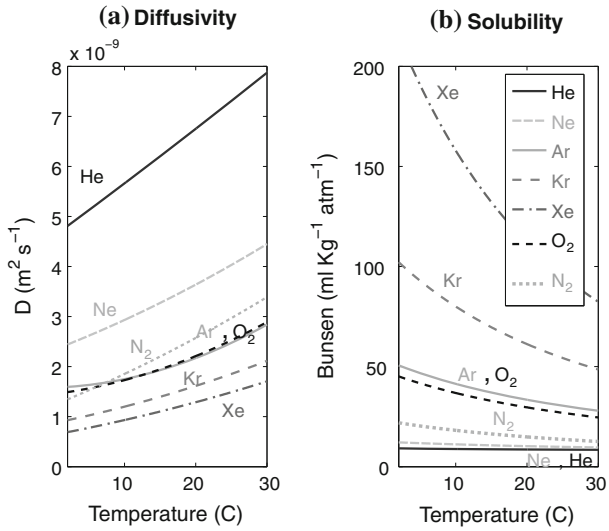

Fig. 1 **a** Molecular diffusivities of the noble gases, oxygen, and nitrogen as a function of temperature, as calculated from the diffusivity values of Jahne et al. (1987) and Wise and Houghton (1966). **b** Solubilities of the five noble gases, nitrogen, and oxygen in seawater as a function of temperature. Solubility values for He are from a modified version of Weiss (1971), Ne, Ar, and N_2 solubilities are from Hamme and Emerson (2004b), Kr solubility is from Weiss and Kyser (1978) and Xe solubility is from Wood and Caputi (1966)

temperature whereas the solubility of the lighter ones (He, Ne) are relatively insensitive to temperature (Hamme and Emerson 2004b; Smith and Kennedy 1983; Weiss 1971; Weiss and Kyser 1978; Wood and Caputi 1966). Additionally, during sea ice formation or melting, the lighter gases are favorably partitioned into ice whereas the heavier gases remain preferentially in the water (e.g. Hood et al. 1998). This broad range in physicochemical characteristics leads to significantly different responses to physical forcing (Fig. 2). Thus, measurements of multiple noble gases made concurrently in seawater allow one to diagnose and quantify physical processes, such as air-sea gas exchange, diapycnal mixing, and subsurface basal glacial melting.

The main source of noble gases to the ocean is from the atmosphere through the process of air-sea gas exchange. The noble gases are usually close to being in equilibrium with the atmosphere, according to Henry Laws constants, although rapid warming or cooling, ice formation or melting, and bubble injection can lead to departures from equilibrium. Additionally, He has two additional sources. ^{4}He is produced by nuclear reactions in rocks, primarily in the Uranium series. Some of this ^{4}He enters the ocean through water-rock processes. Additionally ^{3}He is produced by radioactive decay from atmospheric tritium.

Noble gas measurements can be combined with dissolved biologically active gases, such as O_2 or N_2, to yield quantitative insights into biogeochemical processes. O_2 and N_2 can be used as geochemical tracers for quantifying rates of important biological processes such as net community production and denitrification. However, physical processes such as air-sea gas exchange and thermal forcing affect O_2 and N_2, making direct interpretation of those gas records difficult. Argon has a very similar solubility and diffusivity to O_2, and thus can serve as an abiotic analogue to O_2. Thus, the difference between O_2 and Ar can serve as a tracer for biological productivity. Additionally, Ar can be used in conjunction with nitrogen to construct basin-scale estimates of denitrification.

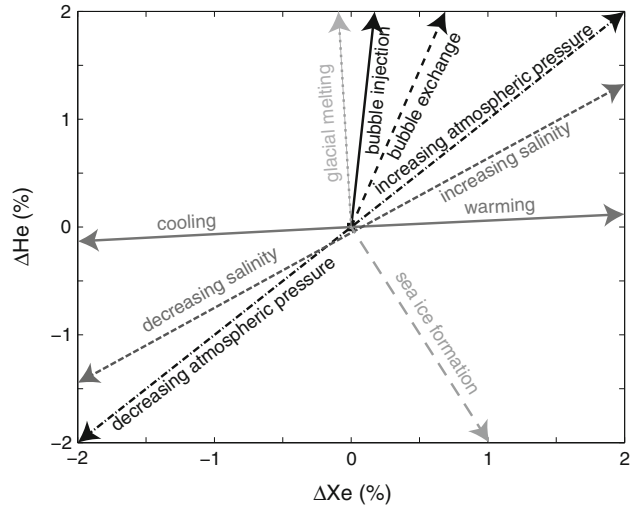

Fig. 2 Schematic depicting the effect of different physical processes on saturation anomalies of He and Xe. Because of the differences in solubilities and diffusivities of the noble gases, different physical processes have differing effects on the gases, allowing the gases to be powerful tools for separating and quantifying physical processes

2 Analytical Methods

2.1 Sample Collection

The standard protocol for measuring noble gases in seawater is to collect a sample of seawater, extract the gases from the water, and measure the gases on a mass spectrometer. Water samples are generally drawn on the deck of the ship from Niskin bottles mounted on a CTD rosette system. It is important to draw the samples soon after the rosette is retrieved, and immediately after the Niskin is vented for sampling, as exchange with the head-space created from drawing water from the Niskin will compromise the integrity of the dissolved gases (Takahashi et al. 1988). Samples of seawater can be transferred to copper tubes (Weiss 1968; Young and Lupton 1983), stainless steel cylinders (Lott and Jenkins 1998), or pre-evacuated custom-made glass bottles (Emerson et al. 1999) for storage (although the last is not suitable for helium studies). In all cases, great care must be taken when sampling to avoid bubbles entering the sample containers. This can be achieved by presoaking any transfer tubing that is used, tapping on walls of sample containers as the sample is drawn, keeping the temperature of sample containers similar to temperature of the water (i.e. avoid letting the containers sit in the sun before collecting samples since the gases in the seawater may exsolve due to warming on contact with the container), and carefully watching for any bubbles in tubing, neck of bottle, etc.

The lighter noble gases are more diffusive than the heavier ones and are not well contained by o-rings. If samples are collected in stainless steel cylinders, which have o-rings in the plug valves at the end of the cylinders, it is best to extract the gases from the samples into aluminosilicate glass bulbs within 24–48 h of collection (Lott 2001). If samples are stored in custom-made glass bottles, which contain Louers-Houpert valves that have o-rings, it is best to use valves with two o-rings, to fill the necks with CO_2 to decrease the loss of gas across the valves, and to analyze the samples within at most two months of sample collection (Hamme and Emerson 2004a). In contrast, samples are well preserved in copper tubes for indefinitely long periods.

In the case of stainless steel cylinders, subsequent to sample collection, usually at-sea or in an onshore laboratory, gases are extracted from

the water by essentially boiling the water in a high-vacuum system and transferring the released gas to ~25 cc aluminosilicate glass ampoules that can then be flame-sealed and stored. In the laboratory, these ampoules are attached to the mass spectrometer sample processing system using o-ring seals and the sample is introduced by mechanically snapping the end of the glass flame-seal (Lott and Jenkins 1998). In the case of crimped or clamped copper tube samples, a similar extraction procedure can be used on-shore, but after introduction to the evacuated sample line, samples are stirred at room temperature and the aluminosilicate glass ampoules are chilled with liquid nitrogen. Alternatively, some research groups directly attach copper tube samples to the mass spectrometer and extract "in-line" (Beyerle et al. 2000; Sano and Takahata 2005). For the custom-made glass bottles, no extraction is necessary; the gas partitions between the headspace in the bottle and the water (90–99 % in the headspace, depending on the gas) at a known temperature and the water is drained by vacuum filtration prior to analysis (Emerson et al. 1999).

2.2 Sample Analysis

The noble gases are typically analyzed by quadrupole mass spectrometry (QMS) or magnetic sector mass spectrometry. Some methods analyze for only one or two noble gases (Emerson et al. 1999; Hamme and Emerson 2004a) whereas other systems are set up to analyze for all five noble gases from a single sample (Beyerle et al. 2000; Sano and Takahata 2005; Stanley et al. 2009a). The analysis can be conducted by peak height comparison with a standard or by isotope dilution. If the measurements are conducted on an isotope ratio mass spectrometer, then one gas concentration, often Ar, is determined by isotope dilution and the other gases are determined by ratios to that one gas (Hamme and Severinghaus 2007; Severinghaus et al. 2003). The noble gases are commonly chemically purified, often by use of getters, then condensed onto a charcoal and a stainless steel cryogenic trap at 8 K (Stanley et al. 2009a), onto two charcoal traps with one at liquid N_2 temperature (77 K) and the other at dry ice/acetone temperature (196 K) (Sano and Takahata 2005), or onto a trap at liquid He temperature (4 K) (Hamme and Severinghaus 2007; Severinghaus et al. 2003) Methods that measure all five gases from a single sample have precision of 0.3–1.0 % using a magnetic sector instrument (Beyerle et al. 2000) to 0.1–0.2 % using a series of two automated cryogenic traps and a QMS (Stanley et al. 2009a) and to 0.15–0.17 % for Ar, Kr and Xe only using an isotope ratio mass spectrometer (Hamme and Severinghaus 2007; Severinghaus et al. 2003). Many of the methods also measure a number of different isotopes of each of the noble gases.

When analyzing a sample for a suite of noble gases, one must consider "matrix effects" (also referred to as "chemical slope") of one noble gas on another, either within the mass spectrometer itself (due to issues such as collisions, competition for ionization, etc.), or within the cryogenic trapping systems used for separating the noble gases. Additionally, the presence of other gases in the instrument such as methane, hydrogen, and nitrogen, have been shown to affect noble gas analysis (Stanley et al. 2009a).

High precision helium isotopic analysis is usually performed on a branch tube magnetic sector mass spectrometer using simultaneous collection of the two isotopes. Helium can be readily separated from other gases by chemical gettering and cryogenic separation (Lott and Jenkins 1984, 1998). Because of the large isotope ratio ($^4He/^3He \sim 10^6$) ^4He is measured with a faraday cup and electrometer while ^3He is measured by pulse counting with an electron multiplier. With a stable system, the ultimate limitation to the precision of the measurement is ^3He ion counting statistics. For a "typical" 50–100 g water sample with approximately atmospheric helium isotope ratio, a precision of 0.15 % is commonly achieved.

2.3 Solubilities in Water and Seawater

When exposed to the atmosphere, the noble gases dissolved in seawater will tend to come to

equilibrium concentrations. For each noble gas, these solubility concentrations are a function of temperature, salinity, and pressure. Physical processes such as bubble injection, rapid temperature changes, and ice formation/destruction serve to drive gas concentrations away from solubility equilibrium (Fig. 2), so it is the saturation anomalies (deviations from solubility equilibrium) that are the important observables. Determinations of solubility equilibrium concentrations as a function of temperature and salinity have been made in the laboratory (Hamme and Emerson 2004b; Smith and Kennedy 1983; Weiss 1971; Weiss and Kyser 1978; Wood and Caputi 1966), but with varying degrees of accuracy (e.g. Hamme and Emerson 2004b; Hamme and Severinghaus 2007). The size of noted discrepancies (and hence uncertainties in saturation anomalies) are often significant compared to the effects observed, especially for Xe, and hence limit the quantitative strength of interpretation. It is hoped that the current expansion of interest in oceanic noble gas abundances will motivate a new effort to refine these measurements to at least the quality of the current measurement capability.

3 Air-Sea Gas Exchange

One of the very fruitful applications of noble gases is the determination of air-sea gas exchange fluxes. Air-sea gas exchange is a crucial part of the biogeochemical cycle of climatically important gases (CO_2, DMS, N_2O). Additionally, accurate knowledge of air-sea gas exchange fluxes is imperative when using gases as tracers for biogeochemical processes. Air-sea gas exchange fluxes are very difficult to measure directly and thus most researchers use parameterizations that yield air-sea gas exchange fluxes in terms of easily measured variables such as wind speed. Noble gases are potentially powerful tools for diagnosing air-sea exchange processes, since their distributions are controlled by purely physical and physicochemical mechanisms. Molecular diffusivity, which varies by a factor of seven over the suite of noble gases, plays an important role both in diffusive air-sea gas exchange and in bubble injection processes. Solubility, and in particular its dependence on temperature, which varies by more than an order of magnitude over the suite of noble gases, is an important driver for gas exchange when significant heat transfer occurs, either during radiative warming in the summer months, or in water mass formation processes during the winter. Thus the contrasting behaviors of noble gases are useful diagnostics of a potentially complex interplay between different processes in the oceanic environment.

3.1 Separating Bubble Component from Diffusive Gas Exchange

Wave action at the sea surface forms bubbles (most visibly in "white caps") that can be carried downward many meters in the water column by vertical water motions and turbulence (e.g. Thorpe 1984). Increasing hydrostatic pressure with depth tends to force the bubbles to partially or completely dissolve, tending to enhance dissolved gas concentrations. Helium and Ne are the least soluble noble gases and therefore are most sensitive to bubble processes. Argon, Kr and Xe are the most soluble noble gases with a strong temperature dependence to solubility and are thus more sensitive to diffusive gas exchange. Initial work used a time-series of only two noble gases, He and Ar (Spitzer and Jenkins 1989) or Ne, Ar, and N_2 (Hamme and Emerson 2006) to separate diffusive gas exchange from bubble processes. In both studies, bubble processes were further separated into two end-members (Fuchs et al. 1987; Jenkins 1988b): (1) some bubbles, typically small ones, that dissolve completely and therefore inject air of atmospheric abundances and (2) other bubbles, typically larger ones, that are injected, partially dissolve, and then rise back to the surface, therefore fractionating the noble gases according to permeation rate. Hamme and Emerson (2006) found at the Station ALOHA in the subtropical Pacific that bubble flux was important for Ar—and therefore by extension for O_2—and that the ratio of

completely to partially trapped bubble fluxes is between 1:1 and 2:1.

Including all five noble gases (He, Ne, Ar, Kr and Xe) increases the power of noble gases for constraining air-sea gas exchange rates (Stanley et al. 2006; Stanley et al. 2009b), yielding constraints on the diffusive part of gas exchange to ±10 % and the bubble component to ±15 %. A three-year time-series of all five noble gases in the Sargasso Sea (subtropical North Atlantic) illustrates the difference in response of the noble gases to physical forcing (Fig. 3). Helium and Ne are supersaturated by several percent in the upper 150 m and show relatively little seasonal variation, due to a first order balance between bubble injection and diffusive gas exchange. In contrast, Ar, Kr and Xe show a strong seasonal cycle, with large saturation anomalies in the summer, particularly below the mixed layer, produced by seasonal warming. By combining inverse modeling with the noble gas data, Stanley et al. (2009b) produced a parameterization of air-sea gas exchange that explicitly includes bubble processes, is based on an intermediate and relevant time scale, and has tighter constraints than many existing parameterizations. They too found that bubble injection is important for all noble gases, even the more soluble ones such as Xe, and by extension is likely to be important for CO_2 in high wind speed events. Additionally, they found that completely trapped bubbles, i.e. "injected" ones were much more important than partially trapped ones, i.e. "exchanged" ones, with completely trapped bubbles comprising >90 % of the bubble flux in most cases.

Numerical modeling must be combined with the noble gas data in order to constrain air-sea gas exchange. Bulk mixed layer models (PWP), which have been modified for use with the noble gases (Hamme and Emerson 2006; Spitzer and Jenkins 1989; Stanley et al. 2006; Stanley et al. 2009b) are used in the studies mentioned above. Additionally, Ito et al. (2011) have included Ne and Ar into the off-line ECCO model (MIT-GCM) in order to examine gas exchange and diapycnal diffusivity in the Pacific Ocean.

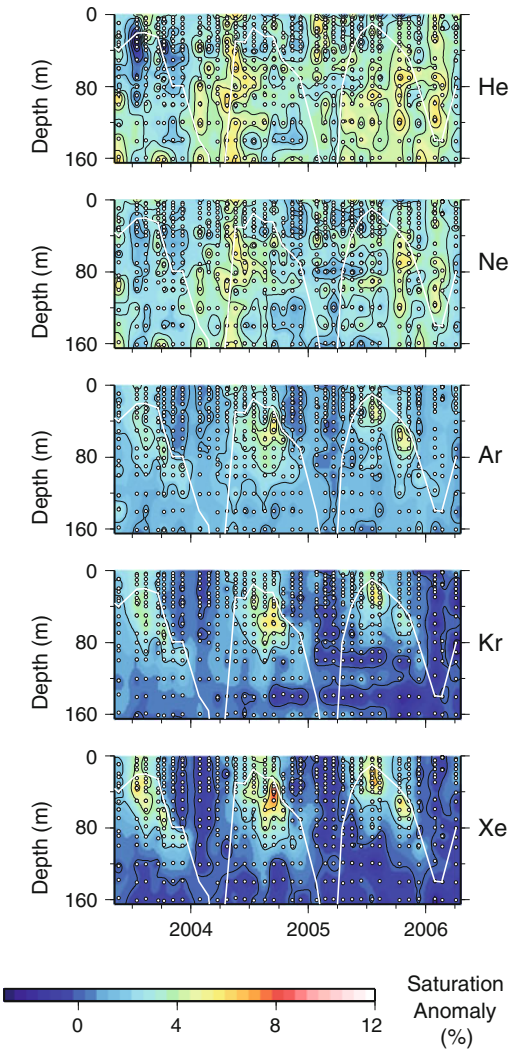

Fig. 3 Saturation anomalies of the five noble gases, calculated from in situ temperature and salinity, in the upper 160 m of the Sargasso Sea, as measured in a three year time-series at the Bermuda Atlantic Time-Series study site. Because the noble gases track physical processes and have a wide range of solubilities and molecular diffusivities, measurements of all five noble gases provide tight constraints on air-sea gas exchange rates. The *white dots* correspond to sample depths and the *thin white line* denotes the mixed layer depth. Figure modified from Stanley et al. (2009b)

Additionally, the noble gas ^3He has been used in conjunction with the gas SF_6 to quantify air-sea gas exchange (Ho et al. 2006, 2011; Nightingale et al. 2000; Salter et al. 2011; Smith et al. 2011; Watson et al. 1991). This approach

yields parameterizations of air-sea gas exchange on time-scales of several days and does not distinguish between bubble-mediated and diffusive gas exchange. The approach rests on the fact that ^{3}He and SF_6, both inert gases, have very different gas transfer rates, with ^{3}He being exchanged quickly and SF_6 being exchanged much more slowly. A known mixture of ^{3}He and SF_6 is deliberately injected into a patch of water. The patch is followed and the decline in gas concentration is measured over several days; the change in the ratio of the gases is used to quantify air-sea gas exchange. Several parameterizations determined by this dual tracer approach are widely used (Ho et al. 2006; Nightingale et al. 2000).

3.2 High Latitude Ventilation

Air-sea gas exchange processes are important in setting gas concentrations during water mass formation in the high latitudes. Water in the high latitudes is rapidly cooled, leading to an undersaturation of some gases, and there has long been the question of the extent to which gases reach equilibrium before the water is subducted. This question is particularly important for evaluating the strength of the solubility pump of CO_2. Noble gases can be used to determine the degree to which gases reach equilibrium. Hamme and Severinghaus (2007) used noble and inert gas concentrations (Ne, Ar, Kr, Xe, and N_2) in the intermediate and deep waters at Station ALOHA in the subtropical North Pacific and a time-dependent model of deep convection in the Labrador Sea to examine the relative importance of bubble injection, gas exchange due to cooling, and sea level pressure for setting deep ocean concentrations of gases. The difference in physicochemical properties of the noble gases allowed separation of the processes. Deep water Ne saturation anomalies are positive (i.e. supersaturated) due to the influence of bubbles and the relative insensitivity to rapid cooling (Fig. 4). In contrast, deep water Ar, Kr and Xe saturation anomalies are negative (i.e. undersaturated) due to rapid cooling. It is clear that it is rapid cooling, and not sea level pressure, that causes these undersaturations

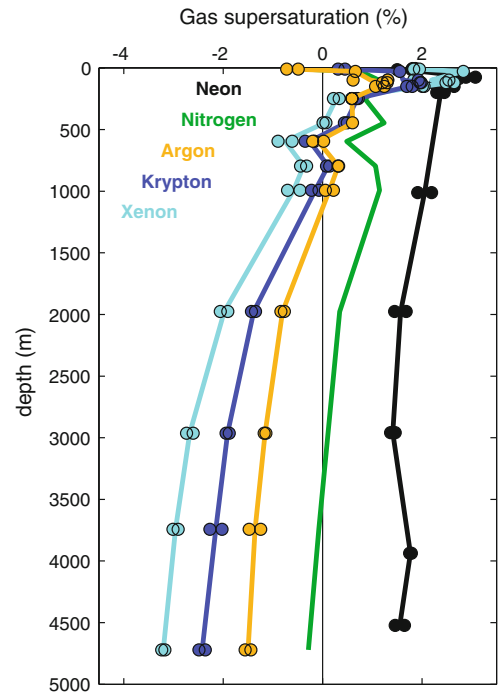

Fig. 4 Depth profiles of Ne, N_2, Ar, Kr and Xe saturation anomalies measured at station ALOHA in the subtropical North Pacific. Equilibrium with the atmosphere is indicated by the *vertical line* at 0 %. *Points* indicate individual samples while the *lines* are average of duplicates. Xe supersaturations were increased by 2 % above the solubility data of Wood and Caputi (1966). Profiles of deep water noble gas saturation anomalies can constrain the extent to which equilibrium is reached during high latitude ventilation. Figure reproduced from Hamme and Severinghaus (2007)

because sea level pressure variations would affect all gases equally but the undersaturation is stronger for Kr and Xe than for Ar.

Noble gas measurements have also been used in conjunction with three box and seven box models, to examine the extent at which high latitude waters reach equilibrium before ventilation. Nicholson et al. (2010) used profiles of Ar, Kr, as well as Ar isotopes from the northwest Pacific, subtropical North Pacific, and tropical Atlantic oceans to estimate the size of the high latitude ventilation area. They showed that the area for high latitude ventilation is much smaller than the area of enhanced preformed nutrients, suggesting that the CO_2 solubility pump is weaker than box models previously predicted.

4 Diapycnal Mixing

Noble gases are powerful tools for constraining diapycnal mixing rates in the ocean interior. Constraining diapycnal mixing rates is important for understanding the transport of heat and nutrients in the ocean. As Bieri et al. (1966) first suggested, noble gas measurements can be used to estimate basin-scale diapycnal diffusivity coefficients. Models of different complexity, ranging from simple theoretical schematics and box models (Henning et al. 2006; Ito and Deutsch 2006; Ito et al. 2007) to GCMs (Henning et al. 2006; Ito et al. 2011) have been used to show the effects of diapycnal diffusivity on Ar saturation. Including other noble gases in the analysis would likely offer better constraints on diapycnal diffusivity since Kr and Xe have stronger temperature dependence to solubility and a smaller contribution from bubbles.

The basic premise behind this approach is that because of the curvature in the dependence of solubility of the heavier noble gases (Ar, Kr, Xe) on temperature, mixing between water of two different temperatures leads to a positive saturation anomaly (Fig. 5). The magnitude of this saturation anomaly depends on the temperature difference of the waters being mixed. The behavior of noble gases is conservative in the ocean interior. Thus the observed saturation anomaly of a noble gas in the ocean interior can be considered a sum of two components: (1) a preformed component based on gas exchange, bubble injection, and sea level pressure variations when the water was subducted and (2) a mixing component that is the product of noble gas solubility, mixing ratio of low latitude surface waters, and temperature gradients (Ito and Deutsch 2006). Therefore measurements of noble gas saturation anomalies along a transport path from an outcrop to the ocean interior can be used to constrain the diapycnal diffusivity rate. Ito et al. (2007) used Ar data from the North Pacific in order to estimate a diapycnal diffusivity rate of $0.35 \pm 0.21 \times 10^{-4}$ m^2 s^{-1}. However, uncertainties arise from interannual variability in air-sea fluxes at the outcrop, bubble effects, strong thermal gradients and sparse sampling.

Modeling studies have shown that this method is most promising for the subtropical gyres (Henning et al. 2006; Ito et al. 2011) and indeed the only study actually using data to determine the mixing rates was in the subtropical gyres (Ito et al. 2007). The approach does not work well if the advective time scale is shorter than the diffusive time scale, for example in the equatorial regions, in the strong Western boundary currents (i.e. Kuroshio or Gulf Stream), or in the unventilated shadow zones (Gehrie et al. 2006; Henning et al. 2006; Ito et al. 2011).

5 Ocean-Cryospheric interaction

The interaction of the ocean with the cryosphere, either by seasonal sea ice formation and destruction, or the subsurface melting of grounded glaciers, plays an important role in modifying the density properties of seawater and hence in the formation of deepwater. The presence of a separate phase, namely ice, creates a potential for affecting the dissolved gas composition of seawater. The creation and destruction of sea ice, for example, may serve to differentially enhance or deplete gases according to their respective solubilities in the ice lattice (Fig. 2). The noble gases are potentially unambiguous tools for detecting and quantifying the relative contributions of these processes because of their conservative nature in seawater. We mention three different applications, two of which have been at least partially exploited, and one that may hold promise in the future.

5.1 Sea Ice Formation and Destruction

In polar regions, rapid extraction of heat can form sea ice, a process that increases the density of the remaining seawater by increasing salinity due to brine rejection. This contributes to the formation of deep and bottom waters and potentially to the planetary scale overturning circulation. The formation of ice serves to fractionate gases based on

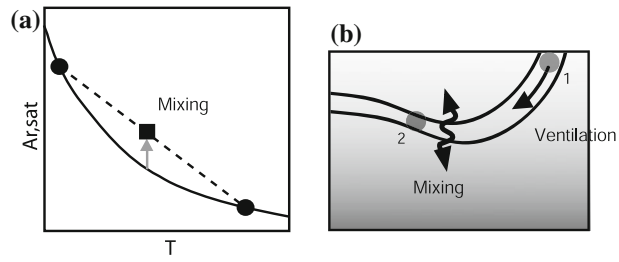

Fig. 5 Cartoons depicting the effect of diapycnal mixing on argon saturation state. **a** Because of the non-linearity of the solubility temperature dependence of Ar (*solid line*, curvature exaggerated for clarity), mixing of two water masses (*filled circles*) produces Ar saturation anomalies above a conservative mixing line (*dash line*). **b** Diapycnal mixing increases the Ar saturation anomaly whereas horizontal ventilation brings the Ar saturation anomaly toward its surface value. The relative strength of diapycnal mixing vs. horizontal ventilation determines the gradient of the Ar saturation anomaly along an isopycnal surface. Figure reproduced from Ito et al. (2007)

their atomic or molecular size: the ice lattice can accommodate only the smaller species while it rejects the larger ones. This was observed in ice covered stratified Antarctic lakes (Hood et al. 1998) where several fold supersaturation in Ar was observed coincident with a several fold undersaturation of He and Ne. This was argued to be the result of the fact that He and Ne were more soluble in ice than in water, while Ar (and by inference Kr and Xe) were much less soluble in ice than in water.

Laboratory experiments confirmed this differential solubility effect in fresh water and seawater for He, Ne, and Ar (Postlethwaite 2002; Runham 2001) and a time-series in a coastal salt water lagoon on Hokkaido (Postlethwaite 2002) showed similar effects. A subsequent noble gas study in the Japan/East Sea by Postlethwaite et al. (2005), combined with oxygen isotopes, provided some evidence of the contribution of sea ice formation in the Tatarskiy Strait to bottom water formation in that basin.

5.2 Basal Melting of Glaciers

The formation of glacial ice is a complex process that results in the entrapment of air bubbles. Glaciers near the coast often flow toward and into the sea where they extend outward. Contact between relatively warmer seawater and the underside of floating ice shelves results in melting of the ice and release of ice-entrapped bubbles at elevated hydrostatic pressure. This in turn leads to large observed excesses of He (Schlosser 1986; Schlosser et al. 1990; Weppernig et al. 1996) and likely other noble gases. The injection of these gases has a slightly different signature than the injection of air bubbles from air-sea gas exchange because the melting of the glacial ice also changes the salinity and temperature of the water (Fig. 2). Schlosser and co-workers (Schlosser 1986; Schlosser et al. 1990; Weppernig et al. 1996) pointed to dissolved He excesses in polar waters as resulting from the sea-water induced melting of the ice shelf at high hydrostatic pressure: a signature of the forced dissolution of atmospheric gases occluded in the ice during melting at depth (Gow and Williamson 1975; Martinerie et al. 1992). In combination with other tracer information (particularly stable isotopes) they very effectively used this to constrain the role of sub-glacial melt-water in the formation of Weddell Sea bottom water.

More recently, this approach has been extended into the southeast Pacific to include Ne, and applied to estimate the volume flux of melt-water from the western Antarctic shelves to be of order 7 mSv (Hohmann et al. 2002). A He–Ne simulation based on a regional coupled ice-ocean circulation model has been published (Rodehacke et al. 2007) that reveals not only the diagnostic potential of He and Ne, but also that they not surprisingly serve to "low-pass filter" seasonal/regional variability on the timescales near the flushing time of the sub-shelf ice

cavern; viz., 2–3 years. He and Ne data, along with the stable isotopic ratio of water ($H_2^{18}O/H_2^{16}O$), have been used on the Ross Ice Shelf to estimate the concentration of glacial meltwater in that environment (Loose et al. 2009). By combining the meltwater concentration with age estimates calculated by CFC transit time distribution curves, Loose et al. (2009) calculated a basal melting rate for the ice shelf.

One challenge, however, with the interpretation of He and Ne anomalies alone is that air injection associated with air bubbles produced by surface waves and forced into solution hydrostatically can generate saturation anomalies in approximately the same ratio as that inferred from glacial melt: 0.78 vs. 0.76 respectively. Although the authors in the above studies make convincing arguments based on the spatial distribution of the anomalies such that the effects are safely attributed to glacial melting, there still exists the potential for an underlying residual ambiguity. The Ar/Ne and Ar/He ratios of the gases trapped in glacial ice are approximately half the atmospheric ratio (Huber et al. 2006). Therefore, measurement of Ar (and also Kr and Xe) anomalies in seawater offers an opportunity to resolve this ambiguity and obtain a more accurate assessment of glacial melt input.

5.3 Underplating of Floating Ice Shelves

Basal melting of ice shelves produces colder and less saline water at depth that, because it is more buoyant than surrounding seawater, tends to flow upward under the shelf, entraining surrounding waters. This Ice Shelf Water (ISW), as it decompresses, becomes supercooled and forms frazil ice crystals that underplate the shelf (Smedsrud and Jenkins 2004). This process results in accretion of large amounts of submarine ice on the base of the shelf (Holland et al. 2007). The formation of marine ice may result in strong fractionation favoring the larger atomic diameter gases (Ar, Kr, and Xe) relative to He (and possibly Ne) in the residual ISW. In principle, measurement of the suite of noble gases in ISW emerging from under, for example, the Ronne Ice Shelf could provide valuable constraints on the magnitude of such processes.

6 Ocean Circulation

Tritium (^3H) decays with a 12.31 year half-life (MacMahon 2006) to ^3He, a stable, noble gas isotope. The primary source of ^3H to the contemporary ocean is from ^3H created by the atmospheric thermonuclear bomb tests in the 1960s. Thus, the $^3H/^3He$ system is most useful for dating water that has been at the surface within the last 50 years. When the water is at the surface, excess ^3He, i.e. ^3He concentration above the solubility value, is almost completely lost due to gas exchange with the atmosphere. ^3He is measured as the $^3He/^4He$ isotope ratio (R) anomaly of the sample (X) relative to the atmospheric standard (A), defined as

$$\delta^3 He = 100\left(\frac{R_X}{R_A} - 1\right)$$

When in equilibrium with air, seawater is depleted in ^3He since it is slightly less soluble than ^4He (Benson and Krause 1980; Weiss 1970), with $\delta^3He \sim -1.7\ \%$. As water descends from the surface layer and ages, excess ^3He builds up and ^3H correspondingly decreases. The sum of ^3He and ^3H, ζ, acts as a dye-like, stable tracer that responds to mixing and dilution and thus is useful for studying ocean circulation and thermocline ventilation (Jenkins 1987, 1991, 1998). Additionally, ^3He (φ) and ^3H (ϑ) concentrations can be combined with the radioactive decay equation to calculate the tritium-^3He age, τ, of the water, a measure of time since a water parcel left the surface (Jenkins 1977; Jenkins 1987; Jenkins, et al. 1972) according to

$$\tau = \frac{1}{\lambda}\log\left(1 + \frac{\varphi}{\vartheta}\right)$$

where λ is the radioactive decay constant for ^3H.

Figure 6 depicts the distribution of tritium-^{3}He age in years on a constant density anomaly horizon ($\sigma_0 = 26.5$ kg m^{-3}) in the Pacific, largely based on World Ocean Circulation Experiment (WOCE) stations taken during the late 1980s and early 1990s. We plot properties on a potential density horizon because the ocean is density stratified and water tends to move along these horizons. This horizon corresponds to the approximate base of the directly ventilated layer in the North Pacific and the main thermocline in the South Pacific (Huang and Qiu 1994, 1998). It lies at a depth of about 200 m in the tropics, deepens to about 500–600 m in the western subtropics, and shoals to the ocean surface in the high latitudes. The distribution of tritium-^{3}He ages is a semi-quantitative representation of the ventilation time-scales of this horizon (see discussion below) and bears a general resemblance to other ventilation tracer age distributions such as CFC-ages (Doney et al. 1997; Warner et al. 1996). Note the penetration of younger waters emanating from the high latitude southeast South Pacific and northwest North Pacific, and the fact that the mid-latitude contour lines show an imprint of the large-scale anticyclonic gyre circulation. The age distributions are also characterized by intense, poorly ventilated shadow zones (Luyten et al. 1983) in the eastern equatorial and subequatorial Pacific. These regions coincide with very low tritium values (and hence weak ventilation) and zonally extended, high nutrient plumes that straddle the equator.

It is possible that the tritium-^{3}He age distributions shown in Fig. 6 may be influenced by an additional source of non-atmospheric ^{3}He, namely volcanic ^{3}He released from sea-floor spreading centers (see Sect. 7). However, despite the relatively large volcanic ^{3}He plumes evident in Pacific deep water, there are several reasons to suspect that volcanic ^{3}He does not strongly influence the shallow tritiugenic ^{3}He distributions in the subtropical and tropical regions. The first stems from the recognition that abyssal waters are more slowly ventilated than the shallow, wind-driven circulation. The deep waters overturn on century-to-millennium time-scales while the shallow thermocline is ventilated on decadal time-scales. Thus, the abyssal volcanic ^{3}He plumes are larger due to longer accumulation times.

Second, it is known from hydrography, tracers, and inverse models that the circulation and exchange of shallow and deep waters in the Pacific are not strongly linked (e.g., Wijffels, et al. 1996; Wijffels, et al. 2001), with the bulk of Pacific deep waters (and hence the volcanic ^{3}He signature) being exported to the Antarctic Circumpolar circulation (Well, et al. 2003). Third, the meridional distribution of excess ^{3}He in the Pacific is dominated in the vertical by a *minimum* at a potential density anomaly level of approximately 26.8–27.0 kg m^{-3} (Jenkins 1996) suggesting little upward transport of volcanic ^{3}He into the thermocline from below. This can be seen in the meridional distribution of this isotope in the Pacific (along 135°W, Fig. 7). In the upper part of the northern subtropical water column, the ^{3}He distribution has a characteristic tritiugenic maximum in the thermocline (at about 500 m depth near 30°N) that shoals southward into the tropics. This maximum, also seen in Atlantic waters (see Jenkins 1988b) bears a striking relationship with the observed tritium distribution (see Fig. 8), tracking the tritium plume penetration southward into the tropics. Note the hemispheric asymmetry in the tritium distributions (and the consequent asymmetry in the tritiugenic ^{3}He) due to the dominant northern hemispheric delivery of this isotope due to the bomb tests (Doney, et al. 1992; Weiss and Roether 1980). A ^{3}He minimum lies below the tritiugenic ^{3}He maximum, separating the ventilated (and tritiated) shallow waters from the deeper volcanic ^{3}He contaminated waters. The depth of this minimum ($\sim$ 800 m) corresponds to the zero in vertical velocity observed in Wijffels' (2001) inverse calculations.

Finally, one needs to consider the comparative magnitudes of the volcanic and tritiugenic ^{3}He fluxes. The global volcanic ^{3}He flux has been estimated to be between 500 and 1,000 mol y^{-1} (Bianchi et al. 2010; Farley et al. 1995), corresponding to an average flux of

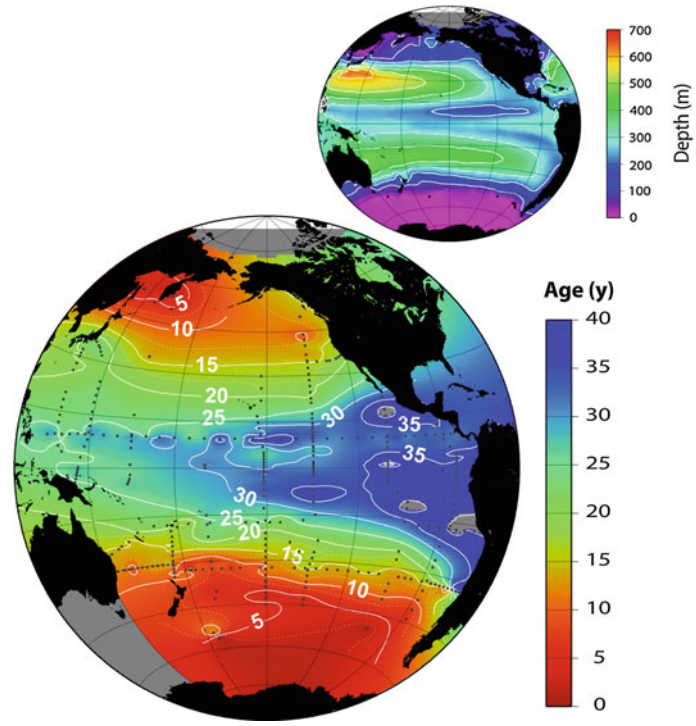

Fig. 6 The distribution of tritium-^{3}He age (in years) on the 26.5 kg m^{-3} potential density anomaly horizon in the Pacific, as measured during the World Ocean Circulation Experiment (1989–1995). *Grey dots* indicate sampling locations. The depth of this horizon ranges from the near surface in high latitude regions to in excess of 600 m in the western subtropics, and shoals to 100–200 m in the tropics (see map in *upper right* of figure)

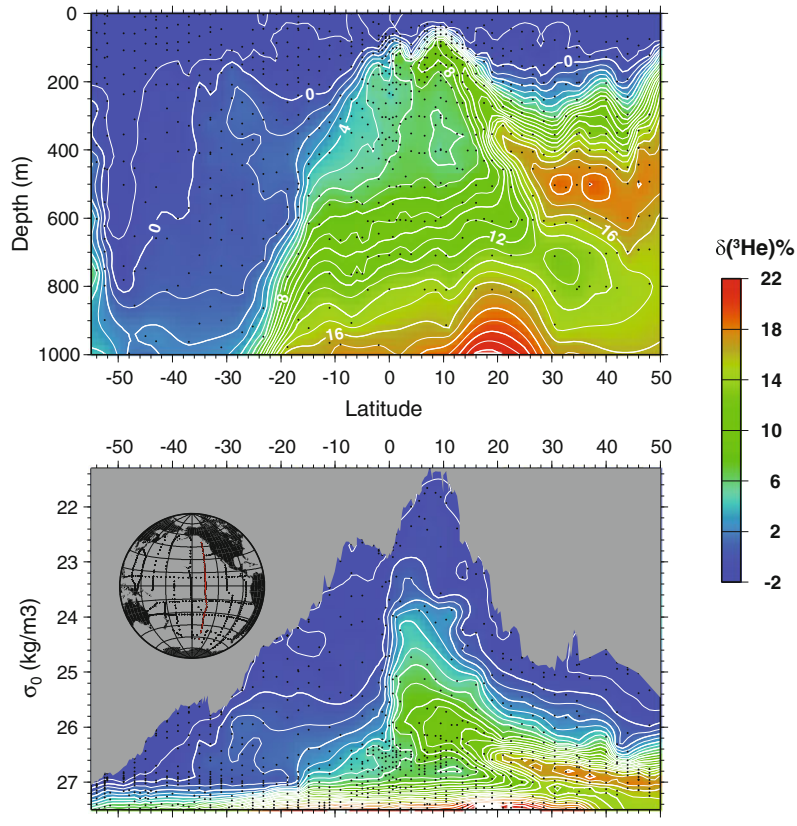

Fig. 7 The distribution of helium isotope ratio anomaly (in percent) plotted as a function of latitude and depth in meters (*upper panel*) and potential density anomaly in kg m^{-3} (*lower panel*) along WOCE line P17(135°W) in 1991. *Black dots* show sample locations. Positive latitude is north, negative is south. The contour (*white lines*) interval is 1 % and measurement precision is 0.15 % (1 sigma).The *grey area* in the *top part* of the *lower panel* corresponds to density anomalies lighter than the shallowest waters for the corresponding locations. Station locations are indicated as a *red line* in the insert map

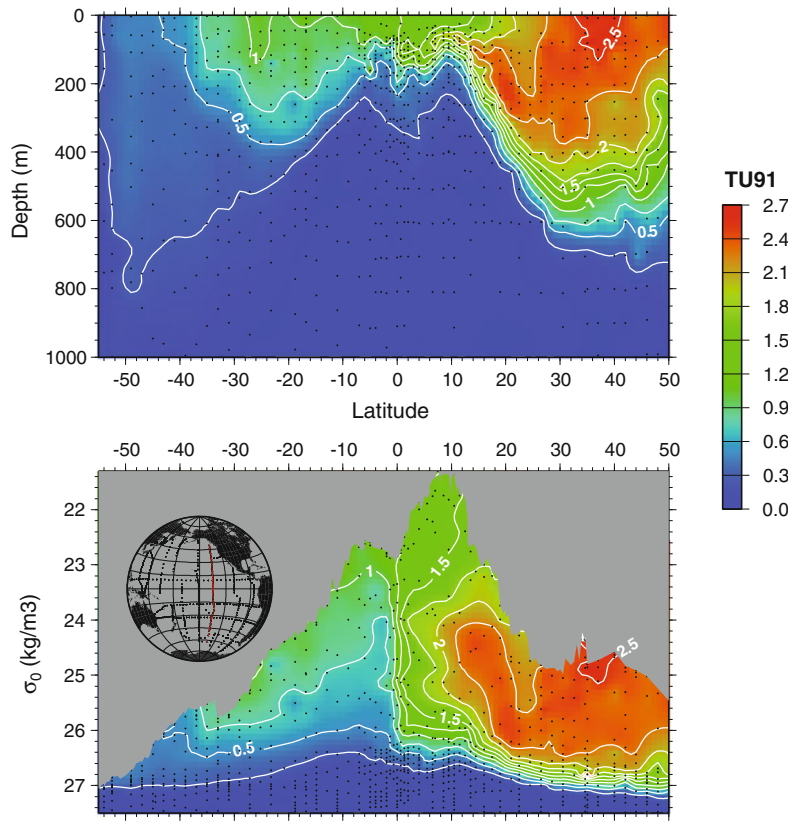

Fig. 8 The distribution of bomb tritium (in $TU_{91} = 10^{18} \times {}^3H/{}^1H$, decay corrected to January 1, 1991) plotted as a function of latitude and depth in meters (*upper panel*) and potential density anomaly in kg m^{-3} (*lower panel*) along WOCE line P17(135°W) in 1991. Positive latitude is north, negative is south. The contour (*white lines*) interval is 0.25 TU_{91} and measurement precision (1 sigma) is 0.005 TU_{91}. The *grey area* in *top part* of the *lower panel* corresponds to density anomalies lighter than the shallowest waters for the corresponding locations. Station locations are indicated as a *red line* in the insert map

approximately 3×10^4 atoms m^{-2} s^{-1}. We can compare this to a basin-wide tritium deposition of ~900 MCi by 1972 (Weiss and Roether 1980), leading to tritiugenic ^{3}He production rate of 1.5×10^5 atoms m^{-2} s^{-1}, or about 5 times larger than the volcanic ^{3}He flux.

Mixing further complicates the tritium-^{3}He age. This can be seen by considering the time-dependent advection–diffusion equation for the age-tracer:

$$\frac{\partial \tau}{\partial t} = \nabla(\kappa \nabla \tau) - \vec{u} \cdot \nabla \tau + 1 + \kappa \left(\frac{\nabla \vartheta}{\vartheta} + \frac{\nabla \zeta}{\zeta} \right) \cdot \nabla \tau$$

[see Jenkins (1987) for a derivation] where κ is the turbulent diffusivity tensor (largely aligned along isopycnal surfaces), ϑ is the tritium concentration and ζ is the sum of tritium and ^{3}He concentrations. The equation closely resembles that of an *ideal age tracer* (one that is advected and diffused) except for the last composite "non-linear" term, largely driven by the fact that tritium (and hence tritiugenic ^{3}He) is a transient tracer. The form of this last term and the typical signs of the ϑ and ζ gradients leads to an augmented "pseudo-velocity" that tends to lower the tritium-^{3}He age relative to that of an ideal ventilation age (Jenkins 1987).

In directly subducted shallow water regimes such as the shallow thermocline in the eastern subtropical gyres, the non-linear contribution to the age is relatively small (Jenkins 1998; Robbins and Jenkins 1998). However, it can be quite significant for indirectly ventilated regions and deeper in the thermocline (Jenkins 1991, 1998). Using an appropriately designed experiment, *i.e.,* by documenting the three dimensional distribution of these (and other) properties, these terms can be adequately evaluated and robust results can be gained (Jenkins 1998). Moreover, they can be crudely accounted for using box models (Jenkins 1980) or transit time distribution models

(Stanley et al. 2012). Estimates of τ can then be combined with oxygen distributions to calculate oxygen utilization rates, a measure of export production (see Sect. 8.3).

The distributions of ^{3}He and ^{3}H in the upper thermocline have been used to investigate thermocline ventilation and shallow ocean circulation in the Northern hemisphere (Jenkins 1998, 2008; Robbins et al. 2000). Jenkins (1998) used a 13 year time-series of ^{3}H and ^{3}He in the Sargasso sea, in combination with measurements of salinity and oxygen, to calculate absolute velocities (given by the ^{3}H and ^{3}He data combined with geostrophy), isopycnal diffusivities, and oxygen consumption rates. The dilution of the inventory of tritium in the thermocline suggested that the gyre could be considered to have two regions: a western one with cross streamline mixing and an eastern one that is principally advectively ventilated. ^{3}He and ^{3}H have also been used to study the ventilation of the lower subtropical thermocline, showing that the Azores current forms a barrier for the southward invasion of mass from isopycnal surface outcrops with only diffusive ventilation across the front for lower thermocline waters (Robbins et al. 2000). More recently, in the East/Japan sea, a time-series of ^{3}He, ^{3}H, and CFC data, used in conjunction with a multi-box model, were used to estimate time-changing water mass formation rates and vertical exchange (Jenkins 2008). Jenkins found that there was an approximate order of magnitude decrease in deep water formation rates since the 1960s, accompanied by a shift from sea ice/brine rejection processes to shallow, open ocean convection as the dominant mode of deep and bottom water ventilation.

7 Ocean-Lithosphere Interactions

It has been known for more than a century that the residence time of helium in the atmosphere against loss to outer space is of the order of a few million years or less (Bryan 1901; Cook 1902; Stoney 1905)—much shorter than the age of the earth—and it was supposed that the present day atmospheric inventory of the more abundant isotope ^{4}He was supported by the degassing of radiogenically produced ^{4}He from the decay of U and Th series isotopes in the solid earth (Turekian 1959). The residence time of the rarer isotope ^{3}He in the atmosphere is even shorter (Axford 1968)—less than a million years—and there was a mystery as to how even its meager atmospheric inventory was supported. Production from the decay of cosmic ray produced tritium (Craig and Lal 1961) is at least an order of magnitude too small, as is the lithogenic production by $^6Li(n,\alpha)^3H \rightarrow {}^3He$ reactions (Andrews 1985). The neutrons for the latter are produced by thermalization of fast neutrons induced by (α, n) reactions in rocks, where the α particles are produced by decay of U and Th series radionuclides.

The discovery of excess ^{3}He in Pacific deep waters (Clarke et al. 1969) led to the realization that this isotope was primordial (inherited during the formation of the earth) and emanating from volcanic activity on the seafloor. This conclusion was briefly contested (Fairhall 1970) but shown to be quantitatively sound (Craig and Clarke 1970). The hypothesis was further borne out by subsequent observations near hydrothermal vents (Jenkins et al. 1978, 1980; Lupton et al. 1980; Sakai et al. 1987) and in basaltic glasses from the sea floor (Kurz and Jenkins 1981; Kurz et al. 1983; Lupton and Craig 1975). It also led to the first firm quantification of the present day degassing rate for the earth. Based on radiocarbon chronometry of abyssal waters, the global ^{3}He degassing rate was estimated to be of the order of 500–1,000 mol y^{-1} (Craig and Clarke 1970) a rate later refined by more sophisticated modeling (Bianchi et al. 2010; Dutay et al. 2004; Farley et al. 1995).

The injection of primordial ^{3}He into the deep waters occurs at mid-ocean ridges, i.e. sites of active mantle upwelling, and at mantle plume hot spots (e.g. Hawaii and Iceland). The injection of buoyant, very hot ($\sim$350 °C) water drives vertical plumes which extend hundreds of meters in the water column and are characterized by massive entrainment of surrounding

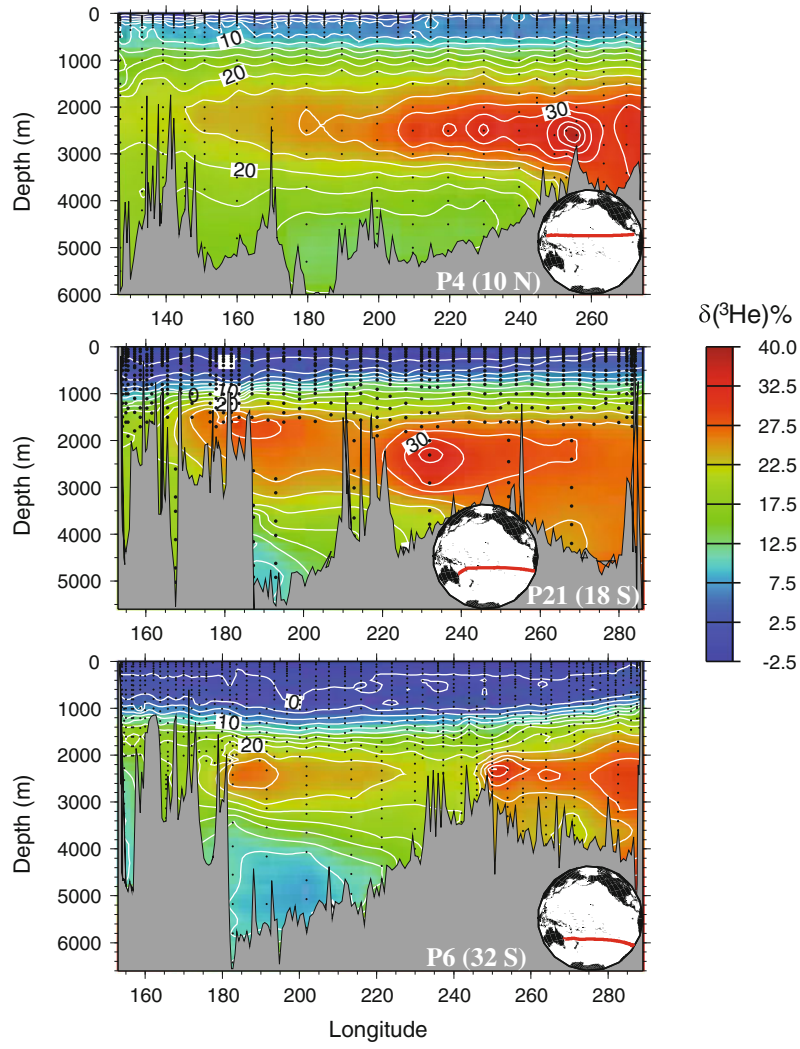

Fig. 9 Zonal distributions of excess ^{3}He (largely geophysical) at three latitudes in the Pacific Ocean measured during the WOCE expeditions. The values presented are the dissolved helium ^{3}He/^{4}He isotope ratio anomaly in percent relative to the atmospheric ratio

waters (McDougall 1990; Speer and Rona 1989). Such activity results in clearly discernible horizontal plumes of ^{3}He that extend from hundreds to even tens of thousands of kilometers (see Fig. 9), tracing deep circulation on basin and global scales. The observation by Lupton and Craig (1981) of a westward emanating ^{3}He plume at ~15°S in the Pacific apparently running counter to the presumed cyclonic abyssal flow (Stommel and Aarons 1960) prompted Stommel (1982) to point out that these deep plumes are actively driven by the injection of buoyant water at depth, thus influencing the large scale abyssal circulation (Speer 1989).

Substantial excesses of this isotope were observed at active hydrothermal sites (e.g. Jenkins et al. 1978). As a stable conservative tracer, excess ^{3}He anomalies are visible for tens of thousands of kilometers (Fig. 9). Combining the observed correlation of ^{3}He and heat in active submarine systems with the known global ^{3}He flux permits estimates of global convective hydrothermal heat fluxes (Jenkins et al. 1978) although such estimates are limited by local decoupling of the two properties and variations over space and time (Lupton et al. 1989). Nonetheless, use of the ^{3}He flux gauge for estimating the hydrothermal input of Fe into the

abyssal Pacific provides useful constraints (Boyle and Jenkins 2008) and can be used to estimate global hydrothermal Fe fluxes (Tagliabue et al. 2010).

Because of its persistence in subsurface waters, ^{3}He excesses can be widely distributed in the ocean, far from its sources. For example, ^{3}He injected into deep waters in the Pacific can be traced into the Antarctic Circumpolar Current (Garabato et al. 2007; Well et al. 2003) and into the Atlantic Ocean (Jenkins and Clarke 1976; Ruth et al. 2000), where slow seafloor spreading rates result in more modest volcanic ^{3}He injections. Ruth et al. (2000) have used optimum multiparameter analysis (Tomczak 1981) to separate a local hydrothermal plume signature in the South Atlantic from background contributions from waters of Pacific origin.

Finally, it should be recognized that isotopic ratio of "terrigenic" helium shows substantial variations due to significant variations in the "mantle" helium isotope ratio (Kurz et al. 1982; Kurz et al. 1983), as well as the contribution of radiogenic ^{4}He due to α-day of U and Th series isotopes and lithogenic helium due to $^6Li(n,\alpha)^3H \rightarrow {}^3He$ reactions (Andrews 1985; Morrison and Pine 1955). It should be possible in principle to evaluate the two contributions by using the saturation anomaly of He in seawater, but the latter is complicated by a variable atmospheric excess driven by surface bubble injection processes (see earlier sections). A variety of schemes have been suggested and used, pioneered first by Bieri and others (Bieri et al. 1964, 1966, 1967; Roether et al. 1998; Well et al. 2001).

8 Biogeochemical Processes

The noble gases, being biologically and chemically inert, cannot give direct information, by themselves, about biological processes in the ocean. However, they can be very useful if combined with biologically active species since the noble gases can constrain physical processes, allowing the biological and physical components to be separated when considering the behavior of the biologically active gas. Gases are useful tracers of biological production for several reasons. First, the measurements are made in situ, requiring no manipulation of the biological communities, and thus avoiding so called bottle effects (Harrison and Harris 1986; Peterson 1980; Scarratt et al. 2006) that radiotracer bottle incubations may include. Second, the gas tracer based estimates integrate over larger temporal and spatial scales than bottle incubations. For the O_2/Ar pair (Sect. 8.1), the time scale is approximately one to two weeks, depending on the depth of the mixed layer and the magnitude of the gas transfer velocity. For the helium flux gauge technique (Sect. 8.2), the integration occurs over the temporal scale of months to a year and the spatial scale reflects the gyre. For the ^{3}H/^{3}He derived apparent oxygen utilization rates (Sect. 8.3), the temporal scale is several years and the spatial scale reflects the gyre to basin. These long temporal and spatial scales allows the gas tracers to give an integrated view of production, rather than a "snapshot" as may be given by radiotracer bottle incubations, and makes them more likely to catch episodic events such as production stimulated by eddies (McGillicuddy et al. 2007) or storms (Lomas et al. 2009). The different gas tracer systems quantify net community production, new production, and export production, all of which should be equal over long temporal and spatial scales (Eppley and Peterson 1979).

8.1 Oxygen and Argon for Net Community Production

Most of the research in the area of using noble gases to quantify biological production has centered around O_2 and Ar. O_2 is produced by photosynthesis and consumed by respiration, making it reflective of net community production. However, O_2 also responds to physical processes such as thermal warming, gas exchange, and mixing. Ar has similar physicochemical properties to O_2 (Fig. 1), namely nearly identical molecular diffusivity in water and $\sim$10 % difference in solubility. These similarities make Ar an ideal abiotic analogue for O_2. In particular, Ar serves as a good analogue for effects due to warming/cooling and to

bubble injection. However, Ar is not a good analogue for vertical fluxes across the mixed layer, since Ar and O_2 are decoupled below the mixed layer and especially below the euphotic zone, with O_2 decreasing much faster due to remineralization of organic matter. If the O_2 and Ar measurements are interpreted in the framework of a physical model, such as a one-dimensional mixed layer model, the vertical fluxes can be accounted for (Hamme and Emerson 2006; Howard et al. 2010; Spitzer and Jenkins 1989). Including other noble gases, such as He, Ne, Kr and Xe in the model can lead to improved constraints on net community production estimates from the O_2/Ar mass balance (Stanley 2007). However, if only mixed layer measurements of O_2 and Ar are made, then assumptions need to be invoked of steady state production, stable mixed layer depths, and negligible transport of O_2 across base of mixed layer. In regions with a lot of vertical mixing/local upwelling such as in large areas of the Southern Ocean, these assumptions, particularly the latter one, fail; a recent modeling study shows that measurements of O_2/Ar made in mixed layer only and without any corrections for O_2 fluxes tends to underestimate net community production by 5–35 % (Jonsson et al).

The utility of the O_2/Ar pair was first recognized in the late 1980s (Craig and Hayward 1987; Spitzer and Jenkins 1989). These studies estimated net community production rates from either profiles of O_2 and Ar made at discrete locations in the Pacific (Craig and Hayward 1987; Emerson et al. 1991) or from seasonal cycles of oxygen and argon made at a single location in the subtropical North Atlantic (Spitzer and Jenkins 1989). Throughout the next two decades, O_2 and Ar were used to calculate net community production rates throughout the world's oceans, including in the Southern Ocean (Cassar et al. 2007; Hendricks et al. 2004; Reuer et al. 2007), Equatorial Pacific (Hendricks et al. 2005; Stanley et al. 2010), subtropical Pacific (Juranek and Quay 2005; Quay et al. 2010), and North Pacific (Howard et al. 2010).

A recent exciting advance is the development of small mass spectrometers that can be taken to sea to measure O_2/Ar continuously in the underway water of a research vessel (Cassar et al. 2009; Kaiser et al. 2005; Tortell 2005). Either a membrane inlet system (Kaiser et al. 2005; Tortell 2005) (in the case of a Membrane Inlet Mass Spectrometer or MIMS) or an equilibrator contact cartridge (in the case of an Equilibrator Inlet Mass Spectrometer or EIMS) (Cassar et al. 2009; Hamme et al. 2012; Stanley et al. 2010) are used in conjunction with a quadrupole mass spectrometer to produce records of net community production with submesoscale resolution. The unprecedented resolution of these NCP records reveals previously unseen variability in NCP, with NCP changing by an order of magnitude on scales as small as tens of kilometers (Fig. 10) (Stanley et al. 2010). Furthermore, in the Western Equatorial Pacific, there is a significant but weak correlation of NCP with temperature and salinity ($R^2 = 0.18$ and 0.33 respectively) with some regions being more strongly correlated and some regions being anticorrelated (Stanley et al. 2010). It is likely that the variations in NCP are related to submesoscale physical processes such as convergence and divergence zones although such a link has not been shown definitively.

8.2 The Helium Flux Gauge for New Production

New production can be estimated from the upward flux of ^{3}He in an approach dubbed the "Helium Flux Gauge" (Jenkins 1988a; Jenkins and Doney 2003). As described in Sect. 6, ^{3}He is the daughter of ^{3}H. Excess ^{3}He is correlated with nitrate in the thermocline because as water ages, it gains in nitrate due to continuing remineralization and gains in ^{3}He due to decay of ^{3}H. When this water is mixed into the euphotic zone, it supplies the nutrients needed for new production and also carries an excess ^{3}He signal. Measurements of ^{3}He in the mixed layer can be combined with a gas exchange relationship to calculate the air-sea flux of excess ^{3}He to the atmosphere. It is imperative that the gas exchange relationship explicitly includes bubbles, since the bubble flux can be a large

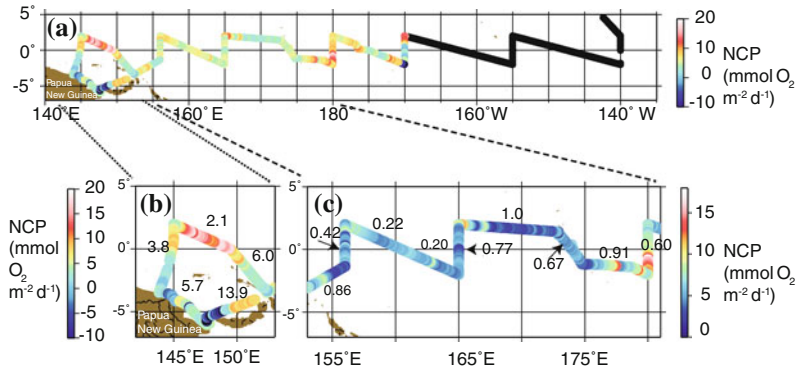

Fig. 10 **a** Net Community Production (NCP) rates through the equatorial Pacific, as determined by O_2/Ar ratios from an equilibrator inlet mass spectrometer. Negative and "blacked-out" values in the central equatorial Pacific reflect upwelling rather than net heterotrophy. The same data are plotted (**b**) in larger format for the region near Papua New Guinea and (**c**) in larger format with a different color scale for the Western Equatorial Pacific. The numbers reflect the variance-to-mean ratio of NCP along sections of the cruise track. The high-resolution records of O_2/Ar show an enormous amount of small scale variability in NCP. Figure modified from Stanley et al. (2010)

component of the helium flux. This excess ^{3}He flux out of the mixed layer must be balanced by a supply of excess ^{3}He from below on annual or longer time-scales and thus gives a measure of the amount of excess ^{3}He being input to the mixed layer. The correlation between excess ^{3}He and nitrate can then be used to calculate the input of nitrate. Thus this calculation predicts new production based on the physically mediated nitrate flux from vertical transport of thermocline waters—it does not take into account nitrate from other sources such as nitrogen fixation, zooplankton migration (Steinberg et al. 2000) or lateral transport of DON (Mahaffey et al. 2004; Williams and Follows 1998).

This method was first used by Jenkins (1988a) to calculate the rate of new production in the Sargasso Sea from a two year time-series of ^{3}He data. Jenkins and Doney (2003) extended the analysis to a six year time-series of ^{3}He data and found that the nutrient flux, though quantitatively consistent with other observations of production rates, cannot be supplied by local processes. Thus they proposed a three dimensional circulation path by which nutrients are returned to the seasonally accessible surface ocean after being remineralized in the thermocline.

8.3 Oxygen Utilization Rates for Export Production

A third way in which noble gases can be used to quantify biological production is through the use of ^{3}He and ^{3}H to calculate oxygen utilization rates. As described in Sect. 6, ^{3}He and ^{3}H can be combined to calculate τ, the mean age of a water parcel, i.e. the time since the water parcel was subducted. The age of the water can be combined with oxygen data to calculate oxygen utilization rates. If enough ^{3}H and ^{3}He data are collected, then true oxygen utilization rates (OUR) can be calculated (Jenkins 1988b). But if ^{3}H and ^{3}He data are only available at limited locations/times, as is more common, then apparent oxygen utilization rates (AOUR) are calculated, with assumptions being made regarding the path of the water and the initial saturation state of oxygen (Jenkins 1980, 2008; Klein et al. 2003; Stanley et al. 2012; Takahata et al. 2008). The vertically integrated AOUR is a measure of the regional export production; it reflects a projection of geographic and horizontally distributed processes working on individual isopycnal layers (Stanley et al. 2012) rather than local export production.

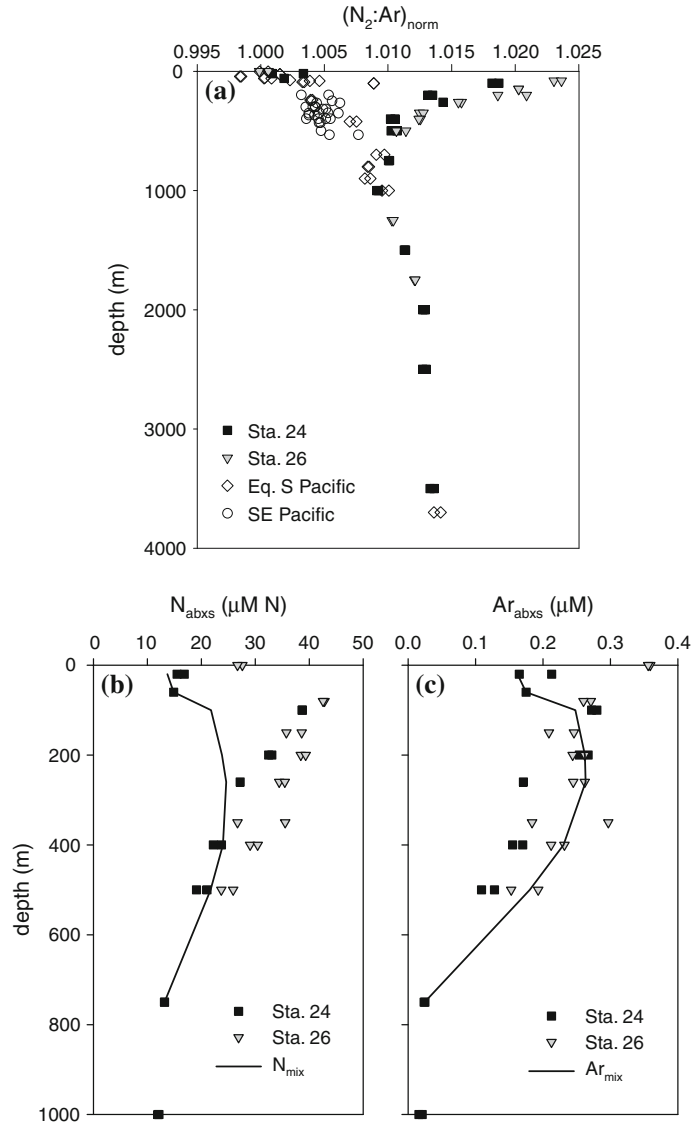

Fig. 11 **a** Profiles of the ratio of the normalized ratio of N_2/Ar, i.e. $(N_2{:}Ar)_{norm}$, throughout the SE Pacific including at two stations (Sta 24 and 26) in the Eastern Tropical South Pacific oxygen deficient zone. N_2, compared to Ar, in oxygen deficient zones is used to calculate denitrification rates. **b** and **c** Depth profiles of observed absolute excess of N_2 and Ar respectively (symbols). The *solid line* denotes the calculated excess due to mixing. Using absolute N_2 and Ar concentrations and a mixing model is an alternative approach for calculating denitrification rates. Figure reproduced from Chang et al. (2010)

8.4 Water Column Denitrification Rates

A fourth application of noble gases to biological processes is the use of N_2/Ar ratios to quantify water column denitrification. Denitrification, i.e. the loss of fixed nitrogen from the ocean, is a key term in the global nitrogen budget but is currently not well constrained, leading to some studies suggesting the nitrogen budget is balanced whereas other studies suggest the budget has a net loss of nitrogen (e.g. Codispoti 2007; Gruber and Sarmiento 1997). Argon can be paired with N_2 to quantify water column denitrification rates (Chang et al. 2010; Devol et al. 2006; Fuchsman et al. 2008; Manning et al. 2010). The basis behind this technique is that all denitrification processes, whether they stem from NO_3 or NH_3, will lead to an increase in N_2. Ar is used to normalize the observed N_2 excesses for physical processes, such as the supersaturation due to mixing (see Sect. 4) and to some extent thermal heating/cooling. The advantages of this technique are that it makes no assumption about the form of

fixed nitrogen consumed, does not rely on the perhaps erroneous assumption of Redfield stoichiometry, and integrates over larger scales than bottle incubations.

Argon has been used in conjunction with N_2 in calculating denitrification rates in two ways. In one method, the N_2/Ar ratio is used (Fig. 11a) (Chang et al. 2010; Devol et al. 2006; Fuchsman et al. 2008; Manning et al. 2010). Profiles of N_2/Ar, normalized to equilibrium values, from oxygen deficient zones (ODZ) show a significant excess of N_2/Ar in the denitrification zone, i.e. region of low O_2, compared to N_2/Ar profiles from other regions of the ocean (i.e. outside of the ODZ). The N_2/Ar excess can be used to calculate the amount of N_2 lost by denitrification processes. This N_2 loss can then be used in conjunction with an estimate of the residence time of water to calculate the denitrification rate.

In the second method (Chang et al. 2010; Fuchsman et al. 2008), absolute N_2 and Ar concentrations are measured by isotope dilution with a spike of ^{36}Ar (Fig. 11b and c). A two-end member mixing model is used to estimate the effects of diapycnal mixing on the N_2 and Ar concentrations. The absolute N_2 excess can then be calculated by the difference in concentration of N_2 from that predicted by the mixing model. Again, estimates of the residence time of the water are needed to convert the excess N_2 loss into a rate of denitrification.

In the Arabian sea, the N_2/Ar method for calculating denitrification rates gave a rate that was twice as high as that predicted by the more typical "Nitrate-deficit" method—a method that relies on the difference between observed nitrate concentration and Redfield N:P ratios (Devol et al. 2006). The difference is likely to result from one of four causes: (1) non Redfieldian stoichiometry of remineralized matter, perhaps due to nitrogen fixers, leading to errors in the nitrate-deficit method; (2) denitrification of NH_3 which is missed by the nitrate deficit method but included in the N_2/Ar method; (3) water column processes between Fe, Mn, I and N leading to production of N_2; (4) sedimentary processes that release N_2 into the overlying water. In the Eastern Tropical South Pacific ODZ, the N_2/Ar method yielded estimates of denitrification that were only 15–30 % larger than those calculated using the nitrate deficit method (Chang et al. 2010).

9 Summary

Noble gases in seawater, whether measured individually (i.e. ^{3}He for circulation or Ar for diapycnal mixing), as a suite (i.e. measurements of He, Ne, Ar, Kr, and Xe made concurrently for air-sea gas exchange) or in conjunction with biologically active gases (such as O_2/Ar and N_2/Ar), are useful tracers of physical and biological processes. A number of applications of noble gases exist presently and it is likely that more applications will be developed. Until recently, the heavier noble gases (Kr and Xe) were not easily measured. Including Kr and Xe in many of the studies mentioned above could improve the information gleaned from the noble gas distributions.

References

Andrews JN (1985) The isotopic composition of radiogenic helium and its use to study groundwater movement in confined aquifers. Chem Geol 49:339–351

Axford WI (1968) The polar wind and the terrestrial helium budget. J Geophys Res 73:6855–6859

Benson BB, Krause D Jr (1980) Isotopic fractionation of helium during solution: a probe for the liquid state. J Solution Chem 9:895–909

Beyerle U, Aeschbach-Hertig W, Imboden DM, Baur H, Graf T, Kipfer R (2000) A mass spectrometric system for the analysis of noble gases and tritium from water samples. Environ Sci Technol 34(10):2042–2050

Bianchi D, Sarmiento JL, Gnanadesikan A, Key RM, Schlosser P, Newton R (2010) Low helium flux from the mantle inferred from simulations of oceanic helium isotope data. Earth Planet Sci Lett 297:379–386

Bieri RH, Koide M, Goldberg ED (1964) Noble gases in seawater. Science 146(3647):1035–1037

Bieri RH, Koide M, Goldberg ED (1966) The noble gas contents of Pacific seawaters. J Geophysical Research 71:5243–5265

Bieri RH, Koide M, Goldberg ED (1967) Geophysical implications of excess helium found in Pacific waters. J Geophys Res 72(10):2497–2511

Boyle E, Jenkins W (2008) Hydrothermal iron in the deep western South Pacific. Geochim Cosmochim Acta 72(12):A107–A107

Bryan GH (1901) The kinetic theory of planetary atmospheres. Philos Trans R Soc (London) 196(1):1–24
Cassar N, Barnett BA, Bender ML, Kaiser J, Hamme RC, Tilbrook B (2009) Continuous high-frequency dissolved O-2/Ar measurements by equilibrator inlet mass spectrometry. Anal Chem 81(5):1855–1864
Cassar N, Bender ML, Barnett BA, Fan S, Moxim WJ, Levy H, Tilbrook B (2007) The Southern Ocean biological response to Aeolian iron deposition. Science 317(5841):1067–1070
Chang BX, Devol AH, Emerson S (2010) Denitrification and the nitrogen gas excess in the eastern tropical South Pacific oxygen deficient zone. Deep-Sea Res Part I-Oceanogr Res Pap 57(9):1092–1101. doi:10.1016/j.dsr.2010.05.009
Clarke WB, Beg MA, Craig H (1969) Excess ^{3}He in the sea: evidence for terrestrial primordial helium. Earth Planet Sci Lett 6:213–220
Codispoti LA (2007) An oceanic fixed nitrogen sink exceeding 400 Tg Na(−1) vs the concept of homeostasis in the fixed-nitrogen inventory. Biogeosciences 4(2):233–253
Cook SR (1902) The permanency of planetary atmospheres, according to the kinetic theory of gases. Mon Weather Rev 52(2):401–407
Craig H, Clarke WB (1970) Oceanic ^{3}He: contribution from cosmogenic tritium. Earth Planet Sci Lett 9: 45–48
Craig H, Hayward T (1987) Oxygen supersaturation in the ocean: biological versus physical contributions. Science 235:199–202
Craig H, Lal D (1961) The production rate of natural tritium. Tellus 13:85–105
Devol AH, Uhlenhopp AG, Naqvi SWA, Brandes JA, Jayakumar DA, Naik H, Gaurin S, Codispoti LA, Yoshinari T (2006) Denitrification rates and excess nitrogen gas concentrations in the Arabian Sea oxygen deficient zone. Deep-Sea Res Part I-Oceanogr Res Pap 53(9):1533–1547. doi:10.1016/j.dsr.2006.07.005
Doney SC, Glover DM, Jenkins WJ (1992) A model function of the global bomb-tritium distribution in precipitation, 1960–1986. J Geophys Res 97:5481–5492
Doney SC, Jenkins WJ, Bullister JL (1997) A comparison of ocean tracer dating techniques on a meridional section in the eastern North Atlantic. Deep-Sea Res I 44(4):603–626
Dutay J-C, Jean-Baptiste P, Campin J-M, Ishida A, Maier-Reimer E, Matear RJ, Mouchet A, Totterdell IJ, Yamanaka Y, Rodgers KB, Madec G, Orr JC (2004) Evaluation of OCMIP-2 ocean models' deep circulation with mantle helium-3. J Mar Syst 48:15–36
Emerson S, Quay P, Stump C, Wilbur D, Knox M (1991) O_2, Ar, N_2, and 222Rn in surface waters of the subarctic ocean: net biological O_2 production. Global Biogeochem Cycles 5:49–69
Emerson S, Stump C, Wilbur D, Quay P (1999) Accurate measurement of O-2, N-2, and Ar gases in water and the solubility of N-2. Mar Chem 64(4):337–347
Eppley RW, Peterson BJ (1979) Particulate organic matter flux and planktonic new production in the deep ocean. Nature 282(677–680):
Fairhall AW (1970) Concerning the source of the excess ^{3}He in the sea. Earth Planet Sci Lett 7(3):249–250
Farley KA, Maier-Reimer E, Schlosser P, Broecker WS (1995) Constraints on mantle ^{3}He fluxes and deep-sea circulation from a general circulation model. J Geophys Res 100(B3):3829–3839
Fuchs G, Roether W, Schlosser P (1987) Excess ^{3}He in the ocean surface layer. J Geophys Res 92:6559–6568
Fuchsman CA, Murray JW, Konovalov SK (2008) Concentration and natural stable isotope profiles of nitrogen species in the Black Sea. Mar Chem 111(1–2): 90–105. doi:10.1016/j.marchem.2008.04.009
Garabato ACN, Stevens DP, Watson AJ, Roether W (2007) Short-circuiting of the overturning circulation in the Antarctic circumpolar current. Nature 447:194–197
Gehrie E, Archer D, Emerson S, Stump C, Henning C (2006) Subsurface ocean argon disequilibrium reveals the equatorial Pacific shadow zone. Geophys Res Lett 33(18):
Gow AJ, Williamson T (1975) Gas inclusions in antarctic ice sheet and their glaciological significance. J Geophys Res Oceans Atmos 80(36):5101–5108. doi:10.1029/JC080i036p05101
Gruber N, Sarmiento JL (1997) Global patterns of marine nitrogen fixation and denitrification. Global Biogeochem Cycles 11(2):235–266
Hamme RC, Cassar N, Lance VP, Vaillancourt RD, Bender ML, Strutton PG, Moore TS, DeGrandpre MD, Sabine CL, Ho DT, Hargreaves BR (2012) Dissolved O2/Ar and other methods reveal rapid changes in productivity during a Lagrangian experiment in the Southern Ocean. J Geophys Res-Oceans 117:C00F12 doi:10.1029/2011JC007046
Hamme RC, Emerson S (2004a) Measurement of dissolved neon by isotope dilution using a quadrupole mass spectrometer. Mar Chem 91(1–4):53–64
Hamme RC, Emerson S (2004b) The solubility of neon, nitrogen and argon in distilled water and seawater. Deep Sea Res I 51(11):1517–1528
Hamme RC, Emerson S (2006) Constraining bubble dynamics and mixing with dissolved gases: implications for productivity measurements by oxygen mass balance. J Mar Res 64(1):73–95
Hamme RC, Severinghaus JP (2007) Trace gas disequilibria during deep-water formation. Deep-Sea Res Part I-Oceanogr Res Pap 54(6):939–950
Harrison WG, Harris LR (1986) Isotope-dilution and its effects on measurements of nitrogen and phosphorus uptake by oceanic microplankton. Mar Ecol Prog Ser 27(3):253–261
Hendricks MB, Bender ML, Barnett BA (2004) Net and gross O-2 production in the Southern Ocean from measurements of biological O-2 saturation and its triple isotope composition. Deep-Sea Res Part I-Oceanogr Res Pap 51(11):1541–1561

Hendricks MB, Bender ML, Barnett BA, Strutton P, Chavez FP (2005) Triple oxygen isotope composition of dissolved O-2 in the equatorial Pacific: a tracer of mixing, production, and respiration. J Geophys Res-Oceans 110(C12):doi:10.1029/2004JC002735

Henning CC, Archer D, Fung I (2006) Argon as a tracer of cross-isopycnal mixing in the thermocline. J Phys Oceanogr 36(11):2090–2105

Ho DT, Law CS, Smith MJ, Schlosser P, Harvey M, Hill P (2006) Measurements of air-sea gas exchange at high wind speeds in the Southern Ocean: implications for global parameterizations. Geophys Res Lett 33(16)

Ho DT, Wanninkhof R, Schlosser P, Ullman DS, Hebert D, Sullivan KF (2011) Toward a universal relationship between wind speed and gas exchange: gas transfer velocities measured with (3)He/SF(6) during the Southern Ocean gas exchange experiment. J Geophys Res-Oceans 116 doi:C00f0410.1029/2010jc006854

Hohmann R, Schlosser P, Jacobs S, Ludin A, Weppernig R (2002) Excess helium and neon in the southeast Pacific: tracers for glacial meltwater. J Geophys Res-Oceans 107(C11):doi:10.1029/2000JC000378

Holland PR, Feltham DL, Jenkins A (2007) Ice shelf water plume flow beneath filchner-ronne ice shelf, Antarctica. J Geophys Res-Oceans 112(C5) doi:C0504410.1029/2006jc003915

Hood EM, Howes BL, Jenkins WJ (1998) Dissolved gas dynamics in perennially ice-covered Lake Fryxell, Antarctica. Limnol Oceanogr 43(2):265–272

Howard E, Emerson S, Bushinsky S, Stump C (2010) The role of net community production in air-sea carbon fluxes at the North Pacific subarctic-subtropical boundary region. Limnol Oceanogr 55(6):2585–2596. doi:10.4319/lo.2010.55.6.2585

Huang RX, Qiu B (1994) Three dimensional structure of the wind-driven circulation in the subtropical North Pacific. J Phys Oceanogr 24(7):1608–1622

Huang RX, Qiu B (1998) The structure of the wind-driven circulation in the subtropical South Pacific Ocean. J Phys Oceanogr 28:1173–1186

Huber C, Beyerle U, Leuenberger M, Schwander J, Kipfer R, Spahni R, Severinghaus JP, Weiler K (2006) Evidence for molecular size dependent gas fractionation in firn air derived from noble gases, oxygen, and nitrogen measurements. Earth Planet Sci Lett 243(1–2):61–73

Ito T, Deutsch C (2006) Understanding the saturation state of argon in the thermocline: the role of air-sea gas exchange and diapycnal mixing. Global Biogeochem Cycles 20(3):doi:10.1029/2005GB002655

Ito T, Deutsch C, Emerson S, Hamme RC (2007) Impact of diapycnal mixing on the saturation state of argon in the subtropical North Pacific. Geophys Res Lett 34(9):doi:10.1029/2006GL029209

Ito T, Hamme RC, Emerson S (2011) Temporal and spatial variability of noble gas tracers in the North Pacific. J Geophys Res-Oceans 116 doi:C08039 10.1029/2010jc006828

Jahne B, Heinz G, Dietrich W (1987) Measurement of the diffusion coefficients of sparingly soluble gases in water. J Geophys Res 92(C10):10767–10776

Jenkins WJ (1977) Tritium-helium dating in the Sargasso Sea: a measurement of oxygen utilization rates. Science 196(4287):291–292

Jenkins WJ (1980) Tritium and He-3 in the Sargasso Sea. J Mar Res 38(3):533–569

Jenkins WJ (1987) ^{3}H and ^{3}He in the Beta Triangle: observations of gyre ventilation and oxygen utilization rates. J Phys Oceanogr 17:763–783

Jenkins WJ (1988a) Nitrate flux into the euphotic zone near Bermuda. Nature 331(6156):521–523

Jenkins WJ (1988b) The use of anthropogenic tritium and He-3 to study sub-tropical gyre ventilation and circulation. Philos Trans R Soc Lond Ser A Math Phys Eng Sci 325(1583):43–61

Jenkins WJ (1991) Determination of isopycnic diffusivity in the Sargasso Sea. J Phys Oceanogr 21(7):1058–1061

Jenkins WJ (1996) Tritium and ^{3}He in the WOCE Pacific program. Int WOCE Newslett 23:6–8

Jenkins WJ (1998) Studying subtropical thermocline ventilation and circulation using tritium and He-3. J Geophys Res-Oceans 103(C8):15817–15831

Jenkins WJ (2008) The biogeochemical consequences of changing ventilation in the Japan/East Sea. Mar Chem 108(3–4):137–147. doi:10.1016/j.marchem.2007.11.003

Jenkins WJ, Beg MA, Clarke WB, Wangersky PJ, Craig H (1972) Excess ^{3}He in the Atlantic Ocean. Earth Planet Sci Lett 16:122–130

Jenkins WJ, Clarke WB (1976) The distribution of ^{3}He in the western Atlantic Ocean. Deep Sea Res 23:481

Jenkins WJ, Doney SC (2003) The subtropical nutrient spiral. Global Biogeochem Cycles 17(4):1110. doi:1110.1029/2003GB002085

Jenkins WJ, Edmond JM, Corliss JB (1978) Excess ^{3}He and ^{4}He in galapagos submarine hydrothermal waters. Nature 272:156

Jenkins WJ, Rona PA, Edmond JM (1980) Excess ^{3}He in the deep-water over the Mid-Atlantic Ridge at 26°N: evidence of hydrothermal activity. Earth Planet Sci Lett 50:39–44

Jonsson BF, Doney SC, Dunne J, Bender M Evaluation of Southern Ocean O2/Ar based NCP measurements in a model framework. J Geophys Res-Oceans

Juranek LW, Quay PD (2005) In vitro and in situ gross primary and net community production in the North Pacific subtropical gyre using labeled and natural abundance isotopes of dissolved O-2. Global Biogeochem Cycles 19(3):doi:10.1029/2004GB002384

Kaiser J, Reuer MK, Barnett B, Bender ML (2005) Marine productivity estimates from continuous O-2/Ar ratio measurements by membrane inlet mass spectrometry. Geophys Res Lett 32(19):doi:10.1029/2005GL023459

Klein B, Roether W, Kress N, Manca BB, d'Alcala MR, Souvermezoglou E, Theocharis A, Civitarese G, Luchetta A (2003) Accelerated oxygen consumption

in eastern Mediterranean deep waters following the recent changes in thermohaline circulation. J Geophys Res-Oceans 108(C9) doi:8107.10.1029/2002jc001454
Kurz MD, Jenkins WJ (1981) The distribution of helium in oceanic basalt glasses. Earth Planet Sci Lett 53:41–54
Kurz MD, Jenkins WJ, Hart SR (1982) Helium isotopic systematics of oceanic islands and mantle heterogeneity. Nature 297(5861):43–47
Kurz MD, Jenkins WJ, Hart SR, Clague D (1983) Helium isotopic variations in volcanic rocks from Loihi Seamount and the islands of Hawaii. Earth Planet Sci Lett 66:388–406
Lomas MW, Lipschultz F, Nelson DM, Krause JW, Bates NR (2009) Biogeochemical responses to late-winter storms in the Sargasso Sea, I-pulses of primary and new production. Deep-Sea Res Part I Oceanogr Res Pap 56(6):843–860
Loose B, Schlosser P, Smethie WM, Jacobs S (2009) An optimized estimate of glacial melt from the ross ice shelf using noble gases, stable isotopes, and CFC transient tracers. J Geophys Res-Oceans 114 doi:C08007.10.1029/2008jc005048
Lott DE (2001) Improvements in noble gas separation methodology: a nude cryogenic trap. Geochemistry, Geophysics, Geosystems 2:10.129/2001GC000202
Lott DE, Jenkins WJ (1984) An automated cryogenic charcoal trap system for helium isotope mass spectrometry. Rev Sci Instrum 55(12):1982–1988
Lott DE, Jenkins WJ (1998) Advances in analysis and shipboard processing of tritium and helium samples. Int WOCE Newslett 30:27–30
Lupton JE, Baker ET, Massoth GJ (1989) Variable ^{3}He/heat ratios in submarine hydrothermal systems: evidence from two plumes over the Juan de Fuca ridge. Nature 337:161–164
Lupton JE, Craig H (1975) Excess He-3 in oceanic basalts: evidence for terrestrial primordial helium. Earth Planet Sci Lett 26(2):133–139
Lupton JE, Craig H (1981) A major helium-3 source at 15S on the East Pacific rise. Science 214(4516):13–18
Lupton JE, Klinkhammer G, Normark WR, Haymon R, MacDonald KC, Weiss RF, Craig H (1980) Helium-3 and manganese at the 21 N East Pacific rise hydrothermal site. Earth Planet Sci Lett 50:115–127
Luyten JR, Pedlosky J, Stommel H (1983) The ventilated thermocline. J Phys Oceanogr 13:292–309
MacMahon D (2006) Half-life evaluations for H-3, Sr-90, and Y-90. Appl Radiat Isot 64(10–11):1417–1419
Mahaffey C, Williams RG, Wolff GA, Anderson WT (2004) Physical supply of nitrogen to phytoplankton in the Atlantic Ocean. Global Biogeochem Cycles 18(1):
Manning CC, Hamme RC, Bourbonnais A (2010) Impact of deep-water renewal events on fixed nitrogen loss from seasonally-anoxic Saanich inlet. Mar Chem 122(1–4):1–10. doi:10.1016/j.marchem.2010.08.002
Martinerie P, Raynaud D, Etheridge DM, Barnola JM, Mazaudier D (1992) Physical and climatic parameters which influence the air content in polar ice. Earth Planet Sci Lett 112(1–4):1–13. doi:10.1016/0012-821x(92)90002-d
McDougall TJ (1990) Bulk properties of "hot smoker" plumes. Earth Planet Sci Lett 99:185–194
McGillicuddy DJ, Anderson LA, Bates NR, Bibby T, Buesseler KO, Carlson CA, Davis CS, Ewart C, Falkowski PG, Goldthwait SA, Hansell DA, Jenkins WJ, Johnson R, Kosnyrev VK, Ledwell JR, Li QP, Siegel DA, Steinberg DK (2007) Eddy/wind interactions stimulate extraordinary mid-ocean plankton blooms. Science 316(5827):1021–1026
Morrison P, Pine J (1955) Radiogenic origin of helium isotopes in rock. Ann N Y Acad Sci 62(3):69–92
Nicholson D, Emerson S, Caillon N, Jouzel J, Hamme RC (2010) Constraining ventilation during deepwater formation using deep ocean measurements of the dissolved gas ratios (40)Ar/(36)Ar, N(2)/Ar, and Kr/Ar. J Geophys Res Oceans 115 doi:C11015. 10.1029/2010jc006152
Nightingale PD, Malin G, Law CS, Watson A, Liss PS, Liddicoat MI, Boutin J, Upstill-Goddard R (2000) In situ evaluation of air-sea gas exchange parameterizations using novel conservative and volatile tracers. Global Biogeochem Cycles 14(1):373–387
Peterson BJ (1980) Aquatic primary productivity and the C-14-Co2 method—a history of the productivity problem. Annu Rev Ecol Syst 11:359–385
Postlethwaite CF (2002) Developing a tool for evaluating the role of seasonal sea ice in deepwater formation. University of Southampton
Postlethwaite CF, Rohling EJ, Jenkins WJ, Walker CF (2005) A tracer study of ventilation in the Japan/East Sea. Deep Sea Res Part II 52(11–13):1684–1704
Quay PD, Peacock C, Bjorkman K, Karl DM (2010) Measuring primary production rates in the ocean: enigmatic results between incubation and non-incubation methods at station ALOHA. Global Biogeochem Cycles 24(3):doi:10.1029/2009GB003665
Reuer MK, Barnett BA, Bender ML, Falkowski PG, Hendricks MB (2007) New estimates of Southern Ocean biological production rates from O-2/Ar ratios and the triple isotope composition of O-2. Deep-Sea Res Part I Oceanogr Res Pap 54(6):951–974
Robbins PE, Jenkins WJ (1998) Observations of temporal changes of tritium-^{3}He age in the eastern North Atlantic thermocline: evidence for changes in ventilation? J Mar Res 56:1125–1161
Robbins PE, Price JF, Owens WB, Jenkins WJ (2000) The importance of lateral diffusion for the ventilation of the lower thermocline in the subtropical North Atlantic. J Phys Oceanogr 30(1):67–89. doi: 10.1175/1520-0485(2000)030<0067:tioldf>2.0.co;2
Rodehacke CB, Hellmer HH, Huhn O, Beckmann A (2007) Ocean/ice shelf interaction in the southern Weddell Sea: results of a regional numerical helium/neon simulation. Ocean Dyn 57(1):1–11
Roether W, Well R, Putzka A, Ruth C (1998) Component separation of oceanic helium. J Geophys Res 103(C12):27931–27946
Runham G (2001) Laboratory determination of the partitioning of He, Ne, and Ar between seawater and ice during freezing. University of Southampton

Ruth C, Well R, Roether W (2000) Primordial 3He in South Atlantic deep waters from sources on the Mid-Atlantic ridge. Deep Sea Res I 47:1059–1075

Sakai H, Tsubota H, Nakai T, Ishibashi J, Akagi T, Gamo T, Tilbrook B, Igarashi G, Kodera M, Shitashima K, Nakamura S, Fujioka K, Watanabe M, McMurtry G, Malahoff A, Ozima M (1987) Hydrothermal activity on the summit of Loihi Seamount. Geochem J 21:11–21

Salter ME, Upstill-Goddard RC, Nightingale PD, Archer SD, Blomquist B, Ho DT, Huebert B, Schlosser P, Yang M (2011) Impact of an artificial surfactant release on air-sea gas fluxes during deep ocean gas exchange experiment II. J Geophys Res Oceans 116 doi:C1101610.1029/2011jc007023

Sano Y, Takahata N (2005) Measurement of noble gas solubility in seawater using a quadrupole mass spectrometer. J Oceanogr 61(3):465–473

Scarratt MG, Marchetti A, Hale MS, Rivkin RB, Michaud S, Matthews P, Levasseur M, Sherry N, Merzouk A, Li WKW, Kiyosawa H (2006) Assessing microbial responses to iron enrichment in the subarctic Northeast Pacific: do microcosms reproduce the in situ condition? Deep Sea Res Part II 53(20–22):2182–2200

Schlosser P (1986) Helium: a new tracer in Antarctic oceanography. Nature 321:233–235

Schlosser P, Bayer R, Flodvik A, Fammelsrod T, Rhohardt G, Munnich KO (1990) Oxygen 18 and helium as tracers of ice shelf water and water/ice interaction in the Weddell Sea. J Geophys Res 95:3253–3263

Severinghaus JP, Grachev A, Luz B, Caillon N (2003) A method for precise measurement of argon 40/36 and krypton/argon ratios in trapped air in polar ice with applications to past firn thickness and abrupt climate change in Greenland and at Siple Dome, Antarctica. Geochim Cosmochim Acta 67(3): 325–343

Smedsrud LH, Jenkins A (2004) Frazil ice formation in an ice shelf water plume. J Geophys Res Oceans 109(C3) doi:C03025 10.1029/2003jc001851

Smith MJ, Ho DT, Law CS, McGregor J, Popinet S, Schlosser P (2011) Uncertainties in gas exchange parameterization during the SAGE dual-tracer experiment. Deep Sea Res Part Ii 58(6):869–881. doi: 10.1016/j.dsr2.2010.10.025

Smith SP, Kennedy BM (1983) The solubility of noble gases in water and NaCl brine. Geochim Cosmochim Acta 47(3):503–515. doi:10.1016/0016-7037(83)90273-9

Speer KG (1989) The stommel and arons model and geothermal heating in the South Pacific. Earth Planet Sci Lett 95:359–366

Speer KG, Rona PA (1989) A model of an Atlantic and Pacific hydrothermal plume. J Geophys Res 94:6213–6220

Spitzer WS, Jenkins WJ (1989) Rates of vertical mixing, gas-exchange and new production—estimates from seasonal gas cycles in the upper ocean near Bermuda. J Mar Res 47(1):169–196

Stanley RHR (2007) Air-sea gas exchange and upper ocean biological production. Ph.D thesis, MIT/WHOI Joint Program

Stanley RHR, Baschek B, Lott DE, Jenkins WJ (2009a) A new automated method for measuring noble gases and their isotopic ratios in water samples. Geochem Geophys Geosyst 10:doi:10.1029/2009GC002429

Stanley RHR, Doney SC, Jenkins WJ, Lott III DE (2012) Apparent oxygen utilization rates calculated from tritium and helium-3 profiles at the Bermuda Atlantic time-series study site. Biogeosciences doi:10.5194/bg-9-1969-2012:9977-10015

Stanley RHR, Jenkins WJ, Doney SC (2006) Quantifying seasonal air-sea gas exchange processes using noble gas time-series: a design experiment. J Mar Res 64(2):267–295

Stanley RHR, Jenkins WJ, Doney SC, Lott III DE (2009b) Noble gas constraints on air-sea gas exchange and bubble fluxes. J Geophys Res Oceans 114:doi:10.1029/2009JC005396

Stanley RHR, Kirkpatrick JB, Barnett B, Cassar N, Bender ML (2010) Net community production and gross production rates in the Western Equatorial Pacific. Global Biogeochem Cycles 24:GB4001, doi:4010.1029/2009GB003651

Steinberg DK, Carlson CA, Bates NR, Goldthwait SA, Madin LP, Michaels AF (2000) Zooplankton vertical migration and the active transport of dissolved organic and inorganic carbon in the Sargasso Sea. Deep Sea Res I 47:137–158

Stommel H (1982) Is the South Pacific helium-3 plume dynamically active? Earth Planet Sci Lett 61:63–67

Stommel H, Aarons AB (1960) On the abyssal circulation of the world ocean—II. An idealized model of the circulation pattern and amplitude in ocean basins. Deep Sea Res 6:217–233

Stoney GJ (1905) Escape of gases from the atmosphere. Mon Weather Rev 7(January):6–9

Tagliabue A, Bopp L, Dutay J-C, Bowie AR, Chever F, Jean-Baptiste P, Bucciarelli E, Lannuzel D, Remenyi T, Sarthou G, Aumont O, Gehlen M, Jeandel C (2010) Hydrothermal contribution to the oceanic dissolved iron inventory. Nat Geosci 3(4):252–256

Takahashi T, Williams RT et al (1988) Alteration of the concentrations of dissolved gases in Niskin bottles during sampling operations. SAVE technical report

Takahata N, Sano Y, Horigucut K, ShiraO' K, Ganio T (2008) Helium isotopes of seawater in the Japan Sea. J Oceanogr 64(2):293–301. doi:10.1007/s10872-008-0023-3

Thorpe SA (1984) A model of the turbulent diffusion of bubbles below the sea surface. J Phys Oceanogr 14:841–854

Tomczak M (1981) A multi-parameter extension of temperature/salinity diagram techniques for the analysis of non-isopycnal mixing. Prog Oceanogr 10:147–171

Tortell PD (2005) Dissolved gas measurements in oceanic waters made by membrane inlet mass spectrometery. Limnol Oceanogr Methods 3:24–37

Turekian KK (1959) The terrestrial economy of helium and argon. Geochim Cosmochim Acta 17:37–43

Warner MJ, Bullister JL, Wisegarver DP, Gammon RH, Weiss RF (1996) Basin-wide distributions of

chlorofluorocarbons CFC-11 and CFC-12 in the North Pacific: 1985–1989. J Geophys Res 101:20525–20542
Watson AJ, Upstill-Goddard RC, Liss PS (1991) Air-sea gas exchange in rough and stormy seas measured by a dual-tracer technique. Nature 349:145–147
Weiss RF (1968) Piggyback sampler for dissolved gas studies on sealed water samples. Deep Sea Res 15: 841–854
Weiss RF (1970) Helium isotope effect in solution in water and seawater. Science 168:247–248
Weiss RF (1971) Solubility of helium and neon in water and seawater. J Chem Eng Data 16:235–241
Weiss RF, Kyser TK (1978) Solubility of krypton in water and seawater. J Chem Eng Data 23(1):69–72
Weiss WM, Roether W (1980) The rates of tritium input to the world oceans. Earth Planet Sci Lett 49:435–446
Well R, Lupton JE, Roether W (2001) Crustal helium in deep Pacific waters. J Geophys Res 106(C7):14165–14177
Well R, Roether W, Stevens DP (2003) An additional deep-water mass in drake passage as revealed by ^{3}He data. Deep Sea Res I 50(9):1079–1098
Weppernig R, Schlosser P, Khatiwala S, Fairbanks RG (1996) Isotope data from ice station Weddell: implications for deep water formation in the Weddell sea. J Geophys Res Oceans 101(C11):25723–25739. doi:10.1029/96jc01895
Wijffels SE, Toole JM, Bryden HL, Fine RA, Jenkins WJ, Bullister JL (1996) The water masses and circulation at 10°N in the Pacific. Deep Sea Res I 43(4):501–544
Wijffels SE, Toole JM, Davis RE (2001) Revisiting the South Pacific subtropical circulation: a synthesis of WOCE observations along 32 S. J Geophys Res 106(C9):19481–19513
Williams RG, Follows MJ (1998) The Ekman transfer of nutrients and maintenance of new production over the North Atlantic. Deep Sea Res Part I Oceanogr Res Pap 45(2–3):461–489
Wise DL, Houghton G (1966) Diffusion coefficients of 10 slightly soluble gases in water at 10–60°C. Chem Eng Sci 21(11):999–1010. doi:10.1016/0009-2509(66)85096-0
Wood D, Caputi R (1966) Solubilities of Kr and Xe in fresh and sea water. In: U.S. Naval Radiological Defense Laboratory, San Francisco, p 14
Young C, Lupton JE (1983) An ultra tight fluid sampling system using cold-welded copper tubing. Eos Transactions AGU 64:735

Noble Gas Thermometry in Groundwater Hydrology

Werner Aeschbach-Hertig and D. Kip Solomon

Abstract

Concentrations of dissolved atmospheric noble gases in water constitute a thermometer, whose application to the groundwater archive provides a method of paleoclimate reconstruction. In addition, noble gases have found wide application as tracers in hydrogeology. This chapter reviews the historical development, the theoretical foundations, the sampling and analytical techniques, as well as the spectrum of applications of this important tool of tracer hydrology. A detailed account of currently available sampling techniques is given, as this information is of great practical importance but not fully available in the scientific literature. The analytical methods are better documented in the literature, although the many lab-specific details and constant development make it hard to provide an authoritative overview, so that this part is kept comparatively short. The focus of the chapter lies on the methods for data reduction and interpretation, which have undergone rapid and important development in the recent past. Nevertheless, in this respect still substantial research needs exist. Finally, this chapter provides an overview of applications of noble gases in groundwater hydrology, which range from the classical paleothermometry and the determination of other paleoclimate parameters such as humidity to various hydrological investigations, such as groundwater dating or the study of water origin and recharge conditions in hydrothermal, glaciated, alluvial, coastal, managed, and mountainous aquifer systems.

W. Aeschbach-Hertig (✉)
Institut für Umweltphysik, Heidelberg University,
Heidelberg, Germany
e-mail: aeschbach@iup.uni-heidelberg.de

D. K. Solomon
University of Utah, Salt Lake City, UT, USA
e-mail: kip.solomon@utah.edu

P. Burnard (ed.), *The Noble Gases as Geochemical Tracers*, Advances in Isotope Geochemistry,
DOI: 10.1007/978-3-642-28836-4_5,

Keywords
Recharge temperatures · Paleoclimate · Excess air · Climate archives · Hydrogeology

1 Introduction

Noble gases have become established and rather widely used tools in groundwater hydrology over the past decades. Their importance in this field derives from the usual advantages of noble gases as tracers: Chemical inertness, well-known and quantifiable sources and sinks (namely: exchange with air or other gas phases and radioactive decay), and low background concentrations. As a result, noble gas data from groundwater lend themselves to a relatively clear and quantitative interpretation.

Nevertheless, noble gases may still be regarded as more specialised tracers compared to the standard methods of isotope hydrology, such as the stable isotopes of water (^{2}H and ^{18}O) or the radioisotopes tritium (^{3}H) and radiocarbon (^{14}C). The main reason for the less frequent application of noble gases is the relative complexity of the analytical methods for noble gas measurements. Still only a few specialised labs worldwide engage in the field of noble gas hydrology. Their services are in high demand, however, as noble gases ideally complement the other methods of isotope hydrology.

One important application concerns age dating of groundwater, where ^{3}H and ^{14}C are the classical methods, complemented by a number of more modern tools (e.g., CFCs, SF_6, ^{36}Cl). Noble gases add another broad and powerful suite of dating methods, namely ^{3}H–^{3}He, radiogenic ^{4}He and ^{40}Ar, and the radioisotopes ^{39}Ar, ^{81}Kr, and ^{85}Kr. As important as these methods are, in this contribution we do not discuss them in any detail, but focus on the other major application of noble gases in groundwater, which is noble gas thermometry.

Dissolved atmospheric noble gases (i.e., Ne, Ar, Kr, and Xe, but not He which often contains radiogenic components) in groundwater provide information on the conditions during groundwater recharge, in particular the recharge or noble gas temperature (NGT). While temperature is the traditional main result of the noble gas thermometer, as implied by the name of the method, more recent research has shown that additional information can be derived from the so-called "excess air". All this information nicely complements the stable isotope data, which also indicate the origin of the groundwater and the climatic conditions under which it was formed. The combination of noble gas temperatures and stable isotopes from groundwater is therefore a powerful approach to paleoclimate reconstruction. At the same time, these tools represent useful tracers of different groundwater components, with wide applications in the field of groundwater hydrology.

1.1 Early History of the Noble Gas Thermometer

The first step towards the development of the noble gas thermometer was a study by Oana (1957), who measured N_2 and Ar concentrations in precipitation and groundwater and compared them to the temperature-dependent atmospheric equilibrium concentrations. They found that the concentrations of these gases in precipitation were close to solubility equilibrium with air and thus varied in accordance with the seasonal temperature cycle. In contrast, the concentrations in groundwater were fairly constant and on average somewhat higher than in precipitation. In a similar approach, Sugisaki (1961) used the seasonal cycle of N_2 and Ar concentrations in groundwater recharged from a stream to determine subsurface travel times and thus flow velocities.

The notion that noble gas concentrations in groundwater could provide paleotemperatures

was established by Mazor (1972), who studied thermal waters of the Jordan Rift Valley in Israel. He found that the dissolved atmospheric noble gases in these hot groundwaters reflected the much cooler modern air temperatures in the recharge areas. He concluded that the thermal waters were of meteoric origin and had retained the noble gas signature that was imprinted during their recharge. Hence, groundwater could serve as an archive of paleoclimate, as it stored the information from dissolved gases over long periods of time.

The idea of deriving a paleotemperature record from noble gases in groundwater was first realised by Andrews and Lee (1979) in a study of the Bunter Sandstone aquifer in England. ^{14}C dating established groundwater ages up to about 35 kyr and thus a record spanning the Holocene and the later part of the last glacial period was obtained. This time frame, essentially dictated by the range accessible by ^{14}C dating, has remained a standard for such studies to the present day. It is of interest as it includes the last glacial maximum (LGM) at around 20 kyr BP. To quantify the temperatures during this coldest period of the last glacial has become a major goal of noble gas paleothermometry, but already the pioneering study of Andrews and Lee (1979) showed a restriction in reaching this goal for cold areas. The record from England showed a gap in ^{14}C ages between 10 and 20 kyr, which was explained by the absence of recharge due to permafrost conditions during the LGM. Groundwater older than 20 kyr was characterized by cool NGTs, 4–7 °C lower than those obtained from groundwater of Holocene age.

Already the pioneers of noble gas thermometry noticed that dissolved noble gas concentrations in groundwater often exceeded the expected atmospheric equilibrium concentrations. Herzberg and Mazor (1979) studied springs in Israel and found substantial air excess in the karstic springs. They attributed this to the presence of air in the karstic systems and suggested that it may be a tracer for karstic waters. However, Andrews and Lee (1979) found Ne concentrations exceeding the equilibrium also in a sandstone aquifer, which they ascribed to the entrainment of microscopic bubbles. They introduced a correction scheme based on subtracting small amounts of air and optimising the agreement between equilibration temperatures indicated by the different gases, which was used for the next two decades.

Heaton and Vogel (1981) coined the term "excess air" for the excess of atmospheric gases above solubility equilibrium, which they observed in N_2 and Ar data from South African groundwaters. They suggested that during groundwater recharge small bubbles of air become trapped and are then carried downwards with the water, to finally dissolve completely under the increased hydrostatic pressure at depth. They noted that the ratio of excess N_2 to Ar was close to the atmospheric ratio, indicating complete dissolution of the bubbles rather than partial dissolution, which would shift the ratio towards that of the solubility equilibrium concentrations. This model of complete dissolution of bubbles, later termed "unfractionated excess air" or UA model, remained the standard assumption for more than a decade.

Heaton and Vogel (1981) also discussed the hydrological significance and possible use of the excess air component. They noted that the physical structure of the unsaturated zone in the recharge area, in particular the size of the pores, may influence the amount of excess air being formed. Furthermore, they suggested that strong intermittent recharge events, as common in semi-arid regions, may favor the entrapment and eventual dissolution of air. This idea was further supported by a study of groundwater in the western Kalahari (Heaton et al. 1983), where systematic variations of excess were found, which seemed to be related to changes in humidity and recharge intensity. Variations of initial nitrate, which was reconstructed as the sum of the measured nitrate and the excess N_2 above solubility equilibrium and excess air, also seemed to be related to paleoclimate variations. This study also showed that dissolved N_2 concentrations can be significantly enhanced as a result of denitrification, making this gas less suitable for paleothermometry than the conservative noble gases. Later studies almost

exclusively used the full suite of atmospheric noble gases for the purpose of temperature reconstruction.

An essential prerequisite for the use of the noble gas thermometer in paleoclimate reconstruction is to show that the noble gas data truly reflect actual temperatures. As the final contact of groundwater with air takes place near the groundwater table, it is assumed that NGTs reflect ground temperatures at the depth of the water table. This correspondence was demonstrated for several sites in Germany by Rudolph et al. (1984). Other fundamental aspects of the method, such as the composition of soil air, the separation of the equilibrium and excess air components, the relationship between soil and air temperature, and the preservation of climatic signals with respect to dispersion, were for the first time comprehensively discussed by Stute and Schlosser (1993).

Their first review of the method remains an important resource to the present day. It has been extended by later reviews of Stute and Schlosser (2000) and Kipfer et al. (2002). This chapter hopes to add to this tradition by updating these previous recapitulations of the state of the art of noble gas thermometry.

1.2 Recent Developments and Outline of this Chapter

Although the foundations of the method were laid in the 1970s and 1980s, the methodological development did not come to a halt. Progress was made with regard to sampling procedures (e.g., passive diffusion samplers, Sanford et al. 1996) as well as with analytical techniques (e.g., combined analysis of Ar, Kr, Xe, Beyerle et al. 2000, or the use of quadrupole mass spectrometers, Poole et al. 1997; Kulongoski and Hilton 2002; Stanley et al. 2009). These developments will be described in more detail in Sect. 2.

As more noble gas data from groundwater accumulated, it transpired that the usual assumption of an atmospheric composition of the excess air component did not always yield satisfactory results. The problem became critical in a classical record from Brazil, published by Stute et al. (1995b) in Science, which gained particular importance in the discussion about the glacial climate in the tropics. In this study, a new model for excess air was introduced, later called the "partial re-equilibration" or PR model. The validity of the PR model and with it the record from Brazil was challenged by Ballentine and Hall (1999), who in parallel with Aeschbach-Hertig et al. (1999) came up with a new optimisation approach to determine NGTs and excess air concentration and composition.

Aeschbach-Hertig et al. (2000) showed that an alternative model for the formation of excess air, the "closed-system equilibration" or CE model, provided an adequate description of the samples from Brazil. This model proved to work also for many other data sets and thus became widely used. Nevertheless, several other models have been proposed in recent years, addressing the equilibration conditions in the unsaturated zone (Mercury et al. 2004; Hall et al. 2005; Sun et al. 2008). The methods to evaluate noble gas data and the various excess air models are discussed in Sect. 3. That section also discusses the methodological questions that revolve around the issue of how well noble gas temperatures represent soil and eventually air temperatures.

Finally, when all methodological questions are addressed, one can turn to applications of the method. A large number of studies have addressed the paleotemperature history since the late last glacial period at various sites. They generally found a temperature difference between the Holocene warm period and the preceding last glacial maximum (LGM) of roughly 5 °C, both in the tropics and in temperate latitudes. Some studies from mid-latitude northern hemispheric sites found significantly larger differences up to 9.5 °C, and even these may underestimate the maximum cooling during the LGM if permafrost prevented groundwater recharge in the coldest periods. All in all, such studies have contributed significantly to our knowledge of the LGM climate state, in particular in the tropics (e.g., Farrera et al. 1999).

Besides paleotemperature reconstruction, the excess air component is increasingly used as a paleoclimate proxy, as suggested by Heaton

et al. (1983) and later by Aeschbach-Hertig et al. (2002a). Last but not least, a variety of other applications of noble gases in groundwater hydrology are possible, ranging from the assessment of river infiltration (Beyerle et al. 1999a) to the investigation of groundwater reorganisation during sea-level rise (Morrissey et al. 2010) or to the study of mountain block recharge (Manning and Solomon 2003). The kaleidoscope of applications of noble gas thermometry is presented in Sect. 4.

Finally, Sect. 5 provides a summary of the present status of research involving noble gas thermometry and an outlook on future research needs in this field.

2 Sampling and Analytical Methods

This section provides an overview of the experimental techniques related to the noble gas thermometer. Special emphasis is placed on sampling procedures, as they are usually only briefly explained in the literature. In contrast, some detailed descriptions of analytical setups do exist, hence we restrict ourselves to a short review to point out the relevant sources in the scientific literature.

2.1 Sampling

The art of sampling dissolved gases in groundwater, especially such a mobile gas as He, lies in resolving the following potential problems:

1. Avoid gas exchange during sampling, i.e., equilibration with air due to contact with the atmosphere, contamination by inclusion of air bubbles, or degassing by formation of gas bubbles in the water.
2. Make sure that the sampled water has not been affected by contact with a gas phase before the sampling, by careful selection of suitable wells or springs.
3. Prevent alteration of the gas content during transport and storage of the samples by using appropriate sample containers.

Standard solutions to these challenges, involving specialised sampling procedures and containers, are discussed in the following.

2.1.1 Preventing Gas Exchange During Sampling

Since highly volatile gases like the noble gases can rapidly escape from the water upon contact with a gas phase, any such contact has to be prevented. In addition to contact with air, the formation of gas bubbles from within the sampled groundwater itself has to be avoided.

The usual solution to these challenges lies in the construction of a tight series of pipes and hoses that connects the water outlet from the well or pump to the sample containers. Standard sample containers are copper tubes, which can be shut vacuum tight on both ends by stainless steel clamps (e.g., Beyerle et al. 2000). Advantages of these samplers are their sturdiness, their ultra-vacuum leak tightness, allowing storage for years without alteration of even the He content, and the possibility to connect them directly with all-metal connections to the vacuum lines used for gas extraction. Moreover, if a solid connection to the well outlet has been established, the sampling system can be pressurised in order to avoid phase separation in supersaturated groundwaters.

More recently, in situ diffusion samplers have been developed, which directly capture the gas in equilibrium with the groundwater within a well. This approach has its advantages, such as avoiding the need for pumping of the well and gas extraction in the laboratory, and largely preventing air contact or degassing during sampling. Disadvantages are the relatively long time needed for the samplers to establish equilibrium with the groundwater and the need for additional measurements of the total dissolved gas content. Hence, the traditional water sampling using copper tubes is still prevalent in studies using the noble gas thermometer.

2.1.2 Selection of Suitable Wells and Springs

Not all wells are suitable for noble gas sampling, because of the requirements of closure against

air or other gas phases and of sufficient pressure to prevent degassing. Closed boreholes are highly desirable, open wells or springs are problematic, because they allow gas exchange. Ideal are artesian wells with sufficient pressure or wells with a submersible pump. Sucking pumps should be avoided, they most likely induce degassing. Pressure tanks often contain a pressurized gas phase, which may exchange with the water. If pressure or storage tanks are present, the water should be taken before it enters the tanks. Sampling after chemical treatment or filtering of the water should also be avoided.

Another important aspect of selecting sites for a noble gas study is whether or not groundwater moving along a single flow path will be collected. In general, unconfined aquifers can be highly stratified with respect to groundwater travel times and thus long well screens (filter zones) can produce samples that are a mixture of flow paths each of which could have recharged at a distinct elevation and temperature. This stratification is sometimes less in confined aquifers, but depends on the distribution of recharge in the unconfined portion of the system. In any event, wells with shorter well screens will sample fewer flow paths and contain water that recharged over a smaller range of temperature and elevation.

The problem of mixtures of groundwater having different recharge temperatures and elevations can be extreme in the case of springs that drain regional flow systems. Springs represent locations where short and long flow paths (young and old groundwater) converge. In general, the more regional the spring the greater the range of travel times and as a result the greater the potential range in recharge temperature and elevation. As discussed elsewhere in this chapter, the relationship between recharge temperature and noble gas concentration is non-linear and as a result, a mixture of groundwater with various concentrations does not map back exactly to the average recharge temperature of the mixture.

Another important consideration in selecting sampling locations is whether or not gas exsolution occurs just before or during sample collection. In flow systems where gases such as CH_4, CO_2, or N_2 are generated in the subsurface, samples can become supersaturated with respect to local pressure conditions en route to the surface as the total fluid pressure declines. Furthermore, groundwater temperatures are generally warmer in the subsurface and at discharge locations than at recharge. As a result, groundwater tends to be supersaturated at typical collection points. If groundwater exsolves gas either just before or during sample collection, the phase separation leads to a re-partitioning of gases between the water and the gas phase. The resulting concentrations and relative proportions of dissolved noble gases can be highly altered making it extremely difficult to extract recharge temperature information.

A very useful instrument for assessing such situations is a total dissolved gas pressure probe (Manning et al. 2003). This instrument consists of a semipermeable membrane connected to a pressure transducer. It senses the sum of all dissolved gases and if this pressure is lower than the total fluid pressure at which a sample can be collected, the risk of gas exsolution is minimal. If samples are collected from a well, this probe can be useful for determining whether or not it is possible to pump the sample to the surface and still maintain sufficient backpressure to prevent gas exsolution; if not, a down-hole bailer or diffusion sampler method may be possible. In springs where groundwater is ascending, the probe can be used to determine the depth above which gas exsolution might occur and can likewise guide the selection of sampling methods.

2.1.3 Standard Protocol for Copper Tube Samplers

The sample containers consist of a copper tube which is mounted on an aluminum rack (Fig. 1). On both ends, the tube is held by stainless steel pinch-off clamps, which are used to create a gas-tight seal. Before connecting to the well, it should be assured that the copper tube is well centered in the rack. The ends of the tube sticking out of the rack on both sides are needed for the connections in the field as well as later in the lab. The copper tube also needs to be

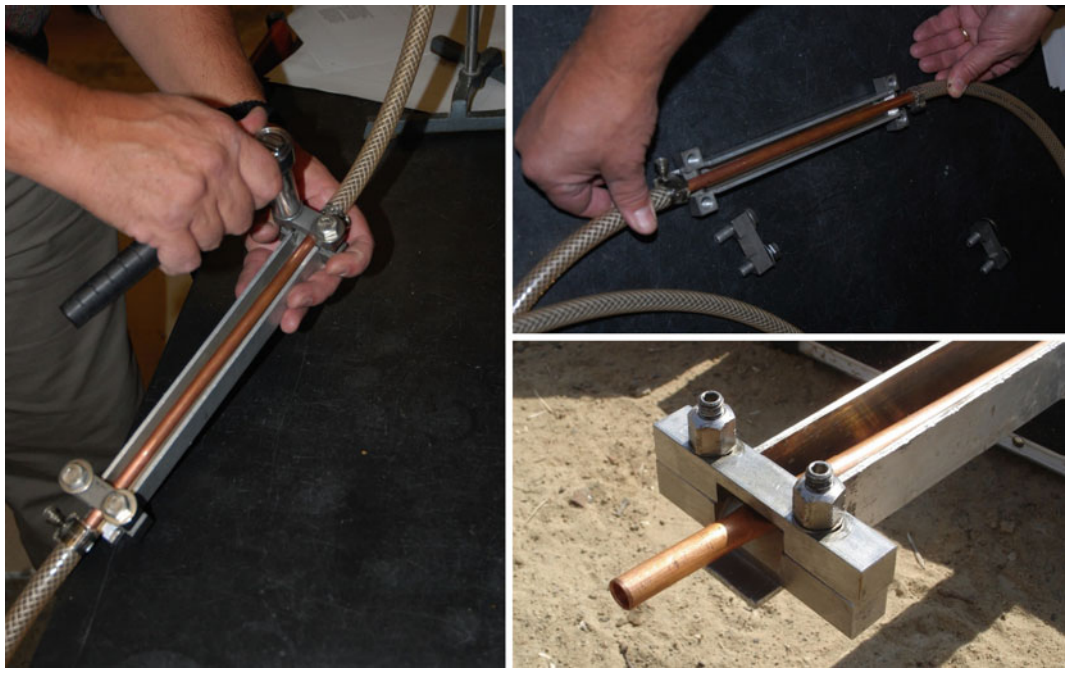

Fig. 1 Copper tube samplers. The picture on the *left* shows the complete sampler with hoses connected on both ends, in the process of closing a clamp. Details of the pinch clamp assembly are visible in the *upper right* photo. A close-up of a pinched-off clamp is shown at the *lower right*

centered in the clamps, to make sure that it can be completely closed. The adjusted copper tube is temporarily fixed in its position by tightening the screws by hand.

The copper tube is connected to the water outlet from the well or pump through flexible plastic tubing. Ideally, a tap near the well head is used. Often, several hoses need to be connected in order to reduce the diameter to the size of the copper tube (Fig. 2a). Unfortunately, suitable well outlets are not always available. For large diameter wells without separate outlet (e.g., agricultural wells in developing countries), a special setup based on fire-fighter equipment can be used, as illustrated in Fig. 2b. A big hose is used to collect all water from the well tube and channel it to a hydrant, where the water flow is split up in a large-volume by-pass flow and a small-diameter tubing for sampling.

The tubing should be tight and strong enough to withstand water pressure, and in order to allow detection of bubbles, at least parts should be transparent. Inner braided PVC tubing has proved to be suitable for this purpose. All connections, also on the copper tube, should be secured with hose clamps (see Fig. 1). In order to safely remove the flushing water and to avoid degassing near the copper tube outlet, it is recommended to attach a tube also at the back end. It is also useful to check that all connections withstand the pressure when the flow is stopped, by squeezing the outlet tube before permanently closing the sampler.

Before sampling, the well should be sufficiently flushed, ideally by pumping several borehole volumes. At least the water standing in the borehole needs to be purged. It is recommended to monitor parameters such as electrical conductivity, temperature, pH and dissolved oxygen during the flushing of the well and start sampling only when these readings have stabilised. The tubing connecting the sampler also has to be flushed and checked for bubbles. Bubbles tend to stick at connections and can be removed by squeezing the hoses or knocking against the tubing. During the whole sampling

Fig. 2 Connection setups for copper tube sampling from wells. Ideally, a plastic tubing of the diameter fitting to the copper tube or only slightly larger is directly connected to a water tap, enabling pressure regulation (*upper left panel*). If only larger diameter outlets are available, multiple hoses (*lower left panel*) or a by-pass construction based on fire-fighter equipment (*right panel*) can be used to reduce the water flow to the sampler. In all pictures, the thin PVC tubing at the end of the installations is eventually connected to the copper tubes. In the *right picture,* surplus water is channeled through the two larger hoses left and right of the sampling connection. Photos by Tim Schneider and Andreas Kreuzer, Heidelberg

procedure, it is recommended to hold the copper tube at a slight upward angle to the horizontal, such that air bubbles can rise along with the water flow and are flushed out of the system. Sometimes, air is sucked in at connections of the tubing, particularly if the diameter of the tubing increases in flow direction. Such configurations should be avoided. Slight leakage of water out of the tubing may be tolerable, but any leakage of air to the inside is prohibitive.

If bubbles form due to gas exsolution from the water, an increase of pressure may help to suppress degassing. A high pressure is generally preferable, limits are set by the stability of the connections. If possible, the pressure should also be regulated such as to avoid noise in the tap or connections, which may indicate turbulence or degassing. Usually, the pressure is fine when the water jet after the copper tube reaches for several meters. If the pressure is low or if it is impossible to avoid bubbles, sampling should be avoided or at least a note should be taken about the adverse sampling conditions.

Once the system is well rinsed, the sample is isolated by first closing the outlet clamp, and then the clamp on the inlet side. If the connections break before the inlet side is closed, the sample is lost and a new copper tube has to be used. The clamps are correctly closed if there is no gap left between their two outer parts. A gas tight seal will occur when the machined gap between the sealing surfaces is the same as the wall thickness of the copper tubing (i.e., two walls are forced together to half of their original thickness). Slight differences in sampler and clamp design exist between different labs, so individual instructions have to be followed. Care should be taken to avoid bending or even

breaking of the outer end-pieces of the copper tubes during sampling and transport. The containers are best packed in boxes, where they can be stacked and fastened.

2.1.4 Passive Diffusion Samplers

Dissolved gases have traditionally been measured using either extraction or equilibrium techniques (Capasso and Inguaggiato 1998). Equilibrium methods have been applied to both the laboratory and field settings. In situ equilibration methods employ the use of a semipermeable membrane that separates and allows for equilibrium between liquid and gas phases. These devices are known as passive diffusion samplers because the dissolved gases must diffuse through the membrane in order to equilibrate with a gas-filled volume (head space).

In order to be used for noble gases, the passive diffusion sampler must have the following attributes. (1) Noble gas samples must ultimately be contained with a material (e.g., metal) that has an extremely low helium permeation rate. Plastics and most glasses will readily exchange light noble gases such as helium. (2) In order to compute the dissolved concentration of a gas using Henry's law, its in situ partial pressure must be known (see Sect. 3). Sheldon (2002) report a system in which gas is ultimately sealed inside copper tubing and the in situ gas pressure is measured with a probe. Gardner and Solomon (2009) report a sampler in which the gas is sealed in nickel tubing and in which the in situ gas pressure can be determined from the pressure inside the sample. Either of these methods makes it possible to utilize passive diffusion samplers for precise noble gas measurements.

Figure 3 illustrates a simple diffusion sampler in which the semipermeable membrane consists of silicone rubber tubing and the sample container is 2 cm long by 4.8 mm OD copper tubing (2 sections of tubing provide a duplicate sample). The sampler is initially filled with air. It is lowered into the well or spring at which time dissolved gases in groundwater diffuse through the silicone tubing and eventually the gas inside the sampler equilibrates with the dissolved gases in groundwater. The sampler remains gas filled as the silicone tubing prevents the permeation of liquid water. The equilibration time depends on the membrane as well as the surface area to volume ratio of the sampler (Sanford et al. 1996). Samplers are typically manufactured such that equilibrium is achieved in about 12 h, but are left in place for 24 h or longer. After equilibration, the sampler is quickly removed from the well or spring, and the copper tubing is sealed with a pinch-off tool before significant re-equilibration with air occurs. In the laboratory, the sample is reopened under vacuum and the gas is expanded into the purification line. The total gas yield is measured with a capacitance (gas independent) manometer, and the subsequent purification and measurement is the same as for conventional copper tube samples.

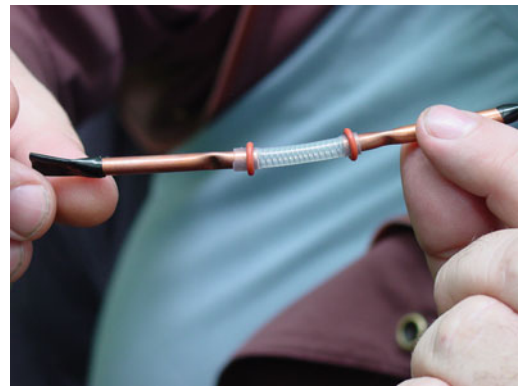

Fig. 3 A simple passive diffusion sampler. Silicone rubber tubing acts as a semipermeable membrane. After equilibration in a well or spring for 24 h, the gas inside the copper tubes is sealed with a pinch-off tool

Some of the general advantages of diffusion samplers are summarized below.

1. Avoids problems associated with the collection of bubbles. This is especially relevant in springs and open boreholes where degassing may not be occurring at the bottom of the spring/bore (and where the sampler can be placed), but where degassing may occur near the surface where the fluid pressure is lower.
2. Small sample size that is easy to ship.
3. Produces gas that usually has a composition that is very close to the air standard used in

most analytical systems; gas extracted from water collected in copper tubes has a composition that is affected by the various solubilities of noble gases and is thus enriched in the heavy noble gases and depleted in the light noble gases relative to an air standard.
4. Laboratory processing time and effort are substantially reduced because the quantitative extraction of gases from water is not needed.

Some of the disadvantages of diffusion samplers include the following.

1. The sampler must be placed inside the well or spring, preferably at the depth of the screen (filter). This is problematic in some public supply wells and when dedicated pumps have been installed.
2. It is necessary to visit the site twice.
3. An accurate in situ temperature measurement must be made in order to convert the measured gas composition and total gas pressure to a dissolved concentration using Henry's law.
4. The simple diffusion sampler illustrated in Fig. 3 requires the in situ measurement of total dissolved gas pressure using a probe. Although probes are commercially available, they are moderately rare and expensive. Furthermore, these probes can sometimes require up to 30 min in the field to equilibrate, and can typically only be submerged to 50 m.

The more advanced diffusion sampler presented by Gardner and Solomon (2009) includes a down-hole valve that can isolate the semipermeable membrane from the sample volume, without altering the pressure inside the sample volume. As a result, the in situ dissolved gas pressure is preserved in this sampler as it is retrieved (the flexibility of the membrane results in a change in internal gas pressure when the simple sampler shown in Fig. 3 is retrieved). This makes it possible to determine the in situ total dissolved gas pressure in the laboratory when the gas is inlet into the process line and thus eliminates the need for an in situ measurement using a probe.

In principle the accuracy and precision of measurements made using in situ diffusion samplers is similar to extraction methods. Gardner and Solomon (2009) compared diffusion samplers with copper tube measurements and found the agreement between the two methods to be within the measurement accuracy of the mass spectrometer (e.g., 1 % for He). Although the diffusion sampler method does depend on the accuracy of the total dissolved gas measurement, Gardner and Solomon (2009) reported a precision of about 0.5 % for the advanced passive diffusion samplers and thus this does not limit the overall precision of the measurement.

2.1.5 Additional Parameters to Measure in the Field

Parameters that can be measured in the field and are very useful for interpreting noble gas data include water temperature, electrical conductivity, dissolved oxygen, and total dissolved gas pressure (TDGP). The collection of samples for the analysis of major ions can also be helpful, especially for provenance studies. The field parameters serve the following functions. First, by monitoring these parameters during well purging, it is possible to evaluate when sufficient water has been removed as indicated by the temporal stability of these parameters. Second, the electrical conductivity can be used to estimate the water salinity, which in turn has a control on the solubility of noble gases; however, in general it is the recharge salinity that is directly used in NGT calculations. Third, parameters such as temperature and TDGP can be essential when using diffusion samplers, as they are needed to convert gas partial pressures to dissolved concentrations using Henry's law. Fourth, dissolved oxygen (DO) can be useful for evaluating the redox state of the water. When the DO value is subtracted from the TDGP, a reasonable estimate of dissolved nitrogen is obtained and this can help evaluate whether or not degassing from excess nitrogen may be occurring.

2.2 Analytical Techniques

The methods used to analyse noble gases from water samples vary in many details between

different laboratories. Fundamental differences are related to the main analytical platform, which ranges from sector field static noble gas mass spectrometry to quadrupole mass spectrometers and even gas chromatographic systems. A comprehensive discussion of these systems and the various techniques for the preparation of gas samples appears impossible here. Several systems have been described in detail in the literature. Therefore, this section only gives a brief overview and points out the relevant original papers.

Most published accounts on analytical systems for noble gases from water samples refer to the measurement of He isotopes and Ne only. The analysis of all noble gases requires some additional steps, but the general setups are similar. Descriptions of systems for He, Ne and ^{3}H based on sector field mass spectrometers have been given by Clarke et al. (1976), Bayer et al. (1989), Jean-Baptiste et al. (1992), and Sültenfuß et al. (2009). The only full treatment of a system designed to measure all noble gases was provided by Beyerle et al. (2000). While sector field mass spectrometers with a high resolution are required to measure ^{3}He, the total abundances of the noble gases can be determined by simpler and cheaper methods. Systems based on quadrupole mass spectrometers have been described by Takahata et al. (1997), Poole et al. (1997), Kulongoski and Hilton 2002, and Stanley et al. (2009). Systems based on gas chromatography, combining the analysis of some noble gases (often Ne and Ar, but in principle all noble gases can be analysed) with other gas tracers such as CFS and SF_6, are in use in some labs (Hofer and Kipfer 2007; Mochalski et al. 2006, 2007).

2.2.1 Extraction of Noble Gases from Water

The determination of NGTs requires accurate measurements of dissolved noble gas concentrations from water samples. Hence, both the amounts of noble gases and water have to be determined. The traditional approach involves sampling water and dissolved gases together in copper tubes, followed by a separation of the two phases, the so-called extraction. The amount of extracted noble gases is then analysed as described in the following. The mass of water is easily obtained for groundwater samples of typically 10–45 ml by weighing the full and empty container. The situation is different when passive diffusion samplers are used. In that case, the phase separation has already taken place in the well, saving the extraction step in the lab but requiring a more complicated calculation of dissolved gas concentrations (see Sect. 3). Here, the classical methods to extract gases from water are described, followed by a discussion of the subsequent procedures used to separate and accurately measure noble gases.

The initial phase separation step is usually performed by vacuum extraction. The copper tubes are connected to some extraction volume which is evacuated before the copper tube is opened by re-squeezing the clamped section. The water flows into the extraction vessel where it is shaken or stirred to facilitate degassing. The vessel is connected to a water trap via a capillary (e.g., 0.5 mm ID by about 25 mm long), such that a flow of water vapour transports the liberated gases to the other side of the capillary, which limits both water vapour flow and gas back diffusion. Various designs for the water trap are in use, e.g., stainless steel traps at liquid nitrogen or dry ice temperature or zeolites at room temperature. Depending on the setup, heavy noble gases may be condensed in the water trap, which then has to be heated later on to release them again. Also the degassing times vary between about 5 and 20 min, but in any case very high extraction efficiencies above 99.99 % can be achieved.

When the extraction is completed, the remaining water in the extraction volume is separated from the gas phase behind the capillary. If required, the degassed water can be transferred into a copper tube or a glass bulb and sealed off again to allow ingrowth of tritiogenic ^{3}He for later ^{3}H determination. The gases above the water trap are expanded or actively transferred into the preparation line for further cleaning and separation before being admitted to the mass spectrometer.

2.2.2 Gas Purification and Separation

As the noble gases are only a minor part of the gases extracted from water, it is necessary to purify the gas mixture in order to remove major components such as N_2, O_2, or CO_2 etc. which could impede the noble gas analysis. Moreover, it is generally preferable to separate individual noble gases before they are analysed in the mass spectrometer, in order to avoid interferences between the different gas components; this is particularly important since the abundance of Ar can be about 30,000 times greater than that of Xe.

After the gas has been dried, it is condensed on one or more cold traps. Charcoal traps at liquid nitrogen temperature or stainless steel traps at even lower temperatures created with cryostatic systems can trap the heavier noble gases Ar, Kr, and Xe. Cryostatic cold traps reaching temperatures below 10 K and filled with activated charcoal can trap even the light noble gases He and Ne (Lott and Jenkins 1984). From such traps, the individual noble gases are then released sequentially, by heating to appropriate temperatures. The different gas fractions are finally expanded to the mass spectrometer, passing by getter pumps to remove reactive gases that may be present.

It is not trivial to achieve complete cryogenic separation of the noble gases, in particular Ar and Kr are hard to separate. To avoid this problem, some laboratories have employed a procedure where Ar, Kr, and Xe are not separated but measured in one fraction (Beyerle et al. 2000). The problem with this approach is the enormous difference in abundance of Ar relative to Kr and Xe. The simultaneous measurement is possible by detecting ^{40}Ar on a Faraday cup and counting the main Kr and Xe isotopes on an ion multiplier. However, it depends on the type and tuning of the ion source whether or not the presence of a large amount of Ar does intolerably disturb the Kr and Xe measurement. Fortunately, recent developments in the field of cold traps and their operation have demonstrated new ways to reliably separate Ar and Kr (Lott 2001; Stanley et al. 2009).

The typical samples of several 10 g of water contain enough Kr and Xe to enable their analysis on a Faraday detector. While this has advantages with regard to the precision of the detection compared to ion counting on a multiplier, the difficulty lies in a reliable separation and purification of these two noble gases in the presence of the large quantities of atmospheric gases (mainly N_2) that are released with them from the trap. Hence, the approach of Beyerle et al. (2000), where only a small split of the Ar, Kr, Xe plus air fraction from a water sample is cleaned, has its advantages even if these gases are not measured in one step. Both the purification of the gas mixture by getters and the separation of the different noble gases on cryotraps is much easier for small amounts of gas.

2.2.3 Analysis of Noble Gas Amounts

The standard procedure for the analysis of the different noble gas fractions is based on static noble gas mass spectrometry. The pure noble gas fractions are admitted to a sector field mass spectrometer, usually with permanent gettering to suppress reactive gases and in particular the H_2 background. Ionisation takes place by electron impact in a gas ion source. The ions of the main isotopes such as ^{4}He, ^{20}Ne, ^{22}Ne, ^{36}Ar, and ^{40}Ar are detected on a Faraday cup. Minor isotopes such as ^{3}He, ^{21}Ne, as well as various Kr and Xe isotopes are often counted by an ion multiplier. While most systems currently in use for noble gas analyses on water have only one detector of each type, modern multi-collector instruments enable the measurement of up to five isotopes simultaneously, which should be useful to improve sensitivity and precision of Kr and Xe analyses. Very useful for precise He isotope analyses are furthermore machines with a split flight tube, enabling the parallel detection of ^{3}He and ^{4}He on the respective detectors.

The measurement of isotope ratios is in general not required for applications of the noble gas thermometer, where the focus lies on gas amounts and concentrations in water derived from them. However, it is recommendable to measure isotope ratios of at least the lighter noble gases. The ^{3}He/^{4}He ratio is useful to identify the origin of non-atmospheric He

(mantle versus crustal He) and in young groundwaters for ^{3}H–^{3}He dating. The $^{20}Ne/^{22}Ne$ and the $^{36}Ar/^{40}Ar$ ratios may be useful to detect deviations from the atmospheric ratios due to diffusive fractionation (Peeters et al. 2003).

A single analysis in static noble gas mass spectrometry consists of a time series of signal (peak height) readings, which is extrapolated back to the time of inlet to correct for pumping and memory effects during the measurement. To determine absolute gas amounts, the final (back-extrapolated) signal of each sample fraction is compared to calibration signals of air aliquots that were prepared in exactly the same way as the samples. Most labs use different sizes of air standards (in the range of 0.1 to several cm^3STP of air) in order to correct for possible non-linearity of the sensitivity of the entire analytic process (preparation, ionisation, and detection). Some labs also use regular measurements of pure gas fractions (so-called fast calibrations) to correct for short-term sensitivity fluctuations. Moreover, it is recommendable to regularly analyse water standards, e.g., air-equilibrated water or replicate samples from some large reservoir, in order to check the long-term stability of the entire system.

The precision of calculated NGTs depends directly on the precision of the dissolved concentrations and hence the gas amounts. For example, at low temperatures the solubility of Xe changes by about 4 % per °C of temperature change. Thus, in principle a relative precision of the Xe concentration of 4 % enables a resolution of 1 °C in noble gas thermometry. However, the uncertainty of the derived NGTs increases if large excess air corrections have to be applied, in particular if the excess air is fractionated, introducing an additional parameter in the inversion used to estimate the equilibration temperature (see Sect. 3). Therefore, a high precision of the noble gas analysis is of central importance and uncertainties of about 1 % or less are desirable. Systems based on sector field mass spectrometers have achieved this precision, e.g., Beyerle et al. (2000) reported uncertainties between 0.3 % for Ar and 1.0 % for Xe. Isotope ratios usually have even lower uncertainties.

Because it is not trivial to achieve a stability that enables so precise measurements with quadrupole mass spectrometers, these systems have traditionally been based on the principle of isotope dilution (Poole et al. 1997; Kulongoski and Hilton 2002). With such systems, similar precisions as with sector field machines have been reached (Kulongoski and Hilton 2002). However, a disadvantage of the isotope dilution method is that it does not allow measurement of isotope ratios, at least for the isotopes that are used as spikes.

Very recently, Stanley et al. (2009) have reported on a system based on static quadrupole mass spectrometry, linked with sophisticated cryostatic techniques for gas separation. With this system they achieved amazingly good reproducibilities for noble gas amounts in water samples, below 1 % for all noble gases and even in the range of only a few ‰ for the heavy noble gases in particular, which are most important for temperature determination. These methods therefore appear promising for future analytical development in the field of noble gas thermometry.

3 Data Reduction and Interpretation

3.1 From Raw Data to Noble Gas Concentrations

Analytical procedures as described in the previous section yield signals (currents, counts) that need to be converted to gas amounts by comparison with the signals of air standards, taking non-linearity and fluctuations of sensitivity into account. The details of these calibration procedures vary from lab to lab and will not be described in detail here. We only note that this conversion is an important and critical step in the determination of noble gas concentrations. In particular, it is important that in this step a reasonable error estimation for the gas amounts (and later concentrations) is made. These uncertainties are crucial input quantities for the calculation of NGTs and other parameters, as

described below. The uncertainty of the calibration usually can be estimated quite well from the reproducibility of air standard measurements. It is also highly recommended to check the error estimates by comparison with the reproducibility obtained from repeated water standard measurements.

The step from gas amounts to concentrations is trivial for the case of complete extraction of the gases from water samples. Only a division of the gas amounts by the mass of water is required. This step is more critical for diffusion samplers, which are filled with gas that has equilibrated in situ with dissolved gases in groundwater. The dissolved gas concentration is calculated using Henry's law:

$$C_i = \frac{p_i}{K_i} = \frac{P_{tot} X_i}{K_i}$$

where C_i is the dissolved concentration of the ith gas, K_i is the Henry's law coefficient (that is a function of temperature and salinity), p_i is the partial pressure, P_{tot} is the total in situ gas pressure, and X_i is the wet volume fraction (or mixing ratio) of gas i in the total gas volume. In the laboratory the "wet" gas (i.e., gas plus water vapor) inside the sampler is expanded into the process line and the pressure is measured with a capacitance manometer. By knowing the volume of the process line and lab temperature, the moles of total gas can be calculated (or calibrated using a gas standard of known amount). After purification the number of moles (n_i) of each measured gas is determined, X_i is then calculated as $X_i = n_i/n_{tot}$. In practice, the process volume often includes a water vapor trap in which case the dry volume fraction ($X_i^d = n_i/n_{tot}^d$) is determined. The relationship between the dry volume fraction (X_i^d) and the wet volume fraction (X_i) is $X_i = X_i^d \cdot (1 - p_{\mathrm{H_2O}}/P_{tot})$, where $p_{\mathrm{H_2O}}$ is the saturated water vapor pressure at the temperature in the well where the sampler equilibrated, and P_{tot} is the total ("wet") pressure inside the sampler; P_{tot} is taken to be equal to the total dissolved gas pressure P_{tdg}, and $p_{\mathrm{H_2O}}$ is computed using a standard empirical equation (e.g., Gill 1982) at the temperature inside the well. Thus, the laboratory gas measurements are converted to dissolved concentrations using one of the two following equations, depending on whether the dry or wet volume fraction is measured.

$C_i = \frac{P_{tdg} X_i}{K_i}$ in the case of a wet volume fraction, or

$C_i = \frac{P_{tdg} X_i^d \left(1 - p_{H2O}/P_{tdg}\right)}{K_i}$ in the case of a dry volume fraction.

In both cases, the Henry coefficient (K_i) pertains to the temperature and salinity inside the well.

3.2 From Concentrations to Noble Gas Temperatures

A variety of techniques exist for estimating noble gas recharge temperatures from measured concentrations. A graphical technique can be utilized by plotting the measured concentrations of two gases against each other and comparing these to the expected concentrations for solubility equilibrium at various temperatures. This approach has already been used in early studies based only on Ar and N_2 (e.g., Heaton and Vogel 1981). Even in the classical study of Mazor (1972), such a plot of Kr versus Xe was given. However, it is usually best to plot Ne versus Xe, as these two gases have the biggest differences in solubility and temperature sensitivity.

Figure 4 shows such a plot, where solubility equilibrium concentrations of Xe versus Ne at various temperatures are shown by the dark "solubility" line. A Ne–Xe plot is useful for determining both recharge temperature and excess air, as the Ne concentration depends mostly on excess air while the Xe concentration depends mostly on temperature. The sub-horizontal lines labeled "excess air" in Fig. 4 represent the addition of various amounts of unfractionated excess air. To estimate the recharge temperatures, measured values of Xe and Ne are plotted on Fig. 4. A line that is parallel to the excess air lines is then drawn through the sample point until it intersects the solubility line. The recharge temperature is then estimated by interpolating this line to the values of recharge temperature as shown in the example

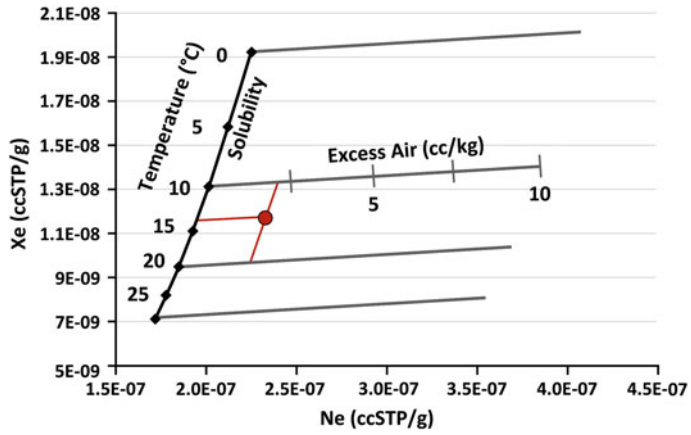

Fig. 4 Xe–Ne plot for graphically estimating recharge temperature and excess air. The example data point is plotted according to the measured concentrations. One *red line* is parallel to the excess air lines and extends to the solubility line. The other *red line* is parallel to the solubility curve and extends to the excess air lines. For this sample the recharge temperature would be about 14 °C with 2 cc/kg excess air

in Fig. 4. The amount of unfractionated excess air can be estimated by interpolating between the solubility line (EA = 0 cc/kg) and the end of the excess air lines (EA = 10 cc/kg for Fig. 4).

An obvious shortcoming of the graphical method is that only the information of two gases is used in any single plot. As usually four atmospheric noble gases (Ne, Ar, Kr, Xe) are available, at least two plots should be drawn. However, the temperature and excess air estimated from these plots may differ, and it is hardly possible to find the best compromise of these estimates in a graphical way. The necessity to find a consistent interpretation of all measured atmospheric gases has led to numerical schemes to determine the NGT. The approach introduced by Andrews and Lee (1979) featured an iterative scheme, where firstly corrections of the measured noble gas concentrations for excess air were performed, and secondly equilibration temperatures for each gas were calculated. This procedure was repeated with increasing excess air corrections, until the variance of the temperatures derived from the different noble gases was minimised. Later, Pinti and van Drom (1998) published a program that performs this iterative correction and minimisation procedure.

One of the shortcomings of the iterative correction method is that is does not provide an objective measure for what constitutes an acceptable agreement between the different noble gas temperatures. This difficulty was solved when, in a curious case of parallel invention, two groups came up with a new approach to perform the separation of noble gas components (Ballentine and Hall 1999; Aeschbach-Hertig et al. 1999). The two fully equivalent algorithms proposed in these papers perform a search for the optimal parameters determining noble gas concentrations in groundwater (equilibration temperature, excess air concentration, fractionation, and other parameters depending on the model, see below). Optimal means that the deviation of the modeled concentrations from the measured ones is minimal. The essential difference of this inverse modeling approach compared to the older iterative method is that now the minimisation goal function uses the deviation from the measured concentrations, with known uncertainties, rather than the variance of the equilibration temperatures obtained from the different gases. One important advantage of this new approach lies in the possibility to use the uncertainties of the measured concentrations as an objective measure of the goodness of the achieved fits.

This measure is provided by the so-called Chi-square test. Chi-square (χ^2) is the sum of the error-weighted deviations between modelled and

measured noble gas concentrations, which is minimised during the model inversion. Assuming that the used model provides a good description of reality, the deviations between the best model fit and the data should be due to analytical errors. Hence, χ^2 should be on the order of magnitude of the number of degrees of freedom (number of constraints, i.e., noble gas concentrations, minus number of free parameters). If the value of χ^2 is high, and the corresponding probability derived from the χ^2-distribution is low, the assumption that the model really describes the processes that created the observed concentrations must be called into doubt. The χ^2-distribution provides an objective measure for how unlikely the observed misfit is, if the model were correct. In practice, a cut-off probability of 1 % has proved reasonable, i.e., fits (or models) with a χ^2-value whose probability is below 1 % should be rejected.

As the procedures introduced by Ballentine and Hall (1999) and Aeschbach-Hertig et al. (1999) are realisations of the general techniques of inverse modelling and parameter estimation, they can make use of various additional features of the theory of non-linear optimisation. One such feature, which constitutes a major advantage of the inverse modelling approach, is that the procedure to find the minimum of χ^2 reveals certain properties of the estimated parameters. Chiefly these are the correlations between parameters and the uncertainties of the best estimates of the parameter values. This information is derived from the covariance matrix of the parameters, which itself is calculated from the uncertainties of the fitted concentrations and the Jacobian matrix (matrix of the derivatives of the model-data deviations with respect to the parameters), which has to be calculated during the minimum search. For mathematical details related to the parameter estimation, the reader is referred to the specialised literature (e.g., Bard 1974; Press 1995).

High correlations between the parameters induce also large uncertainties, because they indicate that two parameters cannot be separated well. A change in one parameter induces a shift of the modelled concentrations, which can be nearly compensated by a suitable change in the other parameter(s). This situation occurs for example when the temperature and air pressure during recharge are treated as free parameters along with the amount of excess air (Aeschbach-Hertig et al. 1999; Ballentine and Hall 1999). This means that it is difficult to estimate NGTs if the recharge altitude (and thus atmospheric pressure) is not known. As a result, noble gas studies in mountainous terrain have to use special procedures and additional constraints to resolve this ambiguity (e.g., Manning and Solomon 2003, 2005).

Of more direct importance than the parameter correlations are their uncertainties, which obviously decide if the derived parameters such as NGT provide meaningful information. The inverse fitting procedure yields objective estimates of these crucial quantities. It can be shown by Monte-Carlo simulations that the error estimates are generally reliable (Aeschbach-Hertig et al. 1999). It should be stressed, however, that the error estimates of the parameters depend directly on the uncertainties of the concentrations that are used as fit targets. Hence it is important to have a good knowledge of analytical uncertainties.

3.3 Estimation of Non-Atmospheric Components

Both He and Ar can be produced in the subsurface and corrections must be applied before using these gases for NGT determination. ^{4}He is produced from the decay of U- and Th-series nuclides, and ^{40}Ar is produced from the decay of ^{40}K. The subsurface production of Ne, Kr, and Xe is small and is usually negligible compared to the atmospheric component (Lehmann et al. 1993). The production of ^{4}He is very common, furthermore its solubility is not very sensitive to temperature, therefore He is generally not used for NGT determination. In general it is only possible to separate subsurface from atmospheric sources of He if an atmospheric only component such as Ne is utilized. Also, the ^{3}He/^{4}He ratio of crustal versus mantle He is vastly different. This, combined with the fact

that ^{3}He can be produced from tritium makes it difficult to utilize the He isotope ratio to correct for the subsurface He component.

The situation is more tractable with Ar if it can be assumed that there is no subsurface production of ^{36}Ar. If the solubility and excess air components of Ar are lumped together as simply Ar_{atm}, and designating R_{atm} as the $^{36}Ar/^{40}Ar$ of atmospheric Ar (0.003378), then the terrigenic (subsurface) component of ^{40}Ar is given by:

$$^{40}Ar_{terr} = {}^{40}Ar_{meas} - {}^{36}Ar_{meas}/R_{atm},$$

where the subscripts terr and meas refer to terrigenic and measured (or total) respectively. This assumes that there is no fractionation between ^{36}Ar and ^{40}Ar from either the solubility equilibrium between the atmosphere and water or from the process of excess air formation. Because the assumption of no subsurface production of ^{36}Ar may be difficult to verify, in practice it is common to compare the measured versus atmospheric ratio of $^{36}Ar/^{40}Ar$ and if the measured ratio is less than 0.003378 (indicating the presence of terrigenic ^{40}Ar), simply exclude Ar from the determination of the NGT.

3.4 Excess Air Models: Historical Development

The reliable estimation of noble gas temperatures depends crucially on the use of a model for dissolved noble gas concentrations in water that describes the processes that determined them correctly or at least in a reasonable approximation. There is generally little doubt that a fundamental part of these processes is equilibration of the water with soil air, with the equilibration temperature being the desired quantity in noble gas thermometry. The exact conditions during this equilibration (composition of the gas phase, total and noble gas partial pressures, salinity of the water) may vary, adding a first difficulty to the temperature determination. Even more complexity stems from the finding that most groundwaters contain an additional component of dissolved atmospheric gases, excess air, which may have atmospheric composition or be fractionated with respect to air. More recently, also the case of a deficit of dissolved gases due to degassing has received some attention.

As discussed in the introduction, the fact that an excess of dissolved noble gases is present in many samples was observed already in the pioneering noble gas studies and the term "excess air" was soon introduced by Heaton and Vogel (1981). But only when noble gas data from groundwater accumulated in the 1980s and 1990s, it began to transpire that the traditional correction of measured noble gas concentrations for atmospheric air did not always yield satisfactory results, i.e., converging equilibration temperatures from the different noble gases. This problem is particularly apparent in samples from semi-arid regions, which often contain large amounts of excess air. A systematic trend in the temperatures derived from Ne to Xe indicated that the usual assumption of an atmospheric composition of the excess air component, the "unfractionated air" (UA) model, could not account for the data.

To resolve this situation, which was evident in their classical record from Brazil, Stute et al. (1995b) introduced a new model for excess air, which later was called the "partial re-equilibration" or PR model. The essence of this model is the assumption that, after initial complete dissolution of trapped air bubbles, the excess air is partially lost through diffusion-controlled gas exchange across the water table. As the light noble gases have higher diffusivities than the heavier ones, they are preferentially lost and the remaining excess of dissolved gases is enriched in the heavy noble gases compared to pure air.

Ballentine and Hall (1999) used their new inverse modeling approach for noble gas evaluation to analyse published groundwater data and highlighted the fact that even the PR model did not provide a satisfactory description of some data sets, in particular the one of Stute et al. (1995b) from Brazil. This critique of the Brazilian record based on objective criteria (Chi-square test, see above) posed a crucial challenge to the noble gas thermometer.

This motivated Aeschbach-Hertig et al. (2000) to propose yet another model for the

formation of excess air, the "closed-system equilibration" or CE model. They could show that it provided an adequate description of previously unexplained samples, including the ones from Brazil. The concept of this model, which assumes that trapped air bubbles do not completely dissolve but reach solubility equilibrium with groundwater at an enhanced hydrostatic pressure, probably dates back to Heaton and Vogel (1981). Stute and Schlosser (1993) also mentioned this possibility. Yet, only Aeschbach-Hertig et al. (2000) provided a complete formulation of the model and, using the newly developed inverse techniques, were able to show that it performed better than other models at least for the investigated data sets. It is also important to note that they could show that the model parameters referring to the amount of initially entrapped air and the hydrostatic pressure that forces its partial dissolution seemed realistic in view of the literature about air entrapment in soils.

These developments motivated research into the processes that lead to the formation of excess air. Experimental and numerical studies (Holocher et al. 2002; Holocher et al. 2003) showed that reality is more complex than any of the simple models can represent. Such results motivated a model assuming a more complex chain of steps forming excess air, the so-called "multi-step re-equilibration" (MR) model (Kipfer et al. 2002). This model builds on the concept of partial diffusive degassing of the PR model, but breaks down the process into many small, physically more plausible steps of gas dissolution and partial re-equilibration. Although more realistic, this model has similar limitations as the PR model in practice. One particularly strong argument against the PR and MR models is the usual absence of diffusive isotope fractionation (Peeters et al. 2003), although the power of this diagnostic has later been put into perspective by a new assessment of the diffusivities of noble gas isotopes in water (Bourg and Sposito 2008).

Albeit the immediate problem highlighted by Ballentine and Hall (1999) was reasonably well resolved by the CE model, new attempts to explain excess air kept popping up in the following years. A completely novel approach was proposed by Mercury et al. (2004). Their so-called "negative pressure" (NP) model built on theoretical calculations of thermodynamic properties of water under various pressure conditions (Mercury et al. 2003). The essential idea is that gas solubilities increase if soil water is in a state of tension (negative pressure) due to capillary forces. Water in small pores within the unsaturated zone therefore dissolves noble gases in excess of the atmospheric equilibrium for free water. If this water can reach the saturated zone without losing its excess, a potential mechanism for excess air creation is provided.

The negative pressure effect does not really add a new component but modifies the equilibrium concentrations. The solubility enhancement increases with mass of the noble gases, which does not conform to the usual excess air pattern, where the relative excess decreases with mass. However, an equilibrium component enhanced by a capillary pressure effect plus normal (unfractionated) excess air produces the typical signature of fractionated excess air, which is enriched in heavy noble gases compared to atmospheric air. Potentially, the capillary pressure parameter in the NP model could itself contain paleoclimatic information, as dry conditions in the unsaturated zone are expected to produce more strongly negative pressures than wet conditions.

The notion that available models (in particular the CE model) yield reliable NGTs was put into question in a noble gas paleotemperature study from Michigan (Ma et al. 2004), which found unusually low NGTs of modern samples compared to present-day mean annual air temperatures. Such a comparison between NGTs and air temperature of young samples has usually been the way to demonstrate the reliability of the calculated recharge temperatures. In most previous paleotemperature studies, a quite good correspondence of NGTs of Holocene samples and modern air temperatures was observed and taken as an indication that the noble gas thermometer worked correctly. However, it would be better to compare NGTs to soil temperatures in the recharge area. Such data are often

unavailable, but then groundwater temperatures of shallow wells may serve as a proxy. It would be interesting to review older studies for such comparisons, but it appears that the finding from Michigan is rather unusual.

The discrepancy between NGTs and air as well as soil temperatures found in Michigan motivated Hall et al. (2005) to propose a new model for the formation of dissolved noble gases in groundwater. This model, called "oxygen depletion" (OD) model, is based on the assumption that the composition of soil air deviates from that of atmospheric air as a result of oxygen consumption. It is well known that soil air can have substantially enhanced mixing ratios of CO_2 due to root respiration. If oxygen is consumed but at the same time replaced by an equivalent amount of CO_2, the noble gas partial pressures should not be changed. However, as already pointed out by Stute and Schlosser (1993), preferential removal of CO_2 by dissolution in water and chemical reactions may deplete the sum of O_2 and CO_2 in soil gas. Such a depletion would have to be compensated by an increase of the partial pressures of the other gases, including the noble gases.

Stute and Schlosser (1993) reasoned that this effect should be small with the possible exception of tropical regions with high biological activity. The rather cold environment of Michigan would thus seem to be an unlikely place to observe this effect, but low dissolved oxygen values in a shallow well later confirmed its presence at the site (Sun et al. 2008). Amos et al. (2005) observed regions of Ar and N_2 depletion as well as enrichment in the unsaturated zone as a result of methanogenesis at a hydrocarbon contaminated site in Minnesota. More measurements of the soil gas composition are certainly desirable for a better assessment of the occurrence of the OD effect.

The OD model, as the NP model, does strictly speaking not address the excess air but the equilibrium component. The equilibrium concentrations are modified by assuming enhanced noble gas partial pressures, equivalent to a higher total gas pressure (or lower recharge altitude). To account for the usual enrichment of light noble gases (Ne excess), the OD model, again as the NP model, combines the modified equilibrium component with unfractionated excess air. Thus, it may be seen as a variant of the UA model with enhanced pressure. As discussed above, it is hardly possible to determine pressure, temperature, and excess air simultaneously due to parameter correlations. This problem can be circumvented by assuming at least one parameter (e.g., the OD overpressure factor) to be the same for all samples in a data set (Hall et al. 2005; Castro et al. 2007).

A refined version of the OD model, the so-called "gas diffusion relaxation" (GR) model was proposed by Sun et al. (2008). This model combines the concept of the OD model (enhanced pressure) with diffusive excess air fractionation similar to the PR model. However, in contrast to the PR model, the diffusion process limiting re-equilibration is assumed to take place in the gas phase rather than in the water. This assumption is motivated by the fact that effective diffusion in the gas phase becomes inefficient if the air-filled porosity is very small, as should be the case near the water table. It has the advantage of avoiding strong isotope fractionation, whose absence speaks against the PR model (see above).

In recent years, several studies using noble gases and the ^3H–^3He dating method have encountered conditions where noble gases are depleted rather than enriched compared to atmospheric equilibrium (Lippmann et al. 2003; Thomas et al. 2003; Klump et al. 2006; Stute et al. 2007; Visser et al. 2007; Cey et al. 2009; Blaser et al. 2010). Such degassing can be explained by the formation of a gas phase in the subsurface, as a result of gas producing processes such as denitrification or methanogenesis (Blicher-Mathiesen et al. 1998; Fortuin and Willemsen 2005). The resulting noble gas patterns have not yet been studied in similar detail as those resulting from excess air. Aeschbach-Hertig et al. (2008) have discussed some possible models to describe degassing. They pointed out that the concept of the CE model also applies to situations where dissolved gases partition into gas bubbles, and that this model performs better than other plausible models based on diffusive degassing.

Table 1 Models for dissolved atmospheric noble gas concentrations in groundwater

Model	Equation	Parameters	Reference
EQ	$c_{iw}^{eq}(T,S,P) = \frac{c_a(T,P)}{H_i(T,S)} = \frac{(P-p_{H2O})x_i}{RTH_i(T,S)}$	T, S, P	Solubility equilibrium
UA	$c_{iw}^{UA} = c_{iw}^{eq} + Ac_{ia} = c_{iw}^{eq}(1 + AH_i)$	T, S, P A	Andrews and Lee (1979)
PR	$c_{iw}^{PR} = c_{iw}^{eq}\left(1 + AH_i \cdot \mathrm{e}^{-F_{PR}\left(\frac{D_i}{D_{Ne}}\right)^{\beta}}\right)$	T, S, P A, F_{PR}	Stute et al. (1995b)
MR	$c_{iw}^{MR} = c_{iw}^{eq}\left(1 + AH_i \cdot \sum_{k=1}^{n} \mathrm{e}^{-kF_{MR}\left(\frac{D_i}{D_{Ne}}\right)^{\beta}}\right)$	T, S, P A, F_{MR}, n	Kipfer et al. (2002)
PD	$c_{iw}^{PD} = c_{iw}^{eq}(1 + AH_i) \cdot \mathrm{e}^{-F_{PD}\left(\frac{D_i}{D_{Ne}}\right)^{\beta}}$	T, S, P A, F_{PD}	Lippmann et al. (2003)
CE	$c_{iw}^{CE} = c_{iw}^{eq}\frac{1+AH_i}{1+BH_i} = c_{iw}^{eq}\left(1 + \frac{(1-F_{CE})AH_i}{1+F_{CE}AH_i}\right)$	T, S, P A, B or F_{CE}	Aeschbach-Hertig et al. (2000)
NP	$c_{iw}^{NP} = c_{iw}^{eq,NP}(T,S,P,P_c) + Ac_{ia}$	T, S, P, P_c A	Mercury et al. (2004)
OD	$c_{iw}^{OD} = c_{iw}^{eq}P_{OD} + Ac_{ia} = c_{iw}^{eq}(P_{OD} + AH_i)$	T, S, P, P_{OD} A	Hall et al. (2005)
GR	$c_{iw}^{GR} = c_{iw}^{eq}\left(P_{OD} + AH_i \cdot \mathrm{e}^{-F_{GR}D_i^{\beta}}\right)$	T, S, P, P_{OD} A, F_{GR}	Sun et al. (2008)

3.5 Excess Air Models: Equations

In the following, a summary of the equations of the excess air (or more generally dissolved atmospheric gas) models for groundwater is given. The model equations and parameters are further listed in Table 1. Illustrations of the main mechanisms assumed in the various models are given in Fig. 5. The notation used in this summary follows Aeschbach-Hertig et al. (2008). Indices i refer to the different noble gases (i = He, Ne, Ar, Kr, Xe). All concentrations (in gas: c_{ig}, in water: c_{iw}) are given in molar units (mol/l). The Henry coefficients H_i are dimensionless. Model parameters are given in capital letters, common parameters are:

T equilibration temperature (NGT),
S salinity of the water,
P total atmospheric pressure at recharge,
A volume ratio of dissolved (or trapped) air to water, dimensionless,
F fractionation parameter (subscript referring to model), dimensionless

(A) Basic quantities and relationships

(A1) Henry's law

Gas solubility in water is central to the noble gas thermometer and expressed by Henry's law in various forms. Following the above conventions, it reads:

$$c_{ig} = H_i(T,S)c_{iw}$$

This differs from the form used above in the discussion of the gas concentrations in diffusion samplers. There, another common form of Henry's law was used:

$$p_i = K_i(T,S)C_i$$

where p_i is the partial pressure of gas i in the gas phase and C_i denotes its concentration in water (in any concentration units). K_i is the Henry coefficient in the respective units. If molar concentration units in the water are used, the two forms of the Henry coefficient are related by $K_i = RTH_i$, with the universal gas constant R. The gas solubilities, i.e., the Henry coefficients

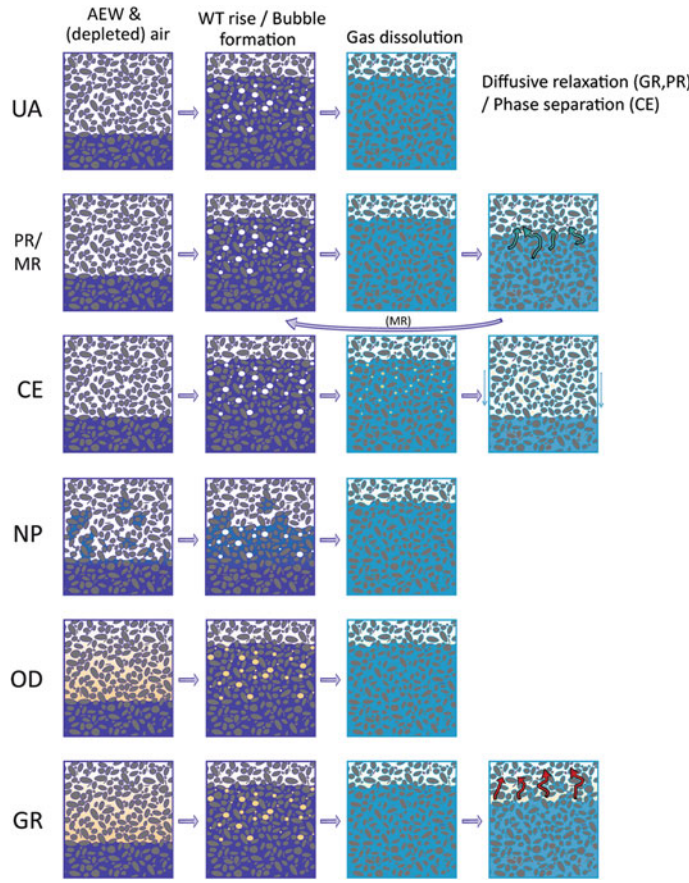

Fig. 5 Schematic illustration of the processes assumed in the various excess air models

H_i or K_i in dependence of T and S, have been determined in numerous studies, e.g., Weiss (1970, 1971), Weiss and Kyser (1978), Wilhelm et al. (1976), Benson and Krause (1976), Smith and Kennedy (1983), Top et al. (1987), and Hamme and Emerson (2004).

(A2) Concentrations of noble gases in air

Since the constant and well-known atmospheric mixing ratios x_i of the noble gases refer to dry air, a correction for water vapor has to be made when calculating the molar noble gas concentrations in air. For the equilibration of water with air, the vapor pressure immediately above the water surface is relevant, which can be assumed to correspond to the saturation water vapor pressure p_{H_2O}. Thus one obtains:

$$c_{ia}(T,P) = \frac{(P - p_{H_2O})x_i}{RT}$$

(A3) Atmospheric equilibrium concentrations

The equilibrium values represent a component of the total dissolved concentrations that is common to all models, except for modifications indicated below.

$$c_{iw}^{eq}(T,S,P) = \frac{c_a(T,P)}{H_i(T,S)} = \frac{(P - p_{H_2O})x_i}{RTH_i(T,S)} = \frac{(P - p_{H_2O})x_i}{K_i(T,S)}$$

See Kipfer et al. (2002) for further details of the calculation of equilibrium concentrations from the solubility data.

(B) Concentrations of Dissolved Atmospheric Noble Gases

(B1) Unfractionated excess air (UA) model

This model has been used traditionally, often without explicit formulation of a model

equation. Following the conventions given above, the model equation reads (compare Aeschbach-Hertig et al. 2008):

$$c_{iw}^{UA} = c_{iw}^{eq}(1 + AH_i)$$

Alternatively, this basic model has frequently been expressed by a dimensional excess air concentration parameter (air amount per water mass or volume, here called A') and the noble gas mixing ratios in air (x_i). This formulation, expressed with molar concentrations, reads (e.g., Aeschbach-Hertig et al. 2000):

$$c_{iw}^{UA} = c_{iw}^{eq} + A'x_i \quad \text{with} \quad A' = A\frac{P - p_{H_2O}}{RT}$$
$$\text{and} \quad A'x_i = Ac_{ia}$$

The advantage of the first equation is that it explicitly shows the proportionality of the equilibrium and excess air components, which both depend linearly on the atmospheric mixing ratios x_i.

(B2) Partial re-equilibration (PR) model

This model has been introduced by Stute et al. (1995b), we use a generalization of the formulation given by Aeschbach-Hertig et al. (2008):

$$c_{iw}^{PR} = c_{iw}^{eq}\left(1 + AH_i \cdot e^{-F_{PR}\left(\frac{D_i}{D_{Ne}}\right)^{\beta}}\right)$$

The parameter F_{PR} expresses the degree of excess air loss due to re-equilibration. D_i are the diffusion coefficients of the noble gases in water. The exponent β is a model parameter from the theory of gas transfer, which in principle can vary between 0.5 and 1 (compare Aeschbach-Hertig et al. 2008). However, the original formulation of Stute et al. (1995b) only considered the case of $\beta = 1$, which corresponds to a stagnant film gas transfer model and seems appropriate for a turbulence-free situation in groundwater.

(B3) Multi-step partial re-equilibration (MR) model

This model was formulated by Kipfer et al. (2002), in our notation it reads:

$$c_{iw}^{MR} = c_{iw}^{eq}\left(1 + AH_i \cdot \sum_{k=1}^{n} e^{-kR_i}\right)$$
$$= c_{iw}^{eq}\left(1 + AH \cdot e^{-R_i}\frac{1 - e^{-nR_i}}{1 - e^{-R_i}}\right);$$
$$R_i = F_{MR}\left(\frac{D_i}{D_{Ne}}\right)^{\beta}$$

The additional parameter n compared to the PR model represents the number of partial degassing steps. It can be set to infinity as a limiting case of the model ($n = 1$ corresponds to the PR model).

(B4) Partial degassing (PD) model

This is the first degassing model, which conceptually resembles the PR model, except that here diffusive gas loss affects the total gas concentration rather than only the excess air component. The concept and equations referring to gas loss relative to solubility equilibrium can be traced as far back as Zartman et al. (1961). If it is considered that excess air may be present before degassing, it can be formulated as follows (compare Aeschbach-Hertig et al. 2008):

$$c_{iw}^{PD} = c_{iw}^{eq}(1 + AH_i) \cdot e^{-F_{PD}\left(\frac{D_i}{D_{Ne}}\right)^{\beta}}$$

A value of $\beta = 0.5$ has been used by Lippmann et al. (2003).

(B5) Closed-system equilibration (CE) model

This model was introduced by Aeschbach-Hertig et al. (2000) and reformulated by Aeschbach-Hertig et al. (2008). The two formulations can be written as:

$$c_{iw}^{CE} = c_{iw}^{eq}\frac{1 + AH_i}{1 + BH_i} = c_{iw}^{eq}\left(1 + \frac{(1 - F_{CE})AH_i}{1 + F_{CE}AH_i}\right)$$

It is important to note that the parameter A in this model has a different meaning than in the other models. It refers to air that is entrapped in the groundwater in the recharge zone, rather than air that is actually dissolved in the water. Only a fraction of this entrapped air is dissolved,

as can be deduced from the final trapped gas to water volume ratio B or alternatively the fractionation factor $F_{CE} = B/A$. Further note that the model describes excess air for $F < 1$ and degassing for $F > 1$.

(B6) Negative pressure (NP) model

In the NP model, proposed by Mercury et al. (2004), the Henry constant and hence the equilibrium component is modified due to (potentially negative) capillary pressure P_c in the unsaturated zone:

$$c_{iw}^{eq,NP}(T,S,P,P_c) = \frac{(P - p_{H_2O})x_i}{K_i(T,S,P_c)}$$

Equations and constants for the calculation of the Henry coefficients (in the form of $k_H = f/X$, with fugacity f and aqueous mole fraction X) as a function of P_c are given in Mercury et al. (2003). The final concentrations according to the NP model include an unfractionated excess air (UA) component and are given by

$$c_{iw}^{NP} = c_{iw}^{eq,NP} + A'x_i = c_{iw}^{eq,NP} + Ac_{ia}$$

(B7) Oxygen depletion (OD) model

Similar to the NP model, the OD model, proposed by Hall et al. (2005), includes a modification of the equilibrium component, this time simply by a constant factor that has usually been called P_{OD} (Sun et al. 2008; 2010), plus an unfractionated excess air component:

$$\begin{aligned} c_{iw}^{OD} &= c_{iw}^{eq}P_{OD} + A'x_i = c_{iw}^{eq}P_{OD} + Ac_{ia} \\ &= c_{iw}^{eq}(P_{OD} + AH_i) \end{aligned}$$

The factor P_{OD} originates from the increase of noble gas partial pressures in soil air to compensate for oxygen depletion. It is equivalent to an increase of the atmospheric pressure parameter P by this factor. As a maximum of 21 % of O_2 in soil air has to be replaced, P_{OD} is limited to the range $1 \leq P_{OD} \leq 1.26$.

(B8) Gas diffusion relaxation (GR) model

Sun et al. (2008) introduced a modification of the OD model, that resembles the PR model and can be written as:

$$\begin{aligned} c_{iw}^{GR} &= c_{iw}^{eq}P_{OD} + A'x_i \cdot \mathrm{e}^{-F_{GR}D_i^{\beta}} \\ &= c_{iw}^{eq}\left(P_{OD} + AH_i \cdot \mathrm{e}^{-F_{GR}D_i^{\beta}}\right) \end{aligned}$$

Here in contrast to the models discussed above, the diffusion constant D_i of gas i refers to the gas phase diffusion in the unsaturated zone. For the gas transfer parameter β, Sun et al. (2008) tested the values 0.5, 2/3, and 1, preferring the middle value on the grounds of best achieving the expected temperature.

3.6 Excess Air Models: Discussion

In summary, at present a large number of models to describe the concentrations of dissolved noble gases in groundwater are available. A first comparison of the performance of some of these model has been provided by Sun et al. (2010). Maybe the most important result of such a comparison is that, while systematic offsets of NGTs and excess air parameters occur between the models, the temperature differences within data sets consistently interpreted with various models agree remarkably well. It follows that conclusions on past temperature changes from noble gas records are quite robust, if all samples of a data set are evaluated with the same model. It is therefore of prime importance not to mix different models when reconstructing paleotemperature records, as this might introduce artificial offsets.

Nevertheless, the current situation is somewhat unsatisfactory. Clearly, many models can be found that provide reasonable fits to four atmospheric noble gas concentrations with three or even more free parameters. The question should not be which model provides the best fit, but which provides accurate information on physically realistic model parameters, such as NGT and the amount of entrapped or dissolved air. Further research is therefore called for, in order to investigate which of the models provide physically realistic descriptions of the underlying processes and unbiased estimates of NGT and the other parameters.

Recent experimental and numerical studies on excess air provided some insights in this

regard. Sprinkling experiments showed that excess air was produced by partial dissolution of entrapped air at a field site with fine-grained sediments, whereas the seepage water simply equilibrated with soil air at the local temperature at a site with coarse sand and gravel (Klump et al. 2007). A laboratory experiment with a sand column in combination with numerical modeling of the process of bubble dissolution showed that the assumption of local equilibrium between water and entrapped gas is reasonable (Klump et al. 2008a). As the column was continuously flushed with equilibrated water, the produced excess air signature varied over time but interestingly often approached the predictions of the simple UA model, even as bubbles were still present.

Although the actual excess air compositions in the experiments of Klump et al. (2008a) did not exactly conform to any of the available excess air models, the CE model often provided acceptable fits. However, the authors cautioned that the fitted excess air parameters may not be realistic, in particular in field situations affected by mixing of waters that reflect different phases of the process of excess air formation. In contrast, the CE model seemed to provide reasonable estimates of the equilibration temperatures and also of the hydrostatic pressure driving bubble dissolution. In a study of a sandstone aquifer system in England, Ingram et al. (2007) had previously arrived at the same conclusion that NGTs and hydrostatic pressures derived from the CE model were realistic.

In principle, detailed numerical modeling of the dynamics of the soil gas—groundwater interaction is required to fully account for the dissolved noble gas concentrations in groundwater, as attempted by Holocher et al. (2003) and Klump et al. (2008a). In addition to modeling the kinetics of bubble dissolution, also the reactive gas transport in the unsaturated zone and the dispersive transport in the saturated zone should be included. Although possible (e.g., compare Amos and Mayer 2006), such a model would certainly contain too many free parameters to be constrained by noble gas data alone. Clearly, reality is more complex than the current "lumped-parameter" type excess air models can describe. Even such elementary processes as mixing of waters with different recharge conditions are not captured. Nevertheless, the simple models have their justification as tools for the interpretation of noble gas data.

A good model should provide a simplified but still in essential respects realistic depiction of the physical processes that lead to excess air as well as degassing. From this point of view we think that the concept of equilibration between groundwater and a trapped gas phase, i.e., the CE model, is a reasonable approach. There may be situations where other models apply, but the prevalence of conditions that enable e.g., diffusive gas loss, strongly negative capillary pressures, or significantly enhanced noble gas partial pressures requires further demonstration.

On the other hand, Sun et al. (2010) showed that the CE model does not always provide an unbiased estimate of NGT. It is true that the CE equations exhibit a certain instability in numerical fit routines and sometimes clearly unphysical solutions with very high values of the parameter for initially entrapped air (A) are obtained. Such solutions, which can be identified by high temperature errors and parameter correlations, should clearly be discarded. Apart from such anomalies, however, the CE model has proven reliable in our experience.

3.7 From Noble Gas Temperatures to a Climate Record

Even if a model has been found that provides good fits to the measured noble gas concentrations and hence enables the formal calculation of NGTs, two issues remain to be addressed before a paleoclimate record is obtained. The first is the question what the derived parameters, in particular the NGT, really measures, i.e., whether and how the proxies can be translated to climate parameters. The climate parameter that one usually wants to reconstruct is the mean annual air temperature (MAAT), which is not identical to the recharge temperature of groundwater. The second issue is the necessity of a good

chronology for the record, including an assessment of smoothing due to mixing, which is always present in groundwater. Stute and Schlosser (1993) have provided a rather comprehensive discussion of these issues, and in fact applied studies have generally relied on their conclusions. Only in recent years have new studies been published that reassess some of the assumptions underlying noble gas paleotemperature records.

3.7.1 Relationship of NGT with Soil and Air Temperature

In concept the noble gas concentrations in groundwater record the temperature and pressure (elevation) at the water table. Stute and Schlosser have provided evidence from several sites that NGTs closely reflect the mean annual ground temperature at the water table (WTT). Klump et al. (2007) showed that NGTs determined from infiltrating soil water at different depths were identical to the corresponding in situ soil temperatures.

Nevertheless, the actual correspondence of NGT and WTT in each case study may depend on the choice of the appropriate noble gas model. If the WTT in the recharge area is known, a comparison with NGTs from young samples may decide the choice of model. Unfortunately, only few studies contain WTT information and explicit comparison with NGT. Castro et al. (2007) have claimed that the OD model stands this test, whereas older, widely used models do not. In contrast, a recent study that contained a detailed comparison of shallow groundwater temperatures (as a surrogate for WTT) and NGTs found no significant bias from using the CE model (Kreuzer et al. 2009). A comprehensive field study conducted by Cey et al. (2009) found good agreement of WTT and NGT derived from the common UA, PR, and CE models.

A reason for disagreement between the real WTT and that inferred from noble gas concentrations may be undetected degassing of the groundwater. In the study of Cey et al. (2009), about 20 % of the samples showed obvious degassing, i.e., Ne concentrations below atmospheric equilibrium, which was explained by gas stripping as a result of denitrification at the agricultural study site. The obviously degassed samples can be either discarded in the analysis or maybe evaluated by an appropriate model. More problematic is the possibility that minor degassing in other samples may be masked by excess air. A modeling experiment demonstrated that a wrong interpretation of such samples, not accounting for weak degassing, could lead to an underestimation of WTT by up to 2 °C.

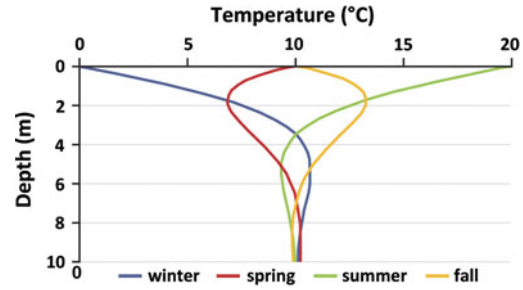

Fig. 6 Simulated soil temperatures in a temperate climate. The mean annual temperature is 10 °C and the air temperature varies from 0 to 20 °C. The dampening of the surface temperature with depth is controlled mostly by the thermal diffusivity, which in turn is a function of the water content and to a lesser extent the mineralogy of the soil. When the water table is more than 10 m below land surface, the annual temperature variations are nearly completely dampened for a typical thermal diffusivity of 0.005 cm^2/s

Even if the equivalence of NGT and WTT is given, the question of the climatological significance of WTT remains. In a conceptually simple system, WTT is assumed to be equal to the soil temperature at a given depth. Soil temperatures vary with depth and time and are frequently modeled using a sinusoidal temperature variation at the land surface through time, along with an extinction in the amplitude of these variations with depth (Hillel 1980). Figure 6 shows simulated temperature versus depth curves for four different seasons in an area with a temperate climate. The mean annual soil temperature (MAST) at the surface in this example is 10 °C with a seasonal fluctuation of 0–20 °C. The attenuation of the seasonal variation with depth depends mostly on the thermal diffusivity, which in turn is a function of the water content and to a lesser extent the mineralogy of the soil.

As shown in Fig. 6, the annual temperature variations at the surface are nearly completely dampened at a depth of 10 m. When the depth to the water table is greater than 10 m, the WTT (and, by inference the NGT) should be similar to the MAST at the surface in this conceptually simple example. However, when the water table is shallow, there could be a range of possible recharge temperatures. If recharge at the water table is continuous throughout the year, hydrodynamic dispersion will tend to mix waters towards the concentrations associated with the mean annual temperature.

Several studies (Stute and Schlosser 1993; Klump et al. 2007; Cey et al. 2009) have shown that the simple model described above can be a reasonable representation of real systems. Stute and Schlosser (1993) discussed the temporal behaviour of soil temperatures and showed that WTT can be expected to be very close to MAST at the surface, unless the water table is very deep, such that the geothermal gradient enhances WTT significantly.

The correspondence between WTT and MAST is presumably a rather robust assumption in the chain relating NGT to mean annual air temperature (MAAT). More critical is the relationship between surface soil and air temperatures (MAST vs. MAAT). There are numerous potential scenarios in which MAAT recorded by weather stations and MAST (or WTT) are not the same. Already Smith et al. (1964) found that generally MAST is slightly (about 1 °C) warmer than MAAT, but significant deviations occur under various soil cover conditions.

Temperature profiles in boreholes have been used to evaluate changes in the land surface temperature over the past several hundred years (e.g., Lachenbruch and Marshall 1986; Harris and Chapman 2001). The extrapolation of borehole temperatures to land surface frequently shows an offset with the meteorological record. For example, Fig. 7 (from Powell et al. 1988) shows the extrapolated borehole temperature at various elevations versus the elevation of land surface. Also shown is the same relationship for the MAAT record from weather stations. While the lapse rate (slope) for the borehole and

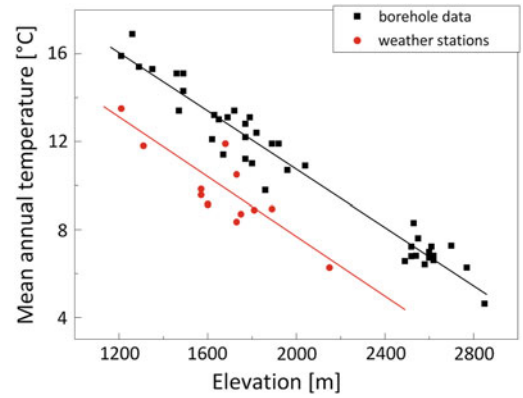

Fig. 7 Mean annual temperature from weather stations (*red circles*) and borehole data extrapolated to the land surface (*black squares*) versus elevation. While the lapse rates (lines fitting the data) have nearly identical slopes, they are offset by about 2.5 °C. Redrawn from Powell et al. (1988)

weather station data are nearly identical, they are offset by about 2.5 °C. Powell et al. (1988) attributed this offset to solar radiation heating the land surface. This effect may be particularly important in warm and arid regions. Beyerle et al. (2003) found that modern NGTs and shallow groundwater temperatures (both presumably indicating WTT and MAST) in the very warm, semi-arid, and sparsely vegetated Sahel zone in Niger were several °C warmer than air temperatures.

Other factors that influence the land surface temperature include snow cover, slope aspect (angle to the sun), and vegetative cover. Bartlett et al. (2004) concluded that snow cover can produce either a warming or cooling effect on the mean temperature of land surface of about ±1 °C. This is due primarily to an insulating effect of the snow that effectively truncates portions of the annual air temperature variations with respect to land surface. Cey (2009) performed detailed modeling of the relationship between WTT and MAAT, and found the strongest and quite significant decoupling during periods of snow cover. Both slope angle and vegetative cover can change the albedo and hence influence the absorption of solar radiation. Additionally, the latent heat associated with evapotranspiration plays an

important role in the energy budget of the land surface. In total, it seems possible that the MAST may deviate from the MAAT measured by weather stations by ± about 2 °C. It further seems likely that such an offset could exist at the water table, but additional field studies under various conditions (snow cover, slope aspect, vegetation, etc.) are needed.

Even if the offset between WTT (or NGT) and MAAT may be estimated for current conditions in the recharge area, a further problem lies in the possibility that this relationship may have changed in the past, due to different climate and thus soil cover (vegetation, snow) conditions (Beyerle et al. 2003; Cey 2009). This problem certainly deserves more attention in future applications of the noble gas thermometer. For example, a recent study from Belgium supports the notion that NGTs close to the freezing point, found in periods around the last glacial maximum, may overestimate actual air temperatures at the time due to the insulating effect of snow cover (Blaser et al. 2010). It is worth noting that paleotemperature reconstructions based on borehole temperatures face essentially the same problem, i.e., that soil temperatures may have changed independently of air temperatures (e.g., Kooi 2008; Mann et al. 2009).

3.7.2 Chronologies for NGT Records

The last but certainly not least difficulty in deriving noble gas paleotemperature records from the groundwater archive is to obtain a reliable time scale. Most studies so far have covered the range of several ten thousand years, in which ^{14}C is the only quantitative dating tool available. The difficulties of radiocarbon dating of groundwater are well-known and a full account of this topic lies far beyond the scope of this article, instead we refer the interested reader to the reviews provided by Kalin (2000) and Geyh (2000). It should also be noted that a recent paleoclimate study from groundwater made use of the paleotemperature information provided by the noble gases to constrain the modeling of past recharge conditions with the aim of improving the ^{14}C dating (Blaser et al. 2010). Thus, NGTs may be used to support ^{14}C dating, rather than only using the ^{14}C ages as a chronology for NGTs.

Even if reliable groundwater ages can be estimated, the problem remains that these can only be mean groundwater transit times, not unique ages of an isolated water sample from a well-defined infiltration event. Dispersion is a natural process in aquifers, and long well screens can further increase the width of the age distribution of the sampled water. These processes will inevitably lead to a smoothing of climate signals contained in groundwater, as discussed by Stute and Schlosser (1993). As a result, the noble gas thermometer applied to groundwater can only provide information on long-term climate changes, similar to reconstructions derived from borehole temperatures. The decisive advantage that makes such low-resolution records attractive nonetheless is that NGTs are independent, physically based and absolute paleotemperatures, which can be compared to the important climate proxy provided by the stable isotopes of the water.

The restriction of low temporal resolution for the noble gas thermometer may be overcome if other archives than groundwater can be made accessible. One such potential archive for the method is pore water in sediments, another option is water trapped in fluid inclusions in minerals. Both systems are discussed in other chapters of this book. Most interesting for paleoclimate reconstruction are probably fluid inclusions in speleothems, as cave deposits constitute a well-datable and increasingly exploited archive. Considerable advances towards using this archive have been made in recent years (Kluge et al. 2008; Scheidegger et al. 2010), but the challenge to develop this approach into a routine method of paleoclimate research remains large.

4 Applications

4.1 Paleotemperature Reconstruction

The reconstruction of paleotemperature records from groundwater is clearly the most straightforward and important application of the noble

gas thermometer. In the following, a brief historical overview of such studies is given, before some recent results are discussed in some more detail.

4.1.1 Historical Overview

Many studies assessed the temperature difference between the Holocene and the preceding LGM or earlier parts of the last glacial period based on the noble gas thermometer. Most studies have been conducted at temperate northern latitudes in Europe and North America. A typical result of these studies has been a Holocene—glacial temperature difference of about 5 °C (Andrews and Lee 1979; Andrews et al. 1985; Phillips et al. 1986; Blavoux et al. 1993; Stute et al. 1995a; Dennis et al. 1997; Beyerle et al. 1998; Clark et al. 1998; Ma et al. 2004; Zuber et al. 2004; Zhu and Kipfer 2010). Only in more recent years, this finding has been confirmed also for East Asia (Edmunds et al. 2006; Kreuzer et al. 2009). As the classical study of Andrews and Lee (1979), however, some of these studies may be affected by a recharge gap during the coldest period of the LGM, indicating that the maximum cooling was higher than 5 °C. Such recharge gaps may be due to permafrost (Beyerle et al. 1998) or very arid conditions during the LGM (Kreuzer et al. 2009).

Several studies from temperate northern latitudes seem to have obtained complete records with a higher Holocene–LGM temperature difference of between 7 and 10 °C (Stute and Deák 1989; Kloppmann et al. 1998; Aeschbach-Hertig et al. 2002b; Klump et al. 2008b; Varsányi et al. 2011). Remarkably, a recent study of this kind, derived from an aquifer in Belgium (Blaser et al. 2010), reported a glacial cooling of 9.5 °C but also indications for the presence of a recharge gap due to permafrost, thus indicating that the maximum cooling in this region was even larger.

Another large group of noble gas paleotemperature studies has focused on tropical and subtropical regions (Heaton et al. 1986; Stute et al. 1992; 1995b; Andrews et al. 1994; Clark et al. 1997; Stute and Talma 1998; Edmunds et al. 1999; Weyhenmeyer et al. 2000; Beyerle et al. 2003; Kulongoski et al. 2004, 2009). Quite remarkably, these studies also generally found a Holocene–LGM temperature difference of close to 5 °C. This result has received significant attention in the paleoclimate community, as it helped to address the question whether or not the tropics were significantly cooler in glacial times (e.g., Broecker 1996; Farrera et al. 1999; Crowley 2000).

Naturally, the noble gas paleothermometer can also be applied to other time scales than the usual Holocene–LGM—late glacial period. Some studies have dealt with much older groundwaters (Beyerle et al. 1999b; Lehmann et al. 2003; Pinti et al. 1997; Lavastre et al. 2010). It has proven difficult to construct reliable temperature records on these long time scales, partly because of the lack of a good dating tool. In fact, Pinti et al. (1997) and Lavastre et al. (2010) have conversely made use of the NGT information as an indication of groundwater age, by comparing NGTs with independent paleoclimate records. Only recently, it has been attempted to use the noble gas method on the shorter time scale of the past millennium, where ^{39}Ar has the potential to provide a very good chronology (Corcho Alvarado et al. 2009).

4.2 Excess Air as a Proxy for Paleohumidity

Another line of research focuses on the potential of the size of the excess air component, usually measured by the relative Ne excess ΔNe, as a climate proxy, following the suggestions of Heaton and Vogel (1981) and Heaton et al. (1983). Wilson and McNeill (1997) provided a systematic analysis of excess air data with regard to lithology, temperature, and precipitation, showing that the latter relationship may be more complex than expected. The hypothesis of Heaton et al. (1983) of high excess air in wet climate phases was supported and refined by the study of Stute and Talma (1998) from the same aquifer in Namibia, which suggested a peak in ΔNe during the transition to a wet phase, related to an increase of the groundwater table.

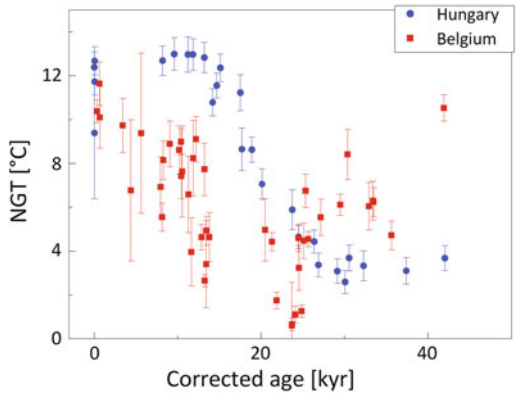

Fig. 8 Two recent European noble gas temperature (NGT) records from Hungary (Varsányi et al. 2011) and Belgium (Blaser et al. 2010) in comparison

Aeschbach-Hertig et al. (2002a) discussed the notion of excess air as a climate proxy in the light of the newly introduced CE model. They suggested that ΔNe is essentially a measure of the amplitude of water table fluctuations in the recharge area. This interpretation has consequently been supported and applied by a number of studies (Beyerle et al. 2003; Kulongoski et al. 2004, 2009; Ingram et al. 2007; Manning and Caine 2007; Klump et al. 2008b; Osenbrück et al. 2009; Zhu and Kipfer 2010). It also seems to be consistent with the findings of laboratory studies on excess air formation (e.g., Holocher et al. 2002; Klump et al. 2008a).

An interesting observation in some studies from tropical regions has been that ΔNe is correlated with stable isotopes (Beyerle et al. 2003; Wieser et al. 2011). This a priori unexpected relationship between completely independent parameters supports the notion that excess air is related to recharge intensity, as the concurrent change in stable isotopes can be interpreted as due to the amount effect. Also striking is the anticorrelation of ΔNe and nitrate found by Osenbrück et al. (2009) in groundwater of the Kalahari. This finding suggests that dry climate periods are related to high nitrate concentrations. Lower groundwater recharge and thus low excess air in dry periods, but continuing release of nitrate from soil organic matter may result in elevated nitrate concentrations.

4.3 Recent Examples

In the following we discuss and compare results from six recent noble gas paleoclimate studies, with regard to the main climate proxies NGT, excess air, and stable isotopes. Taken together, these studies cover the entire northern hemisphere mid-latitudes. All studies have used ^{14}C chronologies, which generally should be interpreted with caution in groundwater. Relative age sequences within each study are certainly more reliable than absolute ages and thus the comparison between the different records.

Two recent European studies have revealed the largest Holocene–LGM temperature differences ever measured by the noble gas thermometer. Varsányi et al. (2011) found a temperature difference of 9.1 ± 0.8 °C in the Pannonian Basin in Hungary, slightly higher than the result that Stute and Deák (1989) had obtained two decades before from a location a bit further north in the Great Hungarian Plain. Blaser et al. (2010) reported an even slightly higher temperature difference of 9.5 ± 0.7 °C from the Ledo-Paniselian aquifer in Belgium. As noted before, this difference does probably not even refer to the LGM, when permafrost seems to have prevented groundwater recharge in the area.

Figure 8 shows the temperature records from Hungary and Belgium in comparison. The NGTs from Hungary are generally a bit warmer than those from Belgium, and in particular they never come close to the freezing point. This may explain why the Hungarian record appears to be continuous, whereas the Belgian data set exhibits a gap between about 15 and 20 kyr, which was interpreted as the coldest period affected by permafrost. The Hungarian record shows a smooth transition from Pleistocene temperatures around 3 °C to Holocene values around 12 °C between about 25 and 15 kyr. As noted above, the absolute ages may not be sufficiently certain to draw conclusions about the exact timing of climate events in both records. With regard to NGTs, an interesting difference between the two records is that in Belgium a

milder pre-LGM glacial period seems to be recorded, which is not apparent in the Hungarian data set.

With respect to excess air, both the studies of Varsányi et al. (2011) and Blaser et al. (2010) did not seem to find interesting signals, as often in studies from temperate, humid climates. In Hungary, Ne concentrations varied between about 2.2 and 2.7 $\times$ 10^{-7} cm^3 STP/g, corresponding to the typical range of 20–50 % ΔNe, except for one sample with a much higher value (possibly air contamination) and two young wells showing clear degassing signatures. Possibly, the cold, Pleistocene samples show a tendency to higher excess air, but this was not discussed in the paper. In Belgium, ΔNe varied between 4 and 36 %, except for a number of samples that were affected by degassing and thus showed negative ΔNe (up to -70 %). An interesting result of this study is that degassing occurred in the time period just after the LGM, possibly related to thawing permafrost.

Stable isotopes in Hungary show a strong climate signal of about 3.5 ‰ in δ^{18}O. The variations of stable isotopes and NGT are highly correlated, providing a neat regional and long-term calibration of the stable isotope paleothermometer (slope of 0.38 ‰/°C). In contrast, in Belgium the stable isotopes vary only little and the correlation with NGTs is weak, as reported by Blaser (2007) but unfortunately not in the paper discussed here. Preliminary data from the study in Belgium were actually already used by Loosli et al. (2001), who showed that the slope of δ^{18}O versus NGT (sensitivity of the stable isotope thermometer) varies systematically over Europe from close to zero at coastal sites to about 0.5 ‰/°C at continental sites. The mean value for non-coastal sites of 0.35 ‰/°C corresponds well to the new result from Hungary.

Three recent noble gas paleoclimate studies from the US have combined NGT and excess air information. Klump et al. (2008b) found a glacial cooling of approximately 7 °C in southern Wisconsin. Excess air was elevated just before the LGM, suggesting a change in recharge dynamics during that period. Kulongoski et al. (2009) studied groundwaters in the Mojave Desert,

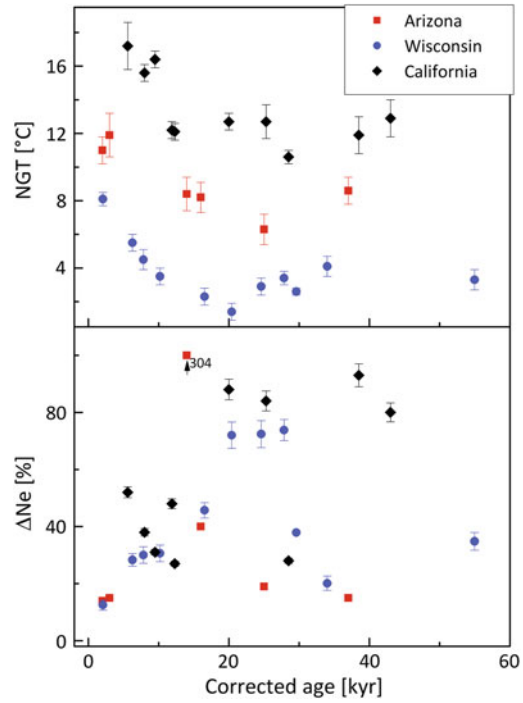

Fig. 9 Three recent US NGT and ΔNe records in comparison: Wisconsin (Klump et al. 2008b), California (Kulongoski et al. 2009) and Arizona (Zhu and Kipfer 2010). The ΔNe record from Arizona contains a sample at around 14 kyr that indicates an extreme peak (off scale, indicated by an arrow, ΔNe = 304 %)

California, which indicated that Late Pleistocene temperatures were about 4 °C cooler than Holocene temperatures. Furthermore, the Pleistocene samples showed higher ΔNe, indicating wetter conditions in that period. Zhu and Kipfer (2010) reported 5–6 °C cooler NGTs during the LGM compared to the late Holocene for Black Mesa, Arizona. They highlighted the finding of enhanced ΔNe during the deglaciation.

Figure 9 shows the NGT and ΔNe records from the recent American studies in comparison. All records indicate that deglacial warming occurred somewhere between 20 and 10 kyr ago, although the limited number of samples and, again, the uncertainties of ^{14}C dating make it difficult to compare the sequences of climate signals between the records. Nevertheless, it is interesting to note that maxima of excess air occurred at different times in these records. The record from California shows a single transition

from high ΔNe in Pleistocene samples to lower values in the Holocene, interpreted as a decrease in the number of large precipitation events, and a transition from wetter to more arid conditions. In Wisconsin, a broad ΔNe peak prior to the LGM is suggested. In Arizona, one extremely high ΔNe value at an age of between 14 and 17 kyr was explained by deglacial recharge pulses coinciding with high water levels independently inferred from numerical groundwater modeling and related to the passage of the southern branch of the jet stream over the area at that time. In summary, excess air data from these records indicate a complex reorganisation of precipitation patterns over North America during the transition from the last glacial period, leading to regionally different climate histories.

Two of the three studies also used stable isotopes to complement their climate records. Klump et al. (2008b) found a good correlation of $\delta^{18}O$ and NGT, with a slope of about 0.7 ‰/°C, indicating a high sensitivity of the stable isotope thermometer in this most northern and continental location of the three studies. Kulongoski et al. (2009) observed smaller changes in stable isotopes, which were interpreted as supporting the evidence from ΔNe for wetter conditions during the Pleistocene.

The final recent study that we would like to discuss comes from East Asia, more precisely the North China Plain, where a glacial—interglacial warming of 4.6 ± 1.2 °C was found (Kreuzer et al. 2009). This study site differs from those in Europe and North America by being influenced by the Asian monsoon, with a strongly seasonal precipitation pattern. It was expected that known past changes of monsoon strength would be reflected in the excess-air record. However, no systematic ΔNe signal was found in this extensive study comprising altogether 52 wells. If anything, an enhanced variability of ΔNe in the modern samples, discussed by von Rohden et al. (2010), was observed. This may be due to perturbed recharge conditions as a result of intensive irrigation.

In contrast to excess air, stable isotopes in the North China Plain show a strong climate signal. Whereas earlier studies had interpreted the change of $\delta^{18}O$ values by about 2 ‰ between the Pleistocene and late Holocene purely as a temperature signal, the comparison with the NGT record revealed that only about half of this change concurred with the deglacial warming. A further increase of $\delta^{18}O$ by about 1 ‰ occurred within the Holocene, where NGTs were quite stable. This trend in stable isotopes was explained by the amount effect, indicating a gradual decrease of monsoon strength during the Holocene. Another increase of $\delta^{18}O$ by roughly 1 ‰ occurred within the past few decades, presumably due to irrigation return flow affected by evaporation and mixing with other water sources (von Rohden et al. 2010). NGT information proved very helpful in disentangling the various effects that influence stable isotopes in the North China Plain aquifers.

4.4 Other Uses of Noble Gases in Groundwater

There are many uses of noble gases in groundwater research other than paleotemperature reconstruction. In general, noble gases can be thought of as indicators of recharge conditions of groundwater, which are useful in various contexts. In the following, a short though hardly comprehensive overview of various applications of noble gases in hydrogeology is given. One field where the use of noble gases has recently attracted particular attention, namely the study of mountain block recharge, is discussed in more detail thereafter.

An application of noble gases that is closely linked with paleotemperature reconstruction is the use of the temperature information as a stratigraphic age marker. As mentioned above, Pinti et al. (1997) and Lavastre et al. (2010) have compared NGTs with independent paleoclimate records on long time scales to derive age estimates. Also in paleotemperature studies on the typical time scale of the LGM–Holocene transition, the NGT increase may serve as an age marker if radiocarbon dating proves too problematic (e.g., Clark et al. 1997; Aeschbach-Hertig et al. 2002b; Zuber et al. 2004).

A very important use of noble gas information, both recharge temperatures and excesss air, occurs in the related field of groundwater dating by gas tracers. Some widely used dating tools for young groundwater (^{3}H–^{3}He, SF_6, CFCs) require knowledge of the recharge temperature and the amount of excess air, in order to perform a component separation and to relate equilibrium concentrations to atmospheric input functions. Numerous such studies have used only the excess air information provided by Ne. Zuber et al. (2005) measured Ar in addition, and increasingly the full suite of noble gases is used (e.g., Althaus et al. 2009; von Rohden et al. 2010; Solomon et al. 2010).

Beyerle et al. (1999a) had already used all noble gases to support the dating, but also as a tracer in a study of river infiltration into shallow groundwater. These authors were able to detect small seasonal recharge temperature variations in very young groundwater. Supporting the dating was only a secondary use of noble gases in a study of Singleton and Moran (2010), where NGTs and excess air provided decisive clues on the recharge sources of young groundwater in a small mountainous catchment.

Several studies have used noble gases to investigate hydrothermal systems, as already pioneered by Mazor (1972). Ciężkowski et al. (1992) and Zuber et al. (1995, 1997) used noble gases along with other tracers to study the age and origin of thermal spring waters in Poland. Gardner et al. (2010) used noble gases in hydrothermal water in a geyser basin of the Yellowstone National Park (USA) to investigate its boiling and mixing with shallow cool water.

Another field where noble gases may have a high potential is the study of groundwater in glaciated areas and of paleowaters formed as glacial meltwater. Vaikmäe et al. (2001) reported unusually high dissolved gas amounts in groundwater of glacial age in the Cambrian-Vendian aquifer in Estonia, which exhibits strongly depleted stable isotope signatures. Such a signature of depleted stable isotopes and enriched excess air may be due to subglacial meltwater recharge, because glacier ice is isotopically depleted and contains a lot of trapped air. However, this signature was not found in the study of Klump et al. (2008b) from Wisconsin, where glacial meltwater may also have been expected.

Unusually high and diagnostic excess air values may also occur at sites of artificial groundwater recharge, linked to rapid and large increases of the water table during groundwater injection. Heilweil et al. (2004) documented large amounts of trapped gas beneath an infiltration pond using a gas-partitioning tracer test and showed that this resulted in up to a factor of 10 decrease in the infiltration rate. Clark et al. (2005) used noble gases to show that trapped air existed beneath an artificial recharge pond, retarding the transport of gaseous tracers. Cey et al. (2008) showed that the distribution of excess air values in groundwaters of California is asymmetric, with an enhanced upper tail resulting from areas impacted by artificial recharge. Heilweil and Marston (2011) reported a plume of very high total dissolved gas pressure (more than 2 atm) migrating through an aquifer beneath a recently filled reservoir. Solomon et al. (2011) found that high dissolved gas pressures in a managed aquifer were due to both air entrapment during artificial recharge and subsequent warming of the injected water.

Noble gases can furthermore be used to study ocean–groundwater interactions, exploiting the different signatures of fresh groundwater and ocean water. Morrissey et al. (2010) used noble gases as a crucial tracer to understand the reorganization of groundwater flow following the sea-level rise at the end of the LGM in the Floridan Aquifer System in south Florida (USA). Greene et al. (2008) provided noble gas evidence for the origin of a Canadian Shield brine from evaporated seawater.

4.5 Mountain Block Recharge

Mountain block recharge (MBR) is the subsurface flow of groundwater into an adjacent basin-fill aquifer (Wilson Guan 2004). MBR is increasingly being recognized as a major source of recharge for basins around the world (e.g., Manning 2011; Magruder et al. 2009; Bouchaou et al. 2008;

Kohfahl et al. 2008; Carrera-Hernández and Gaskin 2008; Kebede et al. 2008). However, there is little direct evidence for MBR and NGT is becoming a powerful investigation tool. One of the potential strengths of NGT in MBR studies is that it may be able to distinguish between infiltration and recharge that occurs in the mountain block from mountain-derived stream flow that infiltrates within the basin itself. For example, MBR would have a high elevation and low temperature noble gas signal whereas stream losses in the basin would have a low elevation, high temperature signal. In contrast, tracers such as the stable isotopes (^{18}O, D) of water would have similar values for MBR versus stream loss in the basin.

While the noble gases offer some advantages over other tracers for studying MBR, evaluating NGT in mountainous systems is complicated by the fact that both the temperature and elevation of recharge are unknown. In theory it is possible to solve for as many as four unknowns (temperature, elevation, and two excess air parameters) when four noble gases are measured. However, elevation and temperature are correlated and this makes the inverse solution rather non-unique (Aeschbach-Hertig et al. 1999; Ballentine and Hall, 1999). Manning and Solomon (2003) showed that uncertainties in noble gas concentrations would need to be less than 0.3 % in order to uniquely resolve a recharge elevation of ±200 m. While this may be possible in terms of laboratory uncertainty, it is unlikely to be the case when uncertainties associated with sampling and excess air models are considered.

Zuber et al. (1995) and Aeschbach-Hertig et al. (1999) pointed out that when both temperature and elevation are unknown, it is possible to derive a set of best-fit solutions as shown in Fig. 10. The solid line in Fig. 10 represents combinations of recharge elevation and temperature that best fit the data. This line is obtained by postulating a recharge elevation, and then solving for the recharge temperature (using the optimization methods described previously). The dashed line in Fig. 10 represents the atmospheric lapse rate. The intersection of the best fit and the atmospheric lapse lines provides an estimate of both the elevation and temperature of recharge.

Manning and Solomon (2003) examined MBR to the Salt Lake Valley, Utah (USA) by developing an empirical lapse rate. This was done by collecting samples from springs in which the physical hydrology constrained the range of possible recharge elevations. They found that the empirical lapse rate was similar to the atmospheric lapse, but the curve was offset by about 2 °C. As described previously, there are many reasons why the temperature at the water table might deviate from the mean annual temperature at land surface. As a result, the lapse line shown in Fig. 10 may be best represented by a lapse area, as shown by the shading. This in turn gives rise to maximum and minimum estimates of both recharge elevation and pressure. For example, the best fit line in Fig. 10 intersects the lower part of the lapse area at a temperature and elevation of about 9 °C and 500 m. These represent the maximum probable recharge temperature and the minimum probable recharge elevation. Similarly, the minimum probable recharge temperature (where the best fit line intersects the upper part of the lapse area) is about 2.5 °C and the maximum recharge elevation is about 2,750 m. Although this is a rather large range of temperatures and elevations (2.5–9 °C and 500–2,750 m), in the case of the MBR study in the Salt Lake Valley, Manning and Solomon (2003) were still able to distinguish MBR from valley recharge. The mean annual temperature in the Salt Lake Valley is about 12 °C and this lies outside of the range of probable NGTs calculated from most groundwater samples.

While adding the additional information of the atmospheric lapse has been useful for constraining NGTs in mountainous regions, some challenges remain. For example, the best fit line from samples does not always have a distinct slope from the atmospheric lapse curve, and in some cases the best fit curve and the atmospheric lapse do not intersect. Constructing an empirical lapse curve can be difficult, and questions remain concerning the extent to which the NGT is reset beneath losing streams in basin fill

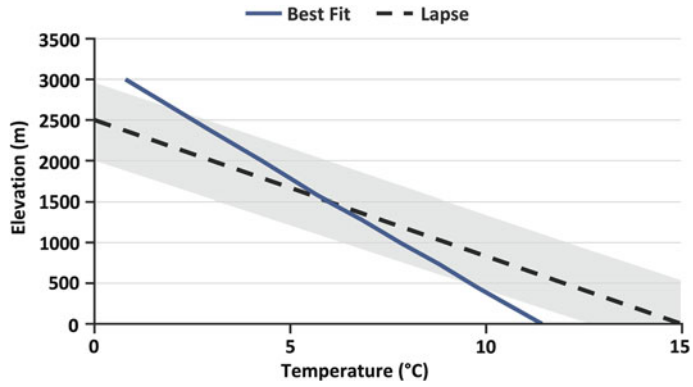

Fig. 10 Relationship between elevation and temperature for the best fit of noble gas concentrations (*solid line*) and the atmospheric lapse curve (*dashed line*). The best fit line was constructed by postulating a range of recharge elevations, and then solving for the best fit recharge temperature for each elevation. The intersection of the best fit line with the atmospheric lapse provides an estimate of the recharge elevation and temperature of the sample (1,500 m and 6 °C for this example). The *shaded area* represents an offset (uncertainty) that may exist between the atmospheric lapse curve and the actual temperature at the water table

aquifers (Manning 2011). For other examples of using NGT to constrain MBR see Thomas et al. (2003), Cederberg et al. (2009), Plummer et al. (2004a, 2004b), and Althaus et al. (2009).

5 Summary and Outlook

In the four decades since the pioneering study of Mazor (1972), the noble gas thermometer has become a mature and widely applied method. Numerous noble gas paleotemperature records have been obtained from groundwaters worldwide, confirming the validity of the concept and the usefulness of the method. In addition to temperature, excess air is now accepted as an indicator of past recharge conditions linked to the strength and variability of recharge and hence ultimately precipitation. Moreover, noble gases have proven useful in a variety of other contexts in hydrogeology.

The main strength of the noble gas thermometer is its ability to provide absolute and reliable paleotemperatures. The fundamental principle of the method consists of the temperature dependence of (noble) gas solubilities in water, which is a precisely known physical relationship. Complications occur due to the presence of excess air, but the present state of theory at least enables reasonable modeling of this component and robust estimation of temperature differences within a paleotemperature record. In principle, if all effects influencing noble gas concentrations during recharge are correctly accounted for, the method delivers absolute past mean annual soil temperatures. The challenge remains to convert them to mean annual air temperatures, but other paleotemperature proxies have the same (borehole temperatures) or even more serious calibration problems.

A fundamental weakness of the noble gas thermometer is its limited applicability. So far, only groundwater has proven to be a reliable archive for this method, although other archives (speleothems, sediment pore waters) should at least in principle be accessible. Groundwater is far from an ideal climate archive. First of all, mixing is inevitably present, limiting the method to low-resolution records. Moreover, dating of the groundwater, i.e., determination of the mean subsurface residence time of the sampled water, is a challenge on the time scales of interest for paleoclimate studies.

On the other hand, the groundwater archive has the advantage of storing past meteoric water, thus allowing direct comparison of NGTs with stable isotope data. The widely applicable stable isotope thermometer can thus be calibrated

against the rather reliable NGTs. Although several studies have reported NGT-based stable isotope temperature sensitivities, it seems that the full potential of this approach has not yet been exploited. As far as we are aware, such information has hardly been used in other paleoclimate studies.

Another advantage of using noble gases in groundwater is that this set of tracers has many other important uses in addition to paleothermometry. Noble gases certainly play a significant role as tracers in groundwater hydrology even without the paleoclimatic implications. Quite possibly, the relative importance of hydrological compared to climatological applications of the noble gases in groundwater research is even increasing. Many promising fields of application have been mentioned above, ranging from groundwater dating to the study of water origin and recharge conditions in hydrothermal, glaciated, alluvial, coastal, managed, and mountainous aquifer systems.

In view of the many examples of successful use of noble gases in groundwater, it is not surprising that the popularity of these tracers is rising. So far, however, the relative complexity and costliness of the experimental techniques have prevented noble gases from being as widely and routinely used in hydrogeology as classical tracers like stable isotopes and tritium. An important question for the future of the method will be whether new analytical methods will make it more easily accessible for new research groups. Ideally, noble gases might become a routine part of geochemical and isotopic studies in hydrogeology.

As noble gases are increasingly used in groundwater research, also by scientists who are not very familiar with the theoretical background expounded in this chapter, it becomes even more important to resolve the most pressing open research questions. These questions all revolve around the evaluation and interpretation of noble gas data, from the raw concentration and isotope data to derived quantities such as NGTs and excess air parameters in the first place, and secondly to environmental parameters such as air temperatures, recharge intensity and elevation, and others.

Research needs therefore focus on the fundamental aspects of the processes and environmental parameters that determine noble gas concentrations in groundwater. Further studies are needed that illuminate the conditions and processes in the soil zone and near the groundwater table, where noble gas concentrations are set. Such research should aim at reducing the current complexity of models for dissolved atmospheric noble gases. It is well possible that no single model exists that describes all possible conditions in the recharge zone. However, it may be feasible to classify typical cases and corresponding models. It cannot be expected that the measurement of four atmospheric noble gases, whose properties vary in very systematic and hence not independent ways, can resolve every detail of the recharge processes. Yet, important information on the general conditions should be recoverable.

A better understanding of the mechanisms of soil air—groundwater interaction is also needed to support current attempts to interpret the excess air component as a proxy for recharge conditions and related climate parameters. The relationship between excess air amount and hydrostatic pressure and amplitude of water table fluctuations is theoretically based in the framework of the CE model (Aeschbach-Hertig et al. 2002a) and experimentally relatively well verified (Holocher et al. 2002; Ingram et al. 2007). But it is doubtful if this mechanism explains the full variability of ΔNe observed in aquifers, as several other factors (lithology, soil air composition, recharge rate, etc.) could play a role. Even less clear is whether parameters of other excess air models, such as the oxygen depletion factor or the capillary pressure can reliably be recovered from the data and beneficially be interpreted in terms of environmental conditions. Also the research on the phenomenon of degassing and its origin is still in its infancy.

For the classical application of noble gases as paleotemperature proxy, the main challenge probably lies in obtaining a better understanding

of how NGTs relate to past mean air temperatures, and how this relationship may have changed over time within a record from a given site. This important issue has long been neglected after the fundamental work of Stute and Schlosser (1993), but in recent years it has become increasingly evident that it has to be taken seriously, at least in hot and dry regions (Beyerle et al. 2003) and in cold, seasonally snow-covered areas (Cey 2009; Blaser et al. 2010).

When recharge occurs in mountainous regions (which is often the case for intermountain basins) both the temperature and elevation are unknown and cannot readily be deduced by an inversion of the noble gas data. Although additional information in the form of an atmospheric lapse rate can sometimes lead to more unique interpretations, additional methodologies are needed. While it could be argued that this non-uniqueness does not affect relative temperature differences in paleotemperature studies, Manning (2011) recently argued that changes in climate may have affected the location and elevation of recharge (i.e., changes from mountain block to mountain front recharge). Because of the importance of mountain precipitation to world-wide water resources, understanding such hydrologic changes due to climate change (in the past and future) is extremely important.

Despite the various complications, in general the direct application of noble gas thermometry in paleoclimate research is sufficiently mature and robust to be more widely applied than at present. The visibility of the noble gas results in the wider paleoclimate community may have somewhat declined since the highly cited Brazil study of Stute et al. (1995b). Simply adding more examples will hardly reverse that trend. The noble gas community would rather benefit from a clarification of the questions about the reliability, accuracy, and climatic significance of NGTs. Moreover, a comprehensive and consistent re-evaluation and compilation of the results that have been obtained to date would be desirable.

In conclusion, we feel that noble gases are well-established tracers in groundwater research, with many fruitful applications in paleoclimate and hydrological studies. Nevertheless, some quite fundamental research needs remain. In addition, many opportunities for new or not yet well-explored applications exist. Thus, the field is open and promising for innovative and venturous scientists.

Acknowledgments We thank Martin Wieser for drawing Fig. 5, Fig. 7, Fig. 8, Fig. 9, Tim Schneider and Andreas Kreuzer for supplying the photographs of Fig. 2, and Lisa Bröder for technical help with the manuscript.

References

Aeschbach-Hertig W, Beyerle U, Holocher J, Peeters F, Kipfer R (2002a) Excess air in ground water as a potential indicator of past environmental changes. In: IAEA (ed) Study of environmental change using isotope techniques IAEA, Vienna, C&S Papers Series 13, pp 174–183

Aeschbach-Hertig W, El-Gamal H, Wieser M, Palcsu L (2008) Modeling excess air and degassing in groundwater by equilibrium partitioning with a gas phase. Water Resour Res 44:W08449. doi:10.1029/2007WR006454

Aeschbach-Hertig W, Peeters F, Beyerle U, Kipfer R (1999) Interpretation of dissolved atmospheric noble gases in natural waters. Water Resour Res 35:2779–2792

Aeschbach-Hertig W, Peeters F, Beyerle U, Kipfer R (2000) Palaeotemperature reconstruction from noble gases in ground water taking into account equilibration with entrapped air. Nature 405:1040–1044

Aeschbach-Hertig W, Stute M, Clark J, Reuter R, Schlosser P (2002b) A paleotemperature record derived from dissolved noble gases in groundwater of the Aquia Aquifer (Maryland, USA). Geochim Cosmochim Acta 66:797–817

Althaus R, Klump S, Onnis A, Kipfer R, Purtschert R, Stauffer F, Kinzelbach W (2009) Noble gas tracers for characterisation of flow dynamics and origin of groundwater: a case study in Switzerland. J Hydrol 370:64–72

Amos RT, Mayer KU (2006) Investigating the role of gas bubble formation and entrapment in contaminated aquifers: reactive transport modelling. J Cont Hydrol 87:123–154

Amos RT, Mayer KU, Bekins BA, Delin GN, Williams RL (2005) Use of dissolved and vapor-phase gases to investigate methanogenic degradation of petroleum hydrocarbon contamination in the subsurface. Water Resour Res 41:W02001. doi:10.01029/02004WR003433

Andrews JN, Fontes J-C, Aranyossy J-F, Dodo A, Edmunds WM, Joseph A, Travi Y (1994) The evolution of alkaline groundwaters in the continental

intercalaire aquifer of the Irhazer Plain Niger. Water Resour Res 30:45–61

Andrews JN, Goldbrunner JE, Darling WG, Hooker PJ, Wilson GB, Youngman MJ, Eichinger L, Rauert W, Stichler W (1985) A radiochemical, hydrochemical and dissolved gas study of groundwaters in the Molasse basin of Upper Austria. Earth Planet Sci Lett 73:317–332

Andrews JN, Lee DJ (1979) Inert gases in groundwater from the Bunter Sandstone of England as indicators of age and palaeoclimatic trends. J Hydrol 41:233–252

Ballentine CJ, Hall CM (1999) Determining paleotemperature and other variables by using an error-weighted, nonlinear inversion of noble gas concentrations in water. Geochim Cosmochim Acta 63:2315–2336

Bard Y (1974) Nonlinear parameter estimation. Academic, New York

Bartlett M, Chapman DS, Harris RN (2004) Snow and the ground temperature record of climate change. J Geophys Res 109:F04008. doi:10.1029/2004JF000224

Bayer R, Schlosser P, Bönisch G, Rupp H, Zaucker F, Zimmek G (1989) Performance and blank components of a mass spectrometric system for routine measurement of helium isotopes and tritium by the ^{3}He ingrowth method. Sitzungsberichte der Heidelberger Akademie der Wissenschaften, Mathemathisch-naturwissenschaftliche Klasse, vol 5, pp 241–279

Benson BB, Krause D (1976) Empirical laws for dilute aqueous solutions of nonpolar gases. J Chem Phys 64:689–709

Beyerle U, Aeschbach-Hertig W, Hofer M, Imboden DM, Baur H, Kipfer R (1999a) Infiltration of river water to a shallow aquifer investigated with ^{3}H/^{3}He, noble gases and CFCs. J Hydrol 220:169–185

Beyerle U, Aeschbach-Hertig W, Imboden DM, Baur H, Graf T, Kipfer R (2000) A mass spectrometric system for the analysis of noble gases and tritium from water samples. Environ Sci Technol 34:2042–2050

Beyerle U, Aeschbach-Hertig W, Peeters F, Kipfer R, Purtschert R, Lehmann B, Loosli HH, Love A (1999b) Noble gas data from the Great Artesian Basin provide a temperature record of Australia on time scales of 10^{5} years. In: IAEA (ed) Isotope techniques in water resources development and management IAEA, Vienna, IAEA-CSP-2/C: 97-103

Beyerle U, Purtschert R, Aeschbach-Hertig W, Imboden DM, Loosli HH, Wieler R, Kipfer R (1998) Climate and groundwater recharge during the last glaciation in an ice-covered region. Science 282:731–734

Beyerle U, Rueedi J, Leuenberger M, Aeschbach-Hertig W, Peeters F, Kipfer R, Dodo A (2003) Evidence for periods of wetter and cooler climate in the Sahel between 6 and 40 kyr BP derived from groundwater. Geophys Res Lett 30:1173. doi:10.1029/2002GL016310

Blaser P (2007) Tracermethoden in der Hydrologie: Kombination verschiedener Methoden und Anwendungen am Beispiel des Ledo-Paniselian-Aquifers in Belgien. PhD thesis, University of Ghent

Blaser PC, Kipfer R, Loosli HH, Walraevens K, Van Camp M, Aeschbach-Hertig W (2010) A 40 ka record of temperature and permafrost conditions in northwestern Europe from noble gases in the Ledo-Paniselian Aquifer (Belgium). J Quaternary Sci 25:1038–1044

Blavoux B, Dray M, Fehri A, Olive P, Gröning M, Sonntag C, Hauquin J-P, Pelissier G, Pouchan P (1993) Palaeoclimatic and hydrodynamic approach to the aquitaine basin deep aquifer (France) by means of environmental isotopes and noble gases. In: IAEA (ed) Isotope techniques in the study of past and current environmental changes in the hydrosphere and the atmosphere IAEA, Vienna, IAEA-SM-329/60: 293-305

Blicher-Mathiesen G, McCarty GW, Nielsen LP (1998) Denitrification and degassing in groundwater estimated from dissolved dinitrogen and argon. J Hydrol 208:16–24

Bouchaou L, Michelot JL, Vengosh A, Hsissou Y, Qurtobi M, Gaye CB, Bullen TD, Zuppi GM (2008) Application of multiple isotopic and geochemical tracers for investigation of recharge, salinization, and residence time of water in the Souss-Massa aquifer, southwest of Morocco. J Hydrol 352:267–287

Bourg IC, Sposito G (2008) Isotopic fractionation of noble gases by diffusion in liquid water: Molecular dynamics simulations and hydrologic applications. Geochim Cosmochim Acta 72:2237–2247

Broecker W (1996) Glacial climate in the tropics. Science 272:1902–1904

Capasso G, Inguaggiato S (1998) A simple method for the determination of dissolved gases in natural waters. An application to thermal waters from Vulcano Island. Appl Geochem 13:631–642

Carrera-Hernández JJ, Gaskin SJ (2008) Spatio-temporal analysis of potential aquifer recharge: application to the Basin of Mexico. J Hydrol 353:228–246

Castro MC, Hall CM, Patriarche D, Goblet P, Ellis BR (2007) A new noble gas paleoclimate record in Texas—basic assumptions revisited. Earth Planet Sci Lett 257:170–187

Cederberg JR, Gardner PM, Thiros SA (2009) Hydrology of northern Utah Valley, Utah County, Utah, 1975–2005 US. Geol Surv Sci Invest Rep 2008–5197:114

Cey BD (2009) On the accuracy of noble gas recharge temperatures as a paleoclimate proxy. J Geophys Res 114:D04107. doi:10.1029/2008JD010438

Cey BD, Hudson GB, Moran JE, Scanlon BR (2008) Impact of artificial recharge on dissolved noble gases in groundwater in California. Environ Sci Technol 42:1017–1023

Cey BD, Hudson GB, Moran JE, Scanlon BR (2009) Evaluation of noble gas recharge temperatures in a shallow unconfined aquifer. Ground Water 47:646–659

Ciężkowski W, Gröning M, Leśniak PM, Weise SM, Zuber A (1992) Origin and age of thermal waters in

Cieplice Spa, Sudeten, Poland, inferred from isotope, chemical and noble gas data. J Hydrol 140:89–117

Clark JF, Davisson ML, Hudson GB, Macfarlane PA (1998) Noble gases, stable isotopes, and radiocarbon as tracers of flow in the Dakota aquifer, Colorado and Kansas. J Hydrol 211:151–167

Clark JF, Hudson GB, Avisar D (2005) Gas transport below artificial recharge ponds: Insights from dissolved noble gases and a dual gas (SF_6 and ^3He) tracer experiment. Environ Sci Technol 39:3939–3945

Clark JF, Stute M, Schlosser P, Drenkard S, Bonani G (1997) A tracer study of the Floridan aquifer in southeastern Georgia: Implications for groundwater flow and paleoclimate. Water Resour Res 33:281–289

Clarke WB, Jenkins WJ, Top Z (1976) Determination of tritium by mass spectrometric measurement of ^3He. Int J Appl Radiat Isotopes 27:515–522

Corcho Alvarado JA, Barbecot F, Purtschert R, Gillon M, Aeschbach-Hertig W, Kipfer R (2009) European climate variations over the past half-millennium reconstructed from groundwater. Geophys Res Lett 36:L15703. doi:10.1029/2009GL038826

Crowley TJ (2000) CLIMAP SSTs re-revisited. Clim Dyn 16:241–255

Dennis F, Andrews JN, Parker A, Poole J, Wolf M (1997) Isotopic and noble gas study of Chalk groundwater in the London Basin, England. Appl Geochem 12:763–773

Edmunds WM, Fellman E, Goni IB (1999) Lakes, groundwater and paleohydrology in the Sahel of NE Nigeria: evidence from hydrogeochemistry. J Geol Soc London 156:345–355

Edmunds WM, Ma JZ, Aeschbach-Hertig W, Kipfer R, Darbyshire DPF (2006) Groundwater recharge history and hydrogeochemical evolution in the Minqin Basin, North West China. Appl Geochem 21:2148–2170

Farrera I, Harrison SP, Prentice IC, Ramstein G, Guiot J, Bartlein PJ, Bonnefille R, Bush M, Cramer W, von Grafenstein U, Holmgren K, Hooghiemstra H, Hope G, Jolly D, Lauritzen SE, Ono Y, Pinot S, Stute M, Yu G (1999) Tropical climates at the Last Glacial Maximum: a new synthesis of terrestrial palaeoclimate data. I. Vegetation, lake levels and geochemistry. Clim Dynam 15:823–856

Fortuin NPM, Willemsen A (2005) Exsolution of nitrogen and argon by methanogenesis in Dutch ground water. J Hydrol 301:1–13

Gardner P, Solomon DK (2009) An advanced passive diffusion sampler for the determination of dissolved gas concentrations. Water Resour Res 45:W06423. doi:10.1029/2008WR007399

Gardner WP, Susong DD, Solomon DK, Heasler HP (2010) Using noble gases measured in spring discharge to trace hydrothermal processes in the Norris Geyser Basin, Yellowstone National Park, U.S.A. J Volcanol Geoth Res 198:394–404

Geyh MA (2000) An overview of ^{14}C analysis in the study of groundwater. Radiocarbon 42:99–114

Gill AE (1982) Atmosphere-ocean dynamics. Academic, New York

Greene S, Battye N, Clark I, Kotzer T, Bottomley D (2008) Canadian Shield brine from the Con Mine, Yellowknife, NT, Canada: noble gas evidence for an evaporated Palaeozoic seawater origin mixed with glacial meltwater and Holocene recharge. Geochim Cosmochim Acta 72:4008–4019

Hall CM, Castro MC, Lohmann KC, Ma L (2005) Noble gases and stable isotopes in a shallow aquifer in southern Michigan: Implications for noble gas paleotemperature reconstructions for cool climates. Geophys Res Lett 32:L18404. doi:10.1029/2005GL023582

Hamme RC, Emerson SR (2004) The solubility of neon, nitrogen and argon in distilled water and seawater. Deep-Sea Res 51:1517–1528

Harris RN, Chapman DS (2001) Midlatitude (30–60°N) climatic warming inferred by combining borehole temperatures with surface air temperatures. Geophys Res Lett 28:747–750

Heaton THE, Talma AS, Vogel JC (1983) Origin and history of nitrate in confined groundwater in the western Kalahari. J Hydrol 62:243–262

Heaton THE, Talma AS, Vogel JC (1986) Dissolved gas paleotemperatures and ^{18}O variations derived from groundwater near Uitenhage South Africa. Quaternary Res 25:79–88

Heaton THE, Vogel JC (1981) "Excess air" in groundwater. J Hydrol 50:201–216

Heilweil VM, Solomon DK, Perkins KS, Ellett KM (2004) Gas-partitioning tracer test to quantify trapped gas during recharge. Ground Water 42:589–600

Heilweil VM, Marston TM (2011) Assessment of managed aquifer recharge from sand hollow reservoir, Washington County, Utah, Updated to Conditions in 2010. U. S. Geological Survey Scientific Investigations Report 2011-5142

Herzberg O, Mazor E (1979) Hydrological applications of noble gases and temperature measurements in underground water systems: examples from Israel. J Hydrol 41:217–231

Hillel D (1980) Fundamentals of soil physics. Academic, New York

Hofer M, Kipfer R (2007) Simultaneous determination of noble gases, N_2, O_2, SF_6, CFC-11 and CFC-12 in water by GC-MS/ECD. In: Proceedings of the 4th mini conference on noble gases in the hydrosphere and in natural gas reservoirs, GFZ Potsdam, Germany, p 68. doi:10.2312/GFZ.mga.011

Holocher J, Peeters F, Aeschbach-Hertig W, Hofer M, Brennwald M, Kinzelbach W, Kipfer R (2002) Experimental investigations on the formation of excess air in quasi-saturated porous media. Geochim Cosmochim Acta 66:4103–4117

Holocher J, Peeters F, Aeschbach-Hertig W, Kinzelbach W, Kipfer R (2003) Kinetic model of gas bubble dissolution in groundwater and its implications for the dissolved gas composition. Environ Sci Technol 37:1337–1343

Ingram RGS, Hiscock KM, Dennis PF (2007) Noble gas excess air applied to distinguish groundwater

recharge conditions. Environ Sci Technol 41:1949–1955

Jean-Baptiste P, Mantisi F, Dapoigny A, Stievenard M (1992) Design and performance of a mass spectrometric facility for measuring helium isotopes in natural waters and for low-level tritium determination by the ^{3}He ingrowth method. Int J Appl Radiat Isotopes 43:881

Kalin RM (2000) Radiocarbon dating of groundwater systems. In: Cook P, Herczeg AL (eds) Environmental tracers in subsurface hydrology, pp 111–144

Kebede S, Travi Y, Asrat A, Alemayehu T, Ayenew T, Tessema Z (2008) Groundwater origin and flow along selected transects in Ethiopian rift volcanic aquifers. Hydrogeol J 16:55–73

Kipfer R, Aeschbach-Hertig W, Peeters F, Stute M (2002) Noble gases in lakes and ground waters. In: Porcelli D, Ballentine C, Wieler R (eds) Noble gases in geochemistry and cosmochemistry, Reviews in Mineralogy and Geochemistry, vol 47, pp 615–700

Kloppmann W, Dever L, Edmunds WM (1998) Residence time of chalk groundwaters in the Paris Basin and the North German Basin: a geochemical approach. Appl Geochem 13:593–606

Kluge T, Marx T, Scholz D, Niggemann S, Mangini A, Aeschbach-Hertig W (2008) A new tool for palaeoclimate reconstruction: Noble gas temperatures from fluid inclusions in speleothems. Earth Planet Sci Lett 269:407–414

Klump S, Cirpka OA, Surbeck H, Kipfer R (2008a) Experimental and numerical studies on excess-air formation in quasi-saturated porous media. Water Resour Res 44:W05402. doi:10.1029/2007WR006280

Klump S, Grundl T, Purtschert R, Kipfer R (2008b) Groundwater and climate dynamics derived from noble gas, ^{14}C, and stable isotope data. Geology 36:395–398

Klump S, Kipfer R, Cirpka OA, Harvey CF, Brennwald MS, Ashfaque KN, Badruzzaman ABM, Hug SJ, Imboden DM (2006) Groundwater dynamics and arsenic mobilization in Bangladesh assessed using noble gases and tritium. Environ Sci Technol 40:243–250

Klump S, Tomonaga Y, Kienzler P, Kinzelbach W, Baumann T, Imboden DM, Kipfer R (2007) Field experiments yield new insights into gas exchange and excess air formation in natural porous media. Geochim Cosmochim Acta 71:1385–1397

Kohfahl C, Sprenger C, Herrera JB, Meyer H, Chacón FF, Pekdeger A (2008) Recharge sources and hydrogeochemical evolution of groundwater in semiarid and karstic environments: a field study in the Granada Basin (southern Spain). Appl Geochem 23:846–862

Kooi H (2008) Spatial variability in subsurface warming over the last three decades; insight from repeated borehole temperature measurements in The Netherlands. Earth Planet Sci Lett 270:86–94

Kreuzer AM, von Rohden C, Friedrich R, Chen ZY, Shi JS, Hajdas I, Kipfer R, Aeschbach-Hertig W (2009) A record of temperature and monsoon intensity over the past 40 kyr from groundwater in the North China Plain. Chem Geol 259:168–180

Kulongoski JT, Hilton DR (2002) A quadrupole-based mass spectrometric system for the determination of noble gas abundances in fluids. Geochem Geophys Geosyst , vol 3. doi:10.1029/2001GC000267

Kulongoski JT, Hilton DR, Izbicki JA, Belitz K (2009) Evidence for prolonged El Nino-like conditions in the Pacific during the Late Pleistocene: a 43 ka noble gas record from California groundwaters. Quaternary Sci Rev 28:2465–2473

Kulongoski JT, Hilton DR, Selaolo ET (2004) Climate variability in the Botswana Kalahari from the late Pleistocene to the present day. Geophys Res Lett 31:L10204. doi:10.1029/2003GL019238

Lachenbruch AH, Marshall BV (1986) Climate change: geothermal evidence from permafrost in the Alaskan Arctic. Science 234:689–696

Lavastre V, La Salle CL, Michelot JL, Giannesini S, Benedetti L, Lancelot J, Lavielle B, Massault M, Thomas B, Gilabert E, Bourles D, Clauer N, Agrinier P (2010) Establishing constraints on groundwater ages with Cl-36, C-14, H-3, and noble gases: a case study in the eastern Paris basin, France. Appl Geochem 25:123–142

Lehmann BE, Davis SN, Fabryka-Martin JT (1993) Atmospheric and subsurface sources of stable and radioactive nuclides used for groundwater dating. Water Resour Res 29:2027–2040

Lehmann BE, Love A, Purtschert R, Collon P, Loosli HH, Kutschera W, Beyerle U, Aeschbach-Hertig W, Kipfer R, Frape SK, Herczeg A, Moran J, Tolstikhin I, Gröning M (2003) A comparison of groundwater dating with ^{81}Kr, ^{36}Cl and ^{4}He in four wells of the Great Artesian Basin, Australia. Earth Planet Sci Lett 211:237–250

Lippmann J, Stute M, Torgersen T, Moser DP, Hall JA, Lin L, Borcsik M, Bellamy RES, Onstott TC (2003) Dating ultra-deep mine waters with noble gases and ^{36}Cl, Witwatersrand Basin, South Africa. Geochim Cosmochim Acta 67:4597–4619

Loosli HH, Aeschbach-Hertig W, Barbecot F, Blaser P, Darling WG, Dever L, Edmunds WM, Kipfer R, Purtschert R, Walraevens K (2001) Isotopic methods and their hydrogeochemical context in the investigation of palaeowaters. In: Edmunds WM, Milne CJ (eds) Palaeowaters in Coastal Europe evolution of groundwater since the late Pleistocene, Special Publications on the Geological Society, vol 189, pp 193–212

Lott DE (2001) Improvements in noble gas separation methodology: a nude cryogenic trap. Geochem Geophys Geosyst, vol 2. doi:10.129/2001GC000202

Lott DE, Jenkins WJ (1984) An automated cryogenic charcoal trap system for helium isotope mass spectrometry. Rev Sci Instrum 55:1982–1988

Ma L, Castro MC, Hall CM (2004) A late Pleistocene–Holocene noble gas paleotemperature record in southern Michigan. Geophys Res Lett 31:L23204. doi:10.1029/2004GL021766

Magruder IA, Woessner WW, Running SW (2009) Ecohydrologic process modeling of mountain block groundwater recharge. Ground Water 47:774–785

Mann ME, Schmidt GA, Miller SK, LeGrande AN (2009) Potential biases in inferring Holocene temperature trends from long-term borehole information. Geophys Res Lett 36:L05708. doi:10.1029/2008GL036354

Manning AH (2011) Mountain-block recharge, present and past, in the eastern Española Basin, New Mexico, USA. Hydrogeol J. doi:10.1007/s10040-010-0696-8

Manning AH, Caine JS (2007) Groundwater noble gas, age, and temperature signatures in an Alpine watershed: valuable tools in conceptual model development. Water Resour Res 43:W04404. doi:10.1029/2006WR005349

Manning AH, Solomon DK (2003) Using noble gases to investigate mountain-front recharge. J Hydrol 275:194–207

Manning AH, Solomon DK (2005) An integrated environmental tracer approach to characterizing groundwater circulation in a mountain block. Water Resour Res 41:W12412. doi:10.1029/2005WR004178

Manning AH, Solomon DK, Sheldon AL (2003) Applications of a total dissolved gas pressure probe in ground water studies. Ground Water 41:440–448

Mazor E (1972) Paleotemperatures and other hydrological parameters deduced from gases dissolved in groundwaters, Jordan Rift Valley, Israel. Geochim Cosmochim Acta 36:1321–1336

Mercury L, Azaroual M, Zeyen H, Tardy Y (2003) Thermodynamic properties of solutions in metastable systems under negative or positive pressures. Geochim Cosmochim Acta 67:1769–1785

Mercury L, Pinti DL, Zeyen H (2004) The effect of the negative pressure of capillary water on atmospheric noble gas solubility in ground water and palaeotemperature reconstruction. Earth Planet Sci Lett 223:147–161

Mochalski P, Lasa J, Śliwka I (2006) Simultaneous Determination of Ne, Ar, and N_2 in Groundwater by Gas Chromatography. Chem Anal 51:825–831

Mochalski P, Sliwka I, Lasa J (2007) Simultaneous determination of Ne, Ar, SF_6, CFC-11 and CFC-12 in groundwater by gas chromatography. In: 4th mini conference on noble gases in the hydrosphere and in natural gas reservoirs, GFZ Potsdam, Germany, pp 86–87. doi:10.2312/GFZ.mga.015

Morrissey SK, Clark JF, Bennett M, Richardson E, Stute M (2010) Groundwater reorganization in the Floridan aquifer following Holocene sea-level rise. Nat Geosci 3:683–687

Oana S (1957) Bestimmung von Argon in besonderem Hinblick auf gelöste Gase in natürlichen Gewässern. J Earth Sci Nagoya Univ 5:103–105

Osenbrück K, Stadler S, Sültenfuß J, Suckow AO, Weise SM (2009) Impact of recharge variations on water quality as indicated by excess air in groundwater of the Kalahari, Botswana. Geochim Cosmochim Acta 73:911–922

Peeters F, Beyerle U, Aeschbach-Hertig W, Holocher J, Brennwald MS, Kipfer R (2003) Improving noble gas based paleoclimate reconstruction and groundwater dating using $^{20}Ne/^{22}Ne$ ratios. Geochim Cosmochim Acta 67:587–600

Phillips FM, Peeters LA, Tansey MK, Davis SN (1986) Paleoclimatic inferences from an isotopic investigation of groundwater in the central San Juan Basin, New Mexico. Quaternary Res 26:179–193

Pinti DL, Marty B, Andrews JN (1997) Atmosphere-derived noble gas evidence for the preservation of ancient waters in sedimentary basins. Geology 25:111–114

Pinti DL, van Drom E (1998) PALEOTEMP: A MATHEMATICA program for evaluating paleotemperatures from the concentration of atmosphere-derived noble gases in ground water. Comput Geosci 24:33–41

Plummer LN, Bexfield LM, Anderholm SK, Sanford WE, Busenberg E (2004a) Geochemical characterization of ground-water flow in the Santa Fe Group aquifer system, Middle Rio Grande Basin, New Mexico. US geological survey on water resources investigation report, p 395

Plummer LN, Bexfield LM, Anderholm SK, Sanford WE, Busenberg E (2004b) Hydrochemical tracers in the middle Rio Grande Basin, USA: 1. conceptualization of groundwater flow. Hydrogeol J 12:359–388

Poole JC, McNeill GW, Langman SR, Dennis F (1997) Analysis of noble gases in water using a quadrupole mass spectrometer in static mode. Appl Geochem 12:707–714

Powell WG, Chapman DS, Balling N, Beck AE (1988) Continental heat flow density. In: Haenel R, Stegena L, Rybach L (eds) Handbook of terrestrial heat-flow density determination, pp 167–222

Press WH (1995) Numerical recipes in C, 2nd edn. Cambridge University Press, New York

Rudolph J, Rath HK, Sonntag C (1984) Noble gases and stable isotopes in ^{14}C-dated palaeowaters from central Europa and the Sahara. In: IAEA (ed) Isotope hydrology 1983 IAEA, Vienna, IAEA-SM-270/17: 467-477

Sanford WE, Shropshire RG, Solomon DK (1996) Dissolved gas tracers in groundwater: simplified injection, sampling, and analysis. Water Resour Res 32:1635–1642

Scheidegger Y, Baur H, Brennwald MS, Fleitmann D, Wieler R, Kipfer R (2010) Accurate analysis of noble gas concentrations in small water samples and its application to fluid inclusions in stalagmites. Chem Geol 272:31–39

Sheldon AL (2002) Diffusion of radiogenic helium in shallow groundwater: implications for crustal degassing. PhD thesis, University of Utah

Singleton MJ, Moran JE (2010) Dissolved noble gas and isotopic tracers reveal vulnerability of groundwater in a small, high-elevation catchment to predicted climate changes. Water Resour Res 46: W00F06. doi:10.1029/2009WR008718

Smith GD, Newhall F, Robinson LH, Swanson D (1964) Soil temperature regimes: their characteristics and predictability USDA, Soil Conservation Service Report SCS-TP-144

Smith SP, Kennedy BM (1983) The solubility of noble gases in water and in NaCl brine. Geochim Cosmochim Acta 47:503–515

Solomon DK, Cole E, Leising JF (2011) Excess air during aquifer storage and recovery in an arid basin (Las Vegas Valley, USA). Hydrogeol J 19:187–194

Solomon DK, Genereux DP, Plummer LN, Busenberg E (2010) Testing mixing models of old and young groundwater in a tropical lowland rain forest with environmental tracers. Water Resour Res 46:W04518. doi:10.1029/2009WR008341

Stanley RHR, Baschek B, Lott DE III, Jenkins WJ (2009) A new automated method for measuring noble gases and their isotopic ratios in water samples. Geochem Geophys Geosyst 10:Q05008. doi:10.1029/2009GC002429

Stute M, Clark JF, Schlosser P, Broecker WS (1995a) A 30'000 yr continental paleotemperature record derived from noble gases dissolved in groundwater from the San Juan Basin, New Mexico. Quaternary Res 43:209–220

Stute M, Deák J (1989) Environmental isotope study (^{14}C, ^{13}C, ^{18}O, D, noble gases) on deep groundwater circulation systems in Hungary with reference to paleoclimate. Radiocarbon 31:902–918

Stute M, Forster M, Frischkorn H, Serejo A, Clark JF, Schlosser P, Broecker WS, Bonani G (1995b) Cooling of tropical Brazil (5 °C) during the last glacial maximum. Science 269:379–383

Stute M, Schlosser P (1993) Principles and applications of the noble gas paleothermometer. In: Swart PK, Lohmann KC, McKenzie J, Savin S (eds) Climate change in continental isotopic records, AGU Geophysical Monograph Series, vol 78, pp 89–100

Stute M, Schlosser P (2000) Atmospheric noble gases. In: Cook P, Herczeg AL (eds) Environmental tracers in subsurface hydrology, pp 349–377

Stute M, Schlosser P, Clark JF, Broecker WS (1992) Paleotemperatures in the Southwestern United States derived from noble gases in ground water. Science 256:1000–1003

Stute M, Talma AS (1998) Glacial temperatures and moisture transport regimes reconstructed from noble gases and delta ^{18}O, Stampriet aquifer, Namibia. In: Isotope techniques in the study of environmental change, Vienna, Austria, IAEA-SM-349: 307–318

Stute M, Zheng Y, Schlosser P, Horneman A, Dhar RK, Datta S, Hoque MA, Seddique AA, Shamsudduha M, Ahmed KM, van Green A (2007) Hydrological control of as concentrations in Bangladesh groundwater. Water Resour Res 43:W09417. doi:10.1029/2005WR004499

Sugisaki R (1961) Measurement of effective flow velocity of ground water by means of dissolved gases. Am J Sci 259:144–153

Sültenfuß J, Roether W, Rhein M (2009) The Bremen mass spectrometric facility for the measurement of helium isotopes, neon, and tritium in water. Isotopes Environ Health Stud 45:83–95

Sun T, Hall CM, Castro MC (2010) Statistical properties of groundwater noble gas paleoclimate models: Are they robust and unbiased estimators? Geochem Geophys Geosyst 11:Q02002. doi:10.1029/2009GC002717

Sun T, Hall CM, Castro MC, Lohmann KC, Goblet P (2008) Excess air in the noble gas groundwater paleothermometer: a new model based on diffusion in the gas phase. Geophys Res Lett 35:L19401. doi:10.1029/2008GL035018

Takahata N, Igarashi G, Sano Y (1997) Continuous monitoring of dissolved gas concentrations in groundwater using a quadrupole mass spectrometer. Appl Geochem 12:377–382

Thomas JM, Hudson GB, Stute M, Clark JF (2003) Noble gas loss may indicate groundwater flow across flow barriers in southern Nevada. Environ Geol 43:568–579

Top Z, Eismont WC, Clarke WB (1987) Helium isotope effect and solubility of helium and neon in distilled water and seawater. Deep-Sea Res 34:1139–1148

Vaikmäe R, Vaullner L, Loosli HH, Blaser PC, Juillard-Tardent M (2001) Paleogroundwater of glacial origin in the Cambrian-Vendian Aquifer of northern Estonia. In: Edmunds WM, Milne CJ (eds) Palaeowaters in Coastal Europe: evolution of groundwater since the late Pleistocene, Special Publications on the Geological Society, vol 189, pp 17–22

Varsányi I, Palcsu L, Kovács LÓ (2011) Groundwater flow system as an archive of palaeotemperature: Noble gas, radiocarbon, stable isotope and geochemical study in the Pannonian Basin, Hungary. Appl Geochem 26:91–104

Visser A, Broers HP, Bierkens MFP (2007) Dating degassed groundwater with $^{3}H/^{3}He$. Water Resour Res 43:W10434. doi:10.1029/2006WR005847

von Rohden C, Kreuzer A, Chen ZY, Kipfer R, Aeschbach-Hertig W (2010) Characterizing the recharge regime of the strongly exploited aquifers of the North China Plain by environmental tracers. Water Resour Res 46:W05511. doi:10.1029/2008WR007660

Weiss RF (1970) The solubility of nitrogen, oxygen and argon in water and seawater. Deep-Sea Res 17:721–735

Weiss RF (1971) Solubility of helium and neon in water and seawater. J Chem Eng Data 16:235–241

Weiss RF, Kyser TK (1978) Solubility of krypton in water and seawater. J Chem Eng Data 23:69–72

Weyhenmeyer CE, Burns SJ, Waber HN, Aeschbach-Hertig W, Kipfer R, Loosli HH, Matter A (2000) Cool glacial temperatures and changes in moisture source recorded in Oman groundwaters. Science 287:842–845

Wieser M, Aeschbach-Hertig W, Schneider T, Deshpande RD, Gupta K (2011) A temperature and monsoon record derived from environmental tracers in groundwater of Northwest India. In: Proceedings of the

international symposium on isotopes in hydrology, marine ecosystems, and climate change studies IAEA, Monaco, IAEA-CN-186-029

Wilhelm E, Battino R, Wilcock RJ (1976) Low-pressure solubility of gases in liquid water. Chem Rev 77:219–262

Wilson GB, McNeill GW (1997) Noble gas recharge temperatures and the excess air component. Appl Geochem 12:747–762

Wilson JL, Guan H (2004) Mountain-block hydrology and mountain-front recharge. In: Hogan JF, Phillips FM, Scanlon BR (eds) Groundwater recharge in a desert environment: the southwestern United States, pp 113–137

Zartman RE, Wasserburg GJ, Reynolds JH (1961) Helium, argon, and carbon in some natural gases. J Geophys Res 66:277–306

Zhu C, Kipfer R (2010) Noble gas signatures of high recharge pulses and migrating jet stream in the late Pleistocene over Black Mesa, Arizona, United States. Geology 38:83–86

Zuber A, Weise SM, Motyka J, Osenbrück K, Rózanski K (2004) Age and flow pattern of groundwater in a Jurassic limestone aquifer and related Tertiary sands derived from combined isotope, noble gas and chemical data. J Hydrol 286:87–112

Zuber A, Weise SM, Osenbrück K (1997) Origin and age of saline waters in Busko Spa (Southern Poland) determined by isotope, noble gas and hydrochemical methods: Evidence of interglacial and pre-Quaternary warm climate recharges. Appl Geochem 12:643–660

Zuber A, Weise SM, Osenbrück K, Grabczak J, Ciężkowski W (1995) Age and recharge area of thermal waters in Ladek Spa (Sudeten, Poland) deduced from environmental isotope and noble gas data. J Hydrol 167:327–349

Zuber A, Witczak S, Rozanski K, Sliwka I, Opoka M, Mochalski P, Kuc T, Karlikowska J, Kania J, Jackowicz-Korczynski M, Dulinski M (2005) Groundwater dating with ^{3}H and SF_6 in relation to mixing patterns, transport modelling and hydrochemistry. Hydrol Process 19:2247–2275

Noble Gases as Environmental Tracers in Sediment Porewaters and Stalagmite Fluid Inclusions

M. S. Brennwald, N. Vogel, Y. Scheidegger, Y. Tomonaga, D. M. Livingstone and R. Kipfer

Abstract

In well-studied aquatic systems such as surface waters and groundwater, noble gases are used extensively as natural tracers to reconstruct palaeoenvironmental conditions, to study transport and mixing, and to identify the geochemical origin of geogenic fluids. It has been suggested that less well-studied aquatic systems such as the porewaters of lacustrine and oceanic sediments and the fluid inclusions present in stalagmites might also be suitable as noble gas archives for environmental studies, but until recently the lack of adequate experimental techniques had hindered the development of noble gas geochemistry in these systems. This chapter reviews recent technical advances in this field and describes the scientific applications that these advances have made possible. The porewaters of lacustrine and oceanic sediments are now well established as noble gas archives in studies of temperature, salinity and mixing conditions that prevailed in the overlying water body in the past, as well as in studies of the transport and origin of solutes and pore fluids in the sediment. The geochemistry of noble gases in stalagmite fluid inclusions is still in the early stages of development. However, the results available to date suggest that stalagmite fluid inclusions have great potential as a noble gas archive in reconstructing palaeoclimatic conditions near caves with suitable stalagmites.

1 Introduction

Noble gases have been used extensively as environmental tracers in lakes, oceans and groundwater since the 1960s. They have proved highly useful in reconstructing palaeoenvironmental conditions, studying transport and mixing in aqueous environments, and in constraining the geochemical origin of geogenic fluids injected into natural water bodies

M. S. Brennwald (✉) · N. Vogel · Y. Scheidegger · Y. Tomonaga · D. M. Livingstone · R. Kipfer
Department of Water Resources and Drinking Water, Eawag, Swiss Federal Institute of Aquatic Science and Technology, CH-8600, Dübendorf, Switzerland
e-mail: matthias.brennwald@eawag.ch

N. Vogel · R. Kipfer
Institute for Geochemistry and Petrology, Swiss Federal Institute of Technology Zurich (ETH), CH-8092, Zurich, Switzerland

P. Burnard (ed.), *The Noble Gases as Geochemical Tracers*, Advances in Isotope Geochemistry,
DOI: 10.1007/978-3-642-28836-4_6,

(for reviews see Ballentine and Burnard 2002; Ballentine et al. 2002; Kipfer et al. 2002; Schlosser and Winckler 2002; Aeschbach-Hertig and Solomon 2012; Stanley and Jenkins 2012).

The concentrations of dissolved noble gases in natural water bodies are determined by various processes involving different noble gas reservoirs (Sect. 2). On the one hand, the partitioning of noble gases between air and water is governed by the exchange of these gases across the air-water interface and by the solubility equilibrium as described by Henry's Law. This allows the concentrations of dissolved atmospheric noble gases (i.e., those derived from the atmosphere) in a water body to be used to reconstruct the temperature and salinity of the water as well as the atmospheric pressure that prevailed during gas exchange. On the other hand, non-atmospheric noble gas isotopes may accumulate in the water either as a result of their in-situ production by radioactive decay and other nuclear reactions or because of the addition of geogenic fluids to the water. The concentrations of such non-atmospheric noble gases can be used to determine the water age (defined as the time that elapsed since the last occurrence of gas exchange between the water and the atmosphere), to quantify the rates at which water and solutes are transported, and to study the accumulation and the geochemical origin of geogenic fluids. These concepts can, in principle, be adapted to other, more unconventional aquatic environments, such as the porewaters of lacustrine and oceanic sediments or water inclusions in stalagmites.

Lakes generally react sensitively to changes in climatic forcing. More than three decades ago, the porewater of lacustrine and oceanic sediments was therefore proposed as a potential noble gas archive for palaeoenvironmental reconstruction (Barnes 1979). In addition, the abundance and relative composition of non-atmospheric noble gases accumulating in the porewater as a result of in-situ production or the injection of geogenic fluids reflect the transport dynamics and the geochemical origin of the pore fluids (Sect. 3.1).

In caves, microscopic water inclusions embedded in the minerals of stalagmites contain a mixture of noble gases that were trapped at the time the inclusions were formed. It has been suggested that the elemental composition of these noble gases may reflect the cave temperature prevailing at that time. Because the ambient air temperature in caves remains relatively constant throughout the year at a value which corresponds closely to the local annual mean soil temperature and to the annual mean air temperature outside the cave, it may be possible to use the noble gases archived in stalagmite water inclusions to reconstruct air temperatures in the distant past (Sect. 4.1).

Until recently, however, a lack of suitable experimental techniques has hindered the development of noble gas geochemistry in lacustrine and oceanic sediment porewater and in stalagmite fluid inclusions. Various research groups have therefore begun to develop new methods of noble gas analysis for these more unconventional aquatic systems (Sects. 3.2 and 4.2).

The resulting experimental advances have meant that lacustrine and oceanic sediment porewaters are now well established as a new type of noble gas archive for environmental studies (Sect. 3.3). New experimental techniques have also allowed the scientific potential of stalagmite fluid inclusions as noble gas archives for palaeoenvironmental research to be assessed (Sect. 4.3).

2 Noble Gases in Aqueous Solution

2.1 Sources and Processes

The noble gas components found in natural waters are characterised in terms of the geochemical reservoirs from which they originate and in terms of the processes by which they enter the water (see also Aeschbach-Hertig and Solomon 2012). Figure 1 illustrates the terminology used in this chapter for the different noble gas components.

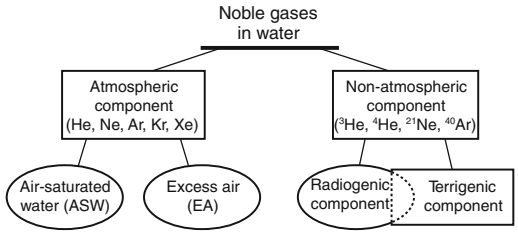

Fig. 1 Terminology and classification of the different noble gas components found in natural waters. Terms associated with geochemical reservoirs are indicated by rectangles and terms associated with the processes governing noble gas abundance by ellipses. Note that radiogenic noble gases are often, but not always, of terrigenic origin (e.g., ^{3}He produced by the radioactive decay of ^{3}H in the atmosphere or the hydrosphere is not terrigenic)

Noble gases from the atmosphere enter the water by gas exchange across the air-water interface and, to a lesser extent, by the (partial) dissolution of air bubbles in the water. The atmospheric noble gas component in the water therefore comprises all noble gases (and their isotopes) that are found in the atmosphere (He, Ne, Ar, Kr and Xe). The non-atmospheric noble gas isotopes originate mainly from the solid earth (terrigenic noble gases), including the rock matrix within which the water is embedded, or from the radioactive decay of ^{3}H in the water. Among the non-atmospheric noble gas isotopes, ^{3}He and ^{4}He have been used most frequently for environmental field investigations so far. Rn, the heaviest naturally occurring noble gas, may also be used as an environmental tracer. However, due to the rapid radioactive decay of the different Rn isotopes (which have half-lives ranging from seconds to days), Rn is most useful as a proxy for rapid transport and mixing processes in surface waters and groundwater (e.g., Hoehn and von Gunten 1989; Bertin and Bourg 1994; Huxol et al. 2012) rather than for the much slower processes dealt with in this chapter. Rn will therefore not be considered further here.

2.1.1 Atmospheric Noble Gases

In meteoric water, the concentrations of dissolved noble gases are dominated by the atmospheric component. When using noble gases as environmental proxies in meteoric water, the noble gas composition of the atmosphere (Table 1) is assumed to be constant in space and time. This assumption is justified because water renewal in the aquatic environment occurs much more rapidly than the evolution of the noble gas composition of the atmosphere (Kipfer et al. 2002).The abundance of atmospheric noble gases dissolved in water is therefore determined solely by the processes governing air-water gas partitioning and by the transport processes occurring within the water body.

Noble Gas Concentrations in Air-Saturated Water

At the water surface, noble gases are partitioned between the atmosphere and the water by exchange across the air-water interface. Because gas exchange usually occurs much faster than the mixing of the water immediately below the air-water interface with the bulk water, solubility equilibrium is attained at the water surface (e.g., Schwarzenbach et al. 2003). The resulting equilibrium concentrations C_i^* in the air-saturated water (ASW) are given by Henry's Law (see also Fig. 2 and Kipfer et al. 2002):

$$P_i = H_i(T,S)C_i^* \qquad i = \text{ He, Ne, Ar, Kr, Xe} \tag{1}$$

where P_i is the partial pressure of the noble gas i in the gas phase; H_i is the Henry coefficient, which is a function of the water temperature T and salinity S; and C_i^* is the equilibrium concentration of noble gas i in the water.

The partial pressure is given by $P_i = (P_{\text{atm}} - e_s(T))v_i$, where P_{atm} is the total atmospheric pressure, $e_s(T)$ is the vapour pressure, and v_i is the volume fraction of gas i in dry air (Table 1).

Excess Air

Excess air is formed by the (partial) dissolution of air bubbles in water. Excess air is of paramount importance in groundwater, whereas it is usually negligible in surface waters (Sect. 3.1). Stalagmites usually contain many air inclusions in addition to water inclusions (Sect. 4.1). Although the air in these inclusions is not dissolved in water, the mathematical treatment of this air component in Sect. 2.1.3 is analogous to that of excess air.

Table 1 Characteristic properties of noble gases

Element	v_i	d_i (Å)	Isotope	R_i (%)
He	$(5.24 \pm 0.05) \cdot 10^{-6}$	2.55	^{3}He	0.000140
			^{4}He	≈100
Ne	$(1.818 \pm 0.004) \cdot 10^{-5}$	2.82	^{20}Ne	90.50
			^{21}Ne	0.268
			^{22}Ne	9.23
Ar	$(9.34 \pm 0.01) \cdot 10^{-3}$	3.45	^{36}Ar	0.3364
			^{38}Ar	0.0632
			^{40}Ar	99.60
Kr	$(1.14 \pm 0.01) \cdot 10^{-6}$	3.65	^{78}Kr	0.347
			^{80}Kr	2.257
			^{82}Kr	11.52
			^{83}Kr	11.48
			^{84}Kr	57.00
			^{86}Kr	17.40
Xe	$(8.7 \pm 0.1) \cdot 10^{-8}$	4.04	^{124}Xe	0.0951
			^{126}Xe	0.0887
			^{128}Xe	1.919
			^{129}Xe	26.44
			^{130}Xe	4.070
			^{131}Xe	21.22
			^{132}Xe	26.89
			^{134}Xe	10.430
			^{136}Xe	8.857

Volume fraction in dry air, v_i (Ozima and Podosek 2002); atomic diameter, d_i (Huber et al. 2006); relative atomic isotope abundance in air, R_i (Ozima and Podosek 2002).

2.1.2 Non-atmospheric Noble Gases

Noble gases that are not of atmospheric origin can also accumulate in the aquatic environment. Noble gas isotopes can be produced in situ by radioactive decay and other nuclear reactions, and they can also be released into the aquatic environment from the solid earth. The concentrations of these radiogenic or terrigenic noble gas isotopes can provide information on water residence times and the dynamics of relevant fluid transport processes.

Relative to the atmospheric noble gas concentrations, non-atmospheric He usually shows the highest concentrations of all terrigenic noble gas isotopes (Mamyrin and Tolstikhin 1984; Ozima and Podosek 2002; Solomon 2000). This is mainly because of (i) the high rate of He production by the radioactive decay of U and Th isotopes in the crust coupled with the low degree of He retention in rock (radiogenic He, typical ^{3}He/^{4}He ratio $\approx 10^{-8}$), and (ii) the release of primordial and radiogenic He from the earth's mantle (typical ^{3}He/^{4}He ratio $\approx 10^{-5}$). In addition, the radioactive decay of ^{3}H bound to water molecules produces considerable amounts of ^{3}He (known as tritiogenic ^{3}He; see, e.g., Solomon and Cook 2000). ^{3}H is produced naturally by spallation in the atmosphere. It is also a by-product of earlier nuclear weapons testing in the atmosphere. The latter resulted in a distinct ^{3}H

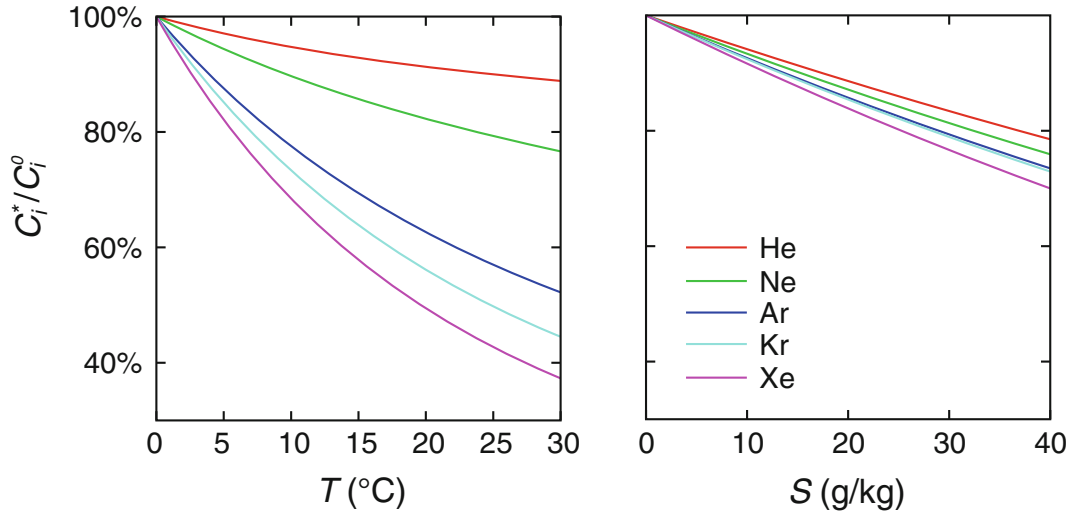

Fig. 2 Noble gas equilibrium concentrations in air-saturated water (C_i^*) as a function of water temperature T (left) and salinity S (right, for a sea-salt solution). The concentrations are normalised to the ASW concentrations C_i^0 at $T = 0$ °C and $S = 0$ g/kg, respectively. Concentrations were calculated using the solubility data recommended by Kipfer et al. (2002)

maximum in the atmosphere in the 1960s, temporarily increasing the global inventory of terrestrial ^{3}H by several orders of magnitude. On local spatial scales the use of ^{3}H in technological applications can also affect ^{3}H concentrations in the aquatic environment.

Apart from the isotopes of He, other isotopes of radiogenic origin found in the aquatic environment include ^{40}Ar and, to a lesser extent, ^{21}Ne. However, in most cases their presence is masked by higher concentrations of ^{40}Ar and ^{21}Ne of atmospheric origin (for an extended discussion see Kipfer et al. 2002).

2.1.3 Disentangling and Quantifying the Various Noble Gas Components

From the above discussion it follows that the overall concentration of each of the noble gases in water is given by the sum of the ASW concentration, the excess air component ("EA"), and the terrigenic He ("terr") and tritiogenic ^{3}He ("trit") components (note that except for He, all non-atmospheric noble gas components are neglected as to their abundance is extremely low):

$$\begin{aligned}
{}^3\mathrm{He}_{\mathrm{tot}} &= {}^3\mathrm{He}_{\mathrm{ASW}}(T,S,P_{\mathrm{atm}}) + {}^3\mathrm{He}_{\mathrm{EA}} + {}^3\mathrm{He}_{\mathrm{terr}} + {}^3\mathrm{He}_{\mathrm{trit}} \\
{}^4\mathrm{He}_{\mathrm{tot}} &= {}^4\mathrm{He}_{\mathrm{ASW}}(T,S,P_{\mathrm{atm}}) + {}^4\mathrm{He}_{\mathrm{EA}} + {}^4\mathrm{He}_{\mathrm{terr}} \\
\mathrm{Ne}_{\mathrm{tot}} &= \mathrm{Ne}_{\mathrm{ASW}}(T,S,P_{\mathrm{atm}}) + \mathrm{Ne}_{\mathrm{EA}} \\
\mathrm{Ar}_{\mathrm{tot}} &= \mathrm{Ar}_{\mathrm{ASW}}(T,S,P_{\mathrm{atm}}) + \mathrm{Ar}_{\mathrm{EA}} \\
\mathrm{Kr}_{\mathrm{tot}} &= \mathrm{Kr}_{\mathrm{ASW}}(T,S,P_{\mathrm{atm}}) + \mathrm{Kr}_{\mathrm{EA}} \\
\mathrm{Xe}_{\mathrm{tot}} &= \underbrace{\mathrm{Xe}_{\mathrm{ASW}}(T,S,P_{\mathrm{atm}}) + \mathrm{Xe}_{\mathrm{EA}}}_{\text{atmospheric}} \quad \underbrace{\qquad\qquad}_{\text{non-atmospheric}}
\end{aligned} \tag{2}$$

Experimental analysis yields only the overall concentrations (the left-hand side of Eq. 2), but not the individual components, which are needed to interpret the noble gas data in terms of T, S, P_{atm}, excess air, and the accumulation of terrigenic and radiogenic He isotopes.

Depending on the type of environment and archive (surface-water body and sediments, or cave and stalagmites), the values of some of these environmental parameters can be constrained using independent information. For instance, P_{atm} can be determined from the altitude of the water surface of a lake or the altitude of the recharge area of a groundwater system. The values of the remaining unknown parameters can then be estimated by regression from the measured data

analogously to the techniques used in surface waters and groundwater (Aeschbach-Hertig et al. 1999; Ballentine and Hall 1999). These techniques have been used widely to infer the groundwater temperature that prevailed during the last occurrence of gas exchange between groundwater and soil air. This temperature is known as the "noble gas temperature" and the procedures used to determine it are known as the "noble gas thermometer" (Mazor 1972).

2.2 Experimental Methods

Water samples taken in the field need to be transported to a laboratory that is specially equipped for the extraction and analysis of noble gases (see also Aeschbach-Hertig and Solomon 2012). In the laboratory, the concentrations of dissolved noble gases are determined from the amounts of each noble gas in the water sample and the mass of the water sample. Because noble gases are only slightly soluble in water, contact between the water samples and air (or any other gas reservoir) must be avoided during sampling, transport, storage and processing.

Conventional bulk water samples from surface waters or groundwater are allowed to expand into a vacuum system to extract the dissolved noble gases from the water (e.g., Bayer et al. 1989; Jean-Baptiste et al. 1992; Beyerle et al. 2000; Sültenfuss et al. 2009). The analysis of noble gases from sediment porewater or stalagmite water inclusions requires additional experimental steps to separate the water from its confining matrix prior to the vacuum extraction process. This critical step, which must be carried out in such a way that the water sample is not exposed to air or to any other gas, needs to be adapted to the type of sample (Sects. 3.2 and 4.2). After separation from the matrix, the dissolved gases are extracted from the water and transferred to a vacuum system to purify and separate out the different noble gases. The gas amounts and isotope ratios are then determined by static mass spectrometry using peak-height comparison (e.g., Beyerle et al. 2000).

The minimum sample size required for noble gas analysis is determined by the sensitivity of the mass spectrometer, the degree of dilution of the sample during the extraction and purification of the sample gas, and the detection limit of the analytical system. Taking these factors together, the practical minimum sample size required for a typical analytical system is approximately 0.1–1 mg of water.

3 Lacustrine and Oceanic Sediments

3.1 Noble Gases in Sediment Porewater

Because gas exchange across the air-water interface is rapid, noble gas concentrations at the surface of lakes and the ocean correspond closely to ASW concentrations as computed from the water temperature, salinity and atmospheric pressure (Sect. 2.1.1).

For the purpose of this chapter, concentrations of excess air are assumed to be negligible in surface waters. Small amounts of excess air are observed only in large lakes and in the ocean, where excess air can be produced by the dissolution of bubbles entrained by breaking waves (Craig and Weiss 1971; Bieri 1971) or by the addition of meltwater from air-rich ice (Hohmann et al. 2002; Loose et al. 2009). The resulting noble gas excesses are usually ≤ 5 % for Ne and even less for the heavier noble gases (Craig and Weiss 1971; Peeters et al. 2000).

The vertical distribution of heat and conservative solutes (e.g., noble gases and salts) in the water column is dominated by vertical transport resulting from advection and macroscopic turbulence ("eddy diffusion", Lerman et al. 1995). The atmospheric noble gas concentrations observed at a given water depth are therefore coupled to the temperature and salinity of the water at that depth. They therefore correspond closely to the ASW concentrations calculated from this water temperature and salinity, as confirmed experimentally by, for instance,

Aeschbach-Hertig et al. (1999) and Peeters et al. (2000).

During sedimentation, part of the open water just above the sediment-water interface is incorporated into the sediment pore space. The noble gas concentrations in this porewater therefore carry information about the temperature and salinity of the bottom water in the past (see examples discussed in Sect. 3.3.1). Analogously, dissolved chloride concentrations and the $\delta^{18}O$ signature in the sediment porewater have been used to reconstruct palaeoenvironmental conditions in the ocean (Adkins et al. 2002; Schrag et al. 1996, 2002). However, geochemical alteration of the chloride concentrations in the porewater may mask the palaeosalinity information (e.g., Austin et al. 1986; Swart 2000). Also, the $\delta^{18}O$ signature in sea water depends not only on water temperature and salinity, but also on the volumes of reservoirs of freshwater (ice, groundwater), which change in response to different climate conditions. Further, $\delta^{18}O$ in the porewater may even be affected by the recrystallisation of dissolved carbonates (Swart 2000). By contrast, the concentrations of dissolved atmospheric noble gases are unaffected by such secondary processes and thus provide a direct measure of water temperature and salinity in the past.

While the noble gas signature in the bottom water is recorded and buried in the sediment, molecular diffusion acts at the same time to smooth out the noble gas profiles. This smoothing will, in principle, result in a loss of information with regard to the past noble gas signature in the water body, leading to a loss of information about the corresponding past environmental conditions. To assess the relative importance of sediment burial (advection) and diffusion for the archived noble gas signature, the distances by which solutes are transported by sediment burial or diffusion need to be compared (see also Strassmann et al. 2005, and references therein):

- Sediment burial: The sediment burial velocity relative to the sediment surface is governed by the rates of sediment accumulation and compaction. For simplicity, compaction is assumed to be so small, that the vertical porewater offset relative to the sediment matrix is negligible. The porewater burial velocity is therefore approximately equal to the sediment accumulation rate (s). Within a given time interval Δt, the porewater is transported downwards a distance Δz_{adv}:

$$\Delta z_{adv} \approx s\Delta t \tag{3}$$

- Diffusion: In contrast to advection, the characteristic transport length ($\Delta z_{diff,i}$) of a diffusive process increases with the square root of the elapsed time according to the Einstein-Smoluchowski equation (e.g., Einstein 1905; Grathwohl 1998; Schwarzenbach et al. 2003):

$$\Delta z_{diff,i} \approx \sqrt{\phi D_i \Delta t} \tag{4}$$

where ϕ is the sediment porosity and D_i is the effective diffusivity of the noble gas i in the sediment, given by:

$$D_i = D_i^0/a \tag{5}$$

where D_i^0 is the molecular diffusivity of gas i in bulk water and $a \geq 1$ is a scaling factor describing the effect of diffusion retardation in the sediment. This scaling factor takes into account the tortuosity of the sediment matrix, but also accounts for any other effects that may result in the retardation of diffusion in the porewater (Sect. 3.3.3).

The diffusive smoothing of vertical noble gas profiles can be considered negligible when the diffusive transport length ($\Delta z_{diff,i}$) is negligible compared to the advective transport length (Δz_{adv}); i.e., when $\Delta z_{diff,i} \ll \Delta z_{adv}$. Combining Eqs. (3), (4) and (5), and assuming $\phi \approx 1$ yields:

$$D_i^0/a \ll s^2\Delta t \approx sL \Leftrightarrow Pe = \frac{sL}{D_i^0/a} \gg 1 \tag{6}$$

where Pe is the Peclet number and L is the sediment-depth range considered. With $L \approx s\Delta t$ (still neglecting compaction), the importance of diffusion for smoothing the noble gas profiles therefore depends on the sediment accumulation rate and the time range considered. Strassmann et al. (2005) showed that in a "typical" sediment

a step-like Xe profile would be smoothed out by diffusion over appoximately 2 m in 10^2 years, 5 m in 10^3 years, and 20 m in 10^4 years. A scaling factor $a \approx 2$ was assumed in these calculations to reflect the tortuosity of the sediment matrix. These results illustrate that even if diffusion does smooth out the noble gas profiles, the palaeoenvironmental information is retained in the sediment over a large depth range L (i.e., if $Pe \gg 1$).

Apart from the reconstruction of palaeoenvironmental conditions, noble gases dissolved in sediment porewater have been shown to be sensitive tracers for the transport of solutes and pore fluids within the sediment column and for the exchange of solutes and fluids between the sediment and the overlying water body (see examples discussed in Sect. 3.3.2). The transient behaviour of radiogenic He isotopes accumulating in the porewater is especially suitable for studying the dynamics of the transport of solutes and fluids in the sediment. In addition, the $^3He/^4He$ ratio of the different He components reflects the geochemical origin and history of the pore fluids.

3.2 Experimental Methods

Peeper methods have been used to sample dissolved He in sediment porewater (Stephenson et al. 1994). A peeper is a dialysis sampler which is buried in the sediment. A gas-permeable membrane separates the sediment porewater from the sample cells, which are filled with gas or water. However, peepers need to be left at the sampling site for several days or weeks to allow the He in the sample cells to equilibrate with the He in the surrounding porewater (Dyck and Da Silva 1981). Because of their lower diffusivity, the heavier noble gases would require even longer equilibration times. Also, gases are lost rapidly from the sample cells during peeper retrieval and sample processing as a result of degassing caused by the decrease in hydrostatic pressure. Finally, peepers may not be suitable for sampling at great water depths because the membranes of the peeper cells collapse under the hydrostatic pressure exerted.

A wireline tool has been used for the in-situ sampling of porewater in marine sediment drill holes to quantify He fluxes through the sediment-water interface (Barnes 1973; Barnes and Bieri 1976; Barnes 1979, 1988; Sano and Wakita 1987). This non-standard sampler is complicated to operate and gas leakage may occur from the samples. Torres et al. (1995) and Winckler (1998) determined He, Ne, Ar, Kr and Xe concentrations in samples obtained using this tool, but it was also noted that gas bubbles may form in the system during sampling. Hence, the noble gas concentrations in the sample can vary in an uncontrollable manner because of gas exchange between the sample and the gas bubbles. Also, contamination with the drilling fluid or the water used to fill the in-situ sampler may occur (Winckler 1998).

To overcome the shortcomings of the methods described above, Brennwald et al. (2003), Chaduteau et al. (2007) and Tomonaga et al. (2011a) developed new experimental methods that rely on simple, robust, and standard sedimentological equipment. In the following, these state-of-the art methods will be described in detail.

3.2.1 Sampling

Sediment cores are collected in plastic tubes (liners) using a gravity corer or a similar coring device. After recovering the sediment core, about 30 g of bulk sediment is sampled from the desired sediment depths. Similar to noble gas sampling in bulk water (e.g., Beyerle et al. 2000), copper tubes are used as sample containers. The copper tubes are connected to the sediment core via fittings that penetrate into the core (Fig. 3a; Brennwald et al. 2003). Sampling ports can be drilled and covered with adhesive tape before coring to minimise the risk of contaminating the sediment with air.

Immediately after collecting the core, the sediment sample is transferred from the liner

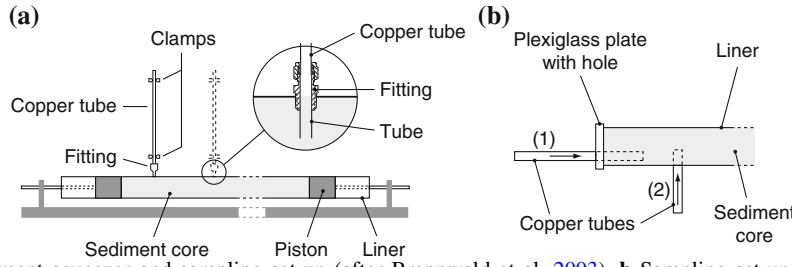

Fig. 3 **a** Sediment squeezer and sampling set-up (after Brennwald et al. 2003). **b** Sampling set-up for direct 'sub-coring' into copper tubes parallel (1) or perpendicular (2) to the axis of the sediment core (after Chaduteau et al. 2007)

into the copper tubes utilising the squeezer set-up shown in Fig. 3a. The copper tubes are flushed with sediment to remove residual air and to expel the sediment fraction which may have exchanged noble gases with the atmosphere while the copper tubes were being mounted. The samples are closed and sealed by pinching off the copper tubes at both ends using the same standard clamps as those used with conventional water samples. This procedure allows the sampling of intact sediment cores and avoids air contamination and gas loss during sampling. By inspection of a layered sediment core after sampling, the uncertainty in sampling depth has been estimated to be less than 5 cm (Brennwald et al. 2004).

An alternative sampling method was developed by Chaduteau et al. (2007). Sediment is sampled in copper tubes by pushing the tubes into the sediment either parallel or perpendicular to the axis of the sediment core (Fig. 3b). This method has the advantage of being less destructive to the sediment core, and of requiring less sediment material because the copper tubes are not flushed with sediment. This "sub-coring" into the copper tubes causes hardly any interference with most other classical sedimentological analyses of the core. Also, the sampling depth within the sediment core is well defined, as there is no offset due to squeezing. This method works best with soft sediments that will easily fill the copper tubes. For other sediments, the squeezing method may be better suited. A disadvantage of the method of Chaduteau et al. (2007) is that it does not allow the copper tubes to be flushed with sediment material, which would help to avoid contamination of the sample with air.

3.2.2 Extraction and Analysis of Dissolved Noble Gases

The methods used to extract dissolved noble gases from conventional water samples (Bayer et al. 1989; Beyerle et al. 2000) cannot be applied directly to the porewater of unconsolidated sediments because the porewater is embedded and trapped in the sediment matrix. Brennwald et al. (2003), Chaduteau et al. (2007) and Tomonaga et al. (2011a) therefore developed other methods of extracting the gases from the porewater.

The method of Brennwald et al. (2003) for extracting the dissolved noble gases from the sediment porewater involves heating and opening the copper tube, which is attached to an evacuated extraction vessel. Heating increases the pressure in the copper tube, causing the whole sediment sample to be extruded explosively into the extraction vessel when the tube is opened. The dissolved noble gases are then extracted into the vacuum of the extraction vessel. The sample gases are transferred into a gas purification system, where the noble gases are cleansed of other gases which would interfere with the subsequent mass spectrometric analysis. This allows the noble gas concentrations to be determined with a standard error of <2 %. In some sediments, however, considerable amounts of radiogenic He can be released from the minerals when the sediment

sample is heated during analysis, resulting in lower accuracy.

To reduce the release of radiogenic He from the sediment minerals by excessive heating, Chaduteau et al. (2007) developed an alternative method for the analysis of dissolved He in porewater. The sediment is transferred from the copper tube to an evacuated glass flask by first briefly flame-heating the copper tube and subsequently flushing it with degassed, hot water. The dissolved He is then extracted from the water in the glass flask at approximately 40 °C with the help of a magnetic stirrer, and is then transferred into the He analysis system. Although untested, this method would seem to be suitable for analysing not only dissolved He, but all other dissolved noble gases also.

Tomonaga et al. (2011a) optimised the extraction process of Brennwald et al. (2003) by centrifuging the sediment samples in the copper tubes to separate the porewater from the sediment matrix. After centrifuging, the part of the copper tube containing pure porewater is separated from the compacted sediment at the sediment-water interface using a third clamp. The porewater in the water-filled part of the copper tube is then analysed in the same way as a standard water sample (e.g., Beyerle et al. 2000). This method completely avoids heating the sediment and therefore guarantees reliable analysis of the concentration and isotopic signature of the He dissolved in the porewater.

Compared to the method of Chaduteau et al. (2007), the method of Tomonaga et al. (2011a) avoids the extra step of producing water free of noble gases, but requires that the sediment sample be centrifuged before analysis. Note also that one has to be careful to avoid gas fractionation when centrifuging gas-rich sediment samples. If gas bubbles form in the sample because of gas supersaturation at the temperature and pressure prevailing in the copper tube, the noble gases originally dissolved in the porewater will partially escape into these bubbles. The gas bubbles are quantitatively removed from the sediment matrix during centrifuging, whereas only a fraction of the porewater is separated from the sediment. Centrifuging gas-rich sediments may therefore result in an undesirable fractionation of noble gases between the compacted sediment and the porewater sample used for analysis, which includes the gas headspace.

3.3 Applications in Environmental Studies

3.3.1 Palaeoenvironmental Conditions

Barnes (1979) was the first to suggest that archived concentrations of atmospheric noble gases dissolved in sediment porewater might be useful as palaeotemperature proxies. Implementation of this idea, however, was long hampered by the lack of suitable experimental methods. This obstacle was removed by the recently developed methods described in Sect. 3.2.

These new methods were applied for the first time by Brennwald et al. (2004) to study the noble gas record in the sediments of Lake Issyk-Kul (Kyrgyzstan, central Asia), one of the worlds largest high-altitude lakes. The lake has no outflow and is therefore slightly saline ($S = 6$ g/kg). Such closed lakes are known to exhibit large changes in lake level and salinity in response to changes in local climate (e.g., Fritz 1996). Analyses of the lake basin morphology and sedimentological proxies showed that during the mid-Holocene the salinity of the lake water was highly variable and that the lake level lay several hundred metres below its present level (e.g., De Batist et al. 2002; Giralt et al. 2003; Ricketts et al. 2001; Romanovsky 2002).

Distinct minima in the concentrations of atmospheric noble gases in the sediment porewater were observed at approximately 90 cm sediment depth (Fig. 4). The effective diffusivities of the noble gases in the sediment porewater were found to be at least two orders of magnitude lower than in the bulk water, implying that the noble gas profiles in the sediment are virtually unaffected by vertical diffusion in the porewater. The ratio of the molecular diffusivity of Ar in water to that of Xe is 2.1. Assuming the diffusive pathways in the pore space to be the same for Ar and Xe, Eqs. (4) and (5) yield $\Delta z_{\mathrm{diff,Ar}}/\Delta z_{\mathrm{diff,Xe}} \approx \sqrt{D^0_{\mathrm{Ar}}/D^0_{\mathrm{Xe}}} \approx 1.5$.

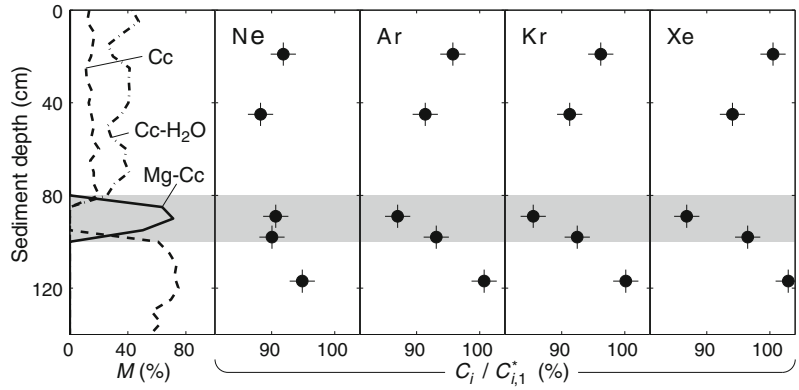

Fig. 4 Mineralogical sediment composition (M) and noble gas concentrations in the porewater (C_i, normalised to present-day ASW noble gas concentrations $C^*_{i,1}$ in the open water) as a function of sediment depth (Brennwald et al. 2004). Cc: calcite. Mg-Cc: magnesian calcite, which is precipitated in water of high salinity. Cc-H_2O: monohydrocalcite

Analogously, $\Delta z_{\mathrm{diff},Ar}/\Delta z_{\mathrm{diff},Kr} \approx 1.3$. However, this diffusive separation disagrees with the measured noble gas data, because, within the vertical resolution of the measurements, the respective concentration minima are all found at the same sediment depth. Brennwald et al. (2004) therefore concluded that diffusion is strongly limited and is insufficient to decouple the Ar, Kr and Xe signals in the porewater from the sediment matrix. The noble gas concentrations at a given sediment depth are therefore essentially determined by the physical conditions prevailing in the overlying water at the time when the sediment was deposited.

The minima in the atmospheric noble gas concentrations at 90 cm sediment depth indicate that either the salinity of the water, its temperature, or both, were considerably higher during the mid-Holocene than they are now. A simple model linking the noble gas concentrations in the deep water of Lake Issyk-Kul to the volume of the lake, and hence to its water level, allowed Brennwald et al. (2004) to infer from the noble gas record of the porewater that the lake level was approximately 300 m lower in the mid-Holocene than it is today (Fig. 5).

In Soppensee, a small Swiss freshwater lake with a maximum water depth of 27 m, noble gas concentration profiles in the sediment porewater

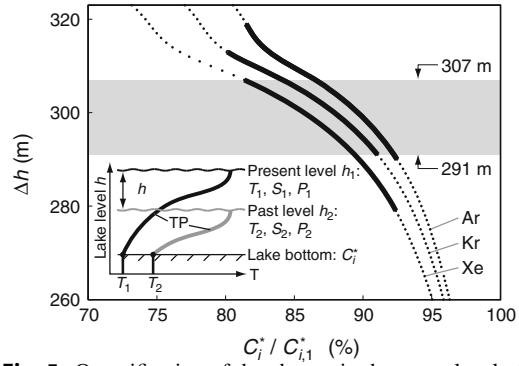

Fig. 5 Quantification of the change in the water level of Lake Issyk-Kul (Brennwald et al. 2004) based on the concentrations of dissolved Ar, Kr and Xe in the porewater. ASW concentrations in the water body (C^*_i) were calculated as a function of the change in lake level Δh. The C^*_i were normalised to present-day ASW concentrations $C^*_{i,1}$ calculated from the present-day temperature (T_1) and salinity (S_1) of the overlying water and the mean atmospheric pressure (P_1) at the water surface. T_2, S_2 and P_2 are the respective values of temperature, salinity and pressure during a period of lower lake level in the past. The annual mean temperature profile in the lake (TP) was used to model C^*_i because the noble gas concentrations in the porewater reflect the annual mean temperature of the deep water (Brennwald et al. 2003). The solid parts of the curves represent the analytical 2σ uncertainty range of the measured minimum concentrations in Fig. 4. In the range 291 m $< \Delta h <$ 307 m (horizontal grey bar), all modelled concentrations simultaneously match the measured minimum concentrations within the limits of analytical uncertainty

were used to study and reconstruct the formation of methane bubbles in the sediment and their release into the overlying water body (Brennwald et al. 2005). The noble gas concentrations in the porewater of Soppensee were found to be much lower than the ASW concentrations of the overlying water (up to 75 % Ne depletion, and increasingly less for Ar, Kr and Xe, which are more soluble). This depletion is greatest just below the sediment surface and decreases steadily with sediment depth.

The decrease in noble gas depletion with the gas solubility is indicative of the loss of dissolved noble gases into a gas phase which was initially free of noble gases (Ballentine et al. 2002; Bosch and Mazor 1988; Holzner et al. 2008; Winckler et al. 2000). Brennwald et al. (2005) attributed this depletion pattern to the stripping of dissolved noble gases into gas bubbles forming in the sediment as a result of supersaturation of the porewater with biogenic CH_4. The escape of these gas bubbles from the sediment results in the observed noble gas depletion of the porewater.

The $^{20}Ne/^{22}Ne$ and $^{40}Ar/^{36}Ar$ ratios in the Soppensee porewater agree with their respective atmospheric equilibrium ratios. Brennwald et al. (2005) assumed that the diffusion of noble gases from the porewater into the gas bubbles would result in their isotopic fractionation in the porewater, as expected from Graham's Law ($D_i/D_j = \sqrt{m_j/m_i}$, where D_i and D_j are the diffusion coefficients of two isotopes i and j of the same element and m_i and m_j are their respective masses). The lack of such an isotopic fractionation indicates that the observed noble gas depletion is not controlled by the kinetics of gas partitioning between the porewater and the gas bubbles. In contrast, a secondary solubility equilibrium between porewater and gas bubbles is attained. Brennwald et al. (2005) therefore used a simple gas equilibration model to estimate the amount of exsolved CH_4, which was found to correspond to about 25 % of the total CH_4 that can be stored in dissolved form in the Soppensee sediments.

Using an argument similar to that used for Lake Issyk-Kul, Brennwald et al. (2005) showed that the lack of isotope fractionation also indicates that the noble gas signature in the porewater at a given sediment depth reflects the intensity of methane ebullition at the time when this sediment was deposited; i.e. that vertical diffusion had virtually no effect on the noble gas profiles in the porewater.

However, the molecular dynamics calculations of Bourg and Sposito (2008) suggest that isotopic fractionation owing to molecular diffusion in water might be much smaller than expected from Graham's Law, which has been validated experimentally only for the diffusion coefficients of ^3He and ^4He (Jähne et al. 1987), but not for the diffusivities of the Ne or Ar isotopes. The lack of experimental data on the extent to which the isotopic fractionation of Ne and Ar is affected by diffusion in water does not allow the importance of diffusion for the noble gas profiles in the Soppensee porewater to be conclusively assessed.

3.3.2 Transport and Geochemical Origin of Pore Fluids

Dissolved noble gases make good tracers for the transport of solutes within the sediment porewater. The transient behaviour of radiogenic He isotopes accumulating in the porewater is particularly useful for studying the transport and geochemical origin of solutes and fluids in the sediment. In a few early studies (Barnes and Bieri 1976; Barnes 1987; Sano and Wakita 1987; Sayles and Jenkins 1982; Winckler 1998), the wireline tool discussed in Sect. 3.2 was used to study the fluxes of He isotopes through oceanic sediments. Stephenson et al. (1994) used a modified peeper (Sect. 3.2) to determine He concentrations when studying the injection of groundwater through the sediment into two small lakes.

Noble gas signatures in the sediment porewater and in the overlying water body of the Black Sea have been used to study the injection of geogenic fluids into the deep water, to determine their geochemical origin and to characterise CH_4 emissions from high-intensity gas seeps in the vicinity of active mud volcanoes (Holzner et al. 2008). Both the He concentrations and their

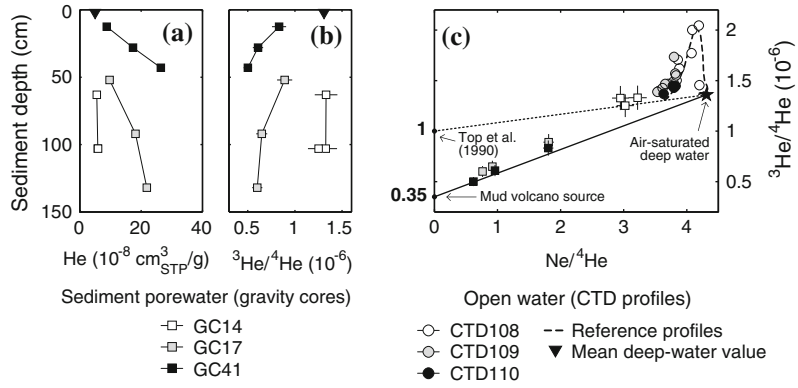

Fig. 6 Noble gas signatures in the sediment porewater (squares) and the open water body (circles, triangle) of the Black Sea, measured near active gas seeps at the Sorokin Trough (sediment cores GC17 and GC41, open-water profiles CTD109 and CTD110) and at a reference site not affected by outgassing (GC14 and CTD108). **a** He concentrations in the sediment porewater. **b** ^{3}He/^{4}He isotope ratios in the sediment porewater. **c** The ^{3}He/^{4}He ratio as a function of the Ne/^{4}He ratio for the sediment porewater, the open water at the seep area and the mean open-water reference profile (dashed line). Straight lines indicate mixing between ASW and a seafloor source with a ^{3}He/^{4}He ratio of 10^{-6} (dotted line) as determined by Top et al. (1990) for the southern Black Sea, and with a mud-volcano source with an estimated ^{3}He/^{4}He ratio of $3.5{\cdot}10^{-7}$ (solid line). After Holzner et al. (2008)

vertical gradients in the sediment porewater were found to be much greater near the gas seeps than at a reference site located approximately 200 km from the gas seeps that is unaffected by mud volcanism. The terrigenic He component of the pore fluids and of the open water body (Fig. 6) shows a ^{3}He/^{4}He ratio of approximately $3.5 \cdot 10^{-7}$ near the gas seeps, whereas the terrigenic He at the reference site is enriched in ^{3}He (^{3}He/^{4}He$\approx$ 10^{-6}). These differences in the abundance and in the isotopic signature of the terrigenic He in the sediment porewater illustrate the variability in the flux and the geochemical origin of the He (and the associated pore fluids) released from the Black Sea sediments.

A similar approach was used to study the fluids released from cold CH_4 seeps off the coast of New Zealand (Tomonaga 2010). The He-Ne signatures in the porewater at two sampling sites at Omakere Ridge and one site at Rock Garden (near the Pacific-Australian subduction zone) show a mixture of ASW and terrigenic He. The ^{3}He/^{4}He ratio of the terrigenic He at the two sites at Omakere Ridge is approximately $6 \cdot 10^{-7}$, which indicates that the terrigenic He is mainly of crustal origin. At Rock Garden, the pore fluids have a ^{3}He/^{4}He ratio of approximately $2.5{\cdot}10^{-6}$, which suggests that these fluids are enriched with mantle-derived ^{3}He.

At the Congo-Angola margin, the He dissolved in the sediment pore fluids near cold fluid seeps was found to be a mixture of seawater-derived He and radiogenic He produced in the sediment column or in the underlying crust (Chaduteau et al. 2009). The vertical He concentration profiles in the porewater and the pore-fluid temperature profiles were used to study pore-fluid circulation and to estimate pore-fluid advection rates in the sediment. The porewater He concentration profiles were shown to be more sensitive than the porewater temperature profiles to pore-fluid advection rates.

At the Mid-Okinawa Trough (Japan), ^{3}He/^{4}He and ^{4}He/^{20}Ne ratios in sediment porewater were used to study earth degassing at subduction zones by estimating the fluxes of terrigenic He isotopes through the sediment and into the ocean (Lan et al. 2010). The ^{3}He fluxes observed at a hydrothermally active site amount to about 20 % of the ^{3}He fluxes measured at the East Pacific Rise. Lan et al. (2010) argued that submarine hydrothermal systems in back-arc basins may therefore contribute a significant amount of helium to the ocean.

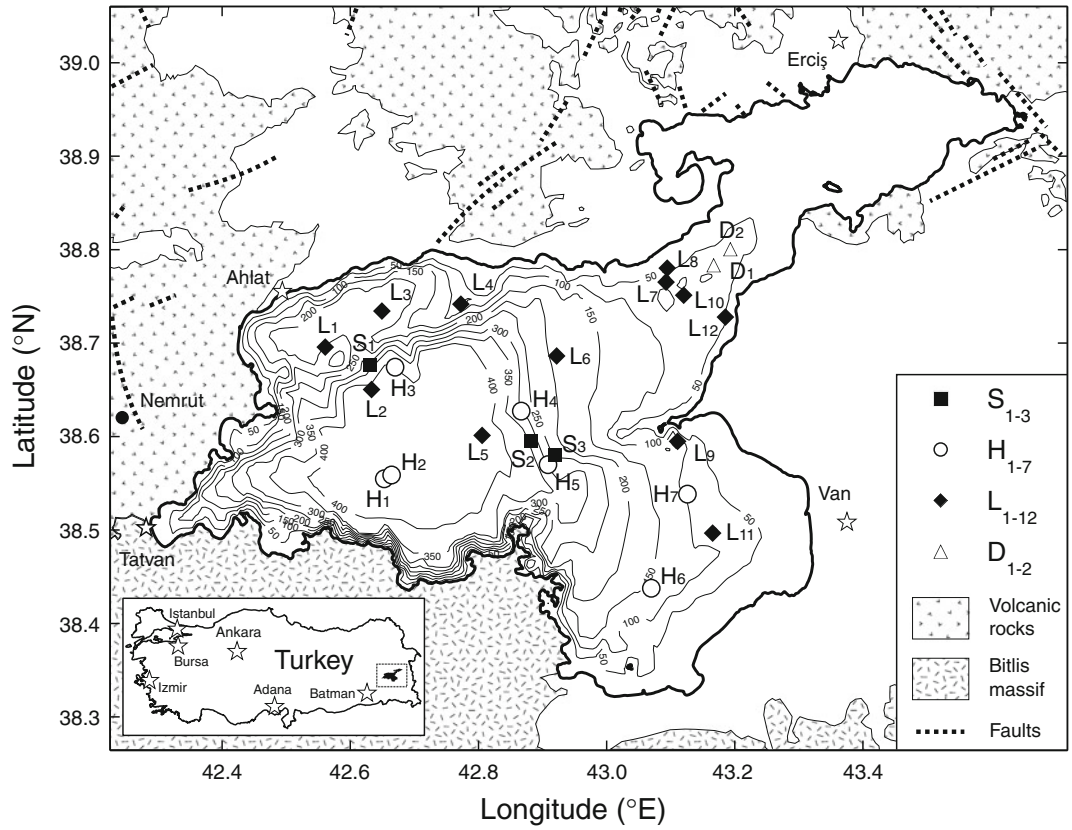

Fig. 7 Geological map of Lake Van, showing the bathymetry of the lake basin and the sediment sampling sites (after Tomonaga et al. 2011b). (**L**) low He fluxes. (**H**) high He fluxes. (**S**) "hot spots" with highest He fluxes. (**D**) noble gas concentrations showing degassing artefacts, possibly caused by bubble formation during sampling

In Lake Van (eastern Anatolia, Turkey), a large, terminal, saline soda lake located in a region of high tectonic and volcanic activity, Tomonaga et al. (2011b) studied the flux of terrigenic He through the sediment. Analysis of the He profiles in 24 sediment cores taken at different sites in the lake showed that the He flux varies strongly within the lake basin, from $0.4 \cdot 10^8$ atoms/m^2/s to $42 \cdot 10^8$ atoms/m^2/s. The largest He fluxes were found at the steep borders of the central, deep part of the lake basin (stations S_1, S_2, and S_3 in Fig. 7). The isotope ratio for the terrigenic He is essentially the same in all sediment cores ($^3He/^4He \approx (2.6–4.1) \cdot 10^{-6}$), which suggests that this He is a mixture of crustal He and mantle He originating from a single, sub-continental source. Tomonaga et al. (2011b) argued that the release of He from the underlying lithosphere is fostered by fault structures that are most likely related to the ongoing subsidence of the circular main basin of the lake and to volcanic activity. This supports the hypothesis that the circular-shaped deep basin was formed by the collapse of an ancient caldera (Litt et al. 2009).

In the estuary of the St. Lawrence River (Québec, Canada), Pitre and Pinti (2010) studied the use of dissolved atmospheric noble gases in sediment porewater as proxies for the dynamics of dissolved or gaseous N_2 produced by nitrate reduction in the sediment. In contrast to previous work, large excesses of atmospheric noble gases with respect to ASW were observed in the porewater samples of these estuarine sediments. The excess increased with increasing atomic mass, which led Pitre and Pinti (2010) to the

hypothesis that the sediments were enriched with noble gases as a result of their sorption on to clay minerals or organic matter in the sediment.

3.3.3 Diffusion and Trapping Mechanisms

Some of the data discussed in Sect. 3.3.1 show that diffusion does not smooth out the noble gas profiles in the sediment enough to cause the information on the environmental history of the overlying water body to be lost, even over sediment depth ranges smaller than the diffusion lengths calculated by Strassmann et al. (2005) (Sect. 3.1). This can only be explained if the corresponding scaling factors a are several orders of magnitudes greater than would be expected from conventional tortuosity models of unconsolidated sediments.

Although a similar suppression of diffusion has been observed for He and H_2 in the porewater of compacted clays (Horseman et al. 1996), this phenomenon is not commonly reported for other gases dissolved in the porewater of slightly compacted lacustrine and oceanic sediments. While little is known about the mechanisms responsible for the suppression of the diffusion of noble gases in sediment porewater, the following conceptual hypotheses can be put forward as possible explanations:

1. Because of the formation of new minerals or because of a geometric realignment of the sediment grains during sedimentation, compaction and early diagenesis, the diameter of the sediment pores or of the channels connecting them can be as small as a few μm or less (e.g., Horseman et al. 1996). In this case the Renkin effect (i.e., the increased viscosity of the water in the vicinity of the pore walls) will result in a reduction of molecular diffusion by several orders of magnitude (Renkin 1954; Grathwohl 1998; Schwarzenbach et al. 2003; Brennwald et al. 2004), as seems to be the case in firn (Beyerle et al. 2003; Huber et al. 2006).
2. A considerable fraction of the pore space might consist of "dead" pores; i.e., pores that are not connected to the main pore space through which diffusive transport occurs on macroscopic scales. Solutes trapped in the dead pores cannot undergo macroscopic transport through the fully connected pore space. Note that conventional transport models axiomatically exclude the possibility of the occurrence of dead pores (e.g., Berner 1975; Imboden 1975; Strassmann et al. 2005), although the retention of solutes in dead pores results in a strong reduction in overall diffusivity within the sediment (e.g., Grathwohl 1998). To our knowledge, however, this axiomatic exclusion of dead pores appears not to be based on solid experimental evidence and may therefore represent an inappropriate model simplification.
3. Microscopic gas bubbles might act as gas reservoirs. In the presence of such gas bubbles in the sediment, a large fraction of the noble gases initially dissolved in the porewater would escape into these bubbles, because noble gases are only slightly soluble in water. This fraction of the noble gas content of the sediment would be excluded from macroscopic diffusion through the porewater (see also the discussion by Tomonaga 2010). As in the case of the postulated dead-pore mechanism, this would result in the effective diffusion of noble gases, and possibly of other volatile gases, being strongly suppressed on a macroscopic scale.
4. Noble gases might be adsorbed on to the sediment matrix; e.g., on to organic matter (Pitre and Pinti 2010). To our knowledge, the quantitative sorption of noble gases on to unconsolidated sediments has not yet been observed. However, if noble gases are indeed adsorbed quantitatively on to the sediment matrix, only the fraction of the noble gases that remain dissolved in the porewater would be subject to diffusion, as the adsorbed fraction would be retained by the sediment matrix. This would result in strong retardation of diffusive noble gas transport in the porewater.

Up until now, however, a systematic and conclusive assessment of these hypotheses has not been possible because of a lack of experimental evidence. Additional studies focusing on the mechanisms described above would be

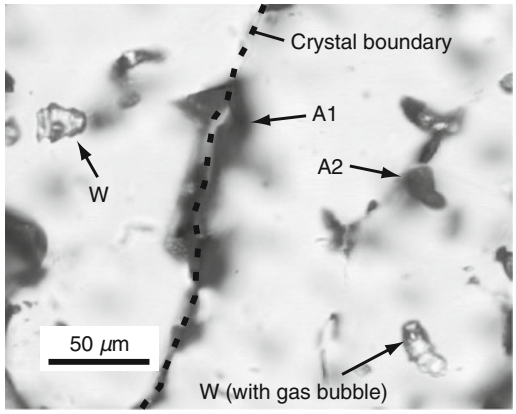

Fig. 8 Photomicrograph of a thin section from a stalagmite (after Scheidegger et al. 2008, 2010). Water inclusions (W) are located within the calcite crystals. Large air inclusions (A1) are observed at the crystal boundaries, whereas smaller air inclusions (A2) also occur within the calcite crystals

required to improve our understanding of how and why macroscopic noble gas diffusion in sediment porewater can be attenuated much more strongly than would be expected from conventional tortuosity models.

4 Stalagmites

4.1 Noble Gases in Stalagmite Fluid Inclusions

Stalagmites are formed in caves by the precipitation of calcite from drip water. The actively growing stalagmite surface is covered by a thin layer of drip water on the order of 0.1 mm thick (Dreybrodt 1980). Gas concentrations in this layer attain solubility equilibrium with the cave air within seconds to minutes. This rapid gas exchange allows the outgassing of excess CO_2, resulting in the precipitation of calcite in the water layer and promoting the growth of the stalagmite. Noble gas concentrations in the water layer, however, can be assumed to correspond closely to ASW concentrations (Sect. 2.1.1).

During stalagmite growth, minute quantities of drip water and cave air are trapped in the bulk calcite as fluid inclusions, which may contain water, cave air, or both. The abundance of the inclusions, and the volumetric ratio of air to water contained within them, vary strongly from stalagmite to stalagmite, and also differ considerably within individual stalagmites (e.g., Kluge et al. 2008). Microscopic investigations have shown that water and air inclusions differ in size and spatial arrangement within individual stalagmites (Scheidegger et al. 2010). Water inclusions are found mainly within the stalagmite calcite crystals, but only rarely at crystal boundaries (Fig. 8). The water inclusions usually do not exceed 50 μm in length. The water abundance per unit mass of calcite typically lies between 0.1 and 1 mg/g (Kendall and Broughton 1978; Schwarcz et al. 1976; Kluge et al. 2008). While air inclusions do occur within calcite crystals (intra-crystalline inclusions), they occur predominantly along grain boundaries between the calcite crystals (inter-crystalline inclusions). Intra-crystalline air inclusions are similar in size and shape to water inclusions (Fig. 8), whereas inter-crystalline air inclusions are larger (20–80 μm long) and more angular (Scheidegger et al. 2010). Air inclusions can account for up to 3 % of a stalagmite's volume (Badertscher et al. 2007; Scheidegger et al. 2010).

Once a fluid inclusion has been formed, it is no longer in contact with the cave air. Using the He and Ar diffusion data of Musset (1969) and Copeland et al. (2007), Kluge (2008) estimated noble gas diffusivities in calcite at room temperature to be about 10^{-25} m^2/s. The diffusion of noble gases through the calcite surrounding a fluid inclusion therefore has a negligible effect on the noble gas concentrations in the inclusions even on time-scales of several 100 ka. The concentrations of dissolved noble gases in a given water inclusion can thus be assumed to reflect the temperature and salinity of the drip water at the time the inclusion was formed. The salinity of the drip water entering the cave is usually so low that it has no effect on noble gas solubilities. The concentrations of noble gases in water inclusions can therefore expected to be related directly and quantitatively to cave palaeotemperatures.

In most caves, temperatures remain constant throughout the year at a value corresponding

approximately to the annual mean air temperature outside the cave (e.g., McDermott et al. 2005; Poulson and White 1969; Smithson 1991). Noble gas records in stalagmite water inclusions are thus expected to allow regional palaeotemperatures to be reconstructed over long periods of time. Stalagmites are especially valuable as a source of such information because of their global distribution. This is in contrast to ice cores, which can supply similar information, but only for polar or high-altitude regions.

Stalagmites have therefore become a major focus for palaeoclimate studies over the past few decades. Stalagmite calcite contains precise, high-resolution $\delta^{13}C$, $\delta^{2}H$ and $\delta^{18}O$ records covering time-scales of up to 10^5 years (e.g., Badertscher et al. 2011; Cheng et al. 2009; Fleitmann et al. 2009; Henderson 2006; Wang et al. 2008). Also, the signatures of $\delta^{2}H$ and $\delta^{18}O$ in water inclusions have been used to study palaeoclimate conditions (Fleitmann et al. 2003; Griffiths et al. 2010; van Breukelen et al. 2008; Wainer et al. 2011). These stable-isotope records are controlled by different environmental variables and processes such as temperature-dependent isotope fractionation during calcite formation, the local precipitation regime, the hydrological cycle, and amounts of precipitation. The complex interplay of these variables and processes makes it difficult to interpret stalagmite isotope records clearly and unequivocally (e.g., Lachniet 2009). Use of the noble gas thermometer to provide an independent estimate of the temperature at which stalagmite water inclusions were formed would therefore not only provide valuable palaeoclimate information in its own right; it would also help to overcome some of the limitations involved in interpreting stalagmite stable-isotope records, thereby contributing to exploiting their full potential.

Determination of the concentrations of noble gases dissolved in the water of stalagmite fluid inclusions was until recently not feasible, mainly because of the lack of adequate extraction methods that would allow water and air inclusions to be separated. As noble gases are much more abundant in air inclusions than in water inclusions, their concentrations in water inclusions are often masked by the comparatively large amounts of noble gases released from air inclusions during the extraction process. The noble gas excess from the air inclusions is mathematically analogous to the excess-air component in groundwater Eq. (2). Noble gas temperatures in groundwater may be determined even in the presence of moderate amounts of excess air (e.g., Aeschbach-Hertig et al. 1999). However, if the excess-air component is large (i.e., if $Ne_{EA}/Ne_{ASW} \gtrsim 10$ in Eq. (2)), it will mask the ASW component to such a degree that the noble gas thermometer becomes unreliable. For the successful determination of noble gas temperatures from stalagmite water, it is of paramount importance to minimise the proportion of noble gases in the final sample that are derived from air inclusions.

4.2 Experimental Methods

Different approaches have been used to extract noble gases from stalagmite fluid inclusions (Sects. 4.2.2 and 4.2.3). Ayliffe et al. (1993) and Kluge et al. (2008) crushed stalagmites in vacuo to release noble gases from fluid inclusions. Kluge et al. (2008) applied this technique successfully to a stalagmite from Bunker Cave (Germany) that had an exceptionally low air-water volume ratio. However, the authors could not derive meaningful noble gas temperatures by applying their crushing method to more typical stalagmites with higher air-water volume ratios, because the noble gases released from the air inclusions masked the noble gas concentrations in the water inclusions.

Scheidegger et al. (2010, 2011) therefore explored alternative approaches that would reduce the contribution of noble gases derived from air inclusions to the final result. These approaches were all based on the authors' observation that most of the air inclusions in stalagmites occur along grain boundaries and can be opened preferentially by gently crushing a sample to yield grains approximately the same size as that of its intrinsic crystals, whereas the intra-crystalline water inclusions remain

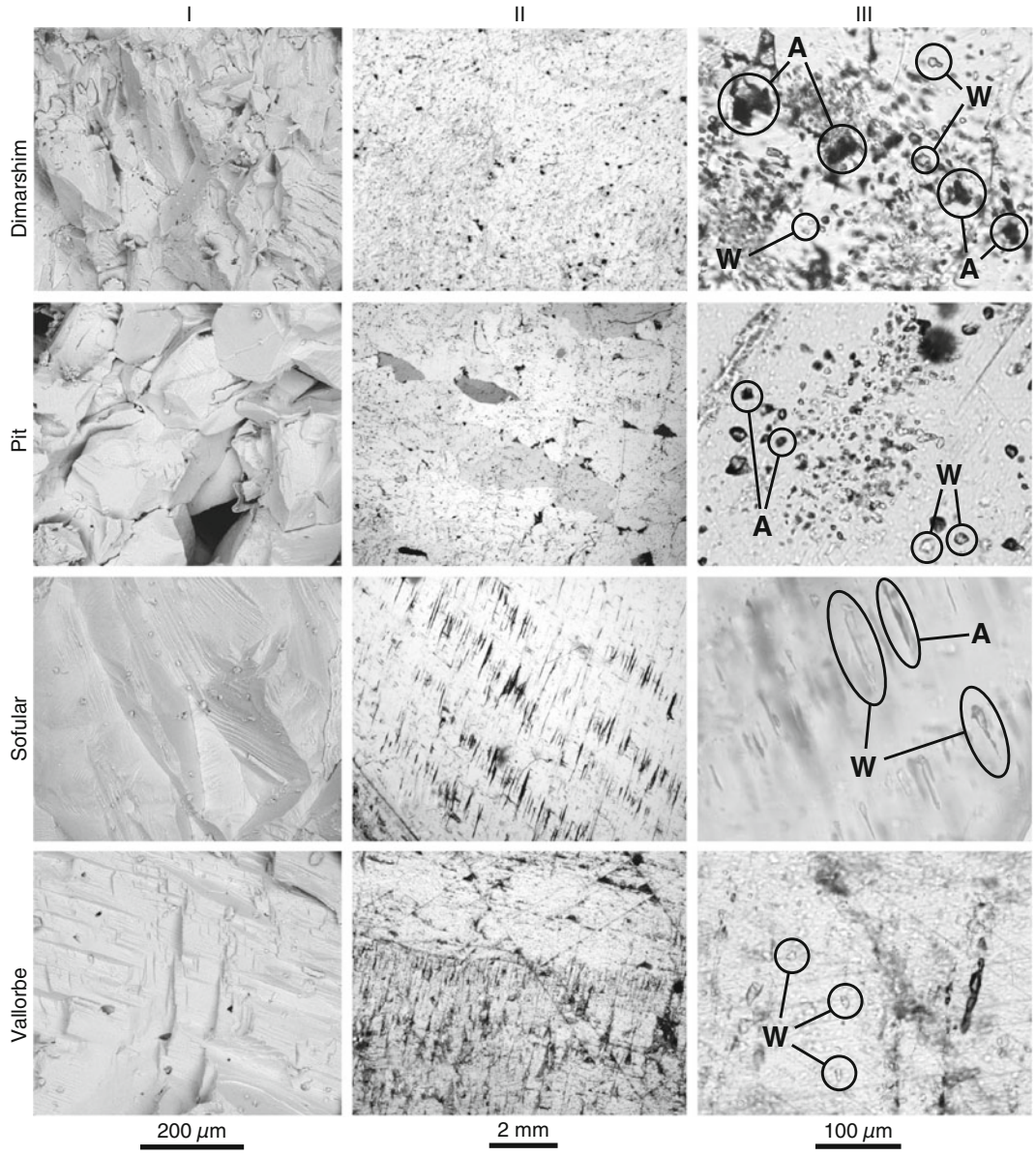

Fig. 9 Petrographic information on stalagmites from Dimarshim Cave and Pit Cave (both Socotra Island, Yemen), Sofular Cave (Turkey), and Vallorbe Cave (Switzerland) (after Scheidegger 2011). **I** SEM images showing the calcite texture of freshly crushed fractions. **II** Photographs of thick sections taken using an optical microscope at low magnification in cross-polarised light. **III** Photographs of thick sections taken using an optical microscope showing typical water (W) and air (A) inclusions

mostly intact. The noble gases extracted from the calcite in a second extraction step are thus derived primarily from water inclusions. The resulting noble gas signatures indeed revealed a much lower contribution of noble gases from air inclusions, making feasible a mathematical correction of the remaining air-related noble gas component (Scheidegger et al. 2010). Unfortunately, however, the procedures used to reduce the amount of noble gases released from

the air inclusions introduce other complexities into the noble gas signatures, thus still often preventing the straightforward calculation of meaningful noble gas temperatures (Sect. 4.3).

A seemingly obvious way of avoiding the problems associated with the release of noble gases from air inclusions would be to spot-drill individual water inclusions in vacuo with a laser. However, because of the small amount of water contained in a single inclusion and the low concentrations of noble gases in this water, the noble gas content of each inclusion is very small. To obtain amounts large enough for all stable noble gases to be analysed reliably, 10^4–10^5 water inclusions would have to be opened up (assuming typical detection limits for the mass-spectrometric noble gas analysis system), thus rendering this approach impracticable.

4.2.1 Sample Selection

As mentioned above, not all stalagmite samples are equally suited for the determination of noble gas temperatures. To be suitable, samples should have a water content of about 0.1 mg/g or higher (e.g. Kluge et al. 2008) and, equally importantly, the air-water volume ratio should not exceed a certain limit to avoid the ASW component from the water inclusions being masked by the noble gases released from the air inclusions. Kluge et al. (2008) give as an upper limit an air-water volume ratio of 0.5.

Microscopic investigation of the samples to be analysed for noble gases is therefore highly recommended. Scheidegger et al. (2011) used scanning electron microscopy and optical microscopy to study samples of different stalagmites. A selection of the images obtained is illustrated in Fig. 9. In addition to yielding information on the size and spatial distribution of air and water inclusions, these images also provide information on the size of individual calcite crystals. This information is essential for determining the grain size to which a given stalagmite sample needs to be pre-crushed in order to separate air and water inclusions most effectively (Sect. 4.2.2). The size of water inclusions in comparison to the crystal size and texture of the host calcite can also provide information about the temperature required to assure quantitative gas extraction during heating (Sect. 4.2.3).

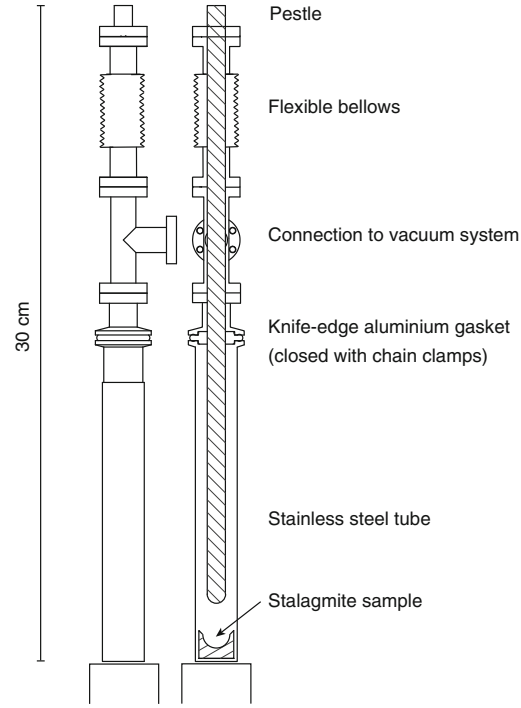

Fig. 10 Stainless steel vacuum crusher used to extract gases from fluid inclusions (after Scheidegger 2011). The pestle is connected to the main chamber via a flexible bellows. The sample is crushed by striking the top of the pestle with a hammer

4.2.2 Crushing

Crushing in Vacuo

Several different devices for crushing a stalagmite sample in vacuo have been described in the literature. Kluge et al. (2008) used a cylindrical cell containing a steel ball, controlled by an external magnet, as a crusher. Badertscher et al. (2007) and Kluge et al. (2008) reported experiments in which a sample is placed in a copper tube which is evacuated and then squeezed with a vice to crush the sample. Scheidegger et al. (2010) used a pestle-operated vacuum crusher (Fig. 10) in which the pestle and the cylinder holding the sample are connected via a flexible bellows. The sample is crushed by striking the

top of the pestle with a hammer. Following the crushing, the gases released from the sample are allowed to expand into a gas purification line leading to the noble gas mass spectrometer.

In an attempt to separate the gases released from the air inclusions from those released from the water inclusions, Scheidegger et al. (2010) applied several consecutive crushing steps to each sample, often followed by a final heating step (Sect. 4.2.3).

Crushing in a Gas Atmosphere

For stalagmites with typical air-water volume ratios, simple stepwise crushing in vacuo often does not allow the noble gases contained in water inclusions to be separated sufficiently well from the noble gases contained in air inclusions. Scheidegger et al. (2010, 2011) therefore explored the possibility of crushing stalagmite samples to a predefined grain size in different gas atmospheres. The appropriate grain size (e.g., 350–700 μm, Scheidegger et al. 2011), which should be close to the natural crystal size of the sample, is determined by microscopic inspection prior to crushing (Sect. 4.2.1). The sample is crushed using a stainless-steel mortar and pestle. After each gentle hammer stroke on the pestle, the sample is sieved to separate crystals of the desired size from larger crystal aggregates, and the large crystal aggregates are then crushed again. The crushing and sieving process is repeated until the whole sample consists of grains no larger than the predefined grain size. The air content of the resulting grains is 10^2–10^3 lower than that of a bulk stalagmite sample, because the air inclusions located at the grain boundaries are indeed preferentially opened during the crushing process (Scheidegger et al. 2011).

After crushing and sieving stalagmite samples in air and in a glove box flushed with N_2 (of purity 6.0), Scheidegger et al. (2010) found that in both cases residual atmospheric heavy noble gases were adsorbed on to the freshly produced grain surfaces. During the subsequent extraction of noble gases from these grains by heating (Sect. 4.2.3), the adsorbed noble gases were released together with the noble gases extracted from the fluid inclusions (Sect. 4.3.2). This increased the resulting concentrations of heavy noble gases considerably, so that in most cases, no meaningful noble gas temperature could be derived from the resulting data. Flushing the glove box with He (of purity 6.0) and further reducing the concentrations of residual heavy noble gases in the He atmosphere with a sorption pump installed in the glove box reduced the Kr and Xe residuals to negligible levels (Scheidegger et al. 2011). To prevent a crushed sample being exposed to air when transferring it to the noble gas purification line, it was first loaded into a stainless steel container sealed with a valve before removing it from the glove box.

4.2.3 Heating

Kluge et al. (2008) heated their vacuum-crushed samples to 50 °C to quantitatively transfer the extracted water into the analytical system (Sect. 4.2.4). In contrast, Scheidegger et al. (2010) heated their crushed samples up to 600 °C to open the intra-crystalline inclusions, which were assumed to be filled predominantly with water. Scheidegger et al. (2010) emphasised that the applied temperature must not exceed the threshold at which excessive amounts of gases such as CO_2 or H_2 are formed, as these prevent reliable determination of the amount of water released (Sect. 4.2.4). CO_2 is produced during the decomposition of calcite to CaO and CO_2 at temperatures $\gtrsim$600 °C (Faust 1950). H_2 is produced during the interaction of water released from the sample with the hot metal surfaces of the vacuum sample container. Scheidegger et al. (2010) found that at temperatures $\gtrsim$400 °C, the partial pressure of H_2 and the corresponding (non-stoichiometric) loss of H_2O exceed the limits below which the amount of water released from the sample can be reliably determined (Sect. 4.2.4). Best results were achieved by heating the

sample for 1 h to temperatures between 300 °C and 400 °C (Scheidegger et al. 2011).

4.2.4 Quantification of the Water Mass

Due to the low water content of stalagmites, typical stalagmite samples of 1–5 g yield no more than few milligrammes of water upon crushing or heating. Accurate determination of such a small mass of water is challenging and cannot easily be accomplished merely by weighing a sample before and after the water is extracted. Instead, the mass of water released is determined manometrically (Ayliffe et al. 1993; Kluge et al. 2008; Scheidegger et al. 2010). This requires the extracted water to be transferred quantitatively to a tempered expansion vessel large enough to prevent the water vapour from condensing. A pressure gauge is then used to determine the vapour pressure inside this vessel. Using the ideal-gas law, the water mass is then calculated from the vapour pressure, the temperature, and the volume of the expansion vessel.

To avoid bias in the determination of the mass of water, the gas pressure in the expansion vessel must be generated essentially by the water vapour only. Formation of excessive amounts of other gases (e.g., CO_2 or H_2) must therefore be avoided during the extraction process (Sect. 4.2.3). If this requirement is met, the manometric method allows the mass of a few milligrammes of water to be determined with a standard error of about 1 % (Scheidegger et al. 2010).

4.3 First Applications of the Noble Gas Thermometer

The occurrence of both air and water inclusions in stalagmites suggests that the noble gas signatures in stalagmite samples should reflect a simple binary mixture of air and ASW. Noble gas data from Bunker Cave stalagmite samples with exceptionally low air-water volume ratios are indeed consistent with this expectation (Sect. 4.3.1). However, results from other stalagmite samples with more typical air-water volume ratios indicate a more complex picture involving additional gas components, such as fractionated air or lattice-trapped noble gases (Sect. 4.3.2).

4.3.1 Stalagmites from Bunker Cave (Germany)

Kluge et al. (2008) studied two stalagmites from Bunker Cave (Germany) with air-water volume ratios of 0.03–0.08, which is exceptionally low. It was therefore not necessary to reduce the air content of these samples by pre-crushing, and precise noble gas temperatures could be derived from the measured Ne, Ar, Kr and Xe concentrations as described in Sect. 2.1.3.

From six samples of one Bunker Cave stalagmite covering the time frame from 10.8–11.7 ka BP, a mean noble gas temperature of 2.9 °C with a standard deviation of 0.7 °C was determined. The noble gas temperatures derived from the different samples agreed with each other within their error limits. One sample from a second stalagmite with a U/Th age of 1.3 ± 0.3 ka yielded a noble gas temperature of 7.1 ± 0.8 °C. The temperature difference of about 4 °C agrees with the results of other palaeotemperature reconstructions (e.g., Davis et al. 2003), which imply similar temperature changes in central and western Europe. However, while the absolute noble gas temperatures obtained are not unreasonable for central Europe, Kluge et al. (2008) could not exclude a possible bias, because their values seem to be slightly lower than would be expected from other palaeotemperature reconstructions in the Bunker Cave region. Kluge et al. (2008) therefore emphasised that the accuracy of noble gas temperatures derived from stalagmite fluid inclusions needs to be tested on modern stalagmites, for which a direct comparison with instrumental cave temperature records would be possible.

4.3.2 Stalagmites from Central Europe and the Middle East

To test different noble gas extraction methods, Scheidegger et al. (2010, 2011) determined noble gas concentrations in more than 50

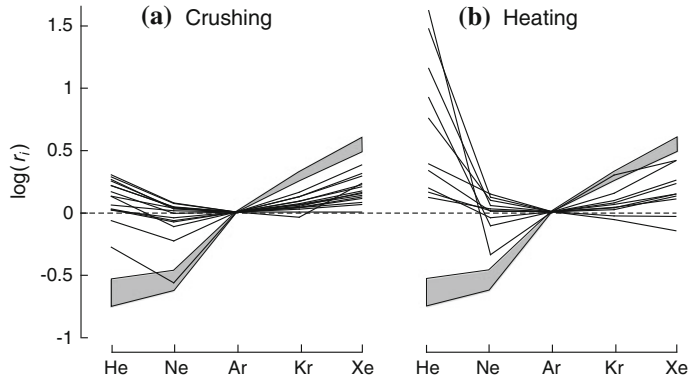

Fig. 11 Normalised elemental ratios r_i observed (**a**) after crushing stalagmite samples in vacuo (Sect. 4.2.2), and (**b**) after subsequently heating the same samples (Sect. 4.2.3), where $r_i = (i/\mathrm{Ar})_{\mathrm{sample}}/(i/\mathrm{Ar})_{\mathrm{air}}$ with i = He, Ne, Ar, Kr, Xe (after Scheidegger et al. 2010). The noble gas compositions of ASW (water temperatures 0–30 °C, grey areas) and of air (dashed lines) are shown for comparison

stalagmite samples from Switzerland (Blättlerloch, Beatus Cave, Feés Cave, Vallorbe Cave), Germany (Bunker Cave), Turkey (Sofular Cave), Oman (Qunf Cave), and Yemen (Dimarshim Cave) covering a variety of climatic regions and time ranges (0–100 ka BP). The analytical errors of the noble gas concentrations ranged between 2 and 5 %.

Pre-crushing did indeed substantially reduce the noble gas contributions from air inclusions relative to those from water inclusions. However, it was still not possible to derive statistically acceptable noble gas temperatures by regression from the Ne, Ar, Kr, and Xe concentrations as described in Sect. 2.1.3. This was attributed to the fact that Eq. (2) assumes a binary mixture of ASW and air, whereas the results also showed contributions from additional noble gas components, such as adsorbed air (Sect. 4.2.2) or He and Ne trapped in the calcite lattice (see below). The elemental compositions of these additional components are poorly constrained and therefore cannot be included quantitatively in Eq. (2), thus precluding the robust determination of noble gas temperatures.

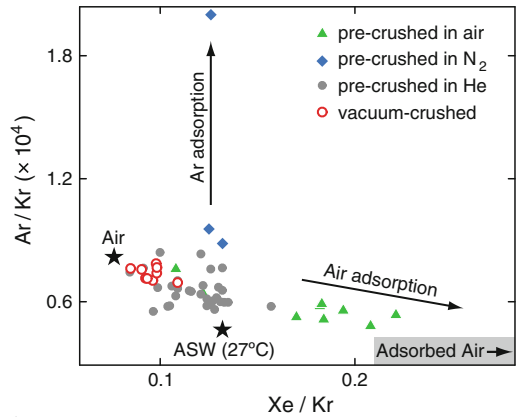

Fig. 12 Relationship between the Ar/Kr and Xe/Kr ratios in the gas extracted from Dimarshim stalagmite samples using different pre-crushing methods (pre-crushing in air, in N_2, in extra-pure He, or in vacuo). The grey area indicates the Ar-Kr-Xe composition of air adsorbed on to calcite grains (data on adsorbed air extends to higher Xe/Kr ratios lying outside the range of the plot; see Scherer et al. 1994; Ozima and Podosek 2002)

He and Ne Trapped in the Calcite Lattice?

In addition to the ASW and air components, excesses of He and Ne have been observed in various stalagmites (Ayliffe et al. 1993; Kluge 2008; Scheidegger et al. 2010) regardless of the extraction method employed (i.e., crushing in vacuo, crushing in a gas atmosphere, or heating; see Fig. 11). The He and Ne excesses therefore seem to be present naturally in the stalagmite samples.

Ayliffe et al. (1993) and Scheidegger et al. (2010) hypothesised that the excesses of He and Ne might be due to the trapping of He and Ne atoms in crystallographic voids within the calcite structure during crystal growth. The maximum diameter of a sphere that would fit into

these voids is approximately 3 Å (Scheidegger et al. 2010). Such voids would be large enough to accommodate an atom of He or Ne, but not of Ar, Kr or Xe, which have diameters >3 Å (Table 1). This hypothesis is supported by evidence from the Martian meteorite GaG 476, in which substantial Ne excesses ("extra Ne") were found (Mohapatra et al. 2009). This extra Ne is likely to be of terrestrial atmospheric origin: during the process of recrystallisation that accompanied terrestrial weathering, atmospheric Ne was probably trapped in newly formed calcite crystals (Ulrich Ott, 2009, Max Planck Institute for Chemistry, Mainz, Germany, personal communication).

Scheidegger et al. (2010) observed that the He/Ne ratio of the excess He and Ne resulting from gas extraction by heating was higher than that resulting from extraction by crushing (Fig. 11). They attributed this to He enrichment resulting from temperature-enhanced diffusion from the calcite, as the diffusivity of He is higher than that of Ne.

Ar-Kr-Xe Signatures in Fluid Inclusions

Figure 12 shows a typical example of the Ar-Kr-Xe signatures, based on samples from a Dimarshim Cave stalagmite, to which Scheidegger et al. (2010, 2011) had applied the whole suite of extraction methods discussed in Sects. 4.2.2 and 4.2.3. The Ar-Kr-Xe data from most samples are located within the mixing triangle of air, ASW, and adsorbed air (the latter with a broad range of elemental compositions). Samples pre-crushed in air clearly show the effect of the adsorption of the heavy noble gases on to the freshly produced grain surfaces (Scheidegger et al. 2010). Samples pre-crushed in N_2 suffer from Ar excesses resulting from excessive residual Ar in the N_2 protective gas. The Ar-Kr-Xe composition in the vacuum-crushed samples is similar to that of air because the air released from the air inclusions masks the ASW component from the water inclusions. The Ar-Kr-Xe composition of the samples pre-crushed in extra-pure He is closest to that of ASW, and many of these samples show Xe/Kr ratios indistinguishable from that of ASW. This led Scheidegger et al. (2010, 2011) to conclude that pre-crushing in extra-pure He substantially reduces the contribution of noble gases derived from air inclusions and also reduces the adsorption of Kr and Xe to negligible levels. They therefore considered this method to be the most suitable for reliable noble gas temperature determination, although artefacts cannot always be ruled out. Such artefacts can result, for instance, from the adsorption of residual heavy noble gases from the protective He atmosphere (Sofular Cave samples were crushed without using a sorption pump in the glove box), or from Kr and Xe deficits associated with the incomplete extraction of noble gases from the fluid inclusions (possibly because of insufficient heating). Nevertheless, 12 out of 30 noble gas temperatures calculated from the Kr and Xe concentrations in an extended Dimarshim Cave data set (Scheidegger 2011) agree to within analytical error with the modern cave temperature of 27 °C. This cave temperature has remained approximately constant since the mid-Holocene (e.g., Wanner et al. 2008). Likewise, 3 out of 9 noble gas temperatures derived from Kr and Xe concentrations in stalagmite samples from Sofular Cave are identical to the modern cave temperature of 12 °C. Also, Kr and Xe concentrations in 4 out of 7 samples from Vallorbe Cave are conceptually consistent with a binary mixture of air and ASW.

5 Summary, Outlook and Future Research

The recent methodological advances in the extraction of noble gases from the porewater of unconsolidated sediments (Sect. 3.2) represent an essential step forward in overcoming the experimental limitations that have hampered the development of terrestrial noble gas geochemistry in sediment porewater for decades. The experimental methods described in Sect. 3.2 can be employed by any noble gas laboratory equipped for the analysis of terrestrial water samples, thus allowing the laboratory to expand its activities to include the analysis of the porewater of unconsolidated sediments.

From a conceptual point of view, the key conclusion of recent sediment porewater studies is that in some sediments the noble gases diffusivities in the sediment porewater are similar to their corresponding molecular diffusivities in bulk water. In other sediments, however, the noble gases are quantitatively trapped in the sediment and diffusion is therefore strongly suppressed (Sects. 3.3.1 and 3.3.3). This trapping results in a stratigraphical control of the noble gas record in the sediment, which allows a time-scale to be associated with it. However, the mechanisms responsible for trapping the noble gases have yet to be identified. A mechanistic understanding of the suppression of diffusion would be required to fully establish the conceptual basis required for noble gases to be utilised as proxies for environmental conditions or as tracers of pore-fluid transport.

The physical mechanisms responsible for the trapping of noble gases in the porewater of unconsolidated sediments are not yet fully understood. However, the experimental tools necessary to study the noble noble gas isotopes dissolved in sediment porewater are now available. Specifically, it is now possible to assess the feasibility of using the concentrations of atmospheric noble gases in the porewater to reconstruct the geochemical evolution of the pore fluids, and to reconstruct past environmental conditions (such as the palaeosalinity of the ocean). Recently, during a scientific drilling programme in Lake Van (Litt et al. 2009, 2011), sediment samples for noble gas analysis were retrieved at depths of more than 200 m below the sediment surface. The highly compacted bulk sediments were squeezed into copper tubes using a hydraulic press. Such a hydraulic squeezer can, in principle, be used during any scientific drilling campaign in which lacustrine or oceanic sediments are recovered (e.g., the Integrated Ocean Drilling Program, IODP, or the International Continental Scientific Drilling Program, ICDP). Of particular interest are oceanic sediments from marginal seas, whose geochemical and physical conditions are expected to react very sensitively to climate change and tectonic activity. Preliminary results from the Sea of Japan (East Sea) suggest that the concentrations of atmospheric noble gases in the sediment porewater might reflect changes in freshwater input and in the mixing conditions of the water body during the last glaciation, as discussed by Lee and Nam (2003).

The sampling techniques developed for the analysis of noble gases in lacustrine and oceanic sediments might also be useful in groundwater studies. Up until now, groundwater dating using transient tracers (e.g., $^{3}H/^{3}He$, terrigenic He, CFCs, SF_6, etc.), and the reconstruction of environmental conditions from atmospheric noble gas concentrations, have been restricted to water samples taken from groundwater wells tapping flowing groundwater. However, available groundwater wells are often not located at the optimum position to address a specific scientific problem. Also, the groundwater flowing into the wells usually originates from a large and often poorly defined domain around the well. A better spatial resolution of the information on groundwater flow paths, water residence time and the environmental conditions pertaining throughout the aquifer is therefore desirable in many groundwater studies. For instance, studies on groundwater contaminants and their rates of natural attenuation and removal from the groundwater (e.g., Aeppli et al. 2010; Amaral et al. 2010; Klump et al. 2006) would greatly benefit from the availability of spatially accurate and highly resolved information on water residence time. One way forward in improving the spatial resolution would be to obtain drill cores from aquifers, or even adjacent aquicludes, at locations that are determined by the specific scientific problem to be addressed (see also Mazurek et al. 2011 for a review of similar porewater tracer analyses in drill cores from 'tight' rock formations). Porewater samples for the analysis of dissolved gases at high spatial resolution could then be taken from these drill cores at the exact depths required by adapting the sampling techniques developed for noble gas analysis in lacustrine and oceanic sediments; e.g., using a hydraulic porewater squeezer.

Stalagmite fluid inclusions, viewed as a noble gas archive, have great potential in palaeoenvironmental research. The recent experimental

advances described in Sect. 4.2 now make possible the precise and accurate determination of the concentrations of noble gases dissolved in the minute amounts of water contained in these inclusions. It has become clear that the concentrations of dissolved noble gases in stalagmite water inclusions do indeed contain useful palaeotemperature information. This has been demonstrated convincingly for samples with very low air-water volume ratios and also for some samples with more typical air-water volume ratios (Sect. 4.3).

However, despite recent experimental progress it is not yet possible to use stalagmites with typical air-water volume ratios for the routine determination of noble gas temperatures that are of immediate relevance to state-of-the-art palaeotemperature reconstruction. This is because all extraction procedures that have been suggested so far either release too much air from the fluid inclusions or introduce artefacts that affect the determination of the noble gas concentrations in the water inclusions. In the case of Kr and Xe, contamination by adsorption on to the sample grains is effectively reduced by pre-crushing the stalagmite samples in extra-pure He. However, this is not true for Ar. Extracting the noble gases by crushing bulk stalagmite samples in vacuo would prevent such adsorption effects altogether. However, the large amounts of noble gases released from the air inclusions that are opened by crushing in vacuo usually mask the relatively small amounts of noble gases extracted from the water inclusions. This is because existing vacuum crushers do not allow the noble gases derived from air inclusions to be removed before extracting the noble gases from water inclusions. An obvious step towards routine noble gas analysis for the robust determination of noble gas temperatures would therefore be to pre-crush and then sieve out stalagmite grains of appropriate sizes in vacuo. Carrying out both pre-crushing and sieving in vacuo would allow uncontaminated calcite crystals of a suitable grain size to be prepared so that the noble gases can then be extracted from the intra-crystalline water inclusions (Vogel et al. 2012). Combining the crushing, sieving and subsequent heating steps in vacuo is likely to be technically challenging. However, in light of the great potential that stalagmite water inclusions have as a noble gas archive for palaeotemperature reconstruction, an attempt at implementing such an all-vacuum procedure would seem to be justified.

It is clear that the concentrations of dissolved noble gases in stalagmite water inclusions can provide valuable information on palaeotemperatures. However, preliminary studies have shown that the gases contained in stalagmite air inclusions should perhaps not be viewed merely as "contamination" that complicates the determination of noble gas concentrations in the water inclusions, but that they may possibly also contain additional information that can aid in interpreting the noble gas concentrations in the water inclusions. By applying the experimental techniques of trace-gas analysis in ice cores to stalagmite samples, Badertscher et al. (2007) and Scheidegger (2011) found the air inclusions to be enriched with CO_2 and CH_4 relative to atmospheric air. Gas inclusions in stalagmites from poorly ventilated caves showed volumetric CO_2 concentrations of up to ~ 10 % (Badertscher 2007). An increased CO_2 partial pressure at the stalagmite surface would reduce the partial pressures of the noble gases during gas-water partitioning before separation of the water inclusions from the cave air. The increased CO_2 partial pressure would therefore result in lower noble gas concentrations, which would need to be taken into account when calculating noble gas temperatures.

In addition, the trace gases in air inclusions might contain useful information about the evolution of cave climates. Badertscher et al. (2007) and Scheidegger (2011) observed that the concentrations and isotopic compositions of CO_2 and CH_4 changed with the age of the stalagmite samples. The gas inclusions thus seem to record the CO_2 and CH_4 composition of the cave air, which is, for instance, related to the processes and rates of biogeochemical turnover in the soil overlying the cave.

It would seem obvious that the new experimental methods described here should also be applied to determine noble gas concentrations in minute amounts of water in other materials containing fluid inclusions. Papp et al. (2010) and

Scheidegger (2011) applied these methods to analyse noble gases in fluid inclusions in mollusc shells and corals. However, Scheidegger (2011) found that such biogenic carbonates seem to have very low noble gas concentrations. Shells are known to contain organically bound water, which is formed by biochemical processes and has never been in contact with the surrounding water body. This organically bound water is therefore expected to exhibit lower noble gas concentrations than the surrounding water body. In order to exploit the noble gas concentrations in biological shells as proxies for environmental conditions, new methods would need to be developed to isolate those parts of the organism which contain water that is unaffected by biological processes from the parts of the organism which contain water that is affected by such processes.

The newly developed methods have also been applied to the porewater of consolidated clays that have been targeted as possible host rocks for nuclear waste deposits (Scheidegger 2011). This porewater was shown to be strongly enriched in radiogenic ^{4}He and ^{40}Ar, indicating a long residence time of the porewater within the clays. However, the atmospheric noble gas concentrations determined exceeded the expected atmospheric equilibrium concentrations. Scheidegger (2011) speculated that the clay samples lose water preferentially as a result of surface drying during storage and during evacuation of the gas extraction system, whereas the (heavy) noble gases are retained in the sample (see also, e.g., Osenbrück et al. 1998; Rübel et al. 2002; Mazurek et al. 2011). Although it is too early to draw final conclusions from these preliminary results, the data do seem to imply that the concentrations of noble gases dissolved in the porewater of consolidated sediments reflect the hydrogeochemical origin of the porewater and might allow the characteristic residence time of pore fluids in formations with very low permeability to be estimated. Such analyses might therefore provide assistance in studying the temporal evolution of sedimentary basins.

The new techniques for analysing noble gases in the porewater of unconsolidated sediments make possible a new experimental approach to the study of gas/liquid partitioning in other unconventional "aquatic" environments, such as blood or other body fluids. We sampled human blood in copper tubes, where the blood coagulated. The blood plasma was separated from the coagulated blood (erythrocytes) for noble gas analysis using the centrifuging method of Tomonaga et al. (2011a). For comparison, we also analysed the noble gas concentrations in the remaining erythrocyte fraction using the extrusion method of Brennwald et al. (2003). The concentrations of Kr and Xe in the plasma exceeded their respective ASW concentrations in fresh water, whereas He and Ne concentrations in the plasma were slightly lower than ASW concentrations (Fig. 13). In addition, the erythrocyte fraction showed an enrichment of all atmospheric noble gases relative to the plasma. These results indicate clearly the potential that noble gases possess as tracers to study gas partitioning in body liquids and living tissues; for instance, in analysing gas-exchange processes in the lung.

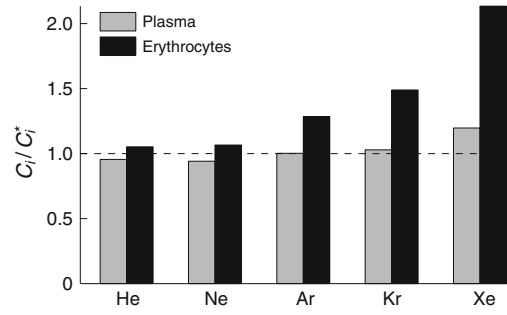

Fig. 13 Noble gas concentrations in human blood plasma and in the erythrocyte fraction remaining after centrifuging (C_i, see text), normalised to the relevant ASW concentrations in fresh water (C_i^*) computed using $T = 36.5$ °C and $P_{atm} = 0.973$ atm (the atmospheric pressure at the altitude where the blood samples were taken)

These examples show that the new experimental methods are powerful tools for studying gas/liquid partitioning in new and sometimes unusual systems and environments. These new methods open up entirely new fields and applications in which terrestrial noble gas geochemistry can play an important role in tracing physical processes—we just have to free our minds and go and find them.

References

Adkins J, McIntyre K, Schrag P (2002) The salinity, temperature, and $\delta^{18}O$ of the glacial deep ocean. Science 298:1769–1773. doi:10.1126/science.1076252

Aeppli C, Hofstetter TB, Amaral HIF, Kipfer R, Schwarzenbach RP, Berg M (2010) Quantifying in-situ transformation rates of chlorinated ethenes by combining compound-specific stable isotope analysis, groundwater dating, and carbon isotope mass balances. Environ Sci Technol 44(10):3705–3711. doi:10.1021/es903895b

Aeschbach-Hertig W, Solomon DK (2012) Noble gas thermometry in groundwater hydrology. In: Burnard PG (ed) The Noble Gases as geochemical tracers. Advances in Isotope Geochemistry Springer, New York.

Aeschbach-Hertig W, Peeters F, Beyerle U, Kipfer R (1999) Interpretation of dissolved atmospheric noble gases in natural waters. Water Resour Res 35(9): 2779–2792. doi:10.1029/1999WR900130

Amaral H, Berg M, Brennwald MS, Hofer M, Kipfer R (2010) $^{13}C/^{12}C$ analysis of ultra-trace amounts of volatile organic contaminants in groundwater by vacuum extraction. Environ Sci Technol 44:1023–1029. doi:10.1021/es901760q

Austin JA, Schlager W, Comet PA, Droxler AW, Eberli GP, Fourcade E, Freeman L, Fulthorpe C, Harwood G, Kuhn G, Lavoie D, Leckie M, Melillo AJ, Moore A, Mullins HT, Ravenne C, Sager WW, Swart P, Verbeek JW, Watkins DK, Williams C (1986) Site 628: Little Bahama Bank. In: Proceedings of the Ocean drilling program, part A: initial reports, College Station, TX (Ocean Drilling Program), vol 101, pp 213–270

Ayliffe LK, Turner G, Burnard PG (1993) Noble gas contents of speleothem inclusion fluids: potential as indicators of precipitation temperature. In: Terra Nova Abstracts, vol 5, p 646

Badertscher S, Fleitmann D, Cheng H, Edwards LR, Göktürk OM, Zumbühl A, Leuenberger M, Tüysüz O (2011) Pleistocene water intrusions from the Mediterranean and Caspian seas into the Black Sea. Nature Geosci 4:236–239. doi:10.1038/NGEO1106

Badertscher SV (2007) Charakterisierung von Einschlüssen in Stalagmiten zur Bestimmung der Paläotemperatur. Master's thesis, ETH Zürich, Switzerland

Badertscher SV, Scheidegger Y, Leuenberger M, Nyfeler P, Fleitmann D, Wieler R, Kipfer R (2007) Trace gas content in air inclusions in speleothems as a new paleoclimate archive. In: Geophysical research abstracts, 4th EGU general assembly, European Geosciences Union, Vienna, Austria, vol 9, p A0491

Ballentine CJ, Burnard PG (2002) Production, release and transport of noble gases in the continental crust. In: Porcelli D, Ballentine C, Wieler R (eds) Noble gases in geochemistry and cosmochemistry, reviews in mineralogy and geochemistry, vol 47. Mineralogical Society of America, Geochemical Society, pp 481–538

Ballentine CJ, Hall CM (1999) Determining paleotemperature and other variables by using an error-weighted, nonlinear inversion of noble gas concentrations in water. Geochim Cosmochim Acta 63(16):2315–2336. doi:10.1016/S0016-7037(99)00131-3

Ballentine CJ, Burgess R, Marty B (2002) Tracing fluid origin, transport and interaction in the crust. In: Porcelli D, Ballentine C, Wieler R (eds) Noble gases in cosmochemistry and geochemistry, reviews in mineralogy and geochemistry, vol 47. Mineralogical Society of America, Geochemical Society, pp 539–614

Barnes R (1973) An in situ interstitial water sampler for use in unconsolidated sediments. Deep-Sea Res 20:1125–1128. doi:10.1016/0011-7471(73)90026-0

Barnes RO (1979) Operation of the IPOD in situ pore water sampler. In: Sibuet J, Ryan W (eds) Initial reports of the Deep Sea Drilling Project, vol 47, part 2, DSDP, Washington (U.S. Govt. Printing Office), pp 19–22

Barnes RO (1987) Fluid kinematics, fluid residence times, and rock degassing in oceanic crust determined from noble gas contents of Deep Sea Drilling Project pore waters. J Geophys Res 92(B12):12491–12506

Barnes RO (1988) ODP in-situ fluid sampling and measurement: a new wireline tool. In: Mascle A, Moore J (eds) Proceedings of the Ocean Drilling Program, initial reports (Part A), vol 110. ODP, College Station TX, pp 55–63

Barnes RO, Bieri RH (1976) Helium flux through marine sediments of the northern Pacific Ocean. Earth Planet Sci Lett 28(3):331–336. doi:10.1016/0012-821X(76)90194-1

Bayer R, Schlosser P, Bönisch G, Rupp H, Zaucker F, Zimmek G (1989) Performance and blank components of a mass spectrometric system for routine measurement of helium isotopes and tritium by the ^{3}He ingrowth method. Sitzungsberichte der Heidelberger Akademie der Wissenschaften Mathemathisch-naturwissenschaftliche Klasse 5, University of Heidelberg, Germany.

Berner RA (1975) Diagenetic models of dissolved species in the interstitial waters of compacting sediments. Am J Sci 275:88–96

Bertin C, Bourg ACM (1994) Rn-222 and chloride as natural tracers of the infiltration of river water into an alluvial aquifer in which there is significant river groundwater mixing. Environ Sci Technol 28(5): 794–798

Beyerle U, Aeschbach-Hertig W, Imboden DM, Baur H, Graf T, Kipfer R (2000) A mass spectrometric system for the analysis of noble gases and tritium from water samples. Environ Sci Technol 34(10):2042–2050. doi:10.1021/es990840h

Beyerle U, Leuenberger M, Schwander J, Kipfer R (2003) Noble gas evidence for gas fractionation in firn. In: Abstracts of the 13th Annual V.M.

Goldschmidt Conference 2003, Kurashiki, Japan, Geochim. Cosmochim. Acta, vol 67, p A38.
Bieri R (1971) Dissolved noble gases in marine waters. Earth Planet Sci Lett 10(3):329–333
Bosch A, Mazor E (1988) Natural gas association with water and oil as depicted by atmospheric noble gases: case studies from the Southeastern Mediterranean Coastal Plain. Earth Planet Sci Lett 87(3):338–346. doi:10.1016/0012-821X(88)90021-0
Bourg IC, Sposito G (2008) Isotopic fractionation of noble gases by diffusion in liquid water: molecular dynamics simulations and hydrologic applications. Geochim Cosmochim Acta 72:2237–2247. doi:10.1016/j.gca.2008.02.012
Brennwald MS, Hofer M, Peeters F, Aeschbach-Hertig W, Strassmann K, Kipfer R, Imboden DM (2003) Analysis of dissolved noble gases in the pore water of lacustrine sediments. Limnol Oceanogr Methods 1: 51–62, http://aslo.org/lomethods/free/2003/0051.pdf
Brennwald MS, Peeters F, Imboden DM, Giralt S, Hofer M, Livingstone DM, Klump S, Strassmann K, Kipfer R (2004) Atmospheric noble gases in lake sediment pore water as proxies for environmental change. Geophys Res Lett 31(4):L04202. doi:10.1029/2003GL019153
Brennwald MS, Imboden DM, Kipfer R (2005) Release of gas bubbles from lake sediment traced by noble gas isotopes in the sediment pore water. Earth Planet Sci Lett 235(1–2):31–44. doi:10.1016/j.epsl.2005.03.004
van Breukelen MR, Vonhof HB, Hellstrom JC, Wester WCG, Kroon D (2008) Fossil dripwater in stalagmites reveals Holocene temperature and rainfall variation in Amazonia. Earth Planet Sci Lett 275(1–2):54–60. doi:10.1016/j.epsl.2008.07.060
Chaduteau C, Fourré E, Jean-Baptiste P, Dapoigny A, Baumier D, Charlou JL (2007) A new method for quantitative analysis of helium isotopes in sediment pore-waters. Limnol Oceanogr Methods 5:425–432. http://www.aslo.org/lomethods/free/2007/0425.pdf
Chaduteau C, Jean-Baptiste P, Fourré E, Charlou JL, Donval JP (2009) Helium transport in sediment pore fluids of the Congo-Angola margin. Geochem Geophys Geosyst 10(1). doi:10.1029/2007GC001897
Cheng H, Edwards RL, Broecker WS, Denton GH, Kong X, Wang Y, Zhang R, Wang X (2009) Ice age terminations. Science 326(5950):248–52. doi:10.1126/science.1177840
Copeland P, Watson EB, Urizar SC, Patterson D, Lapen TJ (2007) Alpha thermochronology of carbonates. Geochim Cosmochim Acta 71:4488–4511. doi:10.1016/j.gca.2007.07.004
Craig H, Weiss RF (1971) Dissolved gas saturation anomalies and excess helium in the ocean. Earth Planet Sci Lett 10(3):289–296. doi:10.1016/0012-821X(71)90033-1
Davis B, Brewer S, Stevenson A, Guiot J (2003) The temperature of Europe during the Holocene reconstructed from pollen data. Quaternary Sci Rev 22(15–17):1701–1716. doi:10.1016/S0277-3791(03)00173-2
De Batist M, Imbo Y, Vermeesch P, Klerkx J, Giralt S, Delvaux D, Lignier V, Beck C, Kalugin I, Abdrakhmatov K (2002) Bathymetry and sedimentary environment of Lake Issyk-Kul, Kyrgyz Republic (Central Asia): a large, high-altitude, tectonic lake. In: Klerkx J, Imanackunov B (eds) Lake Issyk-Kul: its natural environment, NATO science series IV: earth and environmental sciences, vol 13. Kluwer Academic Publishers, Boston, pp 101–123
Dreybrodt W (1980) Deposition of calcite from thin films of natural calcareous solutions and the growth of speleothems. Chem Geol 29:89–105
Dyck W, Da Silva FG (1981) The use of ping-pong balls and latex tubing for sampling the helium content of lake sediments. J Geochem Explor 14:41–48. doi:10.1016/0375-6742(81)90102-3
Einstein A (1905) Über die von der molekularkinetischen Theorie der Wärme geforderte Bewegung von in ruhenden Flüssigkeiten suspendierten Teilchen. Annalen der Physik 322(8):549–560. doi:10.1002/andp.19053220806
Faust GT (1950) Thermal analysis studies on carbonates: 1 aragonite and calcite. Am Mineral 35:207–224
Fleitmann D, Burns S, Neff U, Mangini A, Matter A (2003) Changing moisture sources over the last 333,000 years in Northern Oman from fluid inclusion evidence in speleothems. Quaternary Res 60:223–232. doi:10.1016/S0033-5894(03)00086-3
Fleitmann D, Cheng H, Badertscher S, Edwards RL, Mudelsee M, Goektuerk OM, Fankhauser A, Pickering R, Raible CC, Matter A, Kramers J, Tuysuz O (2009) Timing and climatic impact of Greenland interstadials recorded in stalagmites from northern Turkey. Geophys Res Lett 36: L10707. doi:10.1029/2009GL040050
Fritz SC (1996) Paleolimnological records of climatic change in North America. Limnol Oceanogr 41(5): 882–889
Giralt S, Riera S, Leroy S, Buchaca T, Klerkx J, De Batist M, Beck C, Bobrov V, Brennwald MS, Catalan J, Gavshin V, Julia R, Kalugin I, Kipfer R, Lignier V, Lombardi S, Matychenkov V, Peeters F, Podsetchine V, Romanovsky V, Shukonikov F, Voltattorni N (2003) 1,000 years of environmental history of Lake Issyk-Kul. In: Nihoul J, Zavialov P, Micklin P (eds) Dying and dead seas: climatic versus anthropic causes, NATO science series IV: Earth and environmental sciences, vol 36. Kluwer Academic Publishers, Boston, pp 228–253
Grathwohl P (1998) Diffusion in natural porous media, topics in environmental fluid mechanics. Kluwer Academic Publishers, Boston
Griffiths ML, Drysdale RN, Vonhof HB, Gagan MK, Zhao Jx, Ayliffe LK, Hantoro WS, Hellstrom JC, Cartwright I, Frisia S, Suwargadi BW (2010) Younger Dryas-Holocene temperature and rainfall

history of southern Indonesia from $\delta^{18}O$ in speleothem calcite and fluid inclusions. Earth Planet Sci Lett 295(1–2):30–36. doi: 10.1016/j.epsl.2010.03.018

Henderson GM (2006) Caving in to new chronologies. Science 313(5787):620–622. doi:10.1126/science.1128980

Hoehn E, von Gunten HR (1989) Radon in groundwater—a tool to assess infiltration from surface waters to aquifers. Water Resour Res 25(8):1795–1803

Hohmann R, Schlosser P, Jacobs S, Ludin A, Weppernig R (2002) Excess helium and neon in the southeast Pacific: Tracers for glacial meltwater. J Geophys Res-Oceans 107(C11):3198. doi:10.1029/2000JC000378

Holzner CP, McGinnis DF, Schubert CJ, Kipfer R, Imboden DM (2008) Noble gas anomalies related to high-intensity methane gas seeps in the Black Sea. Earth Planet Sci Lett 265(3–4):396–409. doi:10.1016/j.epsl.2007.10.029

Horseman S, Higgo J, Alexander J, Harrington J (1996) Water, gas and solute movement through argillaceaous media. Technical Report CC-96/1, OECD Nuclear Energy Agency, France

Huber C, Beyerle U, Leuenberger M, Schwander J, Kipfer R, Spahni R, Severinghaus JP, Weiler K (2006) Evidence for molecular size dependent gas fractionation in firn air derived from noble gases, oxygen, and nitrogen measurements. Earth Planet Sci Lett 243(1–2):61–73. doi:10.1016/j.epsl.2005.12.036

Huxol S, Brennwald MS, Hoehn E, Kipfer R (2012) On the fate of ^{220}Rn in soil material in dependence of water content: Implications from field and laboratory experiments. Chem Geol 298–299:116–122. doi:10.1016/j.chemgeo.2012.01.002

Imboden DM (1975) Interstitial transport of solutes in non-steady state accumulating and compacting sediments. Earth Planet Sci Lett 27(2):221–228. doi:10.1016/0012-821X(75)90033-3

Jähne B, Heinz G, Dietrich W (1987) Measurement of the diffusion coefficients of sparingly soluble gases in water. J Geophys Res 92(C10):10767–10776

Jean-Baptiste P, Mantisi F, Dapoigny A, Stievenard M (1992) Design and performance of a mass-spectrometric facility for measuring helium-isotopes in natural-waers and for low-level tritium determination by the He-3 ingrowth method. Appl Radiat Isotopes 43(7):881–891. doi:10.1016/0883-2889(92)90150-D

Kendall AC, Broughton PL (1978) Origin of fabrics in speleothems composed of columnar calcite crystals. J Sediment Petrol 48:519–538

Kipfer R, Aeschbach-Hertig W, Peeters F, Stute M (2002) Noble gases in lakes and ground waters. In: Porcelli D, Ballentine C, Wieler R (eds) Noble gases in geochemistry and cosmochemistry, reviews in mineralogy and geochemistry, vol 47. Mineralogical Society of America, Geochemical Society, pp 615–700

Kluge T (2008) Fluid inclusions in speleothems as a new archive for the noble gas thermometer. PhD thesis, University of Heidelberg, Germany

Kluge T, Marx T, Scholz D, Niggemann S, Mangini A, Aeschbach-Hertig W (2008) A new tool for palaeoclimate reconstruction: noble gas temperatures from fluid inclusions in speleothems. Earth Planet Sci Lett 269(3–4):408–415

Klump S, Kipfer R, Cirpka OA, Harvey CF, Brennwald MS, Ashfaque KN, Badruzzaman ABM, Hug SJ, Imboden DM (2006) Groundwater dynamics and arsenic mobilization in Bangladesh assessed using noble gases and tritium. Environ Sci Technol 40(1):243–250 doi:10.1021/es051284w

Lachniet MS (2009) Climatic and environmental controls on speleothem oxygen-isotope values. Quat Sci Rev 28(5–6):412–432. doi:10.1016/j.quascirev.2008.10.021

Lan TF, Sano Y, Yang TF, Takahata N, Shirai K, Pinti DL (2010) Evaluating earth degassing in subduction zones by measuring helium fluxes from the ocean floor. Earth Planet Sci Lett 298(3–4):317–322. doi:10.1016/j.epsl.2010.07.049

Lee E, Nam S (2003) Freshwater supply by Korean rivers to the East Sea during the last glacial maximum: a review and new evidence from the Korea Strait region. Geo-Marine Lett 23(1):1–6. doi:10.1007/s00367-003-0118-1

Lerman A, Imboden D, Gat J (1995) Physics and chemistry of lakes. Springer, Berlin. doi:10.1002/iroh.19960810312

Litt T, Krastel S, Sturm M, Kipfer R, Örcen S, Heumann G, Franz S, Ülgen U, Niessen F (2009) 'PALEOVAN', International Continental Scientific Dilling Program (ICDP) site survey results and perspectives. Quaternary Sci Rev 28:1555–1567. doi:10.1016/j.quascirev.2009.03.002

Litt T, Anselmetti FS, Cagatay MN, Kipfer R, Krastel S, Schmincke HU (2011) A 500,000-year-long sediment archive drilled in Eastern Anatolia. EOS 92(51):477–479

Loose B, Schlosser P, Smethie WM, Jacobs S (2009) An optimized estimate of glacial melt from the ross ice shelf using noble gases, stable isotopes, and CFC transient tracers. J Geophys Res-Oceans 114:C08007. doi:10.1029/2008JC005048

Mamyrin BA, Tolstikhin IN (1984) Helium isotopes in nature, developments in geochemistry, vol 3, 1st edn. Elsevier, Amsterdam, Oxford, New York, Tokyo

Mazor E (1972) Paleotemperatures and other hydrological parameters deduced from gases dissolved in groundwaters, Jordan Rift Valley, Israel. Geochim Cosmochim Acta 36(12):1321–1336. doi:10.1016/0016-7037(72)90065-8

Mazurek M, Alt-Epping P, Bath A, Gimmi T, Waber HN, Buschaert S, De Cannière P, De Craen M, Gautschi

A, Savoye S, Vinsot A, Wemaere I, Wouters L (2011) Natural tracer profiles across argillaceous formations. Appl Geochem 26:1035–1064. doi:10.1016/j.apgeochem.2011.03.124

McDermott F, Schwarcz H, Rowe P (2005) Isotopes in speleothems. In: Leng M (ed) Isotopes in palaeoenvironmental research, developments in paleoenvironmental research, vol 10. Springer, pp 185–225

Mohapatra RK, Schwenzer SP, Herrmann S, Murty SVS, Ott U, Gilmour JD (2009) Noble gases and nitrogen in Martian meteorites Dar al Gani 476, Sayh al Uhaymir 005 and Lewis Cliff 88516: EFA and extra neon. Geochim Cosmochim Acta 73(5):1505–1522. doi:10.1016/j.gca.2008.11.030

Musset AE (1969) Diffusion measurements and the potassium-argon method of dating. Geophys J Roy Astron Soc 18(3):257–303. doi:10.1111/j.1365-246X.1969.tb03569.x

Osenbrück K, Lippmann J, Sonntag C (1998) Dating very old pore waters in impermeable rocks by noble gas isotopes. Geochim Cosmochim Acta 62(18):3041–3045. doi:10.1016/S0016-7037(98)00198-7

Ozima M, Podosek FA (2002) Noble gas geochemistry, 2nd edn. Cambridge University Press

Papp L, Palcsu L, Major Z (2010) Noble gas measurements from tiny water amounts: fluid inclusions in carbonates of speleothemes and coral skeletons. In: Geophysical Research Abstracts, 7th EGU General Assembly, European Geosciences Union, Vienna, Austria, vol 12, p A432

Peeters F, Kipfer R, Achermann D, Hofer M, Aeschbach-Hertig W, Beyerle U, Imboden DM, Rozanski K, Fröhlich K (2000) Analysis of deep-water exchange in the Caspian Sea based on environmental tracers. Deep-Sea Res I 47(4):621–654. doi:10.1016/S0967-0637(99)00066-7

Pitre F, Pinti DL (2010) Noble gas enrichments in porewater of estuarine sediments and their effect on the estimation of net denitrification rates. Geochim Cosmochim Acta 74:531–539. doi:10.1016/j.gca.2009.10.004

Poulson TL, White WB (1969) The cave environment. Science 165(3897):971–981. doi:10.1126/science.165.3897.971

Renkin EM (1954) Filtration, diffusion, and molecular sieving through porous cellulose membranes. J General Physiol 38:225–243

Ricketts RD, Johnson TC, Brown ET, Rasmussen KA, Romanovsky VA (2001) The Holocene paleolimnology of Lake Issyk-Kul, Kyrgyzstan: trace element and stable isotope composition of ostracodes. Palaeogeogr Palaeoclimatol Palaeoecol 176(1–4):207–227. doi:10.1016/S0031-0182(01)00339-X

Romanovsky VV (2002) Water level variations and water balance of Lake Issyk-Kul. In: Klerkx J, Imanackunov B (eds) Lake Issyk-Kul: its natural environment, NATO science series IV: earth and environmental sciences, vol 13. Kluwer Academic Publishers, London, pp 45–57

Rübel A, Sonntag C, Lippmann J, Pearson F, Gautschi A (2002) Solute transport in formations of very low permeability: profiles of stable isotope and dissolved noble gas contents of pore water in the Opalinus Clay. Mont Terri. Switzerland. Geochim Cosmochim Acta 66(8):1311–1321. doi:10.1016/S0016-7037(01)00859-6

Sano Y, Wakita H (1987) Helium isotopes and heat flow on the ocean floor. Chem Geol 66(3–4):217–226. doi:10.1016/0168-9622(87)90043-1

Sayles FL, Jenkins WJ (1982) Advection of pore fluids through sediments in the Equatorial East Pacific. Science 217:245–248

Scheidegger Y (2011) The use of noble gases in stalagmite fluid inclusions as proxies for the cave temperature. PhD thesis, Swiss Federal Institute of Technology Zurich (ETH), Switzerland. doi:10.3929/ethz-a-006551468

Scheidegger Y, Kluge T, Kipfer R, Aeschbach-Hertig W, Wieler R (2008) Paleotemperature reconstruction using noble gas concentrations in speleothem fluid inclusions. Pages News 16(3):10–12

Scheidegger Y, Baur H, Brennwald MS, Fleitmann D, Wieler R, Kipfer R (2010) Accurate analysis of noble gas concentrations in small water samples and its application to fluid inclusions in stalagmites. Chem Geol 272(1–4):31–39. doi:10.1016/j.chemgeo.2010.01.010

Scheidegger Y, Brennwald MS, Fleitmann D, Jeannin PY, Wieler R, Kipfer R (2011) Determination of Holocene cave temperatures from Kr and Xe concentrations in stalagmite fluid inclusions. Chem Geol 288(1–2):61–66. doi:10.1016/j.chemgeo.2011.07.002

Scherer P, Schultz L, Loeken T (1994) Weathering and atmospheric noble gases in chondrites. Matsuda J (ed) Noble gas geochemistry and cosmochemistry. Terra Scientific Publishing Company, pp 43–53

Schlosser P, Winckler G (2002) Noble gases in ocean waters and sediments. In: Porcelli D, Ballentine C, Wieler R (eds) Noble gases in geochemistry and cosmochemistry, reviews in mineralogy and geochemistry, vol 47. Mineralogical Society of America, Geochemical Society, pp 701–730

Schrag DP, Hampt G, Murray DW (1996) Pore fluid constraints on the temperature and oxygen isotopic composition of the glacial ocean. Science 272:1930–1932

Schrag DP, Adkins J, McIntyre K, Alexander J, Hodell A, Charles D, McManus J (2002) The oxygen isotopic composition of seawater during the Last Glacial Maxiumum. Quaternary Sci Rev 21(1–3):331–342. doi:10.1016/S0277-3791(01)00110-X

Schwarcz HP, Harmon RS, Thompson P, Ford DC (1976) Stable isotope studies of fluid inclusions in speleothems and their paleoclimatic significance. Geochim Cosmochim Acta 40:657–665

Schwarzenbach RP, Gschwend PM, Imboden DM (2003) Environmental Organic Chemistry, 2nd edn. Wiley, New York

Smithson PA (1991) Interrelationships between cave and outside air temperatures. Theoret Appl Climatology 44(1):65–73

Solomon DK (2000) ^{4}He in groundwater. In: Cook P, Herczeg AL (eds) Environmental tracers in subsurface hydrology. Kluwer Academic Publishers, Boston, pp 425–439

Solomon DK, Cook PG (2000) ^{3}H and ^{3}He. In: Cook P, Herczeg AL (eds) Environmental tracers in subsurface hydrology. Kluwer Academic Publishers, Boston, pp 397–424

Stanley R, Jenkins W (2012) Noble gases in seawater as tracers for physical and biogeochemical ocean processes. In: Burnard PG (ed) The Noble Gases as geochemical tracers, Advances in isotope geochemistry. Springer, New York

Stephenson M, Schwartz WJ, Melnyk TW, Motycka MF (1994) Measurement of advective water velocity in lake sediment using natural helium gradients. J Hydrol 154(1–4):63–84. doi:10.1016/0022-1694(94)90212-7

Strassmann KM, Brennwald MS, Peeters F, Kipfer R (2005) Dissolved noble gases in porewater of lacustrine sediments as palaeolimnological proxies. Geochim Cosmochim Acta 69(7):1665–1674. doi:10.1016/j.gca.2004.07.037

Sültenfuss J, Roether W, Rhein M (2009) The Bremen mass spectrometric facility for the measurement of helium isotopes, neon, and tritium in water. Isotopes In Environmental and Health Studies 45(2):83–95. doi:10.1080/10256010902871929

Swart KS (2000) The oxygen isotopic composition of interstitial waters: evidence for fluid flow and recrystalization in the margin of the Great Bahama Bank. In: Proceedings of the Ocean Drilling Program, Scientific Results, vol 166, pp 91–98

Tomonaga Y (2010) Noble gases as tracers for transport of solutes and fluids in lake and ocean sediments. PhD thesis, Swiss Federal Institute of Technology Zurich (ETH), Switzerland. doi:10.3929/ethz-a-006129449

Tomonaga Y, Brennwald MS, Kipfer R (2011a) An improved method for the analysis of dissolved noble gases in the pore water of unconsolidated sediments. Limnol Oceanogr, Methods 9:42–49

Tomonaga Y, Brennwald MS, Kipfer R (2011b) Spatial distribution and flux of terrigenic He dissolved in the sediment pore water of Lake Van (Turkey). Geochim Cosmochim Acta 75(10):2848–2864. doi:10.1016/j.gca.2011.02.038

Top Z, Izdar E, Ergün M, Konuk T (1990) Evidence for tectonism from ^{3}He and residence time of helium in the Black Sea. EOS 71:1020–1021

Torres M, Bayer R, Winckler G, Suckow A, Froelich P (1995) Elemental and isotopic abundance of noble gases in formation fluids recovered in situ from the Chile Triple Junction. In: Lewis S, Behrmann J, Musgrave R, Cande S (eds) Proceedings of the Ocean Drilling Program, Scientific Results, vol 141. ODP, College Station TX, pp 321–329

Vogel N, Scheidegger Y, Brennwald MS, Fleitmann D, Figura S, Wieler R, Kipfer R (2012) Noble gas paleotemperatures and water contents of stalagmites—a new extraction tool and a new paleoclimate proxy. In: Geophysical Research Abstracts, EGU General Assembly 2012, European Geosciences Union, Vienna, Austria, vol 14

Wainer K, Genty D, Blamart D, Daeron M, Bar-Matthews M, Vonhof H, Dublyansky Y, Pons-Branchu E, Thomas L, van Calsteren P, Quinif Y, Caillon N (2011) Speleothem record of the last 180 ka in Villars cave (SW France): Investigation of a large δ^{18}O shift between MIS6 and MIS5. Quaternary Sci Rev 30(1–2):130–146. doi:10.1016/j.quascirev.2010.07.004

Wang Y, Cheng H, Edwards RL, Kong X, Shao X, Chen S, Wu J, Jiang X, Wang X, An Z (2008) Millennial- and orbital-scale changes in the east asian monsoon over the past 224,000 years. Nature 451(7182):1090–1093. doi:10.1038/nature06692

Wanner H, Beer J, Bütikofer J, Crowley T, Cubasch U, Flückiger J, Goosse H, Grosjean M, Joos F, Kaplan J, Küttel M, Müller S, Prentice I, Solomina O, Stocker T, Tarasoc P, Wagner M, Widmann M (2008) Mid- to Late Holocene climate change: an overview. Quaternary Sci Rev 27:1791–1828

Winckler G (1998) Radiogenes Helium im Ozean: Drei Fallstudien. PhD thesis, University of Heidelberg, Germany

Winckler G, Kipfer R, Aeschbach-Hertig W, Botz R, Schmidt M, Schuler S, Bayer R (2000) Sub sea floor boiling of Red Sea brines: new indication from noble gas data. Geochim Cosmochim Acta 64(9):1567–1575. doi:10.1016/S0016-7037(99)00441-X

Extraterrestrial He in Sediments: From Recorder of Asteroid Collisions to Timekeeper of Global Environmental Changes

David McGee and Sujoy Mukhopadhyay

Abstract

Most ^{3}He in deep-sea sediments is derived from fine-grained extraterrestrial matter known as interplanetary dust particles (IDPs). These particles, typically <50 μm in diameter, are sufficiently small to retain solar wind-implanted He with high ^{3}He/^{4}He ratios during atmospheric entry heating. This extraterrestrial ^{3}He ($^{3}He_{ET}$) is retained in sediments for geologically long durations, having been detected in sedimentary rocks as old as 480 Ma. As a tracer of fine-grained extraterrestrial material, $^{3}He_{ET}$ offers unique insights into solar system events associated with increased IDP fluxes, including asteroid break-up events and comet showers. Studies have used $^{3}He_{ET}$ to identify IDP flux changes associated with a Miocene asteroid break-up event and a likely comet shower in the Eocene. During much of the Cenozoic, $^{3}He_{ET}$ fluxes have remained relatively constant over million-year timescales, enabling $^{3}He_{ET}$ to be used as a constant flux proxy for calculating sedimentary mass accumulation rates and constraining sedimentary age models. We review studies employing $^{3}He_{ET}$-based accumulation rates to estimate the duration of carbonate dissolution events associated with the K/Pg boundary and Paleocene-Eocene Thermal Maximum. Additionally, $^{3}He_{ET}$ has been used to quantify sub-orbital variability in fluxes of paleoproductivity proxies and windblown dust. In order to better interpret existing records and guide the application of $^{3}He_{ET}$ in novel settings, future work requires constraining the carrier phase(s) of $^{3}He_{ET}$ responsible for long-term retention in sediments, better characterizing the He isotopic composition of the terrigenous

D. McGee (✉)
Department of Earth, Atmospheric and Planetary Sciences, Massachusetts Institute of Technology, Cambridge, MA, USA
e-mail: davidmcg@mit.edu

S. Mukhopadhyay
Department of Earth and Planetary Sciences, Harvard University, Cambridge, MA, USA
e-mail: sujoy@eps.harvard.edu

P. Burnard (ed.), *The Noble Gases as Geochemical Tracers*, Advances in Isotope Geochemistry,
DOI: 10.1007/978-3-642-28836-4_7,

end-member, and understanding why observed extraterrestrial ^{3}He fluxes do not match the predicted variability of IDP accretion rate over orbital timescales.

1 Introduction

The presence of extraterrestrial material in marine sediments was first proposed by Murray (1876) based upon his observations of magnetic spherules in open-ocean surface sediments collected during the Challenger expedition. Later investigations found similar spherules at high altitudes in the atmosphere and in ice sheets, terrestrial deposits and geologically old marine sediments (Laevastu and Mellis 1955; Fireman and Kistner 1961; Thiel and Schmidt 1961; Fredriksson and Gowdy 1963). Geochemical and mineralogical investigations of cut and polished samples provided evidence consistent with an extraterrestrial origin for at least some of these spherules, including metallic iron cores and high nickel contents (Fredriksson 1956; Fredriksson and Martin 1963). In parallel with this work, studies of meteorites established that extraterrestrial materials contained noble gas signatures clearly distinguishable from terrestrial samples, marked most notably by high ^{3}He concentrations and ^{3}He/^{4}He ratios (e.g., Tilles 1962; Zähringer 1962). Drawing upon these findings, Merrihue (1964) demonstrated that the He isotopic composition of a red clay sample from the south tropical Pacific was inconsistent with any known terrestrial source and was similar to that found in extraterrestrial samples.

Subsequent work has established that most ^{3}He in open-ocean sediments is extraterrestrial, and that this extraterrestrial ^{3}He (^{3}He$_{ET}$) is dominantly brought to Earth's surface by fine (generally <50 μm) interplanetary dust particles (IDPs). IDPs consist of a combination of asteroid and comet debris and carry implanted solar ions with characteristically high ^{3}He/^{4}He ratios. Though all extraterrestrial matter initially contains implanted He, coarser particles attain higher temperatures during atmospheric entry, causing them to lose most of their ^{3}He$_{ET}$ before reaching the Earth's surface. The atmosphere thus acts as a filter, allowing only fine particles to retain ^{3}He$_{ET}$.

Over the past 30 years ^{3}He$_{ET}$ has been identified in Quaternary marine sediments (e.g., Takayanagi and Ozima 1987; Farley and Patterson 1995; Marcantonio et al. 1995) and ice cores (Brook et al. 2000); in marine sediments spanning the Cenozoic (Farley 1995); and in sedimentary rocks as old as 480 Ma (Patterson et al. 1998). When combined with sedimentary accumulation rate estimates, ^{3}He$_{ET}$ data provide insight into past changes in the flux of extraterrestrial material associated with asteroid break-up events and comet showers (Farley 1995; Farley et al. 1998, 2005, 2006; Mukhopadhyay et al. 2001a, b). Because ^{3}He$_{ET}$ traces the accretion of IDPs dominantly smaller than 50 μm, ^{3}He$_{ET}$ fluxes offer a view of accretion rates of extraterrestrial matter that is distinct from that provided by platinum group elements (PGEs) such as iridium, which trace the total extraterrestrial mass flux; large impactors leave PGE anomalies in the sedimentary record but contribute negligible amounts of ^{3}He$_{ET}$ (e.g., Mukhopadhyay et al. 2001a, b). Likewise, collisions in the asteroid belt substantially enhance IDP accretion rates—and thus, ^{3}He$_{ET}$ fluxes—without delivering large impactors (Farley et al. 2006).

As ^{3}He$_{ET}$ accumulation rates have been found to be roughly constant on million-year timescales through most of the Cenozoic, ^{3}He$_{ET}$ can also be used as a constant-flux proxy for calculating sedimentary accumulation rates (Marcantonio et al. 1995, 1996; Mukhopadhyay et al. 2001b, Farley and Eltgroth 2003). This approach has proved particularly valuable in portions of the sedimentary record marked by dramatic changes in sedimentation (e.g., Mukhopadhyay et al. 2001b; Farley and Eltgroth 2003; Murphy et al. 2010). Even in periods of more typical pelagic sedimentation, ^{3}He$_{ET}$-based accumulation rates

allow calculation of fluxes for paleoclimate studies with sub-orbital resolution that are largely independent of age model errors, changes in carbonate preservation and lateral advection of sediments (Winckler et al. 2005; Marcantonio et al. 2009; McGee et al. 2010; Torfstein et al. 2010).

In this chapter we review the current understanding of the sources of IDPs and the carrier phases of extraterrestrial He responsible for long-term retention of He in marine and terrestrial deposits. We then discuss applications of $^3He_{ET}$ to questions of past changes in IDP flux and marine sediment accumulation. We close the chapter with a set of open questions that provide directions for future work.

2 Origin of Extraterrestrial He in IDPs

Interplanetary dust particles originate as asteroid and comet debris and range in size from ~1 μm to 1 mm, with a peak in mass flux near Earth at a diameter of ~200 μm (Love and Brownlee 1993). IDPs are typically porous aggregates of silicate minerals and carbonaceous matter (Nier and Schlutter 1990), with densities averaging ~2 g/cm^3 and ranging from 1 to 6 g/cm^3 (Love et al. 1994). Poynting-Robertson and solar wind drag cause IDP orbits to decay toward the Sun on timescales of 10^4–10^5 years (Burns et al. 1979). This short lifetime requires continuous supply of new IDPs to the inner solar system. IDP sources include asteroid collisions and comets, though the relative importance of these sources is as yet uncertain. Kortenkamp and Dermott (1998b) argued that much of the zodiacal cloud, the diffuse cloud of dust in the plane of the solar system, originates from collisions of a limited number of asteroid families. More recently, modeling by Nesvorný et al. (2010) suggested that Jupiter-family comets might be the most important source of IDPs at distances closer than 5 AU.

As IDPs spiral into the sun they are bombarded by solar wind (SW), which imparts high noble gas concentrations and solar isotopic ratios. SW ions are primarily composed of H and He with particle energies on the order of 1 keV/n (Futagami et al. 1990) and $^3He/^4He$ ratios of 4.48 (±0.15) × 10^{-4} (Benkert et al. 1993). $^3He/^4He$ ratios in IDPs sampled in the stratosphere reach the solar wind value of 4.4 × 10^{-4}, although the majority of the particles have ratios ~2.0–2.7 × 10^{-4} (Fig. 1) (Nier and Schlutter 1990, 1992; Pepin et al. 2000). The lower-than-SW $^3He/^4He$ ratios in most IDPs have led to suggestions that SW He is lost during atmospheric entry and that IDP He instead reflects a distinct population of higher energy solar ions with lower $^3He/^4He$ ratios, called solar energetic particles (SEP; Amari and Ozima 1988; Nier et al. 1990; Pepin et al. 2000). However, study of solar ions implanted during the Genesis mission has recently demonstrated that the heavier isotope is implanted deeper, resulting in depth-dependent isotopic fractionation such that lighter compositions are observed near the surface (Grimberg et al. 2006; Wieler et al. 2007). If so, the lower $^3He/^4He$ ratios observed in IDPs might simply indicate preferential loss of the

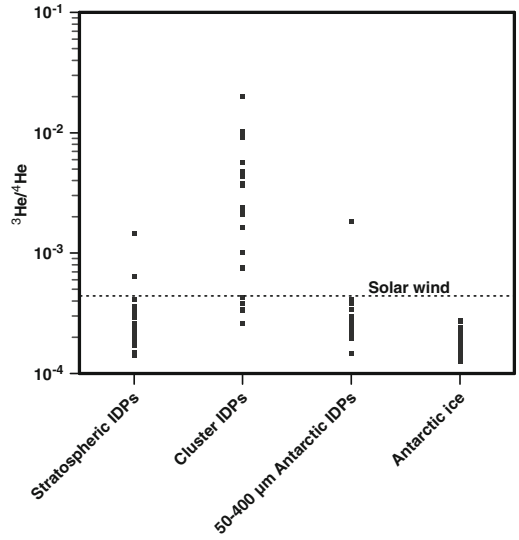

Fig. 1 $^3He/^4He$ ratios of IDPs collected from the stratosphere and from Antarctic ice. Dashed line indicates the $^3He/^4He$ ratio of solar wind (4.48 × 10^{-4}). Note that most IDPs have $^3He/^4He$ ratios similar to or lower than solar wind, while cluster IDPs (fragments of large IDPs) commonly have much higher $^3He/^4He$ ratios, perhaps due to spallogenic He production by galactic cosmic rays. Stratospheric IDPs: Nier et al. (1990), Nier and Schlutter (1992). Cluster IDPs: Nier and Schlutter (1993). 50–400 μm Antarctic IDPs: Stuart et al. (1999). Antarctic ice: Brook et al. (2000)

more shallowly implanted component of solar wind ions during atmospheric entry heating rather than a separate SEP component.

Though most data support a solar source of He in IDPs, some fragments of cluster IDPs collected in the stratosphere—large ($\sim$40 μm) IDPs that break up when impacting the collector surface—have ^{3}He/^{4}He ratios of up to $\sim 1 \times 10^{-2}$ (Fig. 1) (Nier and Schlutter 1993; Pepin et al. 2000, 2001). Spallation reactions from galactic cosmic rays (GCR) or solar cosmic rays (SCR) appear to be the only plausible source of these ^{3}He/^{4}He ratios. In some cases, ^{3}He/^{4}He ratios in deep-sea ferromanganese crusts also indicate the presence of GCR-produced ^{3}He (Basu et al. 2006). However, the ^{3}He flux implied from ferromanganese crusts is a few orders of magnitude lower than that inferred from marine sediments. Furthermore, in magnetic separates from deep sea sediments the measured Ne isotopic compositions appear to be primarily a two component mixture of SW and atmospheric Ne (Fukumoto et al. 1986; Matsuda et al. 1990). Thus, GCR- or SCR-produced ^{3}He appears not to be a major component of the extraterrestrial ^{3}He inventory.

3 IDPs in Terrestrial Deposits

3.1 Determination of Extraterrestrial Noble Gases

In marine sediments and ice cores He is often a two component mixture of extraterrestrial He from IDPs and terrigenous He present in detrital minerals (Fig. 2a). The concentration of extraterrestrial ^{3}He can be estimated using the following equation (Marcantonio et al. 1995):

$$\left[{}^3He_{ET}\right] = \left(\frac{1 - \frac{{}^3He/{}^4He_{TERR}}{{}^3He/{}^4He_{meas}}}{1 - \frac{{}^3He/{}^4He_{TERR}}{{}^3He/{}^4He_{IDP}}}\right) \cdot \left[{}^3He_{meas}\right] \quad (1)$$

where brackets indicate concentrations, 'meas' indicates the measured values, and ^{3}He/^{4}He$_{TERR}$ and ^{3}He/^{4}He$_{IDP}$ denote the ratios for the terrigenous and extraterrestrial endmembers, respectively.

The fraction of ^{3}He$_{ET}$ in the sediments is usually insensitive to the choice of whether the IDP ^{3}He/^{4}He ratio is 4.48×10^{-4} (SW value; Benkert et al. 1993) or the average value of 2.4×10^{-4} observed in stratospheric IDPs (Nier and Schlutter 1990; 1992). The ^{3}He/^{4}He$_{TERR}$ ratio typically varies between 2–4 $\times 10^{-8}$ but occasionally may reach 10^{-7}. When the measured ^{3}He/^{4}He ratios in the sediments are in the 10^{-5} range, the deconvolution is insensitive to the choice of the terrigenous endmember (Fig. 2b; Marcantonio et al. 1995; Farley and Patterson 1995; Mukhopadhyay et al. 2001a; Higgins et al. 2002; Winckler et al. 2005). However, when measured ratios are in the low 10^{-6} to 10^{-7} range, such as in continental margin sediments and other settings with high siliciclastic inputs, studies must consider the sensitivity of ^{3}He$_{ET}$ concentrations to uncertainties in the ^{3}He/^{4}He$_{TERR}$ ratio (e.g., McGee et al. 2010).

The ^{3}He/^{4}He$_{TERR}$ ratio is usually governed by the coupled production of ^{4}He from U and Th decay and ^{3}He from the reaction ^{6}Li(n,α)^{3}H→^{3}He, where the source of the neutrons is the decay of U and Th (Andrews 1985; Mamyrin and Tolstikhin 1984). The ^{3}He/^{4}He production ratio in crustal materials is $\leq 4 \times 10^{-8}$ (Andrews 1985; Mamyrin and Tolstikhin 1984), four orders of magnitude lower than ^{3}He/^{4}He$_{ET}$. This value is similar to values measured for bulk Chinese loess (Marcantonio et al. 1998; Farley 2000; Du et al. 2007; McGee 2010). Some terrigenous samples, however, have ^{3}He/^{4}He ratios of $\sim 10^{-7}$, a factor of 10 higher than the average production rate for the upper continental crust (Marcantonio et al. 1998). Recent work has demonstrated that the fine fraction of Chinese loess (<4 μm) has a factor of 10 higher ^{3}He/^{4}He ratios ($\sim 10^{-7}$) than bulk loess, suggesting that the grain size of terrigenous inputs should be taken into account in choosing ^{3}He/^{4}He$_{TERR}$ (McGee 2010).

A systematic understanding of what controls terrigenous ^{3}He/^{4}He ratios would help in determining ^{3}He/^{4}He$_{TERR}$ for various settings, but at present, the source of high ($\geq 10^{-7}$) ^{3}He/^{4}He ratios in terrigenous sediments is debated. Air-derived ^{3}He appears to be ruled out in sediments even when the measured ^{3}He/^{4}He ratios are

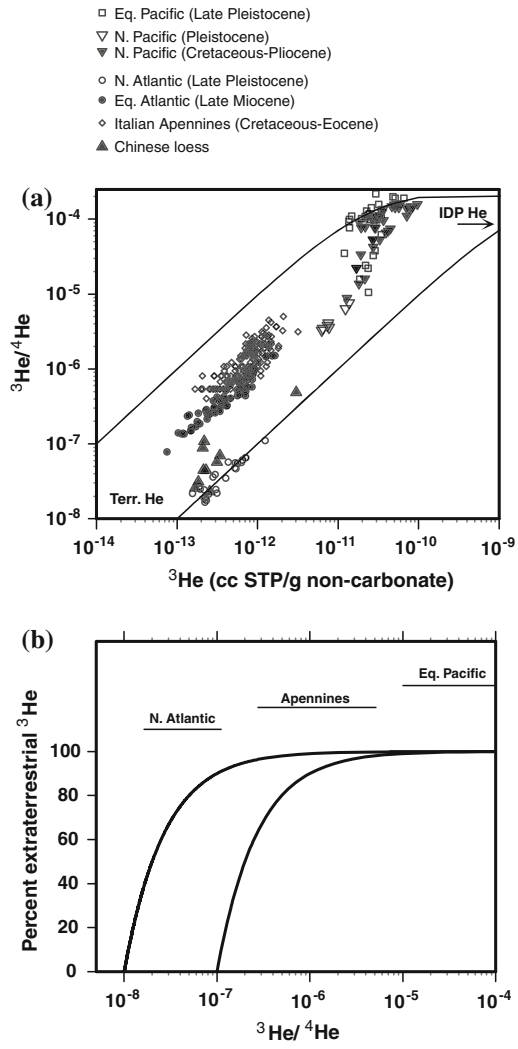

Fig. 2 Mixing between extraterrestrial and terrigenous He in terrestrial sediments. **a** He isotope data from deposits spanning from the late Cretaceous to the Holocene (after Marcantonio et al. 1998). Lines depict mixing between IDP He (^{3}He/^{4}He = 2.4 × 10^{-4}) and two hypothetical terrigenous endmembers. Chinese loess data are shown as a potential terrigenous endmember for North Pacific sediments. ^{3}He concentrations are calculated for the non-carbonate fraction of sediments. Even in IDP-rich samples, sedimentary ^{3}He/^{4}He ratios typically do not exceed 2.4 × 10^{-4}. **b** Plot showing the fraction of ^{3}He that is extraterrestrial for different measured ^{3}He/^{4}He ratios (after Farley 2000). Lines indicate terrigenous endmembers with ^{3}He/^{4}He ratios of 10^{-7} and 10^{-8}; most studies assume ^{3}He/^{4}He ratios of 2–4 × 10^{-8} for the terrigenous endmember. Ranges of measured ^{3}He/^{4}He ratios from selected studies are shown for reference. Equatorial Pacific: Marcantonio et al. (1995); North Pacific: Farley (1995). North Atlantic: McGee et al. (2010). Equatorial Atlantic: Farley et al. (2006). Italian Apennines: Mukhopadhyay et al. (2001a). Chinese loess: Marcantonio et al. (1998), Farley (2000)

close to atmospheric (1.4 × 10^{-6}). Measurements of Ne concentrations in sediments multiplied by the He/Ne ratio of air indicate that in sediments at DSDP Site 607 (Farley and Patterson 1995), LL44-GPC3 (Farley 2000), and Gubbio in the Italian Apennines (Mukhopadhyay et al. 2001a) the percentage of air-derived ^{3}He is ≤1 %. On the other hand, mantle He has been suggested as an important contributor (Marcantonio et al. 1998; Tolstikhin and Drubetskoy

1975) with some volcanic rocks having $^3He/^4He$ ratios on the order of 10^{-5}. Cosmogenic He produced within minerals such as olivines and pyroxene can also have high $^3He/^4He$ ratios. Based on in-vacuo crushing of mantle minerals (e.g., Kurz et al. 1996), Farley (2000) argued that most mantle He (~90 %) would be lost by the time the volcanic material is ground down to grain sizes of a few to few 10 s of microns for transport to the ocean. Additionally, while the globally averaged cosmogenic ^3He production is similar to the flux of $^3He_{ET}$, Farley (2000) argued that cosmogenic He inventory in sediments must be low, since most terrigenous materials are actually derived from a very small percentage of the Earth's surface, and the most common terrigenous minerals (quartz, feldspars, clays) have very low He retentivity. An additional possibility for relatively high $^3He/^4He$ ratios in crustal material is that terrigenous ^3He and ^4He may be held in separate phases that respond differently to weathering, leading some deposits to have elevated $^3He/^4He$ ratios due to preferential loss of radiogenic ^4He (Tolstikhin et al. 1996).

One key uncertainty in determining the correct $^3He/^4He_{TERR}$ for the deconvolution (Eq. 1) is the possibility that samples taken to represent the terrigenous endmember contain IDPs. To the extent that IDPs retain $^3He_{ET}$ during weathering and transport, $^3He/^4He$ ratios in fan sediments and loess deposits—sediments often taken to reflect the terrigenous endmember—may be higher than the true $^3He/^4He_{TERR}$ due to the presence of IDPs. As an example, Marcantonio et al. (1998) found relatively high $^3He/^4He$ ratios in Amazon fan sediments (~$1–2 \times 10^{-7}$). These rapidly accumulating sediments should have low concentrations of directly in-falling IDPs. It is not known whether the high ratios reflect terrigenous sources (possibly enriched in mantle He) (Marcantonio et al. 1998) or additions of IDPs deposited in the Amazon watershed and transported to the fan (Farley 2000). Likewise, the observation that the fine fraction of Chinese loess has higher $^3He/^4He$ ratios than bulk loess (McGee 2010) could result from the fact that IDPs would be concentrated in the fine fraction.

In cases where $^3He_{ET}$ values are sensitive to $^3He/^4He_{TERR}$ and in which $^3He/^4He_{TERR}$ is not known, three approaches have been taken to estimate $^3He/^4He_{TERR}$. The first and most basic approach is to take the lowest $^3He/^4He$ value in the dataset as an upper bound on $^3He/^4He_{TERR}$ (McGee et al. 2010). Second, as IDPs are concentrated in the magnetic fraction of sediments, the $^3He/^4He$ ratio of the nonmagnetic fraction has also been used as an upper bound on $^3He/^4He_{TERR}$ (Fourre 2004). Finally, it has been suggested that step heating of samples may be able to separate terrigenous and extraterrestrial ^3He, based upon the observation in early studies that ^4He is predominantly released at low temperatures (~400 °C), while ^3He is mostly released at >600 °C (Hiyagon et al. 1994; Farley 2000). In this approach, He released below a given temperature (e.g., 500 °C) is taken to be terrigenous, while the remainder of He is taken to be extraterrestrial (Farley 2000); however, recent work employing additional heating steps between 300 and 500 °C has found evidence for extraterrestrial He loss at temperatures of <500 °C (see Sect. 3.2) (Mukhopadhyay and Farley 2006). These recent results suggest that the step heating approach may underestimate $^3He_{ET}$ concentrations as 15–30 % of $^3He_{ET}$ may be released at temperatures <500 °C.

For studies in which the choice of $^3He/^4He_{TERR}$ is critical but $^3He/^4He_{TERR}$ is not known, both lower bound estimates ($^3He/^4He_{TERR} = 2 \times 10^{-8}$) and upper bound estimates using the approaches listed above should be presented. Such an approach would make it clear to the reader whether the assumptions with regards to the $^3He/^4He_{TERR}$ affect the overall conclusions of the work.

3.2 Carrier Phase of $^3He_{ET}$ in Terrestrial Deposits

$^3He_{ET}$ in the geological record is retained for at least 480 Ma (Patterson et al. 1998). However, the identity of the phase(s) responsible for long-term ^3He retention remains unclear, which presents a challenge in understanding how changing redox conditions or sedimentary diagenesis

affect the retention of ^{3}He. Based on magnetic separations and chemical dissolution experiments performed on Quaternary sediments, magnetite and a second non-magnetic phase, probably a silicate, have been suggested as carriers of $^3He_{ET}$ (Fukumoto et al. 1986; Amari and Ozima 1988; Matsuda et al. 1990). The suggestion of magnetite as one of the carriers is, however, problematic. Magnetite in IDPs is not primary but formed during atmospheric entry heating through oxidation of Fe–Ni sulfides, olivine, pyroxene, and poorly ordered silicates (Fraundorf et al. 1982; Brownlee 1985; Bradley et al. 1988). Because magnetite formation during entry heating will involve breaking chemical bonds and diffusion of oxygen, pervasive loss of ^{3}He from the material undergoing the chemical transformation might be expected. ^{3}He retention in silicates is also problematic as the dominant silicate phases in IDPs (olivines and pyroxenes) would be susceptible to diagenetic alteration on the seafloor, while the layer lattice silicates would have low retentivity for ^{3}He. Finally, sequential chemical leaching on recent sediments suggests that refractory phases such as diamond, graphite, SiC, and Al_2O_3 do not account for more than 10 % of the $^3He_{ET}$ (Fukumoto et al. 1986).

More recently, Mukhopadhyay and Farley (2006) carried out chemical leaching experiments of the magnetic and non-magnetic fraction of geologically old sediments (up to 90 Ma). These experiments indicate that similar amounts of ^{3}He are lost from the magnetic and non-magnetic fractions and rule out organic matter and refractory phases such as diamond, graphite, SiC, and Al_2O_3 as the carriers responsible for long-term retention of $^3He_{ET}$. In addition, based on IRM acquisition, Mukhopadhyay and Farley (2006) showed that the magnetic moment of the magnetic and non-magnetic fraction is similar. The result suggests that the magnetite separation technique they and all previous workers used results in approximately half of the magnetite still residing in the non-magnetic fraction. The chemical leaching and the magnetic properties of the magnetic and non-magnetic fraction of the sediments combined suggest a single carrier that might be Fe–Ni metal, Fe–Ni sulfides, or possibly magnetite but more likely a phase that is associated with magnetite. In IDPs collected from the stratosphere olivine and pyroxene grains are frequently rimmed by magnetite a few to a few tens of nm thick that forms during atmospheric entry heating (Bradley et al. 1988). Because magnetite is stable on the ocean floor for tens of millions of years, the magnetite rims may armor the olivines, pyroxenes or poorly ordered silicates against chemical alteration and may also explain the association of the ^{3}He carrier(s) with magnetite.

The presence of a single carrier phase is also strongly supported by step heating experiments (Fig. 3) on the magnetic and non-magnetic fraction of the sediments that demonstrate that the ^{3}He release patterns in the two sediment fractions are identical (Mukhopadhyay and Farley 2006). The step heating experiments indicate two release peaks, one at low temperature (350–400 °C) and one at higher temperature (600–750 °C). Previous work (Amari and Ozima 1985, 1988; Hiyagon 1994) had not noticed the low temperature peak as the step heating experiments started at temperatures in excess of 500 °C. While Farley (2000) had observed a low temperature release peak from step heating experiments in sediments from Site 607B, the ^{3}He/^{4}He ratio for the low temperature release peak was 0.1 R_A and hence, the release was associated with crustal He. Additionally, the new step heating experiments (Mukhopadhyay and Farley 2006) indicate a higher retentivity for ^{3}He over geologic time. For example, extrapolation diffusivities obtained from high-temperature step heating experiments (e.g., Amari and Ozima 1985) to seafloor indicates that greater than 99 % of the extraterrestrial ^{3}He is expected to be lost in 50 Ma, which is at odds with the pelagic clay ^{3}He record from the Central Pacific GPC3 core (Farley 1995). The new step heating experiments indicate that about 20 % of the ^{3}He will be lost through diffusion at seafloor temperatures after 50 Ma, while sedimentary rocks exposed on the Earth's surface for the same amount of time would lose up to 60 % (Mukhopadhyay and Farley 2006). Additionally, if temperatures exceed 70 °C during sediment diagenesis

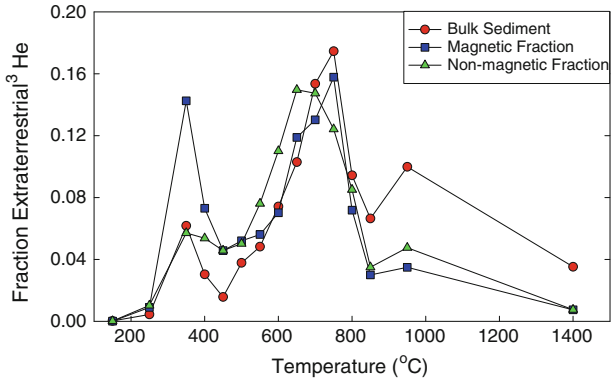

Fig. 3 Extraterrestrial ^{3}He release patterns for bulk, magnetic and non-magnetic fractions of sediments from step heating experiments (Adapted from Mukhopadhyay and Farley 2006). Bulk sediments are from LL44-GPC3 and DSDP Site 596B, while the magnetic and non-magnetic fractions are from LL44-GPC3 sediments. Since multiple experiments for bulk, magnetic and non-magnetic fractions were carried out by Mukhopadhyay and Farley (2006), only the average release pattern for the three sediment types has been shown. Note the very strong similarity in the release patterns for all three sediment types

extensive ^{3}He loss is expected to occur (>90 %) after only a few hundred ka. Thus, care must be taken to compare the extraterrestrial ^{3}He record from different sites and tectonic environments.

3.3 Atmospheric Entry Heating and Grain Size Distribution of $^3He_{ET}$-Bearing IDPs in Terrestrial Deposits

Atmospheric entry heating modifies the extraterrestrial noble gas content of incoming IDPs. Heating during entry causes thermal decomposition of phyllosilicates within IDPs as well as diffusive loss and bubble rupture, all of which contribute to He losses (Stuart et al. 1999). Maximum entry temperatures are proportional to mass and entry velocity; as a result, larger IDPs and IDPs derived from comets (which tend to have higher geocentric velocities than asteroid-derived IDPs) are more likely to be degassed before reaching Earth's surface (Flynn 1989; Love and Brownlee 1991). Hence, ^{3}He in sediments will not reflect the relative abundance of cometary versus asteroid IDPs that enter the Earth's atmosphere but will rather be biased towards the accretion of asteroidal IDPs.

Farley et al. (1997) quantitatively modeled the grain size distribution of IDPs capable of retaining $^3He_{ET}$ after atmospheric entry. Based upon the assumption that IDPs have implanted $^3He_{ET}$ to depths of few hundred nanometers—i.e., ^{3}He is surface area-correlated rather than volume-correlated—and that $^3He_{ET}$ is lost in IDPs heated to more than ~600 °C, Farley et al. (1997) predicted that $^3He_{ET}$ in terrestrial sediments should primarily (>70 %) be contained within IDPs between 3 and 35 μm in diameter. If $^3He_{ET}$ is instead assumed to be volume-correlated, a much broader grain size distribution results, with >70 % of $^3He_{ET}$ contained with grains ranging from ~5 to 150 μm (Farley et al. 1997). Overall, Farley et al. (1997) find that as a result of atmospheric entry heating, $^3He_{ET}$-bearing IDPs represent only ~0.5 % of the total IDP mass flux to Earth of $40 \pm 20 \times 10^6$ g/a (Love and Brownlee 1993) and ~4 % of the total IDP surface area flux.

Since the entry-heating model predicts the size distribution of ^{3}He-bearing particles in sediment (particles not heated to >600 °C), for a given IDP flux and sediment accumulation rate, one can calculate the minimum volume of sediment required to statistically sample the He-bearing IDPs so as not to underestimate the ^{3}He flux. Additionally, predictions can be made of the reproducibility of ^{3}He measurements in sediment aliquots of different sizes (i.e., different area-time products) depending upon whether ^{3}He is surface area-correlated

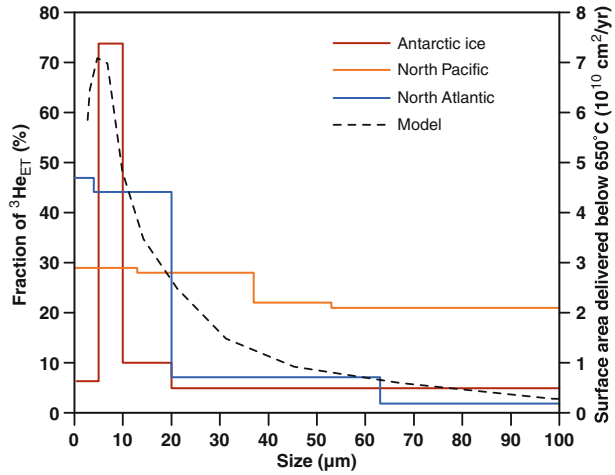

Fig. 4 Grain size distribution of $^3He_{ET}$ in terrestrial deposits and a model of surface area delivery of He-retentive IDPs. Data (*solid lines*) reflects the percent of the total $^3He_{ET}$ in a given grain size fraction. Data from Holocene Antarctic ice (Brook et al. 2009) and 33 Ma North Pacific sediments (Mukhopadhyay and Farley 2006) represent one sample each, while data from the North Atlantic represent the average of six samples from the last glacial period and Holocene (McGee et al. 2010). Model results (*dashed line*) reflect the total IDP surface area delivered by different particle sizes heated to less than 650 °C during atmospheric entry (Farley et al. 1997)

or volume-correlated (Farley et al. 1997). The reproducibility of replicate samples matches predictions from model results if $^3He_{ET}$ is a surface-area correlated component rather than a volume-correlated component (Farley et al. 1997; Patterson and Farley 1998; Mukhopadhyay et al. 2001a). This suggests that $^3He_{ET}$ is primarily contained in a large number of fine grains rather than a small number of large grains. Studies of grain size fractions of deep-sea sediments and ice core particulates also support a correlation of $^3He_{ET}$ content with IDP surface area, finding ~60–90 % of the total $^3He_{ET}$ within size fractions <35 μm (Fig. 4) (Mukhopadhyay and Farley 2006; Brook et al. 2009; McGee et al. 2010).

Though all three studies find that $^3He_{ET}$ is primarily contained in grains <35 μm, each provides a slightly different estimate of the grain size distribution of $^3He_{ET}$ in terrestrial deposits. Data from a sample of Holocene Antarctic ice indicate a sharp peak in $^3He_{ET}$-bearing grains between 5 and 10 μm (Brook et al. 2009); analyses of six samples of Late Quaternary North Atlantic drift sediments indicate a broader peak between 0 and 20 μm (McGee et al. 2010); and data from a sample of 33 Ma North Pacific red clay suggest a broader distribution, with roughly equal $^3He_{ET}$ inventories in the 0–13 and 13–37 μm fractions and only slightly lower $^3He_{ET}$ inventories in the 37–53 μm and >53 μm fractions (Mukhopadhyay and Farley 2006). The differences in these studies may have to do with differences in the time-area product of the samples used (samples with higher time-area products, such as red clays, are more likely to sample rare large IDPs) or with the different methods used for grain size separation. Brook et al. (2009) passed ice melt through filters to separate grain size fractions, while McGee et al. (2010) used settling after adding a chemical dispersant to reduce flocculation of fine grains, and Mukhopadhyay and Farley (2006) used settling without dispersant addition. Settling, and particularly settling without dispersants, is unlikely to quantitatively remove fine grains from coarser size fractions, potentially leading to an overestimation of $^3He_{ET}$ inventories in coarser fractions.

Some large (50–400 μm) IDPs from Antarctic ice appear to have retained $^3He_{ET}$ of both solar and spallogenic origin (Fig. 1) (Stuart et al. 1999), but the grain size and reproducibility measurements cited above suggest that these rare large He-retentive particles do not contribute substantially to the total $^3He_{ET}$ flux. Finally,

we note that Lal and Jull (2005) proposed that instead of ^{3}He in IDPs, spallogenic He within fragments released by meteorites during atmospheric entry is a dominant source of $^3He_{ET}$ in sediments. The hypothesis of Lal and Jull (2005) makes two predictions: (1) approximately 50 % of the ^{3}He is in sediments coarser than 50 μm and (2) high ^{3}He/^{4}He ratios in sediments should be associated with spallogenic Ne. As noted above, the grain size distribution data and reproducibility of $^3He_{ET}$ measurements do not support 50 % of $^3He_{ET}$ being in grain sizes larger than 50 μm. Further, high ^{3}He/^{4}He ratios of 2–3 $\times$ 10^{-4} in sediments have been found to be associated with solar wind Ne and not spallogenic Ne (Fukumoto et al. 1986; Matsuda et al. 1990). Hence, data do not support the hypothesis that fragmentation of meteorites in the atmosphere is the dominant contributor to ^{3}He; they are instead best explained by $^3He_{ET}$ in marine sediments and terrestrial ice being a surface-area correlated component in IDPs.

4 Extraterrestrial He in the Geologic Record

4.1 Extraterrestrial He as a Tracer of Past Variations in IDP Flux

As a tracer of the IDP flux, $^3He_{ET}$ offers a view into past accretion rates of extraterrestrial matter that is quite different from that provided by iridium and other PGEs, which trace the total extraterrestrial mass flux. As demonstrated below, large impacts that leave PGE anomalies may or may not be accompanied by elevated IDP fluxes (Farley et al. 1998; Mukhopadhyay et al. 2001a, b), and elevated IDP fluxes are not always accompanied by large impacts (Farley et al. 2006).

$^3He_{ET}$ fluxes ($f_{He_{ET}}$) are calculated by multiplying the measured $^3He_{ET}$ concentration by the sedimentary mass accumulation rate (MAR):

$$f_{He_{ET}} = \left(\left[{}^3He_{ET}\right] \cdot MAR\right)/R \qquad (2)$$

where [$^3He_{ET}$] is the $^3He_{ET}$ concentration in the sediment (see Eq. 1), MAR is the sedimentary mass accumulation rate and R is the fractional retentivity of ^{3}He (Farley 1995). Though assumptions of constant inputs of hydrogenous cobalt have occasionally been used for MAR calculation (Farley 1995), MARs are usually derived from age models:

$$MAR = \frac{\rho \cdot \Delta z}{\Delta t} \qquad (3)$$

where ρ is the dry bulk density, Δz is a depth interval, and Δt is the time associated with that depth interval. Age models are typically determined from geologic epochs, magnetic chrons or astronomical tuning (e.g., Farley 1995; Farley et al. 1998, 2006; Mukhopadhyay et al. 2001a) and are thus subject to errors in the ages of epoch or chron boundaries or in the identification of astronomical cycles. Age model-based MARs also do not account for sedimentary inputs by lateral advection or slumping. As a result of potential age model errors and spurious $^3He_{ET}$ flux changes caused by changes in lateral advection of sediments, some studies have sought to replicate $^3He_{ET}$ flux excursions in multiple cores or sections (e.g., Farley et al. 1998, 2006). Finally, $^3He_{ET}$ retentivity in the sedimentary record over geological time is not well quantified, and thus the value of R is not known. As a result, the absolute $^3He_{ET}$ flux cannot be determined. Rather, one always calculates the product $f_{He_{ET}} \cdot R$ and the product is termed the implied $^3He_{ET}$ flux (e.g., Farley et al. 1998; Mukhopadhyay et al. 2001a). We note that $^3He_{ET}$ loss by diffusion is expected to increase with age; i.e., R should decrease monotonically with age. However, because $^3He_{ET}$ is retained in the geological record for at least 480 Ma (Patterson et al. 1998), assuming an invariant R in a given sedimentary setting is probably valid over the geologically short ($\sim$a few to a few tens of Ma) timescales over which IDP flux variations would be expected to occur (Farley et al. 1998, 2006). Thus, relative variations in $^3He_{ET}$ fluxes in the sedimentary record over million-year durations are robust even though the absolute values of the fluxes may not be well defined.

The discovery of $^3He_{ET}$ in 480 Ma Ordovician limestones (Patterson et al. 1998) suggests that

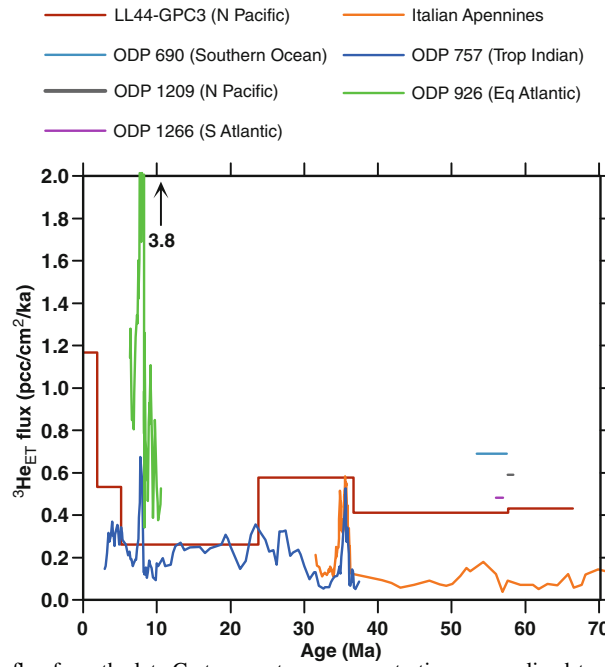

Fig. 5 Records of $^3He_{ET}$ flux from the late Cretaceous to the Pleistocene. Records from LL44-GPC3, ODP 690, ODP 1209 and ODP 1266 represent the average $^3He_{ET}$ fluxes across dated intervals. Records from ODP 757 and ODP 926 reflect the 3-point moving average of "instantaneous" $^3He_{ET}$ fluxes (i.e., the product of a sample's $^3He_{ET}$ concentration and MAR derived from the age model). Data from the Italian Apennines reflect the authors' best estimate based on chron-averaged $^3He_{ET}$ fluxes, $^3He_{ET}$ concentrations normalized to the non-carbonate fraction, and $^3He/^4He$ ratios. The short-lived flux increases at 35 and 8 Ma are shown in greater detail in Fig. 6. Differences in absolute fluxes between records are likely to reflect differences in $^3He_{ET}$ preservation or sediment focusing. LL44-GPC3: Farley (1995). ODP 690: Farley and Eltgroth (2003). ODP 1209: Marcantonio et al. (2009). ODP 1266: Murphy et al. (2010). Italian Apennines: Mukhopadhyay et al. (2001a). ODP 757 and ODP 926: Farley et al. (2006)

IDP accretion rates could be reconstructed over most of the Phanerozoic. The implied accretion rate of extraterrestrial ^3He in the Late Ordovician is $\sim 0.5 \pm 0.2$ pcc STP/cm^2/ka, which is similar to the average flux over the Cenozoic. The Ordovician sediments further demonstrate that $^3He_{ET}$ in sediments is largely carried by IDPs, as co-existing meteorites in the sedimentary section have He concentrations that are similar to or only slightly higher than the ^3He concentration of the host limestones.

At the Permo-Triassic boundary (P/Tr) sections at Meishan, China and Sasayama, Japan, $^3He_{ET}$ has been reported, although not in IDPs but rather in fullerenes delivered through a bolide impact (Becker et al. 2001). However, Farley and Mukhopadhyay's (2001) measurements of ^3He from the Meishan section did not detect $^3He_{ET}$ at or near the vicinity of the P/Tr boundary and thus, they found no evidence for fullerene-hosted $^3He_{ET}$. Additional work by Farley et al. (2005) from the Opal Creek P/Tr section in Canada also found no evidence of extraterrestrial ^3He, and hence, fullerene-hosted $^3He_{ET}$. As a result, whether or not fullerene-hosted $^3He_{ET}$ is present at the P/Tr boundary remains an open question.

In spite of $^3He_{ET}$ being retained for the past 480 Ma, ^3He fluxes are relatively well characterized only for the Cenozoic. The Cenozoic history of $^3He_{ET}$ fluxes was first investigated by Farley (1995) in core LL44-GPC3 from the central North Pacific. The study found roughly constant $^3He_{ET}$ fluxes averaged over epochs from the Late Cretaceous to the Pliocene ($\sim 0.5 \pm 0.2$ pcc STP/cm^2/ka), with highest fluxes in the Oligocene and lowest fluxes in the Miocene (Fig. 5). $^3He_{ET}$ fluxes were also calculated by normalizing to Co concentrations in the sediment, based on the assumption that hydrogenous Co accumulates at a constant rate (Kyte et al. 1993).

Co-based fluxes of $^3He_{ET}$ can be calculated at much higher resolution than epoch-averaged fluxes and show high short-term variability, including peaks just before the K/Pg boundary and during the early Eocene and latest Eocene/early Oligocene. Of these, the first is related to Co-based accumulation rates and is not reflected in $^3He_{ET}$ concentrations, while the latter two are marked by increased $^3He_{ET}$ concentrations in the sediments. One of the most dramatic features of the GPC3 record is a factor of 2 increase in the $^3He_{ET}$ flux from the Pliocene to the Quaternary. This change could reflect (1) a change in IDP flux, (2) diffusional loss of $^3He_{ET}$, (3) an age model error that places the Quaternary/Pliocene boundary too high in the core, or (4) increased lateral advection of sediments to the site during the Quaternary. The Quaternary/Pliocene change in $^3He_{ET}$ flux has not been studied at other sites and offers an important avenue for future work.

Subsequent work investigated the Cretaceous-Eocene portion of the record in greater detail in pelagic limestones exposed in the Umbria-Marche basin of the Italian Apennines (Farley et al. 1998; Mukhopadhyay et al. 2001a). The mean $^3He_{ET}$ flux in the Apennine sections is a factor of 3–5 lower than the mean flux over the same period in the North Pacific core studied by Farley (1995), suggesting either $^3He_{ET}$ loss during the burial and uplift of this section (Mukhopadhyay and Farley 2006) or systematically higher lateral advection of sediments at the North Pacific site. Mukhopadhyay et al. (2001a) found approximately constant $^3He_{ET}$ fluxes from the late Cretaceous through the early Eocene in pelagic limestones in the Italian Apennines. Possible departures from a constant flux occur near the Paleocene/Eocene boundary, with a 2–4-fold increase in $^3He_{ET}$ flux, and during the early Eocene, when a gradual decrease in flux is indicated; however, there are concerns about tectonic disturbances and slumping in this section (Mukhopadhyay et al. 2001a). Significantly, there is no evidence for an increase in $^3He_{ET}$ flux associated with the K/Pg boundary in either the Apennines or an expanded K/Pg section in Morocco. A single asteroid or comet impact is not accompanied by increased accretion rate of IDPs, while a shower of comets generated by perturbation of the Oort cloud leads to an increased terrestrial IDP accretion rate associated with multiple impacts (Farley et al. 1998). Hence, the K/Pg ^3He results suggest that the impactor was not part of a comet shower but rather an asteroid or a lone comet (Mukhopadhyay et al. 2001a, b).

In the latest Eocene, $^3He_{ET}$ fluxes reconstructed from limestones in the Italian Apennines and from an Indian Ocean sediment core document a factor of $\sim$5.5 increase in the IDP accretion rate, with peaks at $\sim$36 and 35 Ma (Farley et al. 1998, 2006). The peaks are accompanied by spikes in Ir concentration in the Apennine section and roughly correspond to the ages of the Chesapeake Bay and Popigai impact structures and tektite layers found in sediments around the world (Fig. 6). The implied increase in IDP flux begins 0.7 Ma before the first Ir spike and gradually decays for almost 1 Ma after the second spike. Two potential mechanisms can account for the simultaneous increase in IDP accretion rates and the delivery of large impactors: a comet shower associated with a perturbation of the Oort cloud or a large collision in the asteroid belt. Farley et al. (1998) preferred the comet shower hypothesis because (1) the observed variations in the dust flux matched Hut et al.'s (1987) predictions of dust enhancement in the inner solar system associated with a comet shower generated by perturbation of the Oort cloud and (2) comet showers would necessarily lead to an increase in both dust and large impactors in the inner solar system. While large collisions in the asteroid belt can enhance dust accretion rates to the Earth, simultaneous delivery of large impactors and dust is not predicted a priori, unless the collision occurs in the close vicinity of one of the several secular and mean-motion resonances in the asteroid belt from which large objects can be ejected on Earth-crossing orbits on timescales of <1 Ma (e.g., Gladman et al. 1997). Furthermore, it is not clear whether the enhancement in dust accretion rate from asteroid belt collisions would match the observed pattern seen in the late Eocene (Farley et al. 1998). Recent work, however, has suggested an

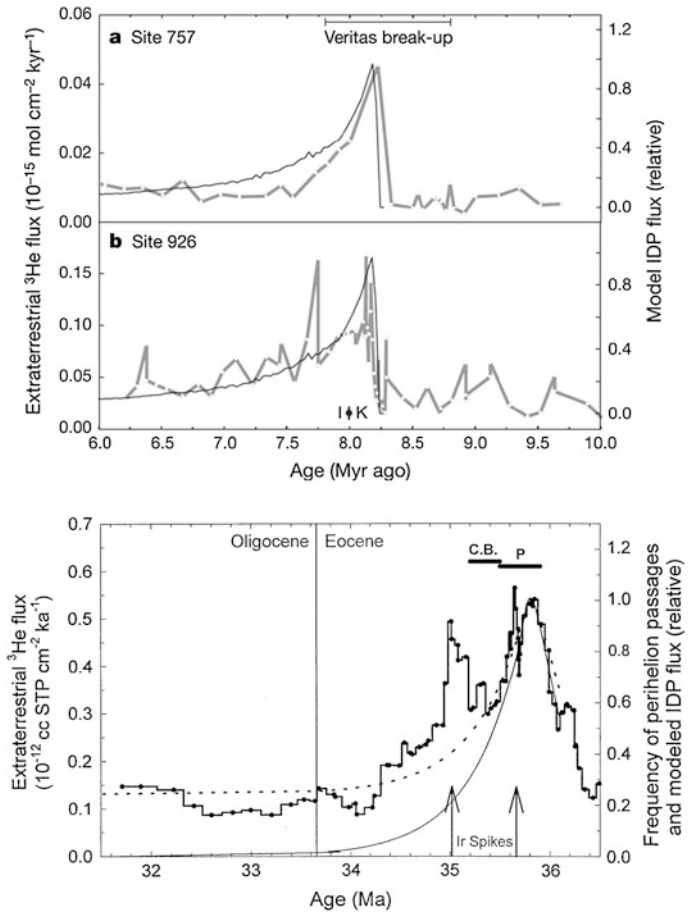

Fig. 6 Insights into past solar system events from variations in the $^{3}He_{ET}$ flux. *Top*—Comparison of late Miocene $^{3}He_{ET}$ fluxes at two sites with flux changes predicted from a model of IDP creation and transport after the Veritas asteroid break-up event (Farley et al. 2006). An independent estimate for the age of this event is shown at the top of the figure. I/K denotes the transition from kaolinite to illite as the dominant clay mineral at Site 926. *Bottom*—A Late Eocene increase in $^{3}He_{ET}$ flux measured in samples from the Italian Apennines (Farley et al. 1998). Independent ages of increases in Ir concentration in marine sediments (a marker of extraterrestrial impacts) and of the Chesapeake Bay and Popagai impact structures are shown. The solid line indicates the modeled increase in IDP flux associated with a comet shower initiated by a perturbation of the Oort cloud; the dashed line is the same result shifted up to reflect pre- and post-event baseline IDP fluxes

L-chondrite composition for the Popigai impactor (Tagle and Claeys 2004) suggesting that the increase in IDP flux may have an asteroidal origin.

$^{3}He_{ET}$ flux again increased transiently in the late Miocene (8.2 Ma) (Fig. 6). The $^{3}He_{ET}$ flux pattern recorded in sediment cores from both the Indian and Atlantic oceans is broadly similar to that of the late Eocene (Farley et al. 2006); in detail, however, the increase in $^{3}He_{ET}$ during the Miocene occurs more abruptly than in the Eocene event, rising a factor of $\sim$4 in <100 ka, followed by a $\sim$1.5 Ma decay to pre-event levels. Unlike the Eocene event, there are no known large impacts of this age. Farley et al. (2006) provided evidence that the event reflects the breakup of a parent asteroid with a diameter greater than 100 km to form the Veritas family of asteroid fragments, an event that has been independently dated to 8.3 $\pm$ 0.5 Ma (Nesvorný et al. 2003). The Veritas family currently orbits at a distance of 3.17 AU and continues to be a

major source of IDPs to the zodiacal cloud (Nesvorný et al. 2006). The breakup event is likely to have formed abundant IDPs, but it is unlikely to have sent any large fragments into Earth-impacting orbits (Farley et al. 2006). Though the link between the Veritas breakup and the $^{3}He_{ET}$ flux increase is compelling, remaining questions include (1) why models indicate a more prolonged decay of IDP flux following the event than is observed and (2) whether a similar peak in $^{3}He_{ET}$ flux is associated with the Karin asteroid breakup event dated to ~5.8 Ma (Nesvorný et al. 2006).

Several studies have investigated the ^{3}He-based IDP accretion rate during the Quaternary, as cyclic variations in IDP accretion rate were suggested as a driver of the 100 ka glacial cycle (Muller and Macdonald 1995). Modeling of the terrestrial accretion rate of asteroid dust predicts 100 ka variations in IDP accretion rate of up to a factor of 2, associated with changes in Earth's orbital inclination (Kortenkamp and Dermott 1998a). $^{3}He_{ET}$ fluxes from the Atlantic and Pacific oceans over the last 2 Ma based on MARs derived from benthic $\delta^{18}O$ data do suggest a 100 ka periodicity in $^{3}He_{ET}$ fluxes over the past 700 ka (Farley and Patterson 1995; Patterson and Farley 1998). Peak fluxes occur during interglacial periods with variations in amplitude ranging from a factor of ~1.5 to ~3.5 between cycles and between cores. Surprisingly, however, the peaks in ^{3}He fluxes are ~180° (50 ka) out of phase with the predicted accretion rate of IDPs based on orbital variations (Kortenkamp and Dermott 1998a). Hence, either the observed peaks in $^{3}He_{ET}$ fluxes are not a consequence of varying IDP accretion rate from space, or the models that predict IDP accretion rates based on variations in Earth's orbital parameters (Kortenkamp and Dermott 1998a) may not be fully capturing all of the accretion processes. For example, Dermott et al. (2001) suggested that accretion of asteroidal dust from the resonant ring of dust around the Earth may be a possible mechanism for inducing a 50 ka lag in the IDP accretion rate. This hypothesis has yet to be verified.

The apparent variations in $^{3}He_{ET}$ flux during the late Quaternary have also been called into question based on observations that the ratio of $^{3}He_{ET}$ to scavenged ^{230}Th—a tracer of sedimentary flux largely independent of age model errors and lateral advection of sediments—remains constant within ±40 % (one standard deviation of the mean) through glacial-interglacial cycles in equatorial Pacific sediments, suggesting relatively constant $^{3}He_{ET}$ flux (Marcantonio et al. 1995, 1996, 1999, 2001b; Higgins et al. 2002) (see Sect. 4.2 for additional discussion). Further, Winckler et al. (2004) found that age model-based $^{3}He_{ET}$ fluxes vary with a 41 ka periodicity in the early Quaternary; this period matches that of contemporaneous glacial-interglacial variability but does not match that of changes in orbital inclination. Winckler and Fischer (2006) also found no changes in $^{3}He_{ET}$ fluxes in Antarctic ice from the last glacial period to the Holocene. Together, these results suggest that the observed 100 ka cycles in late Quaternary $^{3}He_{ET}$ accumulation in marine sediments are a consequence rather than a cause of climate variability, perhaps related to glacial-interglacial changes in sediment focusing or systematic age model errors caused by glacial-interglacial changes in carbonate dissolution (Marcantonio et al. 1996, 2001b; Higgins et al. 2002; Winckler et al. 2004). Variations in extraterrestrial ^{3}He flux of smaller magnitude (±40 %), however, cannot yet be ruled out.

The variations in the ^{3}He-based IDP accretion history discussed above have provided important observational evidence for hypothesized solar system events, such as the possible comet shower in the Late Eocene (Farley et al. 1998), the collision disruption of an asteroid to create the Veritas family 8.3 at Ma (Farley et al. 2006), and the nature of the impactor at the K/Pg boundary (single impactor vs. comet shower). Furthermore, the ^{3}He-based accretion history over the past 70 Ma strongly refutes the speculative hypothesis that mass extinctions in the geological record are driven by quasi-periodic comet showers (Hut et al. 1987). While a comet shower may have occurred in the Late Eocene,

not a single extinction event over the past 70 Ma appears to be associated with comet showers, and one of the largest mass extinction events of the Phanerozoic—the K/Pg boundary event—is clearly not associated with a comet shower (Mukhopadhyay et al. 2001a, b).

4.2 Use of Extraterrestrial ^{3}He to Calculate Sedimentary Accumulation Rates

When the $^3He_{ET}$ concentration in a sedimentary section varies, it implies either a variation in the flux from space or changing MAR. If the flux from space is taken to be constant, then Eq. 2 can be inverted to solve for the sediment MAR. A constant $^3He_{ET}$ flux from space can often be inferred when $^3He_{ET}$ concentrations co-vary with concentrations of a terrigenous sedimentary component (e.g., terrestrial ^{4}He, Fe, or the non-carbonate fraction) or with concentrations of ^{230}Th scavenged from the water column. $^3He_{ET}$-based MARs differ in several important respects from MARs derived from age models. First, $^3He_{ET}$-based MARs can be calculated at each sample depth for which $^3He_{ET}$ measurements are available, while MARs based on age models are calculated as average values between age model tie points. Second, over the last 400 ka (when $^3He_{ET}$ fluxes have been determined by ^{230}Th-normalization, as described below), absolute $^3He_{ET}$-based MARs are independent of sedimentary age models. Finally, if $^3He_{ET}$-bearing IDPs are transported with laterally advected sediments, sediment focusing or winnowing will not substantially change the measured $^3He_{ET}$ concentration at a site; $^3He_{ET}$-based MARs will then "see through" sediment focusing and provide estimates of the vertical rain rate of sediment at a site (e.g., Marcantonio et al. 2001b; McGee et al. 2010). In periods prior to 400 ka, when $^3He_{ET}$ fluxes must be calculated from sedimentary age models, the $^3He_{ET}$ flux estimates may be biased by systematic focusing or winnowing in the sediment, affecting the absolute value of $^3He_{ET}$-based MARs but not the relative changes in MARs.

A critical first step in constructing ^{3}He-based MARs is testing whether $^3He_{ET}$ fluxes are in fact constant over a given period. In late Quaternary marine sediments, $^3He_{ET}$ fluxes have been calculated using ^{230}Th-normalization (Marcantonio et al. 1995, 1996; Higgins et al. 2002). Briefly, ^{230}Th-normalization relies on the approximation that ^{230}Th produced in the water column from the decay of dissolved ^{234}U ($^{230}Th_{xs}$) is scavenged by sinking particles more quickly than it can be laterally mixed as a dissolved species. The flux of $^{230}Th_{xs}$ to the seafloor is then taken to be equal to the (known) production rate of ^{230}Th in the water column, and MARs can be calculated as the ratio of the ^{230}Th production rate to the decay-corrected $^{230}Th_{xs}$ concentration in the sediment (for a review of ^{230}Th normalization, see Francois et al. 2004). ^{230}Th-based MARs have the same properties as $^3He_{ET}$-based MARs mentioned above: namely, they can be computed at high resolution; they are largely independent of age model errors; and they should be only minimally affected by lateral advection of sediments. ^{230}Th-normalization can only be used in sediments from the last ~500 ka due to the radioactive decay of ^{230}Th (half-life 75.7 ka).

Marcantonio et al. (1995, 1996, 2001b) and Higgins et al. (2002) found $^3He_{ET}/^{230}Th_{xs}$ ratios in sediments to be constant to within ±40 % throughout the equatorial Pacific Ocean over the last 200 ka with no systematic glacial-interglacial variability, supporting a near-constant flux of $^3He_{ET}$ during this time period. When $^{230}Th_{xs}$ measurements are used to calculate MARs, these results indicate an average $^3He_{ET}$ accumulation rate of 0.8 ± 0.3 pcc STP/cm^2/ka in the late Quaternary (Fig. 7; all flux estimates are given as mean ± one standard deviation of the mean). Marcantonio et al. (1999) determined a similar $^{230}Th_{xs}$-based $^3He_{ET}$ flux in an eastern equatorial Indian Ocean core for the past 200 ka (1.1 ± 0.4 pcc STP/cm^2/ka). In a core from the Arabian Sea, $^{230}Th_{xs}$-based $^3He_{ET}$ fluxes are 0.4 ± 0.3 pcc STP/cm^2/ka over the past 23 ka, lower than observed at other sites, for reasons that are not clear (see discussion below) (Marcantonio et al. 2001a).

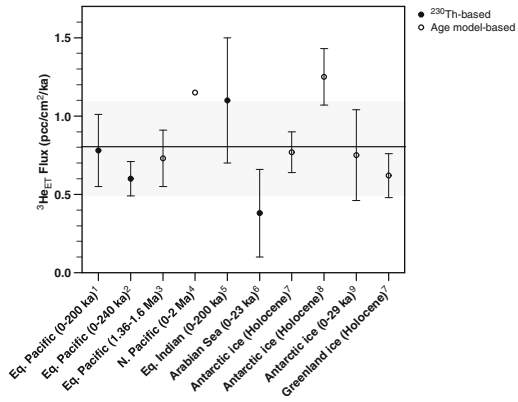

Fig. 7 Estimates of the Quaternary $^{3}He_{ET}$ flux. Fluxes are estimated using both sedimentary and ice core age models (*open circles*) and using ^{230}Th-normalization (*closed circles*). 1-sigma confidence intervals are shown. Most estimates are consistent with a flux of 0.8 ± 0.3 pcc STP $^{3}He_{ET}$/cm^2/ka (indicated by the *line* and *shaded box*). The results do not suggest a latitudinal dependence of $^{3}He_{ET}$ flux. Data sources: Marcantonio et al. (1995), Higgins et al. (2002), Winckler et al. (2004), [4]Farley (1995), Marcantonio et al. (1999), Marcantonio et al. (2001a), Brook et al. (2000), Brook et al. (2009, Winckler and Fischer (2006)

Independent corroboration of $^{3}He_{ET}$ flux estimates from marine sediments comes from measurements of $^{3}He_{ET}$ in ice cores, which find $^{3}He_{ET}$ accumulation rates ranging from 0.62 ± 0.14 to 1.25 ± 0.18 pcc STP/cm^2/ka in four sets of samples of ice from Greenland and Antarctica over the last 30 ka (Brook et al. 2000, 2009; Winckler and Fischer 2006). Similar fluxes have also been found using accumulation rates inferred from an age model in Quaternary samples from the North Pacific core studied by Farley (1995) (~1.2 pcc STP/cm^2/ka) and in equatorial Pacific sediments from the early Quaternary between 1.36 and 1.6 Ma (0.73 ± 0.18 pcc STP/cm^2/ka) (Winckler et al. 2004). Taken together, these results suggest approximately constant (±40 %) $^{3}He_{ET}$ fluxes over the past 1.6 Ma and minimal latitudinal variations in $^{3}He_{ET}$ flux, providing a basis for using $^{3}He_{ET}$ for calculating MARs over this time period. Importantly, these studies establish $^{3}He_{ET}$ as the only constant flux proxy available for paleoflux studies in sediments prior to 500 ka.

$^{3}He_{ET}$ can also been used as a constant flux proxy for MAR calculations in studies ranging back to at least the K/Pg boundary, if $^{3}He_{ET}$ fluxes from space and the fraction of original $^{3}He_{ET}$ lost to diffusion are roughly constant over the timescale of interest. The first assumption does not hold during the late Eocene and late Miocene (see Sect. 4.1), and the second may not be appropriate in transitions between oxic and anoxic sediments, but in much of the late Cretaceous and Cenozoic they appear reasonable. In the carbonate-rich sections that have been studied, $^{3}He_{ET}$ concentrations are relatively constant with respect to the non-carbonate fraction, a rough indicator of relative sedimentation rates, supporting an approximately constant $^{3}He_{ET}$ flux (e.g., Mukhopadhyay et al. 2001a, b; Farley and Eltgroth 2003; Marcantonio et al. 2009).

$^{3}He_{ET}$ fluxes for these earlier periods are typically determined in portions of a given sedimentary section in which the age model is well constrained (usually by orbital tuning or magnetostratigraphy) and that either are adjacent to or span the period of interest. These $^{3}He_{ET}$ fluxes are then applied to the interval of interest, which is often a time of substantial changes in sedimentation when orbital signals are in doubt. Absolute $^{3}He_{ET}$ fluxes for a given time period vary from site to site due to differences in $^{3}He_{ET}$ preservation or sediment focusing (Fig. 5); for example, $^{3}He_{ET}$ fluxes for the late Eocene and early Paleocene are a factor of 3 or more higher in sediment cores from the central and western North Pacific, South Atlantic and Southern Ocean (Farley 1995; Farley and Eltgroth 2003; Marcantonio et al. 2009; Murphy et al. 2010) than in a sediment core from Blake Nose in the North Atlantic (Farley and Eltgroth 2003). To the extent that these differences reflect differences in sediment focusing (which increases $^{3}He_{ET}$ fluxes during a dated interval by laterally advecting IDPs to a core site), $^{3}He_{ET}$-based MARs will be systematically biased low in sites with high focusing but relative changes in accumulation rates will still be robust. As noted above, absolute $^{3}He_{ET}$-based MARs are not independent of the

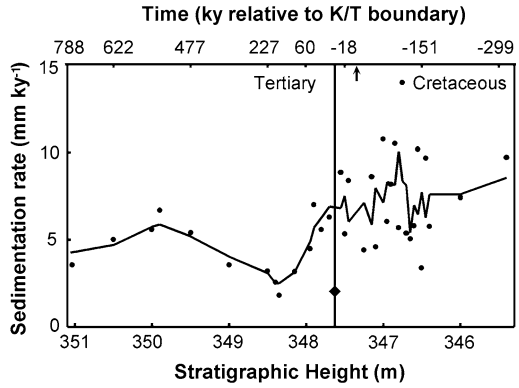

Fig. 8 $^{3}He_{ET}$-based sedimentation rates for the Cretaceous-Paleogene boundary section at Gubbio, Italy (Mukhopadhyay et al. 2001b). Points indicate instantaneous sedimentation rates, while the line is the three-point moving average. The *diamond* indicates the sedimentation rate in the K/Pg (K/T in the figure) boundary clay. Note that the sedimentation rate in the boundary clay is only a factor of ~3 lower than in surrounding carbonate-rich layers. Based upon results at this and two other sections, the authors determined a duration for the K/Pg boundary clay of only 8–11 ka. By combining sedimentation rate estimates with measurements of stratigraphic height, time relative to the K/Pg boundary can be estimated in the rest of the section

chronology used to determine the mean $^{3}He_{ET}$ flux, but relative MAR changes are independent of the chronology within a given core.

$^{3}He_{ET}$ has been used as a constant flux proxy to estimate the duration of two prominent intervals of carbonate dissolution in the late Cretaceous and early Cenozoic: the K/Pg boundary clay and clays associated with the Paleocene-Eocene Thermal Maximum (PETM). Mukhopadhyay et al. (2001b) calculated the mean $^{3}He_{ET}$ flux immediately prior to the K/Pg boundary from Gubbio in the Italian Apennines and then used this flux combined with $^{3}He_{ET}$ concentration data within the boundary clay to determine sedimentation rates and the duration of the K/Pg boundary event (Fig. 8). This was the original purpose of measuring Ir in the boundary clay (Alvarez et al. 1980), but while the asteroid impact created an Ir spike at the boundary, $^{3}He_{ET}$ shows little change. This is to be expected as the large impactor should have been degassed and therefore would not have left a ^{3}He signature in the sedimentary record. Dividing the density and thickness of the clay by the $^{3}He_{ET}$-based MAR of the clay, Mukhopadhyay et al. (2001b) found durations for the boundary event of only 7.9 ± 1.0 ka and 10.9 ± 1.6 ka in two Apennine sections and 11.3 ± 2.3 ka in an expanded K/Pg section in Tunisia.

Farley and Eltgroth (2003) and Murphy et al. (2010) used a similar approach to estimate the duration of the PETM carbonate dissolution event in sediment cores from the Southern Ocean (ODP Site 690), South Atlantic (ODP Site 1266) and North Atlantic (ODP Site 1051). All three cores had age models established by astronomical calibration (in which variations in sediment composition are tuned to orbital changes) that had previously been used to estimate the durations of the onset, peak and recovery phases of the carbon isotope excursions and carbonate dissolution associated with the event. Farley and Eltgroth (2003) determined a mean $^{3}He_{ET}$ flux during two magnetic chrons spanning the PETM, while Murphy et al. (2010) determined the $^{3}He_{ET}$ flux over six eccentricity cycles preceding the event. These mean fluxes were then combined with $^{3}He_{ET}$ concentration data from PETM sediments to estimate the durations of each phase of the event. In each core, the $^{3}He_{ET}$-based age model suggests that the peak duration of the carbon isotope excursion is longer, and the recovery period shorter, compared to results from cyclostratigraphy (Fig. 9) (Röhl et al. 2000, 2007; Farley and Eltgroth 2003; Murphy et al. 2010). If the $^{3}He_{ET}$ age models are correct, the longer duration of the CIE suggests sustained release of light carbon following the initial rapid burst of light carbon into the ocean–atmosphere system (Murphy et al. 2010). Determination of whether the $^{3}He_{ET}$ or cyclostratigraphic age-model is correct is also essential for evaluation of hypothesized mechanisms for removing excess carbon from the ocean–atmosphere system during and after the PETM. Additionally, the $^{3}He_{ET}$ age-model from Site 690 (Farley and Eltgroth 2003) suggests a faster pace of the PETM event compared to Site 1266 (Murphy

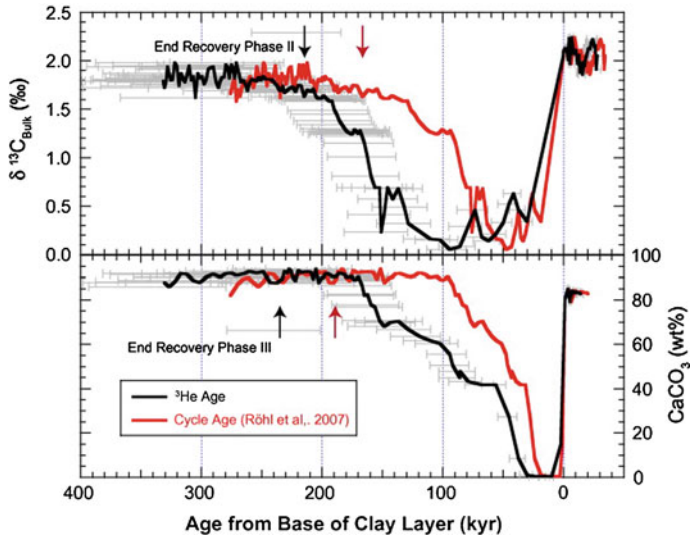

Fig. 9 Age models for the Paleocene-Eocene Thermal Maximum (PETM) based on $^{3}He_{ET}$ (*black*) and cyclostratigraphy (*red*) (Murphy et al. 2010). The panels show the $\delta^{13}C$ and calcium carbonate preservation changes associated with the PETM at ODP Site 1266. Grey error bars reflect the 2σ uncertainty in the $^{3}He_{ET}$-based age model based on the uncertainty of the $^{3}He_{ET}$ flux calibration for the interval. Note that in the $^{3}He_{ET}$-based age model, the duration of the carbon isotope excursion is significantly longer than in the cyclostratigraphic age model, the recovery from the $\delta^{13}C$ excursion is more rapid, and the return to high carbonate preservation is slower. *Arrows* indicate the relative ages of the ends of two phases of the PETM recovery estimated by the two methods, with the $^{3}He_{ET}$-based model indicating a slightly longer (~45 ka) total duration for the PETM event

et al. 2010). The reason for this discrepancy is not completely clear, but may be related to the $^{3}He_{ET}$ flux calibration from Site 690.

$^{3}He_{ET}$-based MARs have also provided the basis for a number of paleoflux studies. As $^{3}He_{ET}$-MARs can be calculated at much higher resolution than age model-based MARs, they allow novel insights into variations in past fluxes—for example, distinguishing whether an increase in the terrigenous fraction of sediments is due to increased terrigenous flux or decreased dilution by other sedimentary constituents. $^{3}He_{ET}$ data from Farley and Eltgroth's (2003) study have been used to determine accumulation rates of excess barium, a productivity proxy, in order to demonstrate that marine productivity did not play a major role in lowering atmospheric CO_2 levels after the PETM (Torfstein et al. 2010). Marcantonio et al. (2009) used $^{3}He_{ET}$ data to determine relative changes in bulk MARs and fluxes of dust and calcium carbonate during the late Eocene prior to the PETM. In addition to identifying orbitally-paced variations in carbonate preservation, this study found that orbital variations in aeolian dust deposition in this greenhouse climate were similar in magnitude to those observed in the icehouse climate of the late Pleistocene. Similarly, Winckler et al. (2005) used $^{3}He_{ET}$-based MARs to determine fluxes of productivity-related trace elements (barium, aluminum, phosphorous) and dust in the equatorial Pacific during a 1 Ma period spanning the mid-Pleistocene transition (MPT). While previous studies normalized productivity proxies to titanium and concluded that productivity increased during the MPT, $^{3}He_{ET}$-normalized fluxes of productivity proxies indicate no change in productivity across the MPT and instead indicate lower fluxes of titanium and ^{4}He from aeolian dust (Winckler et al. 2005).

Given the fact that sedimentary $^{3}He_{ET}$ appears to be predominantly contained in particles <20 μm in diameter (see Sect. 3.3), one concern in using $^{3}He_{ET}$ as a constant flux proxy is that grain size fractionation during lateral advection of sediments by ocean currents

(sediment focusing) will enrich focused sediments in $^3He_{ET}$-bearing IDPs. This fractionation would increase $^3He_{ET}$ concentrations in sites of sediment focusing while decreasing concentrations in winnowed sediments; $^3He_{ET}$-based MARs would then be biased low by sediment focusing and biased high by winnowing. Such an effect was suggested by Marcantonio et al. (2001a), who observed $^3He_{ET}/^{230}Th_{xs}$ ratios in an Indian Ocean core a factor of 1.8 lower than at other sites. To test this suggestion, McGee et al. (2010) measured He and U-Th isotopes in sediments from two cores on the Blake Ridge in the western North Atlantic. The cores are <10 km apart and should thus receive similar vertical fluxes of sediment, but one core received much greater inputs of focused sediments over the past 20 ka. Despite substantial differences in focusing, $^3He_{ET}$-based MARs agree between the two sites and are largely consistent with $^{230}Th_{xs}$-based MARs. Though the uncertainties in $^3He_{ET}$-based MARs in this study are large due to uncertainties in the correction for terrigenous ^3He, the results suggest that $^3He_{ET}$-based MARs are not substantially affected by lateral advection.

The work summarized above builds on the observation that implied $^3He_{ET}$ fluxes at a given site are largely constant over Ma timescales, allowing $^3He_{ET}$ to be used as a constant flux proxy for determining sedimentary mass accumulation rates. In studies seeking to determine variations in fluxes of sedimentary constituents, such as dust and paleoproductivity proxies, ^3He-based MARs currently provide the only means of obtaining data that are independent of age models and capable of resolving sub-orbital flux variations. (Many studies multiply point-by-point concentration data by longer-term average fluxes determined from age models and give the appearance of sub-orbital resolution, but in reality these changes in concentration could reflect either short-term changes in flux or short-term changes in dilution by other sedimentary constituents with no change in flux.) Applications of ^3He-normalization have provided novel insights into the K/Pg and PETM events and into changes in productivity and dust flux during the late Eocene and the mid-Pleistocene transition. Even so, the use of $^3He_{ET}$ as a constant flux proxy has been relatively limited compared to its potential applications.

5 Summary and Future Work

Measurement of $^3He_{ET}$ in marine sediments has provided important insights into past changes in the accretion rates of IDPs. Additionally, $^3He_{ET}$ has shown promise as a constant flux proxy capable of quantifying sub-orbital variability in past sedimentary fluxes and in constraining sedimentary age models, particularly during periods of carbonate dissolution. In looking ahead to future work, several questions offer promising avenues of research. These include:

- Can we improve our ability to distinguish $^3He_{ET}$ from terrigenous ^3He in detrital-rich, rapidly accumulating sediments such as continental margin deposits or lake sediments?
- What phases are responsible for the long-term retention of $^3He_{ET}$ in marine sediments, and is the stability of these phases affected by changing redox conditions? Is $^3He_{ET}$ retained in anoxic sediments, allowing $^3He_{ET}$-based studies of ocean anoxic events?
- What is the relative importance of asteroidal vs. cometary sources of IDPs? Why do the measured $^3He_{ET}$ fluxes not match the predicted variability in IDP accretion rate over orbital timescales?
- What is the pace of environmental change during major climatic transitions? Several major transitions—including those associated with the Eocene–Oligocene, Oligocene–Miocene, and Pliocene–Pleistocene boundaries—have not yet been studied at high resolution, and $^3He_{ET}$ is perhaps the best timekeeper available for such studies.

Acknowledgement The authors would like to thank Ken Farley for reviewing this chapter.

References

Alvarez LW, Alvarez W, Asaro F, Michel HV (1980) Extraterrestrial cause for the cretaceous-tertiary extinction: experimental results and theoretical interpretation. Science 208(4448):1095–1108

Amari S, Ozima M (1985) Search for the origin of exotic helium in deep-sea sediments. Nature 317(6037): 520–522

Amari S, Ozima M (1988) Extraterrestrial noble gases in deep-sea sediments. Geochim Cosmochim Acta 52(5):1087–1095

Andrews JN (1985) The isotopic composition of radiogenic helium and its use to study groundwater movement in confined aquifers. Chem Geol 49:339–351

Basu S, Stuart FM, Klemm V, Korschinek G, Knie K, Hein JR (2006) Helium isotopes in ferromanganese crusts from the central Pacific Ocean. Geochim Cosmochim Acta 70(15):3996–4006. doi:10.1016/j.gca.2006.05.015

Becker L, Poreda RJ, Hunt AG, Bunch TE, Rampino M (2001) Impact event at the permian-triassic boundary: Evidence from extraterrestrial noble gases in fullerenes. Science 291:1530–1533

Benkert JP, Baur H, Signer P, Wieler R (1993) He, Ne, and Ar from the solar wind and solar energetic particles in lunar ilmenites and pyroxenes. J Geophys Res 98(E7):13147–13162

Bradley JP, Sandford SA, Walker RM (1988) Interplanetary dust particles. In: Kerridge J, Mathews MS (eds) Meteorites and the Solar System. University of Arizona Press, Tucson, pp 861–895

Brook EJ, Kurz MD, Curtice J (2009) Flux and size fractionation of He-3 in interplanetary dust from Antarctic ice core samples. Earth Planet Sci Lett 286(3–4):565–569. doi:10.1016/J.Epsl.2009.07.024

Brook EJ, Kurz MD, Curtice J, Cowburn S (2000) Accretion of interplanetary dust in polar ice. Geophys Res Lett 27(19):3145–3148

Brownlee DE (1985) Cosmic dust: collection and research. Ann Rev Earth Planet Sci 13:147–173

Burns JA, Lamy PL, Soter S (1979) Radiation forces on small particles in the solar-system. Icarus 40(1):1–48

Dermott SF, Grogan K, Durda DD, Jayaraman S, Kehoe TJJ, Kortenkamp SJ, Wyatt MC (2001) Orbital evolution of interplanetary dust. In: Grün E, Gustafson BÅS, Dermott SF, Fechtig H (eds) Interplanetary dust. Springer, Berlin, pp 569–641

Du XQ, Wang YH, Ren JG, Ye XR, Lu HY (2007) Helium isotope investigation on magnetic reversal boundaries of loess-paleosol sequence at Luochuan, central Chinese Loess Plateau. Chin Sci Bull 52(17):2407–2412

Farley KA (1995) Cenozoic variations in the flux of interplanetary dust recorded by He-3 in a deep-sea sediment. Nature 376(6536):153–156

Farley KA (2000) Extraterrestrial helium in seafloor sediments: identification, characteristics, and accretion rate over geologic time. In: Peucker-Ehrenbrink B, Schmitz B (eds) Accretion of extraterrestrial matter throughout Earth's history. Kluwer, New York, pp 179–204

Farley KA, Eltgroth SF (2003) An alternative age model for the Paleocene-Eocene thermal maximum using extraterrestrial He-3. Earth Planet Sci Lett 208(3–4): 135–148. doi:10.1016/S0012-821x(03)00017-7

Farley KA, Love SG, Patterson DB (1997) Atmospheric entry heating and helium retentivity of interplanetary dust particles. Geochim Cosmochim Acta 61(11): 2309–2316

Farley KA, Montanari A, Shoemaker EM, Shoemaker CS (1998) Geochemical evidence for a comet shower in the late eocene. Science 280(5367):1250–1253

Farley KA, Mukhopadhyay S (2001) An extraterrestrial impact at the permian-triassic boundary? Science 293:2343

Farley KA, Patterson DB (1995) A 100-Kyr periodicity in the flux of extraterrestrial He-3 to the sea floor. Nature 378(6557):600–603

Farley KA, Vokrouhlicky D, Bottke WF, Nesvorný D (2006) A late miocene dust shower from the break-up of an asteroid in the main belt. Nature 439(7074): 295–297. doi:10.1038/Nature04391

Farley KA, Ward P, Garrison G, Mukhopadhyay S (2005) Absence of extraterrestrial He-3 in permian-triassic age sedimentary rocks. Earth Planet Sci Lett 240(2):265–275. doi:10.1016/J.Epsl.2005.09.054

Fireman EL, Kistner GA (1961) The nature of dust collected at high altitudes. Geochim Cosmochim Acta 24:10–22

Flynn GJ (1989) Atmospheric entry heating: a criterion to distinguish between asteroidal and cometary sources of interplanetary dust. Icarus 77(2):287–310

Fourre E (2004) A 475 kyr record of extraterrestrial 3He and 230Th in North Atlantic sediments: caveats to derive MAR from these tracers. Eos Trans AGU 85(47):Fall Meet Suppl, Abstract PP33A–0910

Francois R, Frank M, van der Loeff MMR, Bacon MP (2004) Th-230 normalization: an essential tool for interpreting sedimentary fluxes during the late quaternary. Paleoceanography 19(1):PA1018. Doi: 10.1029/2003PA000994

Fraundorf P, Brownlee DE, Walker RM (1982) Laboratory studies of interplanetary dust. In: Wilkening LL (ed) Comets. University of Arizona Press, Tucson, pp 383–409

Fredriksson K (1956) Cosmic Spherules in Deep-Sea Sediments. Nature 177(4497):32–33

Fredriksson K, Gowdy R (1963) Meteoric debris from the southern California desert. Geochim Cosmochim Acta 27:241–243

Fredriksson K, Martin LR (1963) The origin of black spherules found in Pacific islands, deep-sea sediments, and Antarctic ice. Geochim Cosmochim Acta 27:245–248

Fukumoto H, Nagao K, Matsuda J (1986) Noble gas studies on the host phase of high $^{3}He/^{4}He$ ratios in deep-sea sediments. Geochim Cosmochim Acta 50:2245–2253

Futagami T, Ozima M, Nakamura Y (1990) Helium ion implantation into minerals. Earth Planet Sci Lett 101(1):63–67

Gladman BJ, Migliorini F, Morbidelli A, Zappala V, Michel P, Cellino A, Froeschle C, Levison HF, Bailey M, Duncan M (1997) Dynamical lifetimes of objects injected into asteroid belt resonances. Science 277(5323):197–201

Grimberg A, Baur H, Bochsler P, Bühler F, Burnett DS, Hays CC, Heber VS, Jurewicz AJG, Wieler R (2006) Solar wind neon from Genesis: implications for the lunar noble gas record. Science 314:1133–1135. doi: 10.1126/science.1133568

Higgins SM, Anderson RF, Marcantonio F, Schlosser P, Stute M (2002) Sediment focusing creates 100-ka cycles in interplanetary dust accumulation on the Ontong Java Plateau. Earth Planet Sci Lett 203(1):383–397

Hiyagon H (1994) Retention of solar helium and neon in IDPs in deep-sea sediments. Science 263:1257–1259

Hut P, Alvarez W, Elder WP, Hansen T, Kauffman EG, Keller G, Shoemaker EM, Weissman PR (1987) Comet showers as a cause of mass extinctions. Nature 329(6135):118–126

Kortenkamp SJ, Dermott SF (1998a) A 100,000-year periodicity in the accretion rate of interplanetary dust. Science 280(5365):874–876

Kortenkamp SJ, Dermott SF (1998b) Accretion of interplanetary dust particles by the Earth. Icarus 135(2):469–495

Kurz MD, Kenna TC, Lassiter JC, Depaola DJ (1996) Helium isotopic evolution of Mauna Kea: first results from the 1 km drill core. J Geophys Res 101:11781–11791

Kyte FT, Leinen M, Heath GR, Zhou L (1993) Cenozoic sedimentation history of the central North Pacific: Inferences from the elemental geochemistry of core LL44-GPC3. Geochim Cosmochim Acta 57(8): 1719–1740

Laevastu T, Mellis O (1955) Extraterrestrial material in deep-sea deposits. Trans Am Geophys Union 36(3):385–389

Lal D, Jull AJT (2005) On the fluxes and fates of He-3 accreted by the Earth with extraterrestrial particles. Earth Planet Sci Lett 235(1–2):375–390. doi: 10.1016/J.Espl.2005.04.011

Love SG, Brownlee DE (1991) Heating and thermal transformation of micrometeroids entering the Earth's atmosphere. Icarus 89(1):26–43

Love SG, Brownlee DE (1993) A direct measurement of the terrestrial mass accretion rate of cosmic dust. Science 262(5133):550–553

Love SG, Joswiak DJ, Brownlee DE (1994) Densities of stratospheric micrometeorites. Icarus 111(1):227–236

Mamyrin BA, Tolstikhin IN (1984) Helium isotopes in nature. Elsevier, Amsterdam

Marcantonio F, Anderson RF, Higgins S, Fleisher MQ, Stute M, Schlosser P (2001a) Abrupt intensification of the SW Indian Ocean monsoon during the last deglaciation: constraints from Th, Pa, and He isotopes. Earth Planet Sci Lett 184(2):505–514

Marcantonio F, Anderson RF, Higgins S, Stute M, Schlosser P, Kubik P (2001b) Sediment focusing in the central equatorial Pacific Ocean. Paleoceanography 16(3):260–267

Marcantonio F, Anderson RF, Stute M, Kumar N, Schlosser P, Mix A (1996) Extraterrestrial He-3 as a tracer of marine sediment transport and accumulation. Nature 383(6602):705–707

Marcantonio F, Higgins S, Anderson RF, Stute M, Schlosser P, Rasbury ET (1998) Terrigenous helium in deep-sea sediments. Geochim Cosmochim Acta 62(9):1535–1543

Marcantonio F, Kumar N, Stute M, Andersen RF, Seidl MA, Schlosser P, Mix A (1995) Comparative study of accumulation rates derived by He and Th isotope analysis of marine sediments. Earth Planet Sci Lett 133(3–4):549–555

Marcantonio F, Thomas DJ, Woodard S, McGee D, Winckler G (2009) Extraterrestrial He-3 in Paleocene sediments from Shatsky Rise: Constraints on sedimentation rate variability. Earth Planet Sci Lett 287(1–2):24–30. doi:10.1016/J.Epsl.2009.07.029

Marcantonio F, Turekian KK, Higgins S, Anderson RF, Stute M, Schlosser P (1999) The accretion rate of extraterrestrial He-3 based on oceanic Th-230 flux and the relation to Os isotope variation over the past 200,000 years in an Indian Ocean core. Earth Planet Sci Lett 170(3):157–168

Matsuda J, Murota M, Nagao K (1990) He and Ne isotopic studies on the extraterrestrial material in deep-sea sediments. J Geophys Res 95(B5):7111–7117

McGee D, Marcantonio F, McManus JF, Winckler G (2010) The response of excess Th-230 and extraterrestrial He-3 to sediment redistribution at the Blake Ridge, western North Atlantic. Earth Planet Sci Lett 299(1–2):138–149. doi:10.1016/J.Epsl.2010.08.029

McGee D (2010) Reconstructing and interpreting the dust record and probing the plumbing of Mono Lake. Dissertation, Columbia University

Merrihue C (1964) Rare gas evidence for cosmic dust in modern pacific red clay. Ann Ny Acad Sci 119(A1): 351–367

Mukhopadhyay S, Farley KA (2006) New insights into the carrier phase(s) of extraterrestrial 3He in geologically old sediments. Geochim Cosmochim Acta 70(19):5061–5073

Mukhopadhyay S, Farley KA, Montanari A (2001a) A 35 Myr record of helium in pelagic limestones from Italy: Implications for interplanetary dust accretion from the early Maastrichtian to the middle Eocene. Geochim Cosmochim Acta 65(4):653–669

Mukhopadhyay S, Farley KA, Montanari A (2001b) A short duration of the cretaceous-tertiary boundary event: evidence from extraterrestrial helium-3. Science 291(5510):1952–1955

Muller RA, Macdonald GJ (1995) Glacial cycles and orbital inclination. Nature 377(6545):107–108

Murphy BH, Farley KA, Zachos JC (2010) An extraterrestrial He-3-based timescale for the Paleocene-Eocene thermal maximum (PETM) from Walvis Ridge, IODP Site 1266. Geochim Cosmochim Acta 74(17):5098–5108. doi:10.1016/J.Gca.2010.03.039

Murray J (1876) On the distribution of volcanic debris over the floor of the ocean—its character, source and

some of the products of its disintegration and decomposition. Proc R Soc Edinb 9:247–261

Nesvorný D, Bottke WF, Levison HF, Dones L (2003) Recent origin of the solar system dust bands. Astrophys J 591(1):486–497

Nesvorný D, Jenniskens P, Levison HF, Bottke WF, Vokrouhlicky D, Gounelle M (2010) Cometary origin of the zodiacal cloud and carbonaceous micrometeorites. Implications for hot debris disks. Astrophys J 713(2):816–836. doi:10.1088/0004-637x/713/2/816

Nesvorný D, Vokrouhlicky D, Bottke WF, Sykes M (2006) Physical properties of asteroid dust bands and their sources. Icarus 181(1):107–144. doi:10.1016/J.Icarus.2005.10.022

Nier AO, Schlutter DJ (1990) Helium and neon in stratospheric particles. Meteoritics 25:263–267

Nier AO, Schlutter DJ (1992) Extraction of helium from individual interplanetary dust particles by step-heating. Meteoritics 27(2):166–173

Nier AO, Schlutter DJ (1993) The thermal history of interplanetary dust particles collected in the Earth's stratosphere. Meteoritics 28(5):675–681

Nier AO, Schlutter DJ, Brownlee DE (1990) Helium and neon isotopes in deep Pacific Ocean sediments. Geochim Cosmochim Acta 54(1):173–182

Patterson DB, Farley KA (1998) Extraterrestrial ^{3}He in seafloor sediments: Evidence for correlated 100 kyr periodicity in the accretion rate of interplanetary dust, orbital parameters, and Quaternary climate. Geochim Cosmochim Acta 62(23/24):3669–3682

Patterson DB, Farley KA, Schmitz B (1998) Preservation of extraterrestrial He-3 in 480-Ma-old marine limestones. Earth Planet Sci Lett 163(1–4):315–325

Pepin RO, Palma RL, Schlutter DJ (2000) Noble gases in interplanetary dust particles, I: the excess helium-3 problem and estimates of the relative fluxes of solar wind and solar energetic particles in interplanetary space. Meteorit Planet Sci 35(3):495–504

Pepin RO, Palma RL, Schlutter DJ (2001) Noble gases in interplanetary dust particles, II: excess helium-3 in cluster particles and modeling constraints on interplanetary dust particle exposures to cosmic-ray irradiation. Meteorit Planet Sci 36(11):1515–1534

Röhl U, Bralower TJ, Norris RD, Wefer G (2000) New chronology for the late paleocene thermal maximum and its environmental implications. Geology 28(10): 927–930

Röhl U, Westerhold T, Bralower TJ, Zachos JC (2007) On the duration of the paleocene-eocene thermal maximum (PETM). Geochem Geophy Geosy 8:Q12002. doi:10.1029/2007GC001784

Stuart FM, Harrop PJ, Knott S, Turner G (1999) Laser extraction of helium isotopes from antarctic micrometeorites: source of He and implications for the flux of extraterrestrial He-3 to earth. Geochim Cosmochim Acta 63(17):2653–2665

Takanayagi M, Ozima M (1987) Temporal variation of ^{3}He/^{4}He ratio recorded in deep-sea sediment cores. J Geophys Res 92(B12):12531–12538

Tagle R, Claeys P (2004) Comet or asteroid shower in the late Eocene? Science 305(5683):492

Thiel E, Schmidt RA (1961) Spherules from the antarctic ice cap. J Geophys Res 66(1):307–310

Tilles D (1962) Primordial gas in the Washington county meteorite. J Geophys Res 67(4):1687–1689

Tolstikhin I, Lehmann BE, Loosli HH, Gautschi A (1996) Helium and argon isotopes in rocks, minerals, and related groundwaters: a case study in northern Switzerland. Geochim Cosmochim Acta 60(9):1497–1514

Tolstikhin IN, Drubetskoy ER (1975) The ^{3}He/^{4}He and $(^{4}He/^{40}Ar)_{rad}$ isotope ratios for earth's crust. Geochem Int 12:133–145

Torfstein A, Winckler G, Tripati A (2010) Productivity feedback did not terminate the paleocene-eocene thermal maximum (PETM). Clim Past 6(2): 265–272

Wieler R, Grimberg A, Heber VS (2007) Consequences of the non-existence of the "SEP" component for noble gas geo- and cosmochemistry. Chem Geol 244:382–390

Winckler G, Anderson RF, Schlosser P (2005) Equatorial Pacific productivity and dust flux during the mid-Pleistocene climate transition. Paleoceanography 20(4): PA4025. doi:10.1029/2005pa001177

Winckler G, Anderson RF, Stute M, Schlosser P (2004) Does interplanetary dust control 100 kyr glacial cycles? Quatern Sci Rev 23(18–19):1873–1878. doi: 10.1016/J.Quascirev.2004.05.007

Winckler G, Fischer H (2006) 30,000 years of cosmic dust in antarctic ice. Science 313(5786):491. doi: 10.1126/Science.1127469

Zähringer J (1962) Ueber die Uredelgase in den Achondriten Kapoeta und Staroe Pesjanoe. Geochimica et Cosmochimica Acta 26(6):665-680. doi: 10.1016/0016-7037(62)90045-5

Application of Noble Gases to the Viability of CO_2 Storage

Greg Holland and Stuart Gilfillan

Abstract

Unequivocable evidence for warming of the climate system is a reality. An important factor for reducing this warming is mitigation of anthropogenic CO_2 in the atmosphere. This requires us to engineer technologies for capture of our carbon emissions and identify reservoirs for storing these captured emissions. This chapter reviews advances made in understanding multiphase interactions and processes operating in a variety of subsurface reservoirs using noble gases. We begin by discussing the types of reservoir available for carbon storage and the mechanisms of viable CO_2 storage, before summarising the physical chemistry involved in data interpretation and the sampling/sample storage techniques and requirements critical to successful sample collection. Theory of noble gas partitioning is interspersed with examples from a variety reservoirs to aid our knowledge of long term CO_2 storage in the subsurface. These include hydrocarbon reservoir and natural CO_2 reservoirs. In these examples we show how good progress has been made in using noble gases to explain the fate of CO_2 in the subsurface, to quantify the extent of groundwater interaction and to understand CO_2 behaviour after injection into oil fields for enhanced oil recovery. We also present recent work using noble gases for monitoring of subsurface CO_2 migration and leakage in CO_2 rich soils, CO_2 rich springs and groundwaters. Noble gases are chemically inert, persistent and environmentally safe and they have the potential to be extremely useful in tracing migration of CO_2. It is imperative that the many upcoming pilot CO_2 injection studies continue to investigate the behaviour of noble gases in the subsurface and develop suitable noble gas monitoring strategies.

G. Holland (✉)
Lancaster Environment Centre, Lancaster University, Lancaster, LA1 4YQ, UK
e-mail: g.holland@lancaster.ac.uk

S. Gilfillan
School of Geosciences, University of Edinburgh, Edinburgh, EH9 3JW, UK
e-mail: stuart.gilfillan@ed.ac.uk

P. Burnard (ed.), *The Noble Gases as Geochemical Tracers*, Advances in Isotope Geochemistry,
DOI: 10.1007/978-3-642-28836-4_8,

1 Introduction

1.1 The Need for CO_2 Storage

Climate change and its effects are emerging as one of the most pressing environmental issues of the 21st century. It is generally accepted that increases in anthropogenic carbon dioxide (CO_2) emissions since the industrial revolution are a key factor in the climate warming observed to date (IPCC 2007). The period between 1995 and 2006 recorded eleven of the twelve warmest years in the instrumental record of global surface temperature, since 1850. The most recent assessment by the Intergovernmental Panel for Climate Change (IPCC) indicated that the global surface temperature has increased by 0.74 ± 0.18 °C between 1906 and 2005 (Fig. 1) (IPCC 2007). The IPCC report clearly stated "Warming of the climate system is unequivocal, as is now evident from observations of increases in global average air and ocean temperatures".

This warming of the Earth's climate has also resulted in a rise of sea levels due to melting of continental ice sheets and thermal expansion of the oceans. The 2007 IPCC report documented that global sea levels rose by 2.7 ± 0.7 mm between 1993 and 2003. The report also predicted a rise of 18–59 cm from 1990 to the 2090s, in addition to an unspecified amount that could come from partial melting of the large ice sheets covering Greenland and Antarctica. More recent studies have shown that this is probably a conservative estimate and rises of up to 1 m are not implausible (Rahmstorf 2010).

It is clear that reduction of CO_2 concentration in the atmosphere is paramount to limiting climate change in the near future and ameliorating the climate in the longer term. IPCC projections suggest a global surface temperature rise of a further 1.1–6.4 °C during the 21st century, as CO_2 concentrations rise from ~370 to ~700 ppm. This rise is largely due to global emissions of CO_2 from burning of fossil fuels at a rate of approximately 25 Gigatonnes of CO_2 equivalent per year (Marland et al. 2008). To reduce this value over the coming decades will require a combined approach of lower emissions from more fuel-efficient/alternative fuel technologies and removal of the on-going CO_2 emissions that produced as a by-product of power generation (Fig. 2).

1.2 What is Geological Carbon Storage?

Geological carbon storage is the final aspect of the Carbon Capture and Storage (CCS) process. The CCS process involves capturing CO_2 from large point source emitters such as power stations, refineries or other industrial processes,

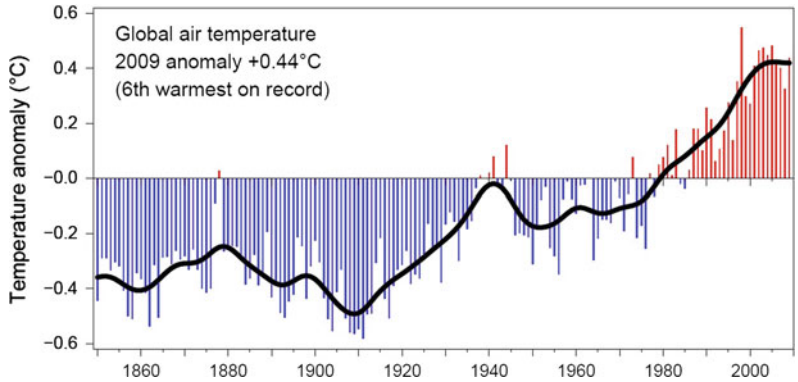

Fig. 1 This time series is compiled jointly by the Climatic Research Unit and the UK Met. Office Hadley Centre showing mean global air temperature over the last ~150 years. The record is being continually up-dated and improved (Brohan et al. 2006)

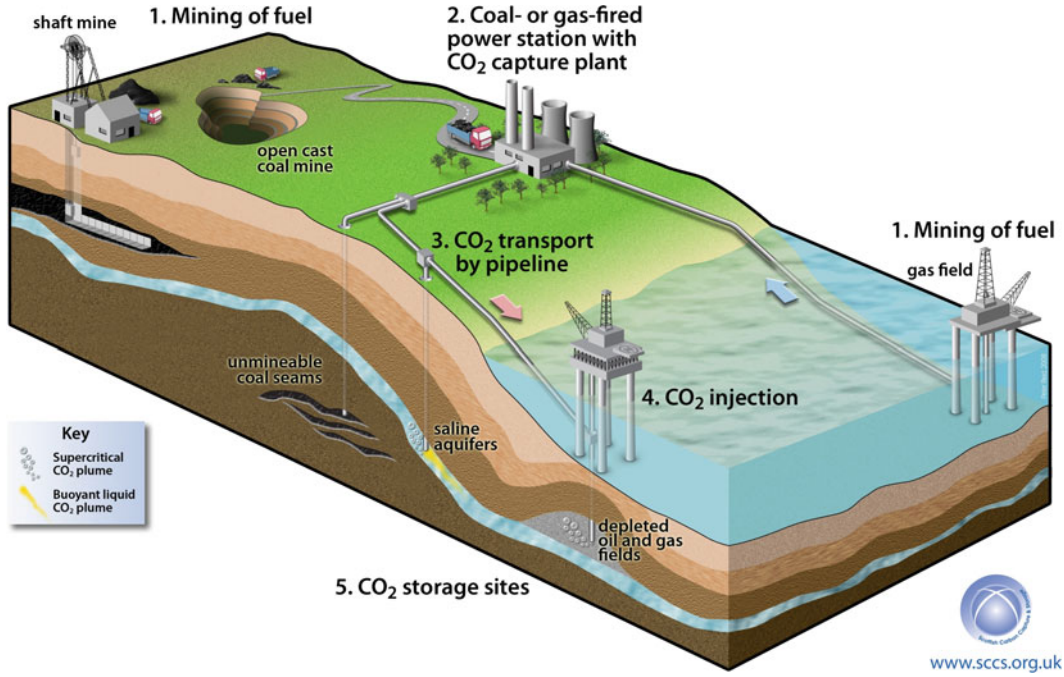

Fig. 2 Diagram illustrating the life cycle chain of fossil fuel use with carbon capture and storage technology. CO_2 capture at the point source of emission allows the CO_2 to be transported to a suitable storage reservoir. Three different subsurface storage sites are being considered and tested; (1) Empty (depleted) oil and gas reservoirs, (2) Saline aquifers and (3) Unminable coal seams. Figure credit to Scottish Carbon Capture and Storage, School of Geosciences, University of Edinburgh

compressing it to produce a supercritical fluid, then transporting, and then injecting it into geological formations that can act as natural underground storage sites. CO_2 becomes a supercritical fluid above the critical temperature of 31.1 °C and critical pressure of 7.39 MPa. Supercritical CO_2 has the properties of both a gas and a liquid, in that it expands to fill its container as a gas would whilst retaining the density of a liquid, making it easier to transport and inject than in gaseous form. The CO_2 injected into the geological carbon storage site must then remain isolated from the atmosphere for a significant period of time (1,000 to 10,000 years). In its simplest form, a geological carbon storage site will consist of a layer of permeable and porous reservoir rock situated beneath a layer of impermeable rock that will act as a seal preventing CO_2 migration to the surface.

There are three main types of proposed underground storage sites:

1.2.1 Depleted Oil and Gas Reservoirs

Oil and gas reservoirs consist of permeable and porous reservoir rocks overlain by impermeable cap rocks that have stored hydrocarbon liquids and gases over many millions of years. Those that have reached the end of their productive life are ideal for CO_2 storage. CO_2 can be pumped into the reservoirs, using the boreholes originally drilled to extract the oil and gas, to fill the empty pore space left by removal of hydrocarbons. The geology of these reservoirs is often well characterized to maximise oil recovery therefore fluid behaviour in these systems is well understood.

However, those reservoirs which have been subjected to the injection of water or gas to increase reservoir pressure and aid oil recovery may require extra production of the hydrocarbons in order to make space for the CO_2 (Haszeldine 2009). This technique is known as enhanced oil recovery (EOR) and can produce 10–15 % more oil. EOR is a mature technology

that has been operating since the early 1970s . In addition, the natural gas industry has been reliant on underground natural gas reservoirs for many decades and enhanced gas recovery (EGR) is also a viable technique. These reservoirs could also be adapted for CO_2 injection and long-term storage. Depleted oil and gas reservoirs are expected to provide potential for storing 920 Gt CO_2 (IEA 2009)—45 % of the total CO_2 output from 2000 to 2050 assuming the IEA's business as usual scenario for CO_2 emissions (i.e. no significant reduction in emissions).

1.2.2 Deep Saline Formations

Saline formations, also known as saline aquifers, are rock formations saturated with salt water that are unsuitable for supplying potable water. These exist worldwide, not just in hydrocarbon provinces and potentially could store large volumes of CO_2. CO_2 injected into these saline formations would partially dissolve into the saline water, storing the CO_2. Additionally, in some cases carbonate minerals could precipitate, locking up the CO_2 permanently. Recent estimates suggest the capacity for storage in geological reservoirs in North West Europe alone could be as much as 800 Gt CO_2 (with most of this in deep saline reservoirs), with other estimates suggesting that up to 10, 000 Gt CO_2 could be stored globally (IEA 2009). However, these estimates are probably somewhat optimistic as they assume static injection efficiency of 5–10 %, when dynamic injection of CO_2 at the Utsira aquifer in the North Sea currently fills only 0.2 % of the pore space. Further study and the injection of CO_2 into other aquifers is required to fully determine the storage capacity and long term storage viability of saline aquifers.

1.2.3 Deep (Un-Minable) Coal Seams

Injection of CO_2 into deep un-mineable coal seams is also a possibility, where the CO_2 will be stored on the surface pores and fractures of the coal. This has the additional benefit of forcing the methane, which is already present within the coal beds, from the coal and so increasing recovery of the coal bed methane. This could offset the cost of CO_2 injection and even if the additional methane extracted is not of economic use, coal can adsorb twice as much CO_2 by volume as methane. Hence, conventional coal bed methane extraction and subsequent CO_2 injection will still result in net storage of CO_2.

1.2.4 Additional CO_2 Storage Options

There are several alternative options for CO_2 storage which include biological sequestration (Marland and Schlamadinger 1999), deep ocean sequestration (Brewer et al. 1999) and CO_2 injection into deep ocean carbonate sediments (House et al. 2006) or basalts (Goldberg et al. 2008) to form carbonate minerals. However, all of these are, with the exception of ocean sequestration, in their infancy and do not offer the necessary volume or security of storage required for large scale CO_2 storage at present (Baines and Worden 2004a).

Injection of large amounts of CO_2 into the marine environment may acidify large amounts of sea water (Haszeldine 2009) and ocean storage is not a permanent method of CO_2 storage. There is a potential risk that CO_2 will over time return to atmosphere, as there is not a distinct physical barrier to prevent the CO_2 from doing so. For these reasons this method of storage has been deemed unsuitable at the current time and is currently outlawed by international marine treaties.

In this chapter we focus on the depleted oil and gas reservoirs as this is the CO_2 storage setting that has received most attention from the scientific community to date and provides important lessons directly relevant to storage in other settings.

1.3 Mechanisms of Viable CO_2 Storage

The key requirement for successful geological CO_2 storage within the Earth is the safety and security of CO_2 retention over significant timescales. It is essential that protocols for monitoring and risk assessing CO_2 storage sites and potential leakage pathways are developed. The

existence of CO_2 reservoirs that have been isolated from the atmosphere for millions of years (Ballentine et al. 2001; Gilfillan et al. 2008) demonstrates the feasibility of storing CO_2 for significant periods of time but understanding the exact behaviour of CO_2 in these systems is of paramount importance. Secure CO_2 storage can be achieved by ensuring that the stored CO_2 is immobile and trapped by one of the four mechanisms outlined below.

1.3.1 Physical Trapping: Stratigraphic and Structural Storage

Supercritical CO_2 has a lower density than water, so when CO_2 is injected into a reservoir it will ascend through the microscopic pore spaces between the grains in the reservoir rock to the top of the reservoir. Therefore, it is essential that a suitable impermeable cap rock such as a shale, clay or mudstone overlies the reservoir to act as a physical barrier to the CO_2 and prevent migration of the CO_2 from the reservoir. Cap rocks of oil and gas fields have trapped buoyant hydrocarbon fluids in this manner for millions of years.

1.3.2 Residual or Hydrodynamic Storage

Microscopic pore spaces which exist between grains in the reservoir rock are analogous to a foam sponge. CO_2 can enter 'dead end' pores in a similar fashion to how air is trapped within a foam sponge. This is known as residual trapping and is the reason why soaking a sponge in water cannot be achieved by submersing it: the sponge requires squeezing to expel the residually trapped air and replace it with water.

1.3.3 Dissolution Storage or Solubility Trapping

As CO_2 is readily soluble in water, it will dissolve in the formation water trapped in the pore spaces within a reservoir. The water containing dissolved CO_2 is denser than the formation water surrounding it. This dense water sinks to the bottom of the reservoir, trapping the CO_2. Provided that the formation water does not migrate from the reservoir this is a secure trapping mechanism.

1.3.4 Mineral Storage or Mineral Trapping

CO_2 dissolves in water to form a weak acid (carbonic acid) and this acid can dissolve and react with the mineral grains present in the reservoir rock. The reaction of the bicarbonate ions produced when the CO_2 dissolves into the formation water with calcium, magnesium and iron from silicate minerals such as micas, clays, feldspars and chlorites will form carbonate minerals. These will be produced in the interior of pores in the reservoir rock and have the potential to 'lock away' the CO_2 within the rock. This is the most permanent trapping mechanism. However, under normal reservoir conditions this process is very slow, typically taking thousands of years (IPCC 2005).

2 Sample Collection and Analytical Techniques

Within the Colorado Plateau and surrounding Rocky Mountain region there are at least nine producing or abandoned gas fields that contain up to 2,800 billion m^3 of natural CO_2 (Allis et al. 2001). These fields act as a natural analogues of CO_2 repository sites and hence intensive studies have been undertaken to provide an understanding of CO_2 behaviour within them. Data included in this chapter are predominantly from five producing gas fields, namely McCallum Dome, (Jackson Co, CO); Sheep Mountain, (Huerfano County, CO); Bravo Dome, (Harding County, NM); McElmo Dome and the related field Doe Canyon, (Montezuma County, CO); St Johns Dome (Apache County, AZ) and eight natural CO_2 seeps at Green River, (Emery and Grand Counties, UT). All of these sites produce CO_2 in extremely high concentrations, averaging 95–99 % CO_2, 1–4 % N_2, 0.1–1 % He and other trace gases (Allis et al. 2001). The majority of these samples were taken directly from producing wellheads that tap the natural gas reservoirs, although samples from several 'shut in' wellheads with high gas pressures were also collected. Well sample sites were chosen on site to

provide a wide range of depths and spatial distribution across the individual reservoirs. Two field-sampling techniques were used to collect these samples.

2.1 Well Head Collection Methods

The first method utilized 'Swagelok©' 300 ml stainless steel sampling cylinders sealed at both ends with high-pressure valves. The cylinders were baked at 150 °C and evacuated prior to sampling use. The cylinders were attached directly to the wellheads before the gas had undergone any form of processing. A length of high pressure hosing was attached to the other end of the cylinder to act as an exhaust. The cylinders were then flushed with gas from the wellhead for 5 min and then purged 6 times. The purging process involves filling the cylinder with well gas, closing the valve to the wellhead, and then releasing the gas. This ensured that there is virtually no air contamination present in the sample. This method was used for wellheads that have high flow rates and typical wellhead pressures ranged from 1.38 to 3.45 MPa.

2.2 Water and Low Pressure Gas Collection Methods

The second collection technique used a 70 cm long piece of 3/8″ diameter refrigeration grade copper tubing as the sample container. This method was used for sampling of low-pressure wellheads with lower flow rates and the Green River seeps. The copper tubing is contained in an aluminium holder with clamping devices at each end and provides approximately 10 cm^3 of gas for analysis (Fig. 3). In the field, high pressure hosing was secured to one end of the copper tubing, which was connected to a gas regulator attached directly to the wellhead by a suitable adapter. The remaining end of the tubing was connected to another section of tubing with a second length of high pressure hosing so a duplicate sample could be obtained. A third length of high pressure hosing was attached to the second length of copper tubing to act as an exhaust and prevent turbulent backflow of atmospheric gases into the sample. Gas from the wellhead was then pumped into both sections of tubing at a regulated pressure of 0.20 MPa (2 atm). The entire line was flushed with gas from the wellhead for 10 min. After flushing, the clamp furthest from the wellhead was closed sealing the end of the copper tube by cold welding. The other clamps were then shut in turn working back up the line to the wellhead. These clamps are then left closed until the samples are ready for analysis. Secure sample storage is achieved as copper is virtually impervious to noble gases (Hilton et al. 2002). Sample analysis was carried out by connecting one end of the copper tube to the mass spectrometer and releasing one of the clamps.

The Green River seeps (Sect. 7.1) were collected using a similar copper tube procedure. All of the seeps were actively releasing CO_2 within pools of water. To sample this gas a plastic funnel connected to a length of high pressure hosing was positioned over the bubbling gas, and submerged into the water. The water provides a seal from the atmosphere, preventing air contamination of the samples. The high pressure hose was directly connected to two copper tubes, allowing duplicate samples to be collected. Gas was allowed to flow freely into the copper tubes for a minimum of 10 min. The clamps were then shut sequentially working back from the clamp furthest from the seep. The water samples collected at St. Johns Dome (Sect. 7.3) and on the Kerr property (Sect. 7.4) were collected in the same manner using copper tubes after flowing water through the tubes for 5 min. The samples were either taken directly from producing well heads or from depth in groundwater pools or wells using a peristaltic pump and a weighed piece of hosing.

2.3 Issues of Long Term Sample Storage

Collection using the high pressure cylinder technique has been the convention in both the commercial and academic sectors. However, re-analysis of a suite of well gas samples after several years of lab storage has highlighted a serious issue, specifically that the double valved

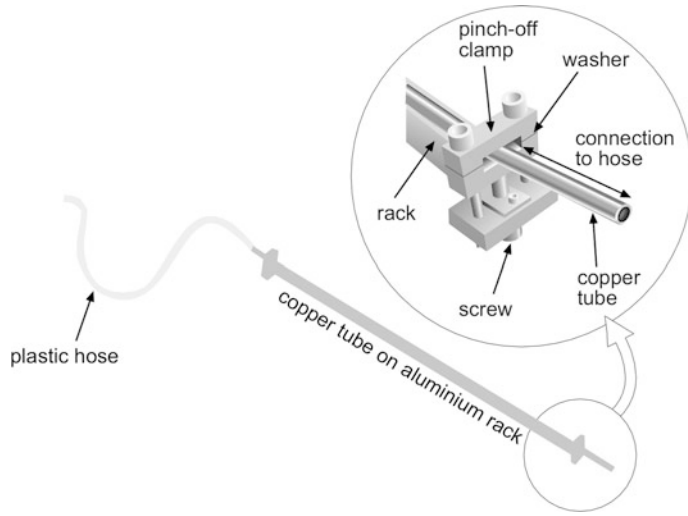

Fig. 3 Schematic of the apparatus used for noble gas sampling with copper tubing [from Becker (2005)]. The plastic hose is attached directly to the well head using a suitable regulator, CO_2 gas is allowed to flow through the copper tube until sample collection is complete. The tubing is then crimped at both ends

Swagelok cylinder approach is prone to air contamination. Over a period of two years, between summer 2005 and summer 2007, samples with $^{40}Ar/^{36}Ar$ ratio of ~22, 000 had been reduced by ingress of air to a $^{40}Ar/^{36}Ar$ ratio ~3,000. The mechanism by which this air contamination had occurred was not specifically identified, but because the partial pressure of noble gases in the atmosphere is significantly higher than in the well gases, any pathway for noble gas transfer will result in an influx of atmospheric noble gases to the cylinders. The high pressure valves were attached to the cylinders via steel screw threads wrapped in PTFE tape and the valve tips were also Teflon based. In a noble gas world where all metal systems are the norm, including linkages and valve tips, it is likely that one or both of these potential weak points are the source of the contamination. Samples are still collected in high pressure cylinders as required by health and safety issues at point of collection and due to commercial shipping regulations but in an attempt to alleviate this problem, the gases are rapidly transferred to an all metal storage device (currently metal spheres with a welded Conflat fitting and a standard copper tipped valve).

2.4 Analytical Techniques Specific to CO_2 Samples

At the University of Manchester, where some of the work reported in this chapter was undertaken, a specific vacuum line was constructed to handle the clean-up requirements of large volumes of well gas. This consisted of a calibrated volume containing a high pressure Baratron® capacitance manometer, a Ti sponge furnace, a Zr-Al SAES getter, cold finger, a quadrupole mass spectrometer and both an ion and turbo pump. The quadrupole was essential for ensuring that the samples had been cleaned up thoroughly prior to admission into the mass spectrometer clean-up/gas extraction line. The separate pumping system also ensured that no hydrocarbon or CO_2 was able to enter the main clean up line.

Well gas samples were extracted from either the copper sample tubes or from stainless steel cylinders into the volume containing a high

pressure Baratron® capacitance manometer. The pressure was recorded, allowing calculation of the volume of CO_2 administered. The sample was then expanded onto a Ti sponge furnace to remove CO_2 and any other active gases. This furnace was preheated to 1,173 K (900 °C) with each sample held at this temperature for 10 min, and then cooled to room temperature over a period of 15 min. Approximately 10 g of Ti sponge material was capable of removing 1 L of CO_2, permitting multiple analyses of the same sample and high precision analyses of the rarer noble gas isotopes of Kr and Xe. These volumes of CO_2 would quickly saturate a Zr-Al SAES getter typically found on noble gas extraction lines and is a necessary step in preparation of CO_2 well gas samples for analysis. Subsequently, the sample was exposed for 10 min with a Zr-Al SAES getter heated to 523 K.

3 Noble gases in Geological Reservoirs

3.1 Introduction

Noble gases are chemically inert elements that exist as extremely volatile gases at standard temperature and pressure. Their lack of reactivity results in no change in their isotopic compositions via chemical processes but allows them to be used as a tracer of physical processes, which can alter both their isotopic and relative elemental compositions. In the context of storage in geological reservoirs, their relative abundances are sensitive to partitioning between different fluid phases such as oil, water and gas, enabling their use as tracers of physical processes even if they have subsequently been partitioned from their host fluids. The three key sources of noble gases in natural gas reservoir fluids are the crust, the atmosphere and the mantle. Each of these possesses different isotopic compositions permitting resolution of the different sources (see Fig. 4).

3.2 Sources of Noble Gases in a Subsurface Reservoir

Noble gases on the Earth are derived from two principle sources: those trapped during the planetary accretion process which are commonly known as ‘primitive’, ‘juvenile’ or ‘primordial’ noble gases (e.g. ^{3}He) and radiogenic noble gases generated by radioactive decay processes within the Earth (e.g. ^{4}He). The radiogenic noble gases are primarily produced by radioactive decay and nucleogenic reactions (Table 1). Minor amounts are also produced by cosmic ray spallation, although this is not relevant to study of CO_2 storage and is not discussed further. The following summary documents these main production mechanisms and focuses on the reactions that are directly relevant to the use of noble gases as tracers in natural gas and CO_2 reservoirs.

3.3 Noble Gas Production

3.3.1 Radiogenic Helium: ^{4}He

^{4}He is produced by any α—decay radioactive pathway which emits α particles. The three most significant radioactive parent isotopes are ^{238}U, ^{235}U and ^{232}Th. Both U and Th are incompatible elements which are concentrated in the continental crust. The majority of crustal rocks contain U and Th in an almost constant weight ratio of 3.3, meaning that ^{4}He production from all three nuclides can be referenced to the abundance of U alone. The ^{4}He production rate expressed in this way is 2.15×10^{-7} cm^3 per gram of U per year (Ozima and Podosek 2001).

3.3.2 Radiogenic Argon: ^{40}Ar

Radiogenic decay of another incompatible element, ^{40}K, results in the production of ^{40}Ar. ^{40}K is strongly partitioned into the crust and therefore ^{40}Ar production is highly significant despite the low isotopic abundance (0.00012) of ^{40}K and only 11 % decaying to ^{40}Ar by electron capture (with the remainder decaying by β decay to ^{40}Ca). Over geologic time the average ^{40}Ar production rate is 3.89×10^{-12} cm^3 per gram of

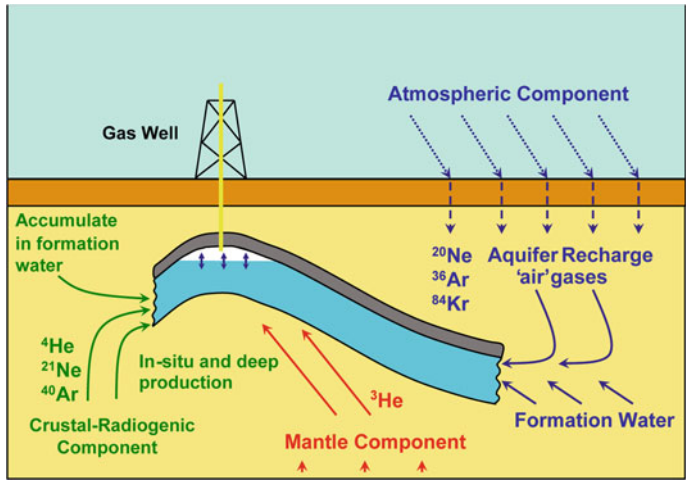

Fig. 4 Schematic diagram of a natural gas reservoir, highlighting the three distinct components and their corresponding isotopes which may occur in a natural gas reservoir. The radiogenic noble gases (e.g. ^{4}He, ^{21}Ne and ^{40}Ar) are produced within the Earth's crust by the radioactive decay of U, Th and K. Atmospheric noble gases (e.g. ^{20}Ne and ^{36}Ar) are input into the gas phase as a result of equilibration with the groundwater at recharge. Within areas of continental extension or magmatic activity mantle derived noble gases (e.g. ^{3}He) may also be present. The distinct elemental and isotopic composition of the noble gases from these three components permits the contribution from each to be quantitatively resolved from any crustal fluid (redrawn from Ballentine et al. 2002)

Table 1 Radiogenic nuclides and their half-lives for noble gases, from Porcelli et al. (2002) and references therein

Nuclide	Half-life	Daughter	Yield	Comments
^{3}H	12.26 a	^{3}He	1	Continuously produced in atmosphere
^{238}U	4.468 Ga	^{4}He	8	
		^{136}Xe	3.6×10^{-8}	Spontaneous fission
^{235}U	0.704 Ga	^{4}He	7	$^{238}U/^{235}U = 137.88$
^{232}Th	14.01 Ga	^{4}He	6	Th/U = 3.8 in bulk Earth
		^{136}Xe	$<4.2 \times 10^{-11}$	No significant production in Earth
^{40}K	1.251 Ga	^{40}Ar	0.1048	^{40}K = 0.01167 % total K
^{244}Pu	80 Ma	^{136}Xe	7.0×10^{-5}	$^{244}Pu/^{238}U = 6.8 \times 10^{-3}$ at 4.56 Ga
^{235}U	0.704 Ga	^{4}He	1	$^{129}I/^{127}I = 1.1 \times 10^{-4}$ at 4.56 Ga

K per year and this has resulted in ^{40}Ar dominating the Ar isotope budget with an isotopic abundance of 99.6 % in the atmosphere.

3.3.3 Krypton and Xenon

Small amounts of fissionogenic Xe and Kr are produced by the fission of ^{244}Pu and ^{238}U. The most significant product of these reactions is ^{136}Xe which is produced at a rate of 4.98×10^{-16} cm^{3}g^{-1}(U) a^{-1} and is accompanied by lesser amounts of ^{131}Xe, ^{132}Xe and ^{134}Xe. Minor amounts of Kr isotopes are also produced by U fission but are not relevant for these discussions so have been omitted.

3.3.4 Nucleogenic Helium and Neon

Alpha particles and neutrons emitted during the decay series of U and Th can bombard lighter elements and cause nuclear reactions producing noble gases. The production of Ne isotopes in the crust is almost entirely due to nucleogenic routes (Table 2). Their rate of production is directly related to radioelement and target-element concentrations and the distribution of the

Table 2 Nucleogenic reactions applicable to this study

Parent	Occurrence	Reaction	Noble gas
Li	Incompatible element, high concentrations in granitic rocks	$^{6}Li(n,\alpha)^{3}He$	^{3}He
O	Major constituent of all Silicates	$^{17}O(\alpha,n)^{20}Ne$	^{20}Ne
O		$^{18}O(\alpha, n)^{21}Ne$	^{21}Ne
Mg	Constituent of Ferro-magnesium rocks e.g. basalts	$^{24}Mg(n, \alpha)^{21}Ne$	^{22}Ne
Mg		$^{25}Mg(n, \alpha)^{22}Ne$	^{22}Ne
F	Igneous terranes, phosphatic and fluorite ore deposits	$^{19}F(\alpha,n)^{22}Na(\beta)^{22}Ne$	^{22}Ne

Data compilation by Ballentine and Burnard (2002) and references therein

target element related to radioelement heterogeneity (Ballentine and Burnard 2002). Additionally, in regions with high U and Th or with unusual compositions, such as high Li contents, nucleogenic ^{3}He production can increase the $^{3}He/^{4}He$ ratios.

3.4 Atmospheric Noble Gases

With the exception of He, which is lost to space, the Earth's noble gases are concentrated in the atmosphere. This is a result of their highly volatile nature, meaning that the atmosphere consists of primordial noble gases that have been outgassed from the Earth's mantle early in its history (e.g. Porcelli and Ballentine 2002) and possibly from external volatile sources such as comets (e.g. Holland et al. 2009).

The noble gas composition of the atmosphere is well constrained (Porcelli et al. 2002; Sarda et al. 1985) and is the standard used as a reference for discussion. With the exception of Ar which is dominated by radiogenic ^{40}Ar and accounts for almost 1 % of the atmosphere, the noble gases are present as trace constituents. The atmosphere contains almost the entire inventory of ^{36}Ar. The $^{40}Ar/^{36}Ar$ ratio of the atmosphere was originally equal to the solar ratio ($<10^{-3}$) but this has been increased to its present value of 295.5 by radiogenic production of ^{40}Ar (Sarda et al. 1985). The atmospheric $^{3}He/^{4}He$ value is commonly referred to as R_A (where R_A is the $^{3}He/^{4}He$ ratio of air at 1.4×10^{-6}). The He inventory of the atmosphere is a combination of material outgassed from the mantle (which is rich in ^{3}He), material produced in and outgassed from the crust (which is rich in ^{4}He), cosmogenic material (rich in ^{3}He) and material lost to space (^{3}He is preferentially lost over ^{4}He as it is lighter and more volatile). The other significant atmospheric noble gases are ^{20}Ne, ^{84}Kr, ^{129}Xe and ^{132}Xe which have characteristic ratios relative to Ar of $^{20}Ne/^{36}Ar = 0.5185$, $^{84}Kr/^{36}Ar = 0.0207$ and $^{130}Xe/^{36}Ar = 0.7237 \times 10^{-3}$ (Ozima and Podosek 2001).

Noble gases from the atmosphere are dissolved in water with the proportions dependent on their respective solubilities and subsequently migrate into basin aquifers, transported by groundwater (Mazor 1972). The fractionation of atmospheric noble gases present in the subsurface natural gases then provides information on the interaction between oil phases, if any, present in the fluid system (Ballentine et al. 1996; Pinti and Marty 1995) and the interactions between water and gas phases, as well as the extent of degassing of the groundwater.

3.5 Crustal Noble Gases

The noble gas inventory of the crust is extremely variable as it is dependent on age, geological history (e.g. degree of metamorphism) and composition of radioactive elements. U, Th and K are enriched in the crust as a result of their incompatible behaviour, and therefore so are ^{4}He and ^{40}Ar, the products of their radioactive decay. Crustal $^{3}He/^{4}He$ ratios are typically within the range of 0.01–0.05 Ra (Ozima and Podosek 2001), but can be significantly higher in Li-rich regions, due to nucleogenic production of ^{3}He (Tolstikhin et al. 1996). The present day $^{4}He/^{40}Ar$ production ratio of the lower, middle and upper crust can be calculated as 3.09, 5.79 and 6.00 (Ballentine and Burnard 2002), using the average crustal composition values of the three separate crust portions. This gives a

production weighted average value of 5.7. ^{36}Ar production in the crust is a minor component compared to the amount of atmosphere-derived ^{36}Ar that is introduced dissolved in the groundwater (Fontes et al. 1991). Fissionogenic Kr and Xe can be significant in regions rich in U, with fissionogenic Xe being characterised by a $^{136}Xe/^{132}Xe$ ratio of 1.733 ± 0.003 and $^{134}Xe/^{132}Xe$ of 1.435 ± 0.003 (Drescher et al. 1998).

3.6 Mantle Noble Gases

The presence of excess ^{129}Xe in the mantle, which is produced by the decay of the extinct ^{129}I with a half-life of 15.7 Ma, implies that the mantle outgassed very early in Earth history (<100 Ma). I–Pu–U systematics requires significant loss of noble gases over this period (Porcelli et al. 2001). Loss of almost all of the primordial ^{36}Ar to the atmosphere and radiogenic production of ^{40}Ar from the decay of ^{40}K has resulted in a high upper mantle $^{40}Ar/^{36}Ar$ ratio, with a upper limit of >35,000 (Burnard et al. 1997; Holland and Ballentine 2006; Moreira et al. 1998). The $^{3}He/^{4}He$ ratios of the mantle are also high and exhibit a distinct difference between the upper and primitive lower mantle sources. The $^{3}He/^{4}He$ signature of oceanic island basalts (OIBs) sourcing the primitive lower mantle is highly variable, typically ranging between 9–32 R_A (Farley and Craig 1994; Trieloff et al. 2000). This is in contrast to the narrow range of $\sim 8 \pm 1$ R_A exhibited by mid ocean ridge basalts (MORB) (Graham 2002), which sample the upper portion of the convective mantle.

4 Understanding the Sources and Processing of Crustal Fluids

4.1 Introduction

As described in the previous section, noble gases are predominantly derived from the atmosphere, the crust and the mantle. We have also seen that the isotopic signatures of these three reservoirs are distinct from one another. These characteristic differences in isotopic composition allow us to distinguish between components.

4.2 Two Component Mixing

The atmosphere has relatively low concentrations of radiogenic/nucleogenic noble gases ^{21}Ne, ^{40}Ar and ^{136}Xe compared to crustal sources. To distinguish between the two, the isotopic ratios can be compared with the atmospheric ratio to identify crustal excess (Ballentine et al. 2002).

In a two component crust/air mixture:

$$\left[{}^{21}Ne\right]_{crust} = \left[{}^{21}Ne\right]_{tot} \times \left[1 - \left({}^{21}Ne/{}^{20}Ne\right)_{air} / \left({}^{21}Ne/{}^{20}Ne\right)_{s}\right] \quad (1)$$

$$\left[{}^{40}Ar\right]_{crust} = \left[{}^{40}Ar\right]_{tot} \times \left[1 - \left({}^{40}Ar/{}^{36}Ar\right)_{air} / \left({}^{40}Ar/{}^{36}Ar\right)_{s}\right] \quad (2)$$

$$\left[{}^{136}Xe\right]_{crust} = \left[{}^{136}Xe\right]_{tot} \times \left[1 - \left({}^{136}Xe/{}^{130}Xe\right)_{air} / \left({}^{136}Xe/{}^{130}Xe\right)_{s}\right] \quad (3)$$

Where subscripts crust and total refer to concentrations and subscripts air and s refer to the isotopic compositions of the atmosphere and sample, respectively.

^{4}He is also produced in significant quantities in the crust but the He system is complicated by the presence of 'primitive' ^{3}He, sourced from the mantle. In order to resolve the mantle/crustal components, ^{3}He can be used. Although He has a low abundance in the atmosphere due to thermal loss, excess air corrections must still be made by using the observed air-derived ^{20}Ne concentrations (Ballentine et al. 2002).

$$\left(\frac{{}^{3}He}{{}^{4}He}\right)_{c} = \frac{\left(\left(\frac{{}^{3}He}{{}^{4}He}\right)_{s} \times \left(\frac{{}^{4}He}{{}^{20}Ne}\right)_{s}\right) \div \left(\left(\frac{{}^{4}He}{{}^{20}Ne}\right)_{air} \times \left(\frac{{}^{3}He}{{}^{4}He}\right)_{air}\right)}{\left(\left(\frac{{}^{4}He}{{}^{20}Ne}\right)_{s} - \left(\frac{{}^{4}He}{{}^{20}Ne}\right)_{air}\right) - 1} \quad (4)$$

Subscripts c, s and air refer to the corrected, measured and air-derived ratios, respectively. Once corrected for excess air, the $^{3}He/^{4}He$ ratio represents the sum of the crust and the mantle, with crustal ^{4}He given by:

$$\left[{}^{4}He\right]_{c} = \frac{\left[{}^{4}He\right]_{tot} \times \left(\left(\frac{{}^{3}He}{{}^{4}He}\right)_{mantle} - \left(\frac{{}^{3}He}{{}^{4}He}\right)_{c}\right)}{\left(\left(\frac{{}^{3}He}{{}^{4}He}\right)_{mantle} - \left(\frac{{}^{3}He}{{}^{4}He}\right)_{crust}\right)} \quad (5)$$

Where subscripts mantle, crust and c refer to the mantle, crust and air corrected values.

4.3 Three Component Mixing

In many crustal fluid reservoirs, a significant magmatic component is present in the fluids, in addition to the air and radiogenic components. Typically, all three components, including that of the atmosphere can be observed in the noble gases. In principle, it is possible to correct out the air component using an unambiguously air derived isotope. In practice, this is problematic because this correction depends on no (or at least well quantified) elemental fractionation in an individual sample which is often not the case. However, due to the large differences in isotopic composition of the mantle, crust and atmosphere end-members of Ne, this isotopic system alone can be used to make the correction for the atmospheric component (Fig. 5). This is because any sample that contains a mix of these components must plot within the envelope defined by the well-known $^{20}Ne/^{22}Ne$ and $^{21}Ne/^{22}Ne$ air and crust end members and the resolved mantle end member values of 12.5 for $^{20}Ne/^{22}Ne$ and 0.06 for $^{21}Ne/^{22}Ne$ (Ballentine et al. 2005). Hence, the Ne isotope system is a particularly useful tracer within natural gas reservoirs as the contribution from the mantle, crust and atmosphere to any sample can be resolved. In the following sections we shall see that Ne isotopic composition provides the most striking evidence of the different proportions of atmosphere, crust and mantle inputs to subsurface gas systems.

4.4 Role of Stable Isotopes

In many natural reservoirs, the dominant CO_2 source and basin scale processes that act on it are poorly constrained. This is primarily a reflection of the multiple origins of CO_2 in the subsurface which include methanogenesis, oil field biodegradation, kerogen decarboxylation, hydrocarbon oxidation, decarbonation of marine carbonates and degassing of magmatic bodies (Jenden et al. 1993; Wycherley et al. 1999). Carbon isotopes can be measured within natural CO_2 gas and precision is usually better than 0.1 ‰ (Javoy et al. 1986), the $\delta^{13}C(CO_2)$ signature having been used previously to distinguish between different CO_2 sources. However, $\delta^{13}CO_2$ values alone do not provide an unambiguous means to distinguish between mantle-derived CO_2 and CO_2 derived from crustal sources such as the metamorphism of carbonate rocks. This is due to the average mantle carbon and bulk crustal carbon exhibiting an overlapping range of $\delta^{13}CO_2$ of −3 to −8 ‰ (Fig. 6) (Sherwood Lollar et al. 1997). These are the only sources that can produce gas fields containing greater than 99 % CO_2 by volume, which are particularly pertinent as natural CO_2 sequestration analogues.

A much more unambiguous measure of CO_2 origin is provided by comparing the absolute amount of the magmatic noble gas, ^{3}He, to the CO_2 concentration within the gas reservoir, because the mantle $CO_2/^{3}He$ ratio measured in mid-ocean ridge basalts (MORB) has a small range, from 1.0×10^{9} to 1.0×10^{10} (Burnard et al. 2002; Marty and Jambon 1987; Trull et al. 1993), compared with the range observed in natural gases. Figure 7 shows $CO_2/^{3}He$ plotted against CO_2 concentration. Any natural CO_2 sample that plots above this MORB range irrespective of CO_2 content can only be attributed to a CO_2 source containing minimal ^{3}He, providing an unambiguous identification of a crustal CO_2 source. Samples within or below the MORB range contain a magmatic component but have been subjected to possible CO_2 loss, dilution (by addition of other gas species such as CH_4 or N_2) and/or crustal CO_2 addition. Careful study of both the $\delta^{13}C$ (CO_2) isotopes and $CO_2/^{3}He$ ratios can distinguish between these processes and allow CO_2 origins to be determined (Ballentine et al. 2001, 2002; Sherwood Lollar et al. 1994, 1997).

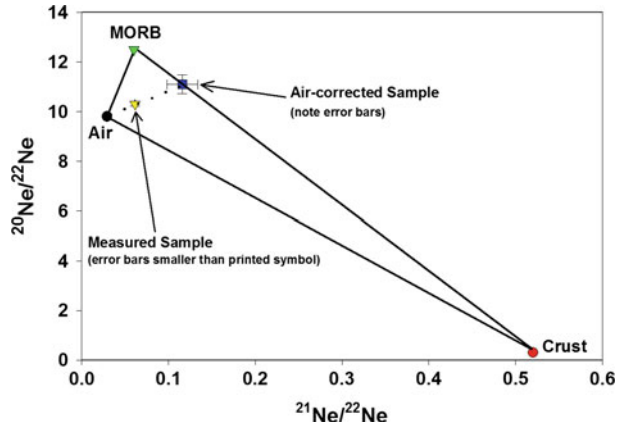

Fig. 5 Plot of $^{20}Ne/^{22}Ne$ against $^{21}Ne/^{22}Ne$ illustrating the three distinct sources of Ne in natural gas reservoirs (redrawn from Ballentine 1997). As the three end member ratios are known it is simple to correct any sample for atmosphere, crust or mantle contributions, taking due account of the error propagation. Example shows correction for the atmospheric contribution. The same procedure can be used for correction of crust and mantle contributions

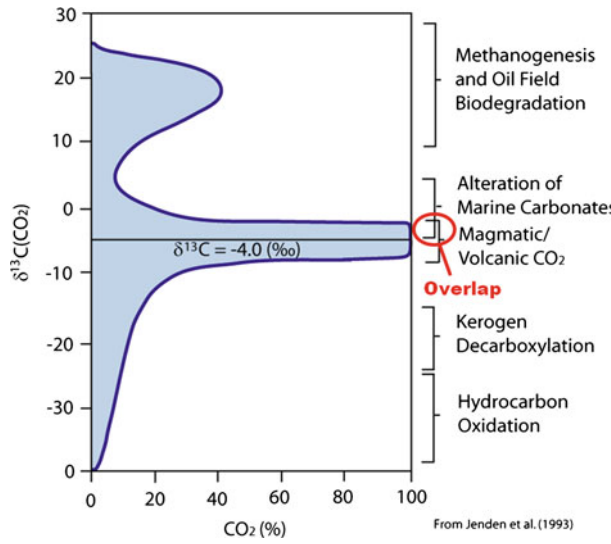

Fig. 6 Plot of CO_2 concentration against the range of $\delta^{13}C$ (%) observed in natural systems. The range of $\delta^{13}C$ values corresponding to a variety of natural processes are also labelled as is the clear overlap in the range of values that exists between magmatic CO_2 and the alteration of marine carbonates. Significantly these are the only sources that can account for reservoirs with high concentrations of CO_2

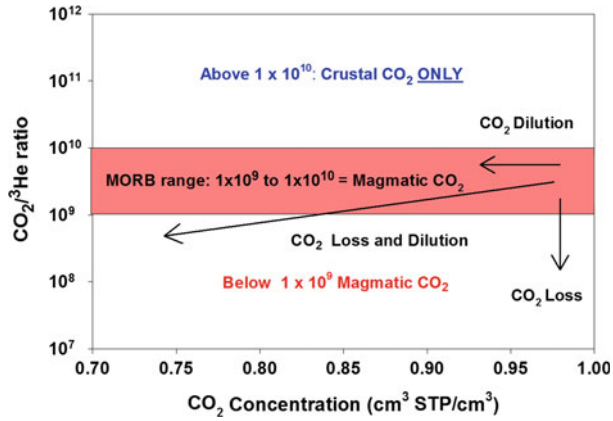

Fig. 7 Plot of CO_2 concentration against $CO_2/^3He$ ratio. The range of $CO_2/^3He$ values exhibited by mid-ocean ridge (MORB) popping rocks is highlighted by the *shaded* region. Any CO_2 that plot within or below this range, must contain a significant quantity of magmatic ^3He, implying a mantle origin for the CO_2. As the crust contains no ^3He, gases sourced from the crust have $CO_2/^3He$ values that plot above the shaded region (Ballentine et al. 2001, 2002; Sherwood Lollar et al. 1999; Zhou et al. 2005)

5 Use of Noble Gases in Natural CO_2 Reservoirs: Colorado Plateau, USA

The study of noble gases in the understanding of water—CO_2—oil interactions is still in the early stages but in principle, noble gases and the combination of noble gases and stable isotope data can provide a quantitative tool for tracing the processes occurring in the hydrogeological system that have direct relevance for long term carbon sequestration.

5.1 Determining the Source and Residence Time of CO_2

Noble gases have been particularly effective in determining the source of CO_2 within natural CO_2 reservoirs. Comparing the concentration of ^3He with the concentration of ^4He (i.e. the $^3He/^4He$ ratio) can identify magmatic contributions to subsurface reservoirs (Ballentine et al. 2002). In a similar fashion, the concentration of ^3He can be compared to the concentration of CO_2 within a natural CO_2 reservoir to determine the origin of the CO_2 (Marty et al. 1992; Oxburgh et al. 1986). Magmatic $CO_2/^3He$ ratios exhibit a small range when compared to other crustal fluids (1×10^9 to 1×10^{10}) (Ballentine et al. 2001) and hence can be used to identify and quantify the amount of mantle CO_2 in a particular reservoir.

Using this technique it has been established that five reservoirs (McCallum Dome, Sheep Mountain, McElmo Dome, Bravo Dome, St Johns Dome) surrounding the Colorado Plateau uplift region of the southwest U.S. primarily contain mantle-derived CO_2 (Fig. 8). Radiometric dating of surface volcanics surrounding these natural CO_2 reservoirs gives an indication of the approximate timing of CO_2 injection. The most recent magmatic event related to the natural CO_2 reservoirs investigated occurred at the Raton-Clayton volcanic field close to Bravo Dome between 10 and 8 ka (Broadhead 1998). The next youngest event is associated with St. Johns Dome, where the last phase of volcanic activity from the nearby Springerville Volcanic field dates from 0.3 to 2.1 Ma (Rauzi 1999). Magmatic activity associated with both the Sheep Mountain and McCallum Dome CO_2 reservoirs occurred in the Late Tertiary (Maughan 1988; Woodward 1983). The oldest intrusive igneous rocks close to a natural CO_2 reservoir are those associated with McElmo Dome, from the nearby Ute Mountain and La Plata Mountain laccoliths which have been dated

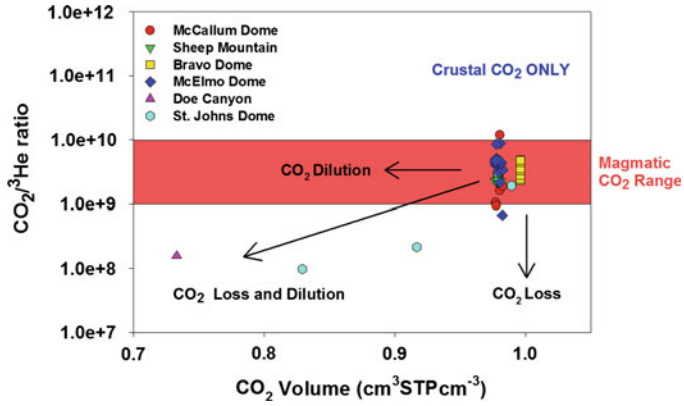

Fig. 8 Plot of $CO_2/^3He$ against CO_2 concentration for all of the reservoirs studied. All error bars are smaller than printed symbols. The *shaded region* highlights the range of $CO_2/^3He$ values measured in pure magmatic samples (MORB). All of the samples from the deep gas fields plot within or below this range, indicating the presence of a significant quantity of magmatic ^3He, implying a mantle origin for the CO_2 within these fields (Gilfillan et al. 2008). Doe Canyon is a small natural CO_2 reservoir related to McElmo Dome

at 40–72 Ma (Stevens et al. 2006). Whilst these ages were determined on surface intrusive igneous rocks, and it is probable that deep igneous activity will have continued for a significant period after these surface rocks were formed, it is clear that several of the natural reservoirs appear to have stored CO_2 for at least a million years. Indeed in two reservoirs CO_2 has been stored for considerably longer, namely McElmo Dome where CO_2 was injected ~40 million years ago (Gilfillan et al. 2008) and in the JM Brown Basset Field which is believed to have contained CO_2 for some 300 million years (Ballentine et al. 2001). In all these fields, $CO_2/^3He$ data show a magmatic origin for the CO_2 gases with evidence of CO_2 depletion relative to ^3He (Fig. 8).

5.2 Determining the Long Term Fate of CO_2

In addition to identifying the source of CO_2, noble gases can also be used to determine the long term fate of natural CO_2. Measured $CO_2/^3He$ ratios from nine CO_2 reservoirs from around the world (specifically the U.S., Europe and China) show a marked decrease in $CO_2/^3He$ ratios with increasing ^4He, (Fig. 9a) and where measured, ^{20}Ne (Gilfillan et al. 2009) (Fig. 9b). As ^3He is almost solely derived from the mantle, there is no source in the shallow crust that could increase its concentration after the premixed CO_2 and ^3He has entered the reservoir. Hence, the reduction in $CO_2/^3He$ can only be explained if the CO_2 component is being reduced relative to ^3He.

Due to its atmospheric origin, ^{20}Ne is a tracer of formation water interaction in crustal fluids. ^4He is a tracer of radiogenic input to a crustal fluid system, and accumulates in the formation water over time (hence its use for formation water dating). Therefore, the correlation between the $CO_2/^3He$ reduction and increasing ^{20}Ne and ^4He concentrations illustrates that contact with the formation water is directly controlling the removal of the CO_2 component in the natural CO_2 reservoirs.

5.2.1 Using Noble Gases and Carbon Isotopes to Identify Long Term Fate of CO_2

In each individual field, the reduction in $CO_2/^3He$ ratios allows the amount of CO_2 lost relative to ^3He to be calculated. Several of the reservoirs show an excess of 90 % loss of CO_2 compared to the highest $CO_2/^3He$ ratio measured (Gilfillan et al. 2009). Using stable carbon isotopes in conjunction with noble gas data it is

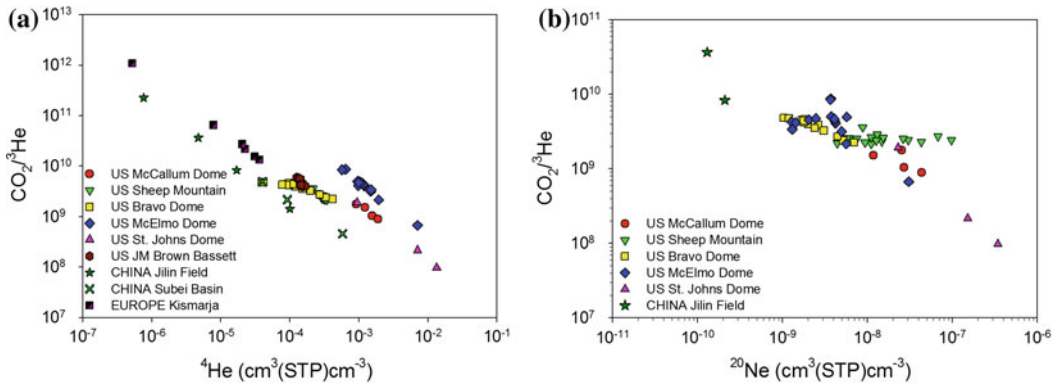

Fig. 9 **a** CO_2-rich gas fields from around the world also show a strong correlation between decreasing $CO_2/^3He$ and increasing ^4He concentrations. ^4He accumulates in the formation water over time and further indicates the importance of formation water in controlling the mechanism of subsurface CO_2 removal (Gilfillan et al. 2009). **b** $CO_2/^3He$ variation plotted against ^{20}Ne in samples from natural CO_2 reservoirs from around the world. There is a general trend in this data set of decreasing $CO_2/^3He$ with increasing ^{20}Ne. ^3He is conservative within the gas phase. Variations in $CO_2/^3He$ therefore represent subsurface removal of CO_2 from the emplaced CO_2 phase. As the only subsurface source of the ^{20}Ne which is now in the CO_2 phase is the formation water, the sink that is reducing CO_2 must be linked to the formation water which is in contact with the CO_2 (Gilfillan et al. 2009)

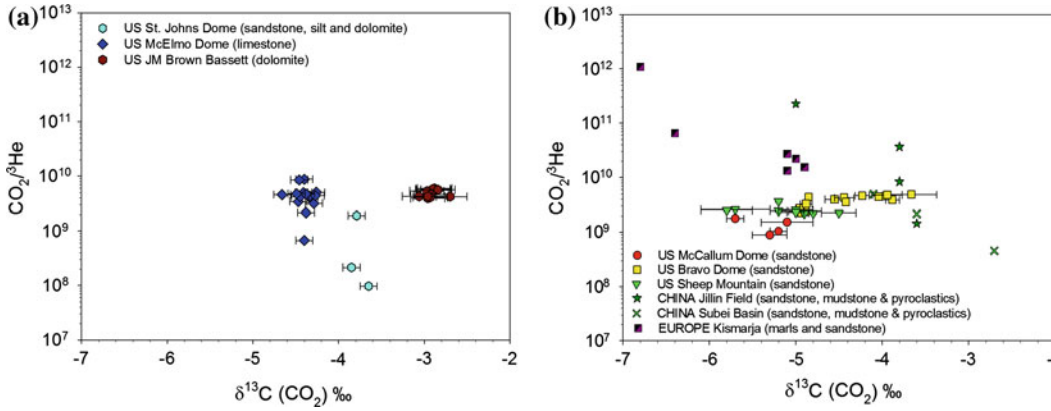

Fig. 10 Plot of $CO_2/^3He$ against $\delta^{13}C$ (CO_2) for all of the reservoirs in the study. The carbonate dominated reservoirs exhibit very little variation in $\delta^{13}C$ (CO_2) value, both within the individual reservoirs and between different reservoirs (*left*). The reservoirs which had a predominantly siliciclastic lithologies reservoirs exhibited a wider range of $\delta^{13}C$ (CO_2) values within and between the reservoirs (*right*) (Gilfillan et al. 2009)

possible to determine how much of this CO_2 component is being lost by dissolution into the formation water or by precipitation of new carbonate minerals. This is because precipitation of new carbonate minerals is a chemical process which strongly alters the $\delta^{13}C$ (CO_2) isotope values as a result of the preferential incorporation of ^{13}C in the precipitate. As both ^{12}C and ^{13}C have similar solubility, dissolution of CO_2 into the formation water has a lesser effect on the $\delta^{13}C$ (CO_2) isotope values, although this is also pH dependent.

All of the natural CO_2 reservoirs investigated exhibited a small range of carbon isotope values, despite large reductions in the CO_2 component relative to ^3He. This shows that the majority of the CO_2 is being removed by dissolution into the formation water. Individual reservoir lithologies

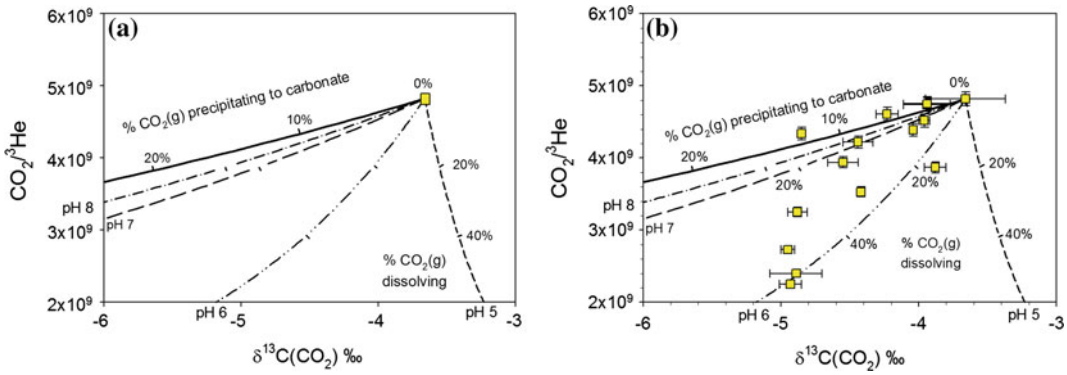

Fig. 11 **a** Model of evolution of gas phase $CO_2/^3He$ ratio and $\delta^{13}C$ of the CO_2 under Bravo Dome reservoir conditions. Using a combination of noble gas and $\delta^{13}C(CO_2)$ stable isotopes determination and quantification of the different mechanisms of CO_2 removal from natural CO_2 reservoirs is possible. This is because $\delta^{13}C(CO_2)$, the stable carbon isotope value of the residual CO_2 phase, is changed, or 'fractionated', by different amounts depending on the loss mechanism. Specifically, precipitation of CO_2 as carbonate minerals has a distinct fractionation from CO_2 dissolving to into the formation water in the reservoir. **b** Plot of $\delta^{13}C(CO_2)$ against $CO_2/^3He$ for the siliciclastic Bravo Dome field as CO_2 gas is either dissolved under different pH (*dashed lines*) or precipitated in an open system by Rayleigh fractionation (*solid line*). The Bravo Dome samples exhibit up to 18 % CO_2 loss by carbonate precipitation and up to 60 % dissolved into the formation water (Gilfillan et al. 2009)

exhibited a clear control on the variation of $\delta^{13}C$ (CO_2) isotopes both within and between the individual natural reservoirs. Within the carbonate dominated reservoirs very little variation in $\delta^{13}C$ (CO_2) values is observed compared to the much wider range of values which were exhibited in the siliciclastic dominated reservoirs (Fig. 10).

Evidence to suggest that precipitation of new carbonate minerals is responsible for some reduction of the CO_2 component is found only in sandstone-dominated reservoirs. This was particularly the case in the Bravo Dome CO_2 reservoir, where the measured values for one sample indicated that up to 18 % of the CO_2 component could have been precipitated (Fig. 11). The dataset from Sheep Mountain indicates that a maximum of 10 % of the CO_2 could have also have been removed by precipitation (Fig. 12a). However, the remaining four siliciclastic and all three of the carbonate dominated reservoirs, such as McElmo Dome (Fig. 12b) showed very little evidence of precipitation and it is clear that CO_2 dissolution into the formation water is the only significant CO_2 sink over geological timescales (Gilfillan et al. 2009).

5.2.2 Using Noble Gases and Carbon Isotopes to Determine Reservoir pH Conditions

Combining the $CO_2/^3He$ ratio reduction with the corresponding fractionation of the $\delta^{13}C$ (CO_2) isotopes also permits determination of the reservoir pH conditions under which the CO_2 dissolution into the formation water is occurring (Fig. 11). This is the result of the different carbon stable isotope fractionation factors which act on CO_2 gas dissolving either to bicarbonate (HCO_3^-) or carbonic acid (H_2CO_3) (Deines et al. 1974). The proportion of CO_2 dissolving to each species is directly controlled by pH, meaning that the $\delta^{13}C$ (CO_2) fractionation trend can be used to determine the pH conditions under which dissolution is occurring (Fig. 11). This is a significant breakthrough in the understanding of natural CO_2 reservoir conditions, as subsurface pH measurements are notoriously difficult to obtain. As with $\delta^{13}C$ (CO_2) values, the reservoir lithology exhibits a clear control on the pH range observed in the different CO_2 reservoirs. A pH range of 5.0–5.3 was observed in the six siliciclastic reservoirs, compared to the higher values of 5.4 to 5.8 determined for the

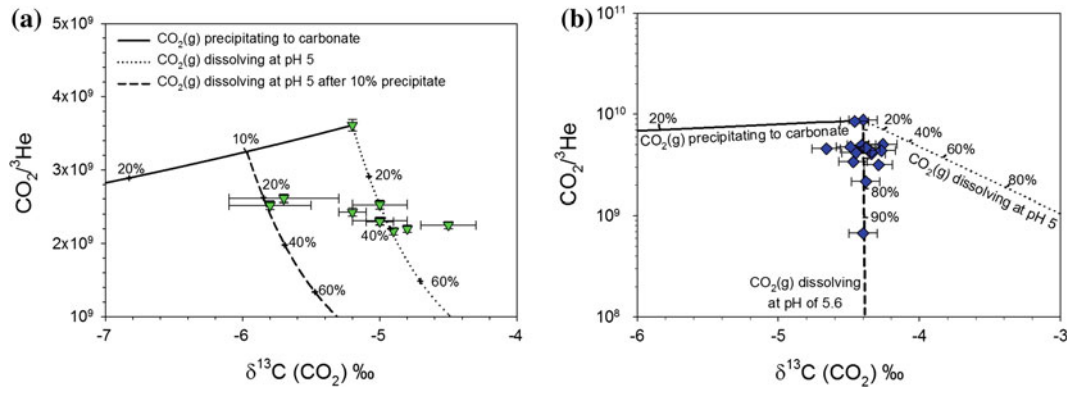

Fig. 12 **a** Plot of $\delta^{13}C$ (CO_2) against $CO_2/^3He$ for the siliciclastic Sheep Mountain field. Whilst the majority of the dataset is consistent with dissolution of CO_2(g) at pH = 5, a number of data points require approximately 10 % of the CO_2(g) precipitating as carbonate, together with dissolution of CO_2(g) into the formation water at a pH of = 5 in a two process model similar to that outlined for Bravo Dome. **b** Plot of $\delta^{13}C(CO_2)$ against $CO_2/^3He$ for the carbonate McElmo Dome field. This shows the relationship between $CO_2/^3He$ and $\delta^{13}C$ (CO_2) observed in the majority of the CO_2 reservoirs. This relationship indicates that the dominant CO_2 sink in these natural systems is dissolution into the formation water. Error bars represent analytical uncertainty on the measured data points

three carbonate reservoirs. This can be accounted for by the buffering capacity provided by additional bicarbonate ions which originate from the dissolution of carbonate minerals in the carbonate-dominated reservoirs. The pH ranges recorded in the natural reservoirs are also consistent with the subsurface pH value of 5.7 observed in the recent CO_2 injection experiment in the Frio formation in Texas (Kharaka et al. 2006).

5.3 Physical Chemistry of Dissolved Noble Gases

The different noble gas isotope systems can tell us about the different proportions of air or crustal derived noble gases within a reservoir but they cannot shed light on the physical processes that occur within these reservoirs. This is because processes such as degassing and phase interactions do not alter the isotopic compositions unless the timescales over which they occur are short than the noble gas diffusion rates. Therefore one must identify the relative solubilities of the noble gases to determine their complex histories within a reservoir, acknowledging that each reservoir will have unique physical conditions and therefore unique 'starting' compositions upon which physical processes leave their fractionating fingerprints. To begin with we must quantify noble gas solubilities in different phases under reservoir conditions to establish these initial noble gas compositions within a reservoir.

Fundamentally, the solubility of noble gases in solution is governed by Henry's law:

$$p_i = K_i x_i \tag{6}$$

where p_i is the partial pressure of gas i in equilibrium with a fluid containing x_i mole fraction of i in solution and K_i is Henry's constant.

Henry's coefficient varies with pressure, temperature and salinity of the fluid. However at the temperatures and pressures found in crustal fluid systems, empirical data are not available. Consequently the equation must be modified to include non-ideality in both the gas and liquid phase. The modified equation then becomes:

$$\phi_i p_i = \gamma_i K_i x_i \tag{7}$$

where Φ is the gas phase fugacity coefficient and γ is the liquid phase activity coefficient.

In the gas phase, the real molar volume can be calculated from:

$$PVm/RT = 1 + B(T)/V_m + C(T)/V_{m^2} \quad (8)$$

From which the fugacity coefficient can be derived via:

$$\Phi(P,T) = \exp[B(T)/V_m + (C(T) + B(T)^2/2V_{m^2} \quad (9)$$

Where P is the total pressure, R is the gas constant, T is the temperature and B(T) and C(T) the temperature dependant first and second order virial coefficients.

Non ideality in the liquid phase cannot be determined using equations of state because of the complexity of solute/solute and solvent/solute interactions. γ is considered to be independent of pressure therefore deviation from ideality caused by temperature and electrolyte concentration is assessed from empirically derived data. For a more extensive review of physical chemistry in liquid and gas phase see Ballentine and Burnard (2002).

5.4 Noble Gas Fractionation and Partitioning Between Phases

Of more direct relevance to assessment of subsurface CO_2 storage using noble gases, is the modelling of solubility fractionation between subsurface phases in open and closed systems (Ballentine et al. 1996; Hiyagon and Kennedy 1992; Pinti and Marty 1998; Torgersen and Kennedy 1999; Zartman et al. 1961). Noble gases alone can also be used to identify interactions between different fluid phases. In the simplest scenario, equilibration of a large gas/water volume ratio in the subsurface would be expected to cause near quantitative degassing of the formation water and result in a gas phase that inherits the formation water noble gas isotopic and elemental composition. This composition would be expected to be similar to the calculated air saturated water (ASW) noble gas composition, determined using appropriate recharge conditions (for the Bravo Dome field used as the example here an ASW $^{20}Ne/^{36}Ar$ of 0.152 was determined assuming air equilibration at 10 °C and a small excess air component of 10 % Ne (Kipfer et al. 2002). As the subsurface gas/water volume ratio decreases the least soluble gases will tend to be enriched in the gas phase until $V_{gas}/V_{water} \rightarrow 0$ when the limit of the enrichment is controlled by the relative solubility of the respective gases. For example, the maximum enrichment of the Ne relative to Ar in the gas phase though phase equilibrium degassing is K_{Ne}/K_{Ar} where K_{Ne} and K_{Ar} are the respective Henry's constants for Ne and Ar (e.g. Ballentine et al. 1991, 2002). K_{Ne} and K_{Ar} for average field conditions predict a maximum enrichment of Ne relative to Ar from ASW values by a factor of ~ 2 corresponding to a maximum $^{20}Ne/^{36}Ar$ of 0.304, which is significantly lower than the range of $^{20}Ne/^{36}Ar$ values (0.314–0.617) observed in the Bravo Dome dataset (Fig. 13). The Sheep Mountain data exhibits even more extreme $^{20}Ne/^{36}Ar$ values which range from 0.530 to 2.496. Clearly both datasets cannot be explained by simple equilibration between the CO_2 and formation water phases and must be explained by a more complex equilibration history.

5.4.1 Solubility Controlled Phase Fractionation

Henry's Law (Eq. 1) defines the fractionation between the gas phase and the liquid phase with which it is in equilibrium. Again assuming ideal gas behaviour, this can be rewritten to relate the concentration in the gas phase, C_g^i, to the concentration in the fluid phase, C_l^i, via Henry's constant K_l^d :

$$C_g^i = K_i^d C_l^i \quad (10)$$

The equilibrium concentrations are also dependent on the gas/liquid volume ratio (V_l/V_g), related by

$$[i]_g = [i]_T \left(V_l/V_g K_i^d + 1\right)^{-1} \quad (11)$$

Where $[i]_g$ is the number of moles in the gas phase and $[i]_T$ is the total number of moles. As

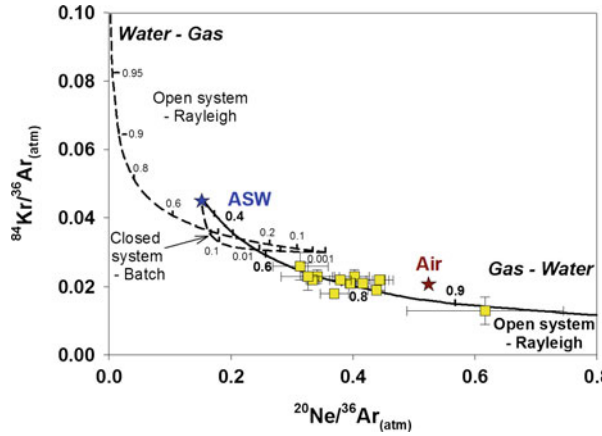

Fig. 13 Plot of $^{20}Ne/^{36}Ar_{(atm)}$ against $^{84}Kr/^{36}Ar_{(atm)}$ for the Bravo Dome field. Also plotted are the Air and ASW values and the calculated Rayleigh and Batch fractionation curves for a gas phase exsolving from a groundwater that has an initial ASW composition (Eq. 6) (*dashed lines*). The *tick marks* on the *dashed lines* represent the proportion of Ar remaining in the groundwater phase. Also plotted is the Rayleigh fractionation line (Eq. 15) which would be produced by a gas phase dissolving into a water phase initially containing no noble gases (*solid line*). This is the re-dissolution model discussed in the text (Eq. 17). The *bold tick marks* on the solid fractionation line represent the proportion of Ar *lost* from the gas phase. The fractionation pattern observed in the air derived ratios can be explained by the re-dissolution model (Gilfillan et al. 2008)

$V_l/V_g \rightarrow 0$, $[i]_g \rightarrow [i]_T$. Giving Henry's constant units of molality leads to:

$$A_g = A_r \left[\frac{22400 T \rho_1 V_1}{1,000 \times 273 \frac{\gamma_A}{\phi_A} K_i^m V_g} + 1 \right]^{-1} \quad (12)$$

where:

A	number of moles
ρl	the density of the liquid l (g/cm^3)
T	Temperature
Vl, g	Volume of liquid l, or gas g in cm^3
Ki^m	Henry's constant (Kg atm/mol)

This determines the partitioning between the gas and liquid phase and makes it possible to calculate the volume of gas with which a liquid has equilibrated by using only one noble gas concentration in the liquid phase. This method assumes that during each stage of degassing, V_{gas}/V_{water} is small and by iteratively equilibrating small volumes of gas with progressively degassed groundwater, one can calculate the number of single stage equilibration episodes that must have occurred to produce an observed loss of the noble gas in question. Summing the volumes of gas defines the total of volume of gas exsolved from the groundwater, hence the gas/groundwater volume ratio (e.g. Zhou et al. 2005).

In practice it is often difficult to assess the initial concentrations of noble gases observed in the liquid phase. In this case, the relative fractionation between two different noble gases can be employed to determine the extent of fractionation processing.

$$\left(\frac{A}{B}\right)_{gas} = \left(\frac{A}{B}\right)_{groundwater} \frac{\left(\frac{Vg}{Vl} + \frac{1}{K_B}\right)}{\left(\frac{Vg}{Vl} + \frac{1}{K_A}\right)} \quad (13)$$

as

$$\text{as } \frac{Vg}{Vl} \rightarrow 0, \frac{\left(\frac{A}{B}\right)_{gas}}{\left(\frac{A}{B}\right)_{groundwater}} \rightarrow \frac{\frac{rA}{\phi A} K_A}{\frac{rA}{\phi B} K_B} = \alpha \quad (14)$$

Where:

$\left(\frac{A}{B}\right)_{groundwater}$	$\frac{A}{B}$ original groundwater ratio and A & B are different noble gases
$\left(\frac{A}{B}\right)_{gas}$	$\frac{A}{B}$ ratio in the gas phase

α	Fractionation coefficient calculated for the gas/groundwater system
K_A, K_B	Henry's constants for gases A and B
r_A, r_B	Groundwater phase activity coefficients
ϕ_A ϕ_B	Gas phase fugacity coefficients

5.4.2 Rayleigh Fractionation (Open System)

Noble gas partitioning from a water phase into a gas phase (degassing) can also follow the Rayleigh fractionation law, provided that the gas phase is continually removed. Rayleigh fractionation can be expressed as:

$$\left(\frac{A}{B}\right)_{groundwater} = \left(\frac{A}{B}\right)_0 f^{\alpha-1} \quad (15)$$

$$\alpha = \frac{\frac{rA}{\phi A} K_A^{groundwater}}{\frac{rA}{\phi B} K_B^{groundwater}} \quad (16)$$

Where:

$\left(\frac{A}{B}\right)_{groundwater}$	$\frac{A}{B}$ ratio in the groundwater and A and B are different noble gases
$\left(\frac{A}{B}\right)_0$	The original groundwater phase $\frac{A}{B}$ ratio
f	Fraction of B remaining in the groundwater phase

Equally, one may also consider the opposite situation, in which noble gases in the gas phase are re-dissolved into groundwater that has been previously stripped of noble gases, as might occur during contact with a CO_2 phase. In this case, the ratio A/B will evolve in the opposite direction, given by:

$$\left(\frac{A}{B}\right)_{groundwater} = \left(\frac{A}{B}\right)_0 f^{\left(\frac{1}{\alpha}-1\right)} \quad (17)$$

In principle, multiple stages of exsolution and dissolution could increase the magnitude of fractionation in a gas phase over that predicted by the phase equilibrium model limit (Zartman et al. 1961). In this case a gas phase exsolved from the water with a low gas/water volume ratio will have an elevated $^{20}Ne/^{36}Ar$ ratio. This could be re-dissolved into a smaller volume of water by a change in physical conditions such as a pressure increase, a decrease in temperature and salinity, or mixing with unsaturated (with respect to the gas phase) water. This would create a local increase in both the formation water noble gas concentration and the magnitude of noble gas fractionation in solution. Subsequent formation of a gas phase in equilibrium with the now modified formation water could result in a fractionation significantly in excess of that predicted by the single stage equilibrium model. For this process to occur the pressure/temperature conditions must fluctuate, and the resulting fractionated gas phase volume must be very small compared to the fluid/water volume required to produce significant fractionation (Ballentine et al. 2002). This is unlikely to have occurred on a gas field scale so it can be discounted as a viable mechanism to account for the extreme values observed in the Bravo Dome and Sheep Mountain datasets.

A second possible mechanism considered is non-equilibrium diffusion. Torgersen et al. (2004) have proposed that variable enrichments of noble gases can be accounted for by incomplete emptying followed by partial filling of lithic grains and half spaces, similar to the mechanism proposed by Pinti et al. (1999) for air diffusion into fresh pumice. They further demonstrate that both elemental and isotopic compositions of Ne and Ar show clear mass-dependent fractionation (Pinti et al. 1999). Whilst the significant mantle and crustal Ne contributions to the Colorado Plateau reservoirs makes subtle isotopic fractionation in Ne hard to identify, no significant mass-dependent fractionation in either the $^{38}Ar/^{36}Ar$ ratios or elemental abundance patterns was observed meaning that non-equilibrium diffusion could be ruled out (Holland and Ballentine 2006).

Another mechanism which could account for the extreme $^{20}Ne/^{36}Ar$ fractionation is interaction of the gas with an oil phase. This is because Ar (and also Kr and Xe), relative to Ne, is more soluble in oil than water meaning that

equilibration of the groundwater with an oil phase could increase the $^{20}Ne/^{36}Ar$ of the water phase (Bosch and Mazor 1988). Subsequent degassing of the groundwater into the gas phase could then result in higher $^{20}Ne/^{36}Ar$ ratios in the gas. This has been suggested as an explanation for elevated $^{20}Ne/^{36}Ar$ ratios measured in the Indus Basin, Pakistan (Battani et al. 2000) and Mexico gas fields (Sarda et al. 2000), where the term double-distillation is used. However, there is no evidence of significant hydrocarbon components in the Bravo Dome CO_2 field and hence, oil interaction can be discounted as a valid explanation of the high $^{20}Ne/^{36}Ar$ ratios. Additionally, in the Indus study there is a correlation between the $^{20}Ne/^{36}Ar$ and $1/^{36}Ar$ ratios but no such correlation exists in the Bravo Dome or Sheep Mountain datasets.

Having ruled out the above mechanisms, a more appropriate model must be devised to explain the high $^{20}Ne/^{36}Ar$ ratios observed in the Colorado Plateau CO_2 reservoirs. One such model is a two stage partial re-dissolution model (Gilfillan et al. 2008). The preservation in some samples near ASW ratios suggests that some degree of 'gas stripping' of the formation water noble gas composition has occurred with complete removal of noble gases into the gas phase. Stage one involves such a complete degassing to provide an ASW starting composition for stage II, which consists of Rayleigh fractionation (open system) of the noble gases from the gas phase into the noble gas stripped formation water (potentially as a result of stage 1).

Neither closed system batch fractionation nor open system Rayleigh degassing models of gas exsolving from an ASW groundwater phase can account for the observed maximum fractionation of $^{20}Ne/^{36}Ar_{(atm)}$ and $^{84}Kr/^{36}Ar_{(atm)}$ in the Bravo Dome reservoir (Fig. 13). The values can however, be explained by the re-dissolution model. It is proposed that gas stripping of the reservoir formation water occurs during the injection and movement of magmatic CO_2 through the formation water during the initial reservoir filling stage. This is corroborated by the orders of magnitude lower ^{20}Ne concentration in the gas phase than that predicted by groundwater degassing (Fig. 14). The CO_2 migrates as a separate phase and as it is an excellent solvent, would have had the capacity to quantitatively partition any gases from the water phase into the CO_2, effectively 'stripping' the formation water of its dissolved gas content. This will produce a CO_2 reservoir with an ASW-like composition which will also have incorporated any radiogenic-crustal noble gases that had previously accumulated in the formation water. At this stage the formation water will be saturated with respect to CO_2, but completely depleted with respect to the atmosphere-derived noble gases.

In the Bravo Dome system, coherent fractionation of the crustal radiogenic and formation water-derived noble gases indicates that the formation water and CO_2 were well mixed prior to the fractionation occurring, hence the fractionation process must have occurred after the ASW gas stripping. Subsequent charges of magmatic CO_2 would then pass through the gas stripped formation water but will only dilute the ASW-derived and crustal-radiogenic noble gases in the CO_2 trapping structure. Bravo Dome preserves a clear ^{20}Ne concentration gradient, increasing from west to east in the field. It is argued this both corroborates the model and indicates the reservoir filling direction, which may still be ongoing, to be from the west (Baines and Worden 2004b).

Following reservoir filling the noble gases now in the CO_2 phase will then re-equilibrate with the degassed formation water. This re-equilibration will occur under either open system or closed system conditions depending on the available volume of water for re-equilibration and if there is significant water migration or recharge. For open system conditions, the re-dissolution process will follow a Rayleigh fractionation path. Under closed system conditions, the trend will be the exact reverse of that calculated for batch fractionation of a gas phase exsolving from water. Under the Bravo Dome reservoir conditions, the open system Rayleigh fractionation re-dissolution model accounts for all of the mantle corrected $^{20}Ne/^{36}Ar_{(atm)}$ and $^{84}Kr/^{36}Ar_{(atm)}$ ratios that are observed in the field (Fig. 13). The conceptual model is also

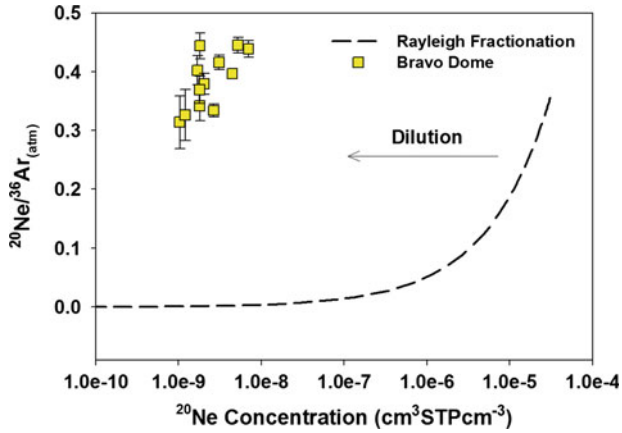

Fig. 14 Plot of $^{20}Ne/^{36}Ar_{(atm)}$ against $^{20}Ne_{(atm)}$ for the samples from the Bravo Dome field. Also plotted are the predicted ^{20}Ne concentration values assuming Rayleigh Fractionation of a gas phase exsolving from the groundwater. The predicted concentrations are several orders of magnitude greater than the observed concentrations, implying that the atmospheric noble gases within the reservoir have been significantly diluted, most probably by injection of magmatic CO_2

presented as a cartoon (Fig. 15) from Gilfillan et al. (2008).

5.4.3 Quantifying the Extent of Water Interaction

Using the open system re-dissolution model outlined above, the fractionation of the measured gas phase $^{20}Ne/^{36}Ar$ ratios from the initial ASW formation water value can be used to define the proportion of ^{36}Ar lost from the gas phase into solution. Using this value it is then straightforward to calculate the initial concentration of ^{36}Ar, $^{36}Ar_{init}$, within the gas phase prior to the re-dissolution process (Zhou et al. 2005). Using the concentration of ^{36}Ar in ASW it is then possible to calculate, for each sample, the volume of water required to have been gas 'stripped' to supply the $^{36}Ar_{init}$ to provide the Stage 1 Water/Gas volume ratio. For Bravo Dome system, Stage 1 Water/Gas volume ratio ranges from 0.0005 to 0.071 cm^3 of water per cm^3 gas (STP) (Table 3). Under reservoir conditions 1 cm^3 of groundwater can hold 4.66 cm^3 of CO_2 (STP) in solution (Spycher and Pruess 2005). This results in a water/gas ratio of 0.215 and is far higher than the largest estimated Stage 1 V_{Water}/V_{Gas} Bravo Dome value. This is consistent with the CO_2 gas charging the reservoir as a separate and distinct phase, and hence is consistent with the proposed CO_2 'stripping' of the formation model (Fig. 15).

One can then calculate the volume of water, under reservoir conditions (Table 3), that the noble gases of the CO_2 phase must re-dissolve into, in order to fractionate the $^{20}Ne/^{36}Ar$ values from ASW (0.152) to the values observed. For the Bravo Dome reservoir these vary from 0 to 104 cm^3 water per cm^3 gas (RTP) (RTP = Reservoir Temperature and Pressure), which corresponds to 0–1.51 cm^3 water per cm^3 gas (STP). The volume of degassed water required to fractionate the $^{20}Ne/^{36}Ar$ from ASW to observed values is far larger than the volume of water 'stripped' to supply the gases, by up to a factor of 50. Little, if any, CO_2 will dissolve in this water while it remains CO_2 saturated. This analytical technique is able to quantify on a sample by sample basis the volume of water the CO_2 in this storage analogue has interacted with both (1) on reservoir filling; and (2) subsequent to reservoir filling.

5.4.4 Adsorptive Fractionation

Several studies have suggested that physical fractionation processes such as adsorption can result in a relative gas abundance pattern that is

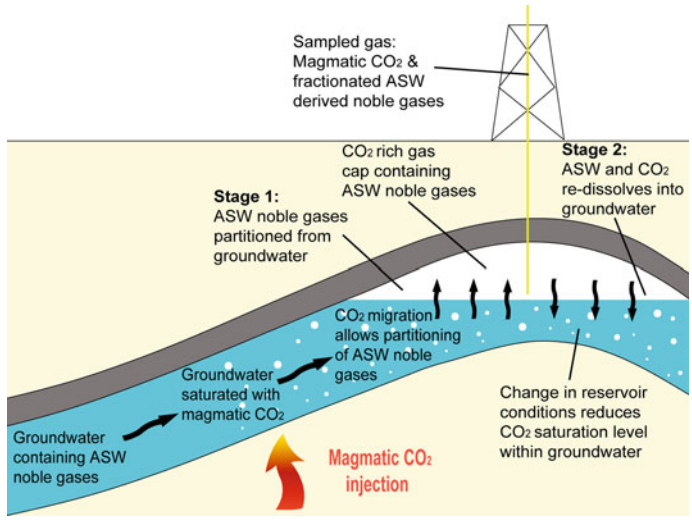

Fig. 15 Cartoon illustrating the two stage degassed formation water and re-dissolution model. *Stage 1*: Magmatic CO_2 injection into the formation water causes the water to become fully saturated in CO_2, with excess gas forming a free CO_2 phase. The free CO_2 phase migrates upwards, stripping dissolved air-derived noble gases and accumulated crustal/radiogenic noble gases as it does so. This results in formation water which is fully saturated in CO_2 and completely degassed with respect to ASW and crustal derived noble gases (and N_2). When this CO_2 containing the noble gases stripped from the formation water encounters a trapping structure, it provides the first reservoir fluid charge. Subsequent charges of CO_2 provide no more ASW and crustal noble gases, and serve only to dilute the original ASW and crustal noble gas rich CO_2. Reservoir scale preservation of concentration gradients in ASW-derived noble gases therefore provide an indication of CO_2 filling direction (cf Bravo Dome, St Johns). *Stage 2*: When recharge of the CO_2 cap stops, the noble gases begin to re-dissolve into the gas stripped groundwater. This results in a fractionation of the ASW-derived noble gases. The magnitude of this fractionation depends on the volume of water in contact with the gas phase and whether open or closed system fractionation conditions are present. Hence, only limited CO_2 re-dissolution can, and only as result of a change in reservoir conditions or CO_2 precipitation as new carbonate minerals causing a reduction of the CO_2 saturation level of the formation water. Figure reproduced from Gilfillan et al. (2008)

highly enriched in heavy noble gas isotopes (Kr and Xe). $^{130}Xe/^{36}Ar$ enrichment factors up to ~600 relative to air and ~200 relative to water in equilibrium with air having been observed. (Fanale and Cannon 1971; Kennedy et al. 1990, 2002; Torgersen et al. 2004). These components cannot be directly determined from ASW by distillation or re-equilibration with oil, gas or oil–gas systems and thus require desorption of these gases from organic matter into fluids (Kennedy et al. 2002; Torgersen and Kennedy 1999). Evidence for this hypothesis is provided by the fact that large quantities of Xe can be adsorbed onto carbon-rich materials at room temperature (Fanale and Cannon 1971; Podosek 1980). Recent work by Torgersen et al. (2004) has reported that these enrichments of noble gases could be accounted for by incomplete emptying followed by incomplete filling of lithic grains and half spaces.

5.4.5 Diffusive Fractionation

Maximum diffusive fractionation will occur under non-equilibrium conditions when the different diffusion properties of the noble gases and CO_2 control the partitioning rate from water into the gas phase. The fractionation or diffusion coefficient of a ratio A/B can be calculated using the Graham's law of diffusion:

$$\alpha_{\frac{A}{B}} = \sqrt{\frac{M_B}{M_A}} \tag{18}$$

where:

A and B	Isotopes
M_A, M_B	Mass of A and B

Table 3 Calculated formation water noble gas concentrations (cm^3STPcm^{-3}) and ratios (Gilfillan et al. 2008)

Field and well	Observed $^{20}Ne/^{36}Ar$	Proportion ^{36}Ar lost to stage 2 water	Measured ^{36}Ar $cm^3(STP)cm^{-3}$ ($\times 10^{-8}$)	$^{36}Ar_{init}$ $cm^3(STP)cm^{-3}$ ($\times 10^{-8}$)	Stage 1 V_{water}/V_{Gas} (STP)	Stage 2 V_{water}/V_{Gas} (STP)	Stage2 V_{water}/V_{Gas} (RTP)
Bravo Dome							
BD01	0.362	0.786	0.212	0.992	0.0090	1.261	87.01
BD02	0.426	0.841	1.25	7.87	0.0714	1.502	103.60
BD03	0.430	0.843	0.881	5.62	0.0510	1.513	104.39
BD04	0.406	0.826	0.222	1.27	0.0115	1.429	98.57
BD05	0.385	0.809	0.873	4.56	0.0414	1.351	93.24
BD06	0.349	0.772	0.299	1.31	0.0119	1.206	83.23
BD07	0.279	0.661	0.191	0.562	0.0051	0.883	60.95
BD08	0.314	0.726	0.505	1.84	0.0167	1.057	72.94
BD09							0.00
BD10	0.395	0.818	0.499	2.73	0.0248	1.389	95.83
BD11	0.152	0.00	0.0549	0.0547	0.0005		0.00
BD12							0.00
BD13	0.347	0.770	0.406	1.76	0.0160	1.199	82.73
BD14	0.296	0.695	0.290	0.948	0.0086	0.969	66.86
BD12b	0.430	0.843	0.0494	0.315	0.0029	1.513	104.39

Hence, for the $^{20}Ne/^{36}Ar$ ratio $\alpha = 1.34$, and for the $^{84}Kr/^{36}Ar$ system $\alpha = 0.655$. As these values depend on the relative mass of the noble gas species, they are independent of the individual reservoir conditions. While some natural gas reservoirs show evidence of isotopic fractionation by diffusion (Zhou et al. 2005) others do not (Holland and Ballentine 2006; Holland et al. 2009).

6 Use of Noble Gases in Hydrocarbon Fields Relevant to CO_2 Storage

6.1 Tracing of CO_2 Injected for EOR, Mabee Oil Field Texas

Noble gas tracing has been used successfully for large-volume groundwater tracing in several different locations (Castro and Goblet 2003; Castro et al. 1998). Nimz and Hudson (2005) undertook an investigation to determine whether noble gases could also be used for CO_2 tracing. This study involved an analysis of noble gas tracer costs, availability, detection limits, and a comparison with other potential tracers.

At the time of the study no CO_2 storage operations were being conducted in which a noble gas tracer could be added therefore the work was undertaken at an active EOR location, the Mabee Oil field in Texas. Fortunately, the CO_2 being injected into the subsurface in the Permian Basin of West Texas contains unique and readily identifiable noble gas isotopic characteristics as the CO_2 originates from the extensive CO_2 reservoirs from the Colorado Plateau region previously discussed in this chapter. This CO_2 is transported via pipelines to West Texas. Therefore, Nimz and Hudson did not have to artificially add noble gases to the CO_2 stream and wait months or years for them to arrive at monitoring wells, they simply investigated the noble gas composition of the producing wells at the field.

Nimz and Hudson collected CO_2 from the pipeline prior to it being injected in the oil field and produced gases from 13 producing oil wells in the Mabee field. The gases extracted from all the Mabee field wells is collected and combined into a single pipeline and which is then mixed

with incoming 'fresh' Colorado Plateau CO_2 and re-injected into the field. This 'blend' of CO_2 was also collected for noble gas analysis. This allowed comparison of the isotopic composition of the injected CO_2 with the CO_2 produced from wells a significant distance from the original injection point. This provided an excellent analogue of tracing in an engineered storage site where noble gases could be injected along with CO_2 and then their distribution could be monitored through outlying wells. It should be noted that the concentrations of noble gases in the injected natural CO_2 from the Colorado Plateau reservoirs is significantly lower than those that would arise from the addition of a spike of artificial noble gases, meaning the study represents a much more difficult monitoring situation than would arise in an engineered storage site.

The wells sampled are shown in Fig. 16, along with the wells that were injecting CO_2 during the period of sampling. As injection had been taking place for many years, the entire field has been subject to injected CO_2 flood.

Nimz and Hudson found that the incoming CO_2 ($KMCO_2$) was isotopically similar to the CO_2 found in McElmo Dome, indicating that the majority of the CO_2 injected into the Mabee field at the time of the study was from McElmo Dome (Fig. 17a). This was somewhat surprising for two reasons; firstly as the operators of the field thought they were receiving CO_2 from Bravo Dome and secondly as there are several CO_2 fields that feed the CO_2 pipeline and hence a more mixed noble gas composition was expected.

Compared to $KMCO_2$ the Mabee production wells all exhibited more 'air like' noble gas composition. This was thought to be the result of either the baseline oil reservoir composition (present prior to CO_2 injection commencing) or from the large amount of water that is also injected into the field with CO_2. (This is because EOR operation in Mabee is a water alternating gas/CO_2 type (WAG), where water and CO_2 are injected into the field at separate times). It was possible to rule out atmospheric contamination during sampling as a cause of this component as the $^{20}Ne/^{36}Ar$ trend recorded from the samples

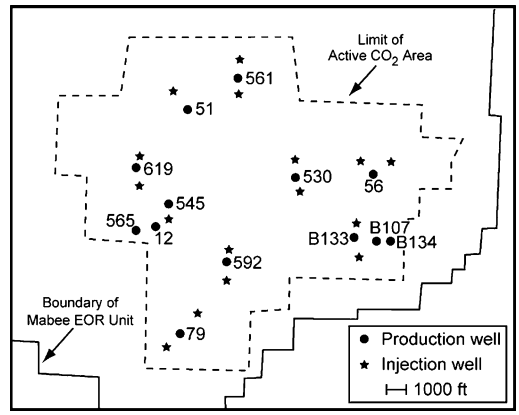

Fig. 16 Map of the southern portion of the Mabee EOR field. The production wells that Nimz and Hudson sampled are shown with adjacent sample numbers. The injection wells shown are those that were known to be active during the sampling period. There are numerous other production wells which are not shown, these occur on approximately 1,000 ft spacings (Nimz and Hudson 2005)

was not close to the fractionation trend expected if the injected $KMCO_2$ was in contact with the atmosphere (Fig. 17c). Instead the samples plotted close to the expected fractionation which would occur if the $KMCO_2$ was in contact with air saturated water (ASW), indicating that the injected water in the field had a strong influence on the noble gas composition of the samples.

From Fig. 17 it is apparent that an additional component must be present in the ASW component because a clear excess in crustal radiogenic ^{40}Ar and nucleogenic ^{21}Ne relative to the predominantly air-derived ^{36}Ar and ^{20}Ne was recorded. This excess component can be clearly seen in Fig. 17b as the trend exhibited by the Mabee samples toward a position with elevated ^{40}Ar relative to excess ^{21}Ne. The radiogenic origin of ^{21}Ne and ^{40}Ar requires this additional component must be crustal in origin.

A similar crustal component was observed in the Xe isotope composition. The samples were found to be enriched in crustal radiogenic $^{132-136}Xe$ relative to atmosphere derived ^{130}Xe. Figure 18d illustrates this excess ^{132}Xe relative to the ASW and air fractionation trends. Unfortunately it was not possible to collect a sample of the

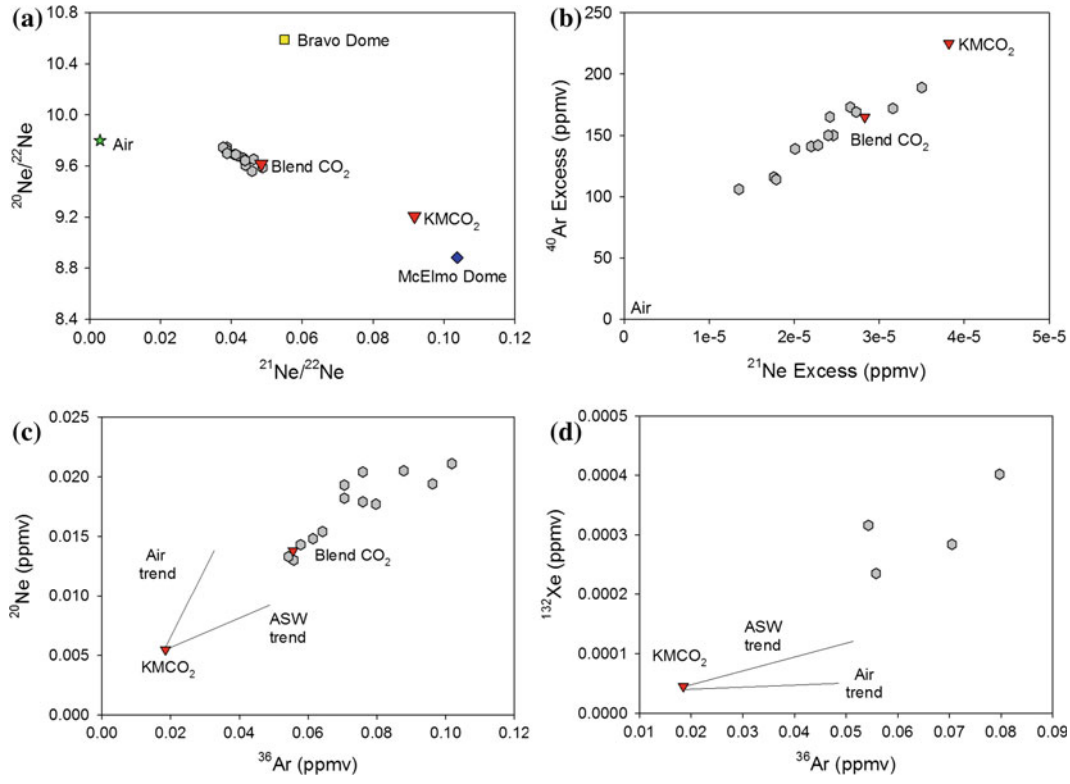

Fig. 17 **a** Plot of $^{20}Ne/^{22}Ne$ against $^{21}Ne/^{22}Ne$ for the individual Mabee oil field samples (*in grey*), $KMCO_2$, which is the composition measured from the incoming CO_2 supply pipeline prior to injection and Blend CO_2 which is from the return pipeline and contains a mix of gases from all the active wells the incoming supply pipeline CO_2. Also plotted is the average Bravo Dome and McElmo Dome ratios from Gilfillan et al. 2008. It is clear to see that the $KMCO_2$ did not originate from Bravo Dome as the operators of Mabee had believed. **b** Plot of the excess ^{40}Ar against excess ^{21}Ne compared to the concentration of air for the Mabee samples including the incoming pipeline CO_2 ($KMCO_2$) and the Blend CO_2. This shows clear mixing between the excess radiogenic ^{21}Ne and ^{40}Ar from the injected $KMCO_2$ and atmospheric air. However the trend does not intersect the origin indicating that an additional crustal component, enriched in ^{40}Ar over ^{21}Ne, must be present. **c** ^{20}Ne concentration plotted against ^{36}Ar concentration. This illustrates that the atmospheric air component in the Mabee samples did not originate from contamination during sampling as the samples do not plot near the fractionation trend expected if the injected $KMCO_2$ was in contact with atmospheric air. They plot on a similar trajectory to what would be expected if the samples were mixing with ASW but with elevated initial ^{20}Ne and ^{36}Ar concentrations. **c** ^{20}Ne concentration plotted against ^{36}Ar concentration. This illustrates that the atmospheric air component in the Mabee samples did not originate from contamination during sampling as the samples do not plot near the fractionation trend expected if the injected $KMCO_2$ was in contact with atmospheric air. They plot on a similar trajectory to what would be expected if the samples were mixing with ASW but with elevated initial ^{20}Ne and ^{36}Ar concentrations. **d** Plot of ^{132}Xe concentration plotted against ^{36}Ar concentration. This plot shows ^{132}Xe concentrations in the Mabee samples are enhanced relative to both the ASW and air fractionation trends starting from an initial $KMCO_2$ composition

injected WAG water in the oil field and hence it is unclear if the crustal radiogenic component was present in this water. However, it is clear from the results of the study that if the groundwaters are the source of crustal radiogenic noble gases, they must have been isolated from atmospheric input for a significant period of time. It is believed that the radiogenic component may originate from the oil reservoir itself as the noble gas compositions measured in the samples from the oil field can be explained by a simple two-component mixture of $KMCO_2$ and a native subsurface component

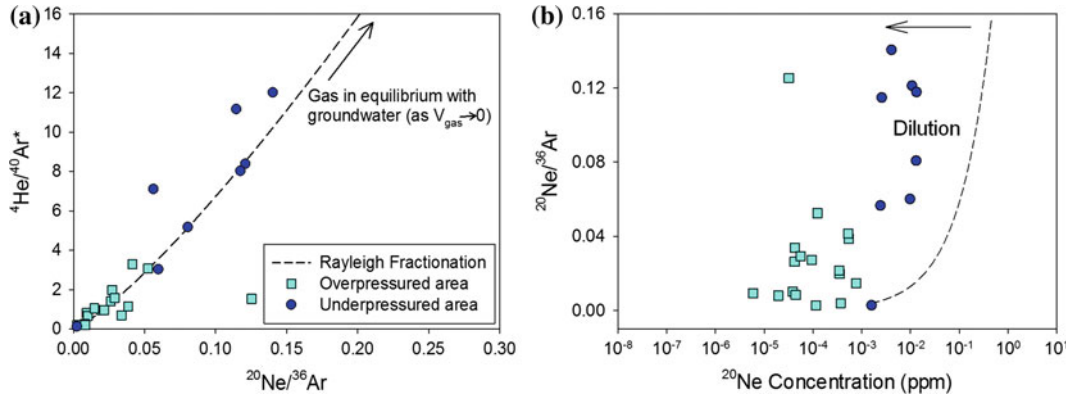

Fig. 18 **a** Water-derived and crustal-derived noble gas show evidence of coherent fractionation trend, which can be modelled as Rayleigh fractionation of a gas phase progressively exsolving from ASW water with a radiogenic component (recalculated and replotted from Zhou et al. 2005). **b** Ne concentrations predicted from the Rayleigh fractionation model are significantly higher than observed, requiring dilution of the groundwater-derived noble gases

which had air-like neon isotope ratios along with a slightly enhanced ^{20}Ne concentration relative to ^{36}Ar, excess ^{40}Ar and enhanced $^{132-136}Xe$ relative to ^{130}Xe.

The key conclusions from this study were: (a) the noble gas tracer was not overprinted in the oil reservoir because the noble gas composition of all of the production gas samples can only be explained by the presence of the $KMCO_2$ component. This is despite the presence of a crustal radiogenic component and a possible WAG component, showing that even if the injected CO_2 moved significantly from the active injection area, the $KMCO_2$ component would still be identifiable, proving that noble gases can be used as tracers of CO_2 migration in a deep reservoir; (b) the sampled $KMCO_2$ had a ^{132}Xe concentration of 1.62×10^{-7} ppmv, which is two orders of magnitude above what would be required for groundsurface monitoring indicating that ^{132}Xe could be used as a tracer of injected CO_2 within the subsurface and probably as a tracer of the migration of deep CO_2.

The noble gas compositions observed in the Mabee Field were very systematic and formed linear trends with only small deviations that could be accounted for by the presence of other known subsurface components, such as a crustal component. This coherent and systematic behaviour of the noble gas system bodes well for using noble gases as tracers of CO_2 in the subsurface. The systematic results obtained from the Mabee study clearly show that even very small isotope variations can be detected using existing noble gas analysis techniques. The isotope variations that would result from injection of artificial noble gas tracers would be much easier to detect and hence Nimz and Hudson demonstrated that noble gases could be used as reliable and robust tracers of CO_2 migration within an engineered storage site.

6.2 Noble Gas Tracing of Groundwater/Coalbed Methane Interaction, San Juan Basin, USA

Coal beds that are not of economic interest for coal extraction are becoming increasingly important as a possible sink for anthropogenic CO_2 emissions (Klara et al. 2003; Pashin and McIntyre 2003). Groundwater plays an important role in CO_2 sequestration in coalbeds in a similar fashion to the controls it exerts on CO_2 storage in CO_2 reservoirs. Consequently noble gases can be used to develop a model of groundwater interaction with coal beds that can inform on the CO_2 sequestering process.

The San Juan Basin natural gas field, located in northwestern New Mexico and southwestern

Colorado in the USA, is a case-type coalbed methane system which was investigated by Zhou et al. (2005). Data from the San Juan field show $^{20}Ne/^{36}Ar$ ratios significantly lower than air but $^{84}Kr/^{36}Ar$ and $^{130}Xe/^{36}Ar$ mostly higher than air which suggests, like the CO_2 fields in the previous section, an open system Rayleigh fractionation process but one in which gas is continuously exsolved and then lost from the system. This can be modelled and, in the case of San Juan data, displayed as the variation in radiogenic $^{4}He/^{40}Ar$ with atmospheric $^{20}Ne/^{36}Ar$. In contrast to the Bravo Dome data, the data converge at the origin when $V_{gas} \rightarrow \infty$ and noble gases have fully exsolved from the fluid phase (Fig. 18a).

However, noble gas data show us this is not the complete story. Using ASW as an initial fluid composition that plausibly fits the San Juan data allows us to predict the ^{20}Ne concentration at any stage of the degassing process (i.e. at any $^{20}Ne/^{36}Ar$). The observed ^{20}Ne concentrations are orders of magnitude lower than predicted (Fig. 18b), as also observed in the CO_2 gas fields of SW USA. In the Bravo Dome CO_2 system, this was explained by CO_2 injection stripping the noble gases from the groundwater, owing to the higher solubilities of noble gases in CO_2 than in water (i.e. the re-dissolution model). However, large scale CO_2 migration is not present in the San Juan basin and hence another explanation is required. The model suggested by Zhou et al. (2005) is that a CH_4 component devoid of any noble gases, and therefore isolated from any groundwater since formation, has diluted the CH_4 component that does contain noble gases from the Rayleigh fractionation process as shown in Fig. 19 (adapted from Zhou et al. 2005).

Further evidence of phase interaction can be identified using the heavy noble gases. In a plot of $^{20}Ne/^{36}Ar$ v $^{130}Xe/^{36}Ar$ (Fig. 13 in Zhou et al. 2005), San Juan data show significant but variable excesses of Xe above that predicted from Rayleigh fractionation. When these Xe data are corrected for the dilution effect of the CH_4 desorbed from the coal bed (the ratio of $[^{20}Ne]$ observed divided by $[^{20}Ne]$ modelled), the Xe excesses disappear and the model fits the data excellently. This independent evidence of a dilution effect from Xe enriched coal corroborates the model presented in Fig. 19. This in turn shows that groundwater is not the only control on coal biodegradation and therefore groundwater alone does not determine the viability of coal beds as a CO_2 sequestration reservoir: other important factors include overpressure that may help maintain the integrity/isolation of coal bed seams.

As described in the Sect. 5, step-wise equilibrium degassing can approximate Rayleigh fractionation if at each stage of degassing, V_{gas}/V_{water} is small. In this case study, the differences between the modelled and observed Ne concentration can be quantified (Fig. 18b). Using this dilution ratio together with calculations of gas production history as performed on the CO_2 data in Sect. 5 (for details of this case study see Table 3 Zhou et al. 2005) one can quantify the volumes of water associated with a gas producing well. Assuming coal bed thickness and specific porosity, one can calculate the volume of water involved in gas production of specific wells. Expressed as radii from the well, in the San Juan field these volumes vary from 16 to 242 m (Zhou et al. 2005). This is significantly smaller than the distance between wells. This in turn indicates there is no need for dynamic groundwater flow between wells on the timescale of well gas production and, in this case, suggest that more CH_4 wells can be drilled without adversely affecting existing well gas production.

In the context of the carbon sequestration, this information is important for understanding reservoir connectivity and the presence of absence of continuous water flow through a basin in light of the evidence that the majority of CO_2 sequestration analogues contain CO_2 dissolved in groundwater (see Sect. 5). In

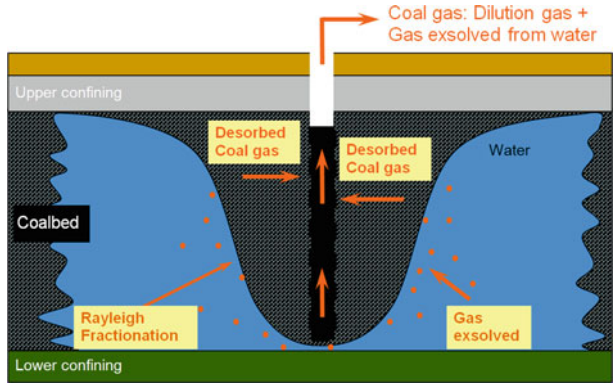

Fig. 19 Cartoon of Rayleigh fraction and dilution model adapted from Zhou et al. 2005. Gas exsolved from the ASW is heavily fractionated and diluted with gas desorbed from the coal bed that has not previously interacted with the groundwater system and is therefore devoid of noble gases

exhausted CO_2 reservoirs or basins undergoing enhanced oil recovery, this type of analysis may also provide information on the extent to which new drilling may increase the storage capacity of a potential subsurface CO_2 storage site.

7 Use of Noble Gases for Monitoring of Subsurface CO_2 Migration and Leakage

7.1 Noble Gases as Tracers of CO_2 Leakage at Green River Springs, Utah, USA

Wilkinson et al. (2010) examined naturally occurring noble gas tracers and isotopic ratios from surface gas samples from a suite of natural CO_2 springs. These springs provide an analogue for some time in the future, when a very severe failure of a containment site has been detected after injection operations have ceased. In the imagined scenario, there was a reservoir of artificially injected CO_2 which existed as a discrete fluid together with shallower aquifers which also contain natural CO_2. It was imagined that a baseline survey had not been undertaken prior to CO_2 storage commencing, so there was only proxy information available from regional archives to identify the chemistry and gas contents of the diverse shallower CO_2 sources and aquifers. The key questions that the study aimed to address were; could CO_2 migration from an injection zone, through the overburden, to the surface, be quantified? Could different sources of CO_2 be discriminated?

The group of CO_2-rich springs sampled by Wilkinson et al. (2010) were located 10 km south of the town of Green River, southwest Utah. They are CO_2-charged springs associated with the Little Grand Wash and Salt Wash faults lying at the northern end of the Paradox Basin in south west Utah. These control the present day flow of gas and groundwater to the surface (Heath 2004; Shipton et al. 2004) with both being part of a series of steeply dipping (70–80°) WNW trending normal faults that are found in the region. Springs of CO_2-rich water and free gas, an active CO_2 charged geyser, and both active and fossil travertine deposits are associated with the Little Grand Wash fault zone. The most notable spring is the cold-water CO_2-charged Crystal Geyser, which erupts to heights of up to 25 m at 4–12 h intervals (see Shipton et al. 2004 for further details). In addition to Crystal Geyser, numerous CO_2-charged springs are associated with the Salt Wash fault zone (see Heath (2004) for further details).

The gases emitted by the Green River Springs are predominantly CO_2 but also include nitrogen and trace noble gases (Heath 2004). Prior to the study of Wilkinson et al. CO_2 and other gases in

the springs were considered to originate from a combination of sources including mantle-degassing, clay-carbonate reactions, the thermal metamorphism of carbonates or atmospheric and soil gas recharge combined with diagenetic reactions such as the maturation of organic material.

In order to calculate crustal and mantle inputs to the CO_2, Wilkinson et al. first quantified the amount of air present in each sample. This was calculated using the measured $^{40}Ar/^{36}Ar$ ratio for each spring using the following formula:

$$\left[^{40}Ar\right]_{air} = \left[^{40}Ar\right]_{meas} \times \left(^{40}Ar/^{36}Ar\right)_{air} / \left(^{40}Ar/^{36}Ar\right)_{meas} \quad (19)$$

The proportion of air-derived Ar was found to be high (33–91 %) as a result of the high ^{40}Ar content of the atmosphere, compared to the much lower crust and mantle contributions. Figure 20 clearly shows how the amount of dissolved air in the samples was controlling both the $^{40}Ar/^{36}Ar$ and $^{4}He/^{20}Ne$ ratios. Using the air-derived ^{40}Ar concentration, it was straightforward to calculate the air contribution to the total erupted CO_2 using the known $CO_2/^{40}Ar$ for air of 0.0398 (Porcelli et al. 2002). The air contribution to the CO_2 was found to be insignificant (0.00003 to 0.00018 volume % CO_2).

The measured $^{3}He/^{4}He$ of the gases erupting from the springs showed a small variation from 0.224 to 0.265 R_a, with the exception of Pseudotenmile geyser which exhibited a higher ratio of 0.386 R_a. This spring was also noted to have a very slow gas discharge rate, possibly enabling atmospheric noble gases to become dissolved in the spring water to form a component of the measured gas, possibly explaining the higher $^{3}He/^{4}He$ ratio observed.

Using the established technique (Craig et al. 1978) the authors attempted to correct the measured $^{3}He/^{4}He$ ratios for the air component, leaving just the crust and mantle input. However, the correction was very small and significantly less than the precision of the data. This was unsurprising given the measured range of $^{4}He/^{20}Ne$ of 313 to 13,002, significantly above the air value of 0.288 (Ballentine et al. 2002). All of the $^{3}He/^{4}He$ ratios were significantly higher than the crustal $^{3}He/^{4}He$ ratio of 0.02 R_a but also lower than the sub-continental mantle ratio of 6 R_a (Fitton et al. 1991). Using these end-member values, it was possible to calculate the proportion of the He from both crustal and mantle sources using the following formula (from Ballentine et al. (2002)).

$$^{4}He_{crust} = \left(^{4}He_{measured} \times {}^{3}He/^{4}He_{mantle} - {}^{3}He/^{4}He_{measured}\right) / \left(^{3}He/^{4}He_{mantle} - {}^{3}He/^{4}He_{crust}\right) \quad (20)$$

The crustal contribution to ^{4}He in the samples ranged from 94 to 97 % with the remainder originating from the mantle. It was also possible to calculate the crustal contribution to the measured ^{3}He concentration using the known continental crust $^{3}He/^{4}He$ ratio of 0.02 R_a. Only 5–8 % of the total ^{3}He originated from the crust with the remainder from the mantle.

The known range of mantle $CO_2/^{3}He$ ratios was used (1×10^{9} to 1×10^{10}) to calculate the proportion of CO_2 which had originated from both the mantle and crust, knowing the atmosphere contribution to the CO_2 was negligible. An unknown is the crustal $CO_2/^{3}He$ ratio, which is variable (O'Nions and Oxburgh 1988). However, a simple mass balance approach allowed the crustal $CO_2/^{3}He$ ratio to be calculated.

$$^{3}He_{mantle} \times CO_2/^{3}He_{mantle} + {}^{3}He_{crust} \times CO_2/^{3}He_{crust} = 1 \quad (21)$$

The results of these calculations are shown in Table 4. Using a $CO_2/^{3}He$ ratio of 1×10^{9} the crustal contribution of CO_2 is uniformly between 84 and 99 % of the total CO_2. Use of a $CO_2/^{3}He$ ratio of 1×10^{10} gives a wider range of crustal compositions ranging from 0 % for Tenmile Geyser to 98 % for Big Bubbling Spring. Unfortunately from these results, it is not possible to determine if the crustal component was derived from deep crustal reactions, or from aquifer water that had interacted with crustal minerals. The calculated $CO_2/^{3}He$ ratios for the crust ranged from 5.81×10^{10} to 6.53×10^{12},

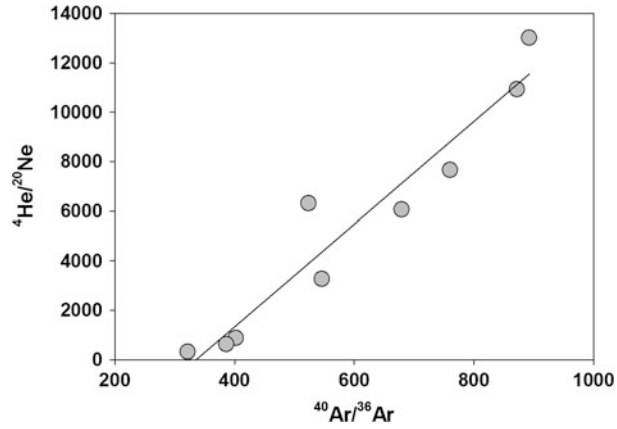

Fig. 20 Plot of $^{4}He/^{20}Ne$ against $^{40}Ar/^{36}Ar$ for the Green River Springs. It is clear that the quantity of dissolved air in the samples is controlling both the $^{40}Ar/^{36}Ar$ and $^{4}He/^{20}Ne$ ratios, with the greatest amount of air in the samples with the lowest ratios

Table 4 Calculated origins of CO_2 erupted at Green River Springs

Sample	Using $CO_2/^3He$ of 1×10^9			Using $CO_2/^3He$ of 1×10^{10}		
	CO_2 origin %		Crust $CO_2/^3He$			Crust $CO_2/^3He$
	Crust	Mantle		Crust	Mantle	
Tumbleweed	98.7	1.3	7.82×10^{11}	86.7	13.3	6.87×10^{11}
Torrey's Spring	96.9	3.1	3.33×10^{11}	68.8	31.2	2.37×10^{11}
Main vent—Crystal Geyser	99.7	0.3	4.88×10^{12}	97.4	2.6	4.77×10^{12}
Side seep—Crystal Geyser	99.5	0.5	2.34×10^{12}	94.6	5.4	2.22×10^{12}
Chaffin Ranch	96.9	3.1	3.45×10^{11}	69.1	30.9	2.46×10^{11}
Small Bubbling Spring	99.6	0.4	3.26×10^{12}	96.2	3.8	3.15×10^{12}
Big Bubbling Spring	99.8	0.20	5.64×10^{12}	98.0	2.0	5.53×10^{12}
Pseudotenmile Geyser	99.7	0.30	6.53×10^{12}	97.0	3.0	6.35×10^{12}
Tenmile Geyser	84.4	15.6	5.81×10^{10}	0	100	–

which are within the range considered by O'Nions and Oxburgh (1988) to be typical of the crust.

In this study noble gas tracers provided substantial constraints on the origins of CO_2 erupted at the Green River Springs, and hence were much more useful than stable isotope data alone. However, due to the lack of measured baseline data on the noble gas composition and CO_2 contents of the different aquifers beneath the springs, noble gases could not provide an unequivocal determination of the origin and transport mechanisms of the CO_2 erupted (Fig. 21).

It was possible to determine that the erupted CO_2 is largely derived from crustal sources, with a 0.2–31 % contribution from the mantle, with the exception of a single spring (Tenmile Geyser) that could be erupting mostly mantle CO_2. This origin for the erupted CO_2 is in contrast to the large, commercially exploited CO_2 accumulations that surround the Colorado Plateau, which are of purely mantle origin. Hence, Wilkinson et al. (2010) were able to determine that the Green River Springs are not derived from these large accumulations. Additionally, they also found that the Green River Springs' noble gases are quite variable in composition,

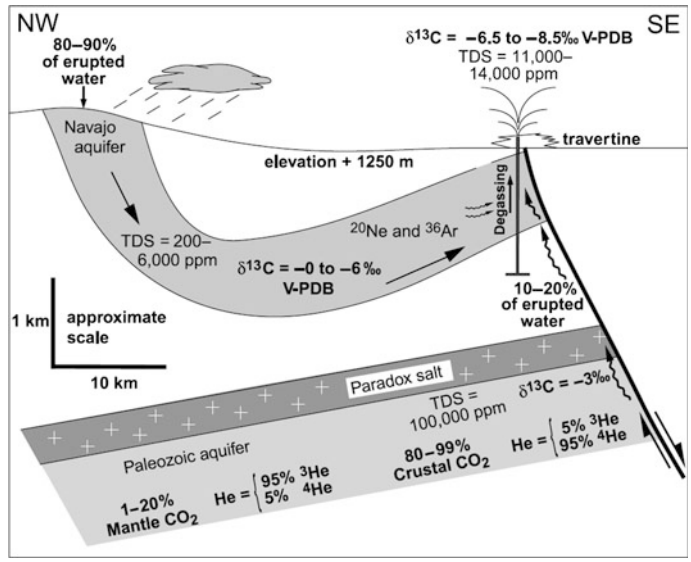

Fig. 21 Cartoon summary of the imagined CO_2 sources beneath the Green River Springs. There is no evidence in the noble gas data for a large subsurface accumulation of free CO_2 (Wilkinson et al. 2010)

arguing against a homogeneous reservoir of free phase CO_2 within the shallow Navajo Aquifer. Nevertheless, they also argue that some ascent of free CO_2 gas must have occurred because the measured surface volumes contained too much CO_2 to have been dissolved in the volume of water erupted at the springs. It is clear from this study that the CO_2 is not derived from a single reaction or source, as had been previously assumed, but is predominantly from crustal diagenetic reactions within the shallow Navajo Aquifer, except for the 1–31 % mantle contribution thought to have originated from the much deeper Paleozoic aquifer.

Whilst the noble gas tracers were not entirely diagnostic of the processes forming the CO_2, with uncertainty still surrounding CO_2 origin and transport mechanisms, the detection of leaks in engineered storage scenarios should be easier as the CO_2 will have a distinctive isotopic composition. Additionally a comprehensive baseline survey will be required at any proposed storage site and with better baseline geochemical data, more would be possible.

7.2 He and Rn in Soil Gases and CO_2 Seeps from the Massif Central, France

An extensive geochemical study of natural CO_2 release at the surface was undertaken by Battani et al. (2010) in Sainte-Marguerite, in the Massif Central region of France. This examined soil gas fluxes and concentrations as well as gas from CO_2 rich bubbling springs. These seeps provide a natural laboratory to study CO_2/fluid/rock interactions and the migration mechanisms of CO_2 migration to the surface. The Sainte-Margurite region is located in the southern part of the Limagne graben and contains many CO_2-rich springs caused extensive natural emissions of CO_2. The springs sampled were associated with two major fault systems dating from the tardi-Hercyian period. The area also contains travertine deposits associated with the CO_2-rich springs.

Soil gas measurements were made over a small area (50 × 100 m) surrounding an ancient thermal bath over two field campaigns in 2006

and 2007. ^{4}He and ^{222}Rn abundance measurements of the soil gases were made in the field and gas samples were also collected for analysis in the laboratory for noble gas abundances, isotopes and $\delta^{13}C$ (CO_2) isotopes. All samples for laboratory analysis were collected using a micro gas chromatograph as a pump to collect gases from depth of 1 m. N_2, Ar and O_2 peaks were monitored during collection to ensure atmospheric gases had been purged from the collection system. Samples of gas were also collected from numerous CO_2 rich bubbling water springs, inferred to be deep gas (Battani et al. 2010).

Measured helium isotopic ratios in the CO_2 exsolving from the bubbling springs ranged from 0.76 to 6.62 R_a. The upper value indicates some samples contain a pure mantle component, given it is above the European Sub Continental Lithopsheric Mantle (SCLM) value of 6 R_a (Gautheron and Moreira 2002) and close to the upper mantle value of 8 R_a (Kurz and Jenkins 1981). Additional evidence of a predominantly mantle origin for the CO_2 came from the measured $\delta^{13}C$ (CO_2) values which were close to −5 %, within the range of mantle derived CO_2 (Marty and Zimmermann 1999). Measured ^{4}He concentrations ranged from 0.12 to 39.12 ppm and somewhat surprisingly the majority of the samples exhibited lower ^{4}He concentrations than the atmospheric value of 5.24 ppm. The low ^{4}He concentrations were particularly unexpected given that the springs emerge from granitic basement which is typically rich in U and Th and hence, as a result of their radioactive decay, also ^{4}He. Battani et al. (2010) argue that this result can only be explained if the fluids migrate rapidly from depth to the atmosphere, and do not interact with crustal fluids. The rapid migration of the CO_2 gas is further confirmed by the observed Ar isotopic fractionation, which is consistent with a Rayleigh type fractionation process. This is illustrated in Fig. 22, which shows that both Ar isotopic ratios ($^{38}Ar/^{36}Ar$ and $^{40}Ar/^{36}Ar$) follow the Mass Fractionation Line (MLF). Such mass fractionated values are a strong indication of a fast migration process which does not allow time for re-equilibration with other fluids. The gas was therefore assumed to travel fast along the deep-rooted faults of the granitic basement.

This is a significantly different scenario to that observed at the Green River Springs in the Colorado Plateau (Sect. 7.1), where the noble gas and $\delta^{13}C$ (CO_2) data indicated that most of the CO_2 was dissolved in water at depth prior to degassing at the surface.

The $\delta^{13}C$ (CO_2) of the soil gas samples ranged between −3 and −5.1 %, slighter heavier than those measured in the CO_2 degassing from the Bubbling Springs, indicating either a crustal or mantle origin of the gas. Battani et al. argued that this was the result of interaction of the gas with the local travertines, which have a $\delta^{13}C$ signature of between 4.4 and 7.4 % (Casanova et al. 1999). Thermal breakdown of travertine would also explain the higher than mantle $CO_2/^{3}He$ ratios which were measured in the gases from some of the bubbling springs. This interaction between soil gas and travertine was consistent with the measured ^{222}Rn activity, as the soil gas samples from above the travertine deposits exhibited higher activities, reaching up to 2×10^{6} Bq/m^{3}. Travertines are between 300 to 10,000 times more enriched in uranium and thorium than typical surface sediments (Casanova et al. 1999). Comparing the soil gases that contained over 50 % by volume of CO_2 with radon activities in excess of 50,000 Bq/m^{3} indicated a strong correlation between the two gases. The enriched Rn activity allowed the authors to identify preferential pathways for migration of gas from depth in the soil gas samples which trended NE-SW aligned to the Allier-river axis, a structure of related to the former opening of the Limagne graben.

The soil gas He concentrations were less diagnostic as both low (less than 5 ppm) or high (over 6 ppm) helium values were exhibited by the samples with high measured high CO_2 concentrations. However, significantly lower than atmosphere values of Ar were measured and this was attributed to the soil gases containing a significant amount of the deep gas flux also found in the bubbling springs. Despite the lack of a clear correlation of high CO_2

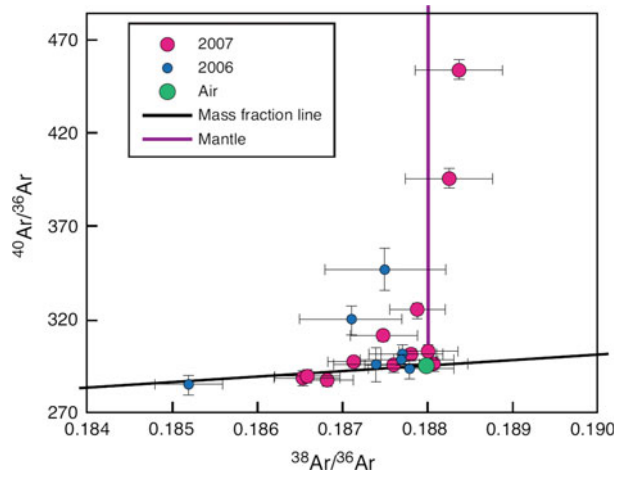

Fig. 22 Plot of $^{40}Ar/^{36}Ar$ against $^{38}Ar/^{36}Ar$ from the CO_2 exsolving from the bubbling springs. This illustrates that the majority of the samples plot along the *black* mass fractionation *black line*. Battani et al. (2010) argued that the increase of some $^{40}Ar/^{36}Ar$ ratios could either be explained by a mantle derived input or the addition of a small component of radiogenic $^{40}Ar^*$. This type of kinetic fractionation is indicative of rapid migration of the fluid

concentrations with He, this study highlighted the role that multiple noble gases (in this case He, Ar and Rn) and C isotopes can play in identifying the migration of CO_2 from depth. It also reinforced the importance of a detailed background geochemical study prior to a storage site being utilised, in order to determine the natural noble gas and C isotope geochemistry which might not be as predicted (i.e lack of ^4He in the deep CO_2 and high natural $^3He/^4He$ as observed in this work).

7.3 He and Ne as Tracers of Natural CO_2 Migration at St. Johns Dome, Arizona, USA

An important aspect of engineered CO_2 storage is the ability to monitor the storage site, and to trace the CO_2 after injection. Future engineered CO_2 storage sites will consist of both the reservoir or saline formation into which the CO_2 is injected, and the overlying suite of rocks above the reservoir or saline formation up to the ground surface. Hence, the overburden will become legally defined as part of the 'storage complex' (EU 2009), and its containment performance needs to be evaluated to ensure that CO_2 can be safely stored over geological timescales. However, it is extremely difficult to unequivocally detect the small releases of anthropogenic CO_2 that could arise from a diffuse leakage of CO_2 from a storage site. This is because there are many natural sources of CO_2 within the crust with overlapping signatures, including breakdown of carbonate minerals or cements, biological activity or hydrocarbon oxidation. Therefore, a more specific and unambiguous method is needed to fingerprint deep-derived CO_2 migration, but it has not yet been understood if fingerprints remain intact during hundreds of metres of migration and diverse interacting geochemical and petrophysical processes.

As an analogue for post-emplacement seepage, Gilfillan et al. (2011) have recently examined natural CO_2 rich springs and groundwater wells in the vicinity of the St. Johns Dome CO_2 reservoir located on the border of Mid-Arizona/New Mexico, USA. Extensive travertine deposits surrounding the CO_2 reservoir highlight a past history of migration of CO_2 rich fluids to the surface. However, there is no evidence that travertine formation is occurring at present and no geysers with gaseous CO_2 are currently found

in the area (Moore et al. 2005). High concentrations of HCO_3^- are common in surface springs, shallow groundwater wells used for irrigation and deeper wells used to obtain cooling water for a coal fired power plant in the region. Previous chemical analysis of these waters implied a possible connection between the formation water within the CO_2 reservoir and the HCO_3^- rich water. This link was not found to be conclusive, due to significant differences in water types (Moore et al. 2005) and the fact that a soil gas survey surrounding these springs and wells was unable to differentiate additional CO_2 flux from that of background biological activity (Allis et al. 2005).

$\delta^{13}C$ measurements have proven to be extremely valuable in tracing CO_2 injected into early CO_2 storage test sites, such as Weyburn (Raistrick et al. 2006). However, in the St. Johns Dome waters there was no clear relationship between the HCO_3^- content of and the $\delta^{13}C_{DIC}$ ratio or sample depth (Fig. 23a). This was in stark contrast to the relationship observed between HCO_3^- concentration and $^3He/^4He$, which showed a distinction between the above air ratios measured in three spring water samples (Willowbank Spring, 24 Bar Ranch and New Mexico Spring—hereafter termed the anomalous springs) and the below air $^3He/^4He$ measured in all of the other samples (Fig. 20b). The above air values in the three springs were attributed to the presence of a small amount of excess ^3He produced by tritium decay, indicating a contribution of recent tritium bearing water. There was also a marked distinction in both the ^3He and ^4He concentrations measured in these three anomalous samples, which were an order of magnitude lower than other water samples (Fig. 23). With the exception of Colorado River Spring, all of the remaining water samples exhibited higher HCO_3^- concentrations which corresponded to lower $^3He/^4He$ ratios (Fig. 23b).

Significantly higher than atmosphere concentrations of ^4He in all of the groundwater wells and majority of surface springs implies the addition of a crustal component that had accumulated radiogenic ^4He. Thus, a portion of the water originated at depth, having circulated in the crust for a significant period of time (Torgersen and Clarke 1985). The ^4He excess was further illustrated by the significantly above air $^4He/^{20}Ne$ measured in all water samples, excluding the similar to air values measured from the three anomalous springs. Figure 24a shows that the low $^3He/^4He$ and high ^4He within the groundwater wells and majority of surface springs (bar the three anomalous springs) could be explained by simple mixing between low $^3He/^4He$ and high ^4He values measured in Wells 10–22 and 22–1X and varying percentages of shallow groundwater (high $^3He/^4He$ with low ^4He concentrations). This clearly illustrated that the excess ^4He fingerprint entrained at depth was retained after migration of the waters to the surface.

As with ^4He, the low $^3He/^4He$ and corresponding high ^3He values within the deep groundwater wells and most surface springs, could be explained by simple mixing between water from Wells 10–22 and 22–1X and air (Fig. 24b). This clearly indicated that all of the waters rich in ^3He must have interacted to some degree with the magmatic CO_2 in the deep reservoir. Furthermore, the fingerprint of high ^3He from magmatic origin, exhibited by the deep CO_2 wells, although diluted, was also retained during transport of water and CO_2 to the surface.

All of the sampled waters, bar the three anomalous air-like springs, exhibited $CO_2/^3He$ ratios which were extremely similar to the range observed in the three deep CO_2 wells (Fig. 25a and b). These results further reinforce the observation that all of the water samples, except for the anomalous springs, contained CO_2 of magmatic origin, which had originated from the CO_2 reservoir. The higher $CO_2/^3He$ ratios observed in the three anomalous springs indicated that they contained CO_2 with less ^3He content compared to that of the deep reservoir, providing further evidence that the anomalous springs contain additional CO_2 from a different source. Several samples exhibited ratios below the lowest observed CO_2 well value of 9.75×10^7, which implied that some of the CO_2 component had been lost relative to ^3He.

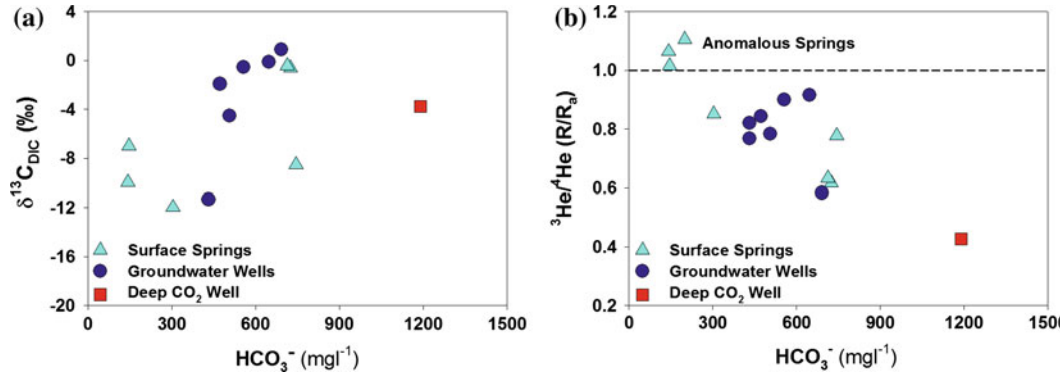

Fig. 23 **a** $\delta^{13}C_{DIC}$ variation plotted against HCO_3^- concentrations for the surface springs, groundwater and CO_2 well sampled at St. Johns. There is no clear relationship between the HCO_3^- concentration of the water and $\delta^{13}C$ or the sample type. **b** $^3He/^4He$ ratios plotted against HCO_3^- concentrations for the surface springs, groundwater and CO_2 well sampled at St. Johns. Values obtained from groundwater wells cluster above $^3He/^4He = 1$, equating to air. A clear correlation exists between increasing HCO_3^- concentrations and decreasing $^3He/^4He$, trending toward the values measured in the deep CO_2 reservoir. A clear distinction existed between the above air $^3He/^4He$ ratios measured in three anomalous spring water samples; Willowbank Spring, 24 Bar Ranch and New Mexico Spring and the other water samples

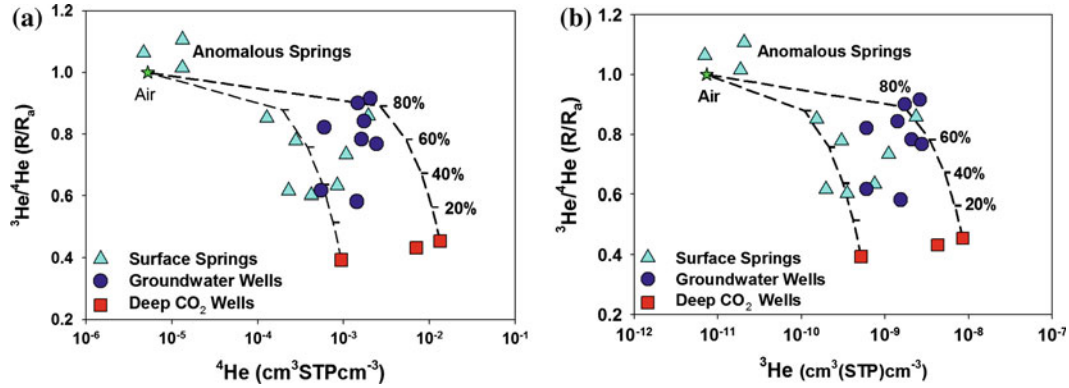

Fig. 24 **a** ^4He plotted against $^3He/^4He$ for the St. Johns waters. *Mixing lines* are plotted from the different compositions of deep groundwater measured from the end member CO_2 wells to 100 % air. The low $^3He/^4He$ and high ^4He within the groundwater wells and majority of surface springs can be explained by simple mixing between the $^3He/^4He$ and ^4He values measured in Wells 10–22 and 22–1X and varying amounts of air (with the per cent air indicated on *tick marks*). This proved that the excess ^4He component entrained at depth was retained and not lost on migration of the waters to the surface. **b** ^3He plotted against $^3He/^4He$ for the St. Johns water samples. As with ^4He, high ^3He concentrations and low $^3He/^4He$ ratios were observed in groundwater wells and majority of the surface springs. These can also be accounted for by the mixing of waters from wells 10–22 and 22–1X and varying amounts of air. This shows that the whilst the high magmatic ^3He signature exhibited by the deep CO_2 wells, although diluted, was retained and not lost as a result of transport water to the surface

Gilfillan et al. (2011) also documented a clear relationship between $CO_2/^3He$ reduction and increases in both ^{20}Ne and especially ^4He (Fig. 25) within the St. Johns water samples. As previously outlined in this chapter, similar relationships have been observed in numerous CO_2 reservoirs around the world (Gilfillan et al. 2009; Sherwood Lollar and Ballentine 2009). Whilst there are means by which crustal CO_2 ($CO_2/^3He > 10^{10}$) could be added to an initial

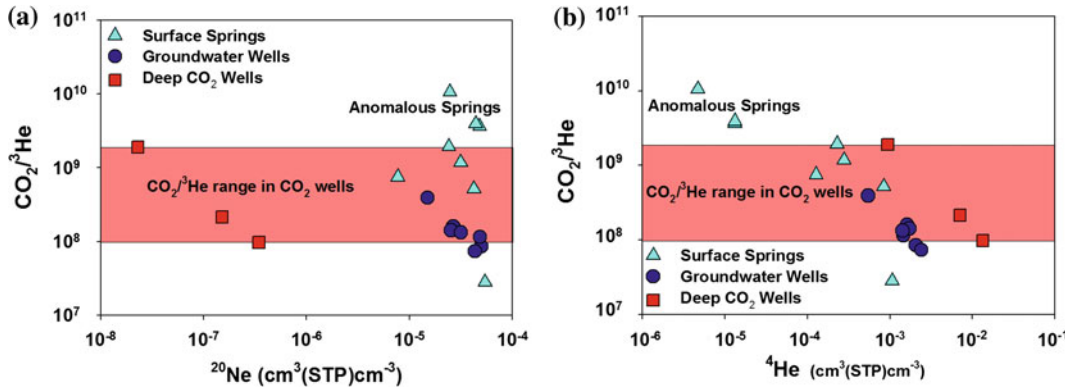

Fig. 25 **a** $CO_2/^3He$ variation plotted against ^{20}Ne for the St. Johns water samples. All of the groundwater springs and the majority of the surface springs exhibit $CO_2/^3He$ ratios which are extremely similar to those measured in the deep CO_2 wells, so implying that they contain dissolved CO_2 which migrated from the CO_2 reservoir. A clear trend of decreasing $CO_2/^3He$ with increasing ^{20}Ne existed in all of the data. As ^3He is a conservative tracer, reduction of $CO_2/^3He$ can only be explained by a reduction of the CO_2 component. As the groundwater is the main source of ^{20}Ne, this CO_2 reduction must be linked to contact with the groundwater. **b** $CO_2/^3He$ variation plotted against ^4He for the St. Johns samples. A clear reduction in the $CO_2/^3He$ ratio corresponds to an increase in ^4He. This can be explained by the mixing of ^4He, which has accumulated in the deep formation water, with the younger shallow groundwater and then migrating from the reservoir, along with dissolved CO_2. This trend is identical to that observed in natural CO_2 reservoirs from around the world (see Fig. 9)

mantle rich CO_2 accumulation (Bradshaw et al. 2004; Cathles and Schoell 2007), there is no plausible mechanism that would allow crustal CO_2 to be added whilst preserving the correlation between $CO_2/^3He$ reduction and increases in noble gases derived from the groundwater. Hence, the changes in $CO_2/^3He$ must be due to CO_2 loss in the subsurface by an amount directly related to the quantity of groundwater that the CO_2 has contacted. As CO_2 is soluble and reactive, the most probable mechanisms of subsurface CO_2 fluid phase removal are dissolution of the CO_2 into the groundwater and/or mineral trapping (Baines and Worden 2004b; Bradshaw et al. 2004). As previously highlighted earlier in this chapter it has been possible in some natural CO_2 reservoirs to distinguish between proportions of CO_2 that were dissolving into the formation water and those which were precipitating as carbonate minerals (Gilfillan et al. 2009). However, due to the lack of any correlation between the $\delta^{13}C$ and $CO_2/^3He$ this was not possible within the St Johns water samples.

The results of this study illustrate that the He and Ne concentrations and $^3He/^4He$ and $CO_2/^3He$ ratios provide characteristic fingerprints, which could be identified in all of the groundwater wells and all but three of the surface springs. The simplest explanation is that the groundwater wells sampled shallow well and spring waters containing noble gases together with magmatic CO_2 derived from the deep reservoir. In this model, the high concentrations of HCO_3^- present in the sampled waters are then the direct result of the migration of dissolved CO_2 from the deep reservoir, illustrating for the first time that CO_2 can be fingerprinted from source to surface using noble gases, particularly He. This paves the way for the use of similar techniques to identify dissolved CO_2 migration from future engineered storage sites.

7.4 Noble Gas Investigation of Alleged CO_2 Leakage at Weyburn

In January 2011 it was extensively reported that the Kerr family had been forced to move from their property located above the Weyburn-Midale Monitoring and Storage Project in Saskatchewan,

Canada. A geochemical consultant from Petro-Find GeoChem Ltd., who was hired on behalf of the Kerr's, reported measurements of $\delta^{13}C$ (CO_2) isotope values in soil gases rich in CO_2 which were similar to those of the CO_2 injected into the deep oil reservoir (Lafleur 2010). The Petroleum Technology Research Centre (PTRC), who are responsible for the environmental monitoring of the Weyburn CO_2-EOR and storage operation, published a detailed response correctly stating that Petrofind had not taken the similar baseline $\delta^{13}C$ (CO_2) isotope measurements conducted prior to the injection into account (Petroleum Technology Research Centre 2011). Also as $\delta^{13}C$ (CO_2) is not a unique tracer, there were several other natural sources that could account for the measured values. Whilst this response went some way to addressing the public perception fears raised by the alleged CO_2 leakage claims, it was clear that more research was required to re-establish confidence in the safety and security of CO_2 stored at Weyburn. This was imperative for both the project itself and the future acceptance of the safety and security of CO_2 storage technologies. The International Performance Centre for Geologic Storage of CO_2 (IPAC-CO_2) undertook a detailed independent incident response protocol focused on the near surface soil gases, the noble gas composition of the shallow groundwaters and a hydrogeological analysis. In the following section we summarise the findings of the noble gas investigation.

In order to determine if migration of dissolved CO_2 from the Weyburn oil field was responsible for the alleged CO_2 anomaly, Gilfillan and Haszeldine (2011) completed noble gas measurements on water samples collected from four groundwater wells surrounding the Kerr quarter, near Goodwater in Saskatchewan. These were compared to the noble gas composition measured from fluids obtained from a production well and CO_2 and water obtained from two separate injection wells on the Weyburn-Midale oil field, located near to the Kerr quarter. The aim of the work was to test the hypothesis that migration of dissolved CO_2, originating from either the free phase CO_2 or water injected into the Weyburn-Midale oil field or from CO_2 contained in the produced fluids, was responsible for the CO_2 anomaly reported at the surface. This focused on dissolved CO_2 in the groundwaters as no free phase CO_2 was present in the sampled well waters and as recent research has shown that the sensitivity of He as a tracer is two orders of magnitude greater in groundwaters than in soil gases (Mackintosh and Ballentine 2012).

Gilfillan and Haszeldine (2011) found that the measured $^4He/^{20}Ne$ ratios in the injected CO_2 and produced fluid samples were significantly above the calculated air saturated water range of 0.250 to 0.296 (Fig. 26). This indicated that atmospheric He input to these samples was minimal. The injected water $^4He/^{20}Ne$ ratio of 1.42 implied that there was a small amount of atmospheric He input in this sample. However, this was considerably above the range of 0.248 to 0.403 observed in the groundwater samples. This overlapped with the air saturated water range (assuming a 0–50 % excess air component and a re-equilibration temperature range on 10 to 25 °C) and indicated that almost the entire of the ^4He dissolved in the groundwaters was of atmospheric origin.

Similarly, there was a distinct difference in $^3He/^4He$ ratios in the different sample types, with the lowest values of 0.173 and 0.179 R_a measured in the produced CO_2 from the Weyburn field (Fig. 26). The injected CO_2 had a similar, albeit slightly higher ratio of 0.193 R_a, with the injected water sample ratio being higher again at 0.295 R_a. The range observed in the groundwater samples of 0.897 to 1.103 R_a was significantly above the ratios observed in the produced fluids, injected water and CO_2 samples, consistent with the $^4He/^{20}Ne$ ratios in indicating that almost the entire of the ^4He in the groundwater samples originated from the atmosphere.

^4He and ^{40}Ar concentrations also exhibited marked distinctions depending on sample type (Fig. 27). The lowest ^4He concentrations were those calculated for water equilibrated with the injected CO_2. The groundwater samples exhibited a measured range of ^4He which was similar to the calculated air saturated water concentration range. This clearly showed that there was no

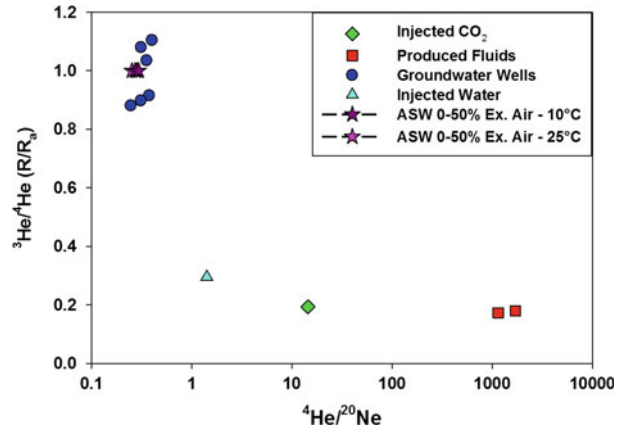

Fig. 26 $^3He/^4He$ ratios plotted against $^4He/^{20}Ne$ ratios. The produced CO_2 and injected CO_2 exhibited ratios well in excess of the air saturated water values. The groundwater wells were extremely close to the air saturated water (ASW) ratio range indicating that almost all of the ^4He they contain is of atmospheric origin (Gilfillan and Haszeldine 2011)

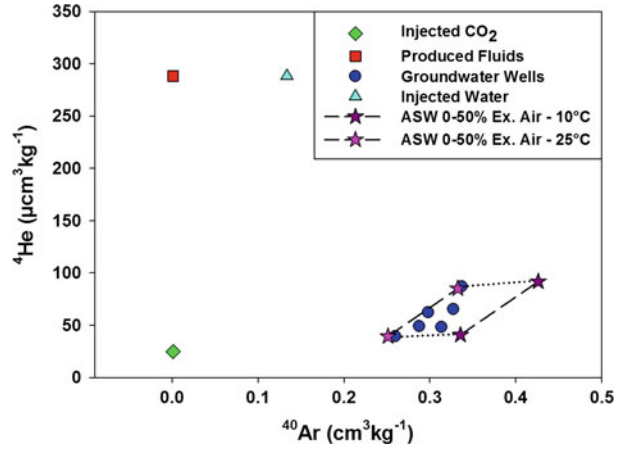

Fig. 27 ^4He concentration plotted against ^{40}Ar concentration. All of the groundwater samples plot within the air saturated water (ASW) concentrations indicating that there is no input of crustal ^4He and the ^{40}Ar is entirely derived from the atmosphere. The lower ASW concentrations are those with no excess air component and the higher values are those with a 50 % excess air component

significant addition of ^4He to the groundwater samples. Measured ^4He concentrations in the injected water were an order of magnitude higher, with the calculated ^4He concentration of water in equilibrium with the produced fluid samples being over another order of magnitude higher still. As with ^4He the lowest ^{40}Ar concentration was that calculated for water in equilibrium with the injected CO_2 under reservoir conditions (Fig. 27). The next highest were those calculated for water in contact with the produced fluids from the Weyburn field with the injected water having an order of magnitude higher ^{40}Ar concentration. The highest concentrations were those observed in the groundwater wells which were within the calculated air saturated water range.

Both ^{20}Ne and ^{36}Ar concentrations exhibited extremely similar concentration groups to ^{40}Ar, with the lowest observed in the calculated water

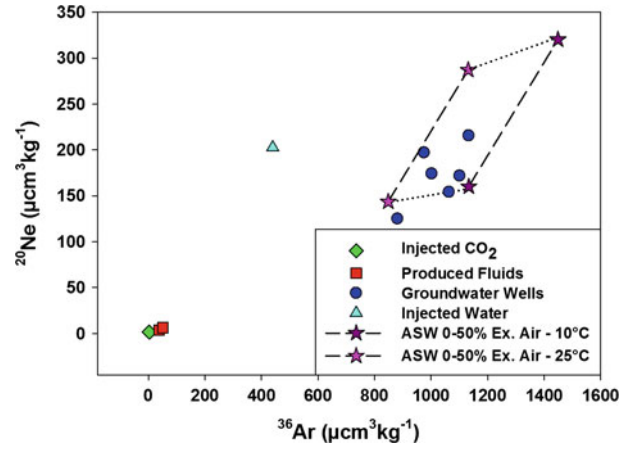

Fig. 28 ^{20}Ne concentrations plotted against ^{36}Ar concentrations. There is a pronounced difference in concentrations between the produced fluids and injected CO_2, the injected water and the groundwater samples. All but one of the groundwater samples can be explained by the calculated air saturated water concentration range, indicating that all of the ^{20}Ne and ^{36}Ar in the waters is atmosphere derived

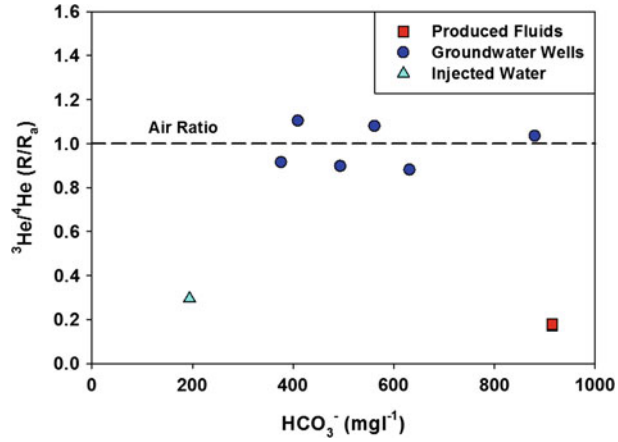

Fig. 29 ^{3}He/^{4}He ratios plotted against HCO_3^- concentrations in the produced reservoir fluids, groundwater wells and water injected into the reservoir surrounding the Kerr quarter. The *black dash line* indicates the air ^{3}He/^{4}He value of 1R$_a$. All of the groundwater wells have ^{3}He/^{4}He ratios which are close to the air ratio and exhibit no relationship between HCO_3^- concentrations and the ^{3}He/^{4}He ratio

concentration equilibrated with the injected CO_2 and highest being those observed in the groundwater wells (Fig. 28). As ^{20}Ne and ^{36}Ar are primarily derived from the atmosphere, this reinforced that the groundwater samples contained only atmospheric noble gases.

Gilfillan and Haszeldine (2011) observed no relationship between the ^{3}He/^{4}He ratio and HCO_3^- concentrations measured in the groundwaters from the Kerr site (Fig. 29). This is in stark contrast to the systematic relationship observed between HCO_3^- concentration and ^{3}He/^{4}He ratios in the St. Johns surface springs and groundwater wells (Sect. 7.3 and Fig. 23b). In the St. Johns Dome dataset there was a clear link between shallow samples and deep sources of CO_2 and He (Gilfillan et al. 2011). The majority of the St. Johns water samples

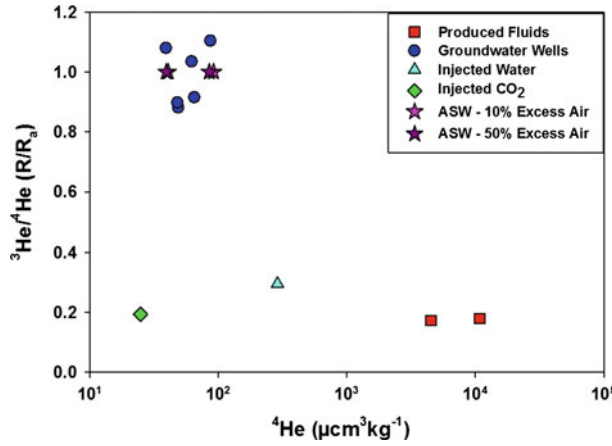

Fig. 30 $^{3}He/^{4}He$ plotted against ^{4}He concentrations in the produced reservoir fluids, groundwater wells and water injected into the reservoir surrounding the Kerr quarter. It is readily apparent that all of the groundwater samples exhibit ^{4}He concentrations which are within the air saturated water concentrations and there is no correlation to the either the injected water, injected CO_2 or produced fluids from the Weyburn oil field

exhibited higher HCO_3^- concentrations which corresponded to lower $^{3}He/^{4}He$ ratios and showed a clear trend towards the lower $^{3}He/^{4}He$ and higher HCO_3^- concentrations recorded in the deep CO_2 well water. In the Kerr groundwaters increased HCO_3^-, indicating increasing concentrations of dissolved CO_2 did not result in any variation in the air like $^{3}He/^{4}He$ ratios.

There was also no relationship observed between $^{3}He/^{4}He$ ratios and the concentration of ^{4}He in the Kerr groundwaters. This strongly implied that there is no addition of deep crustal ^{4}He to the sampled waters surrounding the Kerr quarter and indicates that there was no migration of fluids from depth into the sampled wells. This was again in contrast to the clear relationship between decreasing $^{3}He/^{4}He$ and increasing ^{4}He concentrations observed in the St. Johns groundwaters (Fig. 24a).

In summary, all of the noble gas concentrations and the majority of noble gas ratios measured in the groundwaters from wells surrounding the Kerr quarter were within or very close to the air saturated values. Gilfillan and Haszeldine (2011) found no evidence in any of the noble gas data that there was any presence of deep crustal derived noble gases within the groundwaters surrounding the Kerr quarter. Hence, they found no evidence of the migration of deep CO_2 from the Weyburn oil field into the groundwater on the Kerr quarter or the surrounding area (Fig. 30).

8 Summary and Future Work

Studies of noble gases in natural CO_2 storage analogues have proven to be extremely useful in establishing the viability of geological CO_2 storage. Noble gas data has shown that it is possible to store CO_2 for significant periods of time (up to 40 million years in the case of one reservoir). Measurements of noble gases and carbon stable isotopes have also permitted the identification of the main CO_2 storage processes that act in natural CO_2 reservoirs over geological timescales providing important lessons for engineered storage. These data indicate that the dominant mechanism of CO_2 loss is through dissolution of CO_2 into the formation water within a narrow pH window (pH = 5–5.8). Precipitation of carbonate minerals is only a minor sink, accounting for a maximum of 18 % of CO_2 loss in one of the CO_2 reservoirs.

For CO_2 storage technology to be universally deployed, it is essential that a robust, reliable and inexpensive means to trace the migration of CO_2 within the subsurface exists. Monitoring

during injection will increase confidence that the site characteristics were correctly determined and met. Furthermore, should migration and subsequent surface leakage occur, the ability to track origin and ownership of CO_2 at near and ground surface will be critical for remediation purposes. However, one of the key necessities of any monitoring program will be the detection of any migration, however small, of CO_2 from the storage site. The main problem in detecting migration is the large variation in CO_2 concentrations within the Earth's crust. This makes unequivocally determining if detected small quantities of CO_2 are the result of migration of CO_2 from a storage site extremely difficult. The use of tracers is the main technique that could be used to accurately determine if migration of CO_2 from a storage site has occurred.

Noble gases are chemically inert, persistent and environmentally safe—and possess significant potential as tracers of CO_2 migration within future storage sites. Their ability to trace CO_2 migration within a reservoir is illustrated by the study undertaken at the Mabee EOR field (Sect. 6.1). They have the potential to be extremely useful in tracing migration of CO_2 once it has migrated outside a reservoir as highlighted by the St. Johns Springs and Green River studies (Sects. 7.2 and 7.3), and also can play an important role in investigations of alleged leakage, as outlined by the Weyburn investigation (Sect. 7.4). Hence, there is enormous promise in the use of noble gases to monitor for any leakage of CO_2 or CO_2 rich groundwater from an engineered storage site and so provide a means of reassurance of the security of the storage site. This promise will only be fulfilled if more studies similar to those highlighted in this chapter are undertaken. It is imperative that the many upcoming pilot CO_2 injection studies continue to investigate the behaviour of noble gases in the subsurface and develop suitable noble gas monitoring strategies.

Whilst the aspirations for future CO_2 emissions reduction are in increasing energy efficiency and in developing alternative and renewable energy technologies, these cannot fulfil our current demands for energy. The amount of time that it will take to develop these technologies, and the fact that there are still plentiful supplies of fossil fuels in developing countries, means their combustion will remain the main source of global energy for a considerable time to come. Capturing and storing the CO_2 produced by fossil fuel combustion can drastically reduce CO_2 emissions and this technology can be operational very soon, given the right support. The lessons learned from noble gas studies show that CO_2 can be safely stored on geological timescales and that any migration from a storage site could be detected. CCS has the potential to act as a 'bridge technology' significantly reducing emissions whilst other low carbon energy technologies are developed and deployed. The fossil fuel power plants will be built anyway, as the world needs a reliable economic source of energy. Therefore, the only question to be answered is whether we are willing to build the bridge to capture and store CO_2 emissions from these plants, or prepare to face the climate change consequences.

References

Allis R, Bergfeld D, Moore J, McClure K, MorganC, Chidsey T, Heath JE, McPherson B (2005) Implications of results from CO_2 flux surveys over known CO_2 systems for long-term monitoring.In: Fourth annual conference on carbon capture and sequestration, DOE/NETL, 2–5 May 2005

Allis R, Chidsey T, GwynnW, Morgan C, White S, Adams M, Moore J (2001) Natural CO_2 reservoirs on the colorado plateau and southern rocky mountains: candidates for CO_2 sequestration. DOE/NETL: 1st National conference of carbon sequestration. Procedings Volume

Baines SJ, Worden RH (2004a) Geological storage of carbon dioxide. In: Baines SJ, Worden RH (eds) Geological storage of carbon dioxide. The Geological Society of London, London, pp 1–6

Baines SJ, Worden RH (2004b) The long term fate of CO_2 in the subsurface: natural analogues for CO_2 storage. In: Bains SJ, Worden RH (eds) Geological storage of carbon dioxide. Geological Society, London, pp 59–85

Ballentine CJ, O'Nions RK, Coleman CL (1996) A magnus opus: helium, neon and argon isotopes in a North Sea oilfield. Geochimica Cosmochim Acta 60:831–849

Ballentine CJ (1997) Resolving the mantle He/Ne and crustal 21-Ne/22-Ne in well gases. Earth Planet Sci Lett 152:233–249

Ballentine CJ, Schoell M, Coleman D, Cain BA (2001) 300-Myr-old magmatic CO_2 in natural gas reservoirs of the west Texas Permian basin. Nature 409:327–331

Ballentine CJ, Burgess R, MartyB (2002) Tracing fluid origin, transport and interaction in the crust. In: Porcelli DR, Ballentine CJ, Weiler R (eds) Noble gases in geochemistry and cosmochemistry, pp 539–614

Ballentine CJ, BurnardPG (2002) Production, release and transport of noble gases in the continental crust. In: Porcelli DR, BallentineCJ, Weiler R (eds) Noble gases in geochemistry and cosmochemistry, pp 481–538

Ballentine CJ, Marty B, Lollar BS, Cassidy M (2005) Neon isotopes constrain convection and volatile origin in the Earth's mantle. Nature 433:33–38

Battani A, Deville E, Faure JL, Jeandel E, Noirez S, Tocqué E, Benoît Y, Schmitz J, Parlouar D, Sarda P, Gal F, Le Pierres K, Brach M, Braibant G, Beny C, Pokryszka Z, Charmoille A, Bentivegna G, Pironon J, de Donato P, Garnier C, Cailteau C, Barrès O, Radilla G, Bauer A (2010) Geochemical study of natural CO_2 emissions in the French Massif Central: how to predict origin, processes and evolution of CO_2 leakage. Oil Gas Sci Technol: Rev IFP 65(4):615–633

Battani A, Sarda P, Prinzhofer A (2000) Basin scale natural gas source, migration and trapping traced by noble gases and major elements: the Pakistan Indus basin. Earth Planet Sci Lett 181(1–2):229–249

Becker J (2005) Quantification of Himalayan Metamorphic CO2 fluxes: impact on global carbon budgets. PhD thesis, University of Cambridge, Cambridge. UK

Bosch A, Mazor E (1988) Natural-gas association with water and oil as depicted by atmodspheric Noble Gases—Case studies from the southeastern mediterranean coastal-plain. Earth Planet Sci Lett 87(3): 338–346

Bradshaw J, Boreham C, La Pedalina F (2004) Storage retention time of CO_2 in sedimentary basins; examples from petroleum systems. In: Rubin E, Keith D, Brewer PG, Friederich G, Peltzer ET, Orr FM Jr (1999) Direct experiments on the Ocean disposal of fossil fuel CO_2. Science 284:943–945

Brewer PG, Friederich G, Peltzer ET, Orr FM Jr (1999) Direct experiments on the Ocean disposal of fossil fuel CO2. Science 284(5416):943–945. doi: 10.1126/science.284.5416.943

Broadhead RF (1998) Natural accumulations of carbon dioxide in the New Mexico region—Where are they, how do they occur and what are the uses for CO2? Lite Geol 20:2–6

Brohan P, Kennedy JJ, Harris I, Tett SFB, Jones PD (2006) Uncertainty estimates in regional and global observed temperature changes: a new data set from 1850. J Geophys Res 111(D12):D12106 doi: 10.1029/2005jd006548

Burnard P, Graham D, Turner G (1997) Vesicle-specific noble gas analyses of "Popping Rock": implications for primordial Noble Gases in Earth. Science 276:568–570

Burnard PG, Graham DW, Farley KA (2002) Mechanisms of magmatic gas loss along the Southeast Indian Ridge and the Amsterdam -St. Paul Plateau. Earth Planet Sci Lett 203:131

Casanova J, Bodénan F, Négrel P, Azaroual M (1999) Microbial control on the precipitation of modern ferrihydrite and carbonate deposits from the Cézallier hydrothermal springs (Massif Central, France). Sed Geol 126(1–4):125–145. doi:10.1016/s0037-0738(99)00036-6

Castro MC, Goblet P (2003) Calibration of regional groundwater flow models: working toward a better understanding of site-specific systems. Water Resouces Res 39:1172

Castro MC, Goblet P, Ledoux E, Violette S, de Marsily G (1998) Noble gases as natural tracers of water circulation in the Paris Basin 2. Calibration of a groundwater flow model using noble gas isotope data. Water Resouces Res 34:2467–2483

Cathles LM, Schoell M (2007) Modeling CO_2 generation, migration and titration in sedimentary basins. Geofluids 7:441–450

Craig H, Lupton JE, Horibe Y (1978) A mantle helium component in circum Pacific volcanic gases. In: Alexander EC, Ozima M (eds) Terrestrial rare gases. Japan Science Societies Press, Tokyo, pp 3–16

Deines P, Langmuir D, Harmon RS (1974) Stable carbon isotopes and the existence of a gas phase in the evolution of carbonate groundwaters. Geochim Cosmochim Acta 38:1147–1184

Drescher J, Kirsten T, Schafer K (1998) The rare gas inventory of the continental crust, recovered by the KTB continental deep drilling project. Earth Planet Sci Lett 119:271–281

EU (2009) Directive 2009/31/EC of the European Parliament and of the Council on the geological storage of carbon dioxide. Official J Eur Union L140:114–136

Fanale FP, Cannon WA (1971) Physical adsorption of rare gases on terrigenous sediments. Earth Planet Sci Lett 11:362–368

Farley KA, Craig H (1994) Atmospheric argon contamination of ocean island basalt olivine phenocrysts. Geochim Cosmochim Acta 58:2509–2517

Fitton JG, James D, Leeman WP (1991) Basic magmatism associated with late cenozoic extension in the Western United-States—Compositional variations in space and time. J Geophys Res Solid Earth Planet 96(B8):13693–13711

Fontes J-Ch, Andrews JN, Walgenwitz F (1991) Évaluation de la production naturelle in situ d'argon-36 via le chlore-36: implications géochimiques et géochronologiques. C. R. Acad. 856 Paris 313, Série II, pp 649–654

Gautheron C, Moreira M (2002) Helium signature of the subcontinental lithospheric mantle. Earth Planet Sci Lett 199(1–2):39

Gilfillan SMV, Ballentine CJ, Holland G, Sherwood Lollar B, Stevens S, Schoell M, Cassidy M (2008) The noble gas geochemistry of natural CO_2 gas reservoirs from the Colorado Plateau and Rocky Mountain provinces, USA. Geochim Cosmochim Acta 72:1174–1198

Gilfillan SMV, Lollar BS, Holland G, Blagburn D, Stevens S, Schoell M, Cassidy M, Ding Z, Zhou Z, Lacrampe-Couloume G, Ballentine CJ (2009) Solubility trapping in formation water as dominant CO_2 sink in natural gas fields. Nature 458:614–618

Gilfillan SMV, Wilkinson M, Haszeldine RS, Shipton ZK, Nelson ST, Poreda RJ (2011) He and Ne as tracers of natural CO_2 migration up a fault from a deep reservoir. Int J Greenhouse Gas Control 5(6):1507–1516. doi:10.1016/j.ijggc.2011.08.008

Gilfillan SMV, Haszeldine RS 2011 Report of noble gas, carbon stable isotope and HCO3- measurements from the Kerr Quarter and surrounding area, Goodwater, Saskatchewan. In: Sherk GW (ed) The Kerr investigation: final report, vol. IPAC-CO_2 Research Inc, Regina

Goldberg DS, Takahashi T, Slagle AL (2008) Carbon dioxide sequestration in deep-sea basalt. Proc Nat Acad Sci 105:9920–9925

Graham D (2002) Noble gas isotope geochemistry of Mid-Ocean Ridge and Ocean Island Basalt: characterization of mantle source reservoirs. In: Porcelli D, Ballentine CJ, Wieler R (eds) Noble gases in geochemistry and cosmochemistry 47:247–317

Haszeldine RS (2009) Carbon capture and storage: how green can black be? Science 325:1647–1652

Heath JE (2004) Hydrogeochemical characterization of CO_2 charged fault zones: the Little Grand Wash and Salt Wash fault zones, Emery and Grand counties, Utah. PhD thesis Utah State University, Logan

Hilton D, Fischer T, Marty B (2002) Noble gases and volitile recycling at subduction zones. In: Porcelli DR, Ballentine CJ, Weiler R (eds) Noble gases in geochemistry and cosmochemistry 47:319–370

Hiyagon H, Kennedy BM (1992) Noble gases in CH_4-rich gas fields, Alberta, Canada. Geochimica Cosmochimica Acta 56:1569–1589

Holland G, Ballentine CJ (2006) Seawater subduction controls the heavy noble gas composition of the mantle. Nature 441(7090):186–191

Holland G, Cassidy M, Ballentine CJ (2009) Meteorite Kr in Earth's mantle suggests a late accretionary source for the atmosphere. Science 326:1522–1525

House KZ, Schrag DP, Harvey CF, Lackner KS (2006) Permanent carbon dioxide storage in deep-sea sediments. Proc Nat Acad Sci 103:12291–12295

IEA (2009) Technology roadmap: carbon capture and storage, Paris, p. www.iea.org

IPCC (2005) IPCC special report on carbon dioxide capture and storage. Cambridge University Press, Cambridge

IPCC (2007) Climate change 2007: synthesis report. Contribution of working groups I, II and III to the fourth assessment: report of the intergovernmental panel on climate change. IPCC, Geneva, Switzerland

Javoy M, Pineau F, Delorme H (1986) Carbon and nitrogen isotopes in the mantle. Chem Geol 57:41–62

Jenden PD, Hilton DR, Kaplan IR, Craig H (1993) Abiogenic hydrocarbons in and mantle helium in oil and gas fields. In: Howell DG (ed) The future of energy gases, U.S. Geological Survey Professional Paper 1570. U.S. Geological Survey, pp 31–56

Kennedy BM, Hiyagon H, Reynolds JH (1990) Crustal neon—A striking uniformity. Earth Planet Sci Lett 98:277–286

Kennedy BM, Torgersen T, van Soest MC (2002) Multiple atmospheric noble gas components in hydrocarbon reservoirs: a study of the Northwest Shelf, Delaware Basin, SE New Mexico. Geochim Cosmochim Acta 66:2807–2822

Kharaka YK, Cole DR, Hovorka SD, Gunter WD, Knauss KG, Freifeld BM (2006) Gas-water-rock interactions in Frio Formation following CO_2 injection: implications for the storage of greenhouse gases in sedimentary basins. Geology 34:577–580

Kipfer R, Aeschbach-Gertig W, Peeters F, StuteM (2002) Noble gases in lakes and groundwaters, noble gases in geochemistry and cosmochemistry, pp 615–700

Klara SM, Srivastava RD, McIlvried HG (2003) Integrated collaborative technology, development program for CO_2 sequestration in geologic formations—United States Department of Energy R&D. Energy Convers Manage 44:2699–2712

Kurz MD, Jenkins WJ (1981) The distribution of helium in oceanic basalt glasses. Earth Planet Sci Lett 53(1):41–54. doi:10.1016/0012-821x(81)90024-8

Lafleur P (2010) Geochemical Soil Gas Survey—a site investigation of SW30-5-13-W2 M, Weyburn Field, Saskatchewan. Petro-Find Geochem Ltd, Saskatoon

Mackintosh SJ, Ballentine CJ (2012) Using 3He/4He isotope ratios to identify the source of deep reservoir contributions to shallow fluids and soil gas. Chem Geol 304–305:142–150. doi:10.1016/j.chemgeo.2012.02.006

Marland G, Boden TA, Andres RJ (2008) Global, regional, and national fossil fuel CO_2 emissions, trends: a compendium of data on global change. Carbon Dioxide Information Analysis Center, Oak Ridge National Laboratory, U.S. Department of Energy, Oak Ridge, Tenn., USA

Marland G, Schlamadinger B (1999) The Kyoto Protocol could make a difference for the optimal forest-based CO_2 mitigation strategy: some results from GORCAM. Environ Sci Policy 2:111–124

Marty B, Jambon A (1987) $C/^3He$ in volatile fluxes from the solid Earth: implications for carbon geodynamics. Earth Planet Sci Lett 83:16–26

Marty B, O'Nions RK, Oxburgh ER, Martel D, Lombardi S (1992) Helium isotopes in alpine regions. Tectonophysics 206:71–78

Marty B, Zimmermann L (1999) Volatiles (He, C, N, Ar) in mid-ocean ridge basalts: assesment of shallow-level fractionation and characterization of source composition. Geochim Cosmochim Acta 63(21):3619–3633. doi:10.1016/s0016-7037(99)00169-6

Maughan EK (1988) Geology and petroleum potential, Colorado Park Basin Province, North-Central Colorado. US Geological Survey Open-File Report 88-450 E

Mazor E (1972) Paleotemperatures ans other hydrological parameters deduced from noble gases dissolved in groundwater, Jordan Rift Valley, Israel. Geochimica Cosmochimica Acta 36:1321–1326

Moore J, Adams M, Allis R, Lutz S, Rauzi S (2005) Mineralogical and geochemical consequences of the long-term presence of CO_2 in natural reservoirs: an example from the Springerville-St. Johns Field, Arizona, and New Mexico, USA. Chem Geol 217:365

Moreira M, Kunz J, Allegre C (1998) Rare gas systematics in popping rock: isotopic and elemental compositions in the Upper Mantle. Science 279:1178–1181

Nimz GJ, Hudson GB (2005) The use of noble gas isotopes for monitoring leakage of geologically stored CO_2. In: Thomas DC, Benson SM (eds) Carbon dioxide capture for storage in deep geologic formations. Elsevier, Amsterdam, pp 1113–1128

O'Nions RK, Oxburgh ER (1988) Helium, volatile fluxes and the development of continental crust. Earth Planet Sci Lett 90(3):331–347

Oxburgh ER, O'Nions RK, Hill RI (1986) Helium isotopes in sedimentary basins. Nature 324:632–635

Ozima M, Podosek PA (2001) Noble gas geochemistry, 2nd edn. Cambridge University Press, Cambridge

Pashin JC, McIntyr MR (2003) Temperature-pressure conditions in coalbed methane reservoirs of the Black Warrior basin: implications for carbon sequestration and enhanced coalbed methane recovery. Int J Coal Geol 54:167–183

Petroleum Technology Research Centre 2011 Response to a soil gas study by Petro-Find Geochem Ltd

Pinti DL, Marty B (1995) Noble gases in crude oils from the Paris Basin, France—implications for the origin of fluids and constraints on oil-water-gas interactions. Geochimica Cosmochimica Acta 59:3389–3404

Pinti DL, Marty B (1998) Separation of noble gas mixtures from petroleum and their isotopic analysis by mass spectrometry. J Chromatogr A 824(1):109–117

Pinti DL, Wada N, Matsuda J (1999) Neon excesses in pumice: volcanological implications. J Volcanol Geoth Res 88:279–289

Podosek PA (1980) Sedimentary noble gases. Geochim Cosmochim Acta 44:1875–1884

Porcelli D, Woolum D, Cassen P (2001) Deep earth rare gases: initial inventories, capture from the solar nebula, and losses during Moon formation. Earth Planet Sci Lett 193:237–251

Porcelli D, Ballentine CJ (2002) Models for the distribution of terrestrial noble gases and evolution of the atmosphere. Reviews in Mineralogy and Geochemistry 47:411–480

Porcelli D, Ballentine CJ, Wieler R (2002) An overview of noble gas—Geochemistry and cosmochemistry, noble gases in geochemistry and cosmochemistry, pp 1–19

Rahmstorf S (2010) A new view on sea level rise. Nat Rep Clim Change 4:44–45

Raistrick M, Mayer B, Shevalier M, Perez RJ, Hutcheon I, Perkins EH, Gunter WD (2006) Using chemical and isotopic data to quantify inoic trapping of carbon dioxide in oil field brines. Environ Sci Technol 40:6744–6749

Rauzi SL (1999) Carbon dioxde in the St. Johns—Springerville Area, Apache County, Arizonia. Arizonia Geological Survey, Open-File Report 99-2

Sarda P, Battani A, Prinzhofer A (2000) The 20Ne/36Ar ratio as a tracer for ancient oil: the oil–water and gas-water double distillation model. In: Goldschimidt 2000 vol 5(2). Cambridge Publications, Cambridge, p 876

Sarda P, Staudacher T, Allègre CJ et al (1985) $^{40}Ar/^{36}Ar$ in MORB glasses: constraints on atmosphere and mantle evolution. Earth Planet Sci Lett 72:357–375

Sherwood Lollar B, Ballentine CJ (2009) Insights into deep carbon derived from noble gases. Nat Geosci 2:543–547

Sherwood Lollar B, Ballentine CJ, O'Nions RK (1997) The fate of mantle-derived carbon in a continental sedimentary basin: integration of C/He relationships and stable isotope signatures. Geochim Cosmochim Acta 61:2295–2308

Sherwood Lollar B, O'Nions RK, Ballentine CJ (1994) Helium and neon isotope systematics in carbon dioxide-rich and hydrocarbon-rich gas reservoirs. Geochim Cosmochim Acta 58:5279

Sherwood Lollar B, Slater GF, Ahad J, Sleep B, Spivack J, Brennan M, MacKenzie P (1999) Contrasting carbon isotope fractionation during biodegradation of trichloroethylene and toluene: Implications for intrinsic bioremediation. Org Geochem 30:813–820

Shipton ZK, Evans JP, Kirschner D, Kolesar PT, Williams AP, J H (2004) Analysis of leakage through 'low-peameability' faults from natural reservoirs in the Colorado Plateau, east-central Utah. In: Baines SJ, Worden RH (eds) Geological storage of carbon dioxide. Geological Society, London, pp 43–58

Spycher N, Pruess K (2005) CO2-H2O mixtures in the geological sequestration of CO2. II. Partitioning Chloride Brines at 12–100°C and up to 600 bar. 69(13):3309

Stevens SH, Fox C, White T, Melzer S (2006) Natural CO2 analogs for Carbon Sequestration. Final Report for USDOE

Tolstikhin IN, Lehmann BE, Loosli HH, Gautschi A (1996) Helium and argon isotopes in rocks, minerals, and related groundwaters: a case study in northern Switzerland. Geochim Cosmochim Acta 60: 1497–1514

Torgersen T, Clarke WB (1985) Helium accumulation in groundwater, (i): an evaluation of sources and the continental flux of crustal ^{4}He in the Great Artesian Basin, Australia. Geochim Cosmochim Acta 49:1211–1218

Torgersen T, Kennedy B, van Soest M (2004) Diffusive separation of noble gases and noble gas abundance patterns in sedimentary rocks. Earth Planet Sci Lett 226:477–489

Torgersen T, Kennedy BM (1999) Air-Xe enrichments in Elk Hills oil field gases: role of water in migration and storage. Earth Planet Sci Lett 167:239–253

Treiloff M, Kunz J, Clague DA, Harrison D, Allegre CJ (2000) The nature of pristine noble gases in mantle plumes. Science 288:1036–1038

Trull T, Nadeau S, Pineau F, Polve M, Javoy M (1993) C-He systematics in hotspot xenoliths: Implications for mantle carbon contents and carbon recycling. Earth Planet Sci Lett 118:43

Wilkinson M, Gilfillan SMV, HaszeldineRS, BallentineCJ (2010) Plumbing the depths: testing natural tracers of subsurface CO_2 origin and migration, Utah. In: Grobe M, PashinJC, DodgeRL (eds) Carbon dioxide sequestration in geological media—State of the science. AAPG Studies

Woodward LA (1983) Geology and hydrocarbon potential of the raton basin, New Mexico. In: Fassett JE (ed) Oil and gas fields of the four corners area, vol 3. Four Corners Geological Society, pp 789–799

Wycherley H, Fleet A, Shaw H (1999) Some observations on the origins of large volumes of carbon dioxide accumulations in sedimentary basins. Mar Pet Geol 16:489–494

Zartman RE, Wasserburg GJ, Reynolds JH (1961) Helium, argon and carbon in some natural gases. J Geophys Res 66:277–306

Zhou Z, Ballentine CJ, Kipfer R, Schoell M, Thibodeaux S (2005) Noble gas tracing of groundwater/coalbed methane interaction in the San Juan Basin, USA. Geochim Cosmochim Acta 69:5413–5428

Noble Gas in Oil and Gas Accumulations

Alain Prinzhofer

Abstract

Noble gas geochemistry consists of a series of inert natural tracers which allow quantitative geological modeling relative to the migration, trapping and extraction of hydrocarbon reserves. The noble gas data allow accurate description of complex natural and technological processes involved in identifying and extracting oil and gas discoveries. Among others, the origins of non hydrocarbon gas compounds such as CO_2 present in hydrocarbon accumulations, the physical interactions between hydrocarbon phases and water, the dynamics of oil and gas migration through porous sedimentary rocks, are some of the current applications of noble gases to hydrocarbon exploration in high risk areas. Unconventional hydrocarbon exploration and production, which may represent the future of our hydrocarbon consumption, raise new questions which may also be assessed with these unique tracers. Oil and gas shale production as well as gas hydrates, are future targets which may benefit from the specific properties of noble gases as tracers in hydrocarbon fluids.

The specific properties of noble gas isotopes (chemical inertness, high potential for source characterization, simple physical properties) have been recognized to be of great interest for natural gas characterization. The pioneering work of the Californian Institute of Technology (Zartman and Wasserburg 1961; Wasserburg et al. 1963) presented most of the basic concepts which have been developed in the following 50 years of noble gas geochemistry for hydrocarbon accumulations (non-organic origins of noble gases, chronology of accumulation, crustal versus mantle contamination, meteoric water influence, in situ versus ex situ noble gas exchange with fluids, etc…). Few papers were published in the decades following this application of noble gases (Nagao et al. 1981; Sano et al. 1982; Oxburg et al. 1986; Mazor and Bosh 1987; Bosh and Mazor 1988; Jenden et al. 1988). Only recently, in the past 20 years or so, have a large number of publications from different academic centers shown renewed interest in this methodology with an exponential increase in applications (Ballentine et al. 1991; O'Nions and Ballentine 1993; Ballentine and O'Nions 1994; Sherwood-Lollar et al. 1994; Xu et al. 1995; Ballentine et al. 1996; Torgersen

A. Prinzhofer (✉)
HRT O and G, Av. Atlantica 1130/ 7° andar, Rio de Janeiro, CEP 22021-000, Brazil
e-mail: Alain.Prinzhofer@ipexco.com.br

P. Burnard (ed.), *The Noble Gases as Geochemical Tracers*, Advances in Isotope Geochemistry,
DOI: 10.1007/978-3-642-28836-4_9,

and Kennedy 1999; Battani et al. 2000; Kennedy et al. 2002; Ballentine and Sherwood-Lollar 2002; Prinzhofer and Battani 2003; Kotarba and Nagao 2008; Yu et al. 2010). The last decade confirms this trend, with several scientific groups proposing noble gas geochemical services for commercial oil and gas companies. Very recent interest in shale gas exploration confirms and increases this tendency for further commercial applications of noble gas geochemistry in the petroleum and natural gas industry.

1 Introduction: The Possible Sources and Physical Processes that May Affect HC-Associated Noble Gas Isotopes

1.1 The Three Main Sources of Noble Gas Isotopes in Petroleum and Gas Systems

Noble gas compounds represent a simple family of chemical elements and isotopes, with only five elements (He, Ne, Ar, Kr, Xe with the exception of radon, which has such a short half life that its study represents a distinct and different interest for geologists) and a large number of isotopes, for which only four isotopic ratios are generally used for oil and gas exploration: $^{3}He/^{4}He$, $^{20}Ne/^{22}Ne$, $^{21}Ne/^{22}Ne$ and $^{40}Ar/^{36}Ar$. Considering only subsurface fluids (oil, gas, water), only three main terrestrial reservoirs are implied in noble gas generation Fig. 1:

- Air Saturated Water (ASW)

The Air Saturated Water (ASW) reservoir corresponds to the noble gases present in the subsurface waters, which were previously equilibrated with the atmosphere, via recharge zones of aquifers. Knowing the composition of the atmosphere in terms of concentrations and isotopic ratios of noble gases, and the solubility coefficients between gas and water, it is possible to calculate the composition of this ASW reservoir. The only unknown parameter is the equilibration temperature at the time of the recharge. However, although this variation is paramount when calculating paleo-temperatures

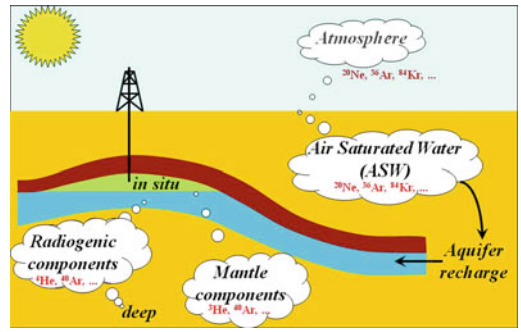

Fig. 1 Shematic diagram of a petroleum system with the different possible origins of noble gases entering into a hydrocarbon accumulation (from Ballentine and O'Nions 1994, modified)

(Weis 1970, 1971; Weis and Kyser 1978; Kipfer et al. 2002), the variation in concentrations is generally sufficiently small to be neglected in petroleum geochemistry, as other processes of exchange between water and hydrocarbons present much larger fractionations than this second order variation.

- Radiogenic isotopes

The radiogenic or nucleogenic contribution comes from minerals. Several nuclear reactions, including the natural radioactive decay of some isotopes in minerals, as well as some nucleogenic reactions may generate excesses of certain noble gas isotopes. The two most important are the production of ^{4}He, due mainly to the radioactive decay of uranium and thorium (and any other α production radioactive process), and ^{40}Ar, generated as the residue of the natural radioactive decay of ^{40}K (another part generating ^{40}Ca). Other isotopes may be generated by more complex processes involving the interaction between neutrons and isotopes of various chemical compounds. The main noble gas isotopes generated through nucleogenic processes are ^{3}He, ^{21}Ne and ^{22}Ne (Morrison and Pine 1955; Sarda et al. 1988; Kennedy et al. 1990; Moreira and Allegre 1998; Ballentine and Burnard 2002). All these noble gas isotopes generated through geological time originate in minerals, which may be present in the sedimentary series, or from deeper horizons such as the metamorphic part of the crust, and the crustal basement composed of various igneous and metamorphic rocks of

different ages. Compare to sedimentary minerals, the continental basement is generally older, and with higher concentrations of the radioactive elements U, Th, K, resulting in greater concentrations of radiogenic isotopes, concentrated mainly in the upper 10 km of the continental crust. Rudnick and Fountain (1995) calculate that 66 % of the radiogenic/nucleogenic budget is concentrated in the 10–15 km top kilometers of the crust, 28 % at intermediate depths of 10–15 to 20–25 km, and that only 6 % of the radiogenic production is generated in the lower part of the crust, i.e. below 25 km. The mechanisms—and their efficiencies—that allow these isotopes to migrate from the basement up to an oil or gas accumulation located in sedimentary series are the limiting processes for the abundance of these isotopes in petroleum systems.

- Mantle fluids

It was discovered some decades ago that in some sedimentary basins, a clear presence of mantle fluids may be demonstrated (Oxburgh et al. 1986; O'Nions and Oxburg 1988). The mantle fluids have a significantly different signature from the other reservoirs in terms mainly of noble gas isotopic ratios. The most commonly used is the $^{3}He/^{4}He$ ratio, which is highly enriched in ^{3}He in the mantle. Normalized to the air value of 1.4×10^{-6}, the upper mantle has values between 6 and 8 times the atmospheric value depending on its location in the mantle: 8Ra2 is the accepted value for MORB (Kurz and Jenkins 1981; Graham 2002), whereas a sub-continental upper mantle has a lower value around 6Ra (Dunai and Baur 1995). The ASW isotopic ratio is of course the air ratio of 1.4×10^{-6}, as there is no measurable isotopic fractionation for helium between a water and vapor phase. However, due to the very low concentration of helium in the air (5 ppm) and its lower solubility coefficient in water compared with other noble gases, the contribution of ASW helium is generally neglected in geologic petroleum reservoirs. Only in superficial gas seeps may this contribution be significant compared to other sources. The $^{3}He/^{4}He$ signature of crustal sources, either sedimentary or from the basement, is around 0.02 Ra. The lower mantle, possibly visible through hot spots, has helium isotopic ratios as high as 50Ra (Stuart et al. 2003). The neon isotopes have also been extensively studied in mantle sources (Sarda et al. 1988; Honda et al. 1991; Moreira and Allegre 1998; Trieloff et al. 2000, 2002; Ballentine et al. 2005). The values for the ratios $^{20}Ne/^{22}Ne$ and $^{21}Ne/^{22}Ne$ vary between 12.5–13.8 and 0.06–0.063 respectively. The $^{40}Ar/^{36}Ar$ isotopic ratios are also very different in the mantle reservoir, as ^{36}Ar is extremely depleted in the mantle. The measured ratios may be as high as 30,000 (Staudacher et al. 1989) or even 40,000 (Burnard et al. 1997).

A summary of the noble gas signatures of these different reservoirs is presented in Table 1, and a schematic sketch of their contribution in an hydrocarbon accumulation is represented in Fig. 1 (from Ballentine and O'Nions 1994, modified).

1.2 The Three Main Processes Affecting Noble Gas Isotopes

Because all the noble gas compounds are strictly chemically inert under geological conditions, only physical processes may affect and fractionate their proportions. I presented in the previous paragraph the nuclear processes generating the radiogenic and nucleogenic noble gas isotopes, and I will deal in this chapter only with non-nuclear physical processes. It is possible to distinguish only three kinds:

1.2.1 Exchange of Noble Gas Compounds Between Phases

The noble gas compounds may originally be present in a gas phase (atmosphere, natural gas accumulations) a liquid phase (water, oil) or a solid phase (minerals with radioactive elements, surface adsorption, hydrates). The hydrocarbon fluids, oil or gas, come principally from degradation of fossil organic matter, and are generated almost without any noble gas content, as the organic matter does not contain gas compounds, and generally almost no radioactive compounds (Ricard et al. 2011). However, the associated shales, rich in organic matter, have generally

Table 1 Average concentrations and isotopic ratios of the principal reservoirs of noble gas compounds affecting a petroleum system

	^{4}He	^{20}Ne	^{36}Ar	^{84}Kr	^{132}Xe	R/Ra	$^{20}Ne/^{22}Ne$	$^{21}Ne/^{22}Ne$	$^{40}Ar/^{46}Ar$
Atmosphere (ppm)	5.24	16.5	31.4	0.65	0.023	1	9.8	0.029	295.5
ASW (20 °C, fresh water) μ mol/m^3	2.04	7.67	47.8	1.83	0.039	1	9.8	0.029	295.5
MORB mantle	36,600	1.04	1	0.029	0.004	8	12.5–13.8	0.06–0.063	40,000
Continental crust	–	–	–	–	–	0.02	0.08–0.10	0.4–0.52	3,000

The atmospheric concentration values are in ppm mol/mol (Porcelli et al. 2002). The ASW concentration values are in micromoles per cubic meter (Kipfer et al. 2002). The MORB concentration values are normalized to the ^{36} Ar concentrations (Burnard et al. 1997, Moreira and Allegre 1998). Only the isotopic ratios of the continental crust have been represented, as the range of variation of noble gas concentrations may be very large
Atmosphere: Porcelli et al. 2002
Mantle: Moreira and Allegre 1998, concentrations normalized to ^{36} Ar
Continental crust: Ballentine and Burnard 2002

high concentrations in Uranium and Thorium, resulting in a potential radiogenic contribution to the hydrocarbon fluids from the source rocks (Torgersen and Kennedy 1999). If noble gases are enriched in an oil or gas phase in the subsurface, this largely results from their exchange between phases, quantified by partition coefficients called either solubility coefficients or Henry coefficients. The phases encountered by hydrocarbons may be either water, or supercritical mantle and hydrothermal fluids, mainly composed of H_2O and CO_2. Another possible exchange between phases, not yet documented in Earth Sciences, is the exchange between fluid phases and hydrates. It is important to note that in the case of hydrate formation, the stability of heavy noble gas hydrates is much larger than the better known stabilities of CH_4 and CO_2 hydrates (Berecz and Balla-Achs 1983; Dyadin et al. 1996). The occurrence of hydrates, either on the sea floor or in peri-glacial areas, have the potential for drastically fractionating the heavy nobles gases (trapped in the hydrate solid phase) versus the light noble gases (never stable in hydrates at natural conditions). However, no quantitative study of these fractionations has been carried so far in Earth Sciences.

The solubility coefficients of noble gases between a gas phase and a water phase have been extensively studied versus temperature and pressure (Crovetto et al. 1981; Smith and Kennedy 1983; Smith 1985; Harvey 1998), and a summary of the values are presented in Table 2. The solubilities may be expressed as Henry's pressures or solubility coefficients. The Henry pressure (expressed in bars) represents the necessary pressure a gas (or its partial pressure) must achieve to reach a concentration of unity in the water. The solubility represents the ratios of concentrations between the water phase and the gas phase for a given thermodynamic equilibrium. It is expressed in mol/m^3/mol/m^3 in Table 2. Following the ideal gas law, the solubility coefficients do not change with absolute pressure, whereas a correction term must be added in the case of non-ideal solutions.

The solubility of noble gases between gas and liquid hydrocarbon phases is less well constrained, as it is dependent on the oil composition, which may be variable. Two sets of solubility coefficients have been obtained by Kharaka and Specht (1988), for a light oil (API of 34) and a heavy oil (API of 25). The solubility of noble gases between oil and water can be calculated by combining the solubilities between water and gas, and between gas and oil. The result is shown in Fig. 2 where the solubilities of the noble gases (in mol/m^3/mol/m^3) between a

Table 2 Values of the solubility coefficients in (mol/m^3)/(mol/m^3), between gas and water, heavy oil (API 25) and gas, and light (API 34) and gas, for atmospheric pressure and temperatures between 10 and 170 °C.

T(°C)	He	Ne	Ar	Kr	Xe
Solubility water/gas (mol/m^3) (mol/m^3) 1 *bar*					
10	0.0089	0.0111	0.0407	0.0795	0.1515
50	0.0090	0.0096	0.0236	0.0388	0.0603
110	0.0125	0.0111	0.0199	0.0281	0.0394
170	0.0209	0.0163	0.0253	0.0326	0.0465
Solubility heavy oil/gas (mol/m^3) (mol/m^3) 1 *bar*					
10	0.0128	0.0111	0.154	0.477	1.491
50	0.0211	0.0198	0.158	0.400	1.080
110	0.0445	0.0474	0.165	0.308	0.666
170	0.0939	0.1131	0.172	0.237	0.411
Solubility light oil/gas (mol/m^3) (mol/m^3) 1 *bar*					
10	0.0192	0.0236	0.163	0.504	2.256
50	0.0269	0.0317	0.149	0.443	1.397
110	0.0449	0.0494	0.130	0.365	0.681
170	0.0749	0.0768	0.113	0.301	0.332

Values calculated from Smith and Kennedy (1983), Smith (1985), Harvey (1998) and Kharaka and Specht (1988)

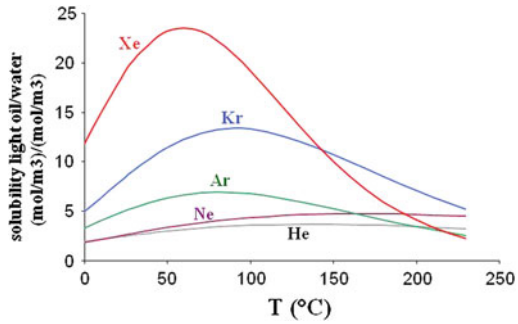

Fig. 2 Relative noble gas solubilities between light oil and water as a function of temperature at atmospheric pressure (from Kharaka and Specht 1988)

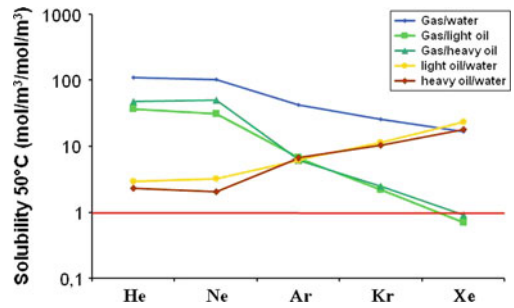

Fig. 3 Partition coefficients of noble gases between oil, water and gas phases, in (mol/m^3)/(mol/m^3) at atmospheric pressure and 50 °C

light oil and water are plotted as a function of temperature. For all the noble gases in the range of temperatures presented Fig. 2, oil always has higher noble gas concentrations than the associated water, indicating that noble gases are more soluble in oil than in water.

It is important to note that the oil considerably enriches the heavy noble gases (mainly Xe and Kr) relative to water for temperatures between 50 and 90 °C. Figure 3 shows noble gas solubilities between different phases at 50 °C, highlighting the fractionation that occurs between gas and oil, favoring heavy noble gases in oil and light ones in gases.

As the initial water may be considered to be ASW, the mass balance of the noble gases between phases will follow simple rules, assuming that the initial water was equilibrated with a gas phase, with an oil phase or with both oil and gas phases. Defining H as the ratio of the volume of oil versus the volume of equilibrated water, and G the ratio of the volume of gas versus the volume of equilibrated water, we may write:

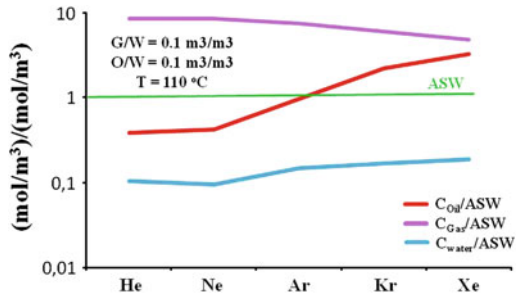

Fig. 4 Concentrations of noble gases in three oil, water and gas, that had originally equilibrated with Air Saturated Water (*ASW*), and with volume ratios gas/water and oil/water of 0.1 m^3/m^3. All the concentrations are normalized to ASW values

$$C_{ASW} = C_W + H.C_H + G.C_G \quad (1)$$

C_H and C_G are calculated versus C_W as:

$$C_H = C_W \text{ solub (oil/water)} \quad (2)$$

$$C_G = C_W \text{ solub (gas/water)} \quad (3)$$

[where solub (x/y) is the concentration of the gas in phase x divided by that in y]. It is possible to calculate, for a given amount of oil, water and gas, the noble gas concentrations in each phase, at equilibrium by writing:

$$C_W = C_{ASW}/(1 + H \text{ solub (oil/water)} + G \text{ solub (gas/water)}) \quad (4)$$

$$C_H = C_W \text{ solub (oil/water)} \quad (5)$$

$$C_G = C_W \text{ solub (gas/water)} \quad (6)$$

An example of the concentration patterns expected is presented in Fig. 4, where the volumetric oil/water and gas/water ratios have been taken at 0.1 m^3/m^3 with an oil gravity of 34° API. The figure shows that the gas phase is enriched in all noble gases versus ASW, with an increasing enrichment for the light noble gas fraction. The oil phase is depleted in light noble gases but enriched in krypton and xenon versus ASW. The water equilibrated with these two phases has lower concentrations than pristine ASW, significantly so for the light noble gases.

This exchange of noble gases between 3 different phases (oil, gas and water) potentially

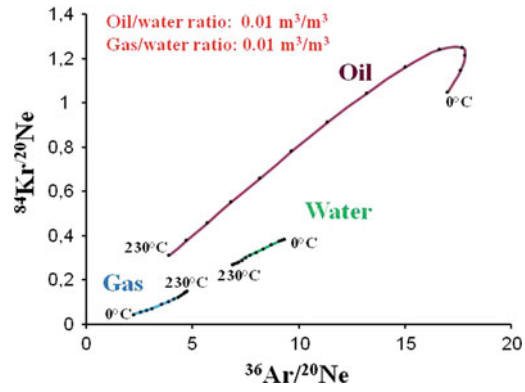

Fig. 5 Evolution of $^{84}Kr/^{20}Ne$ and $^{36}Ar/^{20}Ne$ ratios for oil, water and gas phases at thermodynamic equilibrium, for temperatures varying from 0 to 230 °C, and gas/water and oil/water ratios of 0.01 m^3/m^3. Dots represent temperature steps of 10 °C between 0 and 30 °C, and steps of 20 °C between 30 and 230 °C

presents complex behavior when temperature is taken into account. Figure 5 represents a plot of two ratios of fossil noble gases $^{36}Ar/^{20}Ne$ versus $^{84}Kr/^{20}Ne$. The three trends shown on the figure correspond to the equilibrium of the three phases, with the temperature of equilibration ranging from 0 to 230 °C. The trend for the oil phase is more variable in the diagram, whereas the gas and water trends present a smaller excursion of these two ratios.

1.2.2 Adsorption/Desorption of Noble Gases on the Surface of Solids

The physical sorption of noble gases (as no chemisorption may be envisioned in geological environments with these inert gases) on the surface of solid matter (mineral and organic) may be considered as a particular type of phase change, as described previously. However, the formalism that one may use to describe this process is linked to isothermal adsorption curves. Unfortunately, little experimental data is available on the adsorption properties of noble gases on natural minerals and organic surfaces for geological conditions. Several studies were published in the 60s through the 80s on krypton and xenon, as it was observed that these two elements had anomalously low concentrations in the terrestrial atmosphere compared to meteorites. Fanale and Cannon (1971) provide some Langmuir adsorption isotherms for krypton and

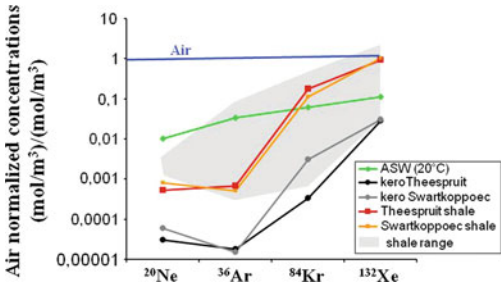

Fig. 6 Air-normalized concentrations of noble gas compounds for kerogen and shale samples (Frick and Chang 1977), expressed in mol/m^3. The concentrations of ASW are also represented

xenon adsorbed on shale and volcanic ash surfaces. However, the importance of adsorption on the organic matter has been only primarily discussed with respect to reduced carbon fractions of meteorites (Yang et al. 1982; Wacker et al. 1985; Wacker 1989). Frick and Chang (1977) further presented results of adsorption on kerogens and shales, and indicated that the preferential adsorption of xenon, and to a lesser degree krypton, is higher for kerogens than for shales. Figure 6 presents the analyzed concentrations of noble gases measured in kerogens and shales (Frick and Chang 1977) compared to air and ASW concentrations. It appears that kerogens fractionate the heavy noble gases from light noble gases. However, their absolute concentrations are lower than in shales and water, meaning that their influence on the noble gas mass balance is smaller. The shales may also present highly fractionated light/heavy noble concentrations, whereas ASW, only controlled by noble gas solubilities, is comparatively less fractionated.

Other constraints on these processes have been obtained through geological case studies. Torgersen and Kennedy (1999) and Zhou et al. (2005) clearly show the importance of adsorption of heavy noble gases (Krypton and Xenon) in geological processes. Torgersen and Kennedy (1999), studying the Elk Hills oil field, USA, show enrichment of Xe/Ar and Kr/Ar relative to air of 576 and 58 times respectively, interpreted as due to preferential adsorption of these on organic-rich shales of the petroleum system. Zhou et al. (2005), studying gases collected in coalbed methane accumulations of the San Juan Basin, USA, also find considerable enrichments of Krypton and Xenon (31 and 146 relatively to ^{36}Ar respectively). These heavy noble gas enrichments are interpreted as due to preferential adsorption on coal macerals. This demonstrates the importance of heavy noble gas adsorption in sedimentary rocks, when severe fractionation is observed between light and heavy noble gases, as was originally suggested by Podosek et al. (1982).

1.2.3 Diffusion in Liquids or in Gas Phases

The fractionation of noble gases between fluid phases (water, oil, gas, supercritical fluids) and during adsorption processes (on mineral and organic surfaces) has been considered so far in the context of thermodynamic equilibrium. The noble gas distribution between rocks and fluids is heterogeneous, implying that equilibrium is not always achieved, and that kinetic processes could affect their concentrations. As pure Darcy flow of a single fluid will not fractionate dissolved species, only diffusion can affect dynamically the absolute and relative concentrations of noble gases. The diffusion coefficients of noble gas are well constrained in pure water (Jähne et al. 1987) and in gases (Reid et al. 1977). Figure 7 summarizes the diffusion coefficients of noble gas in water versus their solubility. Other gas compounds (N_2, CH_4, CO_2, H_2) are added for comparison (Reid et al. 1977). In the oil phase, of course these coefficients depend on the oil composition (viscosity, density, etc…). Modeling the diffusion process in porous rocks is intricate as the geometry and petrography of the matrix will significantly alter the effective diffusion coefficients (Rebour et al. 1997). A slowing down effect always occurs during transport of dissolved gases in porous matrices, due to the reduction of porosity (the noble gases will mainly diffuse in fluid phases filling the porosity), the tortuosity and the permeability of the rocks. These parameters should decrease the effective diffusion coefficients by a constant parameter for all gases. However, it has been noticed (Giannesini et al. 2008; Magnier et al. 2011) that this diffusivity reduction is not the same for the whole

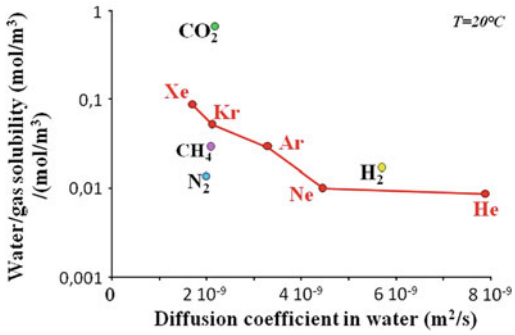

Fig. 7 Correlation between the solubility coefficient of different gases in water [in $(mol/m^3)/(mol/m^3)$ at room temperature and atmospheric pressure] and the diffusion coefficients in water (in m^2/s). Data from Crovetto et al. (1981), Smith and Kennedy (1983), Smith (1985), Harvey (1998) for the solubilities, and Jähne et al. (1987) and Reid et al. (1977) for the diffusion coefficients

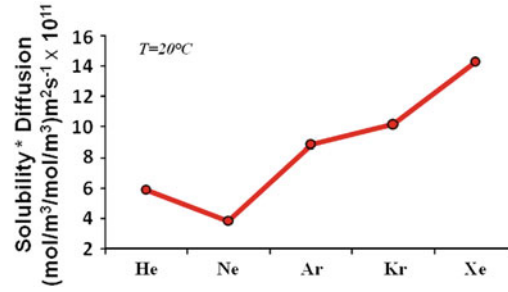

Fig. 8 Product of the solubility and diffusion coefficients in water for the series of noble gas compounds, showing the non-monotonous trend of this key parameter for diffusive fluxes in porous rocks. Same references as Fig. 7

series of noble gas compounds, with a larger flux reduction for the heavier noble gases. This is interpreted as due to the preferential adsorption of the heavy noble gases on the surfaces of minerals and organic compounds present in the sedimentary rocks, adding a chromatographic effect to the simple fluid phase diffusion process. A quantification of this relative retention has been hypothesized to depend on the mineralogy of the rocks and its clay content.

Considering gas diffusion through a simple membrane as an analog to a thin sedimentary layer, the flux of each gas should be proportional to the product of the diffusion coefficient in the membrane and the solubility of the species in the membrane (Crank 1975, here multiplied by the porosity filled with water). For the noble gases, this product is not monotonous, but presents a minimum for neon (Fig. 8). Even if helium is generally considered to be the most mobile noble gas, it can be seen that, in a water membrane, it is not systematically the most mobile. However, considering krypton and xenon adsorption (see previous paragraph and Torgersen and Kennedy 1999; Zhou et al. 2005), this order has to be revised in porous rocks, and generally, a decrease in mobility is indeed correlated with noble gas atomic mass (Magnier et al. 2011). In conclusion, it seems difficult to isolate pure single phase diffusion in sedimentary rocks, as the migration processes always involve a complex combination of physical processes, including advection, water diffusion and adsorption.

1.3 The Atmospheric Noble Gas Isotopes: A Possible Mass Balance Between Water, Oil and Gas Phases

It has been shown that one of the main reservoirs of noble gas isotopes interacting with a petroleum system is ASW. All the atmospheric noble gases are dissolved in the aquifer waters, implying that their original concentrations are known, as their atmospheric concentration and solubility coefficients are well constrained. Some noble gas isotopes are sourced uniquely from ASW, being unradiogenic and with sufficiently low mantle concentrations (compared to ASW) to be neglected; notably ^{20}Ne, ^{36}Ar, ^{84}Kr and ^{132}Xe can be considered to be ASW derived. Therefore, from their concentrations in aquifers, their measured concentrations in a hydrocarbon phase are consequently related to the amount of aquifer water exchanged with the hydrocarbon phase: no interaction at all would imply zero concentrations in the hydrocarbon phase (which is never seen), whereas high oil/water ratios would feed the hydrocarbon phase with high concentrations of these isotopes. Several papers have already demonstrated the geological interest in these fossil interactions recorded by the noble gas isotopes. With well known initial concentrations and

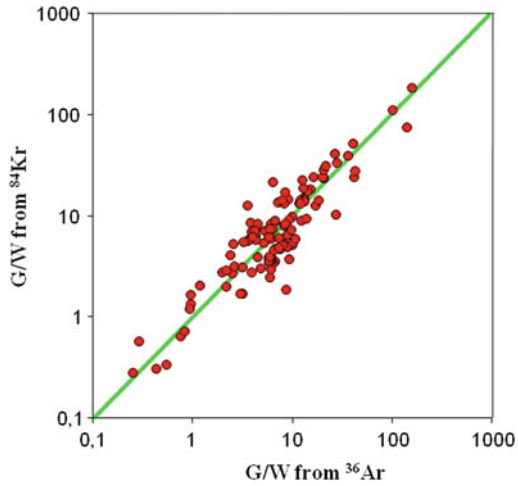

Fig. 9 Correlation of the gas/water ratios (in m^3/m^3) calculated with the concentrations of ^{36}Ar and ^{84}Kr in different gas accumulations worldwide. Data from Ballentine et al. 1991, 1996; Ballentine and Sherwood-Lollar 2002; Prinzhofer and Battani 2003; Gilfillan et al. 2009; Prinzhofer et al. 2010; Battani et al. 2011

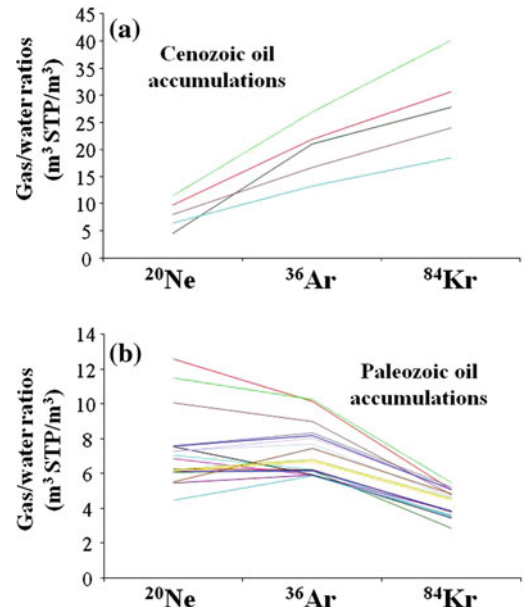

Fig. 10 Calculation of the gas/water ratios calculated with three ASW noble gases, ^{20}Ne, ^{36}Ar and ^{84}Kr. **a** Gas samples accumulated in a Brazilian Cenozoic Basin. **b** Gas samples accumulated in a Brazilian Paleozoic Basin. Prinzhofer and Battani 2003; Prinzhofer et al. 2010

physical properties, exchanges between oil, gas and water phases can readily be traced: Ballentine et al. (1991) investigated noble gas partitioning in the Pannonian Basin, Ballentine et al. (1996) in The Magnus Opus field, with direct measurements of noble gas concentrations in the oil phase, Battani et al. (2000) for the giant gas fields of the Indus Basin, and Prinzhofer et al. (2000) for the gas accumulations of the Mascupana Basin, Mexico.

The basis for all these studies is that it is possible to calculate a Hydrocarbon Gas (G)/Water (W) equilibrium ratio by combining the solubility equation with mass balance equations:

$$G/W = C_{ASW}/C_g - \beta \qquad (7)$$

With G/W as the Gas/Water ratio, C_{ASW} the concentration of the noble gas isotope in the Air Saturated Water, C_g the concentration in the gas phase, and β the solubility of the isotope in water.

However, this calculated Gas (G)/Water (W) ratio may be different depending on the gas used (neon, argon, krypton or xenon). The reason is that a thermodynamic equilibrium is assumed between the two phases, which is rarely the case in sedimentary basins for all the noble gases from helium to xenon. Figure 9 shows that the calculated G/W ratios obtained using ^{36}Ar and ^{84}Kr give the most consistent results, for G/W ratios ranging from 0.2 to 200 m^3/m^3, i.e. three orders of magnitude. The calculated G/W ratios (using ^{20}Ne, ^{36}Ar and ^{84}Kr) appears, for some systems, to be larger for heavier noble gas compounds, whereas for some other petroleum systems, the opposite is observed (Fig. 10). These contrasting behaviors may possibly be interpreted as due to different time scales for the age of accumulation and the age of preservation of the hydrocarbon accumulations. Considering the higher mobility of lighter noble gases, a lack of equilibrium between the accumulating hydrocarbon phase and water would imply larger gas/water ratios for the heavy noble gases, whereas partial gas leakage out of the accumulation would favor the opposite, i.e. larger Gas/Water ratios for the light noble gas compounds. It is interesting to note that for more recent accumulations the dominant process is an absence of equilibration between

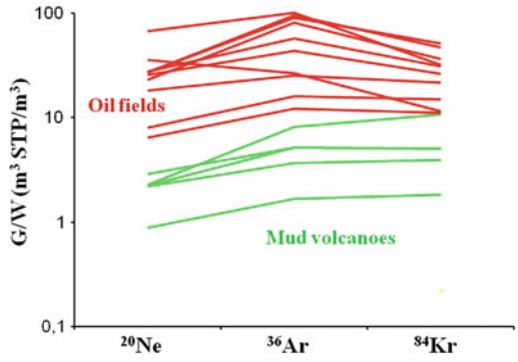

Fig. 11 Gas/Water ratios calculated with ASW noble gases, ^{20}Ne, ^{36}Ar and ^{84}Kr for the oil associated gas samples collected at well heads of oil fields in the Trinidad Islands *in red* and for gas sampled at the head of mud volcanoes from the same area in the Trinidad Islands. Data from Battani et al. 2011

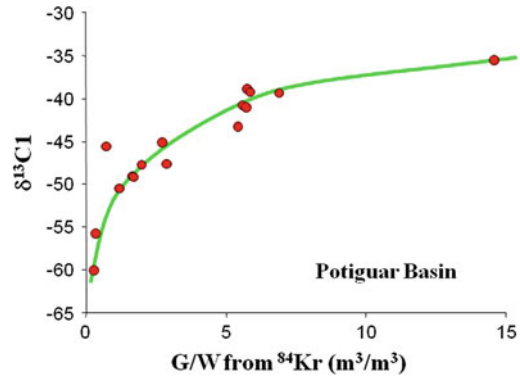

Fig. 12 Correlation between the carbon isotopic ratios of methane and gas/water ratios calculated with ^{84}Kr, for gas samples associated with biodegraded oils of the Potiguar Basin, Brazil (data from Prinzhofer et al. 2010)

hydrocarbon and water, whereas for older geological systems, the dominant factor seems to be loss from the hydrocarbon reservoirs.

Another example of using noble gases to calculate Gas/Water ratios is presented Fig. 11. The gas samples were collected from the Trinidad Islands (Trinidad and Tobago), some (in red) were sampled from oil accumulations, at producing well heads. The gases were collected at the separator, and correspond to the gas in solution in oil at the depth of the geological reservoir. Other samples (in green) were sampled from mud volcanoes. These settings are quite different: the latter correspond to eruptions of mud and hydrocarbon gas from undercompacted layers of the source rocks from which the oil accumulations are derived. This phenomenon is particularly useful as it allows mud and migrating gas to be directly sampled from the "kitchen" of the petroleum system (Battani et al. 2011). Calculating the associated gas/water ratios in these samples, it is clear that all the gases associated with oils present higher gas/water ratios (i.e. less water interaction with the hydrocarbons) compared to gases seeping from mud volcanoes. The association of a gas phase with water and mud, emitted at the same time, can explain the larger exchange with water than for gas compounds dissolved in the oil. Furthermore, gas/water ratios measured on the samples presented consistent quantitative values irrespective of the ASW derived noble gas used (^{20}Ne, ^{36}Ar or ^{84}Kr), indicating good equilibrium between the water and gas phase was reached. The gas/water ratios for the gas associated with oil and sampled from the geological reservoir were estimated to be between 10 and 100 m^3/m^3, whereas gases sampled from mud volcanoes had gas/water ratios between 1 and 10 m^3/m^3.

Figure 12 illustrates a correlation between the carbon isotopic ratio of methane dissolved in oil accumulations, which is sensitive to the extent of bacterial degradation, and the gas/water ratios calculated using ^{84}Kr. Gases that have the lowest gas/water ratios (i.e. most water interaction) have more negative δ^{13}C of methane, indicating an increasing contribution of bacterial methanogenesis. As the bacterial activity is highest at the water interface, an increase of the bacterial activity is consistent with an increase in water–oil interaction. The quantification of the proportion of water required for a given amount of biodegradation is thus possible using noble gas derived Gas/Water ratios.

1.4 Radiogenic Noble Gas Isotopes: Qualitative or Quantitative Estimates of Geological Residence Times of Fluids in the Subsurface

The two most commonly used radiogenic noble gas isotopes in oil and gas exploration are ^{4}He and ^{40}Ar. ^{4}He comes from the natural radioactive decay of ^{235}U, ^{238}U and ^{232}Th, whereas ^{40}Ar is generated through the radioactive decay of ^{40}K. Considering that the ^{40}Ar/^{36}Ar of the atmosphere has a value of 298.6, one may calculate the additional radiogenic ^{40}Ar (commonly known as ^{40}Ar*):

$$^{40}\mathrm{Ar}^{*} = {}^{40}\mathrm{Ar} - 298.6\,{}^{36}\mathrm{Ar} \quad (8)$$

The amount of ^{40}Ar* is a function of the average potassium content of the rocks interacting with the fluid, the proportion of fluid versus rocks (related to the average porosity as $\Phi/(1-\Phi)$. Steiger and Jager (1977) calculated the production of ^{40}Ar* per year and per cubic centimeter (cm^3) of rock as:

$$^{40}\mathrm{Ar}^{*} = 1.05 \cdot 10^{-17}(\mathrm{K})\ \mathrm{cm}^3\,\mathrm{STP}\ \mathrm{cm}^{-3}\,\mathrm{y}^{-1} \quad (9)$$

With an average ^{40}K concentration of 28,000 ppm, we may calculate:

$$^{40}\mathrm{Ar}^{*} = 2.94 \cdot 10^{-13}\,\mathrm{cm}^3\,\mathrm{STP}\ \mathrm{cm}^{-3}\,\mathrm{y}^{-1} \quad (10)$$

The amount of ^{36}Ar, considered as only sourced from ASW, is a function of the concentration of ASW and of the average porosity Φ of the rocks. It is then possible to assess a model age for a crustal fluid related to the ratio ^{40}Ar*/^{36}Ar:

$$\mathrm{T(y)} = \frac{\mathrm{C}^{36\mathrm{Ar}}_{\mathrm{ASW}}\,(\mathrm{cc\,STP/cc})}{2.94 \cdot 10^{-13}} \frac{\Phi}{(1-\Phi)} \frac{^{40}\mathrm{Ar}^{*}}{^{36}\mathrm{Ar}} \quad (11)$$

The same kind of calculation may be done for the generation of ^{4}He, also associated with ^{36}Ar, as the second isotope of helium cannot be considered as a fossil isotope (due to nuclear and possible mantle fluid contributions). Steiger and Jager (1977) calculated the amount of radiogenic ^{4}He generated in rocks:

$$^{4}\mathrm{He} = 1.207 * 10^{-13}\,[\mathrm{U}] + 2.867 * 10^{-14}\,[\mathrm{Th}]\ \mathrm{cm}^3\,\mathrm{STP}\,\mathrm{g}^{-1}\,\mathrm{y}^{-1} \quad (12)$$

From the average crustal concentration of uranium and thorium, the same kind of formula as shown above may give a model age using ^{4}He and ^{36}Ar:

$$\mathrm{T(y)} = \frac{\mathrm{C}^{36\mathrm{Ar}}_{\mathrm{ASW}}\,(\mathrm{cc\,STP/cc})}{1.74\,10^{-12}} \frac{\Phi}{(1-\Phi)} \frac{^{4}\mathrm{He}}{^{36}\mathrm{Ar}} \quad (13)$$

It must be stressed that this kind of modeling implicitly implies a closed system, in relation to the radioactive/radiogenic compounds. As we deal with highly mobile gases such as helium and argon, it is clear that these age calculations should be used with extreme care, as external fluxes of ^{4}He and ^{40}Ar (Zartman and Wasserburg 1961; Sano et al. 1986; Ballentine and Sherwood-Lollar 2002), as well as differential loss of these (Pinti and Marty 1995; Prinzhofer et al. 2010) are common features in geological basins.

1.4.1 Mud Volcanoes from the Makran Area (Pakistan)

The migration of radiogenic isotopes in fluids within porosity, generated by the constitutive rock minerals, has been studied by several authors (Mamyrin and Tolstikhin 1984; Elliot et al. 1993; Ballentine and Burnard 2002). They consider that the rate of release of ^{4}He, as an alpha particle, mobile and with an important initial energy, occurs more easily and at lower temperature than ^{40}Ar, bigger atom and residue of ^{40}K, which needs more energy, i.e. higher temperature in order to enter the fluids within the porosity. Furthermore, it has been suggested that bacterial gas generation may be distinguished from thermogenic generation using these tracers, in part because their generation temperature are quite different (Elliot et al. 1993). As an illustration, Fig. 13 presents geochemical data obtained from mud volcanoes from Makran (Pakistan; Ellouz-Zimmermann et al. 2007). These impressive natural structures (sometimes more than 1,000 m high), are composed of mud and gas expelled from under compacted sediments

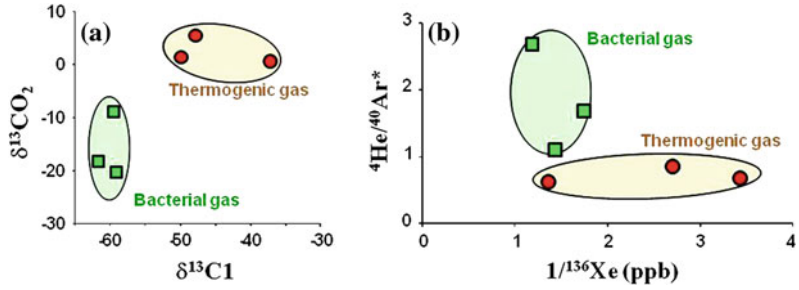

Fig. 13 Two gas families from the Makran (Pakistan) mud volcanoes (Ellouz-Zimmermann et al. 2007). The *green squares* correspond to bacterial gas generation, whereas the *red circles* correspond to thermogenic gases seeping through the mud volcano vents. **a** carbon isotopic signatures of CO_2 and CH_4. **b** $^4He/^{40}Ar^*$ ratios versus the reciprocal of ^{136}Xe concentrations

(Deville et al. 2003). Figure 13a shows the carbon isotopic ratios of methane and carbon dioxide (the two main gas compounds of these mud volcano gases). These gases have either heavy methane and CO_2 $\delta^{13}C$ (red circles), indicating a thermogenic origin for methane and a mineral origin for CO_2 (possible through high temperatures) or else the carbon isotope ratio of methane is in the range of bacterial generation and is associated with light $\delta^{13}C$ of CO_2 of biological origin (green squares).

Combining the data with noble gas isotope analyses (Fig. 13b), the two gas "families" appear significantly different. The $^4He/^{40}Ar^*$ ratios are higher for bacterial gases, explained by the fact that at low temperatures ^{40}Ar is expelled less easily that ^4He from the parent mineral lattice. The concentrations of ASW noble gas isotopes coming from the aquifer, ^{136}Xe in this example, shows that the bacterial gas underwent more interaction with the nearby aquifer water than the thermogenic gas. This can be seen by lower $1/^{136}Xe$, i.e. higher concentrations of ASW noble gas isotopes, associated with a higher Water/Gas ratio.

Radiogenic noble gas isotope ratios also allow an accumulation or exchange period to be tentatively calculated for given gas accumulations, provided the average porosity of the sedimentary system is known (here, the mud of the undercompacted sediments producing the mud volcanoes), assessed using a slightly different formalism by Zhou and Ballentine 2006). Normalizing the concentrations of two radiogenic isotopes (^4He or $^{40}Ar^*$) to an ASW isotope (here ^{36}Ar), the ratio radiogenic/ASW is then a function of both porosity and time. Assuming an average porosity of 15 % for Makran, Fig. 14 then shows the correlation between the model ages calculated using $^4He/^{36}Ar$ and $^{40}Ar/^{36}Ar$. It appears that for all the samples, the calculated age involving helium is younger than that with argon. This may in part be explained by a higher mobility of helium compared to argon and the fact that the memory of argon is probably more significant, rendering a better estimate of the hydrocarbon age with argon. The second observation from the model age is that all thermogenic gases present older ages than bacterial ones, irrespective of the chronological system used (for the $^{40}Ar/^{36}Ar$ dating system, the retention of ^{40}Ar in the minerals associated with the bacterial gases could be an alternate

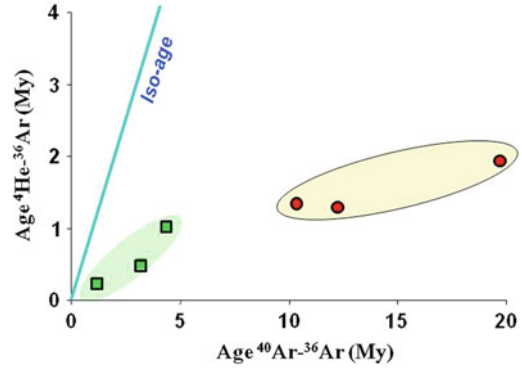

Fig. 14 The age (in million years) calculated for gases from the Pakistan mud volcanoes (see Fig. 13). A correlation exists between the "ages" calculated using ^4He-^{36}Ar and those using ^{40}Ar-^{36}Ar

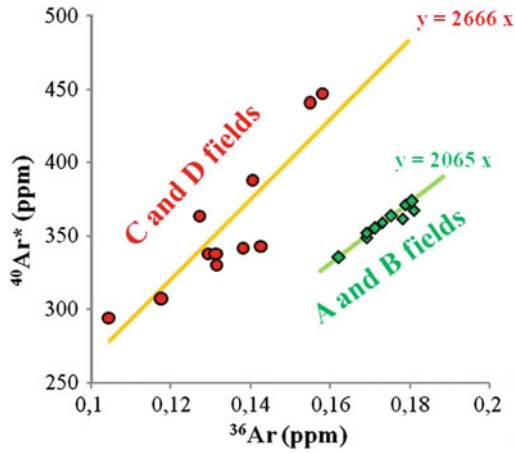

Fig. 15 Correlation between the radiogenic isotope ^{40}Ar* and the fossil ^{36}Ar for two series of oil and gas accumulations in a Paleozoic Basin (Prinzhofer and Battani 2003). The two trends with two different slopes correspond to oil fields with different resident times

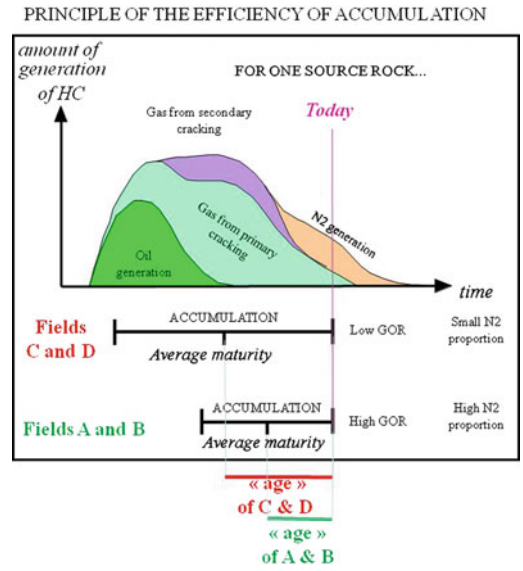

Fig. 16 Schematic sketch representing the relation between the efficiency of accumulation of a hydrocarbon field, its average maturity and its average residence time: For the same maturity history of a source rock; a field with a poor efficiency of accumulation will produce a fluid with higher maturity and lower residence time (and possibly higher nitrogen concentrations)

explanation of these age differences, as discussed above and in the review of Ballentine and Burnard 2002). This is also consistent with a deeper, older origin of the thermogenic gases compared to the more superficial and probably more recent origin of the bacterial gases of the eastern Makran region.

1.4.2 Oil and Gas Accumulation in a Paleozoic Basin, Brazil

Prinzhofer and Battani (2003) presented a case study on a Paleozoic Brazilian basin, consisting of two adjacent anticlinal structures filled with oil and gas. The ratios ^{40}Ar*/^{36}Ar of each of these structures are quite consistent: the concentrations of ^{40}Ar* and ^{36}Ar make an independent positive correlation for each structure, with a correlation line intercepting the origin, and a difference in slope of about 30 % between the two accumulations (Fig. 15). The differences in ^{40}Ar*/^{36}Ar may be interpreted as a difference in hydrocarbon residence times within the two structures. Indeed, it is likely that both isotopes exchange between the hydrocarbon phase and the other phases of the petroleum system (water, minerals). ^{36}Ar originates only from ASW and may be considered as an internal normalization for ^{40}Ar*, whose absolute amount is directly linked to the average residence time of the fluid (assuming that the concentrations of potassium and the porosity of the rocks are similar for both hydrocarbon accumulations, which has been confirmed by geological studies of this area). The fact that hydrocarbon fluids with the greatest residence times (fields C and D) are less mature than the others (fields A and B) corroborates the longer accumulation time. Moreover, this interpretation is in agreement with the more efficiently accumulated fluids generating more mature hydrocarbons (Fig. 16).

2 Sources of Non Hydrocarbon Gases (He, CO_2, N_2)

One of the most commonly used application of noble gas geochemistry in oil and gas exploration is to quantify the origins of non hydrocarbon gas compounds present in accumulations. N_2 and CO_2 are regarded of paramount importance as their presence in large proportions in hydrocarbons

reservoirs changes the reservoir's commercial value. Negative properties are also associated with CO_2, as it is known to acidify water, requiring the use of special well tubing for hydrocarbon production. Moreover, removal of CO_2 implies its subsequent elimination, with all the operational, financial and societal concerns involved (Carbon Capture and Sequestration). Another unwelcome non hydrocarbon gas sometimes in significant quantities is H_2S. Nonetheless this compound is generally autochthonous, generated within oil and gas accumulations (its high reactivity prevents its migration), and it has not been studied using the noble gases to date (as these generally provide information on fluids migrating into a hydrocarbon accumulation). Among non hydrocarbon gases associated with hydrocarbons, helium may be sometimes present in amounts large enough to become economically interesting. The geology and interest of helium will be discussed later.

It has been recognized for many years that some hydrocarbon accumulations present a substantial contribution of mantle noble gas (Oxburgh et al. 1986; Ballentine et al. 1991). The best indicator of mantle fluid contribution has been and remains the helium isotopic ratio, $^3He/^4He$. However, addition of radiogenic ^4He may reduce the isotopic ratio and effectively mask the presence of mantle fluids. Alternative diagrams have recently been suggested, solely using the ^3He concentration in the hydrocarbon phase, or using the ratio $CO_2/^3He$ (Sherwood-Lollar et al. 1997; Ballentine et al. 2002). According to these authors, a magmatic fluid would present a $CO_2/^3He$ ratio between 10^9 and 10^{10}. Any value above this range would suggest that there was no direct mantle contribution, whereas values below this range would correspond to more complex signatures such as partial loss of mantle CO_2. A Brazilian Paleozoic basin rich in evaporites (halite and anhydrite) has $CO_2/^3He$ lower than the mantle value (Prinzhofer and Battani 2003), as can be seen Fig. 17a, which could be interpreted as production of ^3He via nucleogenic reactions. Figure 17b shows the same gases in a $^{40}Ar/^{36}Ar$ versus R/Ra diagram. For mantle and radiogenic Ar contributions, the $^{40}Ar/^{36}Ar$ should increase. But in the case of a mantle contribution, this increase should correlate positively with $^3He/^4He$ (expressed as R/Ra) as the mantle value is around ^8Ra, whereas in the case of a radiogenic contribution, the increase of ^4He would decrease $^3He/^4He$. This is what is observed on Fig. 17b, indicating that there is no evidence for a mantle contribution. The excellent correlation between the two isotopes ^3He and ^4He (Fig. 17c) favors a common origin.

The origin of CO_2 may be characterized using its carbon isotopic ratios (Fig. 18). A low $\delta^{13}C$ value generally indicates an organic carbon origin, whereas a positive (heavy) $\delta^{13}C$ isotopic value is generally associated with oil biodegradation. $\delta^{13}C$ values around -4 per mil are generally linked to a mineral origin of the CO_2, particularly for high proportions of CO_2 (Fig. 18, and Jenden et al. 1993). The two possible origins of mineral CO_2, carbonate decomposition and mantle fluids, cannot be distinguished with carbon isotope ratios alone. The associated noble gases are often used to test the presence of a mantle fluid invading the petroleum system. Figure 19 shows that the gas samples corresponding to high CO_2 concentrations and $\delta^{13}C$ values around -4 ‰ PDB are clearly associated, in this database, to a large mantle contribution, visible with the helium isotopic ratios.

In order to better assess this mantle contribution, a correlation between the isotopic ratios of helium and argon (Fig. 20) shows that two main trends can be identified. A trend with a negative slope, similar to the trend of Fig. 17b, corresponds to addition of radiogenic ^4He and ^{40}Ar, and is related to the natural radioactivity of the sediments and possibly the underlying continental basement. A positive slope corresponds to a mixture with a mantle end-member.

Other mixing diagrams can be used to distinguish different physical processes. For instance, $^{20}Ne/^4He$ versus R/Ra is used to plot various sources of noble gases, notably the atmosphere and ASW, the mantle end-member and a crustal/radiogenic end-member (Fig. 21). It should be mentioned that the crustal end-member must contain a certain amount of ^3He, as a pure ^4He helium end-member would not

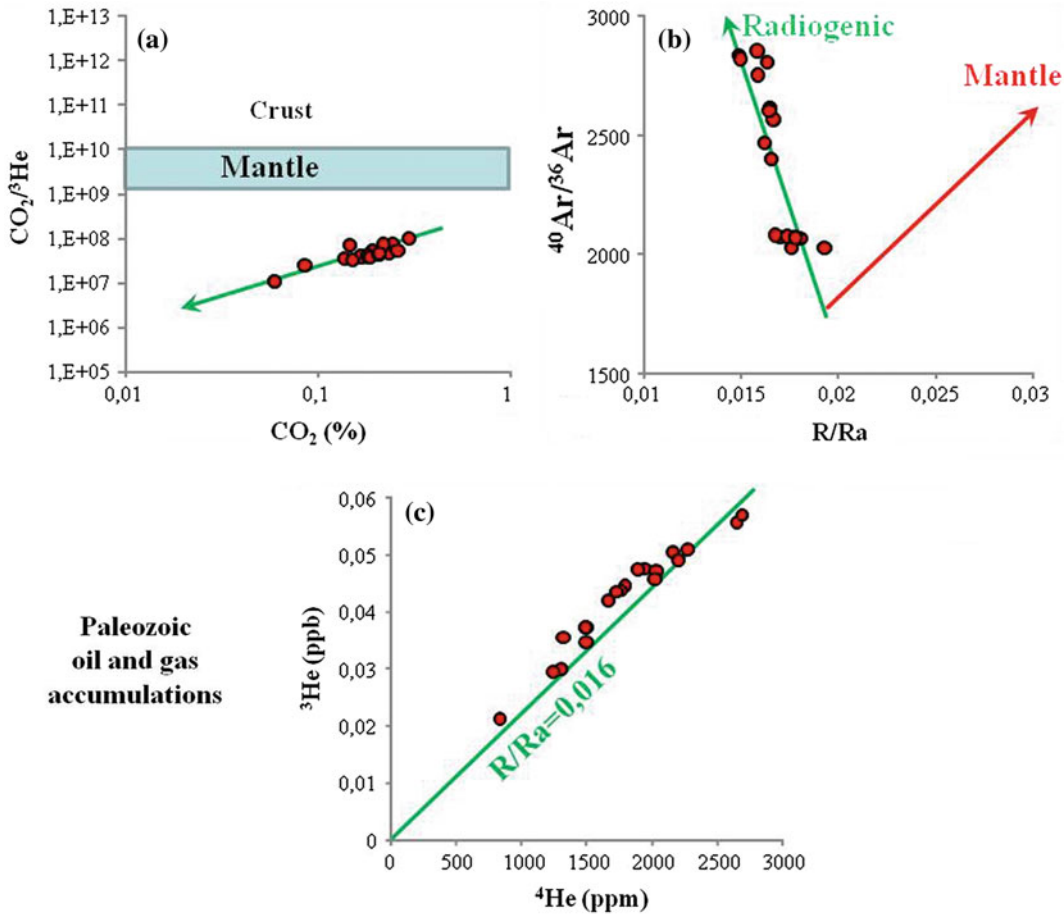

Fig. 17 For oil and gas accumulations in a Paleozoic Basin (Prinzhofer and Battani 2003), diagrams interpreting the possible mantle influence in the hydrocarbon accumulations. **a** Ratios $CO_2/^3He$ versus $^3He/^4He$ normalized to the atmospheric ratio as R/Ra. **b** Correlation between the argon isotopic ratio $^{40}Ar/^{36}Ar$ and the helium isotopic ratio $^3He/^4He$ expressed as R/Ra. **c** Correlation between the concentrations of ^3He and ^4He

explain a large portion of the gas samples, which would have too low $^{20}Ne/^4He$ for a given R/Ra. The radiogenic endmember needs to be around 0.02 Ra, demonstrating that traces of ^3He in gas accumulations may be of purely nucleogenic origin. In such a diagram, it is possible to quantify the proportions of ASW, mantle and crustal sources (considering that the atmospheric component is not present in non air-contaminated samples) for each gas sample.

The neon isotopes may also be used to characterize various sources of a gas accumulation. Figure 22 presents data from Gilfillan et al. (2009) from gas accumulations in the United States composed dominantly of CO_2. Plotting the data in a $^{20}Ne/^{22}Ne$ versus $^{21}Ne/^{22}Ne$, the three end-members mantle, ASW and crustal nucleogenic sources may be clearly indentified. The dataset shows that, depending on the gas province, there are variable contributions from each end-member, with a poorly defined end-member possibly corresponding to the crustal basement, located in the middle of the mixing surface. In this area, three distinct trends may be distinguished, joining the central end-member to each of the well documented trends, i.e. the mantle, the aquifers and the radiogenic poles (see Chap. 8).

An important and not completely resolved question remains: having demonstrated that mantle fluids can contribute to petroleum systems

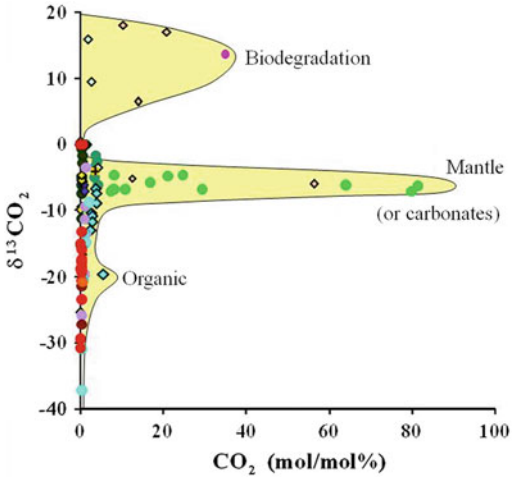

Fig. 18 Relation between the carbon isotopic ratio of carbon dioxide and its concentration in gas accumulations, for different basins wordwide (Ballentine et al. 1991, 1996; Prinzhofer et al. 2000; Ballentine and Sherwood-Lollar 2002; Deville et al. 2003; Prinzhofer and Battani 2003; Ellouz-Zimmermann et al. 2007; Gilfillan et al. 2009; Prinzhofer et al. 2010; Battani et al. 2011)

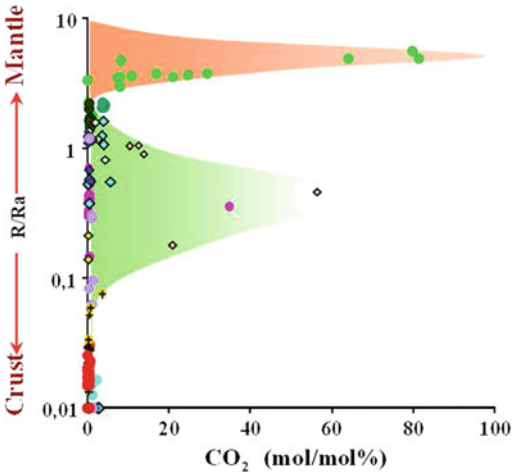

Fig. 19 Helium isotopic ratios of gas accumulations, expressed as R/Ra, versus the carbon dioxide concentrations in the gas accumulations. Same database as Fig. 18

and other gas accumulations, how then do these mantle fluids migrate from their source (the mantle) into the sedimentary sequences? If volcanism is present in the surrounding rocks, this may be the principal carrier of mantle fluids. However, in most cases mantle fluids are present

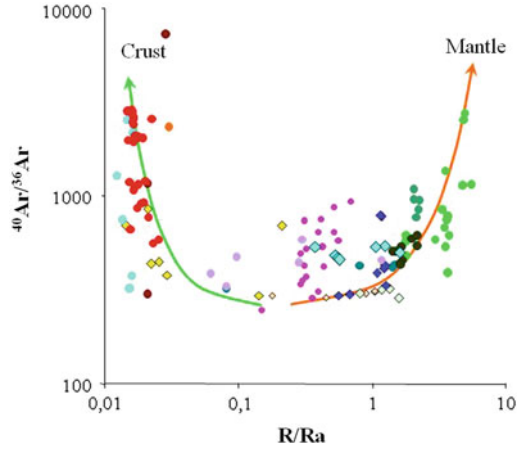

Fig. 20 Correlation between the argon isotopic ratio $^{40}Ar/^{36}Ar$ and the helium isotopic ratio $^{3}He/^{4}He$ expressed as R/Ra for the same database as Fig. 18

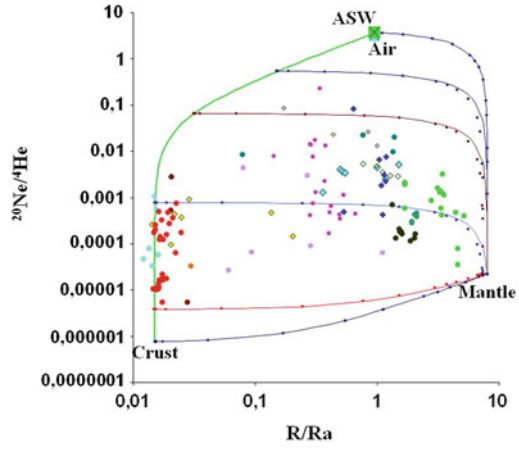

Fig. 21 Mixing diagram using $^{20}Ne/^{4}He$ versus the helium isotopic ratio expressed as R/Ra. The database is the same as for Fig. 18

in sedimentary basins free of local volcanic rocks. Furthermore, a mantle fluid will introduce not only helium but also lower concentrations of heavier noble gases (neon, argon, xenon), possibly overprinted in some cases with ASW contributions, and significant quantities of CO_2. Diffusion cannot be the only migrating process, as the time needed for diffusion through the entire continental crust is too long. Therefore a fluid flux in a constituted phase (supercritical?) is implied. As the porosity of the basement is much too low to permit Darcy, fractures have to be envisioned

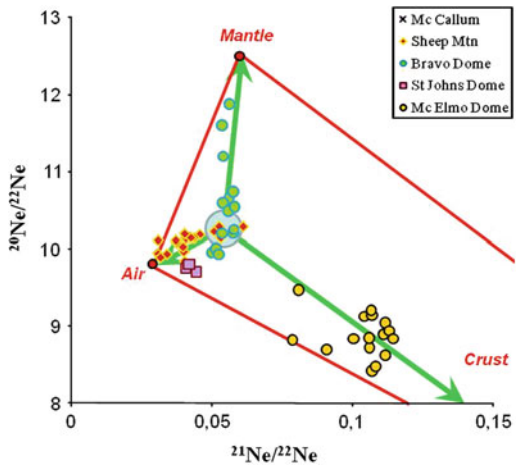

Fig. 22 $^{20}Ne/^{22}Ne$ versus $^{21}Ne/^{22}Ne$ for CO_2-rich gas accumulations studied by Gilfillan et al. (2009)

to allow these fluids to rise through sedimentary reservoirs. Hydraulic fracturing due to the occurrence of supercritical mixture of mantle related CO_2 and H_2O explains large contributions of mantle fluids in metasomatic ore deposits (see Chap. 11). The discovery of mantle lead associated with asphaltenes in the Potiguar Basin (Brazil, Dreyfus 2006), in which mantle helium is also found (Prinzhofer et al. 2010) confirms the metasomatic introduction of mantle fluids through hydraulic fracturing.

3 Control on Migration Processes

It is easy to imagine that helium is more mobile than other gases. In fact, the differential migration efficiency of noble gases may be studied and used for tracing hydrocarbon migration through sedimentary rocks.

The noble gases, being inert chemically, are not affected by chemical or biological processes, precluding complications of mixing chemical and physical processes, as occurs for the carbon isotopic ratio of methane for example. As a result, distinguishing source and migration effects on stable isotope ratios is not always straightforward (Prinzhofer and Pernaton 1997), whereas the noble gas ratios are only affected by physical processes, linked to migration. From the ASW noble gas isotopes, ^{20}Ne, ^{36}Ar, ^{84}Kr or ^{132}Xe, interaction with water that was at equilibrium with the atmosphere (ASW) can be demonstrated. Air itself should not be a significant part of the fluid as there is no direct interaction between deep hydrocarbon fluids and the atmosphere, except in the case of an accidental contamination during gas sampling. Figure 23 presents $^{84}Kr/^{20}Ne$ versus $^{36}Ar/^{20}Ne$ correlations for a database of various oil and gas fields around the world. Figure 24 presents in the same diagram the CO_2-rich accumulations of Colorado, USA (data from Gilfillan et al. 2009). The ratios share the same denominator, therefore a mixing trend between two end-members should plot on a straight line: in a mixture of ASW and the atmosphere, any sample in thermodynamic equilibrium with the surrounding rocks should plot on a straight line joining the ASW—air compositions. From Figs. 23 and 24 this is not the case, and the oil and gas samples plot on a curve passing though the atmospheric end-member, but not through the ASW point (whereas these samples can be demonstrated not to be contaminated by any air contribution during their sampling). Furthermore, these natural samples present a fractionation trend extending to a much larger range than that limited by their possible sources. Contributions from other sources (mantle, organic matter) can be excluded as their absolute concentrations are too small to significantly affect the data. This demonstrates that the noble gases have been fractionated, and that they are not in equilibrium with the surrounding rocks and fluids. As previously presented, only three physical processes may explain these trends: Exchange between phases, diffusion and adsorption. These three processes are linked to the migration of the fluids through the porous rocks, without reaching thermodynamic equilibrium.

In order to interpret and integrate these observations in a more quantitative model of fluid migration, migration experiments have been performed using CO_2, CH_4 or N_2 as the main constituent of the gas phase, with added traces of noble gases (Giannesini et al. 2008; Magnier et al. 2011; Vacquand et al. 2011). As described in the paragraph devoted to noble gas

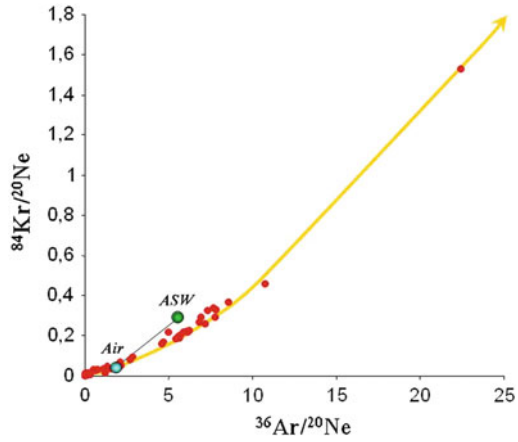

Fig. 23 $^{84}Kr/^{20}Ne$ versus $^{36}Ar/^{20}Ne$ for a large worldwide gas database. The end-members of the atmosphere and of ASW are also shown

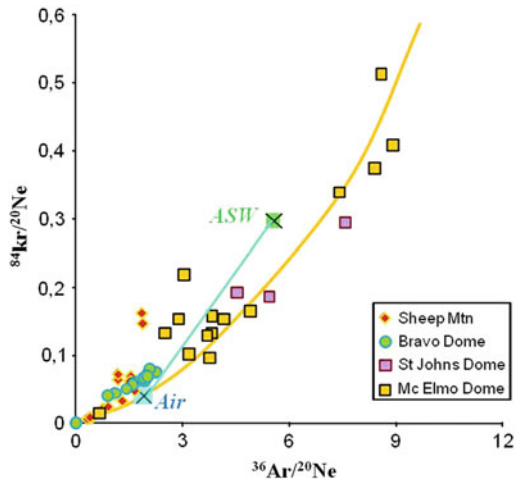

Fig. 24 Same diagram as Fig. 24 for the CO_2-rich gas accumulations studied by Gilfillan et al. (2009)

diffusion, the flux of noble gases in porous rocks is controlled not only by water diffusion, but also by adsorption/desorption of noble gases on mineral surfaces. This last process is largely negligible for helium and neon, but of primordial importance for the heavier noble gases (Ar, Kr, Xe). Combining these experimental results with the observation of natural gas fractionation in Figs. 23 and 24, it should then be possible to use noble gas isotopes in order to quantify migration processes affecting hydrocarbon fluids (oil and gas). The models need then to be assessed at different geometric and temporal scales: geological times, at the basin scale and at the reservoir scale, or human timescales for hydrocarbon migration during oil and gas extraction.

4 Controls on Oil and Gas Production

A new and challenging interest for noble gas geochemistry applied to the oil and gas industry is linked to a better assessment of hydrocarbon production. In fact, one of the big challenges for this century is changing oil and gas resources into reserves, i.e. making production of identified hydrocarbons feasible technically and economically. This concerns both conventional reservoirs (accumulations in sedimentary structures with high permeability) and unconventional reservoirs (rocks with low permeability, such as gas and oil shales, and heavy/viscous oils). The associated porosity is not generally limiting, as porosity controls only the amount of trapped fluids, and not its mobility during extraction. Two series of questions are raised with these issues:

- Characterization of the heterogeneity of the reservoir, in terms of permeability barriers, hydrocarbon saturation, fluid communication between wells, and the 3D image of the producing area,
- Monitoring production, or in other terms, at what stage of production is the reservoir? What is the proportion of currently extracted hydrocarbons versus the total extractable hydrocarbons accumulated in a given structure? What is the relative saturation in gas and in water for a gas shale system, etc…?

Noble gas isotopes, as tracers of physical processes, insensitive to chemical effects, are potentially excellent tracers for these tasks, even if this new application of noble gases is still not yet fully developed. Nevertheless, it has been demonstrated in earlier paragraphs that the hydrocarbon/water ratio can be quantitatively

calculated, and which may be used at the reservoir scale. Additionally, the composition of noble gas in hydrocarbons may vary over several orders of magnitude for both their concentrations and isotopic ratios. Potential heterogeneities may thus be investigated with higher precision using noble gases, as the key parameter for a sensitivity study is the ratio between the range of variation and the accuracy of the measurement. For example, the precision for a $\delta^{13}C$ measurement is about 0.5 per mil, whereas the usual variation of $\delta^{13}C$ for methane in a reservoir is around 30 delta units, and less than 5 delta units for the $C_2 +$ fraction. This gives a selectivity parameter for methane heterogeneity of 60 (30/0.5) and 10 for the C_2 fractions. For the associated helium concentrations, the variations may be from 100 to 2,000 ppm, with an accuracy of about 3 % for the concentration measurement. The resolution between samples is estimated at 120. This overall accuracy is consequently the same for all other noble gas parameters (concentrations and isotopic ratios), increasing significantly the potential to identify or characterize a fluid heterogeneity within a petroleum reservoir, indicative of a lack of mixing in the reservoir. This greater sensitivity to heterogeneities, associated with the fact that the noble gas compounds are only sensitive to physical processes, results in a promising potential for future noble gas applications in oil and gas production, when the usual techniques of production monitoring (geophysics, organic geochemistry) are insufficiently sensitive to provide accurate predictions.

5 Helium as an Important Natural Resource

The only source of helium for humankind is associated with natural gas accumulations, as the atmospheric concentration of helium is only 5 ppm, whereas sustainable helium production requires around 3,000 ppm He. Helium is one of the natural products with the most significant increases in demand (with a price increase of around 25 % for the year 2009). The main applications for helium are cryogenic uses (32 %), pressuring and purging (18 %), inert atmospheres for electronic equipments (18 %), welding (13 %), leak detection (4 %), breathing mixtures (2 %) and other applications (13 %). In some applications, other inert gases could be used, although not for all. Other potential uses of He could become significant if helium reserves were increased accordingly: inflated balloons for ore transportation in countries without road or railways infrastructures (center of Africa for example), heat carrier gas for new generations of nuclear plants, etc…. However, the reserves of helium today (about 8.5 billions of cubic meters) are relatively restricted, and represent about 25 years of production based on present consumption. However, it is important to take into consideration that reserves are calculated solely for the three helium producers at present, i.e. USA, Russia and Algeria. Qatar is building a new helium plant for the biggest gas field on Earth, the North Field. This new plant is expected to supply 25 % of the world production by 2013. The North Field is poorer in helium concentration than the 0.3 % considered today as the cut off value. The Liquefied Natural Gas (LNG) plants which already exist in Qatar allow extraction of commercial concentrations of helium, which appears with the residual non-liquefied part of the natural gas. This first concentration step by gas liquefaction produces a residual gas whose helium concentration is higher than the required 0.3 % cut off value.

More recently, sources of commercial helium have been generated from LNG plants, often located in countries rich in large gas fields. The residual gas (that which cannot be liquefied) in fact concentrates all the helium, as this gas is one of the most difficult to liquefy. Considering the small proportion this residue represents, the helium concentrations become sufficiently large to overcome the cut off value of 0.3 % in a lot of cases, even if the "geological" helium concentration is much smaller (a value of 0.05 % is considered as the pre-LNG cut off limit). Qatar becomes one of the most important country for helium reserves, as they have already built several LNG plants. This new He production

method will certainly change the economics of helium trading, as the market will be more international (for the moment, USA are the major exporter of helium by far), and reserves will grow drastically. It is however, still important to analyze helium concentrations in any gas field discovery, as this gas is not so commonly quantified (problems of sampling quality, as well as the common use of helium as the carrier gas of the gas chromatographic system which quantify the gas compositions).

It is important to note that if today, the reserves of helium are very small, no systematic exploration of this gas has been undertaken yet, meaning that most of the naturally occurring helium fields may be considered as undiscovered (or more precisely, some large gas fields have not been estimated so far for their helium potential).

Geologically speaking, the occurrence of relatively high He concentrations has been difficult to explain. The best known He gas field is the large Hugoton-Panhandle gas field of Texas (Gold and Held 1987; Ballentine and Sherwood-Lollar 2002). In this field, it seems that the absolute amount of helium cannot be explained by helium generated in situ in the basin sediments, as their U + Th concentrations cannot generate the radiogenic ^{4}He accumulated in the reservoir (Ballentine and Sherwood-Lollar 2002). This means that an extra-basinal source of helium needs to be assessed. The crustal basement seems a good candidate, as it is composed of U and Th-rich acid metamorphic and plutonic rocks. However, the transfer mechanism has remained problematic. The fact that helium-rich gas fields are accompanied by non hydrocarbon gas compounds, either N_2 or CO_2, may provide the explanation to helium migration; these non hydrocarbon gases are considered to be generated in metamorphic areas generating nitrogen (Palya et al. 2011), from high temperature decarbonation of carbonates or mantle hydrothermal fluids for CO_2. In all these cases, these extra-sedimentary fluids cross basement rocks before reaching the sedimentary basins, ending up in the gas traps. Mantle fluids were discussed in the paragraph devoted to non

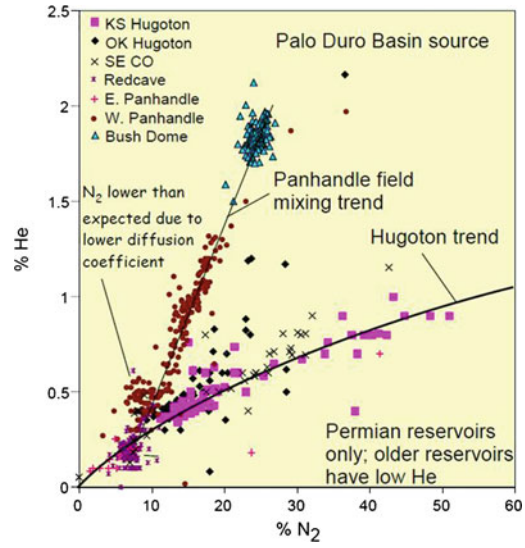

Fig. 25 Correlation between the helium and nitrogen concentrations of the Hugoton, Panhandle and Bush Dome gas accumulations (from Brown 2010)

hydrocarbon gases and migrate from the mantle to the sedimentary basins probably via hydraulic fracturing. It is fairly clear that during their migration, mantle fluids will interact with the rocks in the continental crust located between the mantle formations and the sediments. It may then be considered that these supercritical fluids (CO_2, H_2O, N_2) act as carrier gases for helium, which had been generated in the plutonic rocks of the basement, finishing in the sedimentary trapping systems. This would well explain the excellent correlation observed between nitrogen, helium, neon concentrations as well as nitrogen isotopic ratios in the Hugoton-Panhandle accumulations for example (Fig. 25, from Brown 2010): as for the ratio He/N_2 it may be linked to the specific leaching of the basement, the absolute concentrations related to the dynamics of N_2 metamorphism, and to the radiogenic production of helium in the continental rocks. However, some authors explain, through migration modeling, high helium concentrations gas fields without contributions from extra-basinal fluids (Brown 2010), meaning that further quantitative studies are needed.

References

Ballentine CJ, O'Nions RK, Oxburgh ER, Horvath F, Deak J (1991) Rare gas constraints on hydrocarbon accumulation, crustal degassing and groundwater flow in the Pannonian Basin. Earth Planet Sci Lett 105:229–246

Ballentine CJ, O'Nions RK (1994) The use of natural He, Ne and Ar isotopes to study hydrocarbon-related fluid provenance, migration and mass balance in sedimentary basins. In: Parnell J (ed) geofluids: origin, migration and evolution of fluids in sedimentary basins. Geol Soc Spec Pub, 78: 347–361

Ballentine CJ, O'Nions RK, Coleman ML (1996) A magnus opus: helium, neon and argon isotopes in a North Sea oil field. Geochim Cosmochim Acta 60:831–849

Ballentine CJ, Burnard PG (2002) Production, release and transport of noble gases in the continental crust. In noble gases in geochemistry and cosmoschemistry. Rev Mineral Geochem 47:481–538

Ballentine CJ, Burgess R, Marty B (2002) Tracing fluid origin, transport and interaction in the crust. In noble gases in geochemistry and cosmoschemistry. Rev Mineral Geochem 47:539–614

Ballentine CJ, Sherwood-Lollar BS (2002) Regional groundwater focusing of nitrogen and noble gases into the Hugoton-Panhandle giant gas field USA. Geochim Cosmochim Acta 66(14):2483–2497

Ballentine CJ, Marty B, Lollar BS, Cassidy M (2005) Neon isotopes constrain convection and volatile origin in the Earth's mantle. Nature 433(7021):33–38

Battani A, Sarda P, Prinzhofer A (2000) Basin scale natural gas source, migration and trapping traced by noble gases and major elements; the Pakistan Indus Basin. Earth Planet Sci Lett 181:229–249

Battani A, Prinzhofer A, Deville E, Ballentine CJ (2011) Trinidad mud volcanoes: the origin of the gas. In: Wood L (ed) Mobile shale basins, vol 93. AAPG Memoir, U.S., pp 1–14

Berecz E, Balla-Achs M (1983) Gas hydrates. English translation of gazhidratok. Amsterdam : Series studies in inorganic chemistry N° 4, Elsevier, p 343, ISBN 0444996575

Bosh A, Mazor E (1988) Noble gases association with water and oil as depicted by aztmospheric noble gases: case studies from the southeastern Mediterranean Coastal Plain. Earth Planet Sci Lett 87:338–346

Brown A (2010) Formation of high helium gases: a guide for explorationists 2010 AAPG Conference, New Oleans, Louisiana, USA, April 11–14

Burnard PG, Graham DW, Farley KA (1997) Vesicle-specific noble gas analyses of popping rocks: implication for primordial noble gases in Earth. Science 276:568–571

Crank J (1975) The mathematics of diffusion. Oxford University Press, Oxford, p 424

Crovetto R, Fernandez-Prini R, Japas ML (1981) Solubility of intert gases and methane in H_2O and in D_2O in the temperature range of 300 to 600 K. J Chem Phys 76:1077–1086

Deville E, Battani A, Griboulard R, Guerlais S, Herbin JP, Houzay JP, Muller C, Prinzhofer A (2003) Mud volcanism origin and processes: New insights from Trinidad. Special publication 216 of the Geological Society London on subsurface Sediment mobilisation, pp 475–490

Dreyfus S. (2006) Impact de la migration et de la biodégradation sur les signatures chimiques et isotopiques des traceurs métalliques dans les huiles. PhD. Pau University/IFP, 27th April 2006

Dunai TJ, Baur H (1995) Helium, neon and argon systematics of the European subcontinental mantle: implication for its geochemical evolution. Geochim Cosmochim Acta 59:2767–2783

Dyadin YA, Larionov EG, Mirinskij DS, Mikina TV, Starostina LI (1996) Hydrate formation in the krypton-water and xenon-water systems up to 10 kbars. 2nd international conference on natural gaz hydrates, Toulouse, June 2–6, 1996, pp 59–66

Elliot T, Ballentine CJ, O'Nions RK, Ricchiuto T (1993) Carbon, helium, neon and argon isotopes in a Po Basin (northern Italy) natural gas field. Chem Geol 106:429–440

Ellouz-Zimmermann N, Deville E, Muller C, Lallemant S, Subhani AB, Tabreez AR (2007) Impact of sedimentation on convergent margin tectonics. Example of the Makran accretionary prism (Pakistan). In: Lacombe O, Lavé J, Roure F, Vergés J (eds) Thust belts and Foreland Basins, from fold kinematics to hydrocarbon systems. Springer, pp 327–350

Fanale FP, Cannon WA (1971) Adsorption on the Martian regolith. Nature 230:502–504

Frick U, Chang S (1977) Ancient carbon and noble gas fractionation. Proceedings Lunar Science conference 8th, pp 263–272

Giannesini S, Prinzhofer A, Moreira M, Magnier C (2008) Influence of the bound water on molecular migration of CO_2 and noble gases in clay media. Goldschmidt Conference, Vancouver, Canada

Gilfillan SMV, Sherwood-Lollar B, Holland G, Blagburn D, Stevens S, Schoell M, Cassidy M, Ding Z, Zhou Z, Lacrampe-Couloume G, Ballentine CJ (2009) Solubility trapping in formation water as dominant CO_2 sink in natural gas fields. Nature 458:614–618

Gold T, Held M (1987) Helium-nitrogen-methane systematic in natural gases of Texas and Kansas. J Pet Geol 10(4):415–424

Graham DW (2002) Noble gas isotope geochemistry of mid-oceanic ridge and ocean island basalts: Characterization of mantle source reservoirs. In noble gases in geochemistry and cosmoschemistry. Review in Mineralogy and Geochemistry 47:247–304

Harvey AH (1998) Applications of near-critical dilute-solution thermodynamics. Ind Eng Chem Res 37(8):3080–3088

Honda M, McDougall I, Patterson DB, Doulgeris A, Clague DA (1991) Possible solar noble-gas component in Hawaiian basalts. Nature 349:149–151

Jähne B, Heinz G, Dietrich W (1987) Measurement of the diffusion coefficient of sparingly soluble gases in water. J Geophys Res 92(10):767–776

Jenden PD, Kaplan IR, Poreda RJ, Craig H (1988) Origin of nitrogen-rich natural gases in the California Great Valley: evidence from helium, carbon and nitrogen isotope ratios. Geochim Cosmochim Acta 52:851–861

Jenden PD, Hilton DR, Kaplan IR, Craig H (1993) Abiogenic hydrocarbons and mantle helium in oil and gas fields. In: Howell DG (ed) The future of natural gas, U.S. geological survey professionnal paper, 1570: 31–56

Kharaka YK, Specht DJ (1988) The solubility of noble gases in crude oil at 25–100 1C. Appl Geochem 3:137–144

Kennedy BM, Hiyagon H, Reynolds JH (1990) Crustal neon: a striking uniformity. Earth Planet Sci Lett 98:277–286

Kennedy BM, Torgersen T, Van Soest MC (2002) Multiple atmospheric noble gas components in hydrocarbon reservoirs: a study of the Northwest Shelf, Delaware Basin SE New Mexico. Geochim Cosmochim Acta 66(16):2807–2822

Kipfer R, Aeschbach-Hertig W, Peeters F, Stute M (2002) Noble gas in lakes and ground waters. In noble gases in geochemistry and cosmoschemistry. Rev Mineral Geochem 47:615–689

Kotarba MJ, Nagao K (2008) Composition and origin of natural gases accumulated in the Polish znd Ukrainian parts of the CArepathian region: gaseous hydrocarbons, noble gases, carbon dioxide and nitrogen. Chemical Geol 255:426–438

Kurz MD, Jenkins WJ (1981) The distribution of helium in oceanic basaltic glasses. Earth Planet Sci Lett 53:41–54

Magnier C, Prinzhofer A, Flauraud E, Giannesini S (2011) Effective diffusion rates of CO_2 and associated noble gases in low permeability rocks. Submitted to OGST

Mamyrin BA, Tolstikhin IN (1984) Helium isotopes in nature. Elsevier, Amsterdam, p 273

Mazor E, Bosh A (1987) Noble gas in formations fluids from deep sedimentary basins: a review. Appl Geochem 2:621–627

Moreira M, Allegre CJ (1998) Helium-neon systematic and the structure of the mantle. Chem Geol 147: 53–59

Morrison P, Pine J (1955) Radiogenic origin of the helium isotopes in rocks. Ann N Y Acad Sci 62: 69–92

Nagao K, Takaoka N, Matsubayashi O (1981) Rare gas isotopic compositions in natural gases of Japan. Earth Planet Sci Lett 53:175–188

O'Nions RK, Oxburg ER (1988) Helium, volatile fluxes and the development of the continental crust. Earth Planet Sci Lett 90:331–447

O'Nions RK, Ballentine CJ (1993) Rare gas studies of basin scale fluid movement. Phil Trans R Soc London A 344:141–156

Oxburgh ER, O'Nions RK, Hill RI (1986) Helium isotopes in sedimentary basins. Nature 324(18/24):632–635

Palya AP, Buick IS, Bebout GE (2011) Storage and mobility of nitrogen in the continental crust: evidence from partially melted metasedimentary rocks, Mt. Stafford Australia. Chemical Geology 281:211–226

Pinti DL, Marty B (1995) Noble gases in crude oils from the Paris Basin, France: implications for the origin of fluids and constraints on oil-water-gas interactions. Geochim Cosmochim Acta 59:3389–3404

Podosek FA, Bernatowicz TJ, Kramer FE (1982) Adsorption of xenon and krypton on shales. Geochim Cosmochim Acta 45(12):2401–2415

Porcelli D, Ballentine CJ, Wieler R (2002) An overview of noble gas geochemistry and cosmochemistry. In noble gases in geochemistry and cosmoschemistry. Rev Mineral Geochem 47:1–20

Prinzhofer A, Pernaton E (1997) Isotopically light methane in natural gases: bacterial imprint or segregative migration? Chem Geol 142:193–200

Prinzhofer A, Guzman-Vega MA, Battani A, Escudero M (2000) Gas geochemistry of the Macuspana Basin, Mexico: thermogenic accumulations in sediments impregnated by bacterial gas. Mar Pet Geol 17:1029–1040

Prinzhofer A, Battani A (2003) Gas isotope tracing: an important tool for hydrocarbon exploration. Revue de l'IFP, special publication for B. Tissot's jubilee, June 2003. Oil and gas science and technology. Rev IFP. 58(2): 299–311

Prinzhofer A, Dos Santos Vaz, Neto E, Battani A (2010) Coupled use of carbon isotopes and noble gas isotopes in the Potiguar basin (Brazil): Fluids migration and mantle influence. Mar Pet Geol 27:1273–1284

Rebour V, Billotte J, Deveugele M, Jambon A, le Guen C (1997) Molecular diffusion in water saturated rocks: a new experimental method. J Cont Hydrol 28:71–93

Reid RC, Praunsnitz JM, Sherwood TK (1977) The properties of gases and liquids. McGraw-Hill (ed), p 688

Ricard E, Pecheyran C, Ortega GS, Prinzhofer A, Donard OFX (2011) Direct analysis of trace elements in crude oils by high-repetition-rate femtosecond laser ablation coupled to ICPMS detection. Anal Bioanal Chem 399:2153–2165

Rudnick R, Fountain DM (1995) Nature and composition of the continental crust: a lower crustal perspective. Rev Geophys 33:267–309

Sano Y, Tominaga T, Wakita H (1982) Elemental and isotopic abundance of rare gases in natural gases obtained by a quadrupole mass spectrometer. Geochem J 16:279–286

Sano Y, Watika H, Huang CW (1986) Helium flux in a continental land area from $^3He/^4He$ ratio in northern Taiwan. Nature 323:55–57

Sarda P, Staudacher T, Allegre CJ (1988) Neon isotopes in submarine basalts. Earth Planet Sci Lett 91:73–88

Sherwood-Lollar B, Weise SM, Frape SK, Barker JF (1994) Isotopic constraints on the migration of hydrocarbon and helium gases of southwestern Ontario. Bull Can Pet Geol 42(3):283–295

Sherwood-Lollar B, Ballentine CJ, O′Nions RK (1997) The fate of mantle-derived carbon in a continental sedimentary basin: integration of CHe relationships and stable isotope signatures. Geochim Cosmochim Acta 61(11):2295–2307

Smith SP, Kennedy BM (1983) The solubility of noble gas in water and in NaCl brine. Geochim Cosmochim Acta 47:503–515

Smith SP (1985) Noble gas solubility at high temperature. EOS Trans Am Geophys Union 66:397

Staudacher T, Sarda P, Richardson SH, Allegre CJ, Sagna I, Dmitriev LV (1989) Noble gas in basalt glasses from a Mid-Atlantic Ridge topographic high at 14°N geodynamic consequences. Earth Planet Sci Lett 96:119–133

Steiger RH, Jager E (1977) Subcommission on geochronology: convention on the use of decay constants in geo- and cosmochronology. Earth Planet Sci Lett 36:359–362

Stuart FM, Lass-Evans S, Fitton G, Ellam RM (2003) High $^{3}He/^{4}He$ ratios in picritic basalts from Baffin Island and the role of a mixed reservoir in mantle plumes. Nature 424(6944):57–59

Torgersen T, Kennedy BM (1999) Ar–Xe enrichments in Elk Hills oil field gases: role of water in migration and storage. Earth Planet Sci Lett 167:239–253

Trieloff M, Kunz J, Clague DA, Harrison D, Allegre CJ (2000) The nature of pristine noble gases in mantle plumes. Science 288:1036–1039

Trieloff M, Kunz J, Allegre CJ (2002) Noble gas systematic of the Réunion mantle plume source and the origin of primordial noble gases in Earth's mantle. Earth Planet Sci Lett 200:297–313

Vacquand C, Guyot F, Prinzhofer A, Magnier C (2011) An experimental study of hydrogen migration through water saturated porous rocks. Submitted to OGST

Wacker JF, Zadnik MG, Anders E (1985) Laboratory simulation of meteoritic noble gases. I. Sorption of xenon on carbon: trapping experiments. Geochim Cosmochim Acta 49:1035–1048

Wacker JF (1989) Laboratory simulation of meteoritic noble gases. III. Sorption of neon, argon, krypton and xenon on carbon elemental fractionation. Geochim Cosmochim Acta 53:1421–1433

Wasserburg GJ, Mazor E, Zartman RE (1963) Isotopic and chemical composition of some terrestriam natural gases. In: Geiss J, Goldberg ED (eds) Earth science and meteorites, p 219–240

Weis RF (1970) The solubility of nitrogen, oxygen and argon in water band seawater. Deep-Sea Res 17: 721–735

Weis RF (1971) Solubility of helium and neon in water and seawater. J Chem Eng Data 16:235–241

Weis RF, Kyser TK (1978) Solubility of krypton in water and seawater. J Chem Eng Data 23:69–72

Xu S, Nakai S, Wakita H, Wang X (1995) Mantle-derived noble gases in natural gases from Songliao Basin. China Geochem Cosmochem Acta 59: 4675–4683

Yang J, Lewis RS, Anders E (1982) Sorption of noble gases by solids, with reference to meteorites. I Magnetite and carbon. Geochim Cosmochim Acta 46:841–860

Yu S, Lu X, Xu H, Xie Q, Liu X (2010) Geochemical evidence for differential accumulation of natural gas in Shiwu fault depression, Songliao Basin China. Energy Explor Exploit 28(4):239–258

Zartman RE, Wasserburg GJ (1961) Helium, argon, and carbon in some natural gases. J Geophys Res 66(1):277–306

Zhou Z, Ballentine CJ, Kipfer R, Schoell M, Thibodeaux S (2005) Noble gas tracing of groundwater/coalbed methane interaction in the San Juan Basin USA. Geochim Cosmochim Acta 69(23):5413–5428

Zhou Z, Ballentine CJ (2006) 4He dating of groundwater associated with hydrocarbon reservoirs. Chem Geol 226(3–4):309–327

The Analysis and Interpretation of Noble Gases in Modern Hydrothermal Systems

Yuji Sano and Tobias P. Fischer

Abstract

This chapter describes the practice in the analysis and interpretation of noble gases in modern hydrothermal systems, including sample collection and analytical methods, implications of geographical distribution of helium isotopes in the large scale (100–1000 km) and the small scale (1–100 km), temporal variation of helium isotopes in some volcanoes, and the other noble gas isotope and abundance variations in hydrothermal systems. First, details of sampling method of volcanic and hot spring gases are discussed together with characteristics of two types containers, Giggenbach-type and lead-glass. Second, analytical techniques of noble gas abundances by an isotope dilution method using a QMS-based system, and neon interference on helium isotope measurements by a magnetic sector type mass spectrometer are written precisely. Third, helium isotope variations in three modern volcanic regions, such as hot spot, mid-ocean ridge, and subduction zone are compiled and discussed together with geo-tectonic settings and geophysical data. Fourth, across the island arc variations of helium isotopes are described against recent seismic tomography data in Northeast Japan, Southwest Japan, North Island of New Zealand, and Kamchatka peninsula of Russia. Then smaller size of the isotope variations around the independent volcano such as Mt Ontake and Mt. Nevado del Ruiz are discussed. Fifth, temporal variations of helium and neon isotopes in volcanic discharges

Y. Sano (✉)
Division of Ocean-Earth Systems,
Atmosphere and Ocean Research Institute,
The University of Tokyo, Kashiwano-ha, Chiba,
277-8564, Japan
e-mail: ysano@aori.u-tokyo.ac.jp

T. P. Fischer
Department of Earth and Planetary Sciences,
University of New Mexico, Albuquerque, NM
87131, USA
e-mail: fischer@unm.edu

P. Burnard (ed.), *The Noble Gases as Geochemical Tracers*, Advances in Isotope Geochemistry,
DOI: 10.1007/978-3-642-28836-4_10,

are discussed with examples showing the effects of changes in volcanic activity on noble gas ratios. Sixth, the isotopic compositions of neon, argon, krypton and xenon isotopes in volcanic and hydrothermal systems is discussed and related to mantle and crustal degassing processes. The last section (seven) provides applications of noble gases to traces sources and crustal contamination processes of more abundant gases such as carbon dioxide, methane and nitrogen with examples from well studied hydrothermal systems in New Zealand, Italy, Central America and Greece. In summary noble gases have a wide range of applications in volcanic and hydrothermal systems and are key indicators of tectonic setting, mantle and magma degassing; they provide valuable information on the current activity of a volcano and in combination with major gases can provide insights to understanding other geologically important volatiles such as carbon dioxide, methane and nitrogen.

1 Sampling Methods

1.1 Containers for Collecting and Storage of Fluid Samples

Various kinds of gases and fluids emerge from the solid Earth from volcanoes, thermal springs, low temperature water pools, and natural gas wells in modern hydrothermal systems. Among these, high temperature volcanic fumaroles and thermal springs contain magmatic volatiles, which were dissolved in the magma at depth in the Earth. These are usually acidic volatiles containing HCl, HF, H_2S, and SO_2 (Williams and McBirney 1979) which react severely with metals and would rapidly corrode them. Therefore traditional copper tube with stainless-steel clamp containers (conventionally adopted for collecting water dominated samples) cannot be used. Glass bottles, ampoules, and/or reservoirs are more suitable candidates for collecting and storing acidic gases. There are two types of sampling vessels for fluids in modern hydrothermal system: Giggenbach-type and lead-glass containers. The Giggenbach-type bottle was originally invented and distributed by the German chemist, Werner F. Giggenbach (Giggenbach 1975) and subsequently imitated by many researchers. The bottle consists of an evacuated 300 ml cylindrical, round-bottom flask with a Teflon stopcock and containing approximately 50 ml of 4–6 N NaOH solution (see Fig. 1a). For the heavy noble gases such as Ar and Xe, Giggenbach-type containers are probably useful but have not been extensively used by noble gas geochemists because He permeates through Pyrex glass.

Here, we discuss the problem of He diffusion through glass during storage in the laboratory before analysis. Helium permeation through glass has been experimentally determined by several researchers in the in 1950s–1960s (Altemose 1961; Norton 1953; Rogers et al. 1954). Taking the permeation constant, $K = 9.1 \times 10^{-12}$ and 1.5×10^{-11} ccSTP/sec/cm^2 (area)/mm (thickness)/10 Torr (partial pressure difference) at 25 °C of Pyrex glass (Norton 1953) and assuming that the inner surface area is 280 cm^2 for the Giggenbach-type container (Fig. 1a) and the wall thickness is 0.7 mm, the amount of He permeation becomes 4.1×10^{-4} ccSTP/day if the sample contains 1.3 % He. If the sample inside of the vessel contains 100 ppm He, total amount of He is 3.0×10^{-2} ccSTP and the permeation rate is 3.2×10^{-6} ccSTP/day. It therefore requires more than 10 years to equilibrate with the outside air, simply obtained by the amount divided by the permeation rate. If the sample contains 3 ppm ^{4}He and 20 ppt ^{3}He (typical high temperature volcanic gas; see (Giggenbach et al. 2001), ^{4}He may permeate from the outside to inside at 6.7×10^{-8} ccSTP/day, while that of

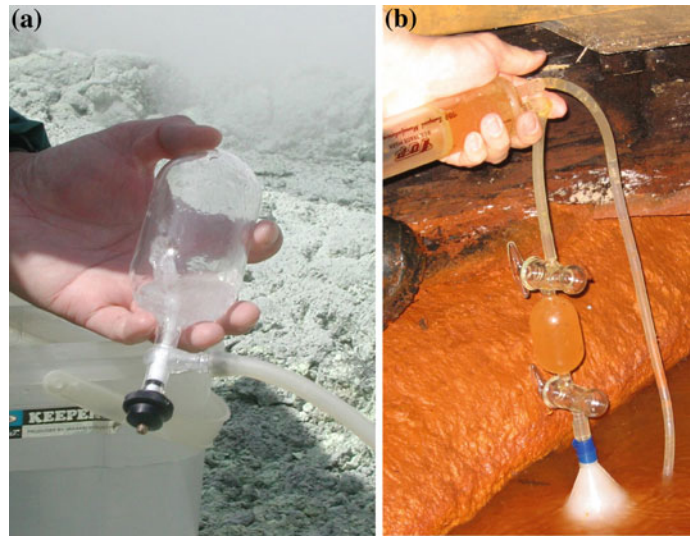

Fig. 1 Sampling vessels of **a** high temperature volcanic gas (Giggenbach-type) and **b** bubbling gas in hot spring (lead-glass container)

^{3}He is reverse, from the inside to the outside at 4.4×10^{-13} ccSTP/day assuming that the ^{3}He permeation constant is the same as that of ^{4}He. In this case, the ^{3}He/^{4}He ratio may decrease about 4 % within a few months of storage time. This suggests that samples collected by a Giggenbach-type containers should be measured as soon as possible.

Figure 1b shows a 50 cm^3 lead glass container with vacuum valves at both ends. The permeation constant of a lead glass (PbO content is 11 %) is 9.4×10^{-12} ccSTP/sec/cm^2/mm at 214 °C and 1.5×10^{-10} at 382 °C (Altemose 1961). Then the permeation constant is extrapolated to about 7.5×10^{-15} ccSTP/sec/cm^2/mm at 25 °C. Adopting this value for lead glass containers with an inner surface area of 74 cm^2 (Fig. 1b), it takes 1,000 years for the ^{3}He/^{4}He ratio of a volcanic gas to decrease by 4 %. The storage time in a laboratory using a lead glass container for 2–3 years is practically accepted and sufficiently long for geochemical research. In addition, there is the possibility of isotopic fractionation accompanying He permeation in glass, because the isotopic diffusivity ratio may correspond to the inverse square-root of the ratio of their masses (Trull and Kurz 1999). This could occur in Giggenbach-type containers, and cautious interpretation of data obtained after a long storage time is required.

1.2 Sampling of Volcanic Gases and Thermal Springs

High temperature volcanic gases (defined here as $T > 400$ °C) contain more than 95 % of water vapor accompanied by variable amounts of CO_2, CO, H_2, CH_4, HCl, SO_2, and H_2S (Williams and McBirney 1979). Noble gases are generally minor components and treated as inert gases together with N_2. It is better to collect a dry gas phase to increase the concentration of noble gases and ideally the water vapor should be separated in the field. Figure 2 shows a block diagram for collecting high temperature volcanic gases. Pure titanium has been adopted for the collection tube from a fumarole source for its chemical and mechanical stability. Copper and stainless tubes are useless, becoming badly corroded in a very short time. The titanium tube is connected to a condenser through a silica tube. Since the flow rate of volcanic gas is high, permeation of He in the silica wall will be negligible. Liquid water drains into the water separator while a dry gas is introduced into the lead glass container. When the flow velocity of the dry gas is slow, a manual pump is connected to the other end of the container and the sample gas is sucked slowly through the apparatus and flushed several times through the container. In the case of medium-temperature fumaroles

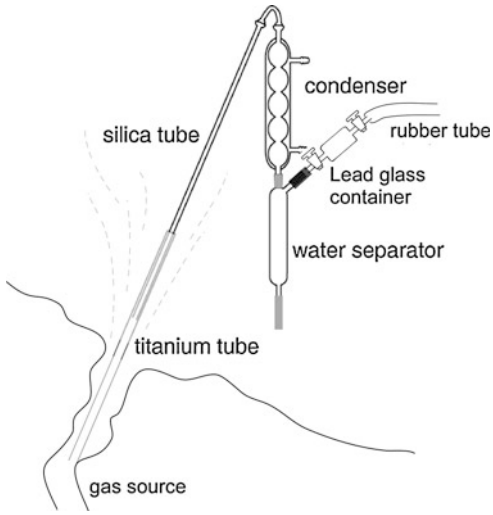

Fig. 2 A schematic diagram of a sampling method for high temperature volcanic gases

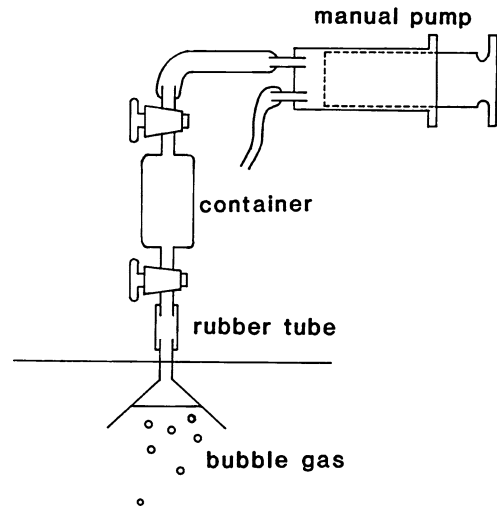

Fig. 3 A schematic diagram of a method for sampling bubbling gases in hot springs

(400 °C > T > 100 °C), the silica tube may be removed and the condenser is directly connected to the titanium tube. For low-temperature fumaroles (T < 100 °C), the condenser and water separator are not necessary. The lead glass container is connected to the titanium tube and the sample gas is drawn in by a manual pump at a low flow rate.

In the thermal spring and drawn fumarole region (T < 100 °C), it is recommended that the gas phase sample is collected when gas bubbles are present. Noble gases preferentially partition into the gas phase rather than liquid water, because of their low solubility (Ozima and Podosek 1983). Collecting with bubbles present results in a lower risk of air contamination. Figures 3 and 1b show a block diagram and a photograph, respectively, for collecting bubbling gases in thermal springs. One end of the lead glass container is connected to an inverted funnel and the other end to a manual pump. First the funnel is put into the spring water and the container is filled with spring water using the pump. Then the funnel is placed over the source of bubbles in the spring. After the water in the funnel has been replaced by gas, the gas in the funnel is transferred into the container by using the manual pump. The inside of the container is flushed several times by passing sample gas through it in order to avoid air contamination. When there is no bubbling, the spring water is collected directly, without the funnel. One end of the lead glass container is connected with a tygon tube and the other end with a manual pump. A tip of the tube is introduced into the spring source and the water sample is transferred into the container by a manual pump. When the spring water is close to neutral in pH, it is possible to collect and store it in a copper tube.

1.3 Advantages and Disadvantages of Lead Glass Container

The advantages of lead glass containers over Giggenbach-type containers is not only the low He permeation but also their use in other geochemical applications. It is possible to directly analyze major and trace chemical compositions of gas samples by means of gas chromatography (Gunter and Musgrave 1966) and/or a quadrupole mass spectrometer system when the sample gas pressure is low (Sano et al. 1992). Then noble gas data are thus interpreted together with the gas chemistry, which is geochemically important. In the case of Giggenbach-type containers, acid species such as CO_2, H_2S, SO_2 and HCl are dissolved in the alkaline solution and are fixed, i.e. do not reacting after sampling.

Even though these species can be measured by titration and/or volumetric method following chemical treatment (Giggenbach 1975), the analytical procedure is more difficult and complex than for lead glass samples.

In addition to the chemical composition, it is also possible to measure the stable isotopes such as $^{13}C/^{12}C$, $^{15}N/^{14}N$ and $^{34}S/^{32}S$ ratios in lead glass container samples (after noble gas measurement). Usually, volcanic gases and hydrothermal fluids contain significant H_2S, which typically interferes with precise measurement of carbon isotopes of CO_2 in gas source mass spectrometers. This is partly due to the fact that hydrogen derived from H_2S may convert a part of CO_2^+ to HCO_2^+ in the ionization chamber (Nishio et al. 1995), which makes the mass number 45/44 ratios higher than the original. Separation of CO_2 from H_2S by simple trapping using coolants (such as liquid nitrogen and acetone with dry ice) is inefficient, because the sublimation point (195 K) of CO_2 is between the boiling point (213 K) and the melting point (188 K) of H_2S. Therefore it is necessary to use a second cold trap containing an evacuated 1 M $CuCl_2$ solution. H_2S reacts with $CuCl_2$ in the solution and precipitates CuS, producing a pure CO_2 gas sample. Sulfur isotopes can be measured from the CuS precipitate after chemical treatment and purification using a continuous flow GC-IR-MS (Grassineau 2006). Nitrogen isotopes can be measured after noble gas study using the remaining gas in the lead glass container. Nitrogen is always in the gas phase together with He and Ar provided an activated charcoal trap at liquid nitrogen temperature is not used. Even though the amount of nitrogen may be as low as 200 pmol, it is nevertheless possible to measure the $^{15}N/^{14}N$ ratio using static vacuum operated mass spectrometers, originally designed for noble gas analysis and modified for nitrogen isotope analysis (Takahata et al. 1998).

The disadvantage of lead glass containers is that it is impossible to retain the redox conditions of sulfur species. After collection of volcanic gases, SO_2 may react with H_2S even in the container at room temperature whereas SO_2 and H_2S are determined separately using a Giggenbach-type container. We can measure H_2S content by alkaline-iodine titration method and total sulfur is determined by gravimetric precipitation of $BaSO_4$ after oxidation using H_2O_2 (Giggenbach 1975). When the noble gases are the main target of the research, the redox condition is not an issue. Therefore we recommend lead glass containers for the collection and storage of volcanic fumarole and thermal spring samples.

2 Analytical Method

2.1 Elemental Abundances of Noble Gases

2.1.1 Extraction of Noble Gases

Noble gas elemental abundances of modern hydrothermal systems imply the concentrations of He, Ne, Ar, Kr and Xe in the gas phase or in liquid water. The former is traditionally expressed by a unit such as ppm (part per million) and ppb (part per billion) volumetrically. For water, this is more conventionally expressed as ccSTP/g (gas volume at standard temperature and pressure dissolved in 1 g liquid water). These concentrations are measured by a gas chromatograph or a mass spectrometer. In the case of thermal spring water samples, noble gases need first to be extracted from the liquid phase. The simplest and easiest way is a head space method. Figure 4 shows a block diagram of a typical noble gas extraction vacuum line. Due to permeation of helium through glass, stainless steel is usually used for all parts of the line. Capacitance manometer pressure gauges are used to determine the pressure precisely. A copper oxide furnace is used to oxidize H_2, H_2S and CH_4. The copper tubes or lead glass containers are connected to a metal extraction vessel with a static (isolated from the pumping system) high vacuum. Then the copper tube clamp is removed or the valve is opened and water is drained and transferred into the extraction vessel. To equilibrate rapidly, the vessel is vibrated by an ultrasonic water bath.

Since the solubility of He and Ne are low in fresh water and brines, most gases partition into

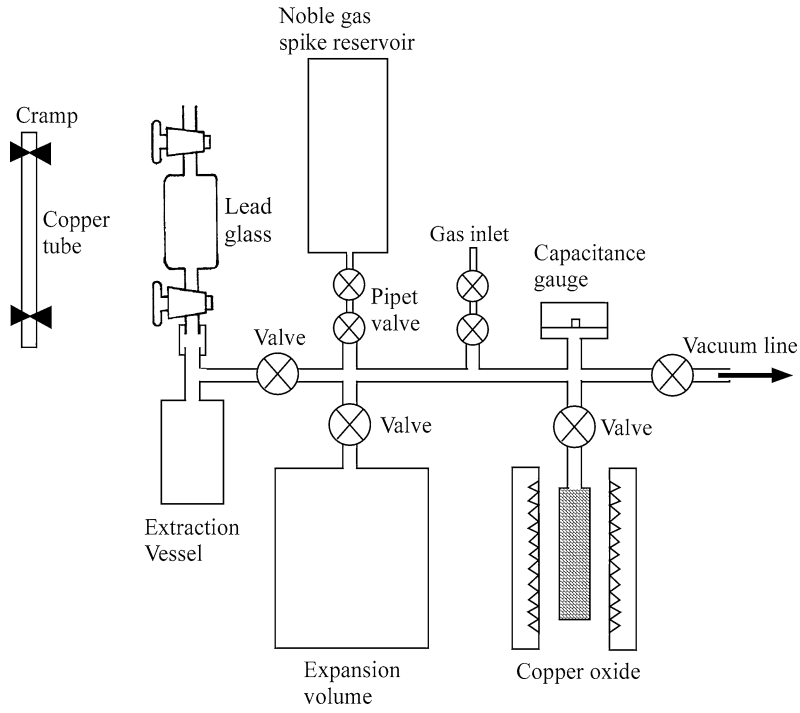

Fig. 4 A schematic diagram of a typical noble gas extraction vacuum line for treating gas/fluid samples

the gas phase at room temperature: only 0.8 % of the total He and 1 % of Ne remain in the liquid phase (solubility data are from Ozima and Podosek (1983)) when the volume of the gas phase is the same as that of liquid. These amounts are usually smaller than the experimental error of He and Ne contents and do not present practical problems. On the other hand, 8.7 % of Xe could remain in the water following extraction (Ozima and Podosek 1983), which is larger than the error and should be corrected after the gas phase measurement. When the gas phase is significantly larger than the liquid phase, the Xe loss should be negligibly small. In order to reduce these losses, Smith and Kennedy (1983) heated the extraction vessel to boil the fluid. In addition, they used a large expansion volume attached to the vacuum line and claimed that more than 99 % of noble gases were extracted from the solution. There is alternative method for extracting noble gases from a liquid phase. In the case of dynamic flow measurement such as a gas chromatography, it is possible to use a helium carrier gas for bubbling the water sample and trap noble gas in a sample loop with activated charcoal held at liquid nitrogen temperature. High sensitivity detectors are required to measure the heavy noble gas (Ar, Kr and Xe) abundances. However this method has not been conducted and documented in the literature.

Abundances of He and Ar in thermal spring gases have been measured by a gas chromatography with a conventional thermo-cupled detector (TCD) for the purpose of earthquake prediction (Sugisaki 1978). Neon contents in volcanic and hot spring gases were also measured by gas chromatography with more sensitive ultra-sonic detector (USD) detectors and He carrier gas (Urabe et al. 1985). Heavier noble gases (Kr and Xe) have been not analyzed by a gas chromatography in a routine manner, because their concentrations are usually lower than the detection limit of the machine. Gas flow measurement using a quadrupole mass spectrometer could also allow He and Ar contents in gas samples to be analysed (Sano et al. 1992), but it is nevertheless difficult to measure Ne, Kr and Xe. All noble gas abundances have been successfully and routinely measured by mass spectrometer, either quadrupole (Sano et al.

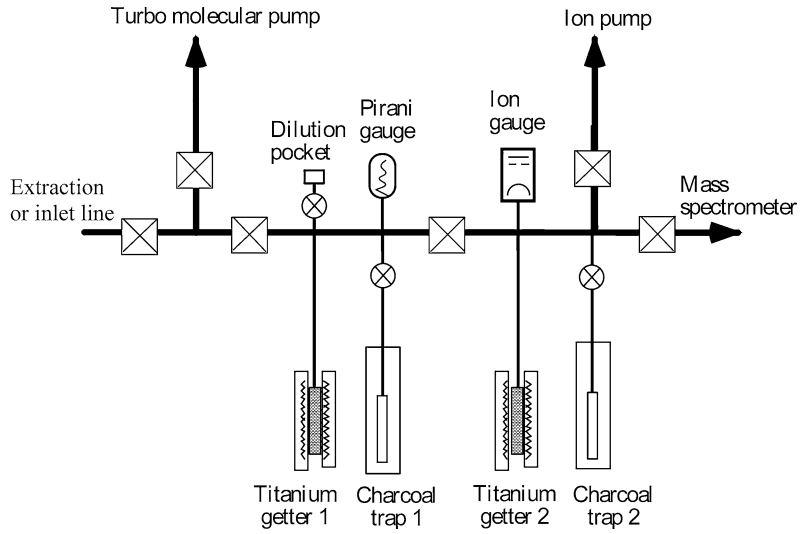

Fig. 5 A schematic diagram of a typical noble gas purification and separation vacuum line

1982) or magnetic reflection type mass spectrometer (Beterle et al. 2000) under a static vacuum operation after purification and separation of noble gases in an ultra-high vacuum line.

2.1.2 Purification and Separation of Noble Gases

Figure 5 shows a block diagram of a typical noble gas purification and separation vacuum line. Since He permeates through normal glass rapidly, stainless steel is used for all parts of the line which consists of two purification and separation sections divided by all-metal, bakeable, bellows valves. The system is evacuated by a turbo molecular pump (for rough vacuum) and sputter ion pump (for ultra-high vacuum). A Pirani gauge and an ionization gauge measure pressure in the first and second sections, respectively.

The outline of purification and separation procedures for noble gases is briefly described in the following section: the gas extracted from a liquid sample or that introduced from a gas inlet is purified by a CuO furnace at 450 °C to decompose H_2, H_2S, CH_4, and other hydrocarbons (Fig. 4). Oxidized gases and the noble gases are transferred to the purification and separation line (Fig. 5). Titanium getter 1 is heated to approximately 850 °C to adsorb active species such as H_2O, CO_2, SO_2 and N_2. When getter 1 is cool, He and Ne are separated from Ar, Kr and Xe lon the activated charcoal trap 1 at liquid nitrogen temperature. Non-adsorbed gases, including He, Ne and small portions of active gases are transferred to the next section. A second purification is repeated using charcoal trap 2. Then purified He and Ne fraction is admitted to the mass spectrometer.

After the He and Ne measurements, the remaining gas is pumped out. The two charcoal traps are heated to about 100 °C to release adsorbed gases and titanium getter 2 is heated to adsorb active species. When the getter is cool, Ar is separated from Kr and Xe by cooling the charcoal traps in dry ice-alcohol baths. Then the Ar fraction is admitted to the mass spectrometer. Usually amount of Ar is too large to measure and needs to be reduced by using a dilution pocket. After the Ar measurement, the vacuum line is pumped out. The two charcoal traps are heated once more and Kr and Xe are released (and minor active gases) by keeping the trap temperature at about 100 °C. The heavier noble gases are purified again by heating a titanium getter 2. Then Kr and Xe are introduced into the mass spectrometer.

2.1.3 Mass Spectrometer of Noble Gas Analysis

Two types of mass spectrometers are used to analyze noble gas abundances; a quadrupole

mass spectrometer (QMS) and a magnetic deflection mass spectrometer, even though they have similar electron impact ion sources. The former has several advantages over the latter, such as simplicity of operation and maintenance, physically small and light, not vulnerable to vibration, a high scanning rate covering a wide range of masses and the low cost of the machine. On the other hand disadvantages are generally low mass resolution, low sensitivity, round peak shapes, and low precision of isotope measurements. In the 1960s, magnetic deflection mass spectrometers were first introduced for noble gases analysis (Canalas et al. 1968; Mazor and Wasserburg 1965; Mazor et al. 1964).

In the 1980s, the first noble gas analysis by QMS were reported by Sano, Tominaga and Wakita (1982). Since then there are several reports of noble gas analysis by using a QMS (Kulngoski and Hilton 2002; Poole et al. 1997) in addition to a magnetic deflection mass spectrometer (Beterle et al. 2000; Igarashi et al. 1987).

Two basic methods are well documented for measuring noble gas abundances by mass spectrometer; the sensitivity method and the isotope dilution method. The former is based on the peak height of the mass spectrum of the most abundant isotopes of the noble gases notably ^{4}He, ^{20}Ne, ^{40}Ar, ^{84}Kr and ^{132}Xe. The intensities of the sample gas are compared with those of a standard gas measured before and immediately after the sample analysis. The precision of the sensitivity method is derived from the reproducibility of the standard gas, which is usually atmospheric noble gases. Generally the reproducibility is 10–20 % by QMS (Sano et al. 1982) and about 1 % by the careful operation of a magnetic deflection mass spectrometer (Beterle et al. 2000). The accuracy of the method for water samples is difficult to assess in some cases, because the recovery of noble gases is not complete or perfect in the extraction method (see the Sect. 2.1.1).

The isotope dilution method provides more precise and accurate data than the sensitivity method. However, an expensive noble gas spike needs to be prepared, enriched (preferably at the 99 % level) in the rare isotopes, usually ^{3}He, ^{22}Ne, ^{38}Ar, ^{78}Kr and ^{124}Xe. In addition, there are some memory effects of the enriched isotopes in the mass spectrometer, making it difficult to measure natural isotopic compositions of noble gases after using these spikes. Usually mixtures of known amounts of these enriched isotopes are stored in a reservoir attached to the extraction line (see Fig. 4). Before opening the clamp of a copper tube or introducing an aliquot of gas samples through the gas inlet, a pipette of the mixed noble gas spike is introduced into the system. Then the noble gases are extracted from the water sample, with thorough mixing of the spike gases with the extracted gases ensured by the vibration of the ultrasonic water bath. After mixing of the sample and spike noble gases, elemental fractionation of noble gases does not affect the analysis, since the mixed spikes behave identically to the natural isotopes. This can work not only against solubility loss but also elemental fractionation due to adsorption by low temperature activated charcoal. Precision of noble gas abundance measurements using the isotope dilution method is limited to the accuracy of the isotopic ratio of the natural isotope to the spike isotope by a mass spectrometer. Table 1 lists a comparison of noble gas abundance analysis of water samples by static mass spectrometer. Recent methods have provided 1 % precision in the abundances in a routine manner.

Noble gas solubilities in water and seawater has been examined and reported in literature (Ozima and Podosek 1983). Generally the heavier noble gases are more soluble than the lighter ones, which discussed in Sect. 2.1. Figure 6 shows experimental noble gas solubility data of brines at different temperatures (Sano and Takahata 2005; Smith and Kennedy 1983; Weiss 1970). For example, Xe is about four times enriched in brine compared to Ar at 0 °C, while Ne is four times depleted. These data are useful for examining noble gas fractionation patterns in hydrothermal systems.

2.1.4 Neon Interference on Helium Isotope Measurements

Purification and separation of noble gases are described in Sect. 2.1.2. After purification, He and Ne are separated from Ar using an activated

Table 1 Comparison of noble gas abundance analyses by a static mass spectrometry

References	Water sample size (cm^3 STP)	Purification and separation	Mass spectrometer	Spike	Method	Precision (%)
Sano et al. (1982)	35	Ti + Zr getter, charcoal	QMS	No	Peak height	10–20
Igarashi et al. (1987)	50	Ti getter, charcoal	Magnetic sector	No	Peak height	10–20
Poole et al. (1997)	n.d.[a]	Zr + Al getter, charcoal	QMS	Yes	Isotope dilution	3[b]
Beterle et al. (2000)	45	Ti getter, charcoal	Magnetic sector	No	Peak height	0.3–1.0
Kulngoski and Hilton (2002)	14	Ti getter, charcoal	QMS	Yes	Isotope dilution	0.9–3.6[c]
Sano and Takahata (2005)	8	Ti getter, charcoal	QMS	Yes	Isotope dilution	0.4–0.9

[a] Sample size was not described
[b] Calculated from the error of equilibrium temperature
[c] Calculated from the average of the error in standard water gas abundances (see Table 6 of the reference)

charcoal trap held at liquid nitrogen temperature and are admitted into the mass spectrometer together. Rison and Craig (1983) reported that varying He/Ne ratios in their mass spectrometer have been found to affect the measured helium isotopic ratio by up to 10 %. If air helium is used as a laboratory standard without separating the neon, measurements on samples with He/Ne ratios similar to air will require little correction, but measurements on samples with quite different He/Ne ratios will result in erroneous values and require major correction: the sample compared to an air standard will generally appear to have a lower $^3He/^4He$ ratio than the real value. It is definitely necessary to separate He from Ne when a precise $^3He/^4He$ ratio is required.

In order to separate He from Ne, a cryogenic charcoal trap is necessary to achieve temperatures lower than liquid nitrogen. Usually cooling is done by a commercial helium expansion refrigerating machine (Reynolds et al. 1978). Sano and Wakita (1988b) reported a modified vacuum line for separation of He from Ne. In Fig. 5, "charcoal trap 2" can be replaced by a cryogenic trap operated by a helium expansion refrigerator. In addition the "ion gauge" is better replaced by an on-line quadrupole mass spectrometer (QMS), allowing separation of He from Ne to be checked using the QMS immediately before admitting the sample into the noble gas mass spectrometer. Figure 7 shows the relationship between the equilibrium ion currents for ^4He and ^{20}Ne by QMS (normalized to 100 % release) and charcoal trap temperature by Sano and Wakita (1988b). The sorption curves agree well with those reported by Reynolds et al. (1978). An excellent separation of He from Ne is achieved at approximately 40 K.

As stated above, varying He/Ne ratios in samples may affect the measured $^3He/^4He$ ratio. Figure 8 shows the relationship between the $^3He/^4He$ ratio of an air standard and co-existing Ne content (expressed here as a $^{20}Ne/^4He$ ratio) on a VG5400 instrument. There is an apparent negative correlation between the $^3He/^4He$ and $^{20}Ne/^4He$ ratios. The measured $^3He/^4He$ ratio of air He + Ne ($^{20}Ne/^4He$ ratio = 3.14 i.e. the air composition) shows a value about 11 % lower than the $^3He/^4He$ ratio of air He only (i.e. Ne free). Thus a sample measured against the air standard with Ne could have a higher $^3He/^4He$ ratio than the true value. Rison and Craig (1983) observed the opposite, notably, a ratio lower than the true ratio was observed when Ne was present in the mass spectrometer. On the other hand, the $^3He/^4He$ ratio of He samples in the presence of Ne measured by a Nuclide instrument showed about 9 % lower values than the

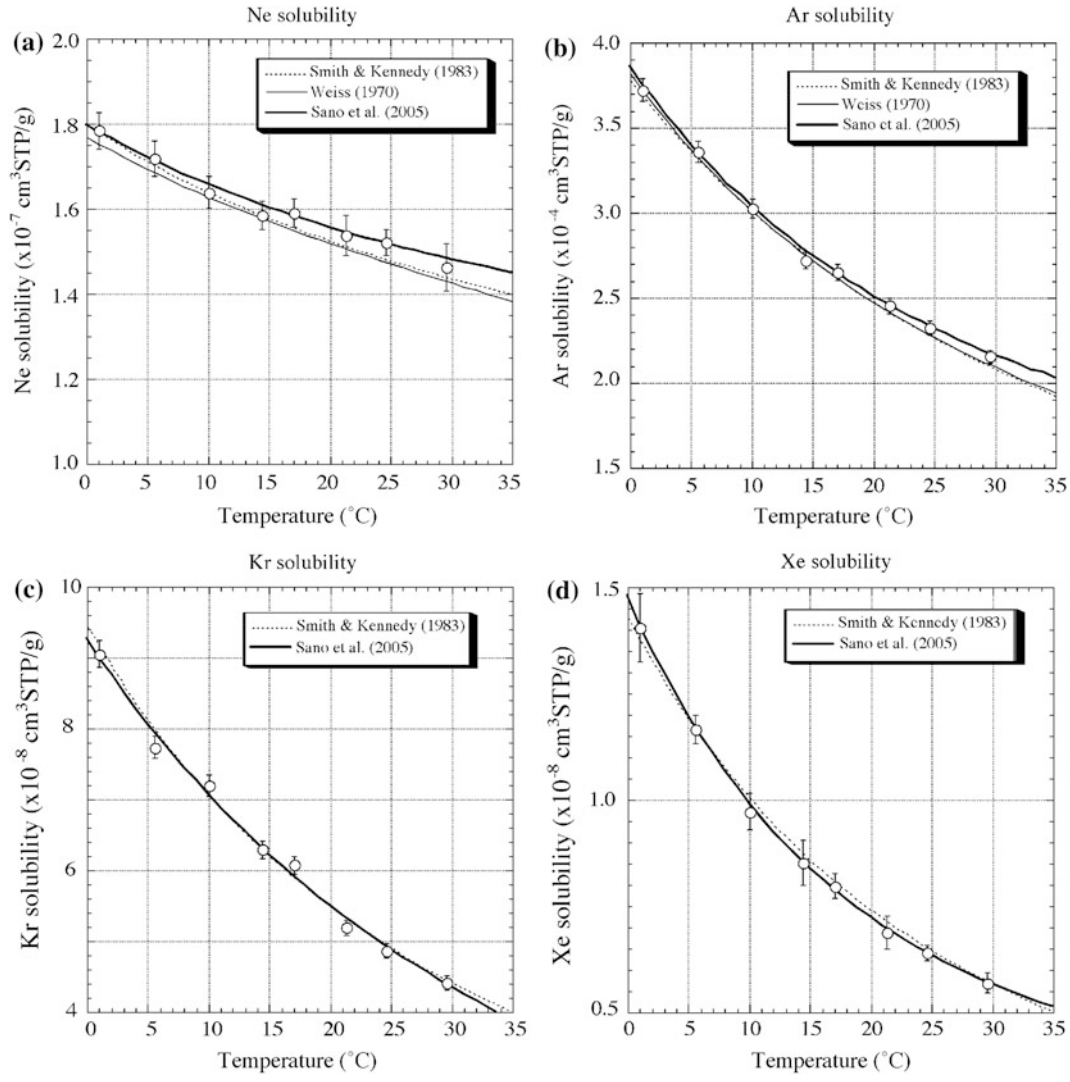

Fig. 6 Noble gas solubility in seawater at different temperatures

true ratios, irrespective of the $^4He/^{20}Ne$ ratio, despite a large range (from 0.97 to 99) in $^4He/^{20}Ne$ (Sano et al. 1998). The effect of Ne on $^3He/^4He$ ratio measurements is spectrometer dependent, and one cannot a priori predict the fractionation trend (such as the negative correlation in Fig. 10). Therefore we recommend that He is separated from Ne when precise measurement of the $^3He/^4He$ ratio is required.

3 Helium Isotopes and Geotectonic Setting on a Large Scale

3.1 Mantle Derived Helium

In the 1960s, the origin of water discharged from modern hydrothermal systems was of great

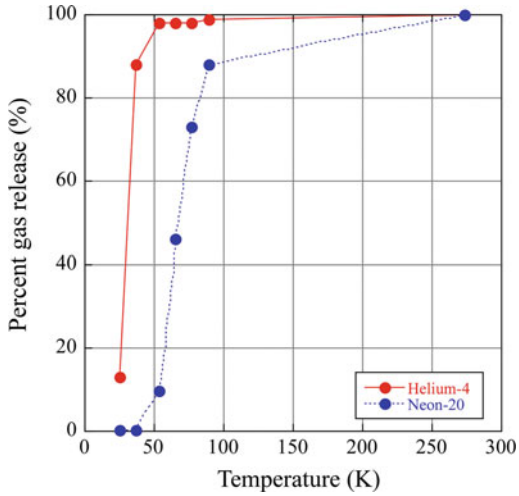

Fig. 7 A relationship between the equilibrium ion currents for ^{4}He and ^{20}Ne by QMS (normalized to 100 % release) and charcoal trap temperature

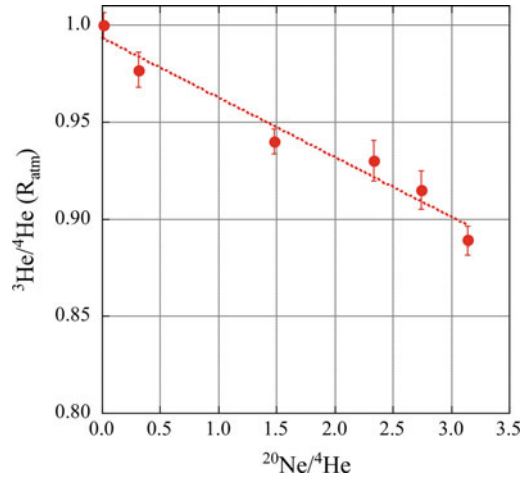

Fig. 8 A relationship between the ^{3}He/^{4}He ratio of an air standard and co-existing Ne content, here expressed as ^{20}Ne/^{4}He ratio, using a VG5400 instrument

interest because of the possible presence of juvenile (or primary, primordial) water from the deep interior of the earth that had never been in contact with aquifers or the hydrologic cycle. The degassing rate of juvenile water is an important parameter in reconstructing the history of the atmosphere and oceans as reported by Rubey (1951). Craig (1963) measured δ^{18}O and δD values of geothermal fluids and concluded that the source of the water and steam was local meteoric precipitation and the contribution of juvenile water was negligibly small. Although the presence of juvenile water was practically rejected, there were further attempts to search for primordial volatile components. Helium was the most prominent candidate for a juvenile element, because the atmospheric He content is sufficiently low for hydrothermal samples to be relatively uncontaminated. In addition, He is one of the most abundant elements in the early solar system (Anders and Grevesse 1989). So He in hydrothermal fluids was a potential candidate for a primordial volatile from deep in the Earth.

Following the study of Aldrich and Nier (1948), analysis of terrestrial ^{3}He/^{4}He ratios ceased for 20 years. In 1969, Clarke et al. (1969) found considerable enrichment of ^{3}He in Pacific deep water relative to the atmospheric ^{3}He/^{4}He ratio. They concluded that the excess ^{3}He was due to leakage of the Earth's primordial mantle ^{3}He into the ocean water. Simultaneously Mamyrin et al. (1969) found that the ^{3}He/^{4}He ratios of volcanic and hot spring gases in the Southern Kurile Islands were significantly higher than that of the atmosphere. They also considered that the excess was derived from deep-seated materials. Since contributions of tritiogenic ^{3}He was negligibly small in these samples, the contribution of primordial He in the mantle was confirmed, known as "mantle derived helium" or simply "mantle helium".

Since then, there has been intense interest in mantle derived helium all over the world. It was observed that natural gases, thermal fluids and rock samples in the same geotectonic regions show quite similar ^{3}He/^{4}He ratios (Lupton 1983). Emission of primordial helium is commonly found in Cenozoic volcanic areas (hot spot, Mid-Ocean Ridge, and subduction zones). Many reviews and textbooks have been published (Mamyrin and Tolstikhin 1984). This section focuses on the ^{3}He/^{4}He ratios of fluid

samples in modern hydrothermal system and geotectonic aspects, which are not well documented elsewhere.

3.2 Hot Spot Regions

Although most active volcanoes are located at plate boundaries, there are exceptions where active volcanism occurs within the plate interiors. This intra-plate volcanism such as Hawaii and Yellowstone is commonly called hotspots, thought be fed by underlying mantle that is anomalously "hot" compared with the ambient asthenospheric mantle. In this context, Iceland is also considered to be a hot spot because of its considerable volcanic output and resultant high elevation relative to other parts of the Mid Atlantic Ridge, despite its location on the boundary between two plates. Morgan (1971) suggested that this volcanism is due to hot mantle plumes that rise as thermal diapirs from the core-mantle boundary. If the hypothesis is correct, hot spot regions should show a more primordial noble gas signature, (that means more enriched in ^{3}He) than volcanism related to plate boundaries such as mid-ocean ridges and subduction zones. This is what is observed. Fluid samples from Hawaii and Iceland commonly show higher ^{3}He/^{4}He ratios than those from plate boundary volcanism, described below.

It is generally accepted that the Hawaiian Islands were produced by the slow movement of a tectonic plate across a stationary "hot spot" (Wilson 1963). The resulting in the islands (Hawaii, Maui, Oahu, and Kauai etc.) becoming progressively older to the northwest. As a result, a systematic change in ^{3}He/^{4}He in these islands is expected due to addition of radiogenic ^{4}He and loss of primordial He as the islands pass over the hotspot. However this is not the case for mineral samples. The highest value of ~32 Ra was found in olivine phenocrysts from Maui and similarly high ratios, ~24 Ra, are found in Kauai phenocrysts, while Hawaii and Oahu xenoliths have relatively low ^{3}He/^{4}He ratios (Rison and Craig 1983). This irregularity may be attributable to significant loss of initial He content during eruptive vesiculation and addition of cosmogenic ^{3}He production by cosmic ray bombardment (Kurz 1986) and accumulation of post-eruptive radiogenic ^{4}He. However, an advantage of studying fluids is that fluid samples are free from these issues. Volcanic gases from Kilauea have ^{3}He/^{4}He ratios of 14.9 Ra (Craig and Lupton 1976) and hydrothermal plumes from Loihi seamount are 16.6 Ra (Kodera et al. 1988). These values are significantly higher than the typical upper mantle value of (8.0 ± 1.5) Ra observed in helium from mid-ocean ridges (MORs: this is described in the next section), and consistent with the plume source having a distinctive He isotope composition compared to the upper mantle source of MORs. In order to further constrain the relationship between ^{3}He/^{4}He ratio and the island's age (or age relative to the hotspot track), He isotope measurements of fluid samples of several Hawaiian islands are required.

Yellowstone is another famous hot spot, located on continental crust (in contrast to the Hawaii and Galapagos hotspots which are located on oceanic crust). Similar to the Hawaiian chain, there is a systematic northwestward progression of volcanism (but rhyolitic in the case of Yellowstone) starting at the McDermitt volcanic field at 16–15 Ma, along with the Eastern Snake River plain (Pierce and Morgan 1992). Since the pioneer work by Craig et al. (1978), intensive ^{3}He/^{4}He ratio surveys have been carried out in Yellowstone by several workers (Evans et al. 2006; Hearn et al.1990; Kennedy et al. 1985; Kennedy et al.1987). Figure 9 shows the geographical distribution of ^{3}He/^{4}He ratios of fluid samples within and around the caldera rim, complied from the literature. Kennedy et al. (1985) pointed out three signatures; (1) The ^{3}He/^{4}He ratios outside the caldera are all low except for a few samples, (2) The ratios are relatively uniform with a value of 7 ± 1 Ra within the caldera, similar to MOR-type He, (3) There are three apparently high ratios, Mud Volcano (15.8 Ra), Gibbon Basin (13.4 Ra), and Crater Hills (10.4 Ra). The low ^{3}He/^{4}He ratios outside the caldera were attributed to dilution of mantle gases with crustal He with a low ^{3}He/^{4}He ratio (0.02 Ra) resulting from the additional

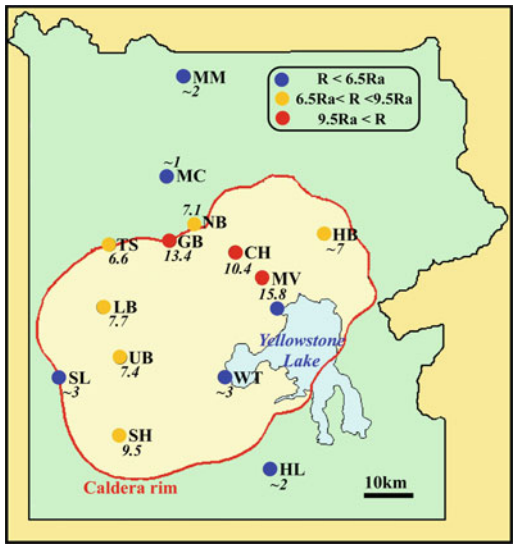

Fig. 9 Geographical distribution of the $^{3}He/^{4}He$ ratios of fluid samples within and around caldera rim in Yellowstone, USA

thickness of crust these fluids had to traverse, considering a scenario where a shallow cooling batholith is present beneath the caldera. The uniform $^{3}He/^{4}He$ ratios within the caldera were either derived from the upper mantle, because the values are similar to MOR-type He, or due to fortuitous mixing between an originally high ratio (plume-type He) with crustal He. The highest $^{3}He/^{4}He$ ratio of 15.8 Ra is remarkably similar to those of the Hawaiian fluids, suggesting a lower mantle origin. Although Christiansen et al. (2002) claimed that the Yellowstone hot spot is of upper mantle origin from a geological point of view, Pierce and Morgan (2009) prefer a deep mantle plume origin from evidence from geophysical imaging.

Iceland, located on the mid-Atlantic ridge is not strictly an intraplate tectonic setting as such and should not be considered as an equivalent to Hawaii and Yellowstone. There is no apparent trail of volcanism such as for the Hawaiian and Yellowstone volcanic chains. Based on seismological studies, low shear velocity anomalies beneath Iceland extended into the upper mantle transition zone, but this is not the case for the adjacent mid-ocean ridge (Ritsema and Allen 2003). The difference between the source of Iceland volcanism and the adjacent ridge volcanism is striking when considering trace element and radiogenic isotope signatures (Langmuir et al. 1978; Schilling 1973; Sun et al. 1975). There are several reports of $^{3}He/^{4}He$ ratios on both solid and fluid samples in Iceland (Breddam et al. 2000; Hilton et al. 1998; Kononov et al. 1974; Kurz et al. 1985; Poreda and Arnorsson 1992; Sano et al. 1985).

An intensive survey of $^{3}He/^{4}He$ ratios in Iceland was at first reported by Kononov et al. (1974). Figure 10 shows the geographical distribution of the $^{3}He/^{4}He$ ratios of fluid samples in Iceland based on the data of Poreda and Arnorsson (1992) together with Kononov et al. (1974) and Sano et al. (1985). The He isotope distribution can be summarized as follows: (1) The $^{3}He/^{4}He$ ratios in the Neo-Volcanic Zone (a divergent plate boundary on the island connecting to the Mid-Atlantic Ridge) vary from values at the high end of the MOR range to extremely high values of 26 Ra. (2) The ratios outside the zone are more variable than those inside, including values even lower than MOR-type He, suggesting a contribution of crustal He. (3) The highest terrestrial $^{3}He/^{4}He$ ratio of a fluid sample, 29 Ra, is found in a moderate temperature spring located in 9 My-old crust in Northwest Iceland. Generally, mantle He in Iceland is considered to be a mixture of MOR-type and plume-type He (Poreda and Arnorsson 1992), consistent with other radiogenic isotope studies such as Sr, Nd and Pb (Langmuir et al. 1978; Schilling 1973; Sun et al. 1975).

Geophysical imaging of these three hot spot regions is discussed here in conjunction with He isotopes. Figure 11 shows P- and S-wave seismic tomograms beneath (a) Hawaii, (b) Yellowstone, and (c) Iceland. In Hawaii, a continuous low-velocity anomaly has been imaged from the surface to the core-mantle boundary (CMB). The root of the anomaly at the CMB is located to the north of the surface volcanism, suggesting an inclined hot conduit toward the south due to mantle flow (Lei and Zhao 2006). In this case, the source of plume-type He may be attributable to the CMB, following the original idea of Morgan (1971). In

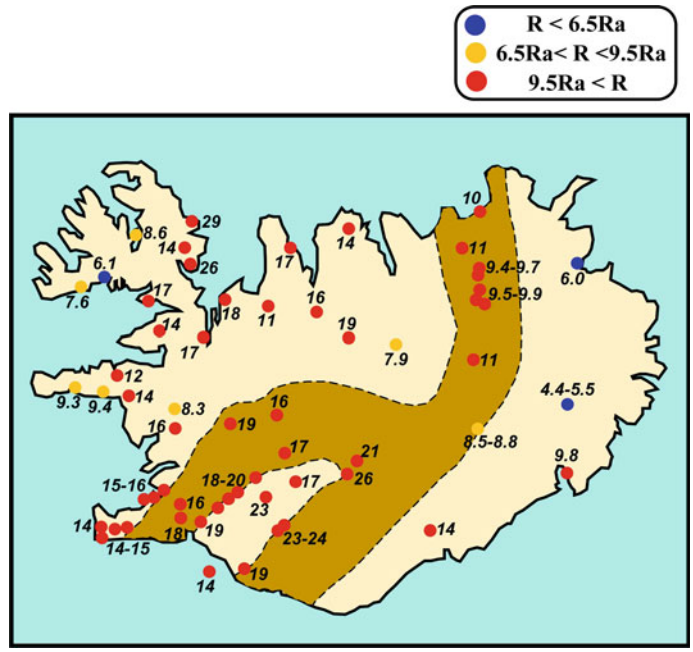

Fig. 10 Geographical distribution of the $^{3}He/^{4}He$ ratios of fluid samples in Iceland. The Neo-Volcanic Zone (extension of the Mid-Atlantic Ridge) is shown by the shaded yellow area

Yellowstone, the existence of a similar conduit beneath the caldera and volcanic fields has been suggested, tilting to the northwest at a depth of 500 km in the mantle transition zone, shown in Fig. 11b (Pierce and Morgan 2009; Yuan and Dueker 2005). Although there is no apparent geophysical evidence for the inferred plume beyond 500 km, Pierce and Morgan (2009) have suggested a much deeper origin, extending to at least 1000 km, based on the large size of the plume head, the track of hot spots, and the divergence of the geoid anomaly. Therefore the source of plume-type He in Yellowstone is probably significantly deeper than the middle upper mantle and may be connected to the lower mantle. In Iceland, low shear velocities, interpreted to be a warm conduit, extended to a depth of 700 km, shown in Fig. 11c (Ritsema and Allen 2003). There is no simple vertical conduit extending to deeper levels (Nolet et al. 2007). Therefore, the nature of the CMB upwelling beneath Iceland remains elusive, but may continue into the lower mantle. Summarizing these three cases (Hawaii, Yellowstone, and Iceland), it seems likely that plume-type He originates at least below the bottom of the upper mantle, (that is the lower mantle) but it is not yet clear if the source of primordial He is connected with the CMB.

Other hot spot regions (listed in (Courtillot et al. 2003; Thorne et al. 2004) where $^{3}He/^{4}He$ ratios higher than MOR-type He have been reported for gas and fluid samples are: Afar (Pik et al. 2006), Azores (Jean-Baptiste et al. 2009), Canary Islands (Hilton et al. 2000; Perez et al. 1996), Cape Verde (Heiweil et al. 2009), Galapagos (Goff et al. 2000), and Reunion (Marty et al. 1993). On the other hand, hydrothermal fluids in Socorro Island (Taran et al. 2002a), Hoggar (Pik et al. 2006), Cameroon (Aka et al. 2004; Pik et al. 2006; Sano et al. 1990) and fluid inclusions of sulfides in Juan de Fuca (Stuart et al. 1994) show the $^{3}He/^{4}He$ ratios equal to or lower than MOR-type He. In addition to hot spot regions, ratios higher than MOR-type He were observed in Manus (Fourre et al. 2006) and North Fiji backarc basin (Ishibashi et al. 1994). These data are listed in Table 2.

Graham (2002) reported the relationship between the $^{3}He/^{4}He$ ratio of ocean island basalts (existence of mantle plumes or thermal upwellings from deep in the Earth) and geologic and tectonic settings. There does not appear to be simple trends between $^{3}He/^{4}He$ ratio and

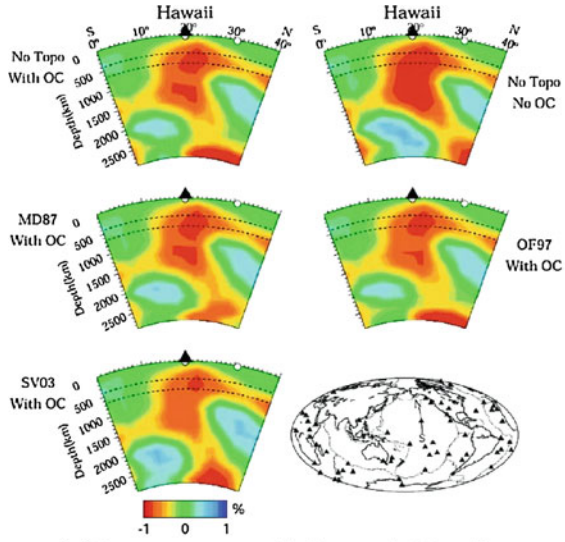

(a) P-wave tomographic images in Hawaii

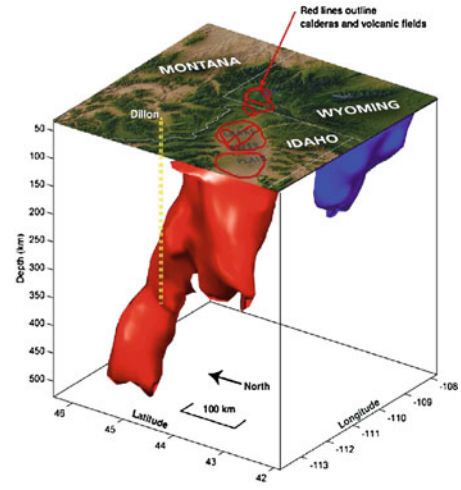

(b) Illustration of warm conduit based on P-wave tomogram in Yellowstone

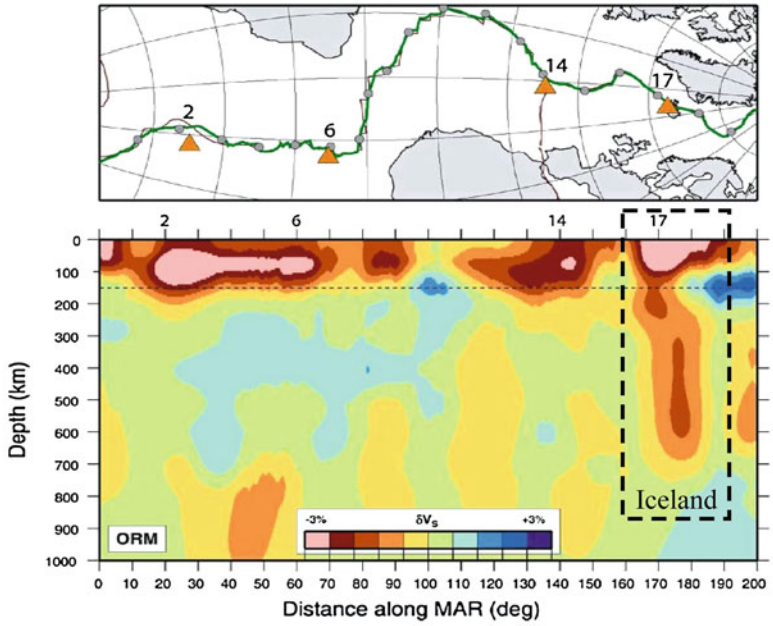

(c) S-wave tomographic image along the Mid-Atlantic Ridge

Fig. 11 Seismic (P- and S-wave) tomograms beneath **a** Hawaii, **b** Yellowstone, and **c** Iceland

buoyancy flux (plume flux), lithosphere age, or plate speed (only crushing analyses were used to avoid post-eruptive addition of cosmogenic ^{3}He and radiogenic ^{4}He). Following the same approach, we discuss below the relationship of fluid samples with geophysical data. Table 2 lists the presence of a linear track (e.g. island chain), buoyancy flux, tomographic characteristics (Courtillot et al. 2003), and S-wave velocity coverage of the CMB surface area (Thorne et al. 2004). It is apparent that there is no correlation between the maximum ^{3}He/^{4}He ratio and the

Table 2 Helium isotopes of fluid samples, linear track, buoyance flux, and tomography of hot spot regions

Hot spot	Helium isotopes		Linear track[a]	Buoyance flux[a]	Tomography[a]	CMB coverage dVs (%)[b]	References
	Min (Ra)	Max (Ra)	(chain of islands)	(×103 kg/s)	500 km deep		
Afar	3	16.4	No	1	Slow	–	Pik et al. (2006)
Azores	5.2	13.5	No?	1.1	Normal	25	Jean-Baptiste et al. (2009)
Cameroon	1.6	6.2	Yes?	–	Normal	14	Sano et al. (1990); Pik et al. (2006)
Canary	6	9.5	No	1	Slow	6.7	Perez et al. (1996); Hilton et al. (2000)
Cape Verde	8.8[d]	11.1[d]	No	1.6	Normal	9.2	Heiweil et al. (2009)
Comores	5.4	5.6	No	–	Normal	31	Pik et al. (2006)
Galapagos	17.1	17.7	Yes?	1	Normal	27	Goff et al. (2000)
Hawaii	14.9	16.6	Yes	8.7	Slow	17	Craig and Lupton (1976); Kodera et al. (1988)
Hoggar	8.6	8.9	No	0.9	Slow	21	Pik et al. (2006)
Iceland	4.4	28.8	Yes?	1.4	Slow	23	Kononov et al. (1974); Poreda et al. (1992)
Juan de Fuca	5.8	7.1	Yes	0.3	Slow	–	Stuart et al. (1994)
Reunion	12.1	12.9	Yes	1.9	Normal	17	Marty et al. (1993)
Socorro	6	6.7	No	–	Slow	38	Taran et al. (2002)
Yellowstone	3	15.8	Yes[c]	1.5	Slow[c]	61	Kennedy et al. (1985); Hearn et al. (1990)
Back-arc basin							
Manus	7.4	11.9	–	–	–	–	Fourre et al. (2006)
North Fiji	9	10	–	–	–	–	Ishibashi et al. (1994)

[a] From Courtillot et al. (2003)
[b] From Thorne et al. (2004)
[c] From Pierce and Morgan (2009)
[d] Corrected air contamination based on the $^{4}He/^{20}Ne$ ratio

existence of a linear track or chain of dated seamounts. On the other hand, the buoyancy flux may be positively correlated with the maximum $^{3}He/^{4}He$ ratio. Figure 12 shows the relationship between these data where the trend is fitted by eye (dotted line) with the exception of Hawaii. Plume-type He may be more present in plumes that have higher buoyancy fluxes, which is consistent with the original idea of a hot spot related to larger volcanic output.

As described in the three cases above (Hawaii, Yellowstone, and Iceland), there is evidence of low velocity zones extending beneath the regions of volcanism to at least the mantle transition zone. In the Afar and Canary Islands (which both have plume-type $^{3}He/^{4}He$ ratios), a slow S-wave velocity anomaly is observed at 500 km depth, whereas there are no velocity anomalies for the Azores, Cape Verde, Galapagos, and Reunion (see Table 2). Yang et al. (2006) reported that the low-velocity anomaly of P-wave extended to at least 400 km depth in the Azores. Silveira and Stutzmann (2002) suggested that there is a striking hot spot

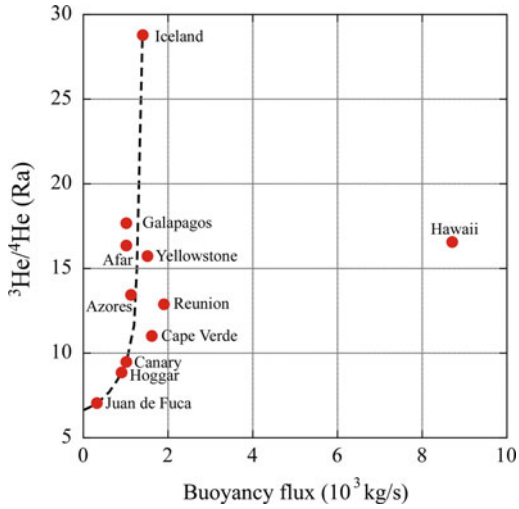

Fig. 12 A relationship between the buoyancy flux and the maximum ^{3}He/^{4}He ratio in hydrothermal fluids from hot spot regions

anisotropy signature beneath the Cape Verdes Islands from S-wave velocity. Based on the differential arrival times of P-to-S conversions, Hooft, Toomey and Solomon (2003) reported an anomalously thin transition zone beneath the Galapagos and that the thermal plume associated with mantle upwelling extended to depths greater than 410 km beneath the hot spot. In Reunion, a similar thinning of the transition zone was found (Li et al. 2001). In a catalogue of deep mantle plumes (Montelli et al. 2006), the volcanism of Reunion and Afar are also classified as potentially deep plumes. However, there is no correlation between the maximum ^{3}He/^{4}He ratio and the S-wave velocity coverage of CMB surface area (Thorne et al. 2004) in Table 2. Therefore, based on the present data it is difficult to assign the source of plume-type He to the CMB region. In summary, plume-type He is generally observed in regions with a high buoyancy flux and a slow shear velocity or anomalous thinning of the mantle transition zone, confirming the lower mantle origin of plume-type He. Finally it is noteworthy that plume-type He in the Manus and North Fiji basins may be related to a small "incipient plume" extending from the westernmost edge of the Pacific super-plume (Montelli et al. 2006), although details are not clear and this should be the focus of future studies.

3.3 Mid-Ocean Ridges

Mid-ocean ridge volcanism occurs where two oceanic plates diverge creating a spreading center. Upper mantle material rises to shallow levels due to the plate separation and melts adiabatically to produce basalt magmas. The lava is quenched on eruption by seawater, forming pillow basalts that have glass-rimmed margins. This glass rim, MORB glass, contains significant quantities of mantle He which has been shown to have a uniform ^{3}He/^{4}He ratio of 6.5–9.5 Ra (Lupton 1983, Graham 2002).

There are numerous modern hydrothermal systems in mid-ocean ridge volcanism. Since the first discovery of hydrothermal fluid venting at the Galapagos spreading center (Corliss et al. 1979), many investigations have been carried out at various locations along plate boundaries. Figure 13 shows the ^{3}He/^{4}He ratio of hydrothermal fluids and/or the estimated vent fluid end member from the plume in the seawater close to the vent (references are listed in Table 3). Even though samples were collected from three different ridge systems, the ^{3}He/^{4}He ratios do not vary significantly, within the range 7.2–9.2 Ra with an average of (8.09 $\pm$ 0.49) Ra (1σ). This value is identical to that of the world-wide average of MORB glass (Hilton et al. 1993) and well within the MOR-type He of (8.0 $\pm$ 1.5) Ra. There is nothing new in this homogeneity since it is already well documented by MORB glass data (Graham 2002). The advantage of using fluid data over MORB glass data is that the relationship between excess ^{3}He and the heat flux and other volatile components such as methane can be investigated, although with the disadvantage that the relation with solid element isotopes (such as ^{87}Sr/^{86}Sr and ^{143}Nd/^{144}Nd) cannot be examined.

Terrestrial heat flow and the He flux in the Earth have similar aspects, although one is a geophysical parameter and the other is geochemical. Both have two distinct origins, primordial (mantle) and radiogenic (crust), and

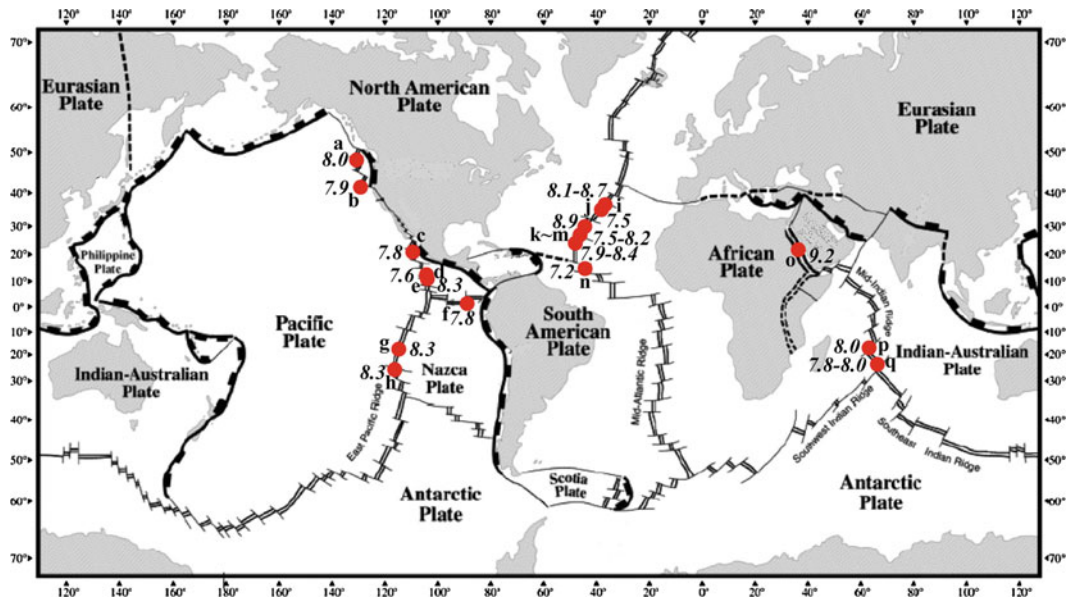

Fig. 13 The $^3He/^4He$ ratio of hydrothermal fluids from mid-ocean ridges and/or that of the estimated end member from hydrothermal plumes in seawater close to the vent. Locations (*a, b, c* etc.) correspond to those in Table 4

their distribution by conduction or convection and diffusion are described by similar equations (Ballentine and Burnard 2002). The global relationship between heat flow and He flux was first discussed by Oxbough and O'Nions (1987). A positive correlation between heat and ^3He emission has been well established in submarine hydrothermal systems in MOR-regions (Jean-Baptiste et al. 2004). Table 3 lists the $^3He/^4He$ ratios of hydrothermal fluid samples from MOR-regions together with ^3He/heat, $CH_4/^3He$ ratios and $\delta^{13}C$ value of CH_4. The average ^3He/heat ratio is calculated to be $(8.6 \pm 3.8) \times 10^{-18}$ mol/J (1σ) for world-wide mid-ocean ridge systems, which is remarkably uniform when taking into account their differences in physical and chemical characteristics. German and Von Damm (2004) summarized the global heat flux from submarine hydrothermal systems. Total seafloor hydrothermal heat flux was estimated 11 TW, while the heat flux due to crystallization of basaltic magma was 2.8 ± 0.3 TW (they called this flux the axial flow restricted to younger oceanic crust, 0–1 Ma). The heat flux associated with cooling of older oceanic crust (1–65 Ma) was defined as off-axis flow consists of 7 ± 2 TW, larger than that of the axial flow.

Craig et al. (1975) originally estimated the ^3He flux from the solid earth to the oceans via hydrothermal venting from ^3He profiles in the oceans, finding a value of ~4.6 atoms cm^2 s^{-1} or a total global flux of 500–1000 mol y^{-1}. Recently Binachi et al. (2010) reported a numerical simulation of the global oceanic ^3He distribution and suggested that the submarine volcanic flux could be about half of Craig's original value. Therefore the global MOR-type ^3He flux may be revised into approximately 2–3 atom/cm^2/s at present.

Methane is one of the most informative tracers for understanding submarine hydrothermal systems in MOR-regions, because it mostly orginates from magmatic process and is typically 10^5–10^7 times enriched over background concentrations in seawater (Welhan and Craig 1983; Welhan et al. 1988). Since ^3He is also derived from MOR-type magma, a uniform $CH_4/^3He$ ratio in global hydrothermal vents and vent plumes is anticipated. However this is not

Table 3 Helium isotopes of hydrothermal fluid samples from mid-ocean ridge regions togeher with other data

	Hydrothermal site	Type	Temperature (°C)	$^{3}He/^{4}He$ (Ra)	$^{3}He/heat$ (10^{-18} mol/J)	$CH_4/^{3}He$ ($\times 10^{6}$)	$^{13}C(CH_4)$ (‰)	References
EPR								
a	Juan de Fuca (48°N)	Vent	345–400	8.0	–	107–217	−55 to −48	Lilley et al. (1993)
b	Juan de Fuca (45°N)	Plume	–	7.9	3.2 ~4.3	–	–	Lupton et al. (1999)
c	East Pacific Rise (21°N)	Vent	373–355	7.8	5.2	3.4–6.5	−18 to −15	Welhan and Craig (1982, 1983)
d	East Pacific Rise (13°N)	Vent	354–381	7.6	11	3.1–3.9	−20 to −17	Merlivat et al. (1987)
e	East Pacific Rise (11°N)	Vent	347	8.3	9.5	4.5–7.0	–	Kim et al. (1984; Welhan et al. (1984)
f	Galapagos	Vent	350	7.8	5.2	12–42	–	Jenkins (1987); Lilley et al. (1983)
g	East Pacific Rise (17–18°S)	Vent	340	8.3	6.2	–	−22 to −24	Charlou et al. (1996); Jean-Baptiste et al. (1997)
h	East Pacific Rise (25°S)	Plume	–	8.3	–	–	–	Takahata et al. (2005)
	East Pacific Rise (27–32°S)	Plume	–	–	5.6–17	2.0–9.7	−27 to −35	Gharib et al.(2005)
MAR								
i	Menez Gwen (37°50N)	Vent	275–284	8.7	18	85	−6.8 to −9.1	Charlou et al. (2000)
	Lucky Strike (37°17N)	Vent	170–330	8.1	6.5	65	−7.2 to −11	Jean-Baptiste et al. (1998)
j	Rainbow (36°14N)	Vent	365	7.5	9.3	100	−16	Jean-Baptiste et al. (2004); Charlou et al. (2002)
k	Broken Spur (29°N)	Vent	356–364	8.9	–	–	–	Jean-Baptiste et al. (2004)
l	TAG (26°N)	Vent	270–366	7.5–8.2	7.7–9.3	–	–	Charlou et al. (1996); Rudnicki and Elderfield (1992)
m	Snake Pit (23°N)	Vent	330–350	7.9–8.4	6.5–12	2.6	–	Rudnicki and Elderfield (1992); Jean-Baptiste et al. (1991)
n	Logatchev (14.45°N)	Vent	320–370	7.2	–	100	−13	Jean-Baptiste et al. (2004); Keir et al. (2009)
o	Red Sea	Brines	22–67	9.2	–	0.66	−16	Faber et al. (1998); Winckler et al. (2001)
CIR								
p	Indian Ridge (19°S)	Plume	–	8.0	–	4	−18	Kawagucci et al. (2008)
q	Indian Ridge (25°S)	Vent	360	7.8–8.0	–	–	−8.6 to −8.7	Gamo et al. (2001)

the case: $CH_4/^3He$ ratios appear to vary between 6.6×10^5 and 2.17×10^8 with an average of 4.4×10^7 (see Table 3). However, it is clear that the Juan de Fuca ridge represents an outlier with high $CH_4/^3He$ ratios and very light carbon isotopes. The Guaymas Basin, Gulf of California, hydrothermal fluids are also characterized by high $CH_4/^3He$ of 3.2×10^9 and light $\delta^{13}C$ (-51 to -43 ‰); these signatures were attributed to thermo-catalytic gases derived from organic material in the sedimentary section (Welhan and Craig 1982; Welhan and Lupton 1987), and it seems possible that Juan de Fuca hydrothermal fluids may also be affected by thermogenic methane. Otherwise $\delta^{13}C_{CH4}$ values are relatively uniform at (-16 ± 7) ‰ (1σ). Ignoring these two outliers, the East Pacific Rise (EPR) and the Mid-Atlantic Ridge (MAR) appear to have different average $\delta^{13}C_{CH4}$ values: -23 ± 6 ‰ for the EPR and -12 ± 4 ‰ for the MAR. In addition, the average $CH_4/^3He$ ratio of the EPR, $(9.4 \pm 9.9) \times 10^6$ which is possibly lower than that of the MAR at $(59 \pm 46) \times 10^6$ (although the data do overlap). These signatures suggest that there may be different CH_4 origins for the EPR and MAR, however the number of data are small and the dispersion of the data is large, therefore the difference needs to be verified in a future study.

Methane derived from MOR hydrothermal systems is apparently abiogenic in origin as discussed above (Welhan and Craig 1983; Welhan et al. 1988), providing direct evidence for the possibility of abiogenic hydrocarbon accumulations. Wakita and Sano (1983) proposed an abiogenic origin for commercial natural gas in Japan based on high $^3He/^4He$ ratios. Since then, intensive research has been carried out to identify abiogenic methane reserves (Sherwood Lollar et al. 1993; Wakita et al. 1990; Welhan 1988). Figure 14 shows the relationship between $\delta^{13}C$ and $CH_4/^3He$ of hydrothermal methane in MOR-and back-arc basins including the Okinawa Trough (Ishibashi et al. 1995), Izu-Bonin (Tsunogai et al. 1994), South Marianas (Gamo et al. 2004) and North Fiji basin

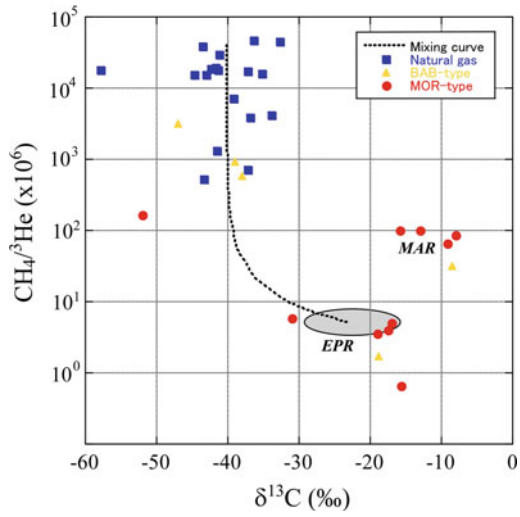

Fig. 14 The relationship between $\delta^{13}C$ of methane and $CH_4/^3He$ ratio in hydrothermal fluids from mid-ocean ridge and back-arc basin regions

(Ishibashi et al. 1994), compared to commercial natural gases in China (JinXing et al. 2008), Japan (Wakita et al. 1990), Thailand (Jenden et al. 1993) and New Zealand (Lyon et al. 1996). The binary mixing curve is calculated based on two end-members: EPR methane with $\delta^{13}C = -23$ ‰ and $CH_4/^3He = 5 \times 10^6$, and biogenic methane with $\delta^{13}C = -40$ ‰ and $CH_4/^3He > 10^{10}$. This curve approximately replicates the distribution of the data even though there is scatter. It is evident that accumulation of EPR methane will not lead to natural gases, suggesting that abiogeic methane is only a minor source of natural gases. Taking into account the total ^3He flux of 2.4×10^{-5} mol/s at MOR-type region and the $CH_4/^3He$ ratio of 4.4×10^7, one would estimate the annual flux of mantle methane to be 3.5×10^{10} mol. On the other hand, global natural gas consumption in 2006 was about 8.5×10^{13} mol (Carbon Dioxide Information Analysis Center, http://cdiac.ornl.gov), three orders of magnitude lager than the annual mantle CH_4 flux. Therefore the abiogenic methane flux at MOR-type regions is negligibly small compared with the present fossil fuel consumption.

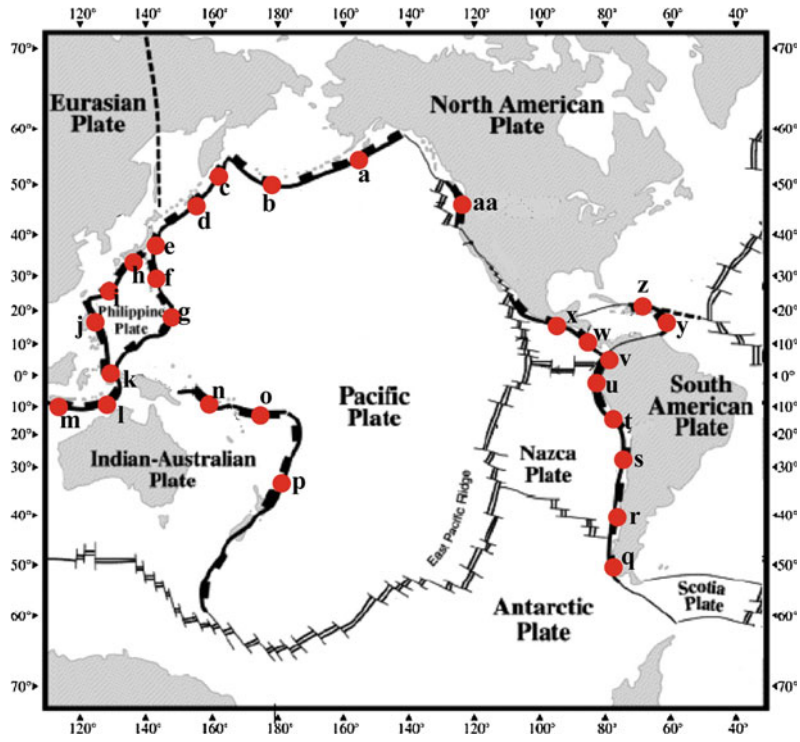

Fig. 15 The cir-cum Pacific region where $^3He/^4He$ ratios of hydrothermal systems have been reported. Locations (*a, b, c* etc.) correspond to those in Table 5

3.4 Subduction Zones

Subduction zone magmatism is notoriously rich in water because the descending oceanic slab releases water into the overlying mantle wedge which decreases the melting temperature of the mantle, causing it to melt and subsequently rise by buoyancy producing chains of volcanoes such as those found in the circum-Pacific "Ring of Fire". MOR-type He may be carried by the magma from the mantle to the surface. One of the first discoveries of elevated terrestrial $^3He/^4He$ ratios was in fact from a subduction zone setting in the volcanic and hot spring gases in the Southern Kurile Islands (Mamyrin et al. 1969). Since then extensive research of He isotopes in hydrothermal gases has been carried out in subduction zones including the circum-Pacific belts, Lesser Antilles, and southern Italy.

The active arc data until 2002 were well compiled and discussed by Hilton et al. (2002). Additional data are now available for the Kamchatka-Kuril region (Taran 2009), the Northeastern Japan arc (Horiguchi et al. 2010; Umeda et al. 2007), the Izu-Bonin arc (Ohno et al. 2011; Sumino et al. 2004), the Southwestern Japan arc (Dogan et al. 2006; Sano et al. 2006; Umeda et al. 2006), the Ryukyu-Taiwan arc (Lee et al. 2008; Yang 2008; Yang et al. 2005), the Sangihe arc in Indonesia (Clor et al. 2005; Jaffe et al. 2004), the Central American system in Nicaragua and Costa Rica (Shaw et al. 2003), South Chile (Ray et al. 2009), the Aegean arc (Shimizu et al. 2005) and Deception island in Antarctica (Kusakabe et al. 2009). Figure 15 shows the circum Pacific region where the $^3He/^4He$ ratios of hydrothermal systems have been reported. Table 4 lists the maximum, minimum, and average ratios together with several geological and geophysical features of subduction zones such as the arc length, taper angle, crustal thickness and magma production from Clift and Vannucchi (2004).

From Table 4, one may summarize circum Pacific He as follows: (1) values vary significantly from 10.1 to 0.01 Ra, a much broader range than for MOR-type He (8.0 ± 1.5) Ra. (2) The highest $^3He/^4He$ ratio of 10.1 Ra (Ambrym

Table 4 Helium isotopes of hydrothermal fluid samples from subduction zones together with other data

	Hydrothermal site	Length (km)	Taper angle (deg)	Thickness of crust (km)	Type*	Magma production (km^3/m.y.)	Age of oceanic plate (Ma)	Number of He isotope data	$^3He/^4He$ max (Ra)	$^3He/^4He$ min (Ra)	$^3He/^4He$ mean (Ra)	References
a	Alaska	2050	7.4	45	A	81	28–60	8	7.89	6.03	7.06	Hilton et al. (2002)
b	Aleutian	1500	9.2	27	A	83	60–65	23	8.0	1.6	5.74	Hilton et al. (2002)
c	Kamchatka	1100	9.2	40	E	108	85–105	54	8.2	1.3	4.9	Taran (2009)
d	Kuril	1100	10.3	25	E	115	105–115	8	8.6	3.9	6.1	Taran (2009)
e	NE Japan	1000	9.8	40	E	135	115–134	78	8.04	0.17	3.66	Horiguchi et al. (2010); Umeda et al. (2007)
f	Izu-Bonin	1300	11	20	E	121	46–53	51	8.22	2.48	6.11	Ohno et al. (2011); Sumino et al. (2004)
g	Mariana	1600	7.1	20	E	121	134–180	6	7.65	5.3	7.04	Hilton et al. (2002)
h	SW Japan	900	9.6	40	A	53	20–25	27	6.16	0.58	3.00	Dogan et al. (2006); Sano et al. (2006)
i	Ryukyu-Taiwan	1000	11.7	30	E	93	46–53	47	8.39	0.09	4.32	Lee et al. (2008); Yang et al. (2005); Yang (2008)
j	Philippine	1000	17.5	32	E	54	42–53	10	7.6	6.9	7.34	Hilton et al. (2002)
k	Sangihe	600			A			41	7.5	0.93	4.6	Clor et al. (2005); Jaffe et al. (2004)
l	Banda	2100	7.9	45	A	103	70–110	28	4.5	0.01	2.18	Hilton et al. (2002)
m	Java	2100	7.9	45	A	103	70–110	26	8.8	4.5	6.69	Hilton et al. (2002)
n	Solomon	2750	10.2	25	E	149	45–54	53	7.54	2.03	6.18	Hilton et al. (2002)
o	New Hebrides	1800			A			9	10.1	4.4	6.42	Jean-Baptiste et al. (2009)
p	Kermadic	1250	6.7	20	E	91	83–120	145	8.23	1.45	5.99	Hilton et al. (2002)
q	South Chile	2000	7.6	45	A	27	24–36	27	6.47	1.5	3.96	Ray et al. (2009)
r	Central Chile	2000	7.4	45	A			18	6.84	0.18	3.9	Hilton et al. (2002)
s	North Chile	2000	7.2	45	E	120	42–46	12	6.02	0.82	2.39	Hilton et al. (2002)
t	Peru	2200	7.2	45	E	104	10–40	10	3.2	2.1	2.56	Simmons et al. (1987)

(continued)

Table 4 (continued)

	Hydrothermal site	Length (km)	Taper angle (deg)	Thickness of crust (km)	Type*	Magma production (km^3/m.y.)	Age of oceanic plate (Ma)	Number of He isotope data	$^3He/^4He$ max (Ra)	$^3He/^4He$ min (Ra)	$^3He/^4He$ mean (Ra)	References
u	Equador	1100	10.2	45	E	86	15–24	5	4.8	2.1	3.22	Hilton et al. (2002)
v	Colombia	1100	10.2	45	E	86	15–24	45	8.84	0.9	5.66	Hilton et al. (2002)
w	Central America	1200	7.6–16.4	32–35	E	86–108	15–24	28	7.6	1.16	4.58	Shaw et al. (2003)
x	Mexico	1700	13.4	40	E	91	105–115	34	7.5	0.4	2.43	Taran et al. (2002)
y	S. Lesser Antilles	850	6	38	A	54	62–82	73	8.6	3.31	6.8	Hilton et al. (2002)
z	N. Lesser Antilles	850	6	38	A	54	62–82	82	8.9	1.53	4.93	Hilton et al. (2002)
aa	Cascades	850	5.7	45	A	47	4–8	19	8.19	1.25	6.07	Hilton et al. (2002)

*A and E show the accretionary and the erosive plate margins, respectively

hot spring, the Vanuatu islands (Jean-Baptiste et al. 2009)), which is apparently higher than MOR-type He. (3) Ratios at the upper end of the MOR range (8.8–8.9 Ra) have been found in the Colombian Andes, Lesser Antilles, and the Sunda arc system in Sumatra and Bali. (4) Considering only the highest ratios measured, comparatively low values (6.5–7.0 Ra) are found in the Ecuadorian Andes, Peruvian Andes and Chilean Andes, and the eastern Sunda/Banda arc, however still within the range of MOR-type He. (4) The lowest ratios (~0.01 Ra) are consistent with addition of radiogenic He produced in a low Li crustal environment (Mamyrin and Tolstikhin 1984).

The highest $^3He/^4He$ ratios found in Vanuatu (Jean-Baptiste et al. 2009) can be attributed to plume-type He, probably derived from the incipient plume at the westernmost edge of the Pacific super-plume (Montelli et al. 2006). This is an apparent outlier in the circum Pacific region with $^3He/^4He$ similar to those of the Manus and North Fiji basins (see the end of Sect. 3.2). Except for Vanuatu, all other samples can be attributed to simple binary mixing between MOR-type mantle He and radiogenic He in the crust. Sano and Wakita (1985a) called this "subduction-type He". The MOR-type He is likely derived from the mantle wedge overlying the subduction slab which is melted by the uprising magma. There are two possible source of radiogenic He in subduction-type He: (1) the subducted slab component, including the oceanic sediment and basement; and (2) shallow derived He resulting from interactions between the rising magma and the continental crust present in the arc. Since He diffusivity in sedimentary matter is high, retention of radiogenic He from the ocean bottom to the mantle wedge is not likely, therefore radiogenic He generated in the descending sediments is likely to be released. However, the contribution from subducted sediments is variable but probably represent a minor component in the sources of arc magmas (Hilton et al. 2002). At accretionary plate margins where oceanic sediments are accumulated in the trench (i.e. not subducted; type

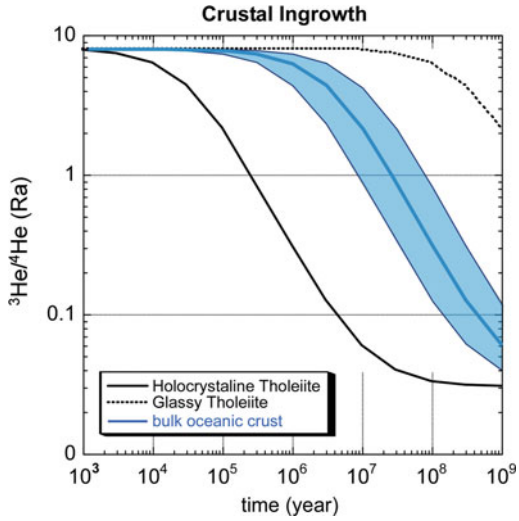

Fig. 16 The decrease in ^{3}He/^{4}He ratio in the oceanic crust by ingrowth of radiogenic He with time. The hatched zone shows the most probable ^{3}He/^{4}He evolution over time

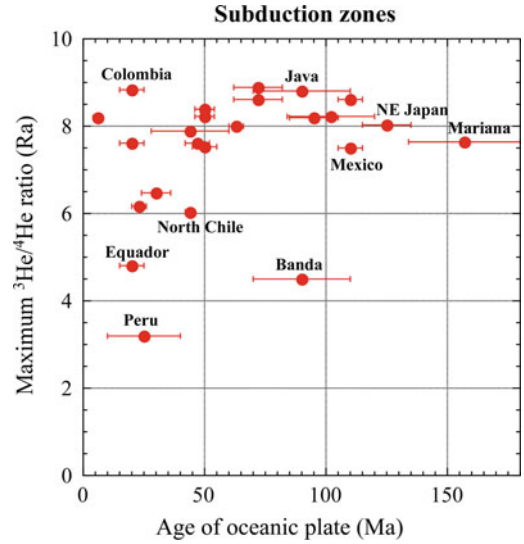

Fig. 17 The relationship between the age of the subducting oceanic plate and the maximum ^{3}He/^{4}He ratio observed in the adjacent arc segment

A in Table 4), the average of the maximum ^{3}He/^{4}He ratio is 7.4 ± 1.3 Ra (1σ). The average is 7.4 ± 1.5 Ra at erosive plate margins (Type E in Table 4), and is undistinguishable from type A. This suggests that the sediment contribution is small and therefore crustal He from the oceanic basement is probably also incorporated in the source of arc magmas.

It is possible to calculate the decrease of ^{3}He/^{4}He ratios (Ra) in the slab over time time (Sano and Nakajima 2008; Torgersen and Jenkins 1982). The initial U, Th and ^{3}He contents are from Tatsumoto (1966) and Dymond and Hogan (1974) for an oceanic basement of tholeiitic composition. Nucleogenic production of ^{3}He and radiogenic ^{4}He are well documented in the reports by Craig and Lupton (1976), Andrews (1985) and Mamyrin and Tolstikhin (1984), allowing the ^{3}He/^{4}He ratio evolution with time to be calculated. Figure 16 shows the aging effect on He isotopes of holocrystalline and glassy tholeiite as defined by Torgersen and Jenkins (1982). The actual initial ^{3}He content in bulk oceanic crust may be between those of holocrystalline (7×10^{-15} ccSTP/g) and glassy tholeiite (7×10^{-11} ccSTP/g). Using the average ^{3}He content of gabbros and peridotites of an oceanic core complex on the Southwest Indian Ridge ($\sim 7 \times 10^{-13}$ ccSTP/g (Kumagai et al. 2003)) as representative of oceanic crust (with an uncertainty of a factor three), even though the lower contents of 0.2 to 2×10^{-13} ccSTP/g was repoted for 11 million year old gabbros from ODP site 735B in the Indian Ocean (Moreira et al. 2003). The probable temporal evolution of the ^{3}He/^{4}He ratio of a slab component is shown by the hatched zone of Fig. 16.

It is possible to compare the relationship between the maximum ^{3}He/^{4}He ratio in a particular arc segment and the age of the subducting oceanic slab. If the radiogenic He produced in and then subducted with oceanic basement is the principle control on He isotopes in arc magmas, there should be a negative correlation between the maximum ^{3}He/^{4}He ratio in the arc segment and the age of oceanic slab. For example, the calculated ^{3}He/^{4}He ratios for 20 and 100 Ma oceanic slabs are 1 and 0.3 Ra, respectively, following the curve of Fig. 16. As a result arc magma from the Kurils, NE Japan, Mariana and Kermadic are expected to show lower maximum ^{3}He/^{4}He ratios than those of SW Japan, Equador, and Cascades. However this is not the case (Fig. 17) rather the results are contrary to

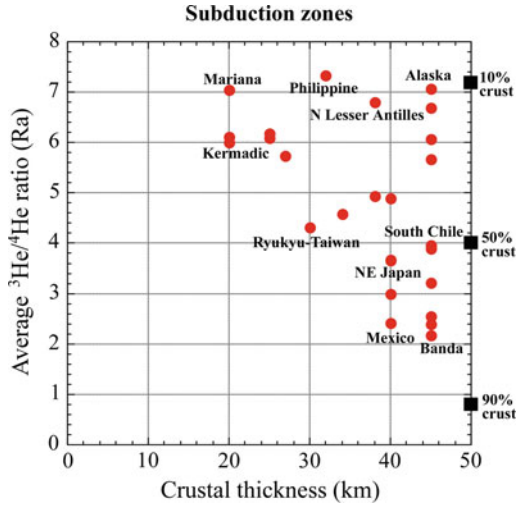

Fig. 18 The relationship between crustal thickness and average ^{3}He/^{4}He ratio in the arc segment

expectations. Except for one outlier (the Banda arc segment), the maximum ratio is lower for younger subducting plate ages. The trend is particularly significant in plates that are younger than 50 Ma. The maximum ratios where older plates are subducted (such as Mexico, NE Japan and the Marianas) are nevertheless well within the MOR range. Therefore it appears that crustal He contributions from both subducted sediments and the basement are negligible in the source of arc magmas. In addition, there is no apparent correlation between the maximum ^{3}He/^{4}He ratio of the segment and the magma production rate, or the taper angle (Table 4).

The principle control that lowers ^{3}He/^{4}He ratios of subduction-type He could therefore be shallow level process after the generation of arc magmas. There are two possible mechanism where crustal He contribution in subduction hydrothermal systems, either at intermediate depths (5–50 km) where the rising magma might assimilate continental crust in the subduction zones or else by subsurface interaction at relatively shallow depths between magmatic fluids and crustal materials. Figure 18 shows the relationship between the crustal thickness of the segment and average ^{3}He/^{4}He ratio. At segments where the crust is thin, such as Mariana and Kermadic trenches, ^{3}He/^{4}He ratios are high and any radiogenic contribution is small. On the other hand, segments with thick crust have variable ^{3}He/^{4}He ratios e.g. from low values of 2 Ra in the Bandaarc to high values of 7 Ra (Alaska). There is a similar relationship between crustal thickness and the maximum ^{3}He/^{4}He ratio. These lines of evidence suggest that magma–crust interactions are the major controls on subduction-type He. Subsurface processes are also important on the local scale where independent volcanoes interact with surrounding hot springs, which is the subject of the next section.

4 Helium Isotopes and Geotectonic Setting on the Small Scale

4.1 Across-Arc Variations

The first order process occurring under trench-arc systems is subduction of an oceanic plate. The general features of He isotopes in subduction zones has been discussed in the previous section. Examining the detailed geographical distribution of the ^{3}He/^{4}He ratios in each arc segment, these data can provide useful information on the geotectonic setting of the region. We focus here on detailed across-arc variations of He isotopes in a few individual subduction zones together with recent seismic tomography data, creating a link between geophysical and geochemical parameters.

4.1.1 NE Japan

The Japanese Islands are located at a triple junction, a point where three plates (the Pacific plate, the Eurasian plate and the Philippine Sea plate) work against one another. The island arc system is divided NE–SW by the "Itoigawa-Shizuoka tectonic line" (I-S TL) into two major tectonic blocks, northeastern (NE) Japan and southwestern Japan (SW). NE Japan is considered as a well-defined island arc system with a deep trench, a frontal arc, a volcanic arc, and a back arc region with a marginal sea. Perpendicular to the trench axis, geophysical data such as terrestrial heat flow, gravity anomaly, and

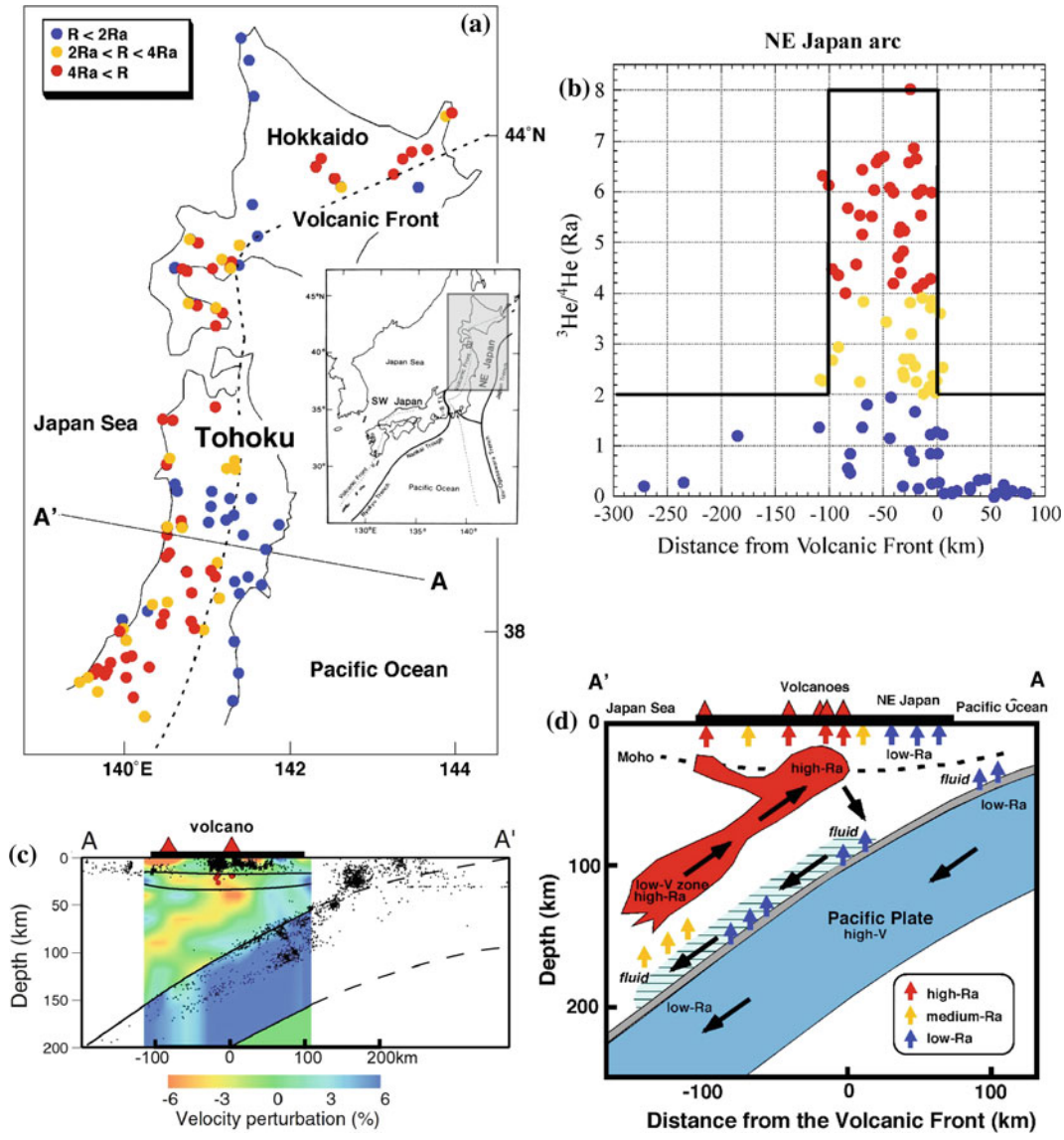

Fig. 19 Geographical distribution of He isotopes in NE Japan (**a**), the relationship between the distance from the volcanic front to the sampling site and the ^{3}He/^{4}He ratio (**b**), a vertical cross-section of S-wave perturbations (**c**), and a schematic diagram of NE Japan to explain the across the arc variation of He isotopes (**d**). Symbol colors reflect ^{3}He/^{4}He ratios: *red* = >4 Ra; *yellow* = 2–4 Ra; *blue* = <2 Ra

seismic velocity vary significantly across the island arc (Yoshii 1977). These geographical and geophysical signatures can in general be well explained by the Pacific plate subducting beneath NE Japan. Since the pioneering work by Nagao et al. (1981), intensive sampling and He isotope measurements have been carried out (Horiguchi et al. 2010; Sano and Wakita 1985b; Sano and Wakita 1988a; Umeda et al. 2007) in this area. The regional NE Japan data are plotted on a map (Fig. 19a) distinguishing high-Ra (red circles) with ratios >4 Ra, medium-Ra (yellow circles) between 4 and 2 Ra, and low-Ra (blue circles) <2 Ra. Assuming that the mantle wedge beneath NE Japan has MOR-type He (8 Ra), the red circles (higher than 4 Ra) show

more than 50 % mantle He contribution to the sample, while the blue indicates less than 25 %.

Figure 19a shows one of the most detailed He isotope maps of a subduction zone. It is apparent that low-Ra samples are located throughout the segment while medium-Ra and high-Ra samples are distributed in a limited region within the volcanic arc, on the western side of the quaternary "volcanic front" in Fig. 19a. The definition of the volcanic front is that "it marks the abrupt appearance of volcanism inward from the trench and along the leading edge of a continent or island arc" (Sugimura et al. 1963). Figure 19b shows the relationship between the distance from the volcanic front to the sampling site and the $^{3}He/^{4}He$ ratio, expressed in Ra. This diagram confirms the observations of Sano and Wakita (1985a) that there is a geographical difference in the $^{3}He/^{4}He$ ratio of the frontal arc and the volcanic arc, being lower on the trench side and higher in the backarc side in NE Japan. Their interpretation was that rising magma is the only material that can introduce MOR-type He from the mantle wedge to the shallow crust. As a result, the $^{3}He/^{4}He$ ratio contrast occurs on the limit of magma introduction, notably the volcanic front (Fig. 19b). In addition, medium-Ra and high-Ra springs are located in a relatively narrow region about 110 km from the volcanic front. In order to understand the distribution further, mechanisms of magma genesis beneath the island arc need to be considered in conjunction with geophysical data.

A dense regional high-sensitivity seismometer network with about 900 stations has been set up in Japan since 1990. Using the large number of natural earthquakes, precise travel-time tomography can be performed. High-quality 3D seismic velocity structure of the upper mantle beneath NE Japan was reported by Nakajima et al. (2001) and Hasegawa and Nakajima (2004). Figure 19c shows a vertical cross-section of S-wave velocity perturbations along line A–A′ in the Fig. 19a map. Zones with low- S-wave velocities are extensively distributed along the volcanic front in the uppermost mantle (perpendicular to the paper) and expand downward to the back arc side of the mantle wedge (along A–A′). Nakajima et al. (2001) suggested that these represent partial melting zones in the mid-crust, directly beneath active volcanoes. They are not directly connected with a deeper portion (the axial point of the front) of the mantle wedge. In traditional views of magma genesis, the volcanic front formed above the location where the volatiles from the subducting slab lower the mantle solidus temperature sufficiently in order to generate partial melting (Tatsumi et al. 1983). However the tomography data (Fig. 19c) suggest that this is not the case, the melting zones are instead located sub-parallel to the subduction slab, with a source that is much deeper than would be predicted for devolatilisation of the slab.

Figure 19d shows a schematic diagram of NE Japan which which rationalizes the He isotope distribution (Sano and Nakajima 2008). The old descending Pacific plate (130 Ma at the trench (Nakanishi et al. 1992)) likely has $^{3}He/^{4}He$ ratios between 0.1 and 0.65 Ra (see Fig. 16 of Sect. 3). These values are consistent with pore waters of deep-sea sediments in the Japan Trench which have $^{3}He/^{4}He$ of ~0.2 Ra (Sano and Wakita 1987). Aqueous fluids with He with these low-Ra compositions are supplied from the slab (including sediments) at different depths to the surface. In addition, the frontal arc area is also affected by radiogenic He ingrowth as there has not been any volcanic activity since 20 million years (Matsuda and Uyeda 1971). Therefore the He isotopes in the fore-arc region are dominated by low-Ra.

Directly beneath the volcanic front, at depths of about 80–130 km, aqueous fluids are generated from the slab, although this does not result in partial melting, but rather these fluids are trapped in overlying materials. Then, at about 100–150 km, a second dehydration may occur and additional fluids are probably produced. Again, these fluids probably react with the overlying mantle, producing a mantle with intermediate $^{3}He/^{4}He$ ratios. As subduction proceeds, fluids hosted in hydrous minerals may be dragged down to depths of 150–200 km. At these depths hydrous minerals become unstable and breakdown (Iwamori 1998), releasing large amounts of

aqueous fluids with intermediate $^{3}He/^{4}He$ ratios. These fluids will migrate upwards and finally initiate partial melting in the mantle region with low S-wave velocities and high $^{3}He/^{4}He$. The melt generated may not move directly upward (due to buoyancy), but is likely transported subparallel to the subducting slab by the upwelling flow, and will meet the Moho directly beneath the volcanic front (Fig. 19d). This melt could be the source of arc magmatism and thus the principle carrier of high $^{3}He/^{4}He$ mantle He. A portion of the flow may reach the Moho on the back-arc side; this separated melt may lead to volcanism in the region, which is hypothesized to be the origin of the 110 km wide high-Ra distributions in Fig. 19b. Despite this, any particular site located far from a volcano may show a crustal He signature (low-Ra) due to interactions with old local lithologies (this is shown in Fig. 19a and described in the following section).

4.1.2 SW Japan

A well-defined island arc system feature has not developed in SW Japan. The Nankai Trough, which corresponds to the trench is not as deep as the Japan Trench. In general, the volcanic front is not as clear here as in NE Japan, with the exception of the Kyushu segment. Heat flow values are relatively high in the trench region (Yamano et al. 1984) and there is no Wadati-Benioff zone longer than a few hundred kilometers. These characteristics are attributed to subduction of the young and warm lithosphere of the Philippine Sea plate beneath the Eurasian plate (Shiono and Sugi 1985), and to the subduction of the Pacific plate beneath the Philippine Sea plate from the east. This has resulted in a complicated surface geology (Taira et al. 1989) and lateral heterogeneity in the structure of the upper mantle (Nakajima and Hasegawa 2007).

Figure 20a shows the geographical distribution of He isotopes in SW Japan using the same definitions for high, medium and low ratios as for NE Japan. These data include all data available in the literature (Matsumoto et al. 2003; Morikawa et al. 2008; Sano et al. 2009; Sano and Wakita 1985b; Umeda et al. 2007; Wakita et al. 1987). Medium-Ra and high-Ra fluids are located primarily in the frontal arc region. In particular high-Ra are found in a region shaped like a backwards letter "L" in southern Kinki district (and not circular (O-shaped), as originally reported by Wakita et al. (1987) which is discussed later). The He data are separated into two groups by a line extending from the fossil Shikoku basin spreading center northward (Okino et al. 1999).

Figure 20b shows the relationship between distance from the volcanic front to the sampling site and the $^{3}He/^{4}He$ ratio in the Chugoku and Shikoku districts, west of the extinct spreading center in Fig. 20a (Sano and Nakajima 2008). High-Ra is located in the volcanic arc while low-Ra occurs throughout the region. This trend is similar to that of NE Japan (Fig. 19b). In contrast, several medium-Ra values are found in the frontal arc region of the Shikoku district, which are defined here as a slab-derived component which is discussed in detail later. Figure 20c shows the relationship in the Kinki district, to the east of the ancient spreading center in Fig. 20a (Sano et al. 2009). This diagram appears anomalous compared to those of NE Japan and the Chugoku and Shikoku districts, there being no contrast in He isotopic composition at the volcanic front. The highest $^{3}He/^{4}He$ ratios, which are equivalent to MOR-type He, are observed even in the frontal arc region. Another anomalous feature is that high-Ra values are found right across the 250 km wide region. This distance is significantly larger than that of NE Japan and Chugoku and Shikoku districts. It appears likely that a different model of magma genesis in the Kinki-district is required.

Figure 21a shows a vertical cross-section of the S-wave velocity perturbations along line B–B′ in Fig. 20a (Nakajima and Hasegawa 2007). A large low-velocity anomaly was found below the Philippine Sea plate down to at least 300 km deep below the Chugoku and Shikoku districts. This zone may be attributable to upwelling—from great depth—of fluid derived from the Pacific plate. Figure 21b shows a schematic diagram of these districts of SW Japan which can explain the across arc variations in He isotopes (Sano and Nakajima 2008). Bearing in mind that the subducting Philippine Sea plate is

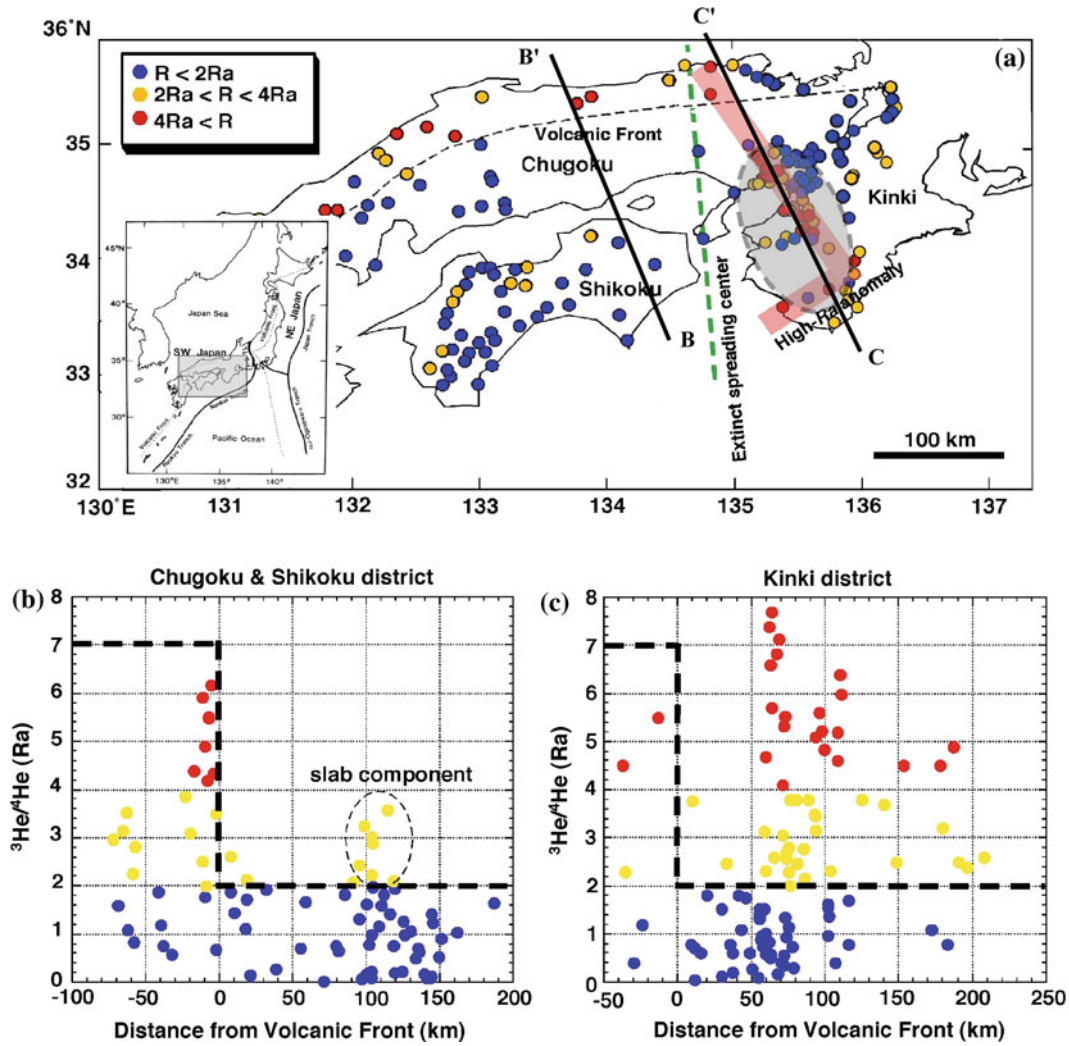

Fig. 20 Geographical distribution of He isotopes in SW Japan (**a**), the relationship between the distance from the volcanic front to the sampling site and the $^3He/^4He$ ratio in Chugoku and Shikoku districts (**b**), and that in Kinki district (**c**)

young (between 15 and 25 Ma (Okino et al. 1994; Shih 1980)), then from Fig. 16 this will lead to $^3He/^4He$ values between 0.4 and 3.4 Ra are present in the slab; medium-Ra fluids will be generated from the Philippine Sea plate. Metamorphic dehydration reactions likely occur at depths of 30–50 km beneath Shikoku district (Hacker et al. 2003; Yamasaki and Seno 2003), suppling abundant aqueous fluids with medium-Ra values which rise through their buoyancy (see Fig. 20b). Furthermore, deep non-volcanic tremors have been observed in the region (Obara 2002), supporting upward flow of aqueous fluids derived from the slab. This mechanism, however, cannot explain the high-Ra fluids in the volcanic arc of the Chugoku district. There is a shallow low-velocity zone towards the Quaternary volcanoes in the Chugoku district visible in the detailed S-wave velocity sections, which connects the large velocity anomaly beneath the Philippine Sea slab by going around the tip of the plate. This seems likely to be the carrier of high-Ra fluids observed in the Chugoku district (see Fig. 21b).

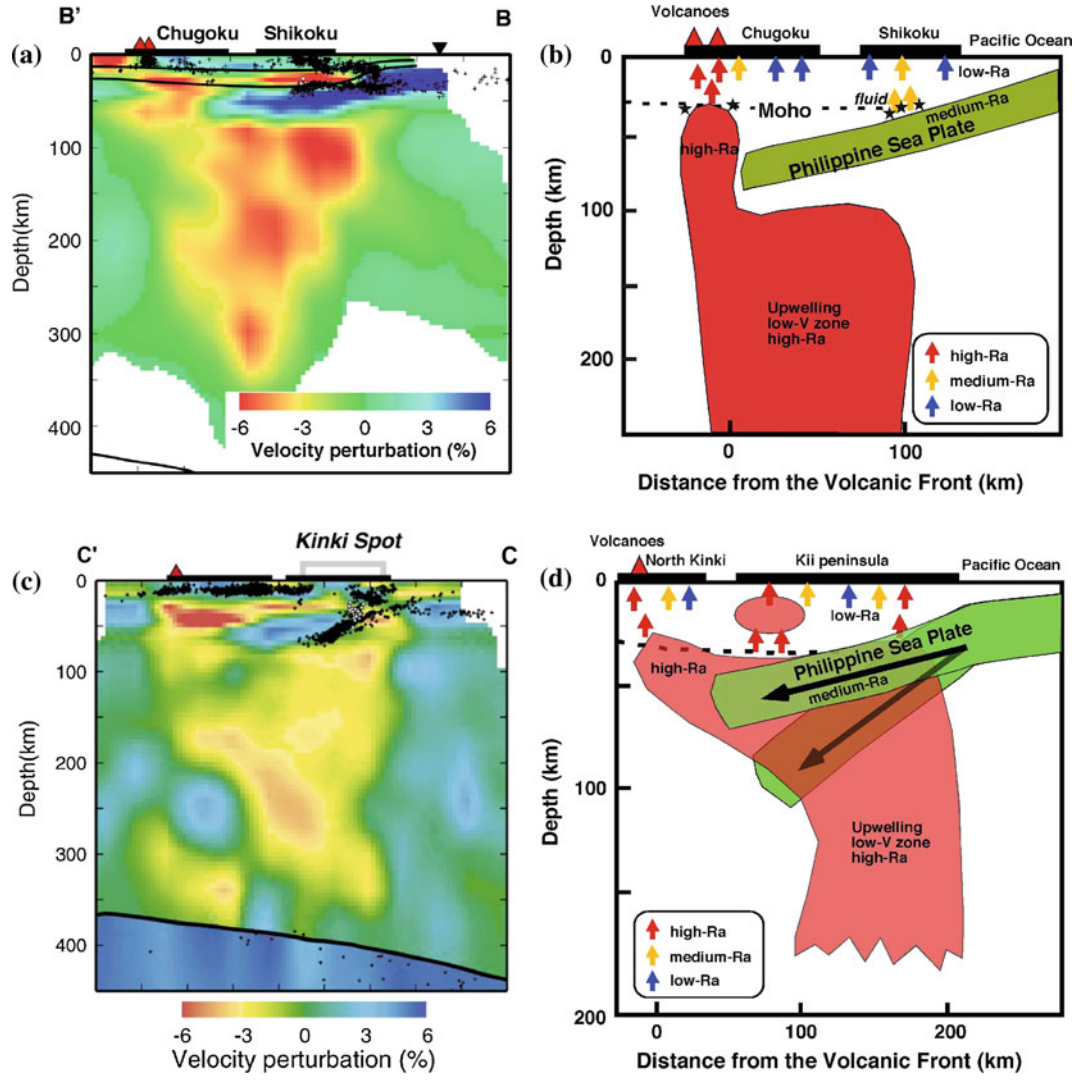

Fig. 21 A vertical cross-section of S-wave perturbations along line B–B′ in Fig. 20a (**a**), schematic diagram of Chugoku and Shikoku districts to explain the across arc variations of He isotopes (**b**), a vertical cross-section of S-wave perturbations along line C–C′ in Fig. 20a (**c**), and a schematic diagram of Kinki district to explain the across arc variations of He isotopes (**d**)

The anomalous distribution of high-Ra in the Kinki district is only observed in one other arc system, Kamchatka (discussed in a later section). Based on the roughly circular distribution of medium- and high-Ra in the district, Wakita et al. (1987) called the region the "Kinki Spot". They suggested that a shallow magma body was present beneath the area, since the region is characterized by high heat flow and molten material at depth is inferred from micro-seismograms (Mizoue et al. 1971). On the other hand, Matsumoto et al. (2003) reported that the anomalous He might be attributable to aqueous fluids expelled from the Philippine Sea plate. Medium-Ra may be supplied from the slab as described in details before (see Fig. 20b). However, it is difficult to preserve high-Ra He in a slab with an age of 15–25 Ma. An upper mantle component is definitely needed in the region. Figure 21c shows a vertical cross-section

of S-wave velocity perturbations along the line C–C′ in Fig. 20a (Nakajima and Hasegawa 2007). A large low-velocity anomaly was again found below the Philippine Sea plate down to at least 300 km below in the Kinki district. Nakajima and Hasegawa (2007) suggested that the shallow low-velocity zone is connected to this large anomaly below the slab, passing through the plate together with the non-volcanic deep tremors. Figure 21d indicates a schematic diagram of the Kinki district which can explain the across-arc He isotope variations (Sano and Nakajima 2008). In order that mantle material can pass through the plate, there needs to be a large fissure or slab tear in the Philippine Sea plate, induced by the change in the dip angle of the subducting oceanic plate. Upwelling material with high-Ra may penetrate through the hypothetical fissure and thus arrive in the shallow crust of the region. Sano and Nakajima (2008) suggested that a slab tear might exist along a fossil spreading center, producing a mechanically fragile lineation. Sano et al. (2009) reported additional He isotope data which emphasize that high-Ra are present in the backwards letter "L" (see Fig. 24a) shaped zone in the southern Kinki district. This evidence supports the idea that the subducted and thus extinct spreading center may have been similar to a mid-ocean ridge with transform faults. Based on receiver function images, the distribution of deep tremor sources, the seismicity and focal mechanisms of intraplate earthquakes, Ide et al. (2010) confirmed that the subducted plate is split along an extinct ridge due to an abrupt change of subduction direction, followed by elastic deformation of the plate and an accumulation of stress near the ancient ridge.

4.1.3 The North Island of New Zealand

New Zealand is situated on the boundary between the Australian and Pacific plates in the southwest Pacific Ocean. This plate boundary extends from the Tonga-Kermadec Trench through New Zealand to the Puysegur Trench. In the North Island of New Zealand, the Pacific plate is being subducted beneath the Australian plate, which leads to the development of an island-arc system (Cole and Lewis 1981), consisting of a shallow structural trench, an accretionary borderland, a frontal ridge, and a volcanic arc and marginal basin with a wedge-shaped Central Volcanic Region. Since subduction occurs obliquely at about 42 mm/yr (DeMetis et al. 1990), the southeastern parts of the North Island are rotating clockwise with respect to the northwest, at rates of 1.6°–3.8 °/Myr. This rotation accommodates the marginal-parallel component of motion between the Pacific and Australian plates (Wallace et al. 2004). The rotation in the southeast has resulted in extension in the Central Volcanic Region which includes the Taupo Volcanic Zone (TVZ). Volcanism in the TVZ ends at Mt Ruapehu with andesitic activity. Other andesitic volcanism occurs in the region of Mt Taranaki, about 130 km west of the TVZ.

Since the pioneer work by Torgersen and Jenkins (1982), several sampling and He isotope measurements have been carried out (Giggenbach et al. 1993; Hulston et al. 2001; Sano and Wakita 1987). These data are complied and plotted on a map (see Fig. 22a) with the same compositional categories as for the NE Japan. The volcanic front is defined clearly on the southeastern margin of the TVZ. We tentatively draw the boundary from Mt Ruapehu to the west, parallel to the Hikurangi Trough (the dotted line in Fig. 22a). Low-Ra samples are located everywhere in the segment except for the Central Volcanic Region, where high-Ra values are concentrated. The number of medium-Ra values is lower than that in NE and SW Japan, suggesting a bimodal He isotope distribution, distinct compared to the examples from Japan.

Figure 22b shows the relationship between the distance from the volcanic front to the sampling site and the $^{3}He/^{4}He$ ratio. High-Ra fluids are limited to the 100 km wide volcanic arc, except for one outlier (the Ngawha geothermal well, about 400 km north of the front). Low-Ra occurs everywhere in the segment, a distribution similar to that of NE Japan. The high-Ra in Ngawha together with a few medium-Ra in northernmost part of the island can be

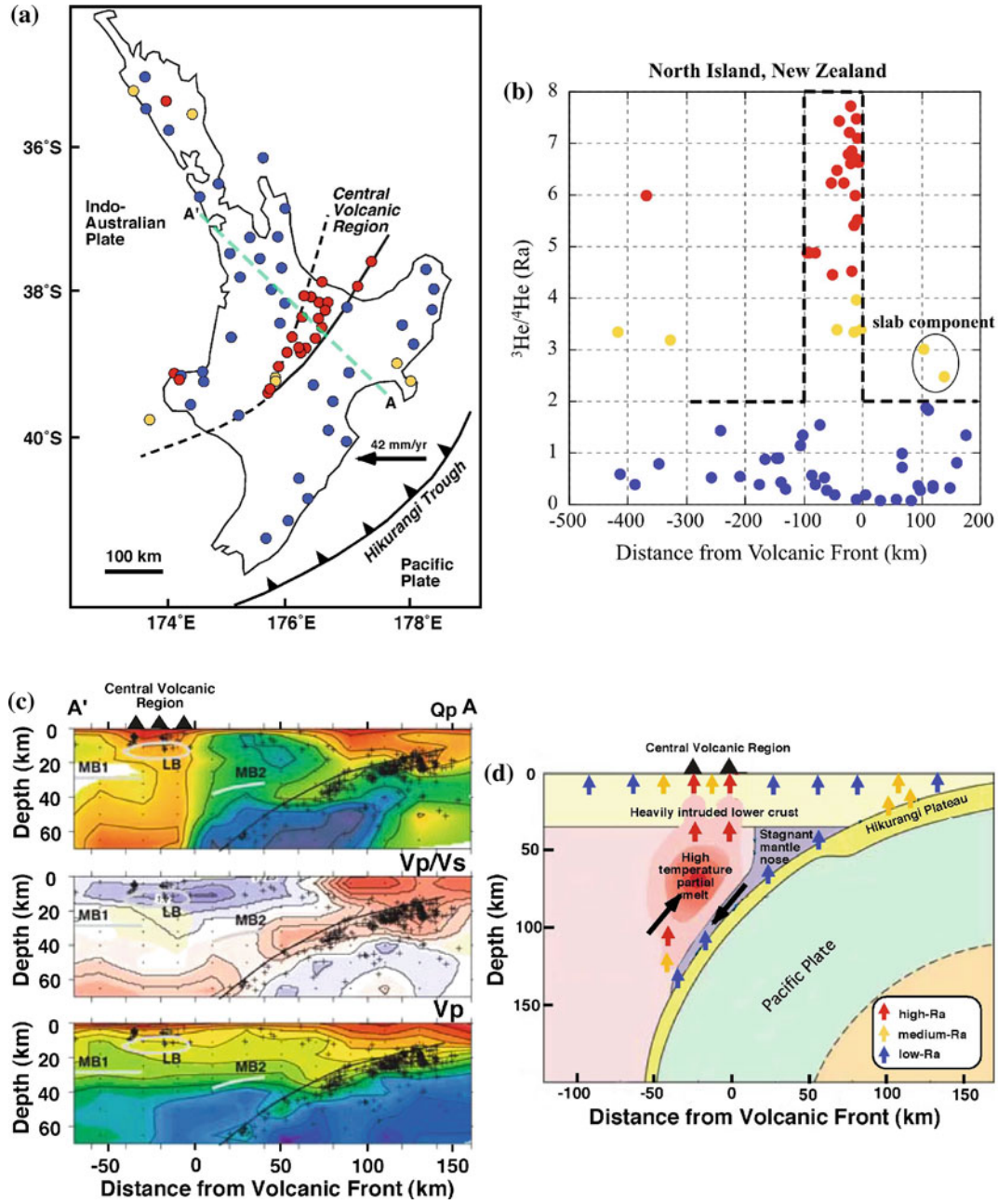

Fig. 22 Geographical distribution of He isotopes in North Island of New Zealand (**a**), the relationship between the distance from the volcanic front to the sampling site and the ^{3}He/^{4}He ratio (**b**), a vertical cross-section of Qp value, Vp/Vs ratio and Vp (**c**), and a schematic diagram of North Island to explain the across arc variations of He isotopes (**d**)

attributed to remnant back-arc type alkali basalt volcanism in the region during the Pleistocene (Giggenbach et al. 1993). The diagram confirms the observations of Sano et al. (1987) that there is a clear contrast in the geographical He isotope distribution between forearc and volcanic arc regions in the North Island: low in the former and high in the latter. The contrast, however, is

not as marked as in NE Japan, rather is similar to that in the Chugoku and Shikoku districts of SE Japan (see Figs. 19b and 20b). There are a few medium-Ra values in the frontal arc region of the North Island, which were collected from mud volcano type springs of accretionary structures associated with compressional tectonics.

Eberhart-Phillips et al. (2008) using waveform data from 2708 earthquakes recorded by dense seismometer deployments in the region reported a three-dimensional attenuation structure of the Hikurangi subduction zone in the central North Island. Figure 22c shows vertical cross-sections of the 3-D Qp, Vp/Vs and Vp models along line A–A′ in the map of Fig. 22a (from Fig. 9 of Eberhart-Phillips et al. (2008) with some modifications). Low-Qp zones (that probably have similar implications as the low S-wave velocity zones in Fig. 19c) are distributed below the Central Volcanic Region down to at least 60 km depth, which could be attributed to upwelling fluid from a deeper region related to the Pacific plate. In addition, low-Qp zones are also found in an area about 100 km southeast of the volcanic front, overlain by a relatively high-Qp zone which extends to the lower crust. Based on the moderately high Qp, high Vp and Vp/Vs region, Eberhart-Phillips et al. (2008) suggested that there is a stagnant mantle "nose" to the southeast of the TVZ with cold, dry and thus viscous materials.

Figure 22d indicates a schematic diagram summarizing the interpretation of the Qp results beneath the TVZ (Eberhart-Phillips et al. 2008) with some modifications to accommodate the He isotope data. The moderate Vp material directly above the dipping seismic zone is probably sinking, entrained by the motion of the subducted slab. This is very similar to that described in the interpretation of NE Japan (Fig. 19d). Under the stagnant wedge mantle and deeper beneath the volcanic front, a viscous blanket appears to be formed with low-Ra and/or medium-Ra material, which may insulate the slab from the high-temperature mantle. In contrast, material with high-Ra in the overlying low Vp region can be interpreted as rising via a return flow within the wedge, again resembling the situation in NE Japan. This flow, rising subparallel to the subduction slab, likely leads to volcanism in the Central Volcanic Region and could be the principle carrier of mantle He with high-Ra. The width of the high-Ra in Fig. 22b may be controlled by the width of the intersection of the rising flow and the Moho on the back-arc side.

Even though general He isotope and seismic tomography features of North Island resemble those of NE Japan, there is a significant difference in the frontal arc region. There are some (few) medium-Ra values found in the forearc of the North Island (a relatively small region of the east coast), which in turn, resembles more the He isotope distribution of Chugoku and Shikoku districts of SW Japan. These medium-Ra localities occur within about 100 km of the volcanic front, suggesting that the medium-Ra source has a similar mechanism in both SW Japan and the North Island of New Zealand, and is likely related to the depth of descending slab. In addition, the medium-Ra zone coincides with increased shallow seismicity (Reynes 1980), supporting the hypothesis that aqueous fluids are rising from the slab in the frontal arcs. However, when we take into account radiogenic ingrowth, the expected He isotope ratios are between 0.13 and 0.8 Ra (the Pacific plate is about 100 Ma in this region (Clift and Vannucchi 2004)), inconsistent with the medium-Ra values observed in the frontal arc. Therefore, there needs to be an additional input of mantle He.

Subduction in the North Island is influenced by the Hikurangi Plateau, a large igneous province on the incoming Pacific plate (Mortimer and Parkinson 1996). The buoyancy of the subducted plateau may have resulted in exposure of the forearc above the shallow portion of the subduction thrust. The age of plateau is unknown but, based on the age of the surrounding crust and correlations with seismic reflectors on the Chatham Rise, it was considered to be at least Mesozoic by Davy and Wood (1994). They further suggested that the Hikurangi Plateau formed due to the interaction of a hotspot or mantle plume with a spreading ridge similar to present

day Iceland. In this case, modification of He isotopes by radiogenic ingrowth would not be the same as for mid-ocean ridges, i.e. the $^3He/^4He$ evolution over time would not follow the curves in Fig. 16. If we assume an initial He isotope ratio of 29 Ra (the Iceland maximum, Table 2) and the same abundances of He, U, and Th in the subducted plateau as in MORB, the expected $^3He/^4He$ ratios are between 0.5 and 2.9 Ra after 100 million years. These values are consistent with those observed in the forearc of the North Island (Fig. 22b), thus possibly explaining the medium-Ra fluids found in this area.

4.1.4 Kamchatka Peninsula of Russia

The Kamchatka-Kuril arc system is one of the most active subduction zones in the north-western Pacific. In southern Kamchatka, the Cretaceous age Pacific plate subducts beneath the Okhotsk plate, leading to the development of a trench-arc system. There are many Holocene volcanoes along the eastern coast of Kamchatka (Braitseva et al. 1995) which generally lie above the 100 km depth contour of the subducting slab (Gorbatov et al. 1999), similar to NE Japan (Fig. 19c). On the northeastern side of Kamchatka, the tectonic setting is more complicated in that the Meiji seamounts, the northernmost segment of the Hawaii-Emperor seamount chain, descend into the subduction zone with the Pacific plate which is also being displaced along the Bering strike-slip fault at about 8 cm/yr (Steblov et al. 2003).

The first discovery of mantle He was made in this region by Mamyrin et al. (1969). Since then, numerous He isotope measurements have been carried out on hydrothermal fluids from the Kamchatka Peninsula (Baskov et al. 1973; Kamensky et al. 1976), although these were generally published in Russian-language journals (Fischer et al. 1998; Taran 1985; Taran et al. 1996). Recently Taran (2009) has compiled a large data set from all published articles. Figure 23a shows the geographical distribution of He isotopes in Kamchatka based on the data by Taran (2009) following the $^3He/^4He$ categories as in NE Japan (Fig. 19). The positions of the volcanic front, and the Kuril-Kamchatka trench and the Bering fault are after Taran (2009) and Jiang et al. (2009), respectively. Most observed values fall into the high-Ra field while the number of low-Ra is relatively small compared to Japan and New Zealand. This may in part due to sampling bias; the sampling strategies were intended to find mantle signatures in Kamchatka.

Figure 23b shows the relationship between the distance from the volcanic front to the sampling site and the He isotopes (essentially the same as Fig. 5 of Taran (2009)). Except for two outliers from the Kronotsky peninsula, there is a clear step-function in the He isotope distribution with high values in the volcanic arc and low $^3He/^4He$ in the forearc, which seems to be a general feature in circum-Pacific trench-arc systems (Sano and Wakita 1985a). The highest $^3He/^4He$ ratio is about 8 Ra, again similar to those in Japan and New Zealand, consistent with MOR-type He in the upper mantle. The possible cause of forearc outliers is discussed later.

Jiang et al. (2009) reported seismic tomography of the Pacific slab edge under Kamchatka using a 3-D P-wave velocity structure of the mantle down to 700 km from 678 P-wave arrivals (75 teleseismic events recorded by 15 portable seismic stations and one permanent station in Kamchatka). Figure 23c shows the vertical cross-section of the 3-D P-wave velocity image along line C–C′ in the map of Fig. 23a (from Fig. 10c of Jiang et al. (2009) with some modifications). The subducting Pacific slab extends below the 660 km discontinuity under southern Kamchatka, while it shortens to the north and terminates near the Aluetian–Kamchatka junction. Their tomographic images also show low-velocity anomalies beneath northern Kamchatka and the Aleutian–Kamchatka junction that may correspond to a large upwelling mantle flow from great depth. In the case of SW Japan, the anomalous zone was attributed to material derived from the interaction between the deep Pacific slab and the upper mantle. In the present case, however, it is difficult to imagine a remnant of a separate subducting slab at great depth. A plume-type source could be responsible for the upwelling material imaged by Jiang et al., even though the

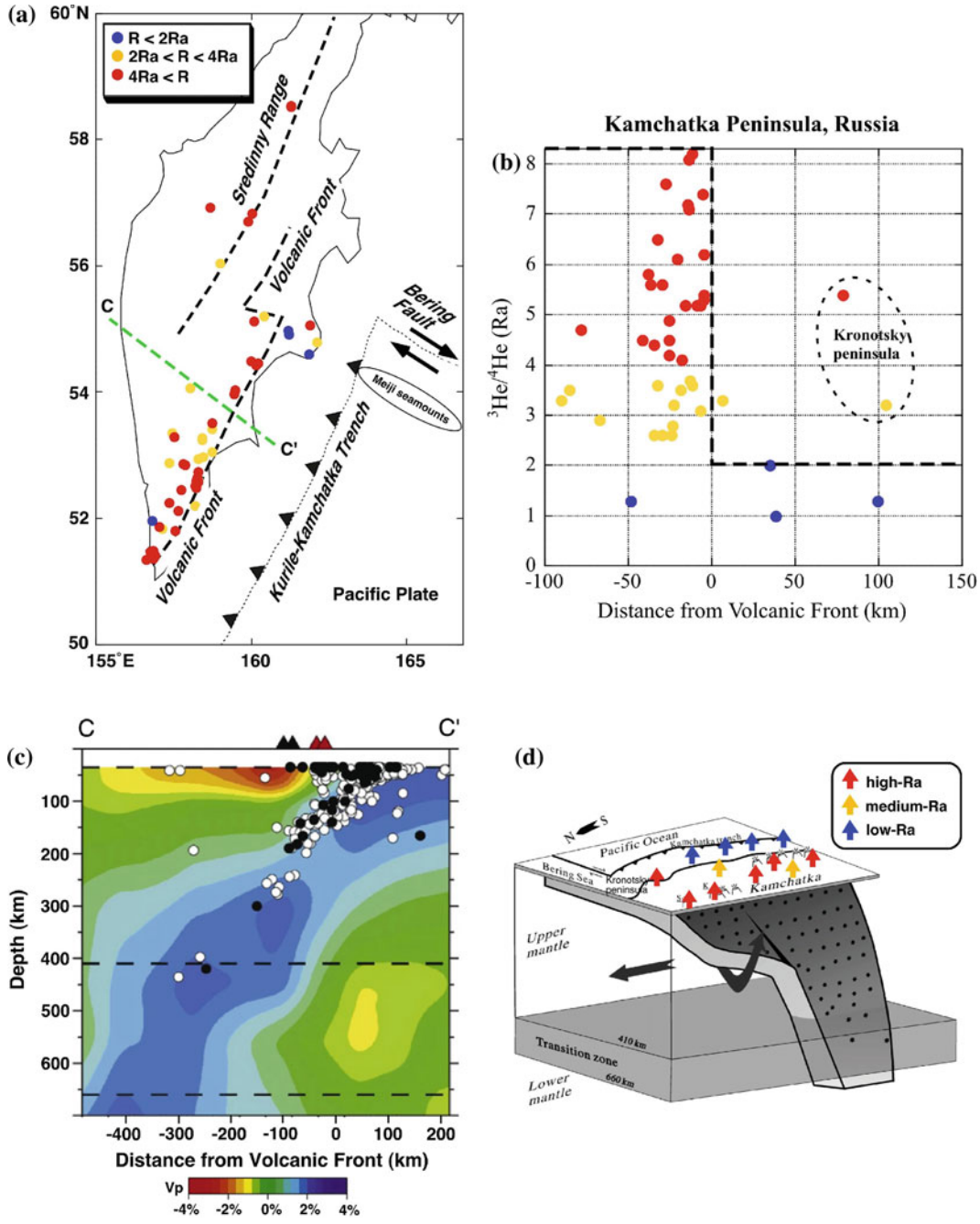

Fig. 23 Geographical distribution of He isotopes in Kamchatka Peninsula of Russia (**a**), a relationship between the distance from the volcanic front to the sampling site and the $^3He/^4He$ ratio (**b**), a vertical cross-section of Vp perturbations (**c**), and a schematic diagram of Kamchatka to explain the across arc variations of He isotopes (**d**)

maximum He isotope ratios in the region fall within the MOR range (Fig. 23b).

Once more, the general features of the He isotope distribution (low in the frontal arc and

high in the volcanic arc) and the seismic tomography (descending Pacific slab and related low-velocity anomalies beneath the volcanic arc) in Kamchatka are similar to NE Japan and the North Island of New Zealand. In contrast, there are anomalous high-Ra and medium-Ra localities found in the frontal Kamchatka arc, about 100 km in front of the volcanic front. Since the estimated age of the Pacific plate is about 100 Ma in the region (Clift and Vannucchi 2004), the expected $^{3}He/^{4}He$ ratio is between 0.13 and 0.8 Ra (based on the ingrowth modeled in Fig. 16), which cannot account for the observed He isotopes. Analogous to the Hikirangu Plateau of the North Island, it is possible that the subducting Meiji seamounts (the northernmost segment of the Hawaii-Emperor seamount chain) provide high $^{3}He/^{4}He$ ratios. Assuming the seamounts have a hot spot He isotope signature and the formation age is that of the surrounding oceanic crust, the expected He isotopes are 0.5 and 2.9 Ra after 100 million years. This hypothesis can explain the medium-Ra locality but not the high-Ra observed in the Kronotsky peninsula, leaving the question open as to how pristine mantle He was supplied to this region.

Figure 23d shows a schematic diagram of the Pacific plate subducting to the west through the mantle transition zone beneath Kamchatka (Jiang et al. 2009) with some modifications to explain the He isotope data. Jiang et al. (2009) suggested that there is a gap in the Pacific Plate associated with loss of subducted lithosphere beneath Sheveluch and Klyuchevskoy volcanoes near the Pacific slab edge. Asthenospheric flow within the upper mantle could therefore allow high $^{3}He/^{4}He$ material to pass through the gap around the slab edge to the north. This could then be the principle carrier of high-Ra He observed in the Kronotsky peninsula. The "gap" hypothesis is similar to the explanation of high-Ra in the Kinki district (Fig. 21d). The combination of He isotopes and seismic tomography are useful tools for evaluating regional tectonic settings.

4.2 Circum-Volcanic Variations in $^{3}He/^{4}He$

It is well documented that there is a large variation of He isotopes in subduction zone hydrothermal systems compared with those of mid-ocean ridges (see Sect. 3.4). These variations are principally attributable to mixing of three components: atmospheric He, mantle He, and crustal He. When the air component is corrected using the $^{4}He/^{20}Ne$ ratio, He in subduction zones is explained by binary mixing between mantle He (from the mantle wedge) with $^{3}He/^{4}He = 8$ Ra, and radiogenic He with 0.02 Ra. There are two possible sources of crustal He, either the subducting oceanic sediments and slab or radiogenic He in the subsurface crustal material, which contaminates mantle He in the volcanic-hydrothermal area. In the first scenario, the slab/sediment derived He would be well mixed with upper mantle material before rising to the magma region of generation whereas shallow contamination would result in He isotope variations around an isolated volcano.

4.2.1 Case Study 1: He Isotope Variations Around Ontake Volcano in Japan

Mt Ontake is an isolated strato-volcano (elevation 3063 m) located in central Honshu, Japan (35°54′N, 137°29′E). There is no other active volcano within a radius of about 40 km. The main rock type is pyroxene andesite. The volcano was believed to be dormant since the last eruptive activity was estimated to have occurred about 23,000 years ago, but the volcano re-erupted on 28 October 1979, forming several new craters and ejecting large amounts of volcanic ash and steam. There are many hot and mineral springs in the area, aligned northwest–southeast of the central cone of the volcano, probably distributed along geo-structurally weak zones. Sano et al. (1984) collected bubbling gases in these springs at various distances from

the central cone of Mt Ontake. Figure 24a shows the sampling sites located within a radius of 25 km of the volcano, and using the same He isotope categories as for NE Japan. The $^3He/^4He$ ratios vary significantly, from 6.15 to 1.71 Ra. It is apparent that high-Ra is located close to the central cone and decreases with distance from the volcano. This is the first example of He isotope variations at the local scale ($\sim$25 km) in an isolated volcano.

Figure 24b shows the spatial evolution of the $^3He/^4He$ ratio, showing a clear inverse correlation between distance and $^3He/^4He$, yet there is no simple relation between $^4He/^{20}Ne$ and distance, suggesting that variable air contamination is not the main control of the He isotope variations. Rather, the observed variation results from dilution of magmatic He by radiogenic He derived from the regional basement rock. Subsequent studies (Sano et al. 1998; Takahata et al. 2003) confirm that the correlation between the $^3He/^4He$ ratio and the distance has been stable during the past 20 years. Thus the magma-fluid flux is probably in quasi-steady state around the volcanic edifice. The gray curve in Fig. 24b is the $^3He/^4He$ ratio decrease predicted by a hydrodynamic dispersion model (discussed in detail below). During volcanic activity most magmatic gases are emitted from the central cone as volcanic gases, however, some gases are also released through fissures or permeable channels in the volcanic edifice. The $^3He/^4He$ ratio of these fissural emissions is reduced by dilution with radiogenic He. However, it is not known if this feature is a general trend of the He isotopes around volcanoes.

4.2.2 Case Study 2: He Isotopes Around Nevado del Ruiz Volcano and the Dispersion Model

Nevado del Ruiz volcano (elevation 5400 m) is located in the Cordillera Central uplift in the west-central Colombian Andes (4°53′N, 75°22′E). The volcanic edifice is composed of andesitic deposits erupted during the past one million years. The broad and flat form of Ruiz is unusual; it is not a typical strato-volcano like Mt Ontake. Williams et al. (1987) carried out intensive sampling and He isotope measurements around Mt Ruiz, showing that. As for Mt Ontake, there is a negative correlation between $^3He/^4He$ and distance from the central crater; this is only the second time this has been observed. Sano et al. (1990) confirmed that the general trend had not changed one year after the initial survey. Figure 25a shows the sampling sites located within a radius of 15 km of the volcano (same He isotope categories as for Mt Ontake). Excluding air-contaminated samples with $^4He/^{20}Ne$ ratios less than one, the $^3He/^4He$ ratios vary significantly from 2.40 to 6.35 Ra (some data are averages of different sampling campaigns). Figure 25b indicates the relationship between the average $^3He/^4He$ ratio and the distance of the sampling site from the central crater.

Sano et al. (1990) developed a hydrodynamic dispersion model to explain the observed He isotope trend around the volcano. Figure 26 shows (a) a schematic cross-section of the Ruiz hydrothermal system and (b) the proposed model. Despite the model being simplistic, it reproduces well the spatial distribution of $^3He/^4He$ ratio around the volcano. Assuming that fluids are supplied from a magma reservoir to the conduit at a constant rate, and that the boundary conditions are such that the height of the piezometric head has the same distribution in any vertical section through the axis of the conduit, one may estimate the fluid flow and thus the He concentration based on the dispersion model. The equation governing He concentration at distance (r) under steady-state, homogeneous and isotropic conditions is as follows:

$$D[1d/rdr(rdC/dr)] - A/r(dC/dr) + (1 - Re)P = 0$$

where D, C, Re and P denote the coefficient of molecular diffusion of He in water, He concentration, retention of radiogenic He in the porous material of the aquifer, and radiogenic production rate of He in the material, respectively. A is a constant, with the dimensions $[L^2/T]$, the same as those of a diffusion constant. The equation can be solved under the boundary

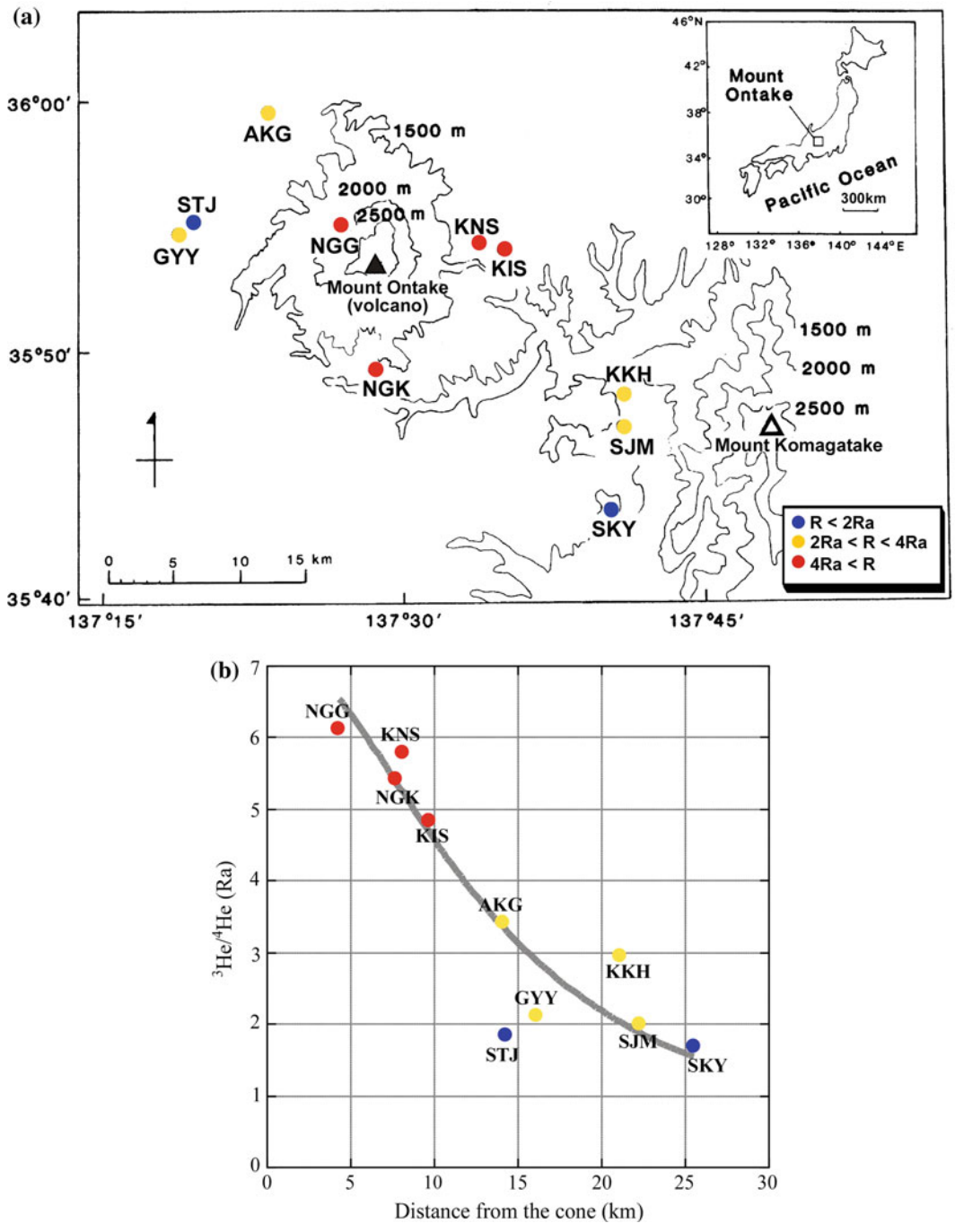

Fig. 24 The sampling sites located within a radius of 25 km of Mt Ontake in central Honshu, Japan, together with their He isotopic compositions (**a**). The relationship between the distance from the sampling site to the central cone and the ^{3}He/^{4}He ratio (**b**)

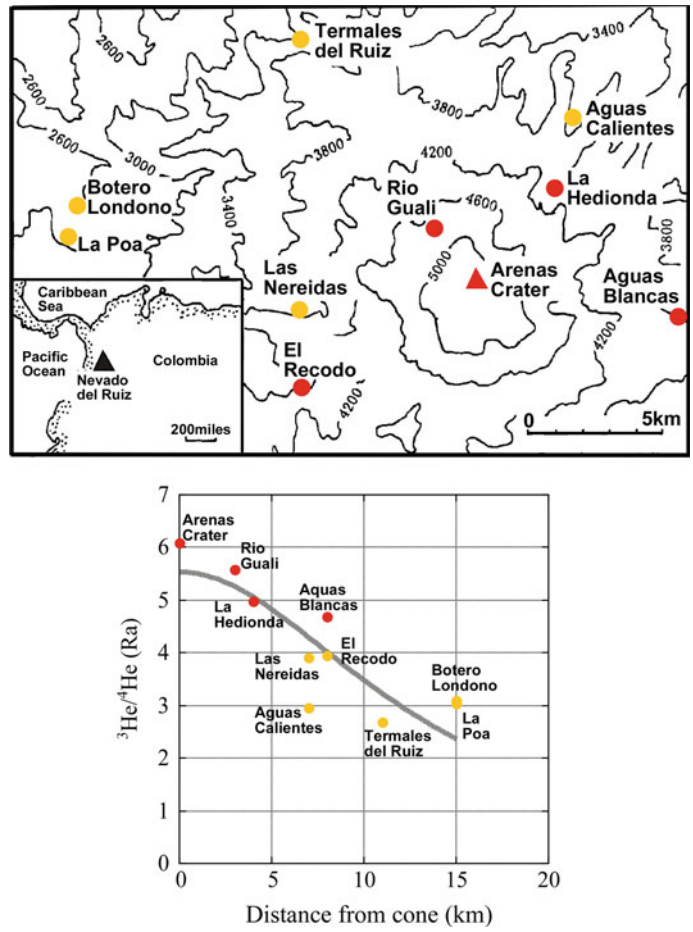

Fig. 25 The sampling sites around Mt Nevado del Ruiz in Colombia together with their He isotopic composition (**a**). The relationship between the distance from the sampling site to the central cone and the ^{3}He/^{4}He ratio (**b**)

condition, $C = C_m$ for $r = 0$ (at conduit) and $C = C_e$ for $r = r_e$ (at the most distant point) as follows:

$$\begin{aligned} C(r) =& (r/re)(A/D)\{(Ce - Cm) \\ & - [(1 - Re)P/(2A - 4D)]r2\} \\ & + \{(1 - Re)P/(2A - 4D)\}r2 + Cm \end{aligned}$$

where C_m is the He concentration at the conduit and C_e is that at the most distant point. Assuming that the above equation is applicable to both ^{3}He and ^{4}He concentrations, the following equation can be derived:

$$^3\mathrm{He}/^4\mathrm{He}(r) = (^3Pr^2 + \alpha^3 C_m)/(^4Pr^2 + \alpha^4 C_m)$$

where ^{3}P, ^{4}P, ^3C_m and ^4C_m denote nucleogenic and radiogenic production rates of ^{3}He and ^{4}He, concentration of ^{3}He and ^{4}He at the conduit, respectively. The constant α equals $(2A - 4D)/(1 - Re)$. Assuming U and Th contents of 3 and 10 ppm in the porous material composing the aquifer, and a density of 2.7 g/cm^3, one may calculate that the production rate of radiogenic ^{4}He (^{4}P) is 1.5 atoms/cm^3 s in the aquifer. Nucleogenic production of ^{3}He (^{3}P) is also estimated to be 3×10^{-8} atoms/cm^3 s based on typical compositions (Mamyrin and Tolstikhin 1984). It is possible to calculate α^3C_m and α^4C_m values by fitting the observed He isotope distribution to the above equation by the least-squares method. The fitted curve (gray line in Fig. 25b) agrees well with the observed ^{3}He/^{4}He ratio variation with distance in the Ruiz hydrothermal system. Thus the simple hydrodynamic dispersion model explains well the variations.

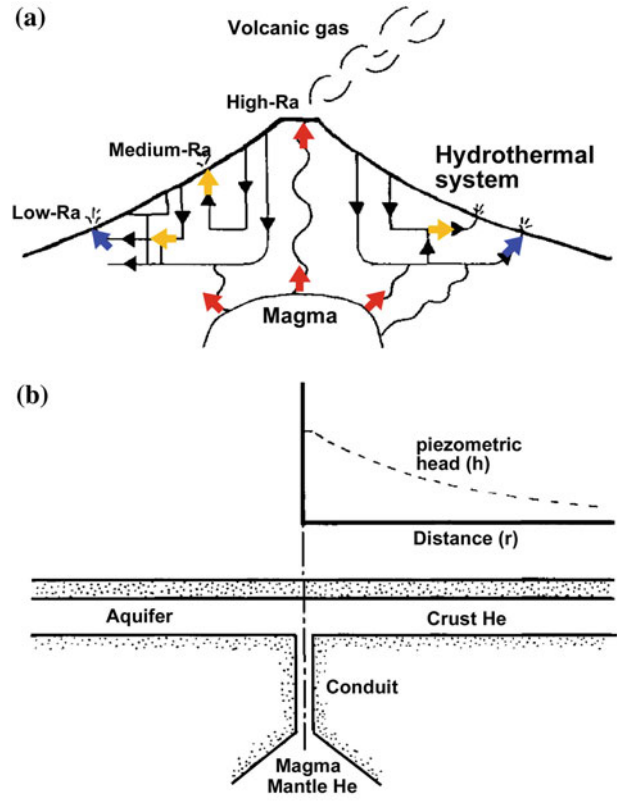

Fig. 26 A schematic cross-section of the Ruiz hydrothermal system (**a**) and the proposed hydrodynamic dispersion model to explain the circum-volcano variation of He isotopes (**b**)

4.2.3 He Isotopes Around Other Independent Volcanoes

In addition to the examples of Mt Ontake and Nevado del Ruiz, there are $^3He/^4He$ data sets around other isolated volcanoes available in the literature, notably Mt Hakone (Sakamoto et al. 1992), Kusatsu-Shirane (Sano et al. 1994), Unzen (Morikawa et al. 2008; Notsu et al. 2001), and the Lesser Antilles islands (van Soest et al. 1998). Figure 27 shows the relationship between the $^3He/^4He$ ratio (corrected for air contamination) and the distance of the sampling site from the central crater in each volcano. The fitted curves (dotted lines) are calculated using the hydrodynamic dispersion model: in general, the model explains the circum-volcano variations, even though the curve may be concave-down (Mt. Kusatsu and Lesser Antilles) or concave-up (Mt. Ontake and Unzen). Table 5 lists a summary of the $^3He/^4He$ ratio variations around the volcanos. There is no clear relationship between $^3C_m/^4C_m$ (the $^3He/^4He$ ratio at the central cone) and rock-type or volcano-type. In addition, there is no correlation between r(1/2) (the distance where $^3He/^4He = 0.5 * {}^3C_m/^4C_m$) and rock-type or volcano-type. Since r(1/2) is related to the dispersion efficiency of the magmatic volatiles in the volcanic edifice, lateral He isotope variations around a volcano may be a useful method for investigating the state of activity of individual volcanoes in the future.

5 Temporal Variation of Helium Isotopes and He/Ne Ratios in Individual Volcanoes

Variations in helium isotopes at a single volcano over time can be expected if the magma chamber gets fed by various sources, i.e. upper mantle versus plume-derived magma. However, such a scenario is unlikely to be observed during

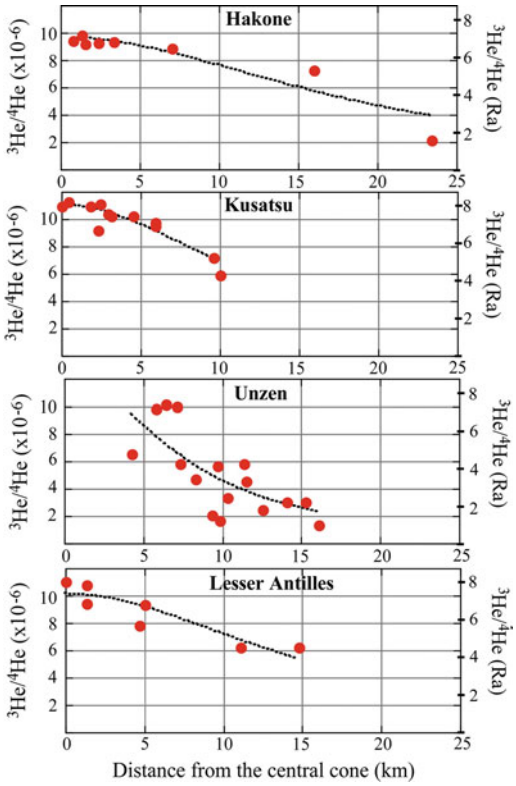

Fig. 27 The relationship between the distance from the sampling site to the central cone and the $^3He/^4He$ ratio in Mt Hakone, Kusatsu-Shirane, Unzen, and Lesser Antilles

sampling campaigns that are usually carried out over several years or several decades at best. Figure 28 schematically summarizes the volcano-hydrothermal processes that can affect the $^3He/^4He$ ratio of a gas or water sample collected at the surface. Most of these processes decrease the $^3He/^4He$ ratio of hydrothermal fluids and only two processes, magma degassing due to depressurization where ^3He preferentially degasses into bubbles, and injection of ^3He-rich fluids (gas or magma), will increase this ratio over time scales that are feasible for volcano monitoring (year to decades). As a result, over time, in any given volcanic system, the $^3He/^4He$ should decrease unless there are perturbations to the magmatic system such as rising magma or injection of new magma. Therefore, $^3He/^4He$ monitoring in volcanic and hydrothermal systems such as hot and cold spring water discharges, fumarole gases, geothermal wells, mud pots and soil gas discharges are a potentially powerful tools for evaluating the state and evolution of a volcano.

5.1 Magma Degassing

Magma degassing and aging will, over time, decrease the $^3He/^4He$ ratio of volcanic discharges; the continuous release of helium from the magma reduces the helium-3 concentration remaining in the melt. The degassed magma is then more susceptible to contamination by radiogenic helium resulting from U and Th decay in the magma itself or from contamination with low $^3He/^4He$ ratio crustal volatiles. These processes have been evaluated in detail (Hilton et al. 1993; Zindler and Hart 1986).

Magma degassing fractionates noble gas abundances due to differences in gas solubilities in magmas (Jambon et al. 1986). The He/Ar ratio of fumaroles and glasses are often used as indicators of degassing. For example, recent work at Oldoinyo Lengai showed that the fumarole He/Ar ratio followed the expected degassing trends as predicted by solubilities and Rayleigh fractionation (Fischer et al. 2009). Gonnermann and Mukhopadhyay (2007) showed that open-system non-equilibrium degassing can explain the He–Ar–Ne characteristics of submarine glasses and fractionation of these gases is kinetically controlled by their diffusivities, where $D_{Ar} \sim D_{Ne} \sim 0.001D_{He}$ (Lux 1987). Such degassing processes should also be reflected in volcanic fumaroles. Noble gas solubility is also controlled by the CO_2 and water content of the magma in such a way that more helium is degassed from magmas with a higher CO_2 content (Nuccio and Paonita 2000). Application of non-equilibrium Rayleigh degassing as well as considerations of the initial CO_2–H_2O contents of magmas has recently been performed by Furi et al. (2010) who show that He–Ar–Ne systematics of Icelandic glasses are predominantly controlled by open-system equilibrium degassing. Nuccio and Paonita (2001) use a quantitative H_2O–CO_2–N_2–noble gas mixture degassing model to show that dissolved H_2O and CO_2 contents strongly affect noble gas

Table 5 Summary of He isotope variaiton around volcano

	Volcano	$^3C_m/^4C_m$ ($\times 10^{-6}$)	r (1/2) (km)	Concave	Rock-type	Volcano-type	Elevation (m)
a	Nevado del Ruiz	7.74	13	No	Andesite	Strato-volcano	5321
b	Ontake	9.92	13	Up	Andesite	Strato-volcano	3063
c	Hakone	9.66	19	No	Basalt + dacite	Complex-volcano	1438
d	Kusatsu	10.1	13	Down	Andesite + dacite	Strato-volcano	2176
e	Unzen	12.2	7.7	Up	Andesite	Complex-volcano	1500
f	Lesser Antilles	10.1	16	Down	Basalt	Three islands: Nevis, Guadeloupe, Martinique	–

r(1/2): distance from the cone to the place where the estimate He isotopic ratio is the half of the maximum ($3C_m/4C_m$)

Table 6 Neon isotopes of hydrothermal fluids

Location		Maximum	N	Average	References
Iceland	$^{20}Ne/^{22}Ne$	10.09	23	9.87	Furi et al. (2010)
	$^{21}Ne/^{20}Ne$	0.0302	23	0.0297	
Yellowstone, USA	$^{20}Ne/^{22}Ne$	10.54	12	10.14	Hearn et al. (1990)
	$^{21}Ne/^{20}Ne$	0.0297	12	0.0292	
Honduras, Central Am.	$^{20}Ne/^{22}Ne$	10.10	11	9.78	Kennedy et al. (1990)
	$^{21}Ne/^{20}Ne$	0.0295	11	0.0292	
Lesser Antilles	$^{20}Ne/^{22}Ne$	10.55	65	9.94	Pedroni et al. (1999)
	$^{21}Ne/^{20}Ne$	n.a.	0	n.a.	
Etna, Italy	$^{20}Ne/^{22}Ne$	10.69	5	10.69	Nakai et al. (1997)
	$^{21}Ne/^{20}Ne$	0.0367	5	0.0343	
Vulcano, Italy	$^{20}Ne/^{22}Ne$	9.89	15	9.76	Tedesco and Nagao (1996)
	$^{21}Ne/^{20}Ne$	0.0397	15	0.0316	
Vesuvius, Italy	$^{20}Ne/^{22}Ne$	9.95	11	9.50	Tedesco et al. (1998)
	$^{21}Ne/^{20}Ne$	0.0451	11	0.0337	
Japan (volcanoes, springs)	$^{20}Ne/^{22}Ne$	10.36	38	9.89	Nagao et al. (1981)
	$^{21}Ne/^{20}Ne$	0.0306	34	0.0292	
Iwojima, Japan	$^{20}Ne/^{22}Ne$	9.996	15	9.88	Sumino et al. (2004)
	$^{21}Ne/^{20}Ne$	0.0299	15	0.0291	
Aegean	$^{20}Ne/^{22}Ne$	10.040	40	9.78	Shimizu et al. (2005); Smith and Kennedy (1985)
	$^{21}Ne/^{20}Ne$	0.0312	40	0.0288	
Valles Caldera, USA	$^{20}Ne/^{22}Ne$	10.07	4	9.97	Smith and Kennedy (1985)
	$^{21}Ne/^{20}Ne$	0.0311	4	0.0300	
Cameroon Line	$^{20}Ne/^{22}Ne$	10.75	11	10.18	Aka et al. (2004); Barfod et al. (1999)
	$^{21}Ne/^{20}Ne$	0.0354	11	0.0313	
Eifel Volcanic Field, Germany	$^{20}Ne/^{22}Ne$	11.21	6	10.133	Aeschbach-Hertig et al. (1996)
	$^{21}Ne/^{20}Ne$	0.0487	6	0.0330	

degassing. In H_2O rich magmas, all noble gases are strongly partitioned into the vapor phase. In contrast, CO_2 rich magmas are able to retain helium longer because CO_2 has to first be released from the melt (Nuccio and Paonita 2001). Application of this model to Vulcano

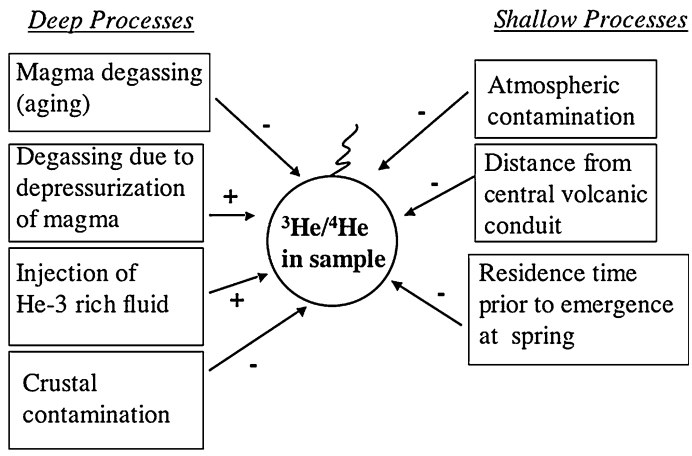

Fig. 28 Schematic depiction of processes that can affect $^{3}He/^{4}He$ ratios in gas and water samples. Plus (+) and minus (−) symbols indicate processes that increase or decrease the $^{3}He/^{4}He$ ratio in the sample, respectively

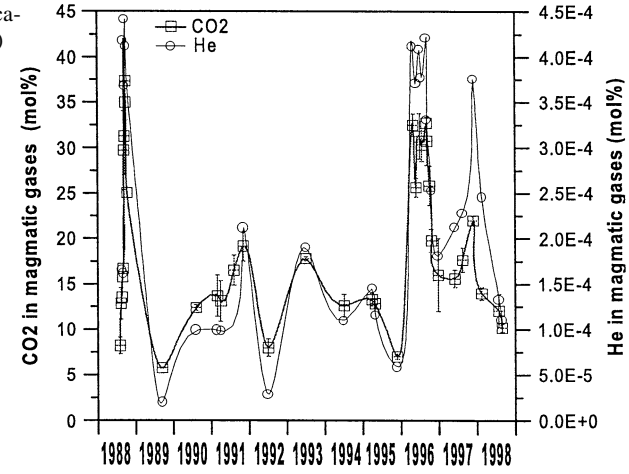

Fig. 29 CO_2 and helium concentrations in volcanic gases of Vulcano (Nuccio and Paonita 2001)

fumarole gases from 1988 to 1998 (Fig. 29) shows that CO_2 and He show clear co-variation and that spikes in CO_2 and He contents of the gas phase represent discrete events of magma degassing caused by depressurization. The peak maximum amplitudes also decrease from 1988 to 1995, which is interpreted to be progressive degassing of a small magma body that has exhausted its less soluble gas species. The significant peak in 1996 likely represents input of new, less degassed magma into the system, followed by a new series of degassing events through 1997. Depressurization rather than crystallization is thought to be the main control on the observed degassing sequence (Nuccio and Paonita 2001). Variations in $^{3}He/^{4}He$ at Vulcano were identified in earlier work by Tedesco and Scarsi (1999) who link He isotope changes to pressure variations in a deep gas reservoir (Fig. 30) and to mixing of deep magmatic fluids with a shallow reservoir (Tedesco 1995). Helium-3 rich magmatic fluids originate from a deep gas reservoir or accumulation chamber and continuously mix with surficial fluids (low $^{3}He/^{4}He$). The oscillations in $^{3}He/^{4}He$ do not correlate with parameters such as temperature or

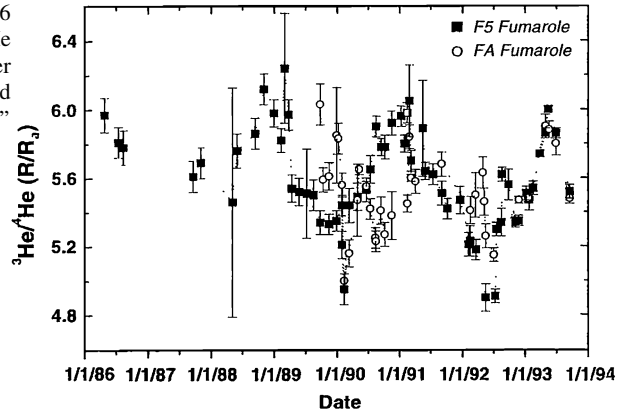

Fig. 30 $^3He/^4He$ variations at Vulcano from 1986 to 1994 (Tedesco and Scarsi 1999). The $^3He/^4He$ ratio oscillations do not correlate with other parameters, such as temperature or seismicity, and are interpreted as reflecting the "normal quiescent" life of the volcano

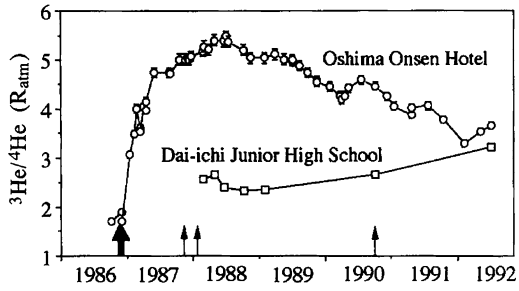

Fig. 31 Correlations of $^3He/^4He$ with eruption cycles in a 92–95 °C steam well (Oshima Onsen Hotel) on the flanks of Izu-Oshima volcano, Japan. (Sano et al. 1995)

seismicity and are interpreted as reflecting the "normal quiescent" life of the volcano (Tedesco and Scarsi 1999).

Clear correlations between $^3He/^4He$ and cycles of eruption were recognized in a 92–95 °C steam well on the flanks of Izu-Oshima volcano, Japan by Sano et al. (1995) (Fig. 31). At Izu–Oshima, small eruptions occurred in November 1987 after a year of quiescence. Prior to the eruptions, the $^3He/^4He$ ratio measured in gases from the well was ~1.8 Ra but shortly after the eruption (within several months) the ratio had increased to ~4 Ra and subsequently peaked at ~5.5 Ra about 18 months after the eruption. The $^3He/^4He$ ratio then gradually declined over the next 4 years to ~4 Ra. The variations in $^3He/^4He$ correlate with $\delta^{13}C$, and the overall trend is interpreted as an increase in the magmatic gas contribution to the system by the eruption with CO_2 acting as a carrier for mantle helium. The subsequent gradual decrease in $^3He/^4He$ results from a combination of depletion of the magmatic gas emission and mixing with crustal helium in the hydrothermal system (Sano et al. 1995).

The $^3He/^4He$ ratios of crater fumaroles at Galeras volcano, Colombia, have also been observed to vary systematically with volcanic activity. Galeras reactivated in 1988 (Williams et al. 1990) and crater fumarole $^3He/^4He$ ratios increased from 5.5 Ra in December 1989 to 7.9 Ra in August 1990, reaching a maximum of 8.84 Ra in May 1992 (Sano et al. 1997). During the time of maximum $^3He/^4He$ ratio, the He content of fumarole gases also increased (Fischer et al. 1997). This suggests that during increased eruptive activity, mantle-derived high $^3He/^4He$ gases entered the magmatic system at Galeras.

Magma degassing can fractionate helium isotopes. During bubble growth, lighter ^3He will diffuse at a higher rate than ^4He and isotopes can be fractionated kinetically. The residual melts will become depleted in ^3He relative to ^4He (Caracausi et al. 2003; Nuccio and Valenza 1998). The fractionation can be modeled as a Rayleigh process:

$$R/R_0 = F^{(k-1)}$$

Where R is the $^3He/^4He$ ratio of the melt, R_0 is the ratio in the melt before degassing, F is the residual fraction of helium after a degassing event, and k is the kinetic fractionation factor ($k = [4/3]^{1/2}$). The above equation predicts that the $^3He/^4He$ ratio will decrease in the melt due to

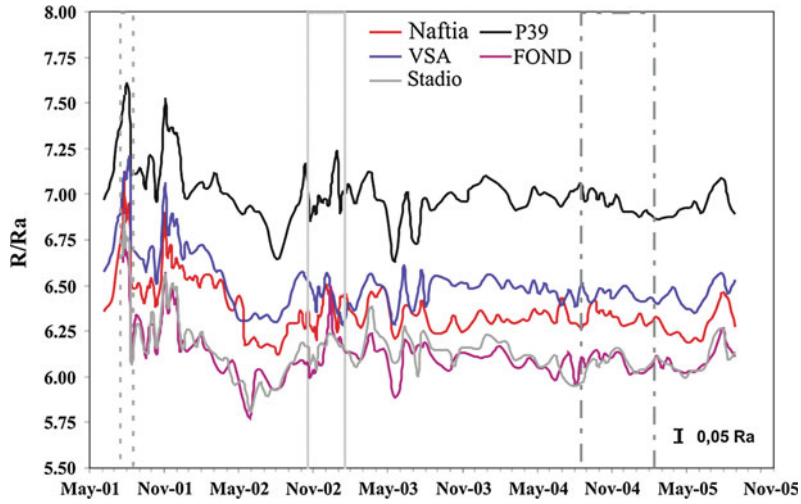

Fig. 32 $^{3}He/^{4}He$ variations of gas emissions observed at five different sites on the periphery of Mt. Etna. Vertical lines indicate eruptive episodes (Rizzo et al. 2006)

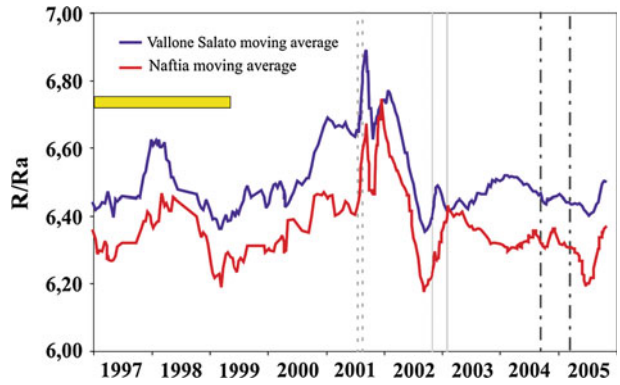

Fig. 33 Time-averaged $^{3}He/^{4}He$ ratios at two sites on Etna Volcano. *Vertical lines* indicate eruptive episodes. Increases and decreases in $^{3}He/^{4}He$ are interpreted as the result of magma degassing due to depressurization and gas exsolution. *Yellow bar* indicates a seismic crisis (Rizzo et al. 2006)

degassing alone; degassing fractionation is interpreted as the key process producing the temporal $^{3}He/^{4}He$ variations observed at Etna Volcano from May 2001 to November 2005 (Rizzo et al. 2006). Figure 32 shows the $^{3}He/^{4}He$ variations of gas emissions observed at five different sites on the periphery of Etna. Decreasing $^{3}He/^{4}He$ ratios are interpreted as the result of progressive magma degassing driven by magma ascent and depressurization. Periods of high $^{3}He/^{4}He$ ratios record either discharge of bubbles that have been kinetically enriched in ^{3}He or the degassing of new inputs of volatile rich magma originating from deeper levels in the plumbing system (Rizzo et al. 2006).

What is particularly interesting about this data set is that all sites record the same increases and decreases in $^{3}He/^{4}He$ which implies the involvement of an extensive, connected magmatic system. Extension of the $^{3}He/^{4}He$ record back to 1997 using data from Caracausi et al. (2003) (Fig. 33) clearly shows that $^{3}He/^{4}He$ changes at both sampling sites synchronously. The high $^{3}He/^{4}He$ ratios in 1997 and the first few months of 1999 suggest a recharge of new volatile-rich magma which then progressively

degassed. The initial increase occurred during a period of explosive and effusive activity at Etna, most probably fuelled by the new, undegassed magma. He isotope ratios increase once more early in 2000 reaching a maximum in August 2001, consistent with a new, massive recharge of the magmatic system; this once more is followed by rapid degassing to the end of 2002. Figure 33 shows that the 2001 and 2002–2003 eruptions occurred during deep recharge and degassing events, whereas the 2004 and 2005 eruptions seem to have lacked any volatile-bearing deep magma recharge event. This is consistent with the observation that the 2004/2005 eruptions were likely caused by failure of the upper parts of the volcanic edifice, rather than a magmatic recharge event (Rizzo et al. 2006). Therefore, as the case of Etna shows, $^{3}He/^{4}He$ ratios can be used as an indicator of magmatic activity. These results are also consistent with conclusions drawn from the geochemistry of the major gases (Caracausi et al. 2003).

5.2 Crustal Contamination

Helium isotopes discharging from volcanic crater fumaroles are also significantly affected by crustal contamination or by influx of fluids that have interacted with crustal reservoirs (i.e. Hilton et al. 1993). Such processes occur on the time-scales of fumarole sampling campaigns and are therefore more likely to be observed. Poas volcano, Costa Rica appears show evidence of such crustal contamination processes during the 10 years of observations. Similar to the above examples, the Poas data set shows systematic changes in $^{3}He/^{4}He$ ratios. Several hydromagmatic eruptions occurred during the sampling period (from 2001 to 2009) and $^{3}He/^{4}He$ ratios vary from ~6.5 to 7.5 Ra, which likely reflect changes in the degree of crust–mantle interaction of the magmatic system. It is an open question whether the hydromagmatic eruptions that occurred during and after 2005 are the result of increased crustal interaction with mantle-derived melts during the sampling interval (Hilton et al. 2010).

5.3 Significance of Baseline Data

At Campi Flegrei Caldera, Italy, $^{3}He/^{4}He$ ratios were systematically measured between 1983 and 1988, but the results obtained from the hottest fumaroles do not show evidence of increasing $^{3}He/^{4}He$ during the 1982–1984 seismic crisis. However, Tedesco et al. (1990) argue that it is possible that the underlying magma chamber in fact has a low $^{3}He/^{4}He$ ratio of 3.2 Ra due to deep crustal contamination. In that case the constant and low $^{3}He/^{4}He$ of Campi Flegrei hydrothermal fluids cannot be taken as indicators for a non-magmatic origin of the seismic events during the crisis. This example shows that it is critical to understand the background $^{3}He/^{4}He$ ratio variations as well as the magmatic end-member compositions in order correctly interpret the helium isotope variations in the context of volcanic activity. This is particularly evident at Unzen volcano where Marty et al. (1989) measured 5.8 Ra in hot spring gases in 1983; an eruption occurred in 1990 and the $^{3}He/^{4}He$ ratio of the same spring increased to 6.7 Ra but then remained stable (between 6.5 and 7.1 Ra) over the next 10 years (Notsu et al. 2001). Without knowledge of the $^{3}He/^{4}He$ ratio prior to the volcanic activity at Unzen, the stable (yet relatively high) post-eruption values could not have been correctly interpreted. Another example of critical pre-activity data is Long Valley Caldera, USA. Between 1986 and 1988, Hilton (1996) measured $^{3}He/^{4}He$ ratios between ~4 and 6 Ra (depending on location) of various springs in the caldera. A few months after a seismic swarm in 1989, one location, the Mammoth Mountain Fumarole, increased from ~3.5 to 5.5 Ra, and $^{3}He/^{4}He$ continued to increase at this fumarole to almost 7 Ra by mid-1990 (Sorey et al. 1993, 1998). At at Mammoth Mountain, Sorey et al. (1998) were able to interpret the rise in $^{3}He/^{4}He$ as the result of a pulse of new gas from a high pressure reservoir following this earthquake swarm and the Landers earthquake *because* they knew before hand that there were other fumaroles in the area that

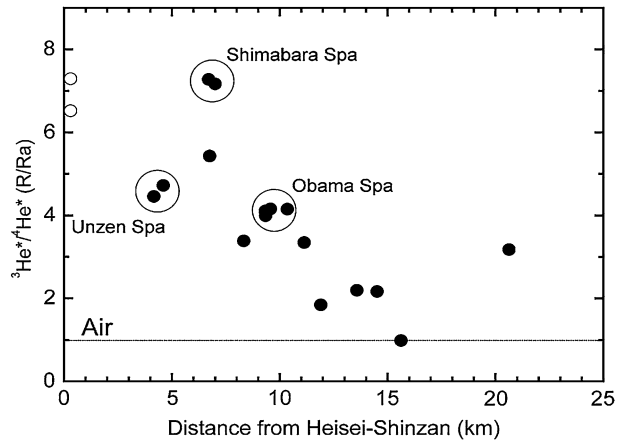

Fig. 34 $^3He/^4He$ ratios versus distance from the central volcanic vent (Heisei-Shinzan, Japan). Shimabara Spa samples have the highest ratios and lie off the correlation line. This is due to sampling of waters with significantly lower residence times by Shamabra hot spring (Morikawa et al. 2008)

had high (~6 Ra) He isotope compositions. During normal (non seismic) activity the high pressure gas reservoir is capped by a low permeability seal which was ruptured during the earthquake swarm, releasing high helium-3 gas.

5.4 Observations in Emissions From Peripheral Locations

Real-time supply of peripheral emissions by magmatic degassing was recognized by Nuccio et al. (2008) at Etna. The $^3He/^4He$ ratios of gases discharging from peripheral locations mirrored the decrease in $^3He/^4He$ trapped in olivines that erupted in 2001 and in 2004–2005. This observation implies that helium isotopes monitor magmatic degassing variations even when samples are collected from springs on the flanks of volcanoes. Morikawa et al. (2008) intensively sampled noble gases in ground-waters around Unzen volcano and related the observed $^3He/^4He$ ratios in different hot spring gases to variations in water residence times. As residence times increase, the ^4He content of the waters increase and the $^3He/^4He$ ratios decrease. Knowledge of water residence times, allowed Morikawa et al. (2008) to determine that the magmatic ^3He flux varied from location to location by a factor of 4. Figure 34 shows that, although there is a general increase of $^3He/^4He$ with decreasing distance to the central magmatic source (Heisei-Shinzan, the conduit for the 1990–1995 eruption), Shimabara Spring lies off this trend. Morikawa et al. (2008) model the residence time of discharges at each spring using the local reservoir rock parameters (U, Th concentrations) and $^3He/^4He$ systematics of the samples, and show that the residence time at Shimabara spring is significantly less than that of Obama and Unzen springs. Therefore, even though Unzen spring is closest to the volcano, slow passage through crustal rocks has resulted in a more significant addition of radiogenic helium-4 at Unzen spring compared to Shimabara spring. This behavior contrasts with many volcanoes where $^3He/^4He$ decreases systematically with distance from the central magmatic conduit as first shown by Sano et al. (1984) with the hydrodynamic dispersion model outlined in the previous section.

Saar et al. (2005) developed a model approach using all noble gases in peripheral hot and cold springs in the Cascades, USA. This procedure allowed them to detect and quantify atmospheric helium contributions that mask crustal and magmatic signals. This approach is useful if samples are extremely air contaminated ($^3He/^4He$ close to 1), but, as shown by Saar et al. (2005) the commonly used He/Ne correction method (Hilton 1996), results in corrected $^3He/^4He$ ratios that agree with the multiple noble

gas technique at better than 10 %. In summary, when evaluating which peripheral springs are most promising for monitoring magmatic activity, distance as well as residence time play important roles and care must be taken to account for atmospheric components.

The following section discusses applications of other noble gases for investigating processes occurring in volcanic and hydrothermal systems.

6 Neon, Argon, Krypton and Xenon Isotope and Abundance Variations in Hydrothermal Systems

In contrast to the data base of helium isotopes in hydrothermal systems, there are still relatively few argon and neon isotopes analyses published to date. Xenon and krypton isotopes in hydrothermal systems are generally dominated by atmospheric components but there are several results that show a mantle-derived contribution, in particular from CO_2 rich wells, which are discussed elsewhere in this volume (see Chap. 8). Since both neon and argon have low concentrations in hydrothermal fluids relative to their concentrations in air, all samples measured to date show various degrees of atmospheric contamination. Therefore, as an application to investigate the mantle or crustal sources of gases in hydrothermal systems, most significance should be given to the highest observed ratios.

6.1 Neon Isotopes

The neon abundance in air is 18.2 ppm, the $^{20}Ne/^{22}Ne_{air} = 9.8 \pm 0.08$, $^{21}Ne/^{22}Ne_{air} = 0.029 \pm 0.0003$. Neon-21 is nucleogenic produced in the reaction $^{18}O(\alpha, n)^{21}Ne$ and $^{24}Mg(\alpha,n)$ (Ozima and Podosek 2002). Like helium, neon is a powerful tracer of heterogeneities in the Earth's mantle. The mantle is characterized by higher $^{20}Ne/^{22}Ne$ and $^{21}Ne/^{22}Ne$ ratios compared to the atmosphere (Honda et al. 1987; Ozima and Zashu 1983; Sarda et al. 1988). Ocean island basalt (OIB) magmas have lower $^{21}Ne/^{22}Ne$ for a given $^{20}Ne/^{22}Ne$ ratio, representing a lower nucleogenic to primordial neon ratio compared to MORB. The global data base to 2002 of neon isotope systematics of MORB and OIB glasses has been reviewed by Graham (2002); see also Chap. 12 of this volume.

Neon isotope systematics of hydrothermal fluids from plumes (Yellowstone and Iceland) (Furi et al. 2010; Hearn et al. 1990) and Arcs (Japan, Aeolian Arc, the Aegean and Central America) (Kennedy et al. 1991; Nagao et al. 1981; Nakai et al. 1997; Shimizu et al. 2005; Sumino et al. 2004; Tedesco and Nagao 1996; Tedesco et al. 1998) are shown in Fig. 35a and b. Table 6 summarizes the neon isotope systematics. Most samples contain a significant air component or are fractionated to high $^{20}Ne/^{21}Ne$ values along the mass fractionation line (MFL). There is no systematic distinction between plume related gases as represented by Yellowstone and Iceland and samples collected from arc related hydrothermal systems. Most samples can be interpreted as the result of mixing between a MORB-type mantle endmember and air. There are, however, two locations (Vesuvius and Vulcano (Tedesco and Nagao 1996; Tedesco et al. 1998)) in the Aeolian arc that extend to extremely high $^{21}Ne/^{20}Ne$ values and fall on the crustal-neon trend of Kennedy, Hiyagon and Reynolds (1990), implying significant crustal contributions. Most notably in the data set of hydrothermal fluids are the samples from Etna (Nakai et al. 1997), geothermal well samples from Valles Caldera, New Mexico (Smith and Kennedy 1985) and samples of CO_2 rich wells from Sao Tome, Cameroon line (Barfod et al. 1999). These three data sets, but especially the samples from Etna and Sao Tome extend to extremely high $^{20}Ne/^{21}Ne$ and $^{21}Ne/^{20}Ne$ ratios and fall precisely on the MORB trend of Sarda et al. (1988). Using helium and radiogenic isotopes in combination with the neon data, Nakai et al. (1997) interpreted the results to represent a recent mixing event of the depleted upper mantle (MORB) with fluids enriched in incompatible elements and radiogenic ^{4}He. The Cameroon Line samples in combination with noble

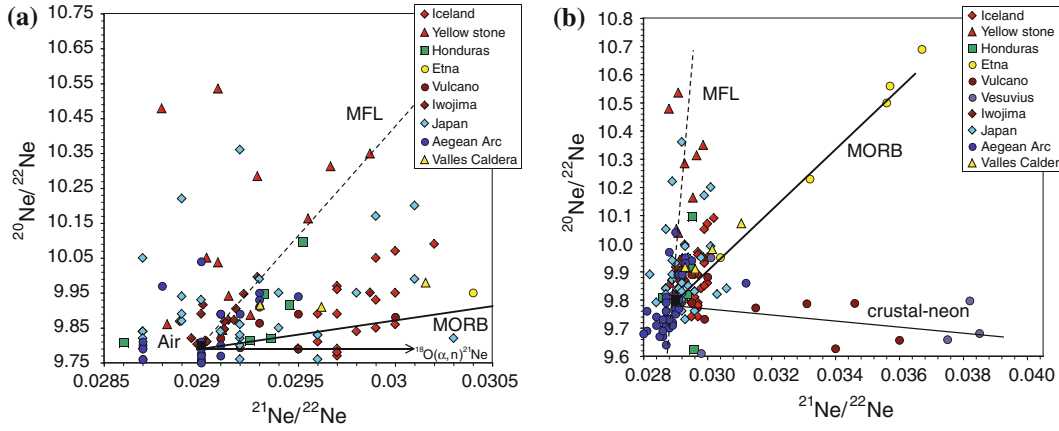

Fig. 35 **a** and **b**: Neon isotope systematics of hydrothermal fluids from plume-affected regions (Yellowstone and Iceland) (Furi et al. 2010; Hearn et al. 1990) and volcanic arcs (Japan, Aeolian Arc, the Aegean and Central America) (Kennedy et al. 1991; Nagao et al. 1981; Nakai et al. 1997; Shimizu et al. 2005; Sumino et al. 2004; Tedesco and Nagao 1996; Tedesco et al. 1998). The mass fractionation line (MFL), MORB and crustal neon trends are shown

gas data from xenoliths of the same region are interpreted by Barfod et al. (1999) to represent a HIMU mantle component. Valles Caldera is located in the Rio Grande Rift of the Continental USA and discharging gases have an upper mantle helium component ($^3He/^4He$ ratios up to 4.8 Ra (Smith and Kennedy 1985)), consistent with mantle (MORB) neon isotope signatures. Samples from another continental rift (the Eifel Volcanic Field, Germany), also show relatively high $^{20}Ne/^{22}Ne$ and $^{21}Ne/^{20}Ne$ ratios extending along the MORB trend to 10.19 and 0.034, respectively (even higher values of 11.21 and 0.0487 are not shown in the Figure) (Aeschbach-Hertig et al. 1996). In summary, neon isotopes have great potential as tracers for contributions from mantle derived fluid sources that can complement helium isotopes. From the data to date, it emerges that gas samples collected from continental rift regions show the highest $^{20}Ne/^{22}Ne$ and $^{21}Ne/^{20}Ne$ ratios and these fall on the MORB trend. This is consistent with the idea that neon (and other volatiles) primarily originate from the upper mantle in these tectonic settings. Most samples from arcs and plume localities fall on or close to the mass fractionation line, however, samples that have the least atmospheric contamination fall on the MORB trend. More data of high quality, low air contamination samples are needed to fully explore the neon characteristics of hydrothermal fluids and to better distinguish upper versus lower mantle (plume) sources.

6.2 Argon Isotopes

The argon abundance in air is 0.934 % with a $^{40}Ar/^{36}Ar$ ratio of 295.5 ± 0.5 and ^{40}Ar is a decay product of ^{40}K (Ozima and Podosek 2002). Hydrothermal fluids are dominated by air-like argon isotopic compositions as shown early on by Mazor and Wasserburg (1965) for samples collected in Yellowstone National Park, USA. The large majority of gas samples from hydrothermal and volcanic systems have $^{40}Ar/^{36}Ar$ ratios that are close to the air value (296). Table 7 summarizes argon isotope systematics of volcanic and hydrothermal fluids globally. Figure 36 shows that a number of samples have $^{40}Ar/^{36}Ar$ values significantly higher than air. As for neon, samples from Etna are enriched in the radiogenic component (^{40}Ar) reaching values up to 1788 (Nakai et al. 1997). The highest values for Vulcano are up to 2082 (Magro and Pennisi 1991; Tedesco and Nagao 1996). For continental rift localities, samples collected from wells in the Eifel reach a $^{40}Ar/^{36}Ar$ ratio of 1060 (Aeschbach-Hertig et al.

Table 7 Argon isotopes of hydrothermal fluids

Location		Maximum	N	Average	References
Iceland	$^{40}Ar/^{36}Ar$				
	$^{38}Ar/^{36}Ar$				
Yellowstone, USA	$^{40}Ar/^{36}Ar$	309.91	25	299.70	Hearn et al. (1990)
	$^{38}Ar/^{36}Ar$	0.1892	12	0.1892	
Central Am.	$^{40}Ar/^{36}Ar$	309.44	11	300.25	Kennedy et al. (1991)
	$^{38}Ar/^{36}Ar$	0.1888	11		
Lesser Antilles	$^{40}Ar/^{36}Ar$	434.82	65	301.08	Pedroni et al. (1999)
	$^{38}Ar/^{36}Ar$	0.1925	65	0.18940	
Etna, Italy	$^{40}Ar/^{36}Ar$	1788	5	1234.70	Nakai et al. (1997)
	$^{38}Ar/^{36}Ar$	0.1927	5	0.1898	
Vulcano, Italy	$^{40}Ar/^{36}Ar$	2082	85	514.01	Magro and Pennisi (1991); Tedesco and Nagao (1996)
	$^{38}Ar/^{36}Ar$	0.1879	15	0.1824	
Vesuvius, Italy	$^{40}Ar/^{36}Ar$	300.47	11	297.72	Tedesco et al. (1998)
	$^{38}Ar/^{36}Ar$	0.1888	11	0.1873	
Japan (volcanoes, springs)	$^{40}Ar/^{36}Ar$	325.00	38	303.86	Nagao et al. (1981)
	$^{38}Ar/^{36}Ar$	n.a.	0	n.a.	
Iwojima, Japan	$^{40}Ar/^{36}Ar$	315	15	297.50	Sumino et al. (2004)
	$^{38}Ar/^{36}Ar$	0.1898	15	0.1871	
Aegean	$^{40}Ar/^{36}Ar$	311.3	40	300.52	Shimizu et al. (2005)
	$^{38}Ar/^{36}Ar$	0.1882	40	0.1877	
Kuriles	$^{40}Ar/^{36}Ar$	302.0	2	300.0	Sano et al. (2001)
	$^{38}Ar/^{36}Ar$	n.a.	0	n.a.	
Indonsesia	$^{40}Ar/^{36}Ar$	309.0	6	300.5	Sano et al. (2001)
	$^{38}Ar/^{36}Ar$	n.a.	0	n.a.	
N. Andes	$^{40}Ar/^{36}Ar$	314.0	2	307.0	Sano et al. (2001)
	$^{38}Ar/^{36}Ar$	n.a.	0	n.a.	
Mexico	$^{40}Ar/^{36}Ar$	334.0	6	303.3	Sano et al. (2001); Taran et al. (2002)
	$^{38}Ar/^{36}Ar$	n.a.	0	n.a.	
Valles Caldera, USA	$^{40}Ar/^{36}Ar$	665.70	4	506.00	Smith and Kennedy (1985)
	$^{38}Ar/^{36}Ar$	0.1871	4	0.1867	
Oldoinyo Lengai, East Africa	$^{40}Ar/^{36}Ar$	947.8	3	518.56	Fischer et al. (2009)
	$^{38}Ar/^{36}Ar$	n.a.	0	n.a.	
Cameroon Line	$^{40}Ar/^{36}Ar$	1648	9	656.1	Aka et al. (2004); Barfod et al. (1999)
	$^{38}Ar/^{36}Ar$	0.1880	5	0.1875	
New Zealand	$^{40}Ar/^{36}Ar$	401	50	317.11	Hulston and Lupton (1996); Torgersen et al. (1982)
	$^{38}Ar/^{36}Ar$	n.a.	0	n.a.	
Eger Rift, Europe	$^{40}Ar/^{36}Ar$	551	4	367.9	Braeuer et al. (2004)
	$^{38}Ar/^{36}Ar$	n.a.	0	n.a.	
Eifel Volcanic Field, Germany	$^{40}Ar/^{36}Ar$	1060	2	725.5	Aeschbach-Hertig et al. (1996)
	$^{38}Ar/^{36}Ar$	n.a.	0	n.a.	

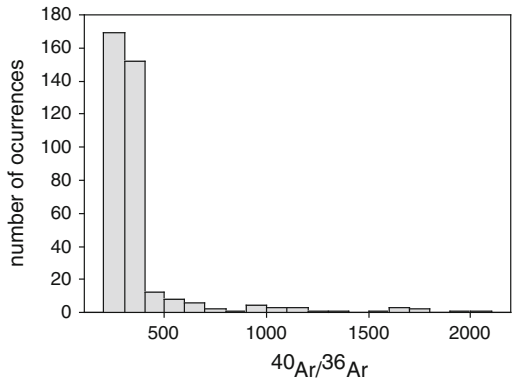

Fig. 36 Variations in $^{40}Ar/^{36}Ar$ values of volcanic and hydrothermal samples. The large majority of samples cluster around the air value of 295

1996). Volcanic fumarole samples from Oldoinyo Lengai carbonatite in the East Africa Rift have values up to 950 (Fischer et al. 2009) and samples from a CO_2 well in Sao Tome (Cameroon Line) reach values up to 1650 (Barfod et al. 1999). With the exception of Etna and Vulcano, $^{40}Ar/^{36}Ar$ ratios of arc volcanoes are dominated by the atmospheric component whereas rift-related gases show the most elevated ratios.

Figure 37a and b show the relationship between $^{40}Ar/^{36}Ar$ and $^{38}Ar/^{36}Ar$. The mass fractionation line (MFL) through the atmospheric component is determined assuming a Rayleigh fractionation process (Ozima and Podosek 2002). Samples that have values lower than the atmospheric values are enriched in the lighter isotope and can be assumed to result from fractionation of the atmospheric value. Enrichment of samples in the radiogenic component (^{40}Ar) is either due to mixing with mantle-derived or crustal ^{40}Ar. The mantle as sampled by MORB has a $^{40}Ar/^{36}Ar$ value of approximately 35,000 (Burnard et al. 1997). Crustal production of ^{40}Ar is dominated by the decay of ^{40}K and the ^{40}Ar content of the crust is directly proportional to the K concentration. ^{36}Ar production in the crust is small compared to the atmospheric background and the $^{40}Ar/^{36}Ar$ production ratio in the crust is 1.57×10^7 (Ballentine and Burnard 2002). Gas samples from Etna and Valles Caldera that plot along the MORB trend in the neon isotope plot also show the highest $^{40}Ar/^{36}Ar$ ratios, suggesting that the upper mantle is a significant contributor of these noble gases to the discharges. Samples from Vulcano, on the other hand, that show crustal neon systematics, are likely to also have crustal Ar, resulting in $^{40}Ar/^{36}Ar$ ratios up to 1100 (Fig. 37) and 2082 (Magro and Pennisi 1991).

6.3 Krypton and Xenon Isotopes

Krypton and Xenon isotopes in hydrothermal and volcanic gases are dominated by the air component. A small anomaly (δ values of 2–3 ‰) in $^{129}Xe/^{130}Xe$ and $^{136}Xe/^{130}Xe$ has been reported for samples in the vicinity of Etna (Mofete dei Palici) by Nakai et al. (1997) and has been interpreted to point towards a MORB anomaly. Further work of Kr and Xe isotopes in pristine and uncontaminated gases is needed to investigate whether there are any significant mantle anomalies. Observed ^{129}Xe excesses relative to air in CO_2-rich well gases and their implications for deep earth and atmospheric formation processes are discussed in another chapter (See Chap. 8 of this volume).

6.4 Patterns of Relative Noble Gas Abundances

Patterns of relative noble gas abundances are generally reported in the F_m notation where $F_m = (^mX/^{36}Ar)/(^mX/^{36}Ar)atm$ and where ^mX represents the noble gas X of mass m. Figure 38 shows the average F values for noble gases collected from hot springs and fumaroles at Yellowstone (Hearn et al. 1990), Japan (Nagao et al. 1981), Vulcano (Tedesco and Nagao 1996), Honduras (Kennedy et al. 1991), Valles Caldera (Smith and Kennedy 1985) and El Chichon Volcano (Taran et al. 1998). The data clearly show that ^4He is significantly enriched in these samples relative to air, consistent with the observation that helium provides the strongest non-atmospheric (mantle or crusalt) signals of all noble gases. Kypton-84 and Xe-132 are slightly enriched relative to air and Ne-22 is depleted. Kennedy et al. (1988) explained the physical processes of noble

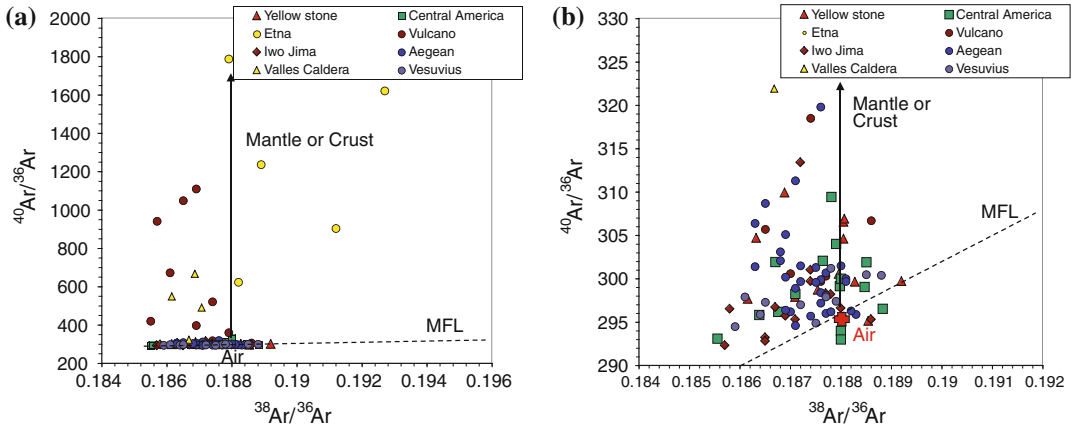

Fig. 37 **a** and **b**: $^{40}Ar/^{36}Ar$ and $^{38}Ar/^{36}Ar$ systematics of volcanic and hydrothermal samples

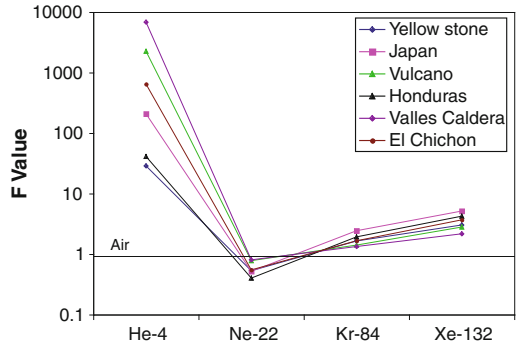

Fig. 38 F-values for noble gas abundances in geothermal systems of various regions. Each line represents the average composition of numerous samples collected

gas abundance patterns in thermal springs. They show that water samples (containing dissolved noble gases) represent a two-component mixture. One component is the surface water of the spring in contact with air. The other component, which is depleted in Ne and enriched in Kr and Xe may be the residuum of a Rayleigh type distillation process that results in a loss of the dissolved gas. In the case of gas samples collected at bubbling springs, the mixing process is more complicated. One component is the gas phase that enters a thermal pool, another component is the gas that is already dissolved in the pool water. Depending on the partial pressure of the gas bubble entering the pool at depth, it will equilibrate with the gas dissolved in the pool water or strip gases out of the water phase into the gas bubble as it rises to the surface. If a gas bubble has to traverse a large distance until it is sampled at the surface (deep pool) then the initial composition of the gas entering the pool is severely modified by gas dissolved in the pool. On the other hand, if a gas bubble only traverses a short distance until it is sampled (a few centimeters) then the sampled gas closely represents the gas entering the pool. The detailed work of Kennedy et al. (1988) therefore implies that variations in noble gas abundance patterns are dependant on sampling strategy and pool morphology rather than processes that occur deeper in the hydrothermal system.

Figure 38 shows that all samples compiled here which include gas and water samples from both fumaroles and bubbling springs have similar noble gas abundance patterns. This observation implies that mixing of air from the surface with a residuum of a Reyleigh distillation process in the water phase either at the surface in the pool or at depth in the hydrothermal system results in the noble gas abundance patterns. As discussed above, Ne, Kr and Xe may have a small but detectable non-atmospheric component.

7 Application of Noble Gases to Evaluate Crustal Contamination Effects on Hydrothermal and Volcanic CO_2, CH_4 and N_2 Discharges

Helium isotope variations are an excellent tracer for crustal contamination of volcanic and hydrothermal gas samples. The average middle crustal $^3He/^4He$ ratio is 0.003 Ra and the average upper crustal $^3He/^4He$ ratio is 0.001 Ra (see review of crustal noble gases in (Ballentine and Burnard 2002) and this volume). The average $^3He/^4He$ ratio of gases released from subduction zone volcanoes and hydrothermal system is 5.37 Ra with maximum ratios well within the MORB rage of 8 ± 1 Ra. The lowest $^3He/^4He$ ratios in subduction zone settings are recorded in locations where magmas traverse thick continental crust, i.e. the Andes have crustal thicknesses up to 70 km. However, low ratios are also recorded in locations with relatively thin crust, i.e. NE Japan (Hilton et al. 2002). When utilizing $^3He/^4He$ ratios to evaluate crustal contamination of gases it is critical to take into account the entire volcanic/hydrothermal setting within which the samples were collected. In particular, it has been recognized that the $^3He/^4He$ ratio in springs decreases systematically with distance from the magmatic source (Sano et al. 1984) and small scale variations have been discussed in a previous section.

7.1 Carbon Dioxide

In addition to evaluating the overall contribution of crustal He to volcanic and hydrothermal discharges, noble gases can be combined with major volatiles such as CO_2, N_2 and CH_4 to investigate their sources. The most widely used application in this respect is to trace the CO_2 contribution from the mantle and subducted sedimentary or carbonate carbon in volcanic arc settings. Figure 39 Giggenbach et al. show a triangular plot of CO_2–^3He–^4He of gases collected from springs and fumaroles in New Zealand volcanic and hydrothermal systems (Giggenbach et al. 1993). The advantage of triangular plots is that processes such as CO_2 removal or mixing of sources can be displayed in straight lines. Figure 39 shows the mantle $CO_2/^3He$ and $^3He/^4He$ ratio of 2×10^9 and 8 Ra, respectively (Marty and Jambon 1987). Crustal gases are assumed to have variable $CO_2/^3He$ ratios from 10^8 to 10^{14} (O'Nions and Oxburgh 1988). The distribution of data points in Fig. 39 shows that some samples with higher than mantle $CO_2/^3He$ ratios can be explained by mixing of mantle CO_2 with crustal CO_2. Such a process would also reduce the $^3He/^4He$ ratios towards crustal values which is the case for a number of samples, particularly ones that are CH_4 dominated. This is also consistent with the fact that CH_4 is predominantly derived from the crust. Higher than mantle $CO_2/^3He$ ratios coupled with crustal $^3He/^4He$ are in some situations the result of carbonates contributed from the crust, i.e. in the Lesser Antilles (van Soest et al. 1998). The CO_2 rich samples, with higher than mantle $CO_2/^3He$, on the other hand, extend to the CO_2 apex of the triangle at mantle $^3He/^4He$ ratios (8 ± 1 Ra). These samples represent processes of CO_2 addition that is not the result of crustal contamination but due to CO_2 contribution from subducted sediments or organic matter (Marty and Giggenbach 1990). In order to further characterize the relative contributions of subducted components, $CO_2/^3He$ is combined with $\delta^{13}C$ of CO_2 to calculate the relative contributions of mantle, subducted organic and carbonate CO_2 using mixing equations (Marty and Jambon 1987; Sano and Marty 1995). A similar approach is used for N_2 (Sano et al. 1998, 2001) and the current global data set has recently been reviewed in Hilton et al. (2002) for subduction zones and globally by Oppenheimer et al. (2012). These approaches generally aim to evaluate the deep C and N that traverses the mantle and crustally contaminated samples are filtered from the data set using a combination of noble gas systematics and gas chemistry (Clor et al. 2005; de Leeuw et al. 2007; Elkins et al. 2006; Ray et al. 2009; Shaw et al. 2003; Zimmer et al. 2004).

Solubility differences in CO_2 and He can result in high $CO_2/^3He$ ratios in springs and fumaroles as

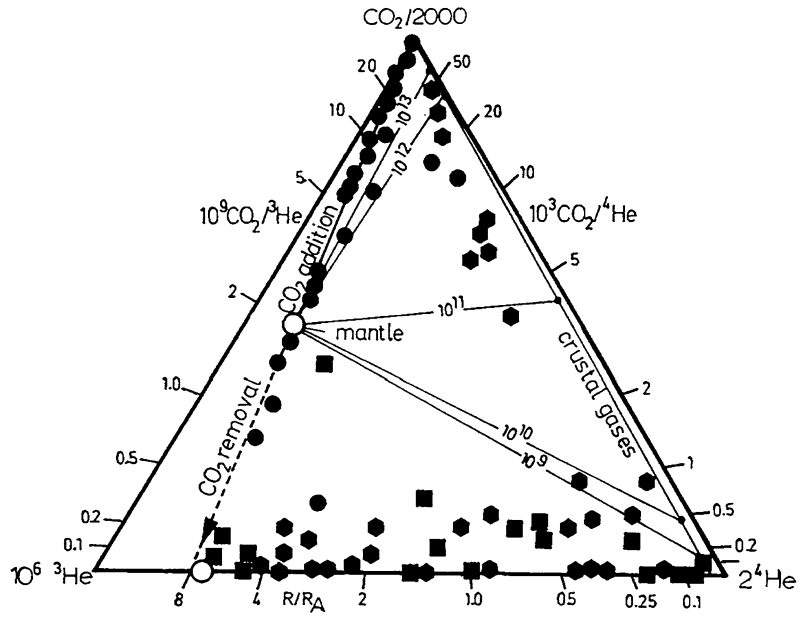

Fig. 39 CO_2–^3He–^4He triangular diagram from Giggenbach et al. (1993). The diagram shows data from volcanic and geothermal systems of New Zealand and magmatic, air, thermogenic and crustal components as well as the predominant gas in each sample

fluids migrate away from the magmatic source. In water up to 100 °C, CO_2 has a greater solubility than He by a factor of 42 (Stephen and Stephen 1963). Therefore He would preferentially partition into a free vapor phase during water degassing, potentially lowering the $CO_2/^3He$ ratio of the sampled gas phase. However because the bulk of the volatiles partition into the gas phase, the $CO_2/^3He$ ratios of the sampled gas phase is expected to approach that of the magmatic value, without significant fractionation. Sampling of a significantly degassed water phase that has been stripped of most of its volatiles would likely result in highly fractionated $CO_2/^3He$ ratios. This effect is clearly seen in water samples where helium content inversely correlates with $CO_2/^3He$ ratios (van Soest et al. 1998).

The samples that fall below the mantle $CO_2/^3He$ value in Fig. 39 are affected by shallow level CO_2 removal. The CO_2 removal process produces N_2 and CH_4-rich gases that may still have high $^3He/^4He$ ratios. The most likely process for CO_2 removal is the conversion to calcite:

$$CO_2 + \text{Ca-Al-silicate} + \text{K-feldspar} = \text{calcite} + \text{K - mica}$$

This reaction is temperature dependant and defines the upper limit of the CO_2 content of gases in equilibrium with crustal rock (Giggenbach 1984; Giggenbach et al. 1993). At high temperatures rising fluids do not react according to this reaction but as they cool to 350 °C and below they lose CO_2 due to conversion to calcite. The process of calcite precipitation has recently been used to explain low $CO_2/^3He$ ratios in Chilean hydrothermal springs where (Ray et al. 2009) showed that $\delta^{13}C$ values of discharging CO_2 positively correlate with water temperature, consistent with an effect due to calcite precipitation. As fluids cool and in the absence of boiling, the solution will remain in full equilibrium with the rock and continue to loose CO_2 to calcite (reaction 1) and to CH_4 according to reaction

$$CO_2 + 8(FeO) + 2H_2O = CH_4 + 8(FeO_{1.5})$$

Where (FeO) and ($FeO_{1.5}$) represent iron in its two oxidation states generally present in minerals of crustal rocks (Giggenbach 1987). The above reaction is very slow compared to the silicate-calcite reaction and only at temperatures below 170 °C does CH_4 become the dominant gas. Therefore, the time required for a CO_2-rich

magmatic gas to convert to a CH_4-rich gas by the above reaction is likely too long to preserve a mantle $^3He/^4He$ ratio (Giggenbach et al. 1993). As shown in Fig. 39, samples that are most affected by CO_2 removal are also CH_4 and N_2 dominated and have low $^3He/^4He$ ratios. A minority of samples, has $CO_2/^3He < 1 \times 10^9$ and mantle $^3He/^4He$ ratios and are still CO_2 dominated. These gases likely experienced only minor and rapid CO_2 loss according to the calcite precipitation reaction (above) and have not resided sufficiently long in the crust to record the addition of significant crustal helium.

A detailed application of CO_2–He systematics by Snyder et al. (2001) showed that $CO_2/^3He$ ratios in geothermal wells along the Central American volcanic front vary from 10.6×10^9 to 71.9×10^9, whereas the ratios are much more variable in springs located behind the volcanic front ranging from 2.55×10^9 to 617.2×10^9. Consistent with Shaw et al. (2003) who looked at the Costa Rican and Nicaraguan segment of the volcanic front, these ratios can be explained by three component mixing of mantle and subducted organic and carbonate carbon. Low $CO_2/^3He$ ratios (lower than volcanic front) may be due to the absence of a subducted carbon component in that region so that the CO_2 budget is dominated by the mantle value ($\sim 2 \times 10^9$). However, the majority of samples behind the volcanic front that has lower than arc $CO_2/^3He$ and also lower $^3He/^4He$ ratios implying that they are affected by CO_2-loss due to the reactions above. De Leeuw et al. (2007) provide a detailed investigation of volcanic front and back-arc gases from El Salvador and Honduras. These authors show that a majority of samples from behind the volcanic front have lower than MORB $^3He/^4He$ ratios and are affected by crustal contamination processes which also caused quite variable $CO_2/^3He$ ratios that extend above and below the volcanic front values.

These examples show that the behavior of ^3He can be quite independent of CO_2 which is often affected by secondary processes. The isotopic composition of He obviously provides a valuable and reliable indicator of its own origin but can be decoupled from the more reactive gases (Giggenbach et al. 1993). On a more global scale O'Nions and Oxburgh (1988) show the mixing relationships of mantle gases with crustal sources (Fig. 40). The crustal $CO_2/^3He$ component ranges widely and depends on factors such as accumulation time of radiogenic He, carbon content of the source material and timing/efficiency of He and C release into gas reservoirs and springs/fumaroles. Of significance in Fig. 40 is that CH_4-dominated samples from the Sacramento Basin can be explained by binary mixtures between mantle and crustal endmembers whereas CO_2-dominated samples from the Massif Central, Hungary or the Engadine do not follow binary mixing trends. As already noted above, $CO_2/^3He$ ratios from bicarbonate mineral springs are likely significantly fractionated by carbonate precipitation such that identification of a mantle and unique curstal component becomes challenging (O'Nions and Oxburgh 1988). In a recent paper Crossey et al. (2009) combine $^3He/^4He$ with CO_2 and stable isotopes systematics as well as water chemistry to decipher the relative contributions of mantle and crustal gases to spring discharges on the Colorado Plateau of the western USA. These authors show that on average approximately 8 % of the CO_2 is of astenosphric and/or mantle origin. The remainder is made up of contributions from shallow crustal carbonates (51 %), shallow organic carbon (14 %) and lithospheric or curstal carbon (29 %).

In summary, when evaluating the CO_2 sources in volcanic and hydrothermal systems, care should be taken to obtain a complete sample suite that includes fumaroles, gas rich bubbling springs and the water phase. The least crustally contaminated samples are expected from magmatic fumaroles and gas-rich bubbling springs close to the volcanic edifice. Gas-poor and water phase samples are likely compromised by degassing, calcite precipitation and crustal contamination processes. Care must also be taken when combining $^3He/^4He$ with other gas species because the noble gas is not affected by secondary processes. In order to most reliably trace

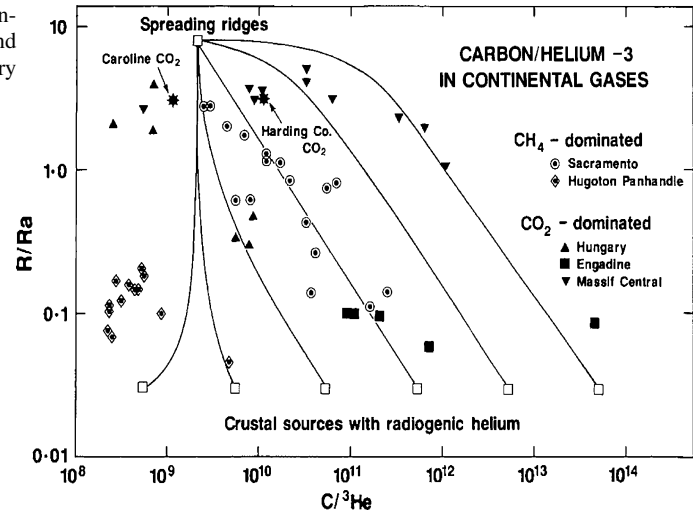

Fig. 40 $^{3}He/^{4}He$ (Ra) and $C/^{3}He$ relationships of continental gases (O'Nions and Oxburgh 1988). Crustal gas sources vary dramatically in $C/^{3}He$ ratio

gas sources, a combination of noble gas, and stable isotopes coupled with gas abundance ratios is likely to produce the best results.

7.2 Methane

Methane is a major component of hydrothermal gases and occurs in trace amounts in volcanic gases (i.e. Giggenbach 1996). The natural occurrence of CH_4 has received considerable attention because it may have played an important role in the evolution of life (Keosian 1960) and is a potent greenhouse gas (Raynoud et al. 1993). The release of CH_4 from sedimentary basins due to volcanic intrusions has recently been advocated as having potentially had a significant effect on past climate change (Ganino and Arndt 2010; Svensen et al. 2004). Four processes are generally responsible for CH_4 production in natural systems (see also Fiebig et al. (2004) and references therein): (1) biologic production by bacterial at temperatures <100 °C (e.g. Rice and Claypool 1981) (2) thermal decomposition of organic matter (thermogenic CH_4 (e.g. Schoell 1988) (3) outgassing of the mantle (e.g. Craig and Lupton 1981; Gold 1979) and (4) formation by Fischer–Tropsch type reactions:

$$CO_2 + 4H_2 = CH_4 + 2H_2O$$

(e.g. (Craig 1953) (Zolotov and Shock 2000)).

The concentration of CH_4 in hydrothermal fluids seems to be mainly controlled by the source output that is comprised of organic matter buried within sedimentary rocks. Thermal decomposition of organic matter in the upper crust produces hydrothermal gases with high CH_4 and extremely high N_2/Ar ratios. In contrast, subduction related volcanic gases have low CH_4 contents and high N_2/Ar due to the contribution of N_2 from subducted sediments (Taran and Giggenbach 2003). Noble gases, especially He isotopes, have been used extensively to further identify the sources of CH_4 in hydrothermal systems (Fiebig et al. 2004; Giggenbach et al. 1993; Jean-Baptiste et al. 1991; Poreda et al. 1988, 1992; Wakita and Sano 1983; Welhan and Craig 1983), in particular, with regard to the formation of CH_4 by Fischer–Tropsch-type reactions.

The Fischer–Tropsch reaction seems to occur at high-temperature mid-ocean ridges only where $\delta^{13}C_{CH4} > -20$ ‰ and low $CH_4/^{3}He$ between 1×10^6 and 6×10^8 are reported and CH_4/CO_2 ratios are consistent with those expected for chemical equilibrium at vent temperatures. Apart from mid-ocean ridges the conditions for this type of reaction do not appear to be met (see Fiebig et al. (2004) and references therein). MORB $CH_4/^{3}He$ ratios are $<80 \times 10^6$

(Charlou et al. 1998; Jean-Baptiste et al. 1991), whereas arc gases exceed the MORB ratios and reach values as high as 10^{12} (Giggenbach et al. 1993; Poreda et al. 1988). The high $CH_4/^3He$ ratios of arc gases imply that CH_4 in these environments is of thermogenic origin. Fiebig et al. (2004) showed in a study of hydrothermal fumarole gas discharges from Nisyros Volcano, Greece, that extraordinarily low $CH_4/^3He$ and $N_2/^3He$ ratios (lower or similar to MORB) imply absence of organic matter in the formation of CH_4. These authors advocate the formation of CH_4 from CO_2 by Fischer–Tropsch type reactions catalyzed by Fe-bearing mineral phases. Taran et al. (2010) showed that gases discharging from Socorro Island, located on the Mathematician Ridge in the Eastern Pacific have extremely high H_2 (20 mol %, in dry gas) and CH_4 (4 mol %, in dry gas) contents with C and He isotope and abundance characteristics indistinguishable from MORB fluids. The reduced conditions of the system favor H_2 generation and reduction of CO_2 to abiotic CH_4 within the high-temperature zone of the volcanic hydrothermal system. Similar to Nisyros, these fluids are characterized by low, MORB-like $CH_4/^3He$ and $CO_2/^3He$ ratios. Figure 41 shows a selected compilation of volcanic and hydrothermal gas discharges from New Zealand, Iceland and Central America. As can be seen in this figure, the New Zealand data set extends to extremely high and variable $CH_4/^3He$ ratios and a shift of data points to lower $^3He/^4He$ ratios indicates significant CH_4 contribution from crustal sources. Data points that cluster around 8 Ra, extending to high $CH_4/^3He$ ratios likely represent thermogenic CH_4 contributions. The low $CH_4/^3He$ ratios at plume-like or MORB-like $^3He/^4He$ ratios as sampled by Iceland and Central America gas discharges are probably the best candidates for containing abiogenic CH_4. Clearly further work on samples from such localities is needed to better constrain the ultimate origin and formation mechanisms of CH_4 in these systems.

7.3 Nitrogen

Nitrogen is a trace component in volcanic gases and originates from the atmosphere, subducted sediments, the mantle or crustal sources (i.e. Giggenbach 1996). As mentioned above, the N–He systematics of volcanic gas discharges from arcs has been reviewed in 2002 (Hilton et al. 2002) and here we focus on the crustal contribution of N to hydrothermal emissions. For example, Jenden et al. (1988) showed that natural gases from the Great Valley, California were composed of three major components: a sedimentary one with N_2/He ratios of 350 and crustal $^3He/^4He$ ratios, an igneous one with N_2/He of around 2000 and a mantle $^3He/^4He$ signature and an extremely N_2-rich gas with N_2/He of >22,000 and a crustal $^3He/^4He$ ratio. This crustal component is thought to have formed through metamorphism of sedimentary rocks deep within the crust. Importantly, the metasedimentary crustal component has N_2/He ratios that are significantly higher than what is found in arc gases (1,000–10,000) where most of the N is of subducted origin (e.g. Sano et al. 2001; Fischer et al. 1998, 2002). In addition to the helium isotope signature, which is expected to be crustal, nitrogen in such metasedimentary gases has a $\delta^{15}N$ signature that is enriched in ^{15}N. For example Mariner et al. (2003) measured gases from hot springs in the Cascades with $\delta^{15}N$ values up to 5.3 ‰ and suggested that they originate from organic-bearing units deposited below Tertiary lava flows. Although only $^3He/^4He$ ratios are reported, the values are significantly lower than MORB or the average arc value indicating significant dilution of the mantle signature with radiogenic helium. Snyder et al. (2003) sampled geothermal gas discharges from wells along the Central American arc and shows that $N_2/^3He$ ratios are only slightly higher than the average arc ratio of 1×10^8.

Inguaggiato et al. (2004) sampled fluids discharging from the forearc region of the Jalisco Block, Mexcio. These fluids are N_2 dominated with

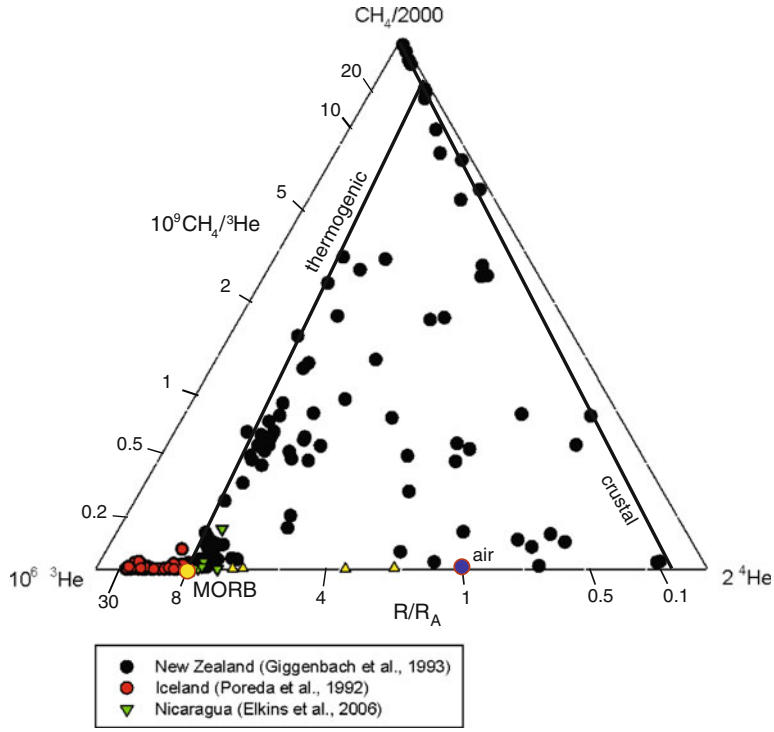

Fig. 41 CH_4–^3He–^4He systematics of volcanic and hydrothermal gas discharges. Note that samples from Iceland, Nicaragua and the southern Andes (*yellow triangles* (Ray et al. 2009)) have significantly lower $CH_4/^3He$ ratios than New Zealand samples which are dominated by thermogenic CH_4

$^3He/^4He$ ratios ranging from 0.6 to 4.5 Ra. The nitrogen isotopes are heavier than air ($\delta^{15}N$ 0.5 to 5.0 ‰) and the excess nitrogen relative to air-saturated water indicates contributions from nonatmospheric sources. The amount of excess nitrogen (calculated using ^{20}Ne contents) correlates with the $\delta^{15}N$ values and samples with almost 100 % excess have $\delta^{15}N$ of +5 ‰. In this region, seafloor sediments are not involved in the subduction process and the authors postulate that contributions of heavy nitrogen from metamorphic rocks located within the continental curst is responsible for the measured $\delta^{15}N$ values (Table 7).

8 Conclusions and Outlook

This chapter reviewed applications of noble gases to modern hydrothermal systems. Clearly, interpretation begins with a suitable sampling technique that is adapted to the fluids that are sampled. Care needs to be taken when collecting acid gases or waters where application of copper tubing will result in leaky and air contaminated samples. Lead-glass bottles are preferable to Pyrex when collecting samples without NaOH solution to concentrate the noble gases and storage time before analyses is in excess of several weeks. For a noble gas survey of a given volcanic or hydrothermal area one should consider collecting samples from bubbling springs, mud-pots, fumaroles and steaming ground. Water samples tend to be more problematic and may be subject to more extensive atmospheric or shallow level crustal contamination, however, they can also yield very good results in particular if some gas phase sampling localities are available for reference. Geothermal wells are also an excellent medium for accessing deep fluids and should be sampled wherever accessible.

The application of noble gases to hydrothermal fluids as opposed to rock samples has some important advantages such as the certainty that

no cosmogenic ^{3}He is contributing to the signal and that sampled fluids represent present day or relatively recent compositions. Another advantage is that usually large amounts of gas can be collected making analyses easier and faster. Disadvantages include higher potential for air contamination and potentially limited area that can be covered by hydrothermal samples.

The by far most useful application of helium isotopes is that the ^{3}He/^{4}He ratio is an ubiquitous and strong signal of mantle derived fluids and therefore can be used to decipher deep and upper mantle sources from crustal and atmospheric sources. The helium isotope ratio is a reliable guide for more extensive noble gas and major gas studies and provides unequivocal evidence for the extent an area receives fluid input from deep within the Earth. The work reviewed in this chapter shows such applications to investigate subduction zone processes, the extent of mantle contribution at hot spots as well as relationships that relate to the migration of magmatic helium away from individual volcanoes.

The strong affinity of high ^{3}He/^{4}He ratios with recent magmatic activity also renders this noble gas as an excellent candidate for volcano monitoring. Currently, the main obstacle to exploring this application is the lack of in situ automated ^{3}He/^{4}He analyses in fumaroles and springs. Future instrument development should advance this area of research and deploy such instruments in bubbling springs, fumaroles, wells and faults that have shown to exhibit signals related to volcanic activity. Such instrumentation would also be extremely useful in earthquake prediction and provide an alternative and complement to the modern geophysical techniques that have so far failed to predict even the largest recent earthquake (Tohoku M9.0 in 2011) despite the continuous seismic record in the area for decades.

Other noble gases, Ne, Ar, Kr, Xe also provide complementary information to helium and can be extensively applied to studies of tectonics, mantle processes and volcanic activity. Their isotopic analyses are less routine than that of helium, although Ar isotopes can easily be analyzed by Quadrupole MS. However, most investigators seem to focus on helium and as a result the hydrothermal database on these companion gases is rather limited. Future studies should include at least Ar isotopes in hydrothermal investigations to further constrain its relationship to helium and better characterize upper and lower mantle Ar isotope ratios and elemental abundances.

Going much beyond the noble gas community is the attractiveness of combining helium isotopes with the main gases, which after all carry this messenger from depth to surface. Interest in abiogenic C sources has spurred research in $CH_4/^3$He ratios but as pointed out in this chapter, even if all CH_4 discharging from the ocean bottom is abiogenic, its flux is three orders of magnitude lower than current anthropogenic natural gas consumption and civilization should not count on alleviating future energy crises with abiogenic hydrocarbon sources. However the formation of abiogenic CH_4 due to low Fischer–Tropsch type reactions has recently been documented utilizing $CH_4/^3$He ratios in combination with C isotope studies and these natural systems may provide relevant analogues for the potential of scaling such reactions to industrial proportions. Combination of helium and argon isotopes with C and N relative abundances and stable isotopic compositions continues to provide a technique that allows for a more unambiguous determination of the relative source contributions (air, crust, mantle, sediments, carbonates) to volcanic and hydrothermal gas discharges than using the stable isotopes alone. Such research is critical when investigating global volatile cycles and the fate of major volatiles in subduction zones as well as the geochemical evolution of the mantle and atmosphere. Future work should include other main components such as water and the halogens which have been neglected in these types of studies so far, although they are of great significance in the planet's geochemical framework and in melt generation processes. Combination of $H_2O/^3$He and HCl/^{3}He parameters with stable isotopes may provide surprising new discoveries on the origins of these elements in various tectonic settings. Again, careful selection of samples and sites becomes essential given the

overwhelming meteoric water contribution to all hydrothermal systems.

In summary, noble gas investigations in hydrothermal systems have provided significant insights into natural processes operating on earth today. Since the first discovery of ^{3}He in natural hot springs and fumaroles by Mamyrin et al. in 1969, the following four decades of research on noble gases and their major gas accomplices show a wide range of applications that we can expect to continue into the future.

Acknowledgments We thank Pete Burnard for putting this volume together and having invited us to contribute. TF acknowledges the US National Science Foundation who supported the writing of this chapter through an NSF IPA appointment and IRD support. YS thanks to Hirochika Sumino for comments on the earlier version of the chapter.

References

Aeschbach-Hertig W, Kipfer R, Hofer M, imboden DM, Wieler R, Signer P (1996) Quantification of gas fluxes from the subcontinental mantle: the example of Laacher See, a maar lake in Germany. Geochim Cosmochim Acta 60(1):31–41

Aka FT, Nagao K, Kusakabe M, Sumino H, Tanyileke G, Ateba B, Hell J (2004) Symmetrical helium isotope distribution on the Cameroon Volcanic Line, West Africa. Chem Geol 203(3–4):205–223

Aldrich LW, Nier AO (1948) The occurrence of ^{3}He in natural sources of helium. Phys Rev 74:1590–1594

Altemose VO (1961) Helium diffusion through glass. J App Phys 32:1309–1316

Anders E, Grevesse N (1989) Abundances of the elements—meteoritic and solar. Geochim Cosmochim Acta 53:197–214

Andrews J (1985) The isotopic composition of radiogenic helium and its use to study groundwater movement in confined aquifers. Chem Geol 49:339–351

Ballentine C, Burnard P (2002) Production, release and transport of noble gases in the continental crust. In: Porcelli D, Ballentine C, Wieler R (eds) Noble gases in geochemistry and cosmochemistry, vol 47. Mineralogical Society of America, Washington, pp 481–529

Barfod D, Ballentine C, Halliday A, Fitton J (1999) Noble gases in the Cameroon line and the He, Ne, and Ar isotopic compositions of high mu (HIMU) mantle. J Geophys Res 104(29–29):527. doi:510.1029/1999JB900280

Baskov YA, Vetsheyn VY, Surikov SN, Tostikhin IN, Malyuk GA, Mishina TA (1973) Isotope composition of H, O, C, Ar and He in hot springs and gases in the Kuril–Kamtchatka volcanic region as indicators of formation conditions. Geochem Int 10:130–138

Beterle U, Aeschbach-Hertig W, Imboden DM, Baur H, Graf T, Kipfer R (2000) A mass spectrometric system for the analysis of noble gases and tritium from water samples. Environ Sci Technol 34:2042–2050

Binachi D, Sarmiento JL, Gnanadesikan A, Key RM, Schlosser P, Newton R (2010) Low helium flux from the mantle inferred from simulations of oceanic helium isotope data. Earth Planet Sci Lett 297:379–386

Braeuer K, Kaempf H, Niedermann S, Strauch G, Weise SM (2004) Evidence for a nitrogen flux directly derived from the European subcontinental mantle in the Western Eger Rift, Central Europe. Geochim Cosmochim Acta 68:4935–4947

Braitseva OA, Melekestsev IV, Ponomareva VV, Sulerzhitsky LD (1995) Ages of calderas, large explosive craters and active volcanoes in the Kurile–Kamchatka region, Russia. Bull Volcanol 57:383–402

Breddam K, Kurz MD, Storey M (2000) Mapping out the conduit of the Iceland mantle plume with helium isotopes. Earth Planet Sci Lett 176:45–55

Burnard PG, Graham DW, Turner G (1997) Vesicle specific noble gas analyses of "popping rock": implications for primordial noble gases in earth. Science 276:568–571

Caracausi A, Italiano F, Paonita A, Rizzo A, Nuccio PM (2003) Evidence of deep magma degassing and ascent by geochemistry of peripheral gas emissions at Mount Etna (Italy): assessment of the magmatic reservoir pressure. J Geophys Res 108(NO. B10):2463

Canalas RA, Alexander EC, Manuel OK (1968) Terrestrial abundances of noble gas. J Geophys Res 73:3331–3334

Charlou J, Fouquet Y, Donval J, Auzende J, Jean-Baptiste P, Stienvenard M, Michel S (1996) Mineral and gas chemistry of hydrothermal fluids along an ultra-fast spreading ridge: East Pacific Rise, 17°S to 19°S (NAUDUR cruise, 1993). Phase separation process controlled by volcanic and tectonic activity. J Geophys Res 101:11591–15899

Charlou JL, Fouquet Y, Bougault H, Donval JP, Etoubleau J, Jean-Baptiste P, Dapoigny A, Appriou P, Rona PA (1998) Intense CH_4 plumes generated by serpentinization of ultramafic rocks at the intersection of the 15∞20′N fracture zone and the Mid-Atlantic Ridge. Geochim Cosmochim Acta 62(13):2323–2333

Charlou J, Donval J, Douville E, Jean-Baptiste P, Radford-Knoery J, Fouquet Y, Dapoigny A, Stievenard M (2000) Compared geochemical signatures and evolution of Menez Gwen (37°50N) and Lucky Strike (37°17N) hydrothermal fluids, south of the Azores Triple junction on the Mid-Atlantic Ridge. Chem Geol 171:49–75

Charlou J, Donval J, Fouquet Y, Jean-Baptiste P, Holm N (2002) Geochemistry of high H_2 and CH_4 vent fluids issuing from ultramafic rocks at the rainbow hydrothermal field (36°14N, MAR). Chem Geol 191:345–359

Christiansen RL, Foulger GR, Evans JR (2002) Upper mantle origin of the Yellowstone hot spot. Geol Soc Amer Bull 114:1245–1256

Clarke WB, Beg MA, Craig H (1969) Excess ^{3}He in the sea: evidence for terrestrial primordial helium. Earth Planet Sci Lett 6:213–220

Clift P, Vannucchi P (2004) Controls on tectonic accretion versus erosion in subduction zones: implications for the origin and recycling of the continental crust. Rev Geophys 42:RG2001

Clor LE, Fischer TP, Hilton DR, Sharp ZD, Hartono U (2005) Volatile and N isotope chemistry of the Molucca Sea collision zone: tracing source components along the Sangihe Arc, Indonesia. Geochem Geophys Geosyst 6:Q03J14. doi:10.1029/2004GC000825

Cole JW, Lewis KB (1981) Evolution of the Taupo Hikurangi subduction system. Tectonophysics 72:1–21

Corliss JB, Dymond J, Gordon LI, Edmond JM, von Herzen RP, Ballard RD, Green K, Williams D, Bainbridge A, Crane K, van Andel TH (1979) Submarine thermal springs on the Galapagos Rift. Science 203:1073–1083

Courtillot V, Davaille A, Besse J, Stock J (2003) Three distinct types of hot spots in the Earth's mantle. Earth Planet Sci Lett 205:295–308

Craig H (1953) The geochemistry of sable carbon isotopes. Geochim Cosmochim Acta 3:53–92

Craig H (1963) The isotopic geochemistry of water and carbon in geothermal areas. In: Nuclear geology on geothermal area (9–13 Sept 1963), pp 17–53. Consiglio Nazionale delle Richerche, Laboratorio di Geologia Nucleare, Pisa

Craig H, Lupton JE (1976) Primordial neon, helium, and hydrogen in oceanic basalts. Earth Planet Sci Lett 31:369–385

Craig H, Lupton JE (1981) Helium 3 and mantle volatiles in the ocean and the oceanic crust. In: The oceanic lithosphere, vol 7, The sea, vol 7, chapter 11. Wiley, London

Craig H, Lupton JE, Welhan JA, Poreda R (1978) Helium isotope ratios in Yellowstone and Lassen Park volcanic gases. Geophys Res Lett 5(897–900):

Crossey LJ, Karlstrom KE, Springer AE, Newell D, Hilton DR, Fischer T (2009) Degassing of mantle-derived CO_2 and He from springs in the southern Colorado Plateau region-Neotectonic connections and implications for groundwater systems. Geol Soc Am Bull 121(7–8):1034–1053

Davy B, Wood RA (1994) Gravity and magnetic modelling of the Hikurangi Plateau. Mar Geol 118:139–151

de Leeuw GAM, Hilton DR, Fischer TP, Walker JA (2007) The He–CO_2 isotope and relative abundance characteristics of geothermal fluids in El Salvador and Honduras: new constraints on volatile mass balance of the Central American Volcanic Arc. Earth Planet Sci Lett 158:132–146

DeMetis C, Gordon RG, Argus DF, Stein S (1990) Current plate motions. Geophys J Intl 101:425–478

Dogan T, Sumino H, Nagao K,Notsu K (2006) Release of mantle helium from the forearc region of the Philippine Sea plate subduction. Chem Geol 233:235–248

Dymond J, Hogan L (1974) The effects of deep-sea volcanism on the gas concentration of ocean water. J Geophys Res 79:877–880

Eberhart-Phillips D, Reyners M, Chadwick M, Stuart G (2008) Three-dimensional attenuation structure of the Hikurangi subduction zone in the central North Island, New Zealand. Geophys J Intern 174:418–434

Elkins L, Fischer TP, Hilton DR, Sharp ZD, McKnight S, Walker JA (2006) Tracing nitrogen in volcanic and geothermal volatiles from the Nicaraguan volcanic front. Geochim Cosmochim Acta 70:5215–5235

Evans WC, Bergfeld D, van Soest MC, Huebner MA, Fitzpatrick J, Revesz KM (2006) Geochemistry of low-temperature springs northwest of Yellowstone caldera: seeking the link between seismicity, deformation, and fluid flow. J Volcanol Geotherm Res 154:169–180

Faber E, Botz R, Poggenburg J, Schmidt M, Stoffers P, Hartmann M (1998) Methane in Red Sea brines. Org Geochem 29:363–379

Fiebig J, Chiodini G, Caliro S, Rizzo A, Spangenberg J, Hunziker JC (2004) Chemical and isotopic equilibrium between CO_2 and CH_4 in fumarolic gas discharges: generation of CH_4 in arc magmatic-hydrothermal systems. Geochim Cosmochim Acta 68:2321–2334

Fischer TP, Sturchio NC, Stix J, Arehart GB, Counce D, Williams SN (1997) The chemical and isotopic composition of fumarolic gases and spring discharges from Galeras Volcano, Colombia. J Volcanol Geotherm Res 77:229–254

Fischer TP, Giggenbach WF, Sano Y, Williams SN (1998) Fluxes and sources of volatiles discharged from Kudryavy, a subduction zone volcano, Kurile Islands. Earth Planet Sci Lett 160:81–96

Fischer TP, Hilton DR, Zimmer MM, Shaw AM, Sharp ZD, Walker JA (2002) Subduction and recycling of nitrogen along the Central American margin. Science 297:1154–1157

Fischer TP, Burnard P, Marty B, Hilton DR, Furi E, Palhol F, Sharp ZD, Mangasini F (2009) Upper-mantle volatile chemistry at Oldoinyo Lengai volcano and the origin of carbonatites. Nature 459:77–80

Fourre E, J-B P, J-L C, J-P D, I J (2006) Helium isotopic composition of hydrothermal fluids from the Manus back-arc Basin, Papua New Guinea. Geochem J 40:245–252

Furi E, Hilton DR, Halldorsson SA, Barry PH, Hahm D, Fischer TP, Gronvold K (2010) Apparent decoupling of the He and Ne isotope systematics of the Icelandic mantle: The role of He depletion, melt mixing, degassing fractionation and air interaction. Geochim Cosmochim Acta 74(11):3307–3332

Gamo T, Chiba H, Yamanaka T, Okudaira T, Hashimoto J, Tsuchida S, Ishibashi J, Kataoka S, Tsunogai U, Kouzuma F, Okamura K, Sano Y, Shinjo R (2001) Chemical characteristics of newly discovered black-

smoker fluid venting and its effluent dispersion at the Rodriguez Triple Junction, Indian Ridge. Earth Planet Sci Lett 193:371–379

Gamo T, Masuda H, Yamanaka T, Okamura K, Ishibashi J, Nakayama E, Obata H, Shitashima K, Nishio Y, Hasumoto H, Watanabe M, Mitsuzawa K, Seama N, Tsunogai U, Kouzuma F, Sano Y (2004) Discovery of a new hydrothermal venting site in the southernmost Mariana Arc: Al-rich hydrothermal plumes and white smoker activity associated with biogenic methane. Geochem J 38:527–534

Ganino C, Arndt NT (2010) Climate changes caused by degassing of sediments during the emplacement of large igneous provinces. Geology 37:323–326

German CR, Von Damm KL (2004) Hydrothermal processes. In: Treatise geochem (The oceans mar geochem), vol 6, pp 181–222

Gharib J, Sansone F, Resing J, Baker E, Lupton J, Massoth G (2005) Methane dynamics in hydrothermal plumes over a superfast spreading center: East Pacific Rise, 27.5°–32.3°S. J Geophys Res 110:B10101

Giggenbach WF (1975) A simple method for the collection and analysis of volcanic gas samples. Bull Volcanol 39(1):132–145

Giggenbach WF (1984) Mass transfer in hydrothermal alteration systems. Geochim Cosmochim Acta 84(2693–2627):2611

Giggenbach WF (1987) Redox processes governing the chemistry of fumarolic gas discharges from White Island, New Zealand. Appl Geochem 2:141–161

Giggenbach WF (1996) Chemical composition of volcanic gases. In: Scarpa R, Tilling R (eds) IAVCEI-UNESCO: monitoring and mitigation of volcano hazards, pp 221–256

Giggenbach WF, Sano Y, Wakita H (1993) Isotopic composition of helium, and CO_2 and CH_4 contents in gases produced along the New Zealand part of a convergent plate boundary. Geochim Cosmochim Acta 57:3427–3455

Giggenbach WF, Tedesco D, Sulisiyo Y, Caprai A, Cioni R, Favara R, Fischer TP, Hirabayashi J, Korzhinsky M, Martini M, Menyailov I, Shinohara H (2001) Evaluation of results from Forth and Fifth IAVCEI Field Workshop on Volcanic Gases, Vulcano Island, Italy and Java, Indonesia. J Volc Geotherm Res 108:283–302

Goff F, McMurtry GM, Counce D, Stimac JA, Roldan-Manzo AR, Hilton DR (2000) Contrasting hydrothermal activity at Sierra Negra and Alcedo volcanoes, Galapagos Archipelago, Ecuador. Bull Volc 62:34–52

Gold T (1979) Terrestrial sources of carbon and earthquake outgassing. J Pet Geol 1:3–19

Gonnermann HM, Mukhopadhyay S (2007) Non-equilibrium degassing and a primordial source of helium in ocean-island volcanism. Nature 449:1037–1040

Gorbatov A, Domínguez J, Suárez G, Kostoglodov V, Zhao D (1999) Tomographic imaging of the P-wave velocity structure beneath the Kamchatka peninsula. Geophys J Int 137:269–279

Graham DW (2002) Noble gas isotope geochemistry of Mid-Ocean Ridge and Ocean Island Basalts: characterization of mantle source regions. In: Porcelli D, Ballentine C, Wieler R (eds) MSA special volume: noble gases, vol 47, pp 247–317

Grassineau NV (2006) High-precision EA-IRMA analysis of S and C isotopes in geological materials. App Geochem 21:756–765

Gunter BD, Musgrave JA (1966) Gas chromatographic measurements of hydrothermal emanations at Yellowstone National Park. Geochim Cosmochim Acta 30:1175–1189

Hacker BR, Peacock SM, Abers GA, Holloway SD (2003) Subduction factory 2. Are intermediate-depth earthquakes in subducting slabs linked metamorphic dehydration reaction? J Geophys Res 108:2030. doi: 2010.1029/2001JB001129

Hasegawa A, Nakajima J (2004) Geophyscial constraints on slab subduction and arc magmatism. In: The state of the planet: frontiers and challenges in geophysics. Geophysical Monograph 150, IUGG, vol 19, pp 1–13

Hearn EH, Kennedy BM, Trudell AH (1990) Coupled variations in helium isotopes and fluid chemistry: Shoshone Geyser Basin, Yellowstone National Park. Geochim Cosmochim Acta 54:3103–3113

Heiweil VM, Solomon DK, Gingerich SB, Verstraeten IM (2009) Oxygen, hydrogen, and helium isotopes for investigating groundwater systems of the Cape Verde Islands, West Africa. Hydrogeol J 17:1157–1174

Hilton DR (1996) The helium and carbon isotope systematics of a continental geothermal system—results from monitoring studies at Long Valley Caldera (California, USA). Chem Geol 127:269–295

Hilton DR, Hammerschidt K, Look G, Friedrichsen H (1993a) Helium and argon isotope systematics of the central Lau Basin and Valu Fa Ridge: evidence of crust/matle interactions in a back-arc basin. Geochim Cosmochim Acta 57:2819–2841

Hilton DR, Hammerschmidt K, Teufel S, Friedrichsen H (1993b) Helium isotope characteristics of Andean geothermal fluids and lavas. Earth Planet Sci Lett 120:265–282

Hilton DR, Gronvold K, Sveinbjornsdottir AE, Hammerschmidt K (1998) Helium isotope evidence for off-axis degassing of the Icelandic hot spot. Chem Geol 149:173–187

Hilton DR, Macpherson CG, Elliott TR (2000) Helium isotope ratios in mafic phenocrysts and geothermal fluids from La Palma, the Canary Islands (Spain): implications for HIMU mantle sources. Geochim Cospmochim Acta 64:2119–2132

Hilton DR, Fischer TP, Marty B (2002) Noble gases in subduction zones and volatile recycling. In: Porcelli D, Ballentine C, Wieler R (eds) MSA special volume: noble gases in geochemistry and cosmochemistry. 47:319–362

Hilton DR, Ramirez CJ, Mora-Amador R, Fischer TP, Furi E, Barry PH, Shaw AM (2010) Monitoring of temporal and spatial variations in fumarole helium

and carbon dioxide characteristics at Poas and Turrialba volcanoes, Costa Rica (2001–2009). Geochem J 44:431–440

Honda M, Reynolds JH, Roedder E, Epstein S (1987) Noble gases in diamonds: occurrences of solar like helium and neaon. J Geophys Res 92:12507–12521

Hooft EEE, Toomey DR, Solomon SC (2003) Anomalously thin transition zone beneath the Galapagos hotspot. Earth Planet Sci Lett 216:55–64

Horiguchi K, Ueki S, Sano Y, Takahata N, Hasegawa A, Igarashi G (2010) Geographical distribution of helium isotope ratios in northeastern Japan. Island Arc 19:60–70

Hulston JR, Lupton JE (1996) Helium isotope studies of geothermal fields in the Taupo Volcanic Zone, New Zealand. J Volcanol Geoth Res 74(3–4):297–321

Hulston JR, Hilton DR, Kaplan IR (2001) Helium and carbon isotope systematics of natural gases from Taranaki Basin, New Zealand. Appl Geochem 16:419–436

Ide S, Shiomi K, Mochizuki K, Tonegawa T, Kimura G (2010) Split Philippine Sea plate beneath Japan. Geophys Res Lett 37:L21304. doi: 10.1029/2010GL044585

Igarashi G, Kodera M, Ozima M, Sano Y, Wakita H (1987) Noble gas elemental and isotopic abundances in deep sea trench in the West Pacific. Earth Planet Sci Lett 86:77–84

Inguaggiato S, Taran Y, Grassa F, Capasso G, Favara R, Varley N, Faber E (2004) Nitrogen isotopes in thermal fluids of a forearc region (Jalisco Block, Mexico): evidence for heavy nitrogen from continental crust. Geochem Geophys Geosyst 5

Ishibashi J, Wakita H, Nojiri Y, Grimaud D, Jean-Baptiste P, Gamo T, Auzende J, Urabe T (1994) Helium and carbon geochemistry of hydrothermal fluids from the North Fiji Basin spreading ridge (southwest Pacific). Earth Planet Sci Lett 128:183–197

Ishibashi J, Sano Y, Wakita H, Gamo T, Tsutsumi M, Sakai H (1995) Helium and carbon geochemistry of hydrothermal fluids from the Mid-Okinawa Trough Back Arc Basin, southwest of Japan. Chem Geol 123(1˙Äì4):1–15

Iwamori H (1998) Transportation of H_2O and melting in subduction zones. Earth Planet Sci Lett 160:65–80

Jaffe LA, Hilton DR, Fischer TP, Hartono U (2004) Tracing magma sources in an arc–arc collision zone: helium and carbon isotope and relative abundance systematics of the Sangihe Arc, Indonesia. Geochem Geophys Geosyst 5:Q04J10. doi:10.1029/2003GC000660

Jambon A, Weber H, Braun O (1986) Solubility of He, Ne, Ar, Kr, and Xe in a basalt melt in the range 1250–1600 °C. Geochemical implications. Geochim Cosmochim Acta 50:401–408

Jean-Baptiste P, Charlou JL, Stievenard M, Donval JP, Bougault H, Mevel C (1991) Helium and methane measurements in hydrothermal fluids from the Mid-Atlantic-Ridge: the Snakepit site at 23°N. Earth Planet Sci Lett 106:17–28

Jean-Baptiste P, Charlou J, Fouquet Y, Dapoigny A, Stievenard M, Donval J, Auzende J (1997) Helium and oxygen isotope analyses of hydrothermal fluids from the East Pacific Rise between 17°S and 19°S. Geo-Marine Lett 17:213–219

Jean-Baptiste P, Bougault H, Vangriesheim A, Charlou J, Radford-Knoery J, Fouquet Y, Needham D, German C (1998) Mantle ^{3}He in hydrothermal vents and plume of the Lucky Strike site (MAR 37°17N) and associated geothermal heat flux. Earth Planet Sci Lett 157:69–77

Jean-Baptiste P, Fouzrr E, Charlou J-L, German CR, Radford-Knoery J (2004) Helium isotopes at the rainbow hydrothermal site (Mid-Atlantic Ridge, 36°14′N). Earth Planet Sci Lett 221(1–4):325–335

Jean-Baptiste P, Allard P, Bani P, Garaebiti E, Pelletier B, Fourré E, Metrich N (2009) Highly variable helium isotope ratios in the Vanuatu volcanic arc. Amer Geophys Union, Fall Meeting 2009, abstract #T21A-1774

Jean-Baptiste P, Allard P, Coutinho R, Ferreira T, FourrÈ E, Queiroz G, Gaspar JL (2009b) Helium isotopes in hydrothermal volcanic fluids of the Azores archipelago. Earth Planet Sci Lett 281(1–2):70–80

Jenden PD, Kaplan IR, Poreda R, Craig H (1988) Origin of nitrogen-rich gases in the Califronia Great Valley: evidence from helium, carbon and nitrogen isotope ratios. Geochim Cosmochim Acta 52:852–861

Jenden PD, Hilton DR, Kaplan IR, Craig H (1993) Abiogenic hydrocarbons and mantle helium in oil and gas field. In: Howell DG (ed) The future of energy gases. US Geol Survey Prof Paper 1570:31–56

Jenkins WJ (1987) ^{3}H and ^{3}He in the beta triangle: observations of gyre ventilation and oxygen utilization rates. J Phys Oceanogr 17:763–783

Jiang G, Zhao D, Zhang G (2009) Seismic tomography of the Pacific slab edge under Kamchatka. Tectonophysics 465:190–203

JinXing D, CaiNeng Z, ShuiChang Z, Jian L, YunYan N, GuoYi H, Xia L, ShiZhen L, GuangYou Z, JingKui M, ZhiSheng L, AnPing H, Chun Y, QingHua Z, YanHua S, Ying Z, ChengHua M (2008) Discrimination of abiogenic and biogenic alkane gases. Sci China Ser D—Earth Sci 51:1737–1749

Kamensky IL, Lobkov VA, Prasolov EM, Beskrovny NS, Kudryavtseva EI, Anufriev GS, Pavlov VP (1976) Components of the upper mantle in gases of Kamchatka. Insight from isotope data (He, Ne, Ar, and C). Geochem Int 1976:682–696

Kawagucci S, Okamura K, Kiyota K, Tsunogai U, Sano Y, Tamaki K, Gamo T (2008) Hydrothermal plumes over the Central Indian Ridge, 18°–20°S. G-Cubed 9:Q10002

Keir R, Schmale O, Seifert R, Sultenfub J (2009) Isotope fractionation and mixing in methane plumes from the Logatchev hydrothermal field. G-cubed 10:Q05005

Kennedy BM, Lynch MA, Reynolds JH, Smith SP (1985) Intensive sampling of noble gases in fluids at Yellowstone: I Early overview of the data; regional patterns. Geochim Cosmochim Acta 49:1251–1261

Kennedy BM, Reynolds JR, Smith SP, Truesdell AH (1987) Helium isotopes: Lower Geysir Basin, Yellowstone National Park. J Geophys Res 92:12477–12480
Kennedy BM, Reynolds JH, Smith SP (1988) Noble gas geochemistry in thermal springs. Geochim Cosmochim Acta 52:1919–1928
Kennedy BM, Hiyagon H, Reynolds JH (1990) Crustal neon: a striking uniformity. Earth Planet Sci Lett 98:277–286
Kennedy BM, Hiyagon H, Reynolds JH (1991) Noble gases from Honduras geothermal sites. J Volcanol Geotherm Res 45(1–2):29–39
Keosian J (1960) On the origin of life. Science 131:479–482
Kim K, Welhan J, Craig H (1984) The hydrothermal vent fields at 13°N and 11°N on the East Pacific Rise: Alvin 1984 results. EOS 68:45
Kodera M, Igarashi G, Ozima M (1988) Noble gases in hydrothermal plumes of Loihi Seamount. Earth Planet Sci Lett 87:266–272
Kononov VI, Mamyrin VA, Polak BG, Khabarin LV (1974) Helium isotopes in gases of Icelandic hydrothermal. Dokl Akad Nauk SSSR 217:172–175
Kulngoski JT, Hilton DR (2002) A quadrupole-based mass spectrometric system for the determination of noble gas abundances in fluids. Geochem Geophys Geosyst 3:U1–U10
Kumagai H, Dick H, Kaneoka I (2003) Noble gas signatures of abyssal gabbros and peridotites at an Indian Ocean core complex. Geochem Geophys Geosyst 4:9107. doi:9110.1029/2003GC000540
Kurz MD (1986) Cosmogenic helium in a terrestrial igneous rock. Nature 320:435–439
Kurz MD, Meyer PS, Sigurdsson H (1985) Helium isotopic systematics within the neovolcanic zones of iceland. Earth Planet Sci Lett 74:291–305
Kusakabe M, Nagao K, Ohba T, Seo J, Park S-H, Lee J, Park B-K (2009) Noble gas and stable isotope geochemistry of thermal fluids from Deception Island. Antarct Antarct Sci 21(3):255–267
Langmuir CH, Vocke RD Jr, Hanson GN, Hart SR (1978) A general mixing equation with applications to Icelandic basalts. Earth Planet Sci Lett 37:380–392
Lee H-F, Yang TF, Lan TF, Chen C-H, Song S-R, Tsao S (2008) Temporal variations of gas compositions of fumaroles in the Tatun Volcano Group, northern Taiwan. J Volcanol Geoth Res 178(4):624–635
Lei J, Zhao D (2006) A new insight into the Hawaiian plume. Earth Planet Sci Lett 241:438–453
Li X, Kind R, Yuan X (2001) Upper mantle structure and transition zone thickness beneath ocean islands from receiver function study. Eos Trans AGU 82(47), Fall Meet Suppl, Abstract S42B-0633
Lilley M, Baross J, Gordon L (1983) Reduced gases and bacteria in hydrothermal fluids The Galapagos spreading center and 21°N East Pacific Rise. In: Rona PA et al (ed) Hydrothermal processes at seafloor spreading centers, plenum, pp 411–419
Lilley M, Butterfield D, Olson E, Lupton J, Macko S, Mcduff R (1993) Anomalous CH_4 and NH_4+ concentrations at an unsedimented mid-ocean-ridge hydrothermal system. Nature 364:45–47
Lupton JE (1983) Terestrial rare gases: isotope tracer studies and clues to primordial components in the mmantle. Ann Rev Earth Planet Sci 11:371–414
Lupton JE, Baker ET, Massoth GJ (1999) Helium, heat, and the generation of hydrothermal event plumes at mid-ocean ridges. Earth Planet Sci Lett 171(3):343–350
Lux GE (1987) The behavior of noble gases in silicate liquids; solution, diffusion, bubbles and surface effects, with applications to natural samples. Geochim Cosmochim Acta 51(6):1549–1560
Lyon GL, Giggenbach WF, Sano Y (1996) Variations in the chemical and isotopic composition of Taranaki gases and their possible causes. N Z Petrol Conf 1:171–174
Magro G, Pennisi M (1991) Noble gases and nitrogen: mixing and temporal evolution in the fumarolic fluids of vulcano, Italy. J Volcanol Geotherm Res 47:237–247
Mamyrin BA, Tolstikhin IN (1984) Helium Isotopes in nature. Elsevier, Amsterdam, p 273
Mamyrin BA, Tolstikhin IN, Anufriyev GS, Kamenskiy IL (1969) Isotopic analysis of terrestrial helium on a magnetic resonance mass spectrometer. Geokhimiya 1969(595–602):
Mariner RH, Evans WC, Presser TS, White LD (2003) Excess nitrogen in selected thermal and mineral springs of the cascade range in Northern California, Oregon, and Washington; sedimentary or volcanic in origin? J Volcanol Geotherm Res 121:99–114
Marty B, Giggenbach WF (1990) Major and rare gases at White Island volcano, New Zealand: origin and flux of volatiles. Geophys Res Lett 17:247–250
Marty B, Jambon A (1987) $C/^3He$ in volatile fluxes from the solid earth: implications for carbon geodynamics. Earth Planet Sci Lett 83:16–26
Marty B, Jambon A, Sano Y (1989) Helium isotopes and CO_2 in volcanic gases of Japan. Chem Geol 76:25–40
Marty B, Appora I, Barrat JAA, Deniel C, Vellutini P, Vidal P (1993a) He, Ar, Sr, Nd and Pb isotopes in volcanic rocks from Afar: evidence for a primitive mantle component and constraints on magmatic sources. Geochem J 27:219–228
Marty B, Meynier V, Nicolini E, Greissharber E, Toutain J (1993b) Geochemistry of gas emanations: a case study of the Rdunion. Hot Spot, Indian Ocean. Appl Geochem 8:141–152
Matsuda T, Uyeda S (1971) On the Pacific-type orogeny and its model-extension of the paired belts concept and possible origin of marginal sea. Tectonophysics 11:5–27
Matsumoto T, Kawabata T, Matsuda J, Yamamoto K, Mimura K (2003) $^3He/^4He$ ratios in well gases in the Kinki district, SW Japan: surface appearance of slab-derived fluids in a non-volcanic area in Kii Peninsula. Earth Planet Sci Lett 216:221–230
Mazor E, Wasserburg GJ (1965) Helium, neon, argon, krypton, and xenon in gas emanations from

Yellowstone and Lassen Volcanic National Parks. Geochim Cosmochim Acta 29:443–454
Mazor E, Wasserburg GJ, Craig H (1964) Rare gases in Pacific Ocean water. Deep-sea Res 11:929–932
Merlivat L, Pineau F, Javoy M (1987) Hydrothermal vent waters at 13°N on the East Pacific Rise: isotopic composition and gas concentration. Earth Planet Sci Lett 84:100–108
Mizoue M, Nakamura M, Seto N, Ishiketa Y (1971) Crustal structure from travel times of reflected and refracted seismic waves recorded at Wakayama micro-earthquake observatory and its substations. Bull Earthquake Res Inst Univ Tokyo 49:33–62
Montelli R, Nolet G, Dahlen FA, Masters G (2006) A catalogue of deep mantle plumes: new results from finite-frequency tomography. Geochem Geophys Geosys 7:Q11007
Moreira M, Blusztajn J, Curtice J, Hart S, Dick H, Kurz M (2003) He and Ne isotopes in oceanic crust: implications for noble gas recycling in the mantle. Earth Planet Sci Lett 216:635–643
Morgan WJ (1971) Convection plumes in the lower mantle. Nature 230:42–43
Morikawa N, Kazahaya K, Fourre E, Takahashi HA, Jean-Baptiste P, Ohwada M, LeGuern FJ, Nakama A (2008a) Magmatic He distribution around Unzen volcano inferred from intensive investigation of helium isotopes in groundwater. J Volcanol Geoth Res 175(1–2):218–230
Morikawa N, Kazahaya K, Masuda H, Ohwada M, Nakama A, Nagao K, Sumino H (2008b) Relationship between geological structure and helium isotopes in deep groundwater from the Osaka Basin: application to deep groundwater hydrology. Geochem J 42:61–74
Mortimer N, Parkinson D (1996) Hikurangi Plateau: a cretaceous large igneous province in the southwest Pacific Ocean. J Geophys Res 101:687–696
Nagao K, Takaoka N, Matsubayashi O (1981) Rare gas isotopic compositions in natural gases of Japan. Earth Planet Sci Lett 53(2):175–188
Nakai S, Wakita H, Nuccio PM, Italiano F (1997) MORB-type neon in an enriched mantle beneath Etna, Sicily. Earth Planet Sci Lett 153:57–66
Nakajima J, Hasegawa A (2007) Tomographic evidence for the mantle upwelling beneath southwestern Japan and its implications for arc magmatism. Earth Planet Sci Lett 254:90–105
Nakajima J, Matsuzawa T, Hasegawa A, Zhao D (2001) Three-dimensional structure of Vp, Vs and Vp/Vs beneath northeastern Japan: implications for arc magmatism and fluids. J Geophys Res 106:21843–21857
Nakanishi M, Tamaki K, Kobayashi K (1992) A new Mesozoic isochron chart of the northwestern Pacific Ocean: Paleomagnetic and tectonic implications. Geophys Res Lett 19:693–696
Nishio Y, Tsutsumi M, Gamo T, Sano Y (1995) Hydrogen effect on the d13C value of CO_2 measured by mass spectrometer with electron impact ionization. Anal Sci 11:9–12
Nolet G, Allen R, Zhao D (2007) Mantle plume tomography. Chem Geol 241:248–263
Norton FJ (1953) Helium diffusion through glass. J Amer Ceramic Soc 36:90–96
Notsu K, Nakai S, Igarashi G, Ishibashi J, Mori T, Suzuki M, Wakita H (2001) Spatial distribution and temporal variation of $^3He/^4He$ in hot spring gas released from Unzen volcanic area, Japan. J Volcanol Geotherm Res 111:89–98
Nuccio PM, Paonita A (2000) Investigation of the noble gas solubility in H_2O–CO_2 bearing silicate liquids at moderate pressure II: the extended ionic porosity (EPI) model. Earth Planet Sci Lett 183:499–512
Nuccio PM, Paonita A (2001) Magmatic degassing of multicomponent vapors and assessment of magma depth: application to Vulcano Island (Italy). Earth Planet Sci Lett 193(3–4):467–481
Nuccio PM, Valenza V (1998) Magma degassing and geochemical detection of its ascent. In: Arehart GB, Hulston JR (eds) Water–rock interaction, pp 475–478 (Balkema AA, Brookfield, Vt)
Nuccio PM, Paonita A, Rizzo A, Rosciglione A (2008) Elemental and isotope covariation of noble gases in mineral phases from Etnean volcanics erupted during 2001–2005, and genetic relation with peripheral gas discharges. Earth Planet Sci Lett 272(3–4):683–690
Obara K (2002) Nonvolcanic deep tremor associated with subduction in southwest Japan. Science 296:1679–1681
Ohno M, Sumino H, Hernandez PA, Sato T, Nagao K (2011) Helium isotopes in the Izu Peninsula, Japan: relation of magma and crustal activity. J Volcanol Geotherm Res 199:118–126
Okino K, Shimakawa Y, Nagano S (1994) Evolution of the Shikoku Basin. J Geomag Geoelectr 46:463–479
Okino K, Ohara Y, Kasuga S, Kato Y (1999) The Philippine Sea: new survey results reveal the structure and the history of the marginal basins. Geophys Res Lett 26:2287–2290
O'Nions RK, Oxburgh ER (1988) Helium, volatiles fluxes and the development of continental crust. Earth Planet Sci Lett 90:331–347
Oppenheimer C, Fischer T, Scaillet B (2012) Volcanic degassing: process and impact. In: Holland HD, Turekian KK, Rudnick RL (eds) The crust, treatise on geochemistry, vol 4, 2nd edn. Elsevier-Pergamon, Oxford
Oxbough ER, O'Nions RK (1987) Helium loss, tectonics, and the terrestrial heat budget. Science 237:1583–1588
Ozima M, Podosek FA (1983) Noble gas geochemistry. Cambridge University Press, Cambridge, p 367
Ozima M, Podosek FA (2002) Noble gas geochemistry. Cambridge University Press, Cambridge
Ozima M, Zashu S (1983) Noble gases in submarine pillow volcanic glasses. Earth Planet Sci Lett 62(1):24–40
Pedroni A, Hammerschmidt K, Friedrichsen H (1999) He, Ne, Ar, and C systematics of geothermal

emanations in the Lesser Antilles arc. Geochim Cosmochim Acta 63:515–532
Perez NM, Nakai S, Wakita H, Hernandez PA, Salazar JM (1996) Helium_3 emission in and around Teide Volcano, Tenerife, Canary Islands, Spain. Geophys Res Lett 23:3531–3534
Pierce KL, Morgan LA (1992) The track of the Yellowstone hot spot: volcanism, faulting and uplift. In: Link PK, Kuntz MA, Platt LB (eds) Regional geology of Eastern Idaho and Western Wyoming. Geological Society of America Memoir, vol 179, pp 1–53
Pierce KL, Morgan LA (2009) Is the track of the Yellowstone hotspot driven by a deep mantle plume?—review of volcanism, faulting and uplift in light new data. J Volcanol Geotherm Res 188:1–25
Pik R, Marty B, Hilton DR (2006) How many plumes in Africa? The geochemical point of view. Chem Geol 226:100–114
Poole JC, McNeill GW, Langman SR, Dennis F (1997) Analysis of noble gases in water using quadrupole mass spectrometer in static mode. Appl Geochem 12:707–714
Poreda RJ, Arnorsson S (1992) Helium isotopes in Icelandic geothermal systems: II. Helium-heat relationships. Geochim Cosmochim Acta 56:4229–4235
Poreda R, Jeffrey PM, Kaplan IR, Craig H (1988) Magmatic helium in subduction-zone natural gases. Chem Geol 71:199–210
Poreda RJ, Craig H, Arnorsson S, Welhan JA (1992) Helium isotopes in Icelandic geothermal systems: I. ^{3}He, gas chemistry, and ^{13}C relations. Geochim Cosmochim Acta 56:4221–4228
Ray M, Hilton D, Munoz J, Fischer T, Shaw A (2009) The effects of volatile recycling, degassing and crustal contamination on the helium and carbon geochemistry of hydrothermal fluids from the Southern Volcanic Zone of Chile. Chem Geol 266:38–49
Raynoud D, Jouzel J, Barnola JM, Chappellaz J, Delmas RJ, Lorius C (1993) The ice record of greenhouse gases. Science 259:926–934
Reynes ME (1980) A microearthquake study of the plate boundary, North Island, New Zealand. Geophys J R Astr Soc 63:1–22
Reynolds JH, Jeffrey PM, McCrory GA, Varga PM (1978) Improved charcoal trap for rare gas mass spectrometry. Rev Sci Instrum 49:547–548
Rice DD, Claypool GE (1981) Generation, accumulation and resource potential of biogenic gas. Am Assoc Petrol Geol Bull 65:5–25
Rison W, Craig H (1983) Helium isotopes and mantle volatiles in the Loihi Seamount and Hawaiian Island basalts and xenoliths. Earth Planet Sci Lett 66:407–426
Ritsema J, Allen R (2003) The elusive mantle plume. Earth Planet Sci Lett 207:1–12
Rizzo A, Caracausi A, Favara R, Martelli M, Paonita A, Paternoster M, Nuccio PM, Rosciglione A (2006) New insights into magma dynamics during last two eruptions of Mount Etna as inferred by geochemical monitoring from 2002 to 2005. Geochem Geophys Geosyst 7:Q06008. doi:06010.01029/02005GC001175
Rogers WA, Burtiz RS, Alpert D (1954) Diffusion coefficient, solubility and permeability for helium in glass. J Appl Phys 25:868–875
Rubey W (1951) Geologic history of sea water. Geol Soc Amer Bull 62:1111–1148
Rudnicki M, Elderfield H (1992) Helium, radon and manganese at the TAG and Snakepit hydrothermal vent fields, 26° and 23°N, Mid-Atlantic Ridge. Earth Planet Sci Lett 113:307–321
Saar MO, Castro MC, Hall CM, Manga M, Rose TP (2005) Quantifzing magmatic, crustal, and atmospheric helium contributions to volcanic aquifers using all stable noble gases: Implications for magmatism and groundwater flow. Geochem Geophys Geosyst 6:Q03008. doi:03010.01029/02004GC000828
Sakamoto M, Sano Y, Wakita H (1992) ^{3}He/^{4}He ratios distribution in and around the Hakone volcano. Geochem J 26:189–195
Sano Y, Marty B (1995) Origin of carbon in fumarolic gas from island arcs. Chem Geol 119:265–274
Sano Y, Nakajima J (2008) Geographical distribution of ^{3}He/^{4}He ratios and seismic tomography in Japan. Geochem J 42:51–60
Sano Y, Takahata N (2005) Measurements of noble gas solubility in seawater by a quadrupole mass spectrometer. J Oceanogr 61:465–473
Sano Y, Wakita H (1985a) Distribution of ^{3}He/^{4}He ratios and its implications for geotectonic structure of the Japanese Islands. J Geophys Res 90:8729–8741
Sano Y, Wakita H (1985b) Geographical distribution of ^{3}He/^{4}He ratios in Japan: imlications for arc tectonics and incipient magmatism. J Geophys Res 90:8729–8741
Sano Y, Wakita H (1987) Helium isotopes and heat flow on the ocean floor. Chem Geol 66:217–226
Sano Y, Wakita H (1988a) Helium isotope ratio and heat discharge rate in Hokkaido island, northeastern Japan. Geochem J 22:293–303
Sano Y, Wakita H (1988b) Precise measurement of helium isotopes in terrestrial gases. Bull Chem Soc Japan 61:1153–1157
Sano Y, Tominaga T, Wakita H (1982) Elemental and isotopic abundances of rare gses in natural gases obtained by a quadrapole mass spectrometer. Geochem J 16(6):279–286
Sano Y, Nakamura Y, Wakita H, Urabe A (1984) Helium-3 emissions related to volcanic activity. Science 224:150–151
Sano Y, Urabe A, Wakita H, Chiba H, Sakai H (1985) Chemical and isotopic composition of gases in geothermal fluids in Iceland. Geochem J 19:135–148
Sano Y, Wakita W, Giggenbach WF (1987) Island arc tectonics of New Zealand manifested in helium isotope ratios. Geochim Cosmochim Acta 51:1855–1860
Sano Y, Kusakabe M, Hirabayashi J, Nojiri Y, Shinohara H, Njine T, Tanyileke G (1990a) Helium and carbon fluxes in Lake Nyos, Cameroon: constraint on next gas burst. Earth Planet Sci Lett 99:303–314
Sano Y, Wakita H, Williams SN (1990b) Helium isotope systematics at Nevado del Ruiz volcano, Colombia:

implications for the volcanic hydrothermal system. J Volcanol Geotherm Res 42:41–52
Sano Y, Sakamoto M, Ishibashi J, Wakita H, Matsumoto R (1992) Helium isotope ratios of pore gases in deep sea sediments, Leg 128. Init Rep Deep Sea Drilling Proj 127(128):747–751
Sano Y, Hirabayashi J, Ohba T, Gamo T (1994) Carbon and helium isotopic ratios at Kusatsu-Shirane volcano, Japan. Appl Geochem 9:371–377
Sano Y, Gamo T, Notsu K, Wakita H (1995) Secular variations of carbon and helium isotopes at Izu-Oshima Volcano, Japan. J Volcanol Geoth Res 64(1–2):83–94
Sano Y, Gamo T, Williams SN (1997) Secular variations of helium and carbon isotopes at Galeras volcano, Colombia. J Volcanol Geotherm Res 77:255–266
Sano Y, Nishio Y, Sasaki A, Gamo T, Nagao K (1998) Helium and carbon isotope systematics at Ontake volcano, Japan. J Geophys Res 103:23,863–823,873
Sano Y, Takahata N, Nishio Y, Marty B (1998b) Nitrogen recycling in subduction zones. Geophys Res Lett 25:2289–2292
Sano Y, Takahata N, Nishio Y, Fischer TP, Williams SN (2001) Volcanic flux of nitrogen from the Earth. Chem Geol 171:263–271
Sano Y, Takahata N, Seno T (2006) Geographical distribution of $^{3}He/^{4}He$ ratios in the Chugoku district, Southwestern Japan. Pure Appl Geophys 163:745–757
Sano Y, Kameda A, Takahata N, Yamamoto J, Nakajima J (2009) Tracing extinct spreading center in SW Japan by helium-3 emanation. Chem Geol 266:50–56
Sarda P, Staudacher T, Allegre CJ (1988) Neon isotopes in submarine basalts. Earth Planet Sci Lett 91(1–2):73–88
Schilling JG (1973) Iceland mantle plume: geochemical study of the Reykjanes Ridge: Sr isotope geochemistry. Nature 246:104–107
Schoell M (1988) Multiple origins of methane in the Earth. Chem Geol 71(1–3):1–10
Shaw AM, Hilton DR, Fischer TP, Walker JA, Alvarado GE (2003) Contrasting He-C relationships in Nicaragua and Costa Rica: insights into C cycling through subduction zones. Earth Planet Sci Lett 214:499–513
Sherwood Lollar B, Frape SK, Wrise SM, Fritz P, Macko SA, Welhan JA (1993) Abiogenic methanogenesis in crystalline rocks. Geochim Cosmochim Acta 57:5087–5097
Shih TC (1980) Magnetic lineations in the Shikoku Basin. Initial Rep Deep Sea Drill Proj 58:783–788
Shimizu A, Sumino H, Nagao K, Notsu K, Mitropoulos P (2005) Variation in noble gas isotopic composition of gas samples from the Aegean arc, Greece. J Volcanol Geoth Res 140(4):321–339
Shiono K, Sugi N (1985) Life of oceanic plate: cooling time and assimilation time. Tectonophysics 112:35–50
Silveira G, Stutzmann E (2002) Anisotropic tomography of the Atlantic Ocean. Phys Earth Planet Inter 132:237–248
Simmons S, Sawkins F, Schlutter D (1987) Mantle-derived helium in two Peruvian hydrothermal ore deposits. Nature 329:429–432
Smith SP, Kennedy BM (1983) The solubility of noble gases in water and NaCl brine. Geochim Cosmochim Acta 47:503–515
Smith SP, Kennedy BM (1985) Noble gas evidence for two fluids in the Baca (Valles Caldera) geothermal reservoir. Geochim Cosmochim Acta 1985:893–902
Snyder G, Poreda R, Hunt A, Fehn U (2001) Regional variations in volatile composition: isotopic evidence for carbonate recycling in the Central American volcanic arc. G-cubed 2:2001GC000163
Snyder G, Poreda RJ, Fehn U, Hunt A (2003) Sources of nitrogen and methane in Central American geothermal settings: noble gas and 129I evidence for crustal and magmatic volatile components. G-cubed 4:9001. doi: 9010.1029/2002GC000363, 002003
Sorey ML, Kennedy BM, Evans WC, Farrar CD, Suemnicht GA (1993) Helium isotope and gas discharge variations associated with crustal unrest in Long_valley Caldera, California, 1989–1992. J Geophys Res 98:15871–15889
Sorey ML, Evans WC, Kennedy BM, Farrar CD, Hainsworth LJ, Hausback B (1998) Carbon dioxide and helium emissions from a reservoir of magmatic gases beneath Mammoth Mountain, California. J Geophys Res 103:15,303–315,323
Steblov GM, Kogan MG, King RW, Scholz CH, Bürgmann R, Frolov DI (2003) Imprint of the North American plate in Siberia revealed by GPS. Geophys Res Lett 30. doi:10.1029/2003GL017805
Stephen H, Stephen T (1963) Solubilities of inorganic and organic componds, I. Binary systems, Part I. Pergamon Press
Stuart FM, Turner G, Duckworth RC, Fallick AE (1994) Helium isotopes as tracers of trapped hydrothermal fluids in ocean- floor sulfides. Geology 22:823–826
Sugimura A, Matsuda T, Chinzei K, Nakamura K (1963) Quantitative distribution of late Cenozoic volcanic materials in Japan. Bull Volcanol 26:125–140
Sugisaki R (1978) Changing He/Ar and N_2/Ar ratios of fault air may be earthquake precursors. Nature 275:209–211
Sumino H, Notsu K, Nakai S, Sato M, Nagao K, Hosoe M, Wakita H (2004) Noble gas and carbon isotopes of fumarolic gas from Iwojima volcano, Izu-Ogasawara arc, Japan: implications for the origin of unusual arc magmatism. Chem Geol 209:153–157
Sun SS, Tatsumoto M, Schilling JG (1975) Mantle plume mixing along the Reykjanes Ridge axis: lead isotope evidence. Science 190:143–147
Svensen H, Planke S, Malthe-Sorenssen A, Jamtveit B, Myklebust R, Eldem TR, Rey SS (2004) Release of methane from a volcanic basin as a mechanism for initial Eocene global warming. Nature 429:542–545
Taira A, Tokuyama H, Soh W (1989) Accretion tectonics and evolution of Japan. In: Ben Avraham Z (ed) The

evolution of the Pacific Ocean Margins. Oxford University Press, New York, pp 100–123
Takahata N, Nishio Y, Yoshida N, Sano Y (1998) Precise isotopic measurements of nitrogen at the sub-nanomole level. Anal Sci 14:485–491
Takahata N, Yokochi R, Nishio Y, Sano Y (2003) Volatile element isotope systematics at Ontake volcano, Japan. Geochem J 37:299–310
Takahata N, Agarwal M, Nishizawa M, Shirai K, Inoue Y, Sano Y (2005) Helium-3 plume over the East Pacific Rise at 25°S. Geophys Res Lett 32:L11608
Taran YA (1985) Fumarolic activity of the Koryak volcano, Kamchatka, in 1983. Volcanol Seismol 5:82–85
Taran YA (2009) Geochemistry of volcanic and hydrothermal fluids and volatile budget of the Kamchatka-Kuril subduction zone. Geochim Cosmochim Acta 73(4):1067–1094
Taran YA, Giggenbach WF (2003) Geochemistry of light hydrocarbons in subduction-related volcanic and hydrothermal fluids. Soc Econ Geol Special Publ 10:61–74
Taran YA, Znamenskiy VS, Yurova LM (1996) Geochemical model of the hydrothermal system of Baransky volcano, Iturup, Kuril islands. Volcanol Seismol 17:471–496
Taran Y, Fischer TP, Pokrovsky B, Sano Y, Armienta MA, Macias JL (1998) Geochemistry of the volcano-hydrothermal system of El Chichon Volcano, Chiapas, Mexico. Bull Volcanol 59(6):436–449
Taran Y, Gavilanes JC, Cortes A (2002a) Chemical and isotopic composition of fumarolic gases and the SO_2 flux from Volcan de Colima, Mexico, between the 1994 and 1998 eruptions. J Volcanol Geoth Res 117(1–2):105–119
Taran YA, Fischer TP, Cienfuegos E, Morales P (2002b) Geochemistry of hydrothermal fluids from an intraplate ocean island: Everman volcano, Socorro Island, Mexico. Chem Geol 188:51–63
Taran Y, Varley NR, Inguaggiato S, Cienfuegos E (2010) Geochemistry of H_2- and CH_4-enriched hydrothermal fluids of Socorro Island, Revillagigedo Archipelago, Mexico. Evidence for serpentinization and abiogenic methane. Geofluids 10(4):542–542–555
Tatsumi Y, Sakuyama M, Fukuyama H, Kushiro I (1983) Generation of arc basalt magmas and thermal structure of the mantle wedge in subduction zones. J Geophys Res 88:5815–5825
Tatsumoto M (1966) Genetic relation of oceanic basalts as indicated by lead isotopes. Science 153:1094–1095
Tedesco D (1995) Fluid geochemistry at Vulcano Island: a change in volcanic regime or continuous fluctuations in the mixing of different systems? J Geophys Res 100:4157–4167
Tedesco D, Nagao K (1996) Radiogenic ^{4}He, ^{21}Ne and ^{40}Ar in fumarolic gases on Vulcano: implication for the presence of continental crust beneath the island. Earth Planet Sci Lett 144(3–4):517–528
Tedesco D, Scarsi P (1999) Intensive gas sampling of noble gases and carbon at Vulcano Island (southern Italy). J Geophys Res 104 B5:10, 499–410, 510
Tedesco D, Allard P, Sano Y, Wakita H, Pece R (1990) Helium-3 in subaerial and submarine fumaroles of Campi Flegrei caldera, Italy. Geochim Cosmochim Acta 54(4):1105–1116
Tedesco D, Nagao K, Scarsi P (1998) Noble gas isotopic ratios from historical lavas and fumaroles at Mount Vesuvius (southern Italy): constraints for current and future volcanic activity. Earth Planet Sci Lett 164 (1–2):61–78
Thorne MS, Garnero EJ, Grand SP (2004) Geographic correlation between hot spots and deep mantle lateral shear-wave velocity gradients. Phys Earth Planet Inter 146:47–63
Torgersen T, Jenkins WJ (1982) Helium isotopes in geothermal systems: Iceland, the Geysers, Raft River, and Steamboat Springs. Geochim Cosmochim Acta 46:739–748
Torgersen T, Lupton JE, Sheppard DS, Giggenbach WF (1982) Helium isotope variations in the thermal areas of New Zealand. J Volcanol Geotherm Res 12(3–4):283–298
Trull TW, Kurz MD (1999) Isotopic fractionation accompanying helium diffusion in basaltic glass. J Mol Struct 485–486:555–567
Tsunogai U, Ishibashi J, Wakita H, Gamo T, Watanabe A, Kajimura T, Kanayama S, Sakai H (1994) Peculiar features of Suiyo Seamount hydrothermal fluids, Izu-Bonin Arc: differences from subaerial volcanism. Earth Planet Sci Lett 126:289–301
Umeda K, Ogawa Y, Asamori K, Oikawa T (2006) Aqueous fluids derived from a subducting slab: observed high ^{3}He emanation and conductive anomaly in a non-volcanic region, Kii Peninsula southwest Japan. J Volcan Geotherm Res 149:47–61
Umeda K, Asamori K, Ninomiya A, Kanazawa S, Oikawa T (2007) Multiple lines of evidence for crustal magma storage beneath the Mesozoic crystalline Iide Mountains, northeast Japan. J Geophys Res - Solid Earth 112(B5):9
Urabe A, Tominaga T, Nakamura Y, Wakita H (1985) Chemical compositions of natural gases in Japan. Geochem J 19(1):11–25
van Soest MC, Hilton DR, Kreulen R (1998) Tracing crustal and slab contributions to arc magmatism in the Lesser Antilles island arc using helium and carbon relationships in geothermal fluids. Geochim Cosmochim Acta 62:3323–3335
Wakita H, Sano Y (1983) ^{3}He/^{4}He ratios in CH_4-rich natural gases suggest magmatic origin. Nature 305:792–794
Wakita H, Sano Y, Mizoue M (1987) High 3He emanation and seismic swarm activities observed in a non-volcanic, frontal arc region. J Geophys Res 92:12539–12546
Wakita H, Sano Y, Urabe A, Nakamura Y (1990) Origin of methane-rich natural gas in Japan: formation of gas

fields due to large-scale submarine volcanism. Appl Geochem 5(3):263–278
Wallace LM, Beavan J, McCaffrey R, Darby D (2004) Subduction zone coupling and tectonic block rotations in the North Island, New Zealand. J Geophys Res 109:B12406. doi:12410.11029/12004JB003241
Weiss RF (1970) The solubility of nitrogen, oxygen and argon in water and seawater. Deep-Sea Res 17:721–735
Welhan JA (1988) Origins of methane in hydrothermal systems. Chem Geol 71:183–198
Welhan JA, Craig H (1982) Biogenic methane in mid-ocean ridge hydrothermal fluids. In: Gwillian WJ (ed) Deep-source-gas workshop technical proceedings, pp 122–129
Welhan JA, Craig H (1983) Methane, hydrogen and helium in hydrothermal fluids. In: Rona PA, Boström K, Laubier L, Smith KL (eds) Hydrothermal processes at seafloor spreading centers. NATO Conf/Ser IV, Mar Sci, vol 12, pp 391–409. Pleanum, New York
Welhan JA, Lupton JE (1987) Light hydrocarbon gases in the Guaymas Basin hydrothermal fluids-thermogenic versus abiogenic origin. Am Assoc Pet Geol Bull 71:215–223
Welhan J, Craig H, Kim K (1984) Hydrothermal gases at 11°N and 13°N on the East Pacific Rise. EOS 65:45
Welhan JA, Poreda RJ, Rison W, Craig H (1988) Helium isotopes in geothermal and volcanic gases of the Western United States, II. Long Valley Caldera. J Volcanol Geoth Res 34(3–4):201–209
Williams H, McBirney AR (1979) Volcanology. Freeman Cooper & Co., San Francisco, p 397
Williams S, Sano Y, Wakita H (1987) Helium-3 emission from Nevado del Ruiz volcano, Colombia. Geophys Res Lett 14:1035–1038
Williams SN, Calvache V ML, Sturchio NC, Zapata G JA, Mendez F RA, Calvache O B, Londoño C A, Gil C F, Sano Y (1990) Premonitory geochemical evidence of magmatic reactivation of Galeras volcano, Colombia. EOS (Transactions, American Geophysical Union) 74(43):690
Wilson JT (1963) A possible origin of the Hawaiian Islands. Can J Phys 41:863–870
Winckler G, Aeschbach-Hertig W, Kipfer R, Botz R, Rubel A, Bayer R, Stoffers P (2001) Constraints on origin and evolution of Red Sea brines from helium and argon isotopes. Earth Planet Sci Lett 184:671–683
Yamano M, Honda S, Uyeda S (1984) Nankai trough—as a hot trench? Mar Geophys Res 6:187–203
Yamasaki T, Seno T (2003) Double seismic zones and dehydration embrittlement of the subducting slab. J Geophys Res 108:2212. doi:2210.1029/2002JB001918
Yang TF (2008) Recent progress in the application of gas geochemistry: examples from Taiwan and the 9th international gas geochemistry conference. Geofluids 8:219–229
Yang TF, Lan TF, Lee HF, Fu CC, Chuang PH, Lo CH, Chen CH, Chen CTA, Lee CS (2005) Gas compositions and helium isotopic ratios of fluid samples around Kueishantao, NE offshore Taiwan and its tectonic implications. Geochem J 39:469–480
Yang T, Shen Y, van der Lee S, Solomon SC, Hung S-H (2006) Upper mantle structure beneath the Azores hotspot from finite-frequency seismic tomography. Earth Planet Sci Lett 250:11–26
Yoshii T (1977) Crust and upper-mantle structure beneath northeastern Japan (in Japanese). Kagaku 47:170–176
Yuan H, Dueker K (2005) Teleseismic P-wave tomogram of the Yellowstone plume. Geophys Res Lett 32:L07304
Zimmer MM, Fischer TP, Hilton DR, Alvarado GE, Sharp ZD, Walker JA (2004) Nitrogen systematics and gas fluxes of subduction zones: insights from Costa Rica arc volatiles. Geochem Geophys Geosyst 5(5). doi:10.1029/2003GC000651
Zindler A, Hart S (1986) Chemical geodynamics. Annu Rev Earth Planet Sci 14:493–571
Zolotov MY, Shock EL (2000) A thermodynamic assessment of the potential synthesis of condensed hydrocarbons during cooling and dilution of volcanic gases. J Geophys Res 105:539–559

Noble Gases and Halogens in Fluid Inclusions: A Journey Through the Earth's Crust

Mark A. Kendrick and Pete Burnard

Abstract

Fluid inclusions provide the only means possible for sampling fluids from the Earth's deep-interior and ancient past. Noble gas isotope analysis can provide quantitative information about the sources of volatile components in fluid inclusions (e.g. atmosphere, crust and mantle), whereas halogens provide complementary information about the fluids, acquisition of salinity and/or the presence of (I-rich) organic components. The aims of this chapter are to: (1) review methods for analysis of noble gases in fluid inclusions, and halogen analysis by the 'noble gas method' (extended ^{40}Ar–^{39}Ar methodology); and (2) summarise case studies of noble gases and halogens in fluid inclusions. The case studies include hydrothermal fluids involved in ore genesis in a range of geological environments encompassing mid-ocean ridge vents, sedimentary basins, near-pluton magmatic environments and metamorphic settings, as well as fluid inclusions in eclogite facies high-grade terranes relevant to subduction recycling processes. In contrast to modern ground waters, the fluid inclusion data suggest that most crustal fluids source some (additional) atmospheric noble gases within the crust (from sediments and hydrous minerals formed during seawater-alteration), and that low salinity fluids can acquire significant Br, as well as I, from organic-rich (meta-)sediments. Fluid–rock interactions are an important control on the composition of deep-crustal fluids; however, the orders of magnitude variation in noble gas isotope compositions and halogen abundances mean that they can preserve information about fluid sources that is overprinted in other stable and radiogenic isotope systems.

M. A. Kendrick (✉)
School of Earth Sciences, University of Melbourne, Victoria, Australia
e-mail: mark.kendrick@unimelb.edu.au

P. Burnard
CRPG- CNRS, Nancy-Université, 54501, Vandoeuvre-lès-Nancy Cedex, France
e-mail: peteb@crpg.cnrs-nancy.fr

1 Introduction

The study of noble gases and halogens dissolved in crustal fluids has found wide application in a range of hydrogeological disciplines (e.g. Kipfer et al. 2002; Ballentine et al. 2002); these

P. Burnard (ed.), *The Noble Gases as Geochemical Tracers*, Advances in Isotope Geochemistry,
DOI: 10.1007/978-3-642-28836-4_11, © Springer-Verlag Berlin Heidelberg 2013

applications can be considerably extended into deeper crustal environments, or the geological past, by the analysis of fluid inclusions. This chapter aims to illustrate: (1) how the noble gas composition of fluid inclusions can help constrain the origin of the major volatile phases, such as H_2O and CO_2, in fluid inclusions (e.g. Kelley et al. 1986; Simmons et al. 1987; Turner et al. 1993); and (2) how additional insights on fluid origins and acquisition of salinity are provided by simultaneous analysis of halogens (Cl, Br, I) with noble gases (e.g. Böhlke and Irwin 1992a; Kendrick et al. 2001a).

Fluid inclusions were initially investigated to search for ancient atmospheric noble gas components (Cadogan 1977; Butterfield and Turner 1985; Turner 1988), and then to study ore deposits (e.g. Kelley et al. 1986; Simmons et al. 1987). The discovery of Simmons et al. (1987) that hydrothermal minerals can preserve mantle-derived ^{3}He proved to be of particular interest for investigating ore genesis, because the mantle is frequently invoked as an important source of heat or exotic metals (e.g. Pirajno 2000). Hydrothermal ore deposits form in a variety of geologic environments from near surface basinal to mid-crustal greenschist or amphibolite facies magmato-metamorphic settings. Fluid inclusions enable metamorphic and magmatic fluids to be sampled from these environments, and in some cases trapping occurs before atmospheric noble gases are introduced via mixing with surface-derived groundwater. The range of fluid inclusions investigated for noble gases has recently been further expanded to include fluid inclusions formed during extensional deformation (Pili et al. 2011), and eclogite facies metamorphism relevant to subduction-recycling processes (Sumino et al. 2010; Kendrick et al. 2011d). As a result, fluid inclusions from ore deposits and metamorphic rocks have greatly expanded the range of crustal fluid types investigated for noble gases.

Basic information concerning the composition of the fluid inclusions major phases (H_2O, CO_2, CH_4, N_2 etc.), salts, and the trapping pressure and temperature conditions can be obtained from petrographic observations of the fluid inclusions and microthermometric heating and cooling experiments (Fig. 1; e.g. Roedder 1984; Bodnar 2003). Furthermore, textural evidence or mineralogical associations can provide information on the relative timing of fluid entrapment (Roedder 1984).

In this chapter we provide an overview of the methods used to analyse noble gases in fluid inclusions and discuss two complementary approaches: (1) noble gas analyses focused on using He–Ar isotope systematics to quantify the presence of mantle and atmospheric components in crustal fluids (e.g. Stuart and Turner 1992; Turner et al. 1993; Stuart et al. 1995; Burnard et al. 1999; Hu et al. 2004; Graupner et al. 2006); and (2) combined noble gas and halogen analysis, which is applied to irradiated samples (e.g. Böhlke and Irwin 1992b; Turner and Bannon 1992; Kendrick et al. 2001a). The combined noble gas and halogen approach represents an extension of ^{40}Ar–^{39}Ar methodology (Table 1; Kendrick 2012), and it enables noble gases to be more closely linked with other fluid tracers than has previously been possible.

Fluid inclusions are providing important new insights on the behaviour of noble gases in the crust (Kendrick et al. 2011a, d). This is illustrated primarily through noble gas and halogen data that illuminate the diverse fluid processes responsible for ore deposition in a range of sedimentary, magmatic and metamorphic environments.

2 Sample Selection

The most important consideration for selecting fluid inclusion bearing samples is that the sample material contains fluid inclusions related to the geological process being investigated. However, the susceptibility of different minerals to post-entrapment modification must also be considered. The two possible modifications of greatest concern for noble gas analysis are: (1) post-entrapment leakage of the light helium isotopes, which are known to diffuse through some of the minerals most commonly used for fluid inclusion studies (e.g. quartz) at relatively

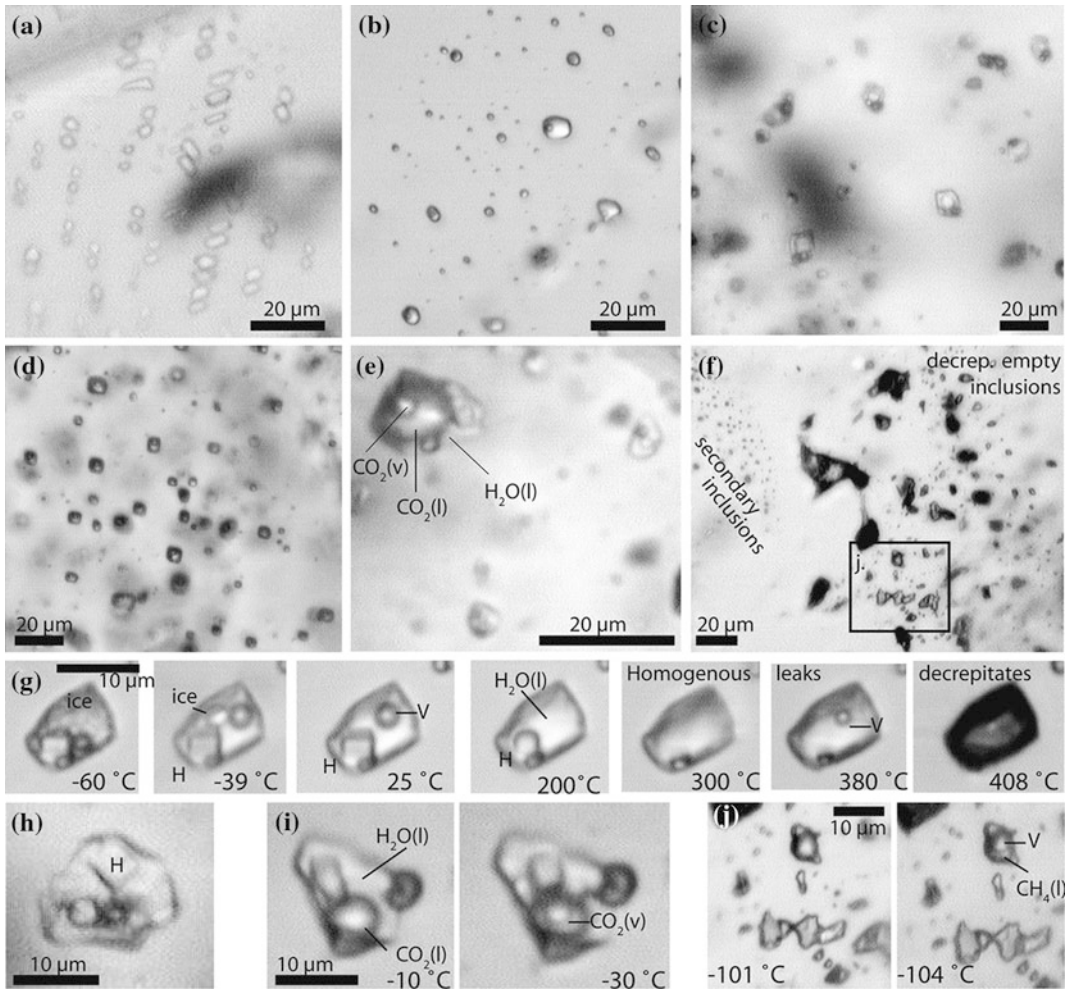

Fig. 1 Fluid inclusions observed in transmitted light during microthermometry. **a** Low temperature monophase water inclusions in birefringent calcite. **b** Two-phase liquid-vapour fluid inclusions. **c** High salinity fluid inclusions with multiple daughter minerals. **d** Liquid CO_2 fluid inclusions. **e** mixed liquid CO_2 and H_2O fluid inclusion containing daughter minerals. **f** Large decrepitated fluid inclusions, medium sized CH_4–N_2 fluid inclusions (see **j**), and a trail of small secondary inclusions. **g** A single daughter bearing fluid inclusion during microthermometry, note homogenisation by halite dissolution and then leakage. **h** Multi-solid fluid inclusion. **i** Mixed CO_2–H_2O fluid inclusion above and below CO_2 homogenisation temperature. **j** Liquid CH_4 fluid inclusion showing critical homogenistion at −102 °C, thus indicating the presence of ~30 vol.% N_2 (Kendrick et al. 2011b). *Abbreviations v* vapour, *l* liquid, *H* halite

low temperatures; and (2) modification of the fluid inclusions noble gas isotope signature by post-entrapment decay of U, Th or K which produce a range of radiogenic noble gas isotopes (e.g. ^{4}He, ^{21}Ne*, ^{40}Ar*, ^{136}Xe*; Ballentine and Burnard 2002).

Note that an asterix is commonly used to denote the radiogenic component of a noble gas isotope. For example, ^{40}Ar has atmospheric and radiogenic sources, whereas ^{40}Ar* has been corrected for atmospheric contributions (e.g. ^{40}Ar* = ^{40}Ar—atmospheric ^{40}Ar). In most fluid

Table 1 Noble gas proxy isotopes produced by irradiation

Parent element	Nuclear reaction	Proxy isotope
Cl	$^{37}Cl(n, \gamma)^{38}Cl(\beta)^{38}Ar$	$^{38}Ar_{Cl}$
Br	$^{79}Br(n, \gamma)^{80}Br(\beta)^{80}Kr$	$^{80}Kr_{Br}$
I	$^{127}I(n, \gamma)^{128}I(\beta)^{128}Xe$	$^{128}Xe_{I}$
K	$^{39}K(n,p)^{39}Ar$	$^{39}Ar_{K}$
Ca	$^{40}Ca(n,\alpha)^{37}Ar$	$^{37}Ar_{Ca}$
U	Fission	$^{134}Xe_{U}$

Extended ^{40} Ar–^{39} Ar methodology enables simultaneous measurement of the halogens, K and U with naturally occurring noble gas isotopes (^{36} Ar, ^{40} Ar, ^{84} Kr, ^{129} Xe, ^{130} Xe) in irradiated samples (Kendrick 2012)

inclusion studies, $^{40}Ar^{*}$ is broadly equivalent to excess ^{40}Ar ($^{40}Ar_{E}$), where, excess ^{40}Ar has been corrected for both atmospheric ^{40}Ar and radiogenic ^{40}Ar produced by in situ decay of ^{40}K (Kendrick et al. 2006b). An asterix is not used for the ^{4}He isotope because the atmospheric contribution to ^{4}He is negligible and ^{4}He is usually assumed to have a purely radiogenic origin in the crust.

2.1 Fluid Inclusion Characterisation

Fluid inclusions can have complex parageneses, primary fluid inclusions trapped during mineral growth are typically identified because they occur in isolated clusters or define mineral growth planes (Roedder 1984). Secondary fluid inclusions are trapped along annealed fractures, and post-date mineral growth (Roedder 1984). Secondary fluid inclusions have ambiguous timing and are often introduced after the geological event of interest; however, secondary fluid inclusions can provide useful information in some situations. For example, secondary inclusions can record the passage of multiple fluid pulses in evolving hydrothermal systems, and might preserve fluids more closely related to gold deposition than primary fluid inclusions in some orogenic gold deposits, where gold is hosted on late fractures within quartz veins (Polito et al. 2001; Fairmaid et al. 2011).

Fluid inclusion bearing samples are usually analysed by either in vacuo crushing or stepped heating of bulk samples. As a result, it is advantageous if sample materials are dominated by a single fluid inclusion type, or a single assemblage of co-genetic inclusions. Sequential analyses (e.g. repeat crushing analyses or stepped heating) can be undertaken to help characterise more complex samples. However, limitations imposed by imperfect sample material need to be considered during interpretation of nobal gas data. It is therefore essential that fluid inclusion samples used for noble gas analysis are studied petrographically in sufficient detail that the nature of the fluid inclusion assemblage can be documented.

2.2 Post-entrapment He Loss

Fluid inclusions can be subject to post-entrapment modifications such as 'necking down' or physical rupture/leakage, which can be identified from fluid inclusions with irregular shapes and variable liquid/vapour volume ratios (e.g. Roedder 1984). In addition, water can leak out of metamorphic fluid inclusions by diffusion of disassociated H^{+} ions, which can significantly alter the fluid inclusions oxidation state or degree of fill (e.g. Mavrogenes and Bodnar 1994; Scambelluri et al. 2001). Fortunately, the heavy noble gases (Ne, Ar, Kr, Xe) have lower diffusivities than H^{+}, and appear to be less prone to diffusional leakage than water (e.g. Kendrick et al. 2011d). However, it is not uncommon for fluid inclusions in quartz to have anomalously low He/Ar ratios, or very low helium abundances that suggest the light helium isotopes are prone to leakage from fluid inclusions in many geological environments (Stuart and Turner 1992; Graupner et al. 2006; Kendrick et al. 2011a).

Previous work indicates dense sulphide minerals, including pyrite and arsenopyrite, reliably trap helium over geological time periods (10^7–10^9 years; Turner and Stuart 1992; Simmons et al. 1987; Burnard and Polya 2004; Kendrick et al. 2011b). Native gold, chalcopyrite, sphalerite, scheelite, fluorite and magnetite also appear suitable helium traps (Stuart and Turner 1992; Eugster et al. 1995; Pettke et al. 1997; Kendrick et al. 2002a, b, 2011c). However, many of these minerals are opaque meaning it is difficult to characterise the nature of their fluid inclusions.

The preservation of helium in minerals like quartz, calcite and feldspar, that are suitable for petrographic study of fluid inclusions is variable (e.g. Stuart and Turner 1992; Graupner et al. 2006; Kendrick et al. 2011a,b). Helium retention probably depends on the nature of lattice dislocations intersecting individual fluid inclusions, and no petrographic criteria have yet been identified for selecting reliable samples.

The best way to test for possible helium leakage is to analyse the full suite of noble gases (He, Ne, Ar, Kr, Xe). If fluid inclusions preserve ^{4}He/^{40}Ar* ratios close to the crustal production ratio, or the He/Ar, Ne/Ar, Kr/Ar and Xe/Ar ratios show systematic behaviour consistent with uniform fractionation in a fluid phase, arguments can be made that significant helium loss has not occurred (e.g. Kendrick et al. 2011b). A real concern is that if helium leakage has occurred, the measured ^{3}He/^{4}He ratio of the trapped fluid could have been compromised by exchange with external fluids.

2.3 Post-entrapment Production of Radiogenic Isotopes

Fluid inclusions trap sufficiently high abundances of noble gas in solution that in situ production of radiogenic noble gas isotopes (e.g. ^{40}Ar*, ^{4}He) from decay of dissolved K, U and Th is only a concern under exceptional circumstances (e.g. Precambrian U deposits). However, it is not unusual for a mineral to contain significant K, U or Th either within its lattice or within minor mineral impurities, and great care must be taken during analysis, to avoid mixing noble gases trapped in fluid inclusions with radiogenic noble gases produced in the mineral host.

Reliable fluid inclusion analyses are most easily obtained from young samples of minerals like quartz, calcite, olivine or sulphide that contain abundant fluid inclusions and very little K, U or Th. However, fluid inclusion and matrix noble gas components can be separated, to some extent, by in vacuum crushing analyses. Optimal separation of the fluid inclusion component is achieved by crushing fluid inclusion rich samples for short durations, because prolonged crushing eventually releases significant noble gas from the mineral matrix (cf. Stuart et al. 1995; Yokochi et al. 2005; Kendrick and Phillips 2009). *In situ* radiogenic noble gas components can be quantified and corrected for if the samples K, Th and U concentrations are measured. The extended ^{40}Ar–^{39}Ar method enables simultaneous measurement of Ar isotopes with K and U (Table 1). Stepped heating enables determination of K and U in mineral as well as fluid inclusions, and wide application of this technique has shown that in situ production of radiogenic ^{40}Ar is negligible for the majority of Paleoproterozoic to recent quartz samples (e.g. Kendrick et al. 2006b, c, 2007, 2008a, b, 2011a, b).

Finally, in addition to ^{4}He ingrowth, there is a potential to produce ^{3}He by neutron capture on Li {^{6}Li(n,α)^{3}He} inside fluid inclusions within some neutron-rich geological environments. This can be significant because ^{3}He can have a very low abundance in hydrothermal fluids and ^{6}Li has a relatively large n-capture cross section (941.1 barns; Chang 2011). High ^{3}He/^{4}He production ratios are most likely in Li-rich fluid inclusions surrounded by U-rich host rocks (Fig. 2; Hu et al. 2009), because U can supply highly penetrative neutrons (without ^{4}He) from distances of $\sim$1 m in silicate rocks (Andrews et al. 1982; Andrews and Kay 1982). However, production *rates* are low, e.g. <10 ^{3}He atoms $g^{-1}a^{-1}$ is estimated for fluid inclusions containing 50 ppm Li surrounded by a host rock with 10 ppm U, meaning in situ ^{3}He production

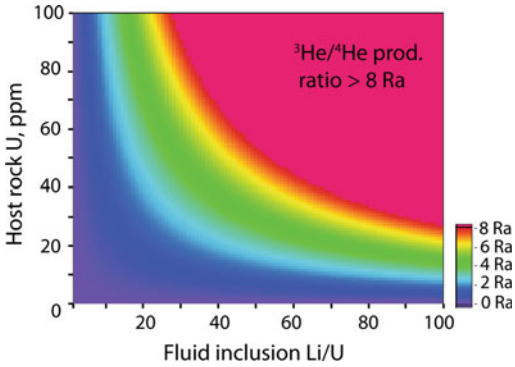

Fig. 2 Contours of ^{3}He/^{4}He production ratios for fluid inclusions with variable Li/U and different host rock U concentrations (which controls the neutron flux). The neutron flux in the rock is calculated following Ballentine and Burnard (2002) for a typical rhyolite composition assuming that U +Th are hosted in silicate phases. Elevated ^{3}He/^{4}He production ratios are possible in Li-rich fluid inclusions, but ^{3}He production rates are low (see text)

is only significant for fluid inclusions with low helium concentrations (see Hu et al. 2009). A second noble gas isotope that could feasibly be generated by this mechanism is ^{36}Ar, which is produced by neutron capture on ^{35}Cl (Fontes et al. 1991; Irwin and Reynolds 1995).

2.4 Post-entrapment Modification by Cosmogenic Production

Cosmogenic production represents the final in situ source of noble gas isotopes, but is only significant for ^{3}He and ^{21}Ne in terrestrial samples (Ozima and Podosek 2002). Cosmic rays are rapidly attenuated in the Earth's atmosphere and significant cosmogenic isotopes are only generated in samples that are within ~1 m of the Earth's surface (Ozima and Podosek 2002). As a result, this complexity can be avoided by selecting shielded samples from rapidly eroding environments, drill core or underground workings.

For He and Ne isotope analysis, it is best to avoid samples that have previously been exposed at the surface, or close to the surface, for periods of more than a few thousand years. The low abundances of ^{3}He and ^{21}Ne in mineral samples, means that relatively minor cosmogenic production could bias results. For example, ^{3}He contents in sulphide minerals are typically on the order of 0.5–50 $\times$ 10^6 atoms g^{-1}. An equivalent concentration could be generated by only ~5–500 kyr exposure at sea level at high latitude (see Niedermann 2002).

3 Analysis

3.1 Sample Preparation

Noble gases in fluid inclusions can be analysed in bulk mineral separates by either *in vacuo* crushing or furnace heating. High purity mineral separates are obtained by hand picking under a binocular microscope. The grain size required for a high purity mineral separate is determined by the sample material. Grains larger than a few mm are avoided because they might contain hidden impurities and can be difficult to load into crushing devices, whereas Crushing samples too finely will open some of the largest fluid inclusions prior to analysis. Scheidegger et al. (2010) demonstrated crushing speleotherm material to <300 μm reduced the presence of undesirable modern air contaminants (Sect. 3.6) by removing inter-crystal air cavities and that increased adsorption of atmospheric noble gases onto fine material was not a significant problem. Mineral separates are usually cleaned in acetone and distilled water with or without ultrasonic agitation; acid cleaning is not possible for soluble sulphide or carbonate minerals.

The irradiation procedure used for combined noble gas and halogen analysis is analogous to ^{40}Ar–^{39}Ar dating (McDougall and Harrison 1999), except Cd-shielding is avoided in order to maximise production of halogen-derived noble gas isotopes from low energy thermal neutrons (Böhlke and Irwin 1992b; Johnson et al. 2000; Kendrick 2012). The noble gas proxy isotopes used to measure Cl, Br, I, K, Ca and U in irradiated samples are summarised in Table 1, and the method is described in detail by Kendrick (2012). Irradiated samples analysed for halogens and the more abundant heavy noble gases can be

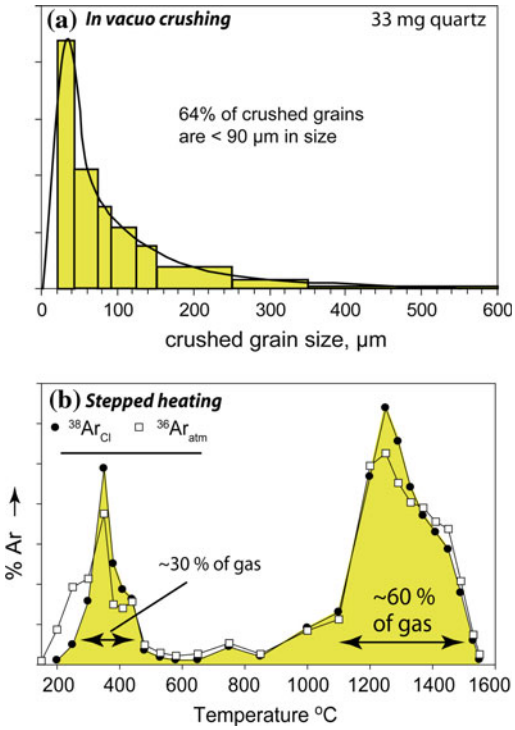

Fig. 3 Noble gas release by: **a** in vacuo crushing in a modified Nupro® valve, note the resulting skewed grain size distribution. **b** Degassing during stepped heating irradiated quartz. The low temperature peak is attributed to noble gas release during decrepitation of >3–4 µm sized fluid inclusions. The high temperature release is attributed to decrepitation of very small fluid inclusions (<1–2 µm), or gases trapped within fluid inclusions that have already leaked and then re-annealed (Fig. 1g; Kendrick et al. 2006c). The relative size of these peaks varies between samples (Kendrick et al. 2006c; Fairmaid et al. 2011). Note that the area under the lines in a and b is equal to 100 % of the sample gas

as small as 10–30 mg. In contrast, noble gas analysis of unirradiated samples for scarce He and Ne isotopes typically require 0.3–1.0 g of sample material. Once loaded into the ultra high vacuum for analysis, the samples are baked at temperatures of <120 °C for 12–48 h, to remove surface contaminants and achieve ultra high vacuum. Higher temperatures are avoided to prevent rupture of fluid inclusions by thermal decrepitation.

3.2 Noble Gas Extraction Methods

Noble gases can be extracted from samples by *in vacuo* crushing, stepped heating or laser ablation, and combinations of these techniques can be employed to provide information about the distribution of noble gases and halogens in the sample (e.g. fluid versus mineral inclusions or different fluid inclusion populations; e.g. Kendrick et al. 2001b, 2006c; Kendrick 2012).

Several crushing apparatus have been designed for fluid inclusion analysis (see Burnard et al. this volume). The different devices vary in efficiency (Kendrick and Phillips 2009), but a significant proportion of the smallest fluid inclusions (often $\ll$10 µm) remain in the coarser fractions of crushed samples in all devices (Fig. 3a). Samples are typically analysed sequentially by multiple crushes to characterise variation in the fluid inclusion population.

Stepped heating can be used to analyse quartz hosted fluid inclusions by thermal decrepitation because quartz it is stable to high temperature and contains negligible K, U or noble gas in its lattice (Fig. 3b; Kendrick et al. 2006c). In contrast, stepped heating of sulphides, sulphates or carbonate can produce potentially damaging pressures of gas (H_2S or CO_2) and is therefore not recommended. Stepped heating can help resolve different fluid inclusion types that have different decrepitation temperatures. For example, liquid carbon dioxide fluid inclusions typically decrepitate at lower temperatures than similarly sized water fluid inclusions. However, fluid inclusion decrepitation temperature is also size dependent (Bodnar et al. 1989). Aqueous fluid inclusions of >5 µm in diameter typically decrepitate between ~200 and ≤700 °C (Stuart et al. 1995; Kendrick et al. 2006c), but very small fluid inclusions of <1–2 µm in diameter are often undecrepitated during microthermometry at temperatures of ~600 °C, and it appears gases are only released from these small inclusions, at temperatures of >1,200 °C

Table 2 Diagnostic noble gas isotope ratios

	$^{3}He/^{4}He$ (R/Ra)	$^{20}Ne/^{22}Ne$	$^{21}Ne/^{22}Ne$	$^{40}Ar/^{36}Ar$
Atmosphere	1	9.8	0.029	299
Crust	<0.1	<9.8	>0.029	299–100,000
Mantle (MORB)	8	12.5	0.058	30,000–40,000

The ^{3} He/^{4} He ratio (R/Ra) is given relative to the atmospheric ratio (Ra) of 1.4×10^{-6} (Mamyrin et al. 1970). Recent determinations of ^{40} Ar/^{36} Ar in modern air are 299 (Lee et al. 2006; Valkiers et al. 2010), compared to the lower value of 296 that is still widely used in the literature (Nier 1950). Atmospheric and representative mantle values from various sources (Graham 2002; Ozima and Podosek 2002; Holland and Ballentine 2006)

(Fig. 3b; Kendrick et al. 2006c). A similar 'bimodal' decrepitation profile has been reported for fluid inclusions in olivine (Tolstikhin et al. 2010); however, there is considerable variability in the degassing profiles of quartz (Fig. 3b; Kendrick et al. 2006c; Fisher and Kendrick 2008; Fairmaid et al. 2011), and bimodal degassing is not a general feature of anhydrous minerals (Stuart et al. 1995). Note that most mineral inclusions, and the mineral lattice, are degassed between ~700 and 1,600 °C depending on their size and composition (see Kendrick et al. 2006b).

Laser ablation was applied in the pioneering studies of Böhlke and Irwin (1992a, b, c) to measure argon isotopes and halogens in ore deposit fluid inclusion wafers. However, based on the quantity of gas released and the performance of 266 nm lasers at that time, it is likely that this was achieved on groups of syngenetic, rather than individual fluid inclusions in the majority of cases (Böhlke and Irwin (1992a, b, c; Irwin and Reynolds 1995; Irwin and Roedder 1995; Kendrick et al. 2001b). More recently, 193 and 213 nm lasers which enable very controlled ablation of quartz have been used to investigate the presence of excess ^{40}Ar in ultra high pressure minerals such as quartz and kyanite (e.g. Sherlock and Kelley 2002). However, routine analysis of individual fluid inclusions remains a distant goal, because in comparison to magmatic glasses which can contain CO_2 vesicles with diameters ranging from >100 μm to mm-size (Burnard et al. 1994, 1997; Raquin et al. 2008), fluid inclusions in crustal environments are often smaller than 10–20 μm making analysis of the scarcest noble gas isotopes (e.g. ^{3}He and ^{22}Ne) unfeasible in individual fluid inclusions.

3.3 Purification

Noble gases released from fluid inclusions are purified using Zr-Al getter pumps that remove the major volatiles (e.g. H_2O, CO_2). A typical purification protocol would be to expose the extracted sample gas to a hot (250 °C) SAES getter for 20 min; then cool the getter over 15 min, prior to final clean up on a second Zr-Al getter pump at 250 °C for 5 min (Stuart et al. 1995). Relatively long gettering times are required due to the slow diffusion of water through the extraction line.

Stepped heating calcite or sulphide releases very large volumes of CO_2 or H_2S, even when the maximum extraction temperature is kept below the mineral breakdown temperature. There are no standard procedures for cleaning up these gases but hot (450 °C) Ag wool is efficient for removing H_2S, and 'flow-through' traps are significantly more effective than 'finger-type' traps (Phillips and Miller 2006; Pujol et al. 2009).

The purified noble gases are usually cryogenically separated into at least light (He+Ne) and heavy (Ar, Kr, Xe) fractions for analysis (e.g. Burnard et al. 1999; Kendrick et al. 2011a; Kendrick 2012). Neon isotope analyses are best if separated from helium using a cryogenic trap; if separation is not possible, the standard must have He/Ne ratios similar to the samples, otherwise uncalibrated mass fractionation effects can occur (Hiyagon 1989).

3.4 Precision Relative to Natural Variation

Fluid inclusion noble gas isotope ratios of helium and argon vary over at least two orders of magnitude (Ballentine et al. 2002; Ozima and Podosek 2002). As a result analytical precision, which varies from best values of <1%, to much higher values, depending on the amount of gas available for analysis, rarely limits data interpretation. However, caution is required for neon isotope analysis because of possible interferences from CO_2 or $^{40}Ar^{++}$ (e.g. Osawa 2004).

Detection limits for halogen measurement by the noble gas method are superior to most conventional techniques and enable Br/Cl and I/Cl ratio measurements with a precision of ~1% in 10 mg sized samples (Böhlke and Irwin 1992a; Johnson et al. 2000; Kendrick 2012; Kendrick et al. 2012). Detection limits for K or U are more variable and depend on the ability to resolve the irradiation produced $^{39}Ar_K$ or $^{134}Xe_U$ proxy isotopes from interfering isotopes such as $^{39}Ar_{Ca}$ and atmospheric xenon (Kendrick 2012).

Machine blanks associated with noble gas measurement are variable depending on recent instrument usage and the noble gas extraction method. Blanks are often very small or negligible for laser ablation and crushing undertaken in modified Nupro® valves (Kendrick et al. 2011c; Kendrick 2012). However, blank corrections sometimes control the uncertainty associated with He and Ne isotope measurements (Kendrick et al. 2011a, b) and are usually important in high temperature heating steps (>1,400 °C).

Robust blank corrections should be 'active' and mimic the sample analysis as closely as possible, by actuating the crusher, firing the laser, moving the parts required to place a sample in the furnace and using an empty foil packet if samples are wrapped in foil. In practice, reported corrections often represent 'passive' blanks in which for example, the crusher was not actuated. Stuart et al. (1995) demonstrated crushing inclusion free quartz using modified Nupro® valves did not contribute to the procedural blank of this crushing device. However, the use of passive blanks is less than satisfactory for some crushing procedures in which friction between moving parts could generate significant blank. Inadequate blank corrections represent a possible source of air-like contaminants present in some noble gas analyses (Sect. 3.5).

3.5 Modern Air Contamination

Noble gas analyses of fluid inclusion bearing samples sometimes give variable compositions that can be partly explained by the presence of a modern air contaminant (e.g. Kelley et al. 1986; Turner and Bannon 1992). Air contamination is usually only a concern for samples with very low noble gas abundances (Ballentine and Barfod 2000). However, modern air contaminants could be significant in fluid inclusion samples if the sample contains 'empty' fluid inclusions filled by air. In cases where modern air contaminants are significant, the noble gases define mixing lines that intersect the composition of modern air (e.g. Turner et al. 1993; Irwin and Roedder 1995).

Analysis of multiple noble gas isotopes (±Cl) enables the presence of modern air contaminants to be rigorously tested. Scheidegger et al. (2010) demonstrated crushing speleotherm material to <300 μm enabled determination of reliable noble gas concentrations for fluid inclusions, because air was efficiently removed from intergrain boundaries. If present, modern air contaminants are usually removed by the first crushing or heating steps of coarser grained materials analysed by crushing or stepped heating in vacuum (e.g. Kendrick et al. 2001a, 2002a). Examples where the presence of modern air contaminants has been conclusively excluded using multi-isotope correlations are highlighted below (e.g. Kendrick et al. 2011a, d). These studies suggest that while caution is required, modern air contamination can be overcome by careful sample preparation, and is significantly less pervasive in fluid inclusion samples than originally envisioned.

3.6 Noble Gas Concentrations

The majority of noble gas analyses reported for fluid inclusion bearing samples report the concentration of noble gas per gram of sample. As this parameter is strongly influenced by the number of fluid inclusions in the sample, and the efficiency of in vacuo crushing (Fig. 3a), it has very little geological significance.

Noble gas concentrations in fluid inclusions can be determined if H_2O is measured manometrically (e.g. Stuart et al. 1995). However, adsorption of water throughout the extraction line represents a significant challenge for these measurements and has only recently been overcome (see Kluge et al. 2008; Scheidegger et al. 2010).

A major advantage of measuring halogens simultaneously with noble gases is that the ^{36}Ar concentration of aqueous fluid inclusions can be calculated based on the measured $Cl/^{36}Ar$ ratio and fluid inclusion salinity (Kelley et al. 1986; Böhlke and Irwin 1992a; Turner and Bannon 1992; Kendrick et al. 2001a, 2002a, b, 2007). The accuracy of the concentration measurement obtained by this technique depends on the homogeneity of the fluid inclusion assemblage and the possible presence of modern air contaminants. The influence of air contaminants is minimised by using the highest $Cl/^{36}Ar$ ratio measured during sequential analysis of a sampled. Accuracy of 10–50 % is suggested for some samples, and as fluid inclusion ^{36}Ar concentrations vary by orders of magnitude, this has provided useful constraints on fluid processes (Sect. 5).

4 Data Terminology and Definitions

4.1 Noble Gas Components

The noble gases have extremely variable isotopic signatures with characteristic values in the mantle, crust and atmosphere (Ozima and Podosek 2002). Combined helium and argon isotope analysis, or neon isotope analysis, can be used to deconvolve contributions from all three reservoirs (Table 2). Crustal fluid inclusions commonly contain mixtures of noble gases from two or more of these reservoirs meaning mixing diagrams are widely used in interpretation of noble gas data. Mixing lines always appear straight in three isotope diagrams that have a common denominator (e.g. $^3He/^4He$ versus $^{40}Ar/^4He$), but mixing trends have curved trajectories in four isotope diagrams (e.g. $^3He/^4He$ versus $^{40}Ar/^{36}Ar$; Langmuir et al. 1978).

Radiogenic noble gas isotopes have predictable abundance ratios (e.g. $^4He/^{40}Ar^*$, $^{21}Ne^*/^{40}Ar^*$ and $^{136}Xe^*/^{40}Ar^*$) controlled by the (U + Th)/K ratio of the host rock (asterix denote radiogenic noble gas isotopes corrected for atmospheric contributions). In contrast, the non-radiogenic noble gases have characteristic abundance ratios (e.g. $^{20}Ne/^{36}Ar$, $^{84}Kr/^{36}Ar$, $^{130}Xe/^{36}Ar$) in air and air saturated water (Ozima and Podosek 2002), but variable compositions in rocks (Table 3). Noble gas abundance ratios can provide useful constraints on fluid sources and physical processes that fractionate noble gases, including H_2O–CO_2 immiscibility (e.g. Kendrick et al. 2001a, 2011a).

1. Air saturated water

Meteoric water and seawater are characterised by atmospheric noble gas isotope signatures (Table 2) and slightly different abundance ratios ($^{20}Ne/^{36}Ar$, $^{84}Kr/^{36}Ar$, $^{130}Xe/^{36}Ar$), because noble gas solubility is influenced by salinity (Smith and Kennedy 1983). However, because both meteoric water and seawater are characterised by enrichment in heavy/light noble gases relative to air, and noble gas solubility is also temperature dependent (Smith and Kennedy 1983), it is difficult to confidently resolve meteoric water from seawater based on noble gas abundance ratios alone. These fluids are therefore commonly referred to with the single moniker of Air Saturated Water (ASW).

2. Modified ASW

Modified Air Saturated Water (MASW) refers to fluids that preserve some of the features of ASW but have been modified during crustal

Table 3 Non-radiogenic noble gases in selected fluid and rock reservoirs

	^{36}Ar mol g^{-1} ($\times 10^{-12}$)	^{20}Ne/^{36}Ar	^{84}Kr/^{36}Ar	^{130}Xe/^{36}Ar	Notes
Air		0.524	0.0207	0.000113	1
Air saturated water					
Meteroic water (0 °C)	75	0.122	0.0428	0.000474	2
Seawater (25 °C)	34	0.175	0.0359	0.000348	3
Bittern Brine (29 °C)	7	0.249	0.0341	0.000285	4
Lithologies					
Dry marine sediments (n = 16)	0.2–12	0.003–0.77	0.04–0.29	0.0007–0.004	5
Carbonate rock (n = 3)	0.1–200	0.05–19	0.02–0.05	Nd.	6
Shale (n = 12)	0.04–6	0.05–6	0.02–0.4	0.0007–0.15	7
Meta-sediments (n = 5)	0.01–0.4	0.2–1.1	nd.	nd.	8
Altered-basalt	0.06–0.3	0.01–0.07	0.03–0.07	0.001–0.004	9
Antigorite-serpentinites (n = 5)	0.09–5	0.06–0.1	0.03–0.06	0.0004–0.002	10
Crystalline basement	0.01–0.7	0.2–6.5	0.01–0.11	0.0001–0.009	11

Notes
1–3 data from Ozima and Podosek (2002)
4 Based on 29 °C NaCl brines (Smith and Kennedy 1983)
5 Unconsolidated sediments or mud (Matsuda and Nagao 1986; Amari and Ozima 1988; Staudacher and Allègre 1988; Schwarz et al. 2005)
6 (Zhou and Ye 2002)
7 (Podosek et al. 1980, 1981)
8 metamorphosed pelagic sediments (Schwarz et al. 2005)
9 (Staudacher and Allègre 1988)
10 (Kendrick et al. 2011d)
11 Includes metamorphic rocks, granites and gneisses, range of relative abundance ratios estimated from Fig. 2 of Drescher et al. (1998)

residence (e.g. Burnard and Polya 2004). The helium isotope system is more easily modified, than heavier noble gases, because the scarce helium isotopes have a very low abundance in ASW (Ozima and Podosek 2002). In addition, α-particles recoil a mean distance of ~20 μm from their parent U nucleus in silicate minerals (Ziegler 1980), and helium has a higher diffusivity than the heavy noble gases (Ozima and Podosek 2002). These processes combine to mean the relative helium abundance in groundwater is altered much more quickly than the relative abundances of the heavy noble gases, and groundwaters rarely preserve either the ^{4}He/^{36}Ar, or atmospheric ^{3}He/^{4}He ratio of ASW. Modifications to noble gas abundance ratios (e.g. ^{20}Ne/^{36}Ar), with initially air saturation values, can occur by diffusion (Torgersen et al. 2004), adsorption/desorption processes (Pitre and Pinti 2010), or interaction with hydrocarbons (Bosch and Mazor 1988).

3. Crustal components

A range of noble gas isotopes are produced in the crust by radioactive decay of U, Th and K (^{4}He and ^{40}Ar*), U fisson (^{136}Xe*, ^{134}Xe*, ^{132}Xe*, ^{131}Xe* and ^{86}Kr*) and α–or n-reactions (including ^{21}Ne* and ^{22}Ne*). For simplicity, noble gas isotopes produced by all these pathways are sometimes collectively referred to simply as radiogenic noble gas isotopes (see Ballentine and Burnard 2002 for review).

Radiogenic noble gas isotopes (e.g. ^{4}He, ^{21}Ne*, ^{40}Ar* and ^{136}Xe*) are released to groundwaters by several process: α-particles (e.g. ^{4}He nuclei) recoil ~20 μm from their parent nuclide (e.g. U or Th) in silicate rocks (Ziegler 1980); noble gases are also released by diffusion, mineral breakdown/dissolution reactions and as a result of fracturing (Honda et al. 1982; Torgersen and O'Donnell 1991). The crust has a mean ^{4}He/^{40}Ar* production ratio of ~5,

but low temperature fluids ($T \leq 200$ °C) are typically enriched in $^{4}He/^{40}Ar^{*}$ as a result of preferential ^{4}He release by recoil ejection and diffusion (Ballentine and Burnard 2002).

The radiogenic noble gas isotopes are often referred to as the crustal noble gas component. However, crustal rocks, especially sediments and rocks altered by ASW (e.g. altered volcanic rocks), also contain substantial quantities of the non-radiogenic atmospheric noble gas isotopes (e.g. ^{20}Ne, ^{36}Ar, ^{84}Kr, ^{130}Xe; Podosek et al. 1980, 1981; Staudacher and Allègre 1988; Kendrick et al. 2011d). The relative importance of these crustally sourced 'atmospheric' noble gas isotopes is negligible in most shallow groundwaters (e.g. Pinti et al. 1997; Kipfer et al. 2002), but can be significant in some sedimentary environments (Kennedy et al. 2002), and is of overwhelming importance in metamorphic fluids (Sect. 5.5; Kendrick et al. 2011d). The ranges of ^{36}Ar abundance in selected fluid and rock reservoirs are summarised in Table 3.

4. Mantle components

Large mantle components are easily recognised in crustal fluids from $^{3}He/^{4}He$ and $^{20}Ne/^{22}Ne$ ratios of more than the atmospheric values (Table 2). Smaller components of mantle-derived noble gas can still be identified from $^{3}He/^{4}He$ ratios of more than $\sim$0.1 Ra (that is typical of the crust) and elevated $^{3}He/^{36}Ar$ ratios. This is because helium has such a low concentration (and low $^{3}He/^{36}Ar$) in ASW, that $^{3}He/^{4}He$ ratios are usually controlled by mixing only mantle and crustal noble gas components.

It has been common practice in the fluid inclusion noble gas literature to use 'mantle' and 'magmatic' almost inter-changeably. However, this practice is discouraged because mantle-derived ^{3}He is common in rift-related sedimentary basins (Oxburgh et al. 1986; O'Nions and Oxburgh 1988), and is decoupled from aqueous basinal fluids in these settings. In addition, crustal melts formed as a result of crustal thickening, without input of mantle heat, will not be associated with ^{3}He anomalies (Stuart et al. 1995), implying some magmatic fluids have crustal $^{3}He/^{4}He$ ratios (Kendrick et al. 2011b).

Despite these caveats, fluid inclusion $^{3}He/^{4}He$ ratios have provided a litmus test for evaluating the involvement of magmatic fluids in many ore deposits (e.g. Stuart et al. 1995; Burnard et al. 1999; Burnard and Polya 2004), and there is no other technique that is more sensitive than the $^{3}He/^{4}He$ ratio for detecting mantle-derived material in the crust.

4.1.1 Fluid Types

In comparison to the terminology traditionally used in noble gas geochemistry which identifies the ultimate origin of noble gases as being atmospheric (non-radiogenic isotopes), crustal (radiogenic isotopes) or mantle (^{3}He), there are multiple ways of designating fluids in the geological literature.

Fluids of interest for understanding ore genesis or metamorphic processes include: meteoric water and seawater (ASW), sedimentary formation waters (which are also known as oil field brines or basinal brines), metamorphic fluids (H_2O or CO_2) produced by breakdown of hydrous or carbonate minerals; and magmatic fluids which can have highly variable salinity and CO_2 content (Cline and Bodnar 1991; Baker 2002). The distinction of these different fluids on the basis of noble gas signatures is illustrated through a series of case studies in Sect. 5.

4.2 Halogens and the Origin of Salinity

Like the noble gases, the halogens (Cl, Br, I) are incompatible elements that have characteristic ratios that vary by orders of magnitude between different geological reservoirs (Table 4). Simultaneous measurement of halogens with noble gases has proven advantageous because while noble gases help constrain fluid source (Sect. 4.1), halogens help constrain the fluids aquisition of salinity (e.g. Böhlke and Irwin 1992c; Yardley et al. 1993; Graupner et al. 2006; Fairmaid et al. 2011; Kendrick et al. 2011c; Fu et al. 2012). The origin of salinity is of special interest in ore deposits because the Cl-ligand is essential for efficient transport of base metals (e.g. Yardley 2005).

Table 4 Halogens in selected fluid and rock reservoirs

	Halogen concentrations	Br/Cl ($\times 10^{-3}$) Molar ratios	I/Cl ($\times 10^{-6}$)	Notes
Seawater	3.5 wt% salt	1.54 ± 0.02	0.84 ± 0.04	1
Bittern brine	~30 wt% salt	1.5–12	0.8–7	2
Halite	100 wt% NaCl	0.05	0.002	3
Rock salt (halite)	100 wt% NaCl	0.04–0.15	0.2	4
Sylvite	100 wt% KCl	0.3	0.07	5
Carnallite	100 wt% $KMgCl_3.6(H_2O)$	0.45	1–2	6
Organic matter	100's of ppm Br + I	(Br/I ~ 1–10)		7
Mica/amphibole	0 to ~1wt% Cl or F	0.05–0.2	1–12	8
Metm. devol. fluids	<5–20 wt% salt	Variable	Variable	9
Metm. desicc. fluids	<100 wt% salt	<40	Variable	10
Magmatic fluids	2–60 wt% salt	0.6–1.8	10–70	11
MORB	10–1,000 ppm Cl	1.6 ± 0.2	40 ± 30	12

Notes

1 Seawater Br/Cl (McCaffrey et al. 1986); 19,350 ppm Cl, 67.3 ppm Br (Drever 1997), 58 ppb I (Fuge and Johnson 1986)

2 Bittern brines produced by evaporation of seawater beyond the point of halite saturation (Zherebtsova and Volkova 1966; Nissenbaum 1977; McCaffrey et al. 1986)

3 Based on precipitation from seawater and partition coefficients of $D_{Br/Cl} \sim 0.03$ and $D_{I/Cl} \sim 0.003$ (where $D_{Br/Cl} = Br/Cl_{halite}/Br/Cl_{seawater}$; Holser 1979; Hermann 1980; Siemann and Schramm 2000)

4 Rock salt I/Cl inferred from fluid data of (Bohlke and Irwin 1992a). Br/Cl based on measure values (McCaffrey et al. 1986) and measured Br abundances of 40–200 ppm (Fontes and Matray 1993; Siemann 2003)

5 Based on precipitation from seawater and partition coefficients of $D_{Br/Cl} \sim 0.2$ and $D_{I/Cl} \sim 0.09$ (Holser 1979)

6 Based on precipitation from seawater and partition coefficients of $D_{Br/Cl} \sim 0.3$ and $D_{I/Cl} \sim 2$–3 (Holser 1979)

7 Concentrations in organic-rich sediments and Br/I in sediments and sedimentary marine pore fluids (Fuge and Johnson 1986; Martin et al. 1993; Muramatsu et al. 2007).

8 Very limited data (n = 2; Kendrick 2012)

9 The salinity range estimated for fluids produced by breakdown of hydrous minerals does not include halogen rich lithologies such as serpentinites or meta-evaporites (Kendrick et al. 2006a).

10 Fluid produced by metamorphic desication e.g. partitioning of $H_2O > Cl > Br$ into mica or amphibole (Markl and Bucher 1998; Svensen et al. 2001), the maximum Br/Cl is inferred from Kendrick et al. (2006a).

11 Variable salinities are expected in magmatic fluids (Cline and Bodnar 1991), reported Br/Cl and I/Cl (Irwin and Roedder 1995; Kendrick et al. 2001a; Nahnybida et al. 2009)

12 Composition of Maquarie Island basalt glasses (Kendrick et al. 2012), see also Schilling et al. (1978) and Jambon et al. (1995)

The principal processes controlling the salinity and Br/Cl–I/Cl composition of surface-derived groundwaters are sub-aerial evaporation and subsequent fluid interaction with evaporite minerals and organic matter (Hanor 1994; Kendrick et al. 2011c). Evaporitic brines preserve seawater Br/Cl and I/Cl ratios up until the point of halite saturation (~30 wt% salts; Zherebtsova and Volkova 1966; McCaffrey et al. 1986). The low compatibility of Br and I in halite means that continued evaporation produces 'residual' halite-saturated brines (bittern brines) that evolve progressively higher Br/Cl and I/Cl ratios up to maximums of $\sim 11 \times 10^{-3}$ and 7×10^{-6}, respectively (Table 4; Zherebtsova and Volkova 1966; Nissenbaum 1977; McCaffrey et al. 1986). In contrast, evaporite deposits have generally low Br/Cl and I/Cl ratios, with the Br/Cl and I/Cl composition depending on the mineralogy of the deposit (e.g. sylvite accomodates more Br than halite; Holser 1979), the presence of Br- and I-rich fluid inclusions (Bein et al. 1991), and the extent of post-depositional evaporite recrystalisation

which preferentially mobilises remaining Br and I relative to Cl (Table 4; e.g. Fontes and Matray 1993). Organic-rich sedimentary rocks represent the Earth's dominant iodine reservoir and organic matter contains high ppm-levels of both I and Br (Collins et al. 1971; Fuge and Johnson 1986; Martin et al. 1993; Muramatsu et al. 2007). Fluid interaction with organic matter does not influence salinity but represents the dominant control of fluid I/Cl, and can exert a significant influence on the Br/Cl ratio (Kendrick et al. 2011c).

Metamorphic fluids can have varied halogen composition and salinity. Fluids produced by devolatilisation of hydrous crustal minerals usually have low salinities (e.g. <5–10 wt% salts; Kendrick et al. 2006a), but higher salinities can be achieved in halogen rich lithologies like serpentinites (Scambelluri et al. 1997) and meta-evaporites (Oliver 1995), or if retrograde hydration reactions lead to fluid desication concentrating salts in a diminishing fluid phase (Markl and Bucher 1998; Svensen et al. 2001). Some metamorphic fluids have higher salinities and higher Br/Cl ratios than can be achieved by sub-aerial evaporation, as a result of preferential incorportation of $H_2O > Cl > Br$ into mica or amphibole (Svensen et al. 2001;Markl and Bucher 1998). The involvement of organic matter remains the dominant control on I/Cl in metamorphic fluids and organic halogen components can sometimes be inferred from characteristic Br/I ratios of between about 1 and 10 (Fairmaid et al. 2011).

The halogen signature of magmatic fluids have been investigated by several workers (e.g. Irwin and Roedder 1995; Banks et al. 2000; Kendrick et al. 2001a; Nahnybida et al. 2009). It seems magmatic fluids have consistently low I/Cl ratios that are close to mantle values (Kendrick et al. 2012), but Br/Cl ratios that encompass mantle-like and lower values (Table 4; Sect. 5.4). The variation in Br/Cl depends in part on the composition of the host rocks through which the magma intrudes (Banks et al. 2000). Phase separation, degassing and crystallisation of Cl-bearing minerals are also likely to contribute to variation in the Br/Cl and I/Cl composition of magmatic fluids; however, systematic variations in halogen ratios that can be explained by these processes have not been documented in fluid inclusions. Furthermore, experimental studies yield contradictory results for fractionation of Br/Cl during phase separation (see Berndt and Seyfried 1990; Liebscher et al. 2006).

5 Fluids in the Earth's Crust: Top to Bottom

The purposes of this section are to provide a historical perspective for noble gas fluid inclusion studies, illustrate how noble gases and halogens distinguish different fluid types and show that fluid inclusions are providing new insights into the behavior of noble gases in a wide variety of crustal environments. The environments investigated are loosely ordered according to their depths in the Earth's crust and the section concludes with a brief comparison of unusual fluid compositions sampled by both fluid inclusions and bore holes.

5.1 Ground Water

Surface-derived fluids in sedimentary aquifers, aged from a few hundred to many thousands of years, commonly preserve non-radiogenic noble gas isotope (^{20}Ne, ^{36}Ar, ^{84}Kr, ^{130}Xe) concentrations close to air saturation levels (e.g. Kipfer et al. 2002). As noble gas solubility is dependent on salinity as well as temperature, many studies have focused on low salinity ground waters and used noble gas concentrations to re-construct the palaeo-temperature of surface recharge (e.g. Andrews and Lee 1979; Aeschbach-Hertig et al. 2000). This information can be combined with groundwater dating techniques (Phillips and Castro 2003), to reconstruct changes in palaeo-climate, and is now being extended even further back into the geological record through the concentration of noble gases in speleothem fluid inclusions (Kluge et al. 2008; Scheidegger et al. 2010, 2011; Brennwald et al. this volume).

Noble gases have higher solubility in gaseous and liquid hydrocarbons than in aqueous fluids

(Smith and Kennedy 1983; Kharaka and Specht 1988; Ozima and Podosek 2002). As the relative solubility of noble gases is systematically related to atomic mass, noble gas concentrations and fractionation of noble gas relative abundance ratios (e.g. $^{20}Ne/^{36}Ar$, $^{84}Kr/^{36}Ar$ and $^{130}Xe/^{36}Ar$), can provide important constraints on groundwater-hydrocarbon interactions (Bosch and Mazor 1988; Ballentine et al. 2002).

Model ages can be calculated for groundwater in sedimentary aquifers based on the fluids ^{4}He concentration (Andrews and Lee 1979; Castro et al. 2007). Models used to calculate ages have varying levels of sophistication. The simplest case assumes the fluid originated as air saturated water with negligible ^{4}He at time zero, and that ^{4}He is acquired from the aquifer rocks at a predictable rate approximating its production within the aquifer. In such a case, the concentration of ^{4}He in the fluid depends only on the residence time of the fluid in the aquifer, the aquifer porosity and aquifer U and Th content (Andrews and Lee 1979). Similar groundwater model ages can also be calculated from the concentrations of the $^{21}Ne^*$ or $^{40}Ar^*$ isotopes. However, important uncertainties in model ages relate to the partial retention of noble gas in aquifer rocks, which is more significant for $^{40}Ar^* > {}^{21}Ne^* > {}^{4}He$; and the possible flux of these isotopes from outside the aquifer (Phillips and Castro 2003; Torgersen 2010).

5.1.1 Applicability to Hydrothermal Fluids?

The well documented behaviour of noble gases in ground water, summarized above and in detail by Kipfer et al. (2002) and Ballentine et al. (2002), cannot be easily applied to higher temperature crustal fluids or hydrothermal ore deposits. Reasons for caution include: (1) most hydrothermal systems have much higher temperatures than <100 °C ground waters; (2) many of the ground waters examined for noble gases preserve O and H isotope signatures similar to meteoric water (e.g. Pinti et al. 1997; Zuber et al. 1997), indicating limited chemical interaction with aquifer rocks, which contrasts starkly with ore fluids (e.g. Taylor 1997); (3) few studies have examined the noble gas systematics of saline ground waters with >10 wt % salts (Zaikowski et al. 1987; Pinti et al. 2011); (4) some 'saline formation waters' involved in ore genesis are much older than typical groundwater (e.g. millions of years old), having possibly had connate origins at the time of sediment deposition in some cases (Hanor 1994; Kharaka and Hanor 2003); (5) hydrothermal fluids with magmato-metamorphic origins did not have a surface origins, meaning initially ASW $^{20}Ne/^{36}Ar$, $^{84}Kr/^{36}Ar$, $^{130}Xe/^{36}Ar$ abundance ratios can not be assumed; (6) the relative solubilities of noble gases in aqueous and carbonic fluids at the pressures and temperatures relevant to magmato-metamorphic environments are poorly known; and (7) the prevalence of fracture generated permeability in most ore deposits and deeper crustal environments means noble gases accumulate within fluids in a fundamentally different way compared to sedimentary aquifers. Ground water model ages are not valid for fracture-hosted fluid regimes because ^{4}He and other radiogenic noble gas isotopes collect in rocks and minerals isolated from fluid flow (Andrews et al. 1989); and stored ^{4}He is rapidly released from locations proximal to newly propagating fractures (Torgersen and O'Donnell 1991). As a result, radiogenic noble gas isotopes (^{4}He, $^{21}Ne^*$, $^{40}Ar^*$, ^{136}Xe) can collect in fracture-hosted fluids much more quickly than they are produced.

5.2 Sediment-Hosted Ore Deposits

Mississippi Valley-type (MVT) ore deposits include a broad family of sediment-hosted epigenetic Pb-Zn-fluorite-barite deposits that form at depths of less than ~1–2 km (Heyl et al. 1974; Sverjensky 1986; Leach et al. 2001). The majority of these deposits are carbonate-hosted but minor mineralisation is found within the Lamotte sandstone beneath the Viburnum trend MVTs of the USA (Viets and Leach 1990), and similar sandstone-hosted Pb-Zn mineralisation is found at Laisvall, and in similar deposits, in Scandinavia (Kendrick et al. 2005).

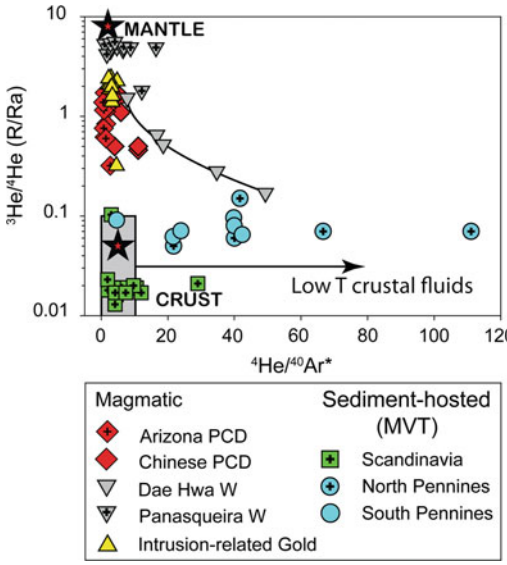

Fig. 4 The ^{3}He/^{4}He versus ^{4}He/^{40}Ar* systematics of selected magmatic and formation water derived ore fluids (Stuart and Turner 1992; Stuart et al. 1995; Burnard and Polya 2004; Hu et al. 1998, 2004; Kendrick et al. 2002b, 2005). The *stars* represent the mean MORB mantle and crustal production ratios, the *grey box* represents the range of compositions expected in crust with variable K:U:Li compositions. Low temperature fluids are typically enriched in ^{4}He relative to ^{40}Ar* (Ballentine and Burnard 2002). Analyses obtained by in vacuo crushing

Mississippi Valley-type ore deposits are associated with $CaCl_2$-rich fluid inclusions with typical salinities of 10–30 wt% salts and homogenisation temperatures of ~60 to ~200 °C (Roedder 1971a; Heyl et al. 1974; Leach and Rowan 1986; Kendrick et al. 2011c). Liquid hydrocarbons are present in the fluid inclusions of some deposits (Gize and Barnes 1987; Etminan and Hoffmann 1989). The ore fluids have δD and δ^{18}O indistinguishable from sedimentary formation waters (Taylor 1997), which can attain Pb and Zn concentrations of ~100 ppm (Carpenter et al. 1974; Ferguson et al. 1993; Hitchon 2006), but even higher Pb and Zn concentrations (e.g. 1,000's of ppm) are reported for ore fluids (Wilkinson et al. 2009).

Mississippi Valley-Type mineralisation occurs in several tectonic settings. In some cases, continent-scale brine migration over 100's of km, occurs through foreland basins as a result of topography driven fluid flow triggered by distal orogenesis (Leach and Rowan 1986; Garven and Raffensperger 1997; Leach et al. 2001). However, the Lennard Shelf deposits in Australia are associated with extension (Wallace et al. 2002), and fluorite-rich MVT ore deposits, typified by the Illinois-Kentucky (USA) and Pennine (UK) districts have been attributed to active rifting with possible involvement of mantle volatiles (Russell and Smith 1979; Plumlee et al. 1995).

The majority of MVT deposits investigated, including fluorite-rich MVT from the Pennines (UK) and Asturias in Spain, are associated with fluid inclusions that have typical crustal ^{3}He/^{4}He ratios of 0.01–0.1 (Fig. 4; Stuart and Turner 1992; Kendrick et al. 2002b, 2005; Sanchez et al. 2010). However, the Illinois-Kentucky fluorspar deposit is associated with fluid inclusions that have slightly elevated ^{3}He/^{4}He ratios of 0.17–0.35 Ra (Kendrick et al. 2002a), indicating a mantle helium component of up to ~6 % in this deposit (Kendrick et al. 2002a). The fluid inclusions from all of the investigated MVT deposits have ^{4}He/^{40}Ar* ratios of much greater than the crustal production ratio of ~5 (Fig. 4), which is consistent with the expectation that ^{4}He collects in low temperature fluids preferentially compared to ^{40}Ar* (Stuart and Turner 1992; Kendrick et al. 2002a, 2005).

Fluid inclusions in carbonate-hosted MVT have typical ^{40}Ar/^{36}Ar of 300–2,000, with the majority <1,000 (Fig. 5b; Böhlke and Irwin 1992a; Stuart and Turner 1992; Turner and Bannon 1992b; Kendrick et al. 2002a, b, 2011c). This range of values is similar to that documented in carbonate sediments (Matsuda and Nagao 1986; Zhou and Ye 2002), and in saline fluids or gases from a large number of sedimentary basins (e.g. Zaikowski et al. 1987; Bosch and Mazor 1988; Ballentine et al. 1991; Zuber et al. 1997 Pinti et al. 2011). In contrast, fluid inclusions in the sandstone-hosted Scandinavian deposits have maximum ^{40}Ar/^{36}Ar of 16,000 (Kendrick et al. 2005). Despite the obvious difference in host lithology, the concentration of ^{40}Ar* in fluid inclusions from the Scandinavian deposits was estimated to exceed

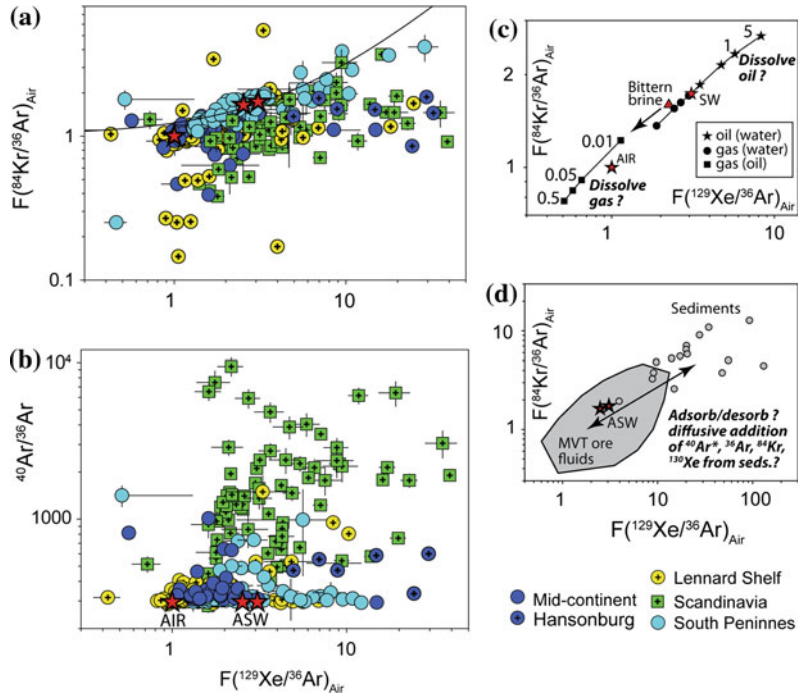

Fig. 5 Noble gas systematics of MVT fluid inclusions. **a** The $^{130}Xe/^{36}Ar$ versus $^{84}Kr/^{36}Ar$ values are expressed as fractionation values such that Air has F = 1 [e.g. $F(Ng/^{36}Ar)_{air} = (Ng/^{36}Ar)_{sample}/(Ng/^{36}Ar)_{air}$; Ng = ^{130}Xe or ^{84}Kr]. Air and air saturated water (*ASW*) are shown as stars, note that the best fit regression through the South Pennine data does not intersect air. **b** $^{40}Ar/^{36}Ar$ is not correlated with $^{129}Xe/^{36}Ar$ indicating the data are not simply explained by the presence of modern air contamination. **c** Noble gas abundance ratios are fractionated by increasing salinity (bittern brine (*triangle*) and seawater (*Star SW*) are shown) or dissolution of noble gas rich hydrocarbons [*stars* oil equilibrated with ASW; *circles* gas equilibrated with ASW; *square* gas equilibrated with oil; fractionation factors calculated for different volume ratios (Bosch and Mazor 1988; Ballentine et al. 2002)]. **d** Noble gas abundance ratios are also fractionated during interaction with sedimentary rocks. Data obtained by laser ablation (Böhlke and Irwin 1992a) and sequential crushing of multiple samples (see Fig. 6; Kendrick et al. 2002a, b, 2005, 2011d). Sedimentary rock data in (**d**) are from Matsuda and Nagao (1986) and Podosek et al. (1980)

what could be reasonably derived from the K-poor sandstone host-rocks or interbedded shale (Kendrick et al. 2005). The high $^{40}Ar/^{36}Ar$ ratios were therefore attributed to fluid interaction with old, K-rich basement rocks, underlying the deposit (Kendrick et al. 2005). This may be significant because the Scandinavian deposits formed close to the Caledonian orogen and in contrast to most MVT deposits, tectonic pumping of fluids through the basement was more likely to have been a driver of fluid flow (Kendrick et al. 2005).

The ore fluids from the Hansonburg MVT were suggested to have maintained air saturation ^{36}Ar and ^{84}Kr concentrations (Böhlke and Irwin 1992a), but the fluids are significantly enriched in $^{130}Xe/^{36}Ar$ (Fig. 5a, b). In contrast, ore fluids in all the other MVT investigated have estimated ^{36}Ar concentrations of greater than air saturation levels (Turner and Bannon 1992; Kendrick et al. 2002a, b, 2005, 2011). The elevated ^{36}Ar concentrations were attributed to the presence of modern air contaminants in several of the early studies (e.g. Sect. 3.5; Stuart and Turner 1992; Kendrick et al. 2002a, b). However, the extensive database now available indicates $^{40}Ar/^{36}Ar$ is not simply correlated with $^{130}Xe/^{36}Ar$ (Fig. 5b), suggesting air contamination is not a major control on measured noble gas compositions. Instead, higher than ASW ^{36}Ar concentrations

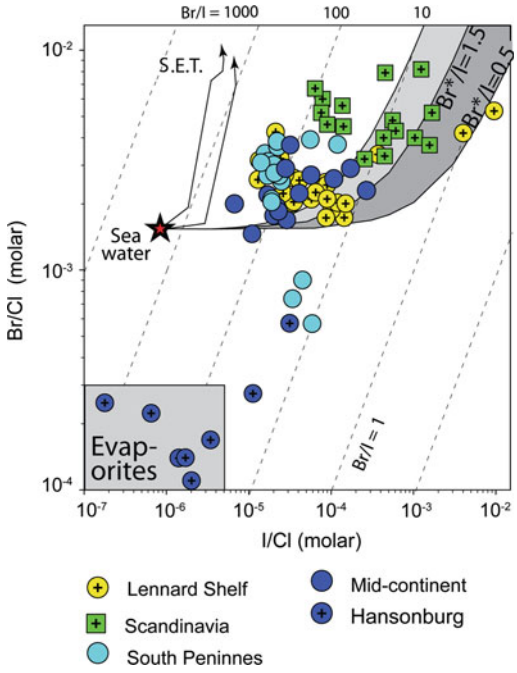

Fig. 6 Halogen systematics of MVT ore fluids, showing individual laser analyses for Hansonburg and sample averages from other locations (Bohlke and Irwin 1992a, b, c; Kendrick et al. 2002a, b, 2005, 2011c). Reference fields include seawater, the seawater evaporation trajectory (S.E.T.; Zherebtsova and Volkova 1966), evaporites (Table 4; Holser 1979; Fontes and Matray 1993), sedimentary marine pore fluids with seawater-corrected Br*/I of 0.5–1.5 (*dark grey envelope*) and organic matter with Br*/I < 10 (*light grey envelope*). The pore fluid trend is defined with data from Fehn et al. (2000, 2003, 2006, 2007); Muramatsu et al. (2001, 2007) and Tomaru et al. (2007a, b, 2009)

appear to be a real characteristic of the MVT ore fluids investigated (Kendrick et al. 2011c).

The ore fluids greater than ASW ^{36}Ar concentrations, and variable ^{84}Kr/^{36}Ar and ^{130}Xe/^{36}Ar ratios, could result from dissolution of hydrocarbons which can have high noble gas concentrations and are present in some MVT fluid inclusions (cf. Figs 5a, c). However, Kendrick et al. (2011c) argued that the most important source of excess ^{36}Ar was recrystallisation of the carbonate aquifer rocks. This was suggested because fractionation of noble gases between an exclusive ASW source and hydrocarbons does not account for the presence of excess ^{40}Ar* in the ore fluids. In contrast, acquisition of noble gases from carbonate rocks, which typically have ^{40}Ar/^{36}Ar slightly above the atmospheric value (Matsuda and Nagao 1986; Zhou and Ye 2002), could potentially account for the presence of excess ^{40}Ar* and the range of fluid inclusion ^{84}Kr/^{36}Ar and ^{130}Xe/^{36}Ar ratios (Fig. 5d; Kendrick et al. 2011c). Noble gases could be released from the carbonates by diffusion, or during the extensive dolomitisation and recrystallization that is usually associated with MVT mineralisation.

A large number of studies have shown MVT ore fluids commonly have greater than seawater Br/Cl ratios (e.g. Crocetti and Holland 1989; Kesler et al. 1995; Viets et al. 1996; Kesler 2007). This has usually been interpreted to indicate acquisition of salinity by sub-aerial evaporation of seawater beyond the point of halite saturation (~30 wt% salts; cf. Chi and Savard 1997). Variable dilution of the brines is then required to produce the observed range of fluid inclusion salinities (10–30 wt% salts). This is significant for interpretation of the noble gas data because air saturated bittern brines, have even lower ^{36}Ar concentrations than seawater (Table 3).

The combined noble gas and halogen method enables precise measurement of iodine, together with Br and Cl which is advantageous for assessing the possible influence of organic matter on fluid Br/Cl ratios (Kendrick et al. 2011c). Sedimentary marine pore fluids associated with CH_4 transport in oceanic sediments (e.g. Muramatsu et al. 2001, 2007; Fehn et al. 2003; Tomaru et al. 2007a, b, 2009) define a linear array in Br/Cl versus I/Cl space that has a seawater intercept and a molar Br*/I slope of 0.5–1.5 (seawater-corrected Br* = Br − 0.0015 × Cl; see Fig. 6 and Kendrick et al. 2011c). Organic matter in sediments usually has higher Br*/I ratios than sedimentary marine pore fluids, with the difference likely to be explained by preferential mobilization of I relative to Br, under some diagenetic conditions (e.g. Martin et al. 1993; Muramatsu et al. 2001; Biester et al. 2004). The majority of MVT ore fluids plot between the seawater evaporation trajectory and the sedimentary pore fluid trend (which has Br*/I of ~0.5−1.5; Fig. 6). As the addition of

organic halogens does not influence salinity, this confirms sub-aerial evaporation as an important source of fluid salinity (Fig. 6; Kendrick et al. 2011c). However, some previous interpretations of fluid Br/Cl that did not allow for organic Br, could have over-estimated the degree of evaporation required to generate a given Br/Cl ratio (cf. Fig. 6), or underestimated the possible importance of evaporite dissolution (Kendrick et al. 2011c).

In the majority of cases, the combined noble gas and halogen data for MVT ore fluids show systematic variation between minerals deposited in different stages of the paragenetic sequence. This has been interpreted to favour fluid migration through independent aquifers providing the potential for fluid mixing at the site of ore deposition (e.g. Crocetti and Holland 1989; Kendrick et al. 2002a, 2011c). Kendrick et al. (2011c) demonstrated that among samples from Lennard Shelf MVT deposits, the fluid inclusions with the highest I/Cl ratio had the lowest ^{36}Ar concentrations. This was suggested to reflect interaction of aqueous fluids and hydrocarbons, with noble gases partitioning into hydrocarbons and organic halogens partitioning into the aqueous fluids that were preferentially trapped as fluid inclusions (Kendrick et al. 2011c).

5.3 Mid-Ocean Ridge VMS Deposits

Volcanogenic massive sulphide (VMS) deposits formed by hydrothermal systems at mid-ocean ridge spreading centres and in back-arc rifts, represent important sites for monitoring global volatile fluxes (Turner and Stuart 1992; Jean-Baptiste and Fouquet 1996), and are major sources of base metals (Robb 2005). Noble gas data are available for vent fluids from a variety of modern systems (e.g. Kennedy 1988; Lupton et al. 1989; Baker and Lupton 1990); in addition, liquid-vapour fluid inclusions trapped at temperatures of between 200 and 360 °C in pyrite, anhydrite, sphalerite and chalcopyrite have been analysed from the East Pacific Rise, Mid-Atlantic Ridge and various back-arc basins (Turner and Stuart 1992; Stuart et al. 1994; Jean-Baptiste and Fouquet 1996; Stuart and Turner 1998; Zeng et al. 2001; Lueders and Niedermann 2010; Webber et al. 2011).

In most cases, the helium and argon isotope systematics of sulphide-hosted fluid inclusions are indistinguishable from vent fluids. The majority of workers have therefore concluded that sulphide-hosted fluid inclusions faithfully retain noble gases (including helium) over millions of years, at ambient seafloor conditions (Turner and Stuart 1992; Jean-Baptiste and Fouquet 1996; Lueders and Niedermann 2010). This is consistent with the diffusion data available for helium in sulphides (Boschmann et al. 1984).

Sulphide fluid inclusions have atmospheric or near atmospheric $^{40}Ar/^{36}Ar$ ratios of 296-310 that reflect the vent fluids dominant origin from seawater (Turner and Stuart 1992; Zeng et al. 2001; Lueders and Niedermann 2010; Webber et al. 2011). The $^{3}He/^{4}He$ ratio of vent fluids vary from typical mantle values (e.g. ~8 Ra; Turner and Stuart 1992; Jean-Baptiste and Fouquet 1996), to significantly lower values (e.g. ~2–4 Ra; Stuart et al. 1994; Zeng et al. 2001; Webber et al. 2011). Jean-Baptiste and Fouquet (1996) found that high temperature minerals preferentially trap the vent fluid and best preserve mantle $^{3}He/^{4}He$ ratios, whereas lower temperature minerals are more likely to contain an ambient seawater component with lower $^{3}He/^{4}He$. Stuart et al. (1994) reported $^{3}He/^{4}He$ data for sulphides from bare-rock and sediment-covered hydrothermal vent systems. This study interpreted variation in fluid inclusion $^{3}He/^{4}He$ to reflect mixing of mantle ^{3}He derived from local basalts and radiogenic ^{4}He associated with sediments overlying some of the spreading centres (Stuart et al. 1994). In a later study, Stuart and Turner (1998) observed vent fluids with small excesses of $^{40}Ar^{*}$ and two distinct groupings of $^{4}He/^{40}Ar^{*}$ that were suggested to reflect magmatic components acquired during different stages of magma degassing (Stuart and Turner 1998).

Vent fluid inclusions typically have heavy noble gas abundance ratios intermediate of seawater and air and are strongly enriched in helium, but some systems also have elevated

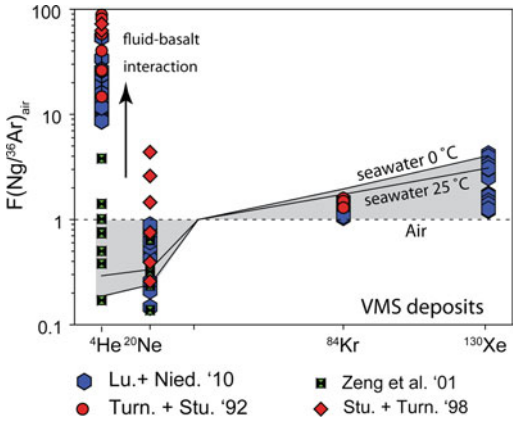

Fig. 7 Noble gas relative abundance patterns for fluid inclusions in VMS deposits from mid-ocean ridge spreading centres and back-arc rifts (Turner and Stuart 1992; Stuart and Turner 1998; Zeng et al. 2001; Lueders and Niedermann 2010). Abundance ratios are normalised to air: $F(Ng/^{36}Ar)_{air} = (Ng/^{36}Ar)_{sample}/(Ng/^{36}Ar)_{air}$; such that Air = 1; Ng = ^{4}He, ^{20}Ne, ^{84}Kr or ^{130}Xe

$^{20}Ne/^{36}Ar$ ratios (Fig. 7; Turner and Stuart 1992; Zeng et al. 2001; Lueders and Niedermann 2010). Luedders and Niedermann (2010) suggested noble gas abundance ratios intermediate of seawater and air could reflect gas loss and re-equilibration of noble gases with vent fluids at elevated temperature; however, these values are also consistent with the presence of modern air contaminants (Sect. 3.5; Turner and Stuart 1992). Modern vent fluids are uniformly depleted in all noble gases relative to seawater (Kennedy 1988; Winckler et al. 2000). The lack of strongly fractionated noble gas abundance ratios could indicate the noble gases all have similarly low solubilities in seawater-derived fluids at vent temperatures.

The salinity of vent fluid inclusions ranges from at least 1.5–15 wt% NaCl eq. (Lueders and Niedermann 2010). Vent fluids can acquire lower than seawater noble gas concentrations, and high salinities, in the residual brines as a result of phase separation (Kennedy 1988; Winckler et al. 2000). In contrast, high noble gas concentrations should be expected in (condensed) vapour phases, and high noble gas concentrations and high salinities might also result from preferential incorporation of $H_2O > Cl > {}^{36}Ar$ into hydrous minerals during hydration of seafloor lithologies (e.g. Bach and Frueh-Green 2010). The combined noble gas and halogen method has not been applied to fluid inclusions in mid-ocean ridge sulphides, but Lueders and Niedermann (2010) reported vent fluid inclusions have variable Br/Cl ratios. The Br/Cl variability is probably related to fractionation of Br and Cl during phase separation, the nature of which is thought to depend strongly on the presence of minor solutes and pressure (e.g. Berndt and Seyfried 1990; Liebscher et al. 2006).

In summary, the range of noble gas compositions recorded by fluid inclusions in seafloor sulphides reflect mixing hot seawater-derived vent fluids and ambient seawater with a magmatic volatile component present in some cases. Seawater-derived fluids are suggested to acquire significant ^{3}He by fluid interaction with young basalts, or underlying gabbros and lithospheric mantle. The presence of a magmatic volatile component may be related to the age of the hydrothermal system (sect. 5. 3. 1).

5.3.1 Helium and Heat

Studies of modern vent fluids indicate that the concentration of ^{3}He is systematically related to the vent fluids temperature, over a large range of temperatures, which is explained because both ^{3}He and heat are ultimately derived from the mantle in mid-ocean ridge settings (e.g. Lupton et al. 1989; Baker and Lupton 1990; Lupton et al. 1999; Baker et al. 2011). Vent fluids above magmatically quiescent mature mid-ocean ridges have low ^{3}He/heat ratios of $0.4–1 \times 10^{-17}$ mol/J; whereas, vent fluids associated with newly erupted lavas have higher ^{3}He/heat ratios of $2–7 \times 10^{-17}$ mol/J, that decrease back toward the lower 'steady state' value over the space of a few years as the magma cools (Baker and Lupton 1990; Lupton et al. 1999).

The ^{3}He/heat ratio carries information about how heat is transferred from the mantle through the crust (Baker and Lupton 1990). High ^{3}He/heat values favour advective transport of heat with magmatic volatiles, whereas low ^{3}He/heat values favour conductive transfer of heat into

circulating seawater (Baker and Lupton 1990; Turner and Stuart 1992). Fluid inclusions provide the potential for extending the study of ^{3}He/heat back into the geological record (Turner and Stuart 1992; Jean-Baptiste and Fouquet 1996). This could be advantageous for further unravelling the causes of ^{3}He/heat variations or determining the periodicity of hydrothermal 'event plumes' observed at some modern spreading centres (cf. Lupton et al. 1999; Baker et al. 2011).

5.4 Magmatic Fluids and Hydrothermal Ore Deposits

5.4.1 'Gold-Only' Ore Deposits

Gold-only ore deposits, in which gold is either the only or by far the dominant economic commodity, include: (1) 'orogenic-gold deposits' (also known as 'lode', 'mesothermal' or 'greenstone' gold; Goldfarb et al. 2001; Groves et al. 2003), and (2) 'intrusion-related gold deposits' (Lang and Baker 2001). These deposits form at crustal depths ranging from <3 to 15 km and because both deposit types can be characterised by very similar low salinity H_2O-CO_2 fluid inclusions, their genesis and distinction is contentious (Sect. 5.5.2; Baker 2002; Mernagh et al. 2007). Magmatic fluids are implicated in intrusion-related gold deposits that are spatially associated with moderately reduced (ilmenite series) I-type felsic magmatism (Lang and Baker 2001; Baker 2002). In contrast, orogenic-gold deposits are variably attributed to the involvement of either distally sourced magmatic fluids or metamorphic fluids (Sect. 5.5.2; Groves et al. 2003; Phillips and Powell 1993; Elmer et al. 2006).

The noble gas systematics of the ~50 Ma greenstone-hosted Ailaoshan gold deposits in SW China provide an example of how noble gases can be used to conclusively demonstrate the involvement of a magmatic fluid in a hydrothermal ore deposit (Burnard et al. 1999; Sun et al. 2009). Fluid inclusions trapped in pyrite and scheelite from Ailaoshan gold deposits have ^{3}He/^{4}He ranging from crustal values of 0.05 Ra up to values of 1.3 Ra that indicate a substantial mantle component (Burnard et al. 1999; Sun et al. 2009). The fluid inclusion ^{40}Ar/^{36}Ar values vary from 300 up to 9,000, and define a parabolic mixing trend in ^{40}Ar/^{36}Ar versus ^{3}He/^{4}He space (Fig. 8a; Burnard et al. 1999; Sun et al. 2009). The shape of the mixing trend is governed by the relative concentrations of the denominator isotopes (e.g. ^{4}He and ^{36}Ar) in the two fluid end-members. This is a general relationship applicable to binary mixing in any four component diagram and the curvature is described by the *r*-value (Langmuir et al. 1978), which in this case is written as (Eq. 1):

$$r = \frac{\left(^{4}He/^{36}Ar\right)_{\text{magmatic}}}{\left(^{4}He/^{36}Ar\right)_{\text{fluid}-2}} \quad (1)$$

where $(^{4}\text{He}/^{36}\text{Ar})_{\text{magmatic}}$ and $(^{4}\text{He}/^{36}\text{Ar})_{\text{fluid-2}}$ represent two fluid end-members. The concentrations of ^{3}He and ^{36}Ar in crustal fluids are such that He-Ar mixing curves are often strongly parabolic (e.g. Fig 8a). As a result, helium can 'appear' to be decoupled from argon, and the ^{40}Ar/^{36}Ar value of the magmatic end-member is only poorly defined as being greater than the highest measured value (Fig 8a). In contrast, the magmatic fluid end-member at Ailaoshan has a well constrained mixed crust-mantle ^{3}He/^{4}He signature of ~1.3 Ra (Fig. 8a).

Caution is always required in the interpretation of mixing diagrams, a mixing model should define the same fluid end-members in diagrams including any combination of different isotopic components. In this instance, the trend in Fig. 8a can be interpreted as a pseudo-binary trend because a third end-member is suggested by plotting the data in a ^{4}He/^{40}Ar versus ^{3}He/^{40}Ar diagram (Fig. 8b; Burnard et al. 1999). The three end-members were interpreted as: (1) a magmatic fluid with ^{3}He/^{4}He of ~1.3 Ra and ^{40}Ar/^{36}Ar of >9,000; (2) a crustal fluid with ^{3}He/^{4}He of <0.05 Ra and ^{40}Ar/^{36}Ar of ~300; and (3) a second crustal fluid that has low ^{4}He/^{40}Ar and a poorly defined ^{3}He/^{4}He intermediate of 0.05 Ra and ASW (Fig. 8b; Burnard et al. 1999). The mixed crust-mantle signature of

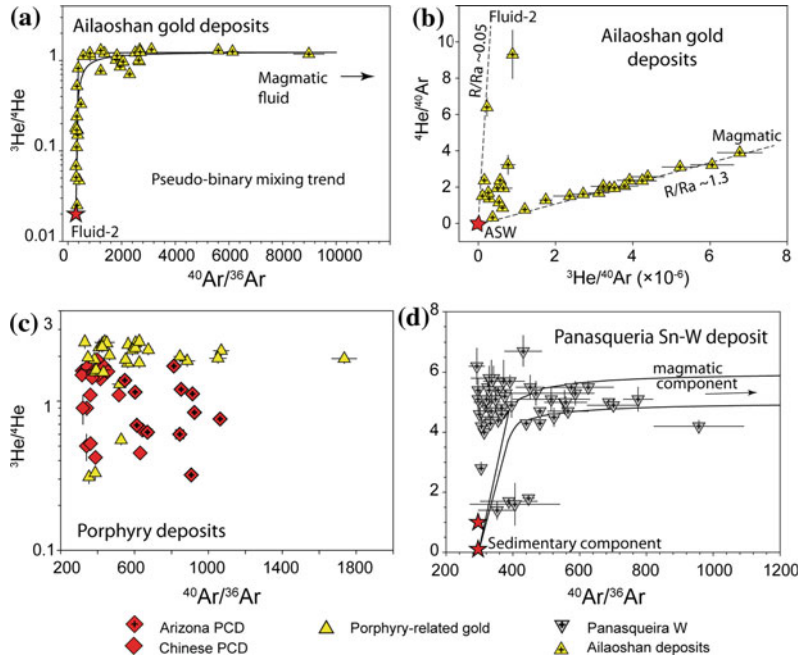

Fig. 8 The He–Ar systematics of fluid inclusions with a magmatic origin in various hydrothermal ore deposits. **a** The Ailaoshan data obtained by 1–3 crushes of 15 sulphide samples exemplify the parabolic shape expected for binary mixing in He–Ar four isotope diagrams (Burnard et al. 1999). **b** However, in this case, a third end-member is revealed by the ^{4}He/^{40}Ar versus ^{3}He/^{40}Ar plot. **c** Porphyry-style ore fluids from Arizonan Porphyry copper deposits (9 samples; Kendrick et al. Kendrick et al. 2001a) and porphyry-related copper and gold deposits of the Red River–Jinshajiang fault belt in SW China (24 samples; Hu et al. 1998, 2004). **d** Fluid inclusion data for granite-associated Panasqueria tin-tungsten deposit, Portugal (12 samples; Burnard and Polya 2004)

noble gases trapped in sulphide and scheelite fluid inclusions is in excellent agreement with scheelite Sr and Nd isotope data, that also indicate a source from a transitional crust-mantle zone (Sun et al. 2009).

Several other Chinese gold-only ore deposits have fluid inclusions with mixed crust-mantle noble gas signatures similar to the Ailaoshan deposits. These include porphyry-related gold deposits along the Red River–Jinshajiang fault belt, south of the Ailaoshan deposits (Fig 8c; Hu et al. 2004); the Bangbu orogenic-gold deposit in Tibet (Wei et al. 2010), and the Dongping orogenic-gold deposit of northern China where fluid inclusions have a maximum ^{3}He/^{4}He of 5.2 Ra (Mao et al. 2003). The mixed crust-mantle noble gas signatures reported for fluid inclusions from all of these deposits are consistent with the involvement of magmatic fluids in a variety of gold-only ore deposits.

In contrast, several orogenic-gold deposits from other parts of the world give maximum fluid inclusion ^{3}He/^{4}He ratios of less than ~0.4 Ra (Pettke et al. 1997; Graupner et al. 2006, 2010; Li et al. 2010; Kendrick et al. 2011b). The lack of high ^{3}He/^{4}He ratios in samples from Phanerozoic deposits is unlikely to be explained by post-entrapment modification (Pettke et al. 1997; Graupner et al. 2006, 2010), conclusively demonstrating that some orogenic-gold deposits are formed from crustal fluids, with a range of ^{3}He/^{4}He similar to MVT ore fluids (Sect. 5.2). These low ^{3}He/^{4}He ratios do not preclude the possible involvement of a magmatic fluid sourced from a largely crustal magma (e.g. Kendrick et al. 2011b), or diluted

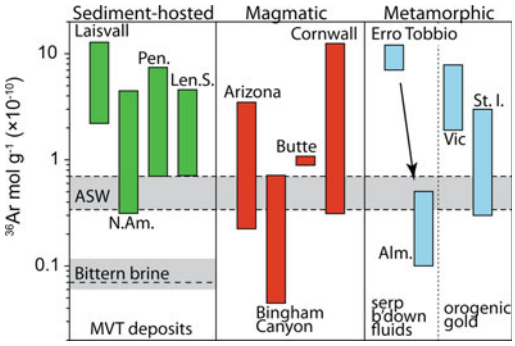

Fig. 9 Apparent ^{36}Ar concentrations determined from fluid inclusion salinity and the maximum Cl/^{36}Ar measured during sequential crushing. Note, analyses shown for Laisvall fluid inclusions have ^{84}Kr/^{36}Ar of 0.04–0.07 and Cl/^{36}Ar is not correlated with ^{40}Ar/^{36}Ar in the Erro Tobbio fluid inclusions, conclusively demonstrating these analyses have not been influenced by modern air contaminants (see text). The range of ASW encompasses 0 °C meteoric water and 25 °C seawater. Data from various sources (Kelley et al. 1986; Turner and Bannon 1992; Irwin and Roedder 1995; Kendrick et al. 2001a, 2002a, b, 2005, 2011a, c; Fairmaid et al. 2011; Fu et al. 2012). *Abbreviations* N.Am. North American mid-continent; Pen. Pennine; Len.S. Lennard Shelf; Alm Almirez (serpentines final breakdown); Vic Victorian Gold deposits; St.I. St. Ives

by modified ASW (Graupner et al. 2006, 2010). However, these dominantly crustal noble gas signatures are also consistent with a dominant role for metamorphic fluids (Sects. 5.5 and 5.6).

5.4.2 Porphyry-Style Ore Deposits

Porphyry-style deposits represent the world's most important source of copper and molybdenum and significant sources of gold (Robb 2005; Sillitoe 2010). Porphyry copper, and porphyry copper-gold or molybdenum, ore deposits are zoned around relatively oxidized (magnetite series) felsic porphyry stocks or dykes, formed from 'I-type' calc-alkaline arc magmas (see Sillitoe 2010 for review). Hydrothermal mineralisation is associated with extensive veining and brecciation at typical emplacement depths of 2–4 km; however, the stocks and dykes act to focus magmatic volatiles, copper and gold, from much larger batholithic intrusions at depth (Sillitoe 2010). The fluid inclusions in porphyry style quartz veins are dominantly aqueous, although significant CO_2 is present in some systems (Roedder 1971b; Rusk et al. 2004). The classic fluid inclusion assemblage associated with high temperature potassic alteration comprises high salinity aqueous fluid inclusions (40–50 wt% NaCl eq.) with coexisting vapour fluid inclusions, that cool from maximum temperatures of >600 °C to temperatures of ~350 °C (e.g. Roedder 1971b; Heinrich 2003). The fluid inclusions provide evidence for cooling of magmatic fluids that have separated into low salinity vapour and high salinity liquid phases during 'hydrothermal boiling' (Roedder 1971b; Heinrich 2003).

Noble gas and halogen data are available from several classic porphyry copper deposits of North America including Bingham Canyon, Butte and several Arizonan deposits including Ray, Pinto Valley, Globe-Miami, Silverbell and Mission (Figs 4 and 8c; Irwin and Roedder 1995; Kendrick et al. 2001a, b). Noble gas data are also available for copper and gold deposits associated with porphyry intrusions along the Red River–Jinshajiang fault belt in SW China (Fig. 8c; Hu et al. 1998, 2004).

The porphyry deposits investigated all have sulphide and quartz hosted fluid inclusions with ^{3}He/^{4}He ratios of 0.3–2.5 Ra and ^{40}Ar/^{36}Ar of 300–3,000 (Hu et al. 1998, 2004; Irwin and Roedder 1995; Kendrick et al. 2001a). The data can be modeled to reflect mixing between a magmatic fluid and modified ASW (e.g. Fig. 8c; Hu et al. 1998, 2004). However, it is interesting that of the deposits in SW China, it is the gold deposits that best define the noble gas mixing trend (Fig. 8c). In general, the noble gases in the porphyry copper deposit fluid inclusions, especially the Arizonan deposits, appear to be 'well mixed' and do not define an obvious trend (Fig. 8c). The generally low ^{40}Ar/^{36}Ar ratios of ore fluids in the Bingham and Arizonan deposits (Fig. 4 and 8c) were originally interpreted to reflect mixing of magmatic fluids with elevated ^{40}Ar/^{36}Ar and meteoric water with ^{40}Ar/^{36}Ar of ~300 (Kendrick et al. 2001a). However, given atmospheric noble gases are recycled through magmatic arcs to some extent (cf. Kendrick et al. 2011d; Staudacher and Allègre 1988),

further work is required to test if the mixed noble gas signatures with high abundances of atmospheric noble gas could be characteristic of magmatic fluids exsolved from porphyry arc magmas. If this proves to be the case, the noble gas signature of porphyry ore fluids could be explained with minimal involvement of meteoric water (cf. Fig. 8c).

Application of the ^{40}Ar–^{39}Ar method to porphyry copper quartz samples has shown the fluid inclusions have variable ^{36}Ar concentrations ranging from air saturation values ($0.3–0.7 \times 10^{-10}$ mol g^{-1}) to much lower concentrations of $0.04–0.1 \times 10^{-10}$ mol g^{-1} (Fig. 9; Irwin and Roedder 1995; Kendrick et al. 2001a). The low ^{36}Ar concentrations could be a characteristic of magmatic fluids (Irwin and Roedder 1995), or the result of gass loss during hydrothermal boiling (Kendrick et al. 2001a). Additional evidence for hydrothermal boiling is provided by variation in $^{40}Ar^*/Cl$ ratios and extreme enrichments in $^{130}Xe/^{36}Ar$ and $^{84}Kr/^{36}Ar$ values (Fig. 10). Hydrothermal boiling reduces the $^{40}Ar^*/Cl$ ratio and increases the Xe/Ar and Kr/Ar ratios of the residual liquid phase, because noble gases are partitioned into the vapour phase on the order Ar > Kr > Xe and Cl is preferentially retained by the liquid phase (Fig. 10; Kendrick et al. 2001a).

Fluid inclusions associated with the majority of porphyry copper ore deposits have a very limited range of Br/Cl and I/Cl (Irwin and Roedder 1995; Kendrick et al. 2001a; Nahnybida et al. 2009), with the Br/Cl values tending to be lower than the MORB mantle value (Fig. 11a; Kendrick et al. 2012). Fluid inclusions in the Silverbell porphyry deposit of Arizona, record higher I/Cl ratios than the majority of porphyry ore fluids (Fig. 11a), and the variation in I/Cl was interpreted to reflect mixing of the dominant magmatic fluid with sedimentary formation waters in this deposit (Kendrick et al. 2001a).

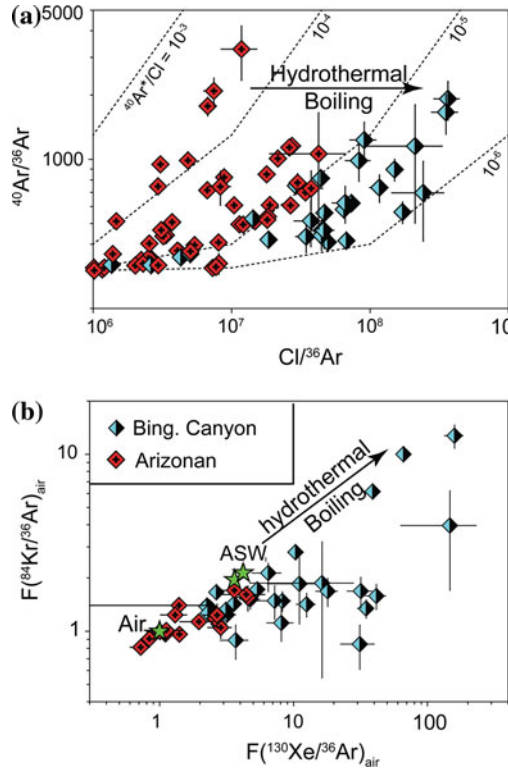

Fig. 10 Noble gas fractionation during hydrothermal boiling of porphyry copper deposit ore fluids (crushing analyses of 19 samples; Kendrick et al. 2001a). Hydrothermal boiling refers to separation of liquid and vapour H_2O phases. **a** $Cl/^{36}Ar$ versus $^{40}Ar/^{36}Ar$, the residual liquid phase has higher $Cl/^{36}Ar$ and lower $^{40}Ar^*/Cl$ ratios than the parent fluid. **b** $F(^{84}Kr/^{36}Ar)_{air}$ versus $F(^{130}Xe/^{36}Ar)_{air}$, the residual liquid phase acquires higher $^{130}Xe/^{36}Ar$ and $^{84}Kr/^{36}Ar$ ratios than the parent fluid. Noble gas abundance ratios are written as F-values [$F(Ng/^{36}Ar)_{air} = [(Ng/^{36}Ar)_{sample}/(Ng/^{36}Ar)_{air}]$; Air = 1; Ng = ^{130}Xe or ^{84}Kr]

5.4.3 Tungsten-Bearing Ore Deposits

Tin-tungsten ore deposits are commonly zoned around reduced (ilmenite series) granites of 'S-type' affinity emplaced at depths of <10 km (Robb 2005). Noble gas data are available for a variety of tin-tungsten deposits including Carrock Fell in the north of England, several occurrences in Cornwall (UK) (Kelley et al. 1986; Turner and Bannon 1992; Böhlke and Irwin 1992c; Irwin and Roedder 1995) and the Panasqueria deposit of Portugal (Burnard and Polya 2004; Polya et al. 2000).

The initial studies applied ^{40}Ar–^{39}Ar methodology to quartz veins and documented fluid inclusion $^{40}Ar/^{36}Ar$ values of between 300 and 2,200, and fluid inclusion ^{36}Ar concentrations of equal to or above air saturation levels (Fig. 9; Kelley et al. 1986; Turner and Bannon 1992).

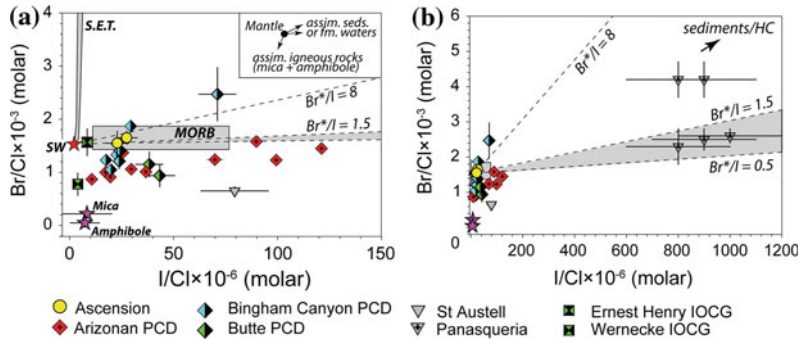

Fig. 11 The halogen systematics of fluid inclusions in magmatic-hydrothermal ore deposits (showing sample means). **a** Fluid inclusions from Ascension granite xenoliths, porphyry-style deposits and St. Austell Sn-W mineralisation, Cornwall (Irwin and Roedder 1995; Kendrick et al. 2001a), are relatively close to MORB composition (Kendrick et al. 2012). Interpreted magmatic fluids involved in iron-oxide copper gold mineralisation (Wernecke, Canada and Ernest Henry, Australia), and igneous mica and amphibole (Kendrick et al. 2007, 2008b; Kendrick 2012) are also shown. Possible causes of compositional variation are shown inset. **b** Fluid inclusions from Panasqueria deposit are strongly enriched in Br and I derived from organic sources (Polya et al. 2000). Note Br*/I indicates the seawater-corrected Br/I ratio that is typical of sedimentary marine pore fluids (see Fig. 6)

Three dimensional ^{40}Ar–^{36}Ar-K-Ca-Cl correlation diagrams were employed by Kelley et al. (1986) and Turner and Bannon (1992) to resolve multiple ^{40}Ar components. In addition to Cl-correlated excess ^{40}Ar* trapped in fluid inclusions, these studies resolved a K-correlated radiogenic ^{40}Ar component, associated with mica impurities in some of the fluid inclusions. The ages of the accidentally trapped mica, in quartz vein fluid inclusions, vary from 250 ± 15 to 270 ± 20 Ma, compared to the probable granite intrusion and mineralisation age of 280–295 Ma (Kelley et al. 1986; Turner and Bannon 1992). The small discrepancy in ages partly reflects the low retentivity of ^{40}Ar in micron-sized mica crystals (Kendrick et al. 2006b), but nonetheless these cooling ages suggest a maximum time period of ~20 Myr between intrusion of the granites and cessation of hydrothermal activity (Kelley et al. 1986; Turner and Bannon 1992).

In comparison to porphyry copper ore fluids exsolved from I-type granites, mineralisation-related fluid inclusions at St Austell have slightly lower Br/Cl and higher I/Cl ratios (Fig. 11a). Assuming the halogens dissolved within these fluids had a dominantly magmatic origin, the difference could reflect anatexis of crustal sedimentary rocks with variable Br/Cl and I/Cl, as opposed to melting dominantly igneous rocks to generate I-type porphyry intrusions (Fig 11a; Irwin and Roedder 1995). Irwin and Roedder (1995) demonstrated that fluid inclusions within granite xenoliths from Ascension Island, that have not had the opportunity of assimilating large amounts of crustal material, preserve MORB-like Br/Cl and I/Cl values (Fig 11a; Irwin and Roedder 1995).

The Panasqueria tin-tungsten deposit of Portugal is hosted by metasediments, overlain by coal bearing sediments, and associated with the ~290 Ma Panasqueria granite (Polya et al. 2000). The Panasqueria granite is of 'S-type' affinity with $^{87}Sr/^{86}Sr$ of 0.713 suggesting ≥50 % of the Sr had a crustal source (see Polya et al. 2000; Burnard and Polya 2004). Quartz-hosted fluid inclusions have salinities of 7–9 wt% NaCl eq. and homogenisation temperatures of 250–260 °C (Polya et al. 2000). Considering the largely crustal origin of the Panasqueria granite, it was surprising that sulphide-hosted fluid inclusions record $^{3}He/^{4}He$ ratios of up to 6.7 Ra (Fig. 8d), implying >75 % of the helium in the ore fluids has a mantle origin (Burnard and Polya 2004). The discrepancy between the $^{87}Sr/^{86}Sr$ and $^{3}He/^{4}He$ isotope

systems was explained by suggesting that after partial crystallisation, a renewed pulse of mantle volatiles and heat passed through the magma chamber resulting in a final pulse of magmatic fluids with disproportionately high $^{3}He/^{4}He$ (Burnard and Polya 2004). Burnard and Polya (2004) suggested mineralisation could have been related to a pulse of mantle-derived fluids that used the granite as a high permeability pathway.

The Panasqueria ore fluids have δD values extending from typical magmatic values of around −40 ‰ to unusually low values of −130 ‰ (Polya et al. 2000). Considering the paleolatitude of the deposit, these low δD values can only be explained by either strong fractionation during magmatic degassing, or fluid interaction with organic-rich sediments and coal (Polya et al. 2000). The fluids have a strongly magmatic $^{3}He/^{4}He$ signature (Fig. 8d), but elevated Br/Cl and I/Cl ratios and low $^{40}Ar/^{36}Ar$ values that are more akin to sedimentary formation waters than typical magmatic fluids (Fig. 11; Polya et al. 2000). The combined noble gas, halogen and δD data could be explained by mixing magmatic fluids and sedimentary formation waters (e.g. Fig. 8d; Burnard and Polya 2004). However, if magmatic fluids acquired the low δD by interaction with organic-rich coals (cf. Polya et al. 2000), the implied fluid-rock ratio of 0.02–0.002 means a magmatic fluid could also have acquired significant Br, I and atmospheric noble gas during interaction with the organic-rich sediments and coal. The K-poor coal was young at the time of ore deposition, meaning it would not have contained significant excess ^{40}Ar (Polya et al. 2000); however, the typical concentrations of atmospheric noble gas in sediments, and the ppm-levels of Br and I in organic matter, would be extremely significant at water-rock ratios of <0.02 (Tables 3 and 4). The key points are therefore that combined noble gas and halogen analysis provides strong evidence for both the involvement of magmatic fluids and extensive fluid interaction with the crustal lithologies overlying the ore deposit (cf. Polya et al. 2000; Burnard and Polya 2004). However, the way these signals were mixed together is to some extent a question of interpretation.

Finally, the Dae Hwa tungsten-molybdenum deposit of South Korea is associated with 'I-type' granite and is famous for its large zoned scheelite crystals. The scheelite zones contain primary fluid inclusions that record a progressive outward decrease in homogenisation temperature (400–200 °C), which on the basis of $\delta^{18}O$, δD and $\delta^{34}S$ was interpreted to reflect dilution of a magmatic fluid by meteoric water (So et al. 1983; Shelton et al. 1987). Noble gases analysed in a representative zoned scheelite crystal have a maximum $^{3}He/^{4}He$ of 2.7 Ra and show inter-zonal variation that is broadly correlated with $\delta^{18}O$ and fluid inclusion homogenisation temperature (Burgess et al. 1992; Stuart et al. 1995). The noble gas data further constrain the magmatic-meteoric mixing model with the magmatic fluid shown to have $^{3}He/^{4}He$ of >2.7 Ra, and the lower temperature fluid recording characteristically elevated $^{4}He/^{40}Ar^{*}$ ratios of up to 50, $^{3}He/^{4}He$ of <0.2 and $^{40}Ar/^{36}Ar$ of ~ 400 (Fig. 4; Burgess et al. 1992; Stuart et al. 1995).

5.5 Metamorphic Fluids and Hydrothermal Ore Deposits

The range of noble gas compositions expected in metamorphic fluids produced by breakdown of hydrous or carbonate minerals in the Earth's crust is poorly constrained (Kendrick et al. 2006a). Metamorphic fluids should have the noble gas isotope signature of either the minerals that breakdown, or perhaps more likely, they could have signatures representative of their source region, as a result of diffusion of noble gases into the fluid phase from the surrounding country rock.

5.5.1 Serpentine Breakdown Fluids

The composition and abundance of noble gases in antigorite-serpentinites was recently investigated to test if serpentine subduction could provide a pathway for transfer of atmospheric noble gases into the Earth's mantle (Kendrick et al. 2011d). The results of this study help illustrate some important features of metamorphic fluids.

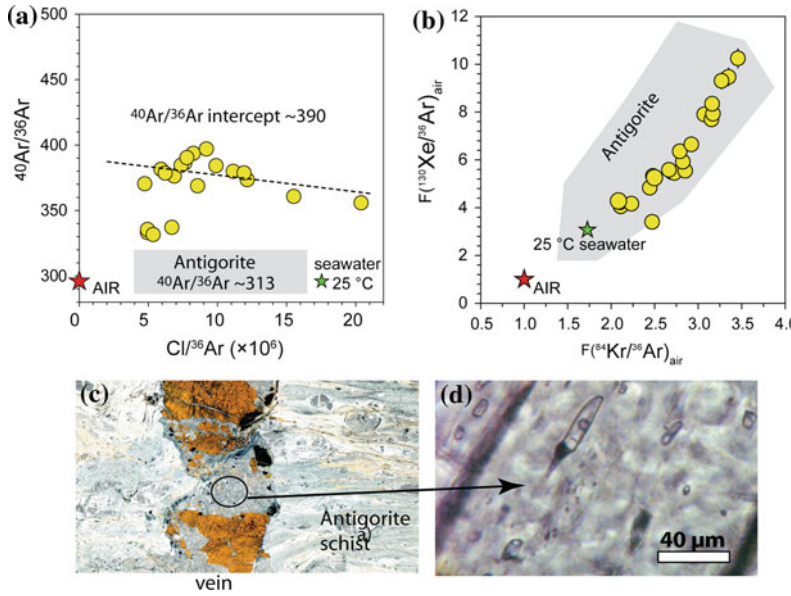

Fig. 12 Serpentinite breakdown fluids from Erro Tobbio, Italy. **a** Fluid inclusion Cl/^{36}Ar versus ^{40}Ar/^{36}Ar and **b** ^{130}Xe/^{36}Ar versus ^{84}Kr/^{36}Ar compositions measured by in vacuo crushing olivine and Ti-clinohumite (F = fractionation value normalised to air; Air = 1). The fluids released by crushing do not define a mixing line with air (**a**) and the fluid inclusions faithfully record the Ar-Kr-Xe isotope signature of the antigorite-schist (modified after Kendrick et al. 2011d). **c** Transmitted light photomicrograph showing a ~1 cm wide olivine-Ti-clinohumite-dioside vein in antigorite schist; and **d** a primary fluid inclusion with visible halite daughter crystal and vapour bubble (photographs courtesy of M. Scambelluri)

Antigorite-serpentinites from Erro Tobbio (Italy) have near atmospheric ^{40}Ar/^{36}Ar ratios of between 300 and 360 and high abundances of ^{20}Ne, ^{36}Ar, ^{84}Kr and ^{130}Xe (Table 3), that were introduced from seawater-derived fluids during seafloor serpentinisation of ultra-mafic lithologies (Kendrick et al. 2011d). Fluid inclusions trapped in olivine bearing veins formed during prograde metamorphism and partial breakdown of antigorite have salinities of up to 40 wt% NaCl eq. (Fig. 12d; Scambelluri et al. 1997), and record ranges of ^{20}Ne/^{36}Ar, ^{84}Kr/^{36}Ar, ^{130}Xe/^{36}Ar and ^{40}Ar/^{36}Ar that are fairly representative of the serpentinite host rocks (Fig. 12; Kendrick et al. 2011d).

Based on a salinity of 40 wt% NaCl eq. and the measured Cl/^{36}Ar ratio, the fluid inclusions (Fig. 12d) are estimated to have a minimum ^{36}Ar concentration of $(9 \pm 1) \times 10^{-10}$ mol g^{-1} (1σ), which is 30 times higher than the concentration of ^{36}Ar in 25 °C seawater (Kendrick et al. 2011d). Note that the range of fluid inclusion ^{40}Ar/^{36}Ar and Cl/^{36}Ar values do not favour the presence of any kind of modern air contaminant, because the mixing line in Fig. 12a does not intersect the composition of air (cf. Sect. 3.5).

The elevated salinity and ^{36}Ar concentration determined for the metamorphic breakdown fluids trapped in the fluid inclusions could reflect any of the following: (1) preferential extraction of ^{36}Ar > Cl > H_2O during partial breakdown of antigorite; (2) diffusive addition of ^{36}Ar and dissolution of water soluble Cl during fluid migration; or (3) retrograde hydration of relic mantle minerals removing H_2O from solution.

These data are relevant to the interpretation of noble gases in fluid inclusions and crustal fluids more generally, because they indicate: (1) high concentrations of ^{36}Ar can be acquired by crustal fluids with a metamorphic origin, or by fluid-rock interaction; (2) crustal fluids can have a range of noble gas concentrations up to values of much greater than ASW (Fig. 9); and (3) the presence of atmospheric noble gases (alone)

does not provide reliable evidence that a fluid originated at the Earth's surface as ASW. The data indicate 'seawater-like' noble gas signatures can have complex histories and can survive metamorphic hydration and dehydration reactions in some cases.

5.5.2 Orogenic-Gold Deposits

Orogenic-gold deposits (e.g. lode-, mesothermal- or greenstone-gold deposits) have formed during periods of orogenesis throughout Earth history (Goldfarb et al. 2001; Groves et al. 2003). They occur in metamorphic terranes and are hosted by quartz and carbonate veins containing low salinity (<10 wt% NaCl eq.) aqueous and CO_2 fluid inclusions (e.g. Mernagh et al. 2007). Low salinity CO_2-bearing fluids could be mobilized by either metamorphic or magmatic processes during orogenesis and the origin of fluids in gold deposits is therefore contentious (Groves et al. 2003).

The metamorphic model explains the global association of gold-only ore deposits with seawater-altered volcanic rocks that occur proximally to, or host, mineralization (Phillips and Powell 1993). Phase equilibrium modeling indicates transitional greenschist-amphibolite facies metamorphism of altered-volcanic rock produces low salinity H_2O-CO_2 fluids similar to gold deposit fluid inclusions (Powell et al. 1991; Phillips and Powell 1993; Elmer et al. 2006). However, the high fluid flux necessary for economic gold mineralization requires externally derived fluids are focused into the mineralization zone (e.g. Yardley et al. 1993; Groves et al. 2003), and many gold deposits are spatially or temporally associated with granites or lamprophyres (e.g. Rock and Groves 1988; Neumayr et al. 2008). Furthermore, magmatic fluids are clearly involved in intrusion-related gold deposits that appear to form a continuum with orogenic-gold deposits (Sect. 5.4.1; Lang and Baker 2001).

Noble gases can help provide new constraints on the origin of gold-related fluids. Seawater-altered volcanic rocks (like serpentinites) are characterized by atmospheric Ne, Ar, Kr and Xe signatures (e.g. Staudacher and Allègre 1988; Burnard and Harrison 2005), but because seawater contains very little helium (Ozima and Podosek 2002), seawater-altered volcanic rocks can retain mantle ^{3}He components for prolonged periods (altered-basalts of Jurassic age have near atmospheric ^{40}Ar/^{36}Ar signatures but ^{3}He/^{4}He ratios of up to 0.4 Ra; Staudacher and Allègre 1988). These limited data suggest fluids generated by metamorphism of altered volcanic rocks are likely to be characterized by low ^{40}Ar/^{36}Ar and variable, but generally low, ^{3}He/^{4}He ratios. In contrast, magmatic fluids are often characterized by high ^{40}Ar/^{36}Ar and high ^{3}He/^{4}He ratios (e.g. Fig. 8; Sect. 5.4.1). Halogens can provide further information because they have a fairly limited range of signatures in magmatic fluids (Fig. 11).

1. Tienshan province, Uzbekistan

The giant Muruntau, Charmitan and related gold deposits of the southern Tienshan gold province, are associated with quartz, scheelite and sulphide-hosted fluid inclusions that have ^{3}He/^{4}He of 0.02–0.4 Ra and ^{40}Ar/^{36}Ar of 300–1200 (Graupner et al. 2006, 2010). The ore fluids from these deposits have high concentrations of atmospheric noble gas that are strongly enriched in ^{20}Ne/^{36}Ar and ^{3}He/^{36}Ar relative to ASW (Fig. 13; Graupner et al. 2006, 2010). These data were interpreted to favour a dominant role for modified air saturated water with the minor mantle component introduced by magmatic fluids sourced from lamprophyres close to the Muruntau and Charmitan deposits (Graupner et al. 2006, 2010), or associated with granitic magmatism (Morelli et al. 2007). While we agree the data are consistent with this interpretation, the discussion above suggests they are equally compatible with a dominant role for metamorphic fluids (Fig. 13). Furthermore, the Muruntau ore fluids have Br/Cl ratios of $(0.6-2.3) \times 10^{-3}$ (Graupner et al. 2006), that are similar to metamorphic fluids in gold deposits from Brussen ($1.6-2.3 \times 10^{-3}$; Yardley et al. 1993); Victoria, Australia ($0.6-3.6 \times 10^{-3}$; Fairmaid et al. 2011; Fu et al. 2012), Alleghany in the Sierra Nevada ($1.2-2.4 \times 10^{-3}$; Böhlke and Irwin 1992c) and the Yilgarn craton of Western Australia ($0.6-3.3 \times 10^{-3}$; Kendrick

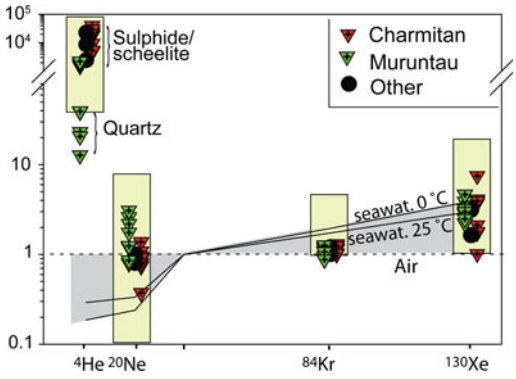

Fig. 13 Noble gas relative abundance ratios for gold-related fluid inclusions from Tienshan gold deposits (Graupner et al. 2006, 2010). Note quartz fluid inclusions are strongly depleted in He relative to Ar in sulphide or scheelite fluid inclusions, but all minerals are strongly enriched in light noble gases relative to ASW. *Yellow boxes* show the range of noble gas abundance ratios in altered oceanic basalts and serpentinites (Staudacher and Allegre 1988; Kendrick et al. 2011d)

et al. 2011b). Therefore further work is still required to establish a strong link between magmatism and gold mineralisation in the Tienshan province.

2. Brusson, NW Italy

Native gold from the 32 Ma Brusson gold deposit of Italy traps fluid inclusions with $^{3}He/^{4}He$ of 0.2 ± 0.1 Ra (2σ) that are within error of crustal values (Table 2), $^{40}Ar/^{36}Ar$ of 330–5,900 (Eugster et al. 1995; Pettke et al. 1997), and $^{136}Xe/^{132}Xe$ values that are slightly enriched in the fission component (Eugster et al. 1995). The fluid inclusions preserve elevated $^{4}He/^{40}Ar^{*}$ and $^{3}He/^{36}Ar$ ratios that together with the gas release spectra favour variable trapping of H_2O and a CO_2 vapour phase enriched in light noble gases (Pettke et al. 1997). The elevated He/Ar ratios also confirm gold is retentive of helium (Eugster et al. 1995; Pettke et al. 1997).

The Brusson vein gold system was further constrained by Sr and Pb isotope data that suggest calc-schists and intercalated meta-ophiolites, underlying the 10 km thick Monte Rosa Nappe, provide the closest possible fluid source (Pettke and Diamond 1997; Pettke and Frei 1996). Two samples of meta-ophiolite gave modern day $^{40}Ar/^{36}Ar$ of 330-670, whereas two samples of metagranite in the Monte Rosa nappe gave modern day $^{40}Ar/^{36}Ar$ of 1,700–4,700 (Pettke et al. 1997). The $^{40}Ar/^{36}Ar$ composition of the fluids (330–5,900) is therefore broadly consistent with the metamorphic model and suggests fluids with low $^{40}Ar/^{36}Ar$ may have acquired additional excess $^{40}Ar^{*}$ during migration through the Monte Rosa nappe. Pettke et al. (1997) suggested the fluids slightly elevated ^{3}He content could have been acquired from the metaophiolites or by fluid interaction with plutonic igneous rocks.

Ion chromatography indicates that the fluid inclusions in these deposits have Br/Cl of $(1.6-2.3) \times 10^{-3}$ and I/Cl of $(2-73) \times 10^{-6}$ (Yardley et al. 1993). The relatively low I/Cl values indicate very little interaction of the fluids with organic-rich sedimentary rocks (cf. Fig. 14).

3. Victoria, Australia

The ~440–360 Ma orogenic-gold deposits in Victoria are hosted by a sedimentary package comprising turbidites and shale, underlain by altered volcanic rocks of Cambrian age (Phillips et al. 2012). Helium data are not yet available for the Victorian gold deposits; however, the regional scale of halogen and Ar-Kr-Xe studies provide some important insights (Fairmaid et al. 2011; Fu et al. 2012).

Low salinity H_2O-CO_2 fluid inclusions have $^{40}Ar/^{36}Ar$ of 300–1,500 in the majority of deposits, but higher values of up to ~5,000 were observed in the regions largest deposits at Stawell and Ballerat (Fairmaid et al. 2011; Fu et al. 2012). The fluid inclusions have elevated ^{36}Ar concentrations of several times air saturation levels (e.g. similar to serpentine breakdown fluids; Fig. 9). The high noble gas concentrations and range of $^{84}Kr/^{36}Ar$ and $^{130}Xe/^{36}Ar$ values were interpreted to result from preferential desorption, or diffusive release, of Ar > Kr > Xe from rock units, and the range of fluid inclusion $^{40}Ar/^{36}Ar$ values was considered representative of altered volcanic source rocks and the meta-sedimentary host rocks (Fairmaid et al. 2011; Fu et al. 2012).

The Br/Cl and I/Cl ratios of gold-related fluids in Victoria encompass a similar range as

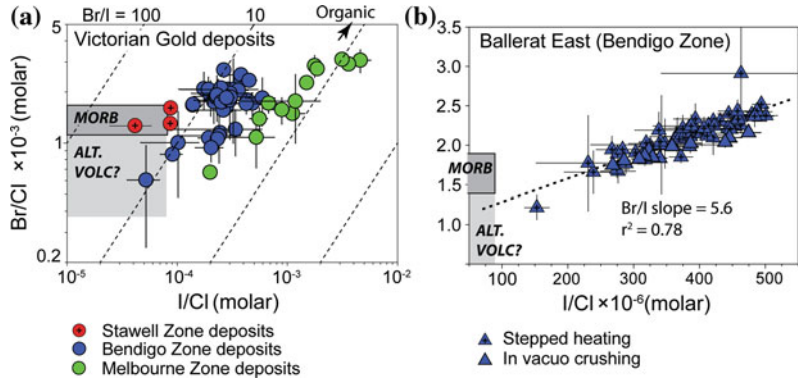

Fig. 14 Fluid inclusion Br/Cl and I/Cl for Victorian gold deposits, Australia. **a** Sample mean and standard deviation, distinguished on the basis of tectonic zone [modified after Fu et al. (2012)]. The Melbourne Zone is shale rich compared to the Bendigo and Stawell Zones. The dashed lines indicate constant Br/I ratios, organic matter has Br/I of ~1–10. **b** Sequential analyses for 13 samples obtained by stepped heating and in vacuo crushing. The best fit slope gives a Br/I ratio of 5.6, that is within the range of organic matter. The intercept is interpreted as altered volcanic rocks (modified after Fairmaid et al. 2011). The MORB field is after Kendrick et al. (2012) and the composition of altered volcanics (*alt. voc.*) is based on adding Cl-rich mica and amphibole to MORB (cf. Fig. 11)

reported for the Muruntau, Brusson and Alleghany deposits (Böhlke and Irwin 1992c; Yardley et al. 1993; Graupner et al. 2006; Fairmaid et al. 2011; Fu et al. 2012). However, the fluid inclusions show systematic variation across Victoria with basalt-like Br/Cl of $(0.9-1.6) \times 10^{-3}$ and I/Cl of $(11-91) \times 10^{-6}$ in the western-most Stawell deposit, and much higher I/Cl values of up to $5{,}200 \times 10^{-6}$ in fluid inclusions from the eastern-most deposits that are situated in the shale-rich Melbourne zone (Fig. 14; Fu et al. 2012). Similar mixing between two halogen components can be observed at the deposit scale, where mixing trends define Br/I ratios of ~6 (Fig. 14b), that are similar to Br/I ratios of organic matter (Fairmaid et al. 2011). As it is known iodine is lost to the fluid phase during metamorphism (Muramatsu and Wedepohl 1998), these data were interpreted to reflect derivation of halogens from two lithologies: altered-basalts and shale (Fairmaid et al. 2011; Fu et al. 2012).

The interpretation of the halogen and noble gas data in Victoria is analogous to stable isotope data which shows the fluids were partially rock-buffered and preserve a range of $\delta^{13}C$ characteristic of both igneous and sedimentary C sources (Fu et al. 2012). While most models for orogenic-gold favour deep metamorphic or magmatic sources for the fluids and gold, it has recently been suggested that diagenetic pyrite within sedimentary rocks in Victoria was the most important gold source (Large et al. 2011; Thomas et al. 2011). The halogen data provide strong supporting evidence for extensive fluid interaction with the sediments; however, the largest gold deposits are not associated with the most I-rich fluids or the most shale-rich parts of the Victorian gold province (Fu et al. 2012).

4. St Ives, Western Australia

The ~2.65 Ga St Ives gold deposits in the Yilgarn craton of Western Australia formed at estimated depths of 5–7 km during late Archean greenschist facies metamorphism of ~2.7 Ga greenstones (Groves et al. 2003; Kendrick et al. 2011c). There was abundant magmatism throughout the terrane overlapping the period of mineralisation and metamorphism, including U-rich potassic granites that were derived from anatexis of ~100–600 Myr old basement rocks (Champion and Sheraton 1997). Noble gas and halogen analyses were used to test if H_2O-CO_2 and CH_4 fluid inclusions associated with gold mineralisation at St Ives had similar origins.

This is significant because independently sourced abiogenic CH_4 has been suggested as a trigger for gold mineralisation (Neumayr et al. 2008), but CH_4 could alternatively have been produced by localised wall-rock reactions (Polito et al. 2001).

In contrast to all the other gold deposits studied to date, fluid inclusions from the St Ives goldfield preserve a huge range in $^{40}Ar/^{36}Ar$, with the highest values in samples containing CH_4 fluid inclusions (Figs.1j and 15). The lowest $^{40}Ar/^{36}Ar$ ratios of <2,000, indicate that some of the fluid inclusions have relatively high abundances of atmospheric noble gas. These values are similar to those observed in the majority of gold deposits and were suggested to represent metamorphic fluids derived from seawater-altered greenstones (Kendrick et al. 2011d). In contrast, the fluids with $^{40}Ar/^{36}Ar$ ratios of 20,000–50,000 were suggested to have had an external origin. It was argued that 100–600 Myr old basement rocks underlying the greenstones at 2.65 Ga represent the most likely source of the strongly radiogenic noble gas isotope signature, because the basement was significantly older than the greenstones and had not been altered by seawater (Kendrick et al. 2011b).

Noble gases could have been released from the basement by either crustal anatexis and exsolution of magmatic fluids from the potassic granites, or they could have been released by basement metamorphism (Kendrick et al. 2011b). It was suggested the fluids were then focused into the site of mineralisation, where atmospheric noble gases derived from the greenstone reduced the fluids $^{40}Ar/^{36}Ar$ ratio (Fig. 15). This interpretation of the noble gas data is analogous to the interpretation of other radiogenic isotopes (Pb and Sr) that also indicate fluid solutes had multiple sources from both the basement and greenstones (Ho et al. 1992). The noble gas data were regarded as being consistent with interaction of independently sourced CH_4 and H_2O-CO_2 during mineralisation (Neumayr et al. 2008); however, the ultimate source of the abiogenic CH_4 remains open to speculation (Kendrick et al. 2011b).

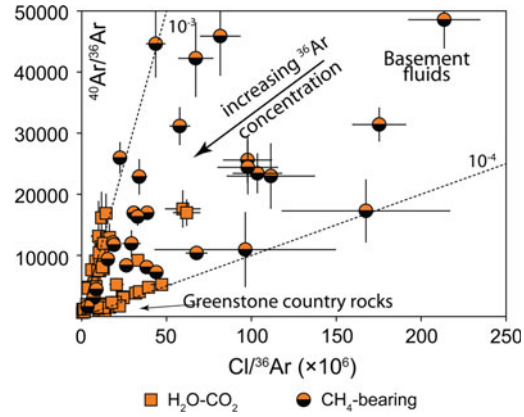

Fig. 15 Fluid inclusion $^{40}Ar/^{36}Ar$ versus $Cl/^{36}Ar$ for quartz and carbonate samples from the St Ives goldfield, Western Australia. The data are corrected for post-entrapment production of $^{40}Ar^*$, based on a mineralisation age of 2.65 Ga. Slopes with constant $^{40}Ar^*/Cl$ are shown for reference. CH_4 fluid inclusions associated with reduced alteration assemblages have higher $^{40}Ar/^{36}Ar$ than H_2O-CO_2 fluid inclusion associated with oxidised alteration assemblages (modified after Kendrick et al. 2011b). Data obtained by sequential crushing and stepped heating of six samples

Interpretation of noble gas signatures in Archean age samples needs to make allowance for high Archean production rates of radiogenic noble gas isotopes. The 1.25 Gyr half life of ^{40}K implies that for any given K content, the $^{40}Ar^*$ production rate was ~4 times higher at 2.65 Ga than it is today. Therefore, the most radiogenic $^{40}Ar/^{36}Ar$ signatures measured for the St Ives ore fluids are comparable to those obtained for magmatic fluids in the Ailaoshan gold deposits (Fig. 8a). Highly radiogenic noble gas components in Archean and Proterozoic age ore fluids are discussed more fully below (Sect. 5.6).

5.5.3 Fluids in Eclogites

Eclogites have mafic composition and are defined as containing garnet and omphacite, but also contain accessory hydrous minerals such as phengite. Eclogites can form by hydration of granulites (e.g. Boundy et al. 1997; Svensen et al. 2001), or prograde metamorphism of

blueschists (Ernst 1971). Fluid inclusions are commonly trapped in omphacite, garnet, kyanite and quartz (Svensen et al. 2001). However, hydrous minerals like phengite represent an important reservoir of excess ^{40}Ar (e.g. Arnaud and Kelley 1995; Kelley 2002; Sherlock and Kelley 2002), and probably other (non-radiogenic) noble gases, reflecting the increased compatibility of noble gases in many hydrous minerals in high pressure environments [see Kelley (2002) for review].

The noble gas content of eclogite fluid inclusions has not yet been systematically investigated. However, based on previous ^{40}Ar/^{39}Ar studies, the trapped argon component within phengite, and eclogite facies fluid inclusions, typically has ^{40}Ar/^{36}Ar in the range of 300–5,000 (Arnaud and Kelley 1995; Reddy et al. 1997; Giorgis et al. 2000; Kendrick 2007). Unsurprisingly noble gases enter the fluid phase when present, but are partitioned into phengite at low water-rock ratios as the fluid phase is consumed by hydration reactions. Eclogite facies minerals often show variable ^{40}Ar–^{39}Ar apparent ages that reflect a heterogenous distribution of extraneous ^{40}Ar*. This is usually interpreted to result from limited fluid mobility during prograde metamorphism, or redistribution of ^{40}Ar* between mineral phases during retrograde chemical exchange (e.g. Boundy et al. 1997; Giorgis et al. 2000; Warren et al. 2011).

The composition of Cl, Br and I was investigated in primary fluid inclusions trapped within omphacite and garnet from the Western Gneiss Region of Norway (Svensen et al. 2001). The high salinity of ~40–50 wt% recorded by these primary fluid inclusions is typical of eclogite facies fluid inclusions (e.g. Fu et al. 2001, 2002). The high salinity of these brines is suggested to result from preferential incorporation of $H_2O > Cl$ into hydrous minerals. Svensen et al. (2001) demonstrated the high salinity brine inclusions (which are much more saline than can be achieved by sub-aerial evaporation), have molar Br/Cl ratios of between 2.2×10^{-3} and 14.3×10^{-3}, and molar I/Cl of between 8×10^{-6} and 29×10^{-6}. The range of Br/Cl values is slightly greater than achieved on the seawater evaporation trajectory (Fig. 16), demonstrating strong fractionation of the halogens can occur during metamorphism at sufficiently low water-rock ratio (Svensen et al. 2001).

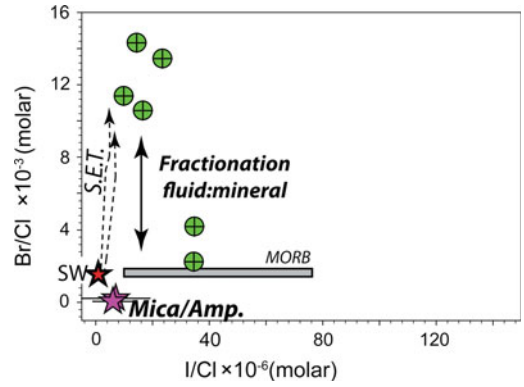

Fig. 16 Halogens in omphacite and garnet hosted primary fluid inclusions showing fractionation during eclogite facies metamorphism (Svensen et al. 2001). The compositions of igneous mica, amphibole (Kendrick 2012) and MORB (Kendrick et al. 2012) are also shown

5.6 Basement Noble Gas Components

In this final section of case studies, we discuss the significance of the highly radiogenic crustal noble gas isotope signatures (e.g. ^{21}Ne/^{22}Ne >0.2, ^{40}Ar/^{36}Ar >30,000, and ^{136}Xe/^{130}Xe > 3) recently reported for fluid inclusions from several Proterozoic or Archean ore deposits in different parts of Australia and Canada (Kendrick et al. 2006a, 2007; 2008a, b; 2011a, b); and we compare the fluid inclusions with CO_2 well gases from Colorado (Gilfillan et al. 2008) and ancient ground waters from South Africa (Lippmann et al. 2003; Lippmann-Pipke et al. 2011).

These highly radiogenic noble gas signatures get special attention because: (1) extra care must be taken to test Proterozoic and Archean age samples for the effects of post-entrapment radiogenic ingrowth; (2) such highly radiogenic noble gas signatures had not been observed in shallow ground waters previously; and (3) the interpretation of strongly radiogenic noble gas isotope signatures requires significant geological

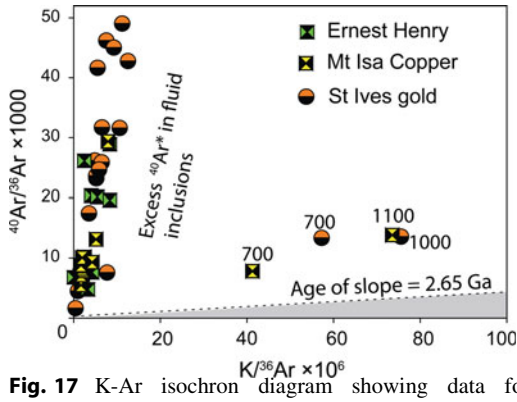

Fig. 17 K-Ar isochron diagram showing data for stepped heating quartz samples from the Proterozoic Mt Isa Inlier and Archean Yilgran Terranes of Australia (see Kendrick et al. 2006a, 2007, 2011a). For clarity, only the samples with very high $^{40}Ar/^{36}Ar$ are shown and uncertainty is not indicated. The highest $K/^{36}Ar$ ratios were obtained for low gas volume steps between 700 and 1,100 °C (cf. Fig. 3b). Sample Q5 from the 2.65 Ga St Ives goldfield had a total correction for in situ production of radiogenic $^{40}Ar^*$ of only 1.8 % (Kendrick et al. 2011b). The fluid inclusions have apparent ages of up to 11 Ga that reflect the presence of excess $^{40}Ar^*$

background, which is illustrated through a case study of the Mt Isa Inlier.

5.6.1 Excluding Radiogenic Ingrowth in Ancient Samples

Several arguments can be made to suggest the noble gas compositions reported for Archean and Proterozoic samples are fairly representative of the fluid inclusions initial composition. Most importantly, stepped heating irradiated quartz from the Mt Isa Inlier and Yilgarn craton yield apparent ^{40}Ar–^{39}Ar ages of up to 11 Ga, that demonstrate the samples do not contain enough K either within their fluid inclusions, or within mineral impurities, to generate the observed $^{40}Ar/^{36}Ar$ ratios (Fig. 17). The low K content of these samples unequivocally demonstrates that the measured $^{40}Ar/^{36}Ar$ ratios of up to 50,000 are representative of the fluid inclusions initial composition (Kendrick et al. 2006a, 2007; 2008a, b; 2011a, b).

Secondly, stepped heating irradiated quartz samples gives $^{134}Xe_U$ concentrations indicating <100 ppb U in the quartz matrix of all Mt Isa samples analysed, and the samples with the highest $^{21}Ne/^{22}Ne$ ratios have concentrations of only 2–20 ppb U (Kendrick et al. 2007, 2008a, 2011a). Crushing released $0.5-4.0 \times 10^{-15}$ mol $^{21}Ne^*$ per gram of these samples (Kendrick et al. 2011a) which is $\ll$100 % of the $^{21}Ne^*$ in the samples (Fig. 3a). Nonetheless, in situ production of the measured $^{21}Ne^*$ over a period of 1.55 Ga, would require a U concentration of 1,000–8,000 ppb [calculated using the equations in Ballentine and Burnard (2002)]. As this is up to 1,000 times greater than the measured U concentrations, it conclusively demonstrates that $^{21}Ne^*$ released by crushing, like $^{40}Ar^*$, represents a trapped component. Similar arguments indicate $^{21}Ne^*$ is also a trapped component in ~2 Ga fluid inclusions from the Kapvaal craton (Lipmann-Pipke et al. 2011), and 2.65 Ga fluid inclusion samples from the Yilgarn (Kendrick et al. 2011b).

The majority of fluid inclusion samples from both the Yilgarn and Mt Isa Inlier have fluid inclusion $^{21}Ne^*/^{40}Ar^*$ and $^{136}Xe^*/^{40}Ar^*$ ratios close to the crustal production ratios that would be expected in high temperature fluids (Kendrick et al. 2011a, b). However, samples dominated by CO_2 fluid inclusions from the Mt Isa Inlier, are systematically enriched in $^{21}Ne^*/^{136}Xe^*$ relative to possible production ratios (Fig 18a). As both $^{21}Ne^*$ and $^{136}Xe^*$ are produced from U, this is impossible to explain by in situ production, but is consistent with fractionation of noble gases between H_2O and CO_2 prior to trapping (Fig. 18a; Kendrick et al. 2011a).

Helium isotope ratios are more sensitive to overprinting than Ne, Ar or Xe isotope ratios. Measured $^4He/^{40}Ar^*$ ratios indicate helium leaked out of Mt Isa quartz samples (Kendrick et al. 2011a); but the $^4He/^{40}Ar^*$ ratios measured for gold-related fluid inclusions from St Ives are in the range of expected Archean production ratios (Fig 18b; Kendrick et al. 2011b). Minor He leakage or in situ production of ^4He in these samples is likely; however, the data are most easily explained if the measured $^3He/^4He$ ratios of ~0.01 Ra remains close to their initial values; and dominantly crustal $^3He/^4He$ ratios are expected in fluids with extremely radiogenic $^{40}Ar/^{36}Ar$, $^{21}Ne/^{22}Ne$ and $^{136}Xe/^{130}Xe$ ratios (Kendrick et al. 2011b). Preservation of near

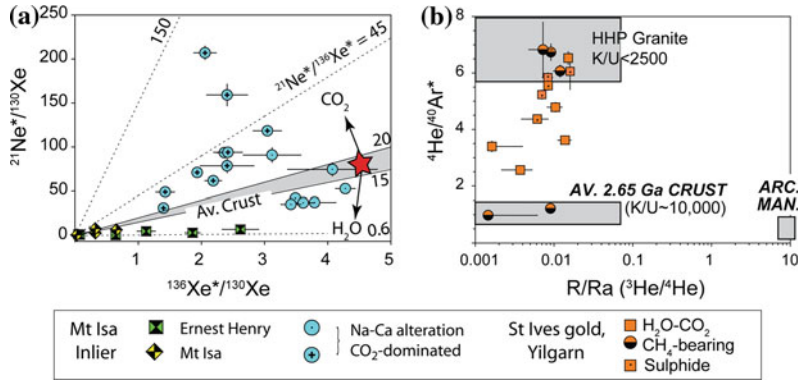

Fig. 18 Fluid inclusion abundance ratios for radiogenic noble gas isotopes. **a** Samples from the Mt Isa Inlier, sequential crushing shows Ne/Xe enrichment in two samples that are dominated by CO_2—only fluid inclusions (Kendrick et al. 2011a). **b** Fluid inclusions from the St Ives goldfield of Western Australia (hosted by 10 quartz and sulphide samples), record $^4He/^{40}Ar^*$ ratios similar to expected production ratios (Kendrick et al. 2011b)

original $^3He/^4He$ ratios requires the samples low salinity water and CH_4- or CO_2-only fluid inclusions have very high (noble gas)/(U + Th) ratios and negligible U and Th.

Finally, the range of $^{136}Xe/^{132}Xe$ reported for Proterozoic and Archean age fluid inclusions (Kendrick et al. 2011a, b) is similar to that reported for fluid inclusions in Phanerozoic gold deposits (Sun et al. 2009), modern well gases (Gilfillan et al. 2008) and fracture-hosted waters from the Witwatersrand basin (Lippmann et al. 2003) (see Table 5). Calculated $^{21}Ne^*/^{22}Ne^*$ ratios for Proterozoic and Archean fluid inclusions range from unusually low values of 0.1, whereas high values would be expected to result from in situ production of $^{21}Ne^*$, up to maximum values that are similar to fracture-hosted ground waters in the Witwatersrand basin (3.3 ± 0.2; Lippmann-Pipke et al. 2011). These observations are all consistent with noble gases in the fluid inclusions being largely representative of their initial compositions.

5.6.2 The Mt Isa Inlier, Australia

The Proterozoic Mt Isa Inlier of northeastern Australia is famous for its high heat producing granites (McLaren et al. 1999; Sandiford et al. 2002) and rich endowment with ore deposits that formed in hydrothermal systems spanning at least 170 Myr of crustal evolution (Oliver 1995; Oliver et al. 2008). Noble gas and halogen data are available for a large number of ore deposits and related alteration from two contrasting settings within the inlier (Heinrich et al. 1993; Kendrick et al. 2006a, b, c, 2007, 2008a, 2011a; Fisher and Kendrick 2008).

Iron-oxide-copper-gold-(± U ± REE) deposits and related regional-scale Na-Ca alteration (albitisation) are found throughout the Eastern Fold Belt (Oliver et al. 2004; Mark et al. 2006; Kendrick et al. 2006a, b, 2007, 2008a, 2011b; Fisher and Kendrick 2008). The Eastern Fold Belt comprises greenschist-amphibolite facies metasediments (including meta-evaporitic calc-schists) intruded by regionally extensive 1,550–1,490 Ma Williams-Naraku Batholiths (Page and Sun 1998; Foster and Rubenach 2006). The iron-oxide-copper-gold deposits are spatially associated with regional faults (Mark et al. 2006). Ernest Henry (166 Mt of 1.1 % Cu and 0.5 ppm Au) and several other deposits overlap intrusion of the 1,550–1,490 Ma Williams-Naraku Batholiths, whereas the Osborne and Starra deposits are suggested to have formed at ~1,595–1,570 Ma (Oliver 1995; Page and Sun 1998; Oliver et al. 2004, 2008; Mark et al. 2006; Duncan et al. 2011). Mineralisation and alteration related fluid inclusions include high salinity brines (e.g. 60 wt% NaCl eq.) and liquid CO_2 trapped at estimated depths of 8–10 km (e.g. Kendrick et al. 2011a). Carbonate veins in regional

Table 5 Crustal fluids with radiogenic noble gas isotope signatures

		Trapping age	$^{3}He/^{4}He$ (R/Ra)	$^{21}Ne/^{22}Ne$	$^{20}Ne/^{22}Ne$	$^{40}Ar/^{36}Ar$	$^{136}Xe/^{132}Xe$	Notes
Fluid inclusions								
Mt Isa	H_2O-CO_2	1.55–1.5 Ga	?	0.36	9.2	40,000	0.71	1
St Ives	CH_4-rich	2.65 Ga	<0.01	0.56	8.3	50,000	0.4	2
Wernecke	H_2O	1.6 Ga	<0.02	0.35	6.6	40,000		3
Ailaoshan	H_2O–CO_2	50 Ma	1.3	0.47	11.5	>9,000	0.45	4
Witwatersrand	?	2 Ga ?	0.01	0.59	8.2	>100,000	0.35	5
Geo-fluids								6
McElmo Dome well gases	CO_2	0	0.17	0.11	8.9	25,000		7
Witwatersrand fracture-hosted	H_2O-CH_4	0	<0.04	0.16	8.9	9,000	0.55	8
Air			1	0.029	9.8	299	0.33	9

Notes
1 Radiogenic signatures in samples dominated by CO_2-only fluid inclusions and H_2O–CO_2 fluid inclusions (Kendrick et al. 2011a)
2 Samples containing CH_4 fluid inclusions H_2O-CH_4 (Kendrick et al. 2011b)
3 (Kendrick et al. 2008b)
4 (Sun et al. 2009)
5 (Lippmann-Pipke et al. 2011)
6 Geo-fluids sampled from depths of 1–3 km are more likely to have mixed with surface–derived groundwater or other atmospheric components than fluid inclusions trapped at depths of 6–10 km
7 (Gilfillan et al. 2008)
8 (Lippmann et al. 2003; Lippmann-Pipke et al. 2011)
9 Table 2 and Ozima and Podosek (2002)

Na-Ca alteration have $\delta^{13}C$ ranging from magmatic values of −6 ‰ to country rock values of −1 ‰ (Oliver 1995; Oliver et al. 1993). Sulphur, O and H isotopes are consistent with, but do not prove, the involvement of magmatic fluids in ore deposition (Mark et al. 2004, 2006). Two major uncertainties in the genesis of these deposits are therefore the extent of magmatic fluid involvement and the role of evaporites in generating high salinity brines (e.g. Barton and Johnson 1996; Pollard 2000, 2001).

The Mt Isa copper deposit (250 Mt of 3.3 wt% Cu) of the Western Fold Belt differs to iron-oxide-copper-gold deposits in several important aspects. Copper mineralization is superimposed on earlier Pb-Zn mineralization; it is hosted by greenschist facies shales (Perkins 1984; Swager 1985), and minor pegmatites represent the only known igneous activity within the Western Fold Belt during the Isan orogeny (Connors and Page 1995). The deposit is associated with mine-scale silica-dolomite rather than regional Na-Ca alteration; copper (with minor cobalt) is the only economic commodity, and iron forms sulphides not oxides (Swager 1985; Heinrich et al. 1989). Fluid inclusions hosted by silica and dolomite alteration are dominantly two phase liquid-vapour with salinities of 5–25 wt% salts (Heinrich et al. 1989). In contrast to the iron-oxide-copper-gold systems, high salinity brine inclusions are lacking and CO_2 is rare (Heinrich et al. 1989; Kendrick et al. 2006a). The S, O and H isotope data indicate the presence of locally derived sedimentary S and are consistent with introduction of additional S as seawater sulphate in evolved basinal brines or

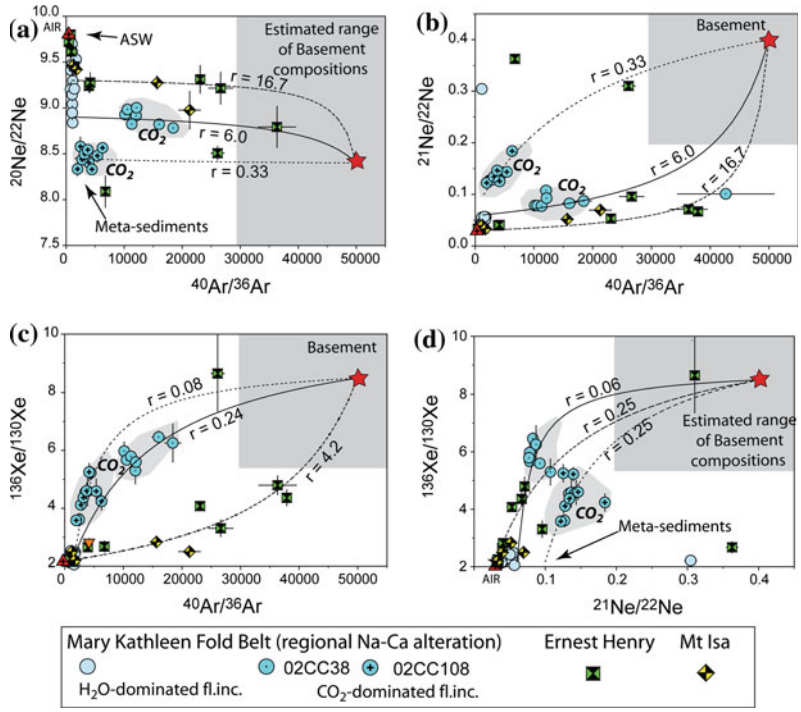

Fig. 19 Noble gas mixing model for fluid inclusions related to ore deposition and regional alteration in the Mt Isa Inlier (Kendrick et al. 2011b). The r-values in each plot describe the mixing trends curvature, where r is related to the relative abundance of the denominator isotopes (e.g. Eq. 1; Sect. 5.4.1; Langmuir et al. 1978). The indicated range of 'estimated basement compositions' is based on typical noble gas abundances in sedimentary and basement rocks (Table 2), realistic K, Th and U concentrations and 600 Myr of radiogenic ingrowth (see Kendrick et al. (2011b) for a full discussion of the model and uncertainties). Data obtained by sequential crushing of 13 samples

derived during metamorphism under oxidizing conditions (Andrew et al. 1989; Heinrich et al. 1989; Painter et al. 1999).

1. Noble gases and halogens

Despite the substantially different geological settings of the iron-oxide-copper-gold mineralization and Mt Isa style copper mineralization (above), the fluid inclusions from both styles of ore deposit have maximum $^{40}Ar/^{36}Ar$ ratios of $\geq$30,000 and combined Ne-Ar-Xe systematics that suggest mixing of noble gases from three very similar reservoirs: (1) ancient basement rocks with highly radiogenic noble gas signatures; (2) air saturated water; and (3) a third component representative of the meta-sedimentary country rocks (Fig. 19a). The mixing model in Fig. 19 is undoubtedly simplification of a complex system (see Kendrick et al. 2011a); however, the model is consistent with both Fold Belts comprising a relatively thin layer of meta-sediments underlain by much older and broadly similar pre-Barramundi basement lithologies (MacCready et al. 1998). The model therefore provides a useful starting point for interpretion of the fluid inclusion noble gas signatures (Kendrick et al. 2011a).

A highly radiogenic basement noble gas signature is expected in magmatic fluids derived from the Williams-Naraku Batholiths in the Eastern Fold Belt, because these intrusions have Nd isotope signatures that indicate a basement source with an average age of ~650–700 Myr at 1,550 Ma (Page and Sun 1998; Mark 2001). Sequential analysis of iron-oxide-copper-gold or Na-Ca alteration related samples, demonstrates the fluid inclusions within each sample have

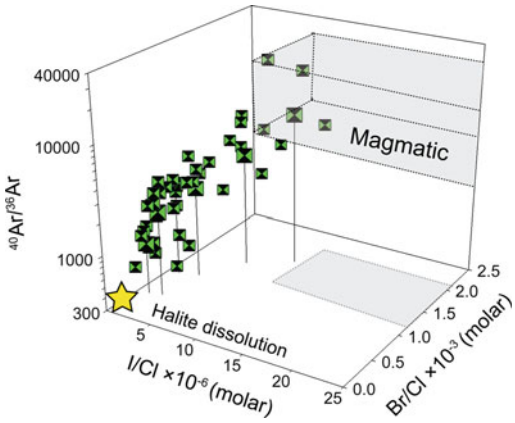

Fig. 20 Fluid inclusion halogen and $^{40}Ar/^{36}Ar$ data obtained by stepped heating Ernest Henry quartz. Individual steps are shown as small symbols, large symbols with drop lines represent weighted means for each sample (modified after Kendrick et al. 2007)

compositions that vary between characteristic limits (see Fig. 19). The noble gas mixing trends defined for the CO_2 fluid inclusions and Ernest Henry ore fluids are comparable to stable isotope data that show mixing of magmatic and metasedimentary C components (cf. Fig. 19a; Oliver et al. 1993). The distinct curvature of mixing trends obtained for samples dominated by CO_2 fluid inclusions compared to H_2O dominated ore fluids, probably results from fractionation of noble gas elemental abundance ratios during CO_2-H_2O interaction (e.g. Fig. 18a; phase separation controls the *r*-values defined in Sect. 5.4.1). The involvement of magmatic fluids in the Ernest Henry deposit is further constrained because the fluids with the most radiogenic noble gas signatures have halogen signatures similar to other magmatic fluids (Fig. 11a), whereas fluids with less radiogenic noble gas signatures are associated with 'halite dissolution' halogen signatures (Fig. 20). Taken together, the data (Figs. 19 and 20) provide strong evidence for magmatic fluids in the Ernest Henry iron-oxide-copper-gold deposit and regional Na-Ca alteration in the northern part of the Eastern Fold Belt (Kendrick et al. 2007, 2008a, 2011a). However, basin derived fluids that interacted with scapolite (or halite) were also present and dominated much of the Na-Ca alteration system (Kendrick et al. 2008a), as well as the southernmost Osborne deposit, which predated intrusion of the Williams-Naraku batholiths (Fisher and Kendrick 2008).

The strongly radiogenic noble gas isotope signature of low salinity fluid inclusions associated with the Mt Isa copper mineralization in the Western Fold Belt is unlikely to reflect the involvement of magmatic fluids but could be explained if: (1) surface-derived basinal fluids were advected into the >10–15 km deep basement (which was the source of the Williams-Naraku batholiths in the Eastern Fold Belt); or (2) basement metamorphism produced a metamorphic fluid that ascended to the site of mineralization (Kendrick et al. 2006a, 2011a). Mt Isa copper related fluid inclusions have much higher Br/Cl than the iron-oxide-copper-gold deposits (Fig. 21a; Heinrich et al. 1993; Kendrick et al. 2006a). If the Mt Isa ore fluids had a surface origin, the Br/Cl data indicate sub-aerial evaporation as the dominant source of salinity (Fig. 21a; Kendrick et al. 2006a). However, Kendrick et al. (2006a) argued an exclusively surface origin was unlikely because: (1) the ^{36}Ar concentration of the silica fluid inclusions with the highest $^{40}Ar/^{36}Ar$ ratios are in the range that would be expected in basement-derived metamorphic fluids (based on typical OH and ^{36}Ar concentrations; Fig. 21b; Kendrick et al. 2006a). (2) there is no evidence for fluid inclusion evidence for hydrothermal boiling; and (3) a much higher ^{36}Ar concentration would be likely in a surface derived fluid that acquired $^{40}Ar/^{36}Ar$ of >> 30,000 (ground waters with air-saturated ^{36}Ar concentrations have $^{40}Ar/^{36}Ar$ of < 500 and meteoric O-H isotope signatures; sect. 5.1; Phillips and Castro 2003) see Kendrick et al. (2006a).

The total variation in fluid inclusion Br/Cl, I/Cl, ^{36}Ar concentration and $^{40}Ar/^{36}Ar$ in silica and dolomite fluid inclusions (Fig. 21), was therefore interpreted to result from mixing basement-derived metamorphic fluids and basinal fluids (best preserved in the dolomite fluid inclusions which have the highest salinity), with an additional contribution of atmospheric noble gases derived from the meta-sedimentary country rocks (Fig. 21; Kendrick et al. 2006a). The involvement

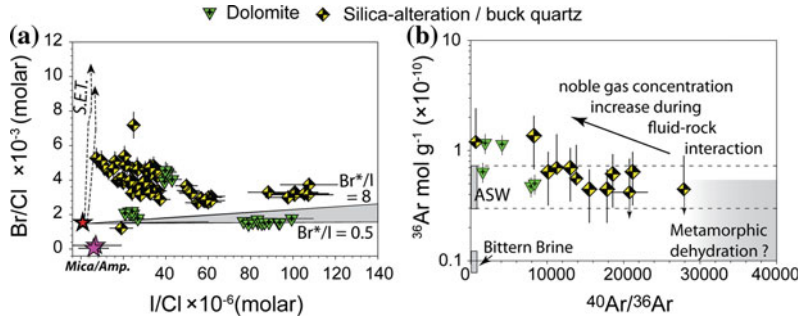

Fig. 21 Noble gas and halogen data for fluid inclusions related to Mt Isa copper mineralisation. **a** sequential Br/Cl and I/Cl analyses of silica-dolomite alteration showing the seawater evaporation trajectory (Zherebtsova and Volkova 1966), the composition of igneous mica and amphibole (Kendrick 2012) and organic Br*/I ratios of 0.5–8. **b** The sample maximum $^{40}Ar/^{36}Ar$ ratio and calculated ^{36}Ar concentration. Bittern brines with 0.07×10^{-10} mol ^{36}Ar g^{-1} and the estimated compositional range of basement-derived metamorphic fluids (Fig. 19; Kendrick et al. 2006c) are shown for reference

of metamorphic breakdown fluids is broadly consistent with mineralization during the latter part of the Isan orogeny (Perkins et al. 1999), but is not consistent with a younger post-orogenic age of ~1,370 Ma (Gregory et al. 2008). However, the younger age is based on Re-Os data that do not define a statistical isochron (cf. Gregory et al. 2008), and is difficult to reconcile with the relative timing of copper mineralization (Perkins 1984; Swager 1985). Assuming mineralization occurred during the Isan orogeny, the <1,500 Ma South Nicholson Group sediments can be excluded as the source of basinal fluids during mineralization (cf. Wilde 2011).

5.6.3 Comparison of Fluid Inclusions and Unusual Geo-Fluids

The CO_2 fluid inclusions associated with Na-Ca alteration in the Eastern Fold Belt of the Mt Isa Inlier (Fig. 19) have Ne, Ar and Xe isotope signatures similar to CO_2 well gases in the Doe Canyon and McElmo Dome gas fields of the Colorado plateau, USA (Table 5; Gilfillan et al. 2008). The CO_2 well gases therefore provide a useful analogue for the CO_2 fluid inclusions and vice versa.

Helium leaked out of the CO_2 fluid inclusions; however, the McElmo Dome well gases have a $^3He/^4He$ ratio of ~0.13–0.17 Ra (Gilfillan et al. 2008), that demonstrate a small mantle helium component could potentially have been present in the CO_2 fluid inclusions. The strongly radiogenic Ne-Ar-Xe signature of the CO_2 fluid inclusions is consistent with a source from a basement-derived 'crustal' magma such as the Williams-Naraku Batholiths (Kendrick et al. 2011a). However, input of a minor mantle component has been suggested as a heat source, to explain the presence of mafic lithologies, and abundant CO_2 fluid inclusions (Oliver et al. 2008). Comparison of the CO_2 fluid inclusions and well gases underlines that the noble gas data (Fig. 19) do not preclude input of a minor mantle component in the Eastern Fold Belt mineral systems (Kendrick et al. 2011a).

The CO_2 gases in the Colorado Plateau have variable magmatic or metamorphic sources but have been trapped in sedimentary reservoirs for millions of years, meaning they are important natural analogues for testing long term CO_2 sequestration and storage (Gilfillan et al. 2009). The CO_2 well gases have undoubtedly interacted with modern ground waters to a much greater extent than CO_2 trapped in fluid inclusions at depths of 8–10 km (cf. Gilfillan et al. 2009; Kendrick et al. 2011a). However, fluid inclusion studies provide new insights on the possible origins of atmospheric noble gases in deeply sourced CO_2 fluids (Kendrick et al. 2011a). The origin of atmospheric noble gases in the well gases has important implications for interpreting the extent of CO_2 well gas interaction with groundwater, and

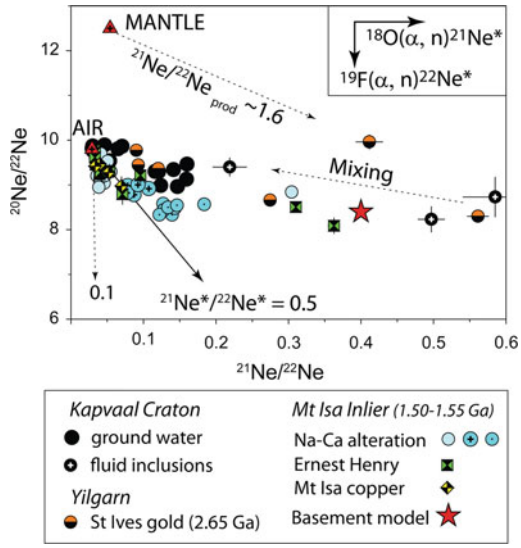

Fig. 22 Neon isotope data for fluids in three Precambrian terranes (Kendrick et al. 2011b, c; Lippmann-Pipke et al. 2011). The average $^{21}Ne^*/^{22}Ne^*$ of ~0.5 determined for the majority of fluids in sedimentary basins is shown for reference (Kennedy et al. 1990; Ballentine and Burnard 2002). Fluid inclusions show much greater variation in neon isotope composition than basinal fluids, with $^{21}Ne^*/^{22}Ne^*$ varying from 0.1 up to 3.3 ± 0.2 (Lippmann-Pipke et al. 2011). The *red star* indicates the estimated composition of Mt Isa's basement the symbols follow Fig. 19

therefore quantifying the long term viability of CO_2 storage (Gilfillan et al. 2009).

Fracture-hosted waters in deep gold mines in South Africa with a dominantly surface origin have extremely radiogenic noble gas signatures similar to fluids inclusions from the Mt Isa Inlier and St Ives goldfield of Western Australia (Table 5; Lippmann et al. 2003; Lippmann-Pipke et al. 2011; Kendrick et al. 2011a, b). These waters contain abiogenic CH_4, the origin of which is of great interest for determining the potential depth of the biosphere (e.g. Lippmann et al. 2003; Lippmann-Pipke et al. 2011). However, interpretation of strongly radiogenic noble gas isotope signatures in modern fracture-hosted ground waters and ancient fluid inclusions is not exactly analogous. The interpretation that strongly radiogenic noble gas isotope signatures in the Mt Isa Inlier and Yilgarn craton had basement origins is based on the premise that at the time of mineralization, both terranes comprised a layer of relatively young meta-sediment, or altered volcanic rocks (e.g. lithologies with significant atmospheric noble gas), underlain by much older igneous basement (with low abundances of non-radiogenic noble gas; cf. Table 3). In contrast, the much greater age of the Kapvaal craton at the present day (>3 Ga), implies that highly radiogenic noble gas signatures could potentially be acquired by fluid interaction with a much greater range of lithologies, making it more difficult to infer a fluid source.

5.6.4 Neon Isotope Systematics of Basement Lithologies

Neon isotope data are conventionally presented in a three isotope diagram (Fig. 22) and the ratio of nucleogenic $^{21}Ne^*$ to nucleogenic $^{22}Ne^*$ is obtained by correcting the data for an atmospheric contribution based on the non-radiogenic ^{20}Ne isotope (implicitly assuming that there is no mantle Ne contribution). Neon data for a variety of natural gases from all over the world have a limited range of $^{21}Ne^*/^{22}Ne^*$, with a best fit value of ~0.52 (Kennedy et al. 1990; Ballentine and Burnard 2002). The $^{21}Ne^*$ and $^{22}Ne^*$ isotopes are produced by alpha particles interacting with ^{18}O or ^{19}F, respectively. The empirically determined

relationship between $^{21}Ne^*/^{22}Ne^*$ and O/F (Hünemohr 1989), indicates the average $^{21}Ne^*/^{22}Ne^*$ of 0.52 determined for fluids in sedimentary basins corresponds an average U mineral O/F ratio of ~113 in sedimentary basins (Kennedy et al. 1990).

In contrast to natural gases in sedimentary basins, fluid inclusions in metamorphic environments have extremely variable $^{21}Ne^*/^{22}Ne^*$ (Fig. 22). The minimum $^{21}Ne^*/^{22}Ne^*$ values of ~0.1, obtained for H_2O dominated fluid inclusions in samples from the Eastern Fold Belt of the Mt Isa Inlier (Fig. 22), are equivalent to an O/F ratio of ~22, that may be representative of U minerals in halogen rich metasediments (Kendrick et al. 2011a). In contrast, much higher $^{21}Ne^*/^{22}Ne^*$ values of up to ~3.3, in the Witwatersrand basin (Lippmann-Pipke, et al. 2011), are equivalent to a U mineral O/F ratio of ~720 that is close to the O/F ratio of average crust (e.g. Rudnick and Gao 2003). Similarly high $^{21}Ne^*/^{22}Ne^*$ values are obtained for fluid inclusions suggested to contain basement-derived noble gases in the Mt Isa Inlier (Kendrick et al. 2011a) and Yilgarn craton (Fig. 22; Kendrick et al. 2011b).

The variable $^{21}Ne^*/^{22}Ne^*$ reported for metamorphic environments indicate U and F are unevenly distributed through the crust and that fluids in low porosity metamorphic environments ($\ll$0.1 % porosity) are much more poorly mixed than fluids in sedimentary basins (Kendrick et al. 2011a, b).

A second important consideration for interpretation of neon data is that, if the anomalous neon signature is representative of an igneous basement source (e.g. Fig. 19), the atmosphere corrected $^{21}Ne^*/^{22}Ne^*$ ratio is unlikely to be representative of the $^{21}Ne/^{22}Ne$ production ratio (Kendrick et al. 2011a, b). This is because comparison with basalt glasses suggests that igneous basement lithologies, that are not exposed to seawater, would probably have had a prominent mantle noble gas component at time zero (basalt glasses have mixed mantle and atmospheric noble gas signatures; e.g. Graham 2002). If the igneous basement had an initially mantle signature, the $^{21}Ne/^{22}Ne$ production ratio would be obtained by a vector from the mantle composition, implying a $^{21}Ne/^{22}Ne$ production ratio of significantly less than the air corrected $^{21}Ne^*/^{22}Ne^*$ ratio (see Fig. 22; Kendrick et al. 2011a, b). It should be noted that the broad mixing trend between the 'anomalous crustal neon' with very high $^{21}Ne/^{22}Ne$ and air does not indicate the basement had an initially atmospheric composition. This trend probably reflects mixing of the distinct basement signature with atmospheric noble gases present in either ground water or meta-sediments (e.g. Fig. 19; Kendrick et al. 2011a, b). Noble gas mixing trends have complicated histories and unravelling the ultimate origin and evolution of noble gases in the Earth's deep crust can be challenging (see Fig. 19 and Sect. 5.6.2; Kendrick et al. 2011a, b).

6 Summary and Conclusions

Noble gases and halogens record a range of distinct compositions in the fluid inclusions of different types of ore deposit (Sect. 5). The isotopes of helium provide a sensitive means for detecting the presence of mantle-derived components and the orders of magnitude variation in noble gas and halogen signatures means they can provide powerful constraints on fluid origins. Considerable advances have been made in improving the interpretation of these signatures over the last 5–10 years.

Investigation of modern pore fluids in marine sediments (Fehn et al. 2000, 2003, 2006, 2007; Muramatsu et al. 2001, 2007; Tomaru et al. 2007a, b, 2009), and regional-scale studies focused on sediment-hosted ore deposits (Fairmaid et al. 2011; Fu et al. 2012), have conclusively demonstrated halogens (Br as well as I) are partly buffered by organic matter in both sedimentary and metamorphic environments (Fig. 14). In addition, the Br/Cl versus I/Cl three element diagram has been demonstrated as a powerful tool for deconvolving organic Br contributions (Fairmaid et al. 2011; Kendrick et al. 2011c).

The investigation of eclogite facies fluid inclusions has provided evidence for halogen fractionation during metamorphism (Svensen et al. 2001; Kendrick et al. 2011d), and new work has started to document the halogen composition of hydrous mineral phases and the MORB mantle (Kendrick et al. 2011d, 2012; Kendrick 2012).

Investigation of noble gases in metamorphic minerals and fluid inclusions has demonstrated atmospheric noble gases are introduced into crustal lithologies during seawater alteration (Kendrick et al. 2011d). Furthermore, fluid inclusions associated with a range of ore deposits in the Mt Isa Inlier have an identifiable contribution of atmospheric noble gas derived from wall-rock (Fig. 19a). In most crustal environments the $^{3}He/^{4}He$ isotope signature of a magmatic fluid is more conservative than the heavy noble gases (e.g. Sect. 5.4.3; Fig. 8). However, fluid interaction with basalt is recognized as an important source of ^{3}He in mid-ocean ridge vent fluids (e.g. Abrajano et al. 1988, 1990; Stuart et al. 1994); and igneous rocks intruded into the crust can preserve mantle $^{3}He/^{4}He$ signatures for 10's of Myr (Staudacher and Allegre 1988; Moreira et al. 2003), suggesting mobilization of ^{3}He during metamorphism is probable.

These observations indicate simplistic interpretations of noble gases in crustal fluids based on equating atmospheric noble gases with the presence of ASW, or diminutive mantle ^{3}He components with a magmatic fluid, are not applicable to high temperature fluids trapped in fluid inclusions. Several examples have been highlighted in this chapter were constraints from noble gases have shown good agreement with other stable (O, H, C, S) or radiogenic (Sr, Nd, Pb) isotope systems, and it has been highlighted that the interpretation of fluid inclusion noble gas isotope signatures is often analogous to other isotope systems (Fig. 19; Fairmaid et al. 2011; Kendrick et al. 2011a, b; Fu et al. 2012). Noble gases can reveal features of hydrothermal systems that are overprinted in other isotopic systems because their signatures vary by such large amounts (e.g. orders of magnitude; Tables 2 and 4), not because they behave 'conservatively': fluid-rock interactions are significant at the low water/rock ratios relevant to many crustal fluids (Table 3).

Finally the behavior of noble gases in the crust depends on the crustal setting (temperature and water-rock ratio) and timescale over which the behavior is observed. Over long time periods, there is a true exchange of noble gases between solid lithological and fluid reservoirs. Atmospheric noble gases initially adsorbed onto sedimentary materials are incorporated into mineral structures during diagenesis (Podosek et al. 1980, 1981); and atmospheric noble gases are trapped in hydrous lithologies formed during seawater alteration (Kendrick et al. 2011d). Trapped atmospheric noble gases are then released to the fluid phase, along with radiogenic noble gas isotopes, during dehydration metamorphism. As a result, most fluid inclusions (with strongly rock-buffered O and H isotope signatures), have ^{36}Ar concentrations of more than air-saturated water (Fig. 9).

6.1 Future Directions

Noble gas and halogen analysis has been demonstrated as a powerful tool for constraining fluid origins in ore deposits and these techniques can be applied to geological processes in other settings. In particular, future work is required to better understand the long term exchange of noble gases between atmospheric and crustal reservoirs. Future studies may therefore combine investigation of fluid inclusion and mineral phases or whole rocks to a much greater extent than has previously been the case (e.g. Pettke et al. 1997).

The available data indicate most geological fluids have elevated noble gas concentrations (Fig. 9), and changes in concentration have been suggested as a means to infer the way in which noble gas isotope signatures are altered during fluid-rock interaction (Fig. 21b; Kendrick et al. 2006a, 2011b). Provided steps are taken to minimise the adsorption of water, manometric

determination of total gas (CO_2, CH_4, H_2O) pressures during fluid inclusion analysis would allow wider determination of noble gas concentrations, enabling these ideas to be more widely evaluated.

Further improvements in fluid inclusion analysis are possible. The work of Scheidegger et al. (2010) has demonstrated that simple variations in sample preparation procedure can help eliminate undesirable modern air contaminants. Laser ablation of individual fluid inclusions is unlikely to be widely applicable; however, 213 and 193 nm lasers could be used for controlled ablation of unusually large fluid inclusions or groups of related fluid inclusion. Opaque sulphide minerals have been demonstrated as robust containers of helium, suggesting routine application of near infra-red microscopy techniques to characterise the fluid inclusions trapped in these minerals is desirable.

Analysis of neon isotopes can be used to test for mantle components in quartz samples that do not always retain helium. Furthermore, rigorous investigation of quartz samples with variable helium retentivities, using transmission electron microscopy, may enable the properties that cause helium leakage to be identified. The potential for helium (and other noble gases) to diffuse into, or out of, fluid inclusions should be studied systematically. Experimental studies establishing a thermodynamic basis for noble gas retention in fluid inclusions hosted by different minerals over a range of temperatures and pressures is desirable.

The combined behaviour of halogens and noble gases during groundwater-hydrocarbon interaction is poorly constrained (Kendrick et al. 2011c). Significant advances noble gases and halogens in could be made by combined investigation of noble gases and halogens in ground waters and fully characterised fluid inclusions (Ballentine et al. 1994; Lippmann-Pipke et al. 2011). These areas provide exciting avenues for future research.

References

Abrajano TA, Sturchio NC, Bohlke JK, Lyon GL, Poreda RJ, Stevens CM (1988) Methane-hydrogen gas seeps, Zambales Ophiolite, Philippines: deep or shallow origin? Chem Geol 71(1–3):211–222

Abrajano TA, Sturchio NC, Kennedy BM, Lyon GL, Muehlenbachs K, Bohlke JK (1990) Geochemistry of reduced gas related to serpentinisation of the zambales Ophiolite, Phillippines. Appl Geochem 5(5–6):625–630

Aeschbach-Hertig W, Peeters F, Beyerle U, Kipfer R (2000) Palaeotemperature reconstruction from noble gases in ground water taking into account equilibration with entrapped air. Nature 405(6790):1040–1044

Amari S, Ozima M (1988) Extra-terrestrial noble gases in deep sea sediments. Geochim Cosmochim Acta 52(5):1087–1095

Andrew AS, Heinrich CA, Wilkins RWT, Patterson DJ (1989) Sulfur isotope systematics of copper ore formation at Mount Isa. Australia Econ Geol 84:1614–1626

Andrews JN, Giles IS, Kay RLF, Lee DJ, Osmond JK, Cowart JB, Fritz P, Barker JF, Gale J (1982) Radioelements, radiogenic helium and age relationships for groundwaters from the Granites at Stripa, Sweden. Geochim Cosmochim Acta 46(9): 1533–1543

Andrews JN, Hussain N, Youngman MJ (1989) Atmospheric and radiogenic gases in groundwaters from the Stripa granite. Geochim Cosmochim Acta 53(8):1831–1841

Andrews JN, Kay RLF (1982) Natural production of tritium in permeable rocks. Nature 298(5872): 361–363

Andrews JN, Lee DJ (1979) Inert gases in groundwater from the Bunter Sandstone of England as indicaters of age and paleoclimate trends. J Hydrol 41:233

Arnaud NO, Kelley SP (1995) Evidence for excess argon during high pressure metamorphism in the Dora Maira Massif (western Alps, Italy), using an ultraviolet laser ablation microprobe ^{40}Ar–^{39}Ar technique. Contrib Miner Petrol 121(1):1–11

Bach W, Frueh-Green GL (2010) Alteration of the oceanic lithosphere and implications for seafloor processes. Elements 6(3):173–178

Baker ET, Lupton JE (1990) Changes in submarien Hydrothermal ^{3}He/Heat ratios as an indicator of magmatic tectonic activity. Nature 346(6284): 556–558

Baker ET, Lupton JE, Resing JA, Baumberger T, Lilley MD, Walker SL, Rubin KH (2011) Unique event plumes from a 2008 eruption on the Northeast Lau Spreading Center. Geochem Geophys, Geosyst 12

Baker T (2002) Emplacement depth and carbon dioxide-rich fluid inclusions in intrusion-related gold deposits. Econ Geol Bull Soc Econ Geol 97(5):1111–1117

Ballentine CJ, Barfod DN (2000) The origin of air-like noble gases in MORB and OIB. Earth Planet Sci Lett 180(1–2):39–48

Ballentine CJ, Burgess R, Marty B (2002) Tracing fluid origin, transport and interaction in the crust. In: Porcelli D, Ballentine CJ, Wieler R (eds) Noble Gases in Geochemistry and Cosmochemistry, vol 47. Geochemical Society/Mineralogical Society of America, pp 539–614

Ballentine CJ, Burnard PG (2002) Production, release and transport of noble gases in the continental crust. In: Porcelli D, Ballentine CJ, Wieler R (eds) Noble gases in geochemistry and cosmochemistry, vol 47. Geochemical society/Mineralogical Society of America, pp 481–538

Ballentine CJ, Mazurek M, Gautschi A (1994) Thermal constraints on crustal rare gas release and migration: evidence from Alpine fluid inclusions. Geochim Cosmochim Acta 58:4333–4348

Ballentine CJ, O'Nions RK, Oxburgh ER, Horvath F, Deak J (1991) Rare gas constraints on hydrocarbon accumulation, crustal degassing and groundwater flow in the Pannonian Basin. Earth Planet Sci Lett 105(1–3):229–246

Banks DA, Green R, Cliff RA, Yardley BWD (2000) Chlorine isotopes in fluid inclusions: determination of the origins of salinity in magmatic fluids. Geochim Cosmochim Acta 64:1785–1789

Barton MD, Johnson DA (1996) Evaporitic-source model for igneous related Fe oxide (REE-Cu-Au-U) mineralization. Geology 24:259–262

Bein A, Hovorka SD, Fisher RS, Roedder E (1991) Fluid Inclusions in Bedded Permian Halite, Palo Duro Basin, Texas: evidence for modification of seawater in evaporite Brine-pools and subsequent early diagenesis. J Sediment Petrol 61(1):1–14

Berndt ME, Seyfried WE (1990) Boron, Bromine and other trace-elements as clues to the fate of chlorine in midocean ridge vent fluids. Geochimica et Cosmochimica Acta 54:2235–2245

Biester H, Keppler F, Putschew A, Martinez-Cortizas A, Petri M (2004) Halogen retention, organohalogens, and the role of organic matter decomposition on halogen enrichment in two Chilean peat bogs. Environ Sci Technol 38(7):1984–1991

Bodnar RJ (2003) Interpretation of data from aqueous-electrolyte fluid inclusions. In: Samson I, Anderson A, Marshall D (eds) Fluid inclusions analysis and interpretation, vol 32. Mineralogical Association of Canada, Vancouver, British Columbia, pp 81–101

Bodnar RJ, Binns PR, Hall DL (1989) Synthetic fluid inclusions: VI. Quantitative evaluation of the decrepitation behaviour of fluid inclusions in quartz at one atmosphere confining pressure. J Metamorph Geol 7:229–242

Böhlke JK, Irwin JJ (1992a) Brine histroy indicated by Argon, Krypton, Chlorine, Bromine and Iodine analyses of fluid inclusions from the Mississippi Valley Type Lead-Fluorite-Barite deposits at Hansonburg, New-Mexico. Earth Planet Sci Lett 110(1–4):51–66

Böhlke JK, Irwin JJ (1992b) Laser microprobe analyses of noble gas isotopes and halogens in fluid inclusions: analyses of microstandards and synthetic inclusions in quartz. Geochim Cosmochim Acta 56:187–201

Böhlke JK, Irwin JJ (1992c) Laserprobe analyses of Cl, Br, I, and K in fluid inclusions: implications for the sources of salinity in some ancient hydrothermal fluids. Geochim Cosmochim Acta 56:203–225

Bosch A, Mazor E (1988) Natural-gas association with water and oil as depicted by atmospheric noble-gases: case studies from the southeastern Mediterranean coastal-plain. Earth Planet Sci Lett 87(3):338–346

Boschmann W, Becker R, Lippolt HJ (1984) Eignungsprufung von Erzmineralien fur U + Th/He Datiering. Verlag-Chemie, 361–373

Boundy TM, Hall CM, Li G, Essene EJ, Halliday AN (1997) Fine-scale isotopic heterogeneities and fluids in the deep crust: a $^{40}Ar/^{39}Ar$ laser ablation and TEM study of muscovites from a granulite-eclogite transition zone. Earth Planet Sci Lett 148(1–2):223–242

Burgess R, Taylor RP, Fallick AE, Kelley SP (1992) $^{40}Ar/^{39}Ar$ laser microprobe study of fluids in different color zones of a hydrothermal scheelite crystal from the Dae-Hwa W Mine, South Korea. Chemi Geol 102(1–4):259–267

Burnard P, Graham D, Turner G (1997) Vesicle-specific noble gas analyses of "popping rock" implications for primordial noble gases in the Earth. Science 276:568–571

Burnard P, Harrison D (2005) Argon isotope constraints on modification of oxygen isotopes in Iceland Basalts by surficial processes. Chem Geol 216(1–2):143–156

Burnard PG, Hu R, Turner G, Bi XW (1999) Mantle, crustal and atmospheric noble gases in Ailaoshan Gold deposits, Yunnan Province, China. Geochim Cosmochim Acta 63(10):1595–1604

Burnard PG, Polya DA (2004) Importance of mantle derived fluids during granite associated hydrothermal circulation: He and Ar isotopes of ore minerals from Panasqueira. Geochim Cosmochim Acta 68(7): 1607–1615

Burnard PG, Stuart F, Turner G (1994) C–He–Ar variations within a dunite nodule as a function of fluid inclusion morphology. Earth Planet Sci Lett 128(3–4):243–258

Butterfield AW, Turner G (1985) Ancient argon in cherts. Terra Cognita 5:201–202

Cadogan PH (1977) Palaeoatmospheric argon in Rhynie chert. Nature 268:38

Carpenter AB, Trout ML, Pickett EE (1974) Preliminary report on the origin and chemical evolution of lead- and zinc-rich oil field brines in central Mississippi. Econ Geol 69:1191–1206

Castro MC, Hall CM, Patriarche D, Goblet P, Ellis BR (2007) A new noble gas paleoclimate record in Texas: basic assumptions revisited. Earth Planet Sci Lett 257(1–2):170–187

Champion DC, Sheraton JW (1997) Geochemistry and Nd isotope systematics of Archaean granites of the Eastern Goldfields, Yilgarn Craton, Australia: implications for crustal growth processes. Precambr Res 83(1–3):109–132

Chang J (2011) Table of Nuclides, KAERI (Korea Atomic Energy Research Institute). Available at: http://atom.kaeri.re.kr/ton/. Retrieved Feb 2011

Chi GX, Savard MM (1997) Sources of basinal and Mississippi Valley-type mineralizing brines: mixing of evaporated seawater and halite-dissolution brine. Chem Geol 143(3–4):121–125

Cline JS, Bodnar RJ (1991) Can economic porphyry copper mineralization be generated by a typical Calc-Alkaline Melt? J Geophys Res Solid Earth and Planets 96(B5):8113–8126

Collins AG, Bennett JH, Manuel OK (1971) Iodine and Algae in Sedimentary Rocks Associated with Iodine-Rich Brines Geol Soc Am Bull 82(9):2607

Connors KA, Page RW (1995) Relationships between magmatism, metamorphism and deformation in the western Mount Isa Inlier, Australia. Precambr Res 71:131–153

Crocetti CA, Holland HD (1989) Sulfur-lead isotope systematics and the composition of fluid inclusions in Galena from the Viburnum trend. Missouri Econ Geol 84:2196–2216

Drescher J, Kirsten T, Schäfer K (1998) The rare gas inventory of the continental crust, recovered by the KTB Continental Deep Drilling Project. Earth Planet Sci Lett 154(1–4):247–263

Drever JI (1997) The geochemistry of natural waters: surface and groundwater environments, vol. Prentice-Hall Inc, Upper Saddle River, New Jersey

Duncan RJ, Stein HJ, Evans KA, Hitzman MW, Nelson EP, Kirwin DJ (2011) A new geochronological framework for mineralization and alteration in the Selwyn-Mount Dore Corridor, Eastern Fold Belt, Mount Isa Inlier, Australia: genetic implications for iron oxide copper–gold deposits. Econ Geol 106(2):169–192

Elmer FL, White RW, Powell R (2006) Devolatilization of metabasic rocks during greenschist-amphibolite facies metamorphism. J Metamorph Geol 24(6):497–513

Ernst WG (1971) Metamorphic Zonations on Presumably Subducted Lithospheric Plates from Japan, California and Alps. Contributions to Mineralogy and Petrology 34(1):43

Etminan H, Hoffmann CF (1989) Biomarkers in fluid inclusions: a new tool in constraining source regimes and its implications for the genesis of Mississippi Valley-type deposits. Geology 17(1):19–22

Eugster O, Niedermann S, Thalmann C, Frei R, Kramers J, Krahenbuhl U, Liu YZ, Hofmann B, Boer RH, Reimold WU, Bruno L (1995) Noble gases, K, U, Th, and Pb in native gold. J Geophys Res-Solid Earth 100(B12):24677–24689

Fairmaid AM, Kendrick MA, Phillips D, Fu B (2011) The origin and evolution of mineralizing fluids in a sediment-hosted orogenic-gold deposit, Ballarat East. Southeastern Australia. Econ Geol 106(4):653–666

Fehn U, Lu Z, Tomaru H (2006) ^{129}I/I ratios and halogen concentrations in pore water of Hydrate Ridge and their relevence for the origin of gas hydrates: a progress report. In: Trehu AM, Bohrmann G, Torres ME, Colwell FS (eds) Proceedings of the Ocean Drilling Program, Scientific Results, vol 204. pp 1–25

Fehn U, Moran JE, Snyder GT, Muramatsu Y (2007) The initial ^{129}I/I ratio and the presence of ′old′ iodine in continental margins. Nucl Instrum Methods Phys Res Sect B 259(1):496–502

Fehn U, Snyder G, Egeberg PK (2000) Dating of pore waters with I-129: Relevance for the origin of marine gas hydrates. Science 289(5488):2332–2335

Fehn U, Snyder GT, Matsumoto R, Muramatsu Y, Tomaru H (2003) Iodine dating of pore waters associated with gas hydrates in the Nankai area. Japan Geology 31(6):521–524

Ferguson J, Etminan H, Ghassemi F (1993) Geochemistry of deep formation waters in the canning Basin, Western Australia and their relationship to Zn-Pb mineralisation. Aust J Earth Sci 40(5):471–483

Fisher L, Kendrick MA (2008) Metamorphic fluid origins in the Osborne Fe oxide–Cu–Au deposit, Australia: evidence from noble gases and halogens. Miner Deposita 43:483–497

Fontes JC, Andrews JN, Walgenwitz F (1991) Evaluation de la production naturelle in situ d'argon-36 via le chlore-36; implications geochimiques et geochronologiques; Evaluation of natural in situ production of argon-36 via chlorine-36; geochemical and geochronological implications. Comptes Rendus de l'Academie des Sciences, Serie 2, Mecanique, Physique, Chimie, Sciences de l'Univers, Sciences de la Terre 313(6):649–654

Fontes JC, Matray JM (1993) Geochemistry and origin of formation brines from the Paris Basin, France 1. Brines associated with Triassic salts. Chem Geol 109:149–175

Foster DRW, Rubenach MJ (2006) Isograd pattern and regional low pressure, high-temperature metamorphism of pelitic, mafic and calc-silicate rocks along an east-west section through the Mt Isa Inlier. Aust J Earth Sci 53:167–186

Fu B, Kendrick MA, Fairmaid AM, Phillips D, Wilson CJL, Mernagh TP (2012) New constraints on fluid sources in orogenic gold deposits, Victoria, Australia. Contrib Miner Petrol 163:427–447

Fu B, Touret JLR, Zheng YF (2001) Fluid inclusions in coesite-bearing eclogites and jadeite quartzite at Shuanghe, Dabie Shan (China). J Metamorph Geol 19(5):531–547

Fu B, Zheng Y-F, Touret JLR (2002) Petrological, isotopic and fluid inclusion studies of eclogites from

Sujiahe, NW Dabie Shan (China). Chem Geol 187(1–2):107–128

Fuge R, Johnson CC (1986) The geochemistry of iodine: a review. Environ Geochem Health 8:31–54

Garven G, Raffensperger JP (1997) Hydrology and geochemistry of ore genesis in sedimentary basins. In: Barnes HL (ed) The Geochemistry of hydrothermal ore deposits. Wiley, New York, pp 125–190

Gilfillan SMV, Ballentine CJ, Holland G, Blagburn D, Lollar BS, Stevens S, Schoell M, Cassidy M (2008) The noble gas geochemistry of natural CO_2 gas reservoirs from the Colorado Plateau and Rocky Mountain provinces, USA. Geochim Cosmochim Acta 72(4):1174–1198

Gilfillan SMV, Lollar BS, Holland G, Blagburn D, Stevens S, Schoell M, Cassidy M, Ding Z, Zhou Z, Lacrampe-Couloume G, Ballentine CJ (2009) Solubility trapping in formation water as dominant CO_2 sink in natural gas fields. Nature 458(7238):614–618

Giorgis D, Cosca M, Li S (2000) Distribution and significance of extraneous argon in UHP eclogite (Sulu terrain, China): insight from in situ $^{40}Ar/^{39}Ar$ UV-laser ablation analysis. Earth Planet Sci Lett 181(4):605–615

Gize AP, Barnes HL (1987) The organic geochemistry of two mississippi valley-type lead-zinc deposits. Econ Geol 82(2):457–470

Goldfarb RJ, Groves DI, Gardoll S (2001) Orogenic gold and geologic time: a global synthesis. Ore Geol Rev 18(1–2):1–75

Graham DW (2002) Noble gas isotope geochemistry of Mid-Ocean Ridge and Ocean Island Basalts: characterisation of mantle source reservoirs. In: Porcelli D, Ballentine CJ, Wieler R (eds) Noble Gases in Geochemistry and Cosmochemistry, vol 47. pp 245–317

Graupner T, Niedermann S, Kempe U, Klemd R, Bechtel A (2006) Origin of ore fluids in the Muruntau gold system: constraints from noble gas, carbon isotope and halogen data. Geochim Cosmochim Acta 70(21):5356–5370

Graupner T, Niedermann S, Rhede D, Kempe U, Seltmann R, Williams CT, Klemd R (2010) Multiple sources for mineralizing fluids in the Charmitan gold (-tungsten) mineralization (Uzbekistan). Miner Deposita 45(7):667–682

Gregory M, Schaefer B, Keays R, Wilde A (2008) Rhenium–osmium systematics of the Mount Isa copper orebody and the Eastern Creek Volcanics, Queensland, Australia: implications for ore genesis. Miner Deposita 43(5):553–573

Groves DI, Goldfarb RJ, Robert F, Hart CJR (2003) Gold deposits in metamorphic belts: overview of current understanding, outstanding problems, future research, and exploration significance. Econ Geol Bull Soc Econ Geol 98(1):1–29

Hanor JS (1994) Origin of saline fluids in sedimentary basins. In: Parnell J (ed) Geofluids: origin, migration and evolution of fluids in Sedimentary Basins, vol 78. Geological Society Special Publication, pp 151–174

Heinrich CA, Andrew AS, Wilkins WT, Patterson DJ (1989) A fluid inclusion and stable isotope study of synmetamorphic copper ore formation at Mount Isa. Australia Econ Geol 84:529–550

Heinrich CA, Bain JHC, Fardy JJ, Waring CL (1993) Br/Cl geochemistry of hydrothermal brines associated with Proterozoic metasediment-hosted copper mineralisation at Mount Isa, northern Australia. Geochim Cosmochim Acta 57:2991–3000

Heinrich CA (2003) Fluid-fluid interactions in magmatic-hydrothermal ore formation. In: Liebscher A, Heinrich CA (eds) Fluid-fluid interactions, vol 65. Mineralogical Society of America, Geochem Soc, pp 363–387

Hermann AG (1980) Bromide distribution between halite and NaCl-saturated seawater. Chem Geol 28:171–177

Heyl AV, Landis GP, Zartman RE (1974) Isotopic evidence for the origin of Mississippi Valley-Type mineral deposits: a review. Econ Geol 69(6):992–1006

Hitchon B (2006) Lead and zinc in formation waters, Alberta Basin, Canada: Their relation to the Pine Point ore fluid. Appl Geochem 21(1):109–133

Hiyagon H (1989) Neon isotope measurement in the presence of Helium. Mass Spectrometry 37:325–330

Ho SE, Groves D, McNaughton NJ, Mikucki EJ (1992) The source of ore fluids and solutes in Archaean lode-gold deposits of Western Australia. J Volcanol Geoth Res 50:173–196

Holland G, Ballentine CJ (2006) Seawater subduction controls the heavy noble gas composition of the mantle. Nature 441(7090):186–191

Holser WT (1979) Trace elements and isotopes in evaporites. In: Burns RG (ed) Marine minerals: Mineralogical Society of America Short Course Notes, vol 6. pp 295–346

Honda M, Kurita K, Hamano Y, Ozima M (1982) Experimental studies of He and Ar degassing during rock fracturing. Earth Planet Sci Lett 59(2):429–436

Hu R-Z, Burnard PG, Bi X-W, Zhou M-F, Peng J-T, Su W-C, Zhao J-H (2009) Mantle-derived gaseous components in ore-forming fluids of the Xiangshan uranium deposit, Jiangxi province, China: Evidence from He, Ar and C isotopes. Chem Geol 266(1–2):86–95

Hu RZ, Burnard PG, Bi XW, Zhou MF, Pen JT, Su WC, Wu KX (2004) Helium and argon isotope geochemistry of alkaline intrusion-associated gold and copper deposits along the Red River-Jinshajiang fault belt, SW China. Chem Geol 203(3–4):305–317

Hu RZ, Burnard PG, Turner G, Bi XW (1998) Helium and Argon isotope systematics in fluid inclusions of Machangqing copper deposit in west Yunnan province, China. Chem Geol 146(1–2):55–63

Hünemohr H (1989) Edelgase in U- and Th-reichen mineralen und die Bestimmung der ^{21}Ne-dicktargetausbeute der ^{18}O(alpha, n)^{21}Ne Kernreaktion in Bereich 4.0-8.8 MeV. In, vol Ph.D. Johannes-Gutenberg University, Mainz

Irwin JJ, Reynolds JH (1995) Multiple stages of fluid trapping in the Stripa granite indicated by laser

microprobe analysis of Cl, Br, I, K, U, and nucleogenic plus radiogenic Ar, Kr, and Xe in fluid inclusions. Geochim Cosmochim Acta 59(2):355–369

Irwin JJ, Roedder E (1995) Diverse origins of fluid inclusions at Bingham (Utah, USA), Butte (Montana, USA), St. Austell (Cornwall, UK) and Ascension Island (mid-Atlantic, UK), indicated by laser microprobe analysis of Cl, K, Br, I, Ba + Te, U, Ar, Kr, and Xe. Geochim Cosmochim Acta 59(2):295–312

Jambon A, Deruelle B, Dreibus G, Pineau F (1995) Chlorine and bromine abundance in MORB: the contrasting behaviour of the Mid-Atlantic Ridge and East Pacific Rise and implications for chlorine geodynamic cycle. Chem Geol 126:101–117

Jean-Baptiste P, Fouquet Y (1996) Abundance and isotopic composition of helium in hydrothermal sulfides from the East Pacific Rise at 13°N. Geochim Cosmochim Acta 60(1):87–93

Johnson L, Burgess R, Turner G, Milledge JH, Harris JW (2000) Noble gas and halogen geochemistry of mantle fluids: comparison of African and Canadian diamonds. Geochim Cosmochim Acta 64:717–732

Kelley S (2002) Excess argon in K-Ar and Ar-Ar geochronology. Chem Geol 188(1–2):1–22

Kelley S, Turner G, Butterfield AW, Shepherd TJ (1986) The source and significance of argon isotopes in fluid inclusions from areas of mineralization. Earth Plan Sci Lett 79:303–318

Kendrick MA (2007) Comment on 'Paleozoic ages and excess ^{40}Ar in garnets from the Bixiling eclogite in Dabieshan, China: New insights from $^{40}Ar/^{39}Ar$ dating by stepwise crushing by Hua-Ning Qiu and JR Wijbrans'. Geochim Cosmochim Acta 71(24):6040–6045

Kendrick MA (2012) High precision Cl, Br and I determination in mineral standards using the noble gas method. Chem Geol 292–293:116–126

Kendrick MA, Baker T, Fu B, Phillips D, Williams PJ (2008a) Noble gas and halogen constraints on regionally extensive mid-crustal Na-Ca metasomatism, the Proterozoic Eastern Mount Isa Block, Australia. Precambr Res 163(1–2):131–150

Kendrick MA, Burgess R, Harrison D, Bjørlykke A (2005) Noble gas and halogen evidence on the origin of Scandinavian sandstone-hosted Pb-Zn deposits. Geochim Cosmochim Acta 69:109–129

Kendrick MA, Burgess R, Leach D, Pattrick RAD (2002a) Hydrothermal fluid origins in Mississippi valley-type ore deposits: combined noble gas (He, Ar, Kr) and halogen (Cl, Br, I) analysis of fluid inclusions from the Illinois-Kentucky Fluorspar district, Viburnum Trend, and Tri-State districts, mid-continent United States. Econ Geol 97(3):452–479

Kendrick MA, Burgess R, Pattrick RAD, Turner G (2001a) Fluid inclusion noble gas and halogen evidence on the origin of Cu-Porphyry mineralising fluids. Geochim Cosmochim Acta 65(16):2651–2668

Kendrick MA, Burgess R, Pattrick RAD, Turner G (2001b) Halogen and Ar-Ar age determinations of inclusions within quartz veins from porphyry copper deposits using complementary noble gas extraction techniques. Chem Geol 177(3–4):351–370

Kendrick MA, Burgess R, Pattrick RAD, Turner G (2002b) Hydrothermal fluid origins in a fluorite-rich Mississippi valley-type deposit: combined noble gas (He, Ar, Kr) and halogen (Cl, Br, I) analysis of fluid inclusions from the South Pennine Orefield, United Kingdom. Econ Geol 97(3):435–451

Kendrick MA, Duncan R, Phillips D (2006a) Noble gas and halogen constraints on mineralizing fluids of metamorphic versus surficial origin: Mt Isa, Australia. Chem Geol 235(3–4):325–351

Kendrick MA, Honda M, Gillen D, Baker T, Phillips D (2008b) New constraints on regional brecciation in the Wernecke Mountains, Canada, from He, Ne, Ar, Kr, Xe, Cl, Br and I in fluid inclusions. Chem Geol 255(1–2):33–46

Kendrick MA, Honda M, Oliver NHS, Phillips D (2011a) The noble gas systematics of late-orogenic H_2O-CO_2 fluids, Mt Isa, Australia. Geochim Cosmochim Acta 75(6):1428–1450

Kendrick MA, Honda M, Walshe J, Petersen K (2011b) Fluid sources and the role of abiogenic-CH_4 in Archean gold mineralization: constraints from noble gases and halogens. Precambr Res 189:313–327

Kendrick MA, Kamenetsky VS, Phillips D, Honda M (2012) Halogen (Cl, Br, I) systemtics of mid-ocean ridge basalts: a Macquarie Island case study. Geochim Cosmochim Acta 81:82–93

Kendrick MA, Mark G, Phillips D (2007) Mid-crustal fluid mixing in a Proterozoic Fe oxide-Cu-Au deposit, Ernest Henry, Australia: Evidence from Ar, Kr, Xe, Cl, Br, and I. Earth Planet Sci Lett 256(3–4):328–343

Kendrick MA, Miller JM, Phillips D (2006b) Part II: Evaluation of ^{40}Ar-^{39}Ar quartz ages: Implications for fluid inclusion retentivity and determination of initial $^{40}Ar/^{36}Ar$ values in Proterozoic samples. Geochim Cosmochim Acta 70:2562–2576

Kendrick MA, Phillips D (2009) New constraints on the release of noble gases during in vacuo crushing and application to scapolite Br-Cl-I and $^{40}Ar/^{39}Ar$ age determinations. Geochim Cosmochim Acta 73(19):5673–5692

Kendrick MA, Phillips D, Miller JM (2006c) Part I. Decrepitation and degassing behaviour of quartz up to 1560 °C: Analysis of noble gases and halogens in complex fluid inclusions assemblages. Geochim Cosmochim Acta 70:2540–2561

Kendrick MA, Phillips D, Wallace M, Miller JM (2011c) Halogens and noble gases in sedimentary formation waters and Zn-Pb deposits: a case study from the Lennard Shelf, Australia. Appl Geochem 26:2089–2100

Kendrick MA, Scambelluri M, Honda M, Phillips D (2011d) High abundances of noble gas and chlorine delivered to the mantle by serpentinite subduction. Nat Geosci 4:807–812

Kennedy BM (1988) Noble gases in vent water from the Juan de Fuca Ridge. Geochim Cosmochim Acta 52(7):1929–1935

Kennedy BM, Hiyagon H, Reynolds JH (1990) Neon: a striking crustal uniformity. Earth Planet Sci Lett 98:277–286

Kennedy BM, Torgersen T, van Soest MC (2002) Multiple atmospheric noble gas components in hydrocarbon reservoirs: a study of the Northwest Shelf, Delaware Basin, SE New Mexico. Geochim Cosmochim Acta 66(16):2807–2822

Kesler SE (2007) Geochemistry of fluid inclusion brines from Earth's oldest Mississippi Valley-type (MVT) deposits, Transvaal Supergroup, South Africa. Chem Geol 237:274–288

Kesler SE, Appold MS, Martini AM, Walter LM, Huston TJ, Kyle JR (1995) Na-Cl-Br systematics of mineralising brines in Mississippi Valley-type deposits. Geology 23:641–644

Kharaka YK, Hanor JS (2003) Deep Fluids in the Continents: I. Sedimentary Basins. In: Treatise on Geochemistry, vol. Pergamon, Oxford, pp 1–48

Kharaka YK, Specht DJ (1988) The solubility of noble gases in crude oil at 25–100 °C. Appl Geochem 3(2):137–144

Kipfer R, Aeschbach-Hertig W, Peeters F, Stute M (2002) Noble Gases in Lakes and Ground Waters. In: Porcelli D, Ballentine CJ, Wieler R (eds) Noble Gases in Geochemistry and Cosmochemistry, vol 47. The Mineralogical Society of America, pp 615–700

Kluge T, Marx T, Scholz D, Niggemann S, Mangini A, Aeschbach-Hertig W (2008) A new tool for palaeoclimate reconstruction: Noble gas temperatures from fluid inclusions in speleothems. Earth Planet Sci Lett 269(3–4):408–415

Lang JR, Baker T (2001) Intrusion-related gold systems: the present level of understanding. Miner Deposita 36(6):477–489

Langmuir CH, Vocke RD Jr, Hanson GN, Hart SR (1978) A general mixing equation with applications to Icelandic basalts. Earth Planet Sci Lett 37(3):380–392

Large RR, Bull SW, Maslennikov VV (2011) A carbonaceous sedimentary source-rock model for carlin-type and orogenic gold deposits. Econ Geol 106(3):331–358

Leach DL, Dwight B, Lewchuk MT, Symons DTA, de Marsily G, Brannon J (2001) Mississippi Valley-type lead-zinc deposits through geological time: implications from recent age-dating research. Miner Deposita 36(8):711–740

Leach DL, Rowan EL (1986) Genetic link between Ouachita Foldbelt Tectonism and the Mississippi Valley-type lead-zinc deposits of the Ozarks. Geology 14(11):931–935

Lee JY, Marti K, Severinghaus JP, Kawamura K, Yoo HS, Lee JB, Kim JS (2006) A redetermination of the isotopic abundances of atmospheric Ar. Geochim Cosmochim Acta 70(17):4507–4512

Li XF, Wang CZ, Hua RM, Wei XL (2010) Fluid origin and structural enhancement during mineralization of the Jinshan orogenic gold deposit, South China. Miner Deposita 45(6):583–597

Liebscher A, Luders V, Heinrich W, Schettler G (2006) Br/Cl signature of hydrothermal fluids: liquid-vapour fractionation of bromine revisited. Geofluids 6:113–121

Lippmann-Pipke J, Sherwood Lollar B, Niedermann S, Stroncik NA, Naumann R, van Heerden E, Onstott TC (2011) Neon identifies two billion year old fluid component in Kaapvaal Craton. Chem Geol 283 (3–4):287–296

Lippmann J, Stute M, Torgersen T, Moser DP, Hall JA, Lin L, Borcsik M, Bellamy RES, Onstott TC (2003) Dating ultra-deep mine waters with noble gases and ^{36}Cl, Witwatersrand Basin, South Africa. Geochim Cosmochim Acta 67(23):4597–4619

Lueders V, Niedermann S (2010) Helium isotope composition of fluid inclusions hosted in massive sulfides from modern submarine hydrothermal systems. Econ Geol 105(2):443–449

Lupton JE, Baker ET, Massoth GJ (1989) Variable 3He/heat ratios in submarine hydrothermal systems: evidence from two plumes over the Juan de Fuca ridge. Nature 337(6203):161–164

Lupton JE, Baker ET, Massoth GJ (1999) Helium, heat, and the generation of hydrothermal event plumes at mid-ocean ridges. Earth Planet Sci Lett 171(3):343–350

MacCready T, Goleby BR, Goncharov A, Drummond BJ, Lister GS (1998) A framework of overprinting orogens based on interpretation of the Mt Isa deep siesmic transect. Econ Geol 93:1422–1434

Mamyrin BA, Anufriyev GS, Kamenskiy IL, Tolstikhin (1970) Determination of the composition of atmospheric helium. Geochemistry International 7:498–505

Mao JW, Li YQ, Goldfarb R, He Y, Zaw K (2003) Fluid inclusion and noble gas studies of the Dongping gold deposit, Hebei Province, China: a mantle connection for mineralization? Econ Geol Bull Soc Econ Geol 98(3):517–534

Mark G (2001) Nd isotope and petrogenetic constraints for the origin of the Mount Angelay igneous complex: implications for the origin of intrusions in the Cloncurry district, NE Australia. Precambr Res 105:17–35

Mark G, Foster DRW, Pollard PJ, Williams PJ, Tolman J, Darvall M, Blake KL (2004) Stable isotope evidence for magmatic fluid input during large-scale Na-Ca alteration in the Cloncurry Fe oxide Cu-Au district, NW Queensland, Australia. Terra Nova 16:54–61

Mark G, Oliver NHS, Carew MJ (2006) Insights into the genesis and diversity of epigenetic Cu-Au mineralisation in the Cloncurry district, Mt Isa Inlier, northwest Queensland. Aust J Earth Sci 53:109–124

Markl G, Bucher K (1998) Composition of fluids in the lower crust inferred from metamorphic salt in lower crustal rocks. Nature 391(6669):781–783

Martin JB, Gieskes JM, Torres M, Kastner M (1993) Bromine and iodine in Peru margin sediments and pore fluids: Implications for fluid origins. Geochim Cosmochim Acta 57(18):4377–4389

Matsuda J, Nagao K (1986) Noble-Gas abundances in a Deep-Sea sediment core from Eastern Equatorial Pacific. Geochem J 20(2):71–80

Mavrogenes JA, Bodnar RJ (1994) Hydrogen movement into and out of fluid inclusions in quartz: experimental evidence and geologic implications. Geochim Cosmochim Acta 58(1):141–148

McCaffrey MA, Lazar B, Holland HD (1986) The evaporation path of seawater and the composition of Br- and K+ with halite. J Sediment Petrol 57:928–937

McDougall I, Harrison TM (1999) Geochronology and Thermochronology by the $^{40}Ar/^{39}Ar$ method, vol Oxford. University Press, New York

McLaren S, Sandiford M, Hand M (1999) High radiogenic heat-producing granites and metamorphism: an example from the western Mount Isa inlier, Australia. Geology 27(8):679–682

Mernagh T, Bastrakov EN, Zaw K, Wygralak AS, Wyborn LAI (2007) Comparison of fluid inclusion data and mineralisation processes for Australian orogenic gold and intrusion related gold systems. Acta Petrol Sin 23:21–32

Moreira M, Blusztajn J, Curtice J, Hart S, Dick H, Kurz MD (2003) He and Ne isotopes in oceanic crust: implications for noble gas recycling in the mantle. Earth Planet Sci Lett 216(4):635–643

Morelli R, Creaser RA, Seltmann R, Stuart FM, Selby D, Graupner T (2007) Age and source constraints for the giant Muruntau gold deposit, Uzbekistan, from coupled Re-Os-He isotopes in arsenopyrite. Geology 35(9):795–798

Muramatsu Y, Doi T, Tomaru H, Fehn U, Takeuchi R, Matsumoto R (2007) Halogen concentrations in pore waters and sediments of the Nankai Trough, Japan: Implications for the origin of gas hydrates. Appl Geochem 22(3):534–556

Muramatsu Y, Fehn U, Yoshida S (2001) Recycling of iodine in fore-arc areas: evidence from the iodine brines in Chiba, Japan. Earth Planet Sci Lett 192(4):583–593

Muramatsu Y, Wedepohl KH (1998) The distribution of iodine in the Earth's crust. Chem Geol 147(3–4):201–216

Nahnybida T, Gleeson SA, Rusk BG, Wassenaar LI (2009) Cl/Br ratios and stable chlorine isotope analysis of magmatic-hydrothermal fluid inclusions from Butte, Montana and Bingham Canyon, Utah. Miner Deposita 44(8):837–848

Neumayr P, Walshe J, Hagemann S, Petersen K, Roache A, Frikken P, Horn L, Halley S (2008) Oxidized and reduced mineral assemblages in greenstone belt rocks of the St. Ives gold camp, Western Australia: vectors to high-grade ore bodies in Archaean gold deposits? Miner Deposita 43(3):363–371

Nissenbaum A (1977) Minor and trace elements in Dead sea water. Chem Geol 19:99–111

Niedermann S (2002) Cosmic-Ray-Produced noble gases in terrestrial rocks: dating tools for surface processes. In: Porcelli CJ, Ballentine CJ, Wieler R (eds) Noble gases in geochemistry and cosmochemistry, vol 47: Reviews in Mineralogy and Geochemistry: Washington DC, Mineralogical Society of America, p 731–777

Nier AO (1950) A redetermination of the relative abundances of the isotopes of carbon, nitrogen, oxygen, argon and potassium. Phys Rev 77:789–793

O'Nions RK, Oxburgh ER (1988) Helium, volatile fluxes and the development of continental crust. Earth Planet Sci Lett 90:331–347

Oliver NHS (1995) Hydrothermal history of the Mary Kathleen fold belt, Mt Isa Block, Queensland. Aust J Earth Sci 42:267–279

Oliver NHS, Butera KM, Rubenach MJ, Marshall LJ, Cleverley JS, Mark G, Tullemans F, Esser D (2008) The protracted hydrothermal evolution of the Mount Isa Eastern succession: a review and tectonic implications. Precambr Res 163(1–2):108–130

Oliver NHS, Cartwright I, Wall VJ, Golding SD (1993) The stable isotope signature of kilometre-scale fracture-dominated metamorphic fluid pathways, Mary Kathleen, Australia. J Metamorph Geol 11:705–720

Oliver NHS, Cleverley JS, Mark G, Pollard PJ, Fu B, Marshall LJ, Rubenach MJ, Williams PJ, Baker T (2004) Modeling the role of sodic alteration in the genesis of iron-oxide-copper-gold deposits, eastern Mt Isa block. Aust Econ Geol 99:1145–1176

Osawa T (2004) A new correction technique for mass interferneces by $^{40}Ar^{++}$ and CO_2^{++} during isotope analysis of a small amount of Ne. J Mass Spectrom Soc Jpn 52(4):230–232

Oxburgh ER, O'Nions RK, Hill RI (1986) Helium isotopes in sedimentary basins. Nature 324(6098):632–635

Ozima M, Podosek FA (2002) Noble Gas Geochemistry, vol. Cambridge University Press

Page RW, Sun S-S (1998) Aspects of geochronology and crustal evolution in the Eastern Fold Belt, Mount Isa Inlier. Aust J Earth Sci 45:343–362

Painter MGM, Golding SD, Hannan KW, Neudert MK (1999) Sedimentologic, petrographic, and sulfur isotope constraints on fine-grained pyrite formation at Mount Isa Mine and environs, Northwest Queensland. Aust Econ Geol 94(6):883–912

Perkins C, Heinrich CA, Wyborn LAI (1999) $^{40}Ar/^{39}Ar$ geochronology of copper mineralisation and regional alteration, Mount Isa. Aust Econ Geol 94:23–36

Perkins WG (1984) Mount Isa Silica Dolomite and Copper Orebodies: the result of a syntectonic hydrothermal alteration system. Econ Geol 79(4):601–637

Pettke T, Diamond LW (1997) Oligocene gold quartz veins at Brusson, NW Alps: Sr isotopes trace the source of ore-bearing fluid to over a 10 km depth. Econ Geol Bull Soc Econ Geol 92(4):389–406

Pettke T, Frei R (1996) Isotope systematics in vein gold from Brusson, Val d'Ayas (NW Italy).1. Pb/Pb evidence for a Piemonte metaophiolite Au source. Chem Geol 127(1–3):111–124

Pettke T, Frei R, Kramers JD, Villa IM (1997) Isotope systematics in vein gold from Brusson, Val d'Ayas (NW Italy).2. (U + Th)/He and K/Ar in native Au and its fluid inclusions. Chem Geol 135(3–4):173–187

Phillips D, Fu B, Wilson CJL, Kendrick MA, Fairmaid AM, Miller JM (2012) Timing of Gold Mineralisation

in the Western Lachlan Orogen, SE Australia: A Critical Overview. Aust J Earth Sci (in press)
Phillips D, Miller JM (2006) $^{40}Ar/^{39}Ar$ dating of mica-bearing pyrite from thermally overprinted Archaean gold deposits. Geology 34:397–400
Phillips FM, Castro MC (2003) Groundwater dating and residence-time measurements. In: Treatise on Geochemistry, vol 5. Elsevier, pp 451–497
Phillips GN, Powell R (1993) Link between gold provinces. Econ Geol Bull Soc Econ Geol 88(5):1084–1098
Pili É, Kennedy BM, Conrad ME, Gratier JP (2011) Isotopic evidence for the infiltration of mantle and metamorphic CO_2-H_2O fluids from below in faulted rocks from the San Andreas Fault system. Chem Geol 281(3–4):242–252
Pinti DL, Béland-Otis C, Tremblay A, Castro MC, Hall CM, Marcil J-S, Lavoie J-Y, Lapointe R (2011) Fossil brines preserved in the St-Lawrence Lowlands, Québec, Canada as revealed by their chemistry and noble gas isotopes. Geochim Cosmochim Acta 75(15):4228–4243
Pinti DL, Marty B, Andrews JN (1997) Atmosphere-derived noble gas evidence for the preservation of ancient waters in sedimentary basins. Geology 25(2):111–114
Pirajno F (2000) Ore deposits and mantle plumes. Kluwer Academic Publishers, Dordrecht
Pitre F, Pinti DL (2010) Noble gas enrichments in porewater of estuarine sediments and their effect on the estimation of net denitrification rates. Geochim Cosmochim Acta 74(2):531–539
Plumlee GS, Goldhaber MB, Rowan EL (1995) Potential role of magmatic gases in the genesis of illinois-kentucky fluorspar deposits: implications from chemical reaction path modelling. Econ Geol Bull Soc Econ Geol 90(5):999–1011
Podosek FA, Bernatowicz TJ, Kramer FE (1981) Adsorption of xenon and krypton on shales. Geochim Cosmochim Acta 45:2401–2415
Podosek FA, Honda M, Ozima M (1980) Sedimentary noble gases. Geochim Cosmochim Acta 44:1875–1884
Polito PA, Bone Y, Clarke JDA, Mernagh TP (2001) Compositional zoning of fluid inclusions in the Archaean Junction gold deposit, Western Australia: a process of fluid wall-rock interaction? Aust J Earth Sci 48(6):833–855
Pollard PJ (2000) Evidence of a magmatic fluid and metal source for Fe-oxide Cu-Au mineralisation. In: Porter TM (ed) Hydrothermal iron oxide copper gold and related deposits: a global perspective, vol. PGC Publishing, Adelaide, pp 27–41
Pollard PJ (2001) Sodic-(calcic) alteration in Fe-oxide-Cu-Au districts: and origin via unmixing of magmatic H_2O-CO_2-NaCl ± $CaCl_2$-KCl fluids. Miner Deposita 36:93–100
Polya DA, Foxford KA, Stuart F, Boyce A, Fallick AE (2000) Evolution and paragenetic context of low δD hydrothermal fluids from the Panasqueira W-Sn deposit, Portugal: new evidence from microthermometric, stable isotope, noble gas and halogen analyses of primary fluid inclusions. Geochim Cosmochim Acta 64(19):3357–3371
Powell R, Will TM, Phillips GN (1991) Metamorphism in archean greenstone belts: calculated fluid compositions and implications for gold mineralization. J Metamorph Geol 9(2):141–150
Pujol M, Marty B, Burnard P, Philippot P (2009) Xenon in archean barite: weak decay of ^{130}Ba, mass-dependent isotopic fractionation and implication for barite formation. Geochim Cosmochim Acta 73(22):6834–6846
Raquin A, Moreira MA, Guillon F (2008) He, Ne and Ar systematics in single vesicles: mantle isotopic ratios and origin of the air component in basaltic glasses. Earth Planet Sci Lett 274(1–2):142–150
Reddy SM, Kelley SP, Magennis L (1997) A microstructural and argon laserprobe study of shear zone development at the western margin of the Nanga Parbat-Haramosh Massif, western Himalaya. Contrib Miner Petrol 128(1):16–29
Robb LJ (2005) Introduction to Ore-Forming Processes, vol. Blackwell Publishing, p 373
Rock NMS, Groves DI (1988) Do lamprophyres carry gold as well as diamonds? Nature 332(6161):253–255
Roedder E (1971a) Fluid-inclusion evidence on the environment of formation of mineral deposits of the Southern Appalachian Valley. Econ Geol 66:777–791
Roedder E (1971b) Fluid inclusion studies on the porphyry-type ore deposits at Bingham, Utah, Butte, Montana, and Climax. Colorado Econ Geol 66(1):98–118
Roedder E (1984) Fluid Inclusions, vol 12. Mineralogical society of America. Bookcrafters, Inc., Chelsea, p 646
Rudnick RL, Gao S (2003) Composition of the Continental Crust. In: Treatise of Geochemistry, vol 3. Elsevier Ltd., pp 1–64
Rusk BG, Reed MH, Dilles JH, Klemm LM, Heinrich CA (2004) Compositions of magmatic hydrothermal fluids determined by LA-ICP-MS of fluid inclusions from the porphyry copper-molybdenum deposit at Butte. MT Chem Geol 210(1–4):173–199
Russell MJ, Smith FW (1979) Plate separation, alkali magmatism and fluorite mineralisation in Northern and Central England. Transac Inst Min Metall Sect B-Appl Earth Sci 88(FEB):B30
Sanchez V, Stuart FM, Martin-Crespo T, Vindel E, Corbella M, Cardellach E (2010) Helium isotopic ratios in fluid inclusions from fluorite-rich Mississippi Valley-Type district of Asturias, northern Spain. Geochem J 44(6):E1–E4
Sandiford M, McLaren S, Neumann N (2002) Long-term thermal consequences of the redistribution of heat-producing elements associated with large-scale granitic complexes. J Metamorph Geol 20(1):87–98
Scambelluri M, Bottazzi P, Trommsdorff V, Vannucci R, Hermann J, Gòmez-Pugnaire MT, Lòpez-Sànchez Vizcaino V (2001) Incompatible element-rich fluids released by antigorite breakdown in deeply subducted mantle. Earth Planet Sci Lett 192(3):457–470

Scambelluri M, Piccardo GB, Philippot P, Robbiano A, Negretti L (1997) High salinity fluid inclusions fromed from recycled seawater in deeply subducted alpine serpentinite. Earth Planet Sci Lett 148:485–499

Scheidegger Y, Baur H, Brennwald MS, Fleitmann D, Wieler R, Kipfer R (2010) Accurate analysis of noble gas concentrations in small water samples and its application to fluid inclusions in stalagmites. Chem Geol 272(1–4):31–39

Scheidegger Y, Brennwald MS, Fleitmann D, Jeannin PY, Wieler R, Kipfer R (2011) Determination of Holocene cave temperatures from Kr and Xe concentrations in stalagmite fluid inclusions. Chem Geol 288(1–2):61–66

Schilling JC, Unni CK, Bender ML (1978) Origin of chlorine and bromine in the oceans. Nature 273: 631–636

Schwarz WH, Trieloff M, Altherr R (2005) Subduction of solar-type noble gases from extraterrestrial dust: constraints from high-pressure low-temperature metamorphic deep-sea sediments. Contrib Miner Petrol 149(6):675–684

Shelton KL, Taylor RP, So CS (1987) Stable isotope studies of the Dae Hwa tungsten-molybdenum mine, Republic or Korea: evidence of progressive meteoric water interaction in a tungsten-bearing hydrothermal system. Econ Geol 82(2):471–481

Sherlock S, Kelley S (2002) Excess argon evolution in HP-LT rocks: a UVLAMP study of phengite and K-free minerals, NW Turkey. Chem Geol 182(2–4): 619–636

Siemann MG (2003) Extensive and rapid changes in seawater chemistry during the Phanerozoic: evidence from Br contents in basal halite. Terra Nova 15(4):243–248

Siemann MG, Schramm M (2000) Thermodynamic modelling of the Br partition between aqueous solutions and halite. Geochim Cosmochim Acta 64(10):1681–1693

Sillitoe RH (2010) Porphyry copper systems. Econ Geol 105(1):3–41

Simmons SF, Sawkins FJ, Schlutter DJ (1987) Mantle derived helium in two Peruvian hydrothermal ore deposits. Nature 329:429–432

Smith SP, Kennedy BM (1983) The solubility of noble gases in water and in NaCl brine. Geochim Cosmochim Acta 47:503–515

So CS, Shelton KL, Seidemann DE, Skinner BJ (1983) The Dae Hwa tungsten-molybdenum mine, Republic of Korea: a geochemical study. Econ Geol 78(5):920–930

Staudacher T, Allègre CJ (1988) Recycling of oceanic crust and sediments: the noble gas subduction barrier. Earth Planet Sci Lett 89(2):173–183

Stuart FM, Burnard PG, Taylor RP, Turner G (1995) Resolving mantle and crustal contributions to ancient hydrothermal fluids: He–Ar isotopes in fluid inclusions from Dae Hwa W–Mo mineralisation, South Korea. Geochim Cosmochim Acta 59(22):4663–4673

Stuart FM, Turner G (1992) The abundance and isotopic composition of the noble gases in ancient fluids. Chem Geol 101:97–109

Stuart FM, Turner G (1998) Mantle-derived ^{40}Ar in mid-ocean ridge hydrothermal fluids: implications for the source of volatiles and mantle degassing rates. Chem Geol 147(1–2):77–88

Stuart FM, Turner G, Duckworth RC, Fallick AE (1994) Helium-isotopes as tracers of trapped hydrothermal fluids in ocean-floor sulphides. Geology 22(9):823–826

Sumino H, Burgess R, Mizukami T, Wallis SR, Holland G, Ballentine CJ (2010) Seawater-derived noble gases and halogens preserved in exhumed mantle wedge peridotite. Earth Planet Sci Lett 294(1–2):163–172

Sun XM, Zhang Y, Xiong DX, Sun WD, Shi GY, Zhai W, Wang SW (2009) Crust and mantle contributions to gold-forming process at the Daping deposit, Ailaoshan gold belt, Yunnan, China. Ore Geol Rev 36(1–3):235–249

Svensen H, Banks DA, Austreim H (2001) Halogen contents of eclogite facies fluid inclusions and minerals: Caledonides, western Norway. J Metamorph Geol 19:165–178

Sverjensky DA (1986) Genesis of Missisippi Valley-type lead-zinc deposits. Annu Rev Earth Planet Sci 14:177–199

Swager CP (1985) Syndeformational Carbonate-replacement model for the copper mineralization at Mount Isa, Northwest Queensland: a microstructural study. Econ Geol 80:107–125

Taylor HP (1997) Oxygen and hydrogen isotope relationships in hydrothermal mineral deposits. In: Barnes HL (ed) Geochemistry of hydrothermal ore deposits. Wiley, New York, pp 229–302

Thomas HV, Large RE, Bull SW, Maslennikov V, Berry RF, Fraser R, Froud S, Moye R (2011) Pyrite and pyrrhotite textures and composition in sediments, laminated quartz veins, and reefs at bendigo gold mine, Australia: insights for ore genesis. Econ Geol 106(1):1–31

Tolstikhin I, Kamensky I, Tarakanov S, Kramers J, Pekala M, Skiba V, Gannibal M, Novikov D (2010) Noble gas isotope sites and mobility in mafic rocks and olivine. Geochim Cosmochim Acta 74(4):1436–1447

Tomaru H, Fehn U, Lu ZL, Matsumoto R (2007a) Halogen systematics in the Mallik 5L–38 gas hydrate production research well, Northwest Territories, Canada: Implications for the origin of gas hydrates under terrestrial permafrost conditions. Appl Geochem 22(3):656–675

Tomaru H, Fehn U, Lu ZL, Takeuchi R, Inagaki F, Imachi H, Kotani R, Matsumoto R, Aoike K (2009) Dating of dissolved iodine in pore waters from the gas hydrate occurrence offshore Shimokita Peninsula, Japan: ^{129}I Results from the D/V Chikyu Shakedown Cruise. Resour Geol 59(4):359–373

Tomaru H, Lu Z, Snyder GT, Fehn U, Hiruta A, Matsumoto R (2007b) Origin and age of pore waters

in an actively venting gas hydrate field near Sado Island, Japan Sea: Interpretation of halogen and ^{129}I distributions. Chem Geol 236(3–4):350–366

Torgersen T (2010) Continental degassing flux of ^{4}He and its variability. Geochem Geophys Geosyst 11

Torgersen T, Kennedy BM, van Soest MC (2004) Diffusive separation of noble gases and noble gas abundance patterns in sedimentary rocks. Earth Planet Sci Lett 226(3–4):477–489

Torgersen T, O'Donnell J (1991) The degassing flux from the solid earth: release by fracturing. Geophys Res Lett 18(5):951–954

Turner G (1988) Hydrothermal fluids and argon isotopes in quartz veins and cherts. Geochim Cosmochim Acta 52:1443–1448

Turner G, Bannon MP (1992) Argon isotope geochemistry of inclusion fluids from granite-associated mineral veins in Southwest and Northwest England. Geochim Cosmochim Acta 56(1):227–243

Turner G, Burnard P, Ford JL, Gilmour JD, Lyon IC, Stuart FM (1993) Tracing fluid sources and interactions. Philisophical transactions of the Royal Society London A 344:127–140

Turner G, Stuart F (1992) Helium heat ratios and deposition temperatures of sulfides from the ocean-floor. Nature 357(6379):581–583

Viets JG, Hofstra AH, Emsbo P (1996) Solute composition of fluid inclusions in sphalerite from North American and European Mississippi Valley-Type ore deposits: ore fluids derived from evaporated seawater. Soc Econ Geol Spec Publ 4:465–482

Viets JG, Leach DL (1990) Genetic implications of regional and temporal trends in ore fluid geochemistry of Mississippi valley: type deposits in the Ozark region. Econ Geol 85:842–861

Valkiers S, Vendelbo D, Berglund M, de Podesta M (2010) Preparation of argon primary measurement standards for the calibration of ion current ratios measured in argon. Int J Mass Spectrom 291(1–2):41–47

Wallace MW, Middleton HA, Johns B, Marshallsea S (2002) Hydrocarbons and Mississippi Valley-type sulfides in the devonian reef complexes of the eastern Lennard Shelf, Canning Basin, Western Australia. In: Keep M, Moss SJ (eds) The Sedimentary Basins of Western Australia 3: Proceedings of the Petroleum Exploration Society of Australia Symposium, Perth, WA., vol., Perth, WA, pp 795–816

Warren C, Sherlock S, Kelley S (2011) Interpreting high-pressure phengite $^{40}Ar/^{39}Ar$ laserprobe ages: an example from Saih Hatat, NE Oman. Contrib Miner Petrol 161(6):991–1009

Webber AP, Roberts S, Burgess R, Boyce AJ (2011) Fluid mixing and thermal regimes beneath the PACMANUS hydrothermal field, Papua New Guinea: Helium and oxygen isotope data. Earth Planet Sci Lett 304(1–2):93–102

Wei HX, Sun XM, Zhai W, Shi GY, Liang YH, Mo RW, Han MX, Yi JZ (2010) He-Ar-S isotopic compositions of ore-forming fluids in the Bangbu large-scale gold deposit in southern Tibet, China. Acta Petrol Sin 26(6):1685–1691

Wilde AR (2011) Mount Isa copper orebodies: improving predictive discovery. Aust J Earth Sci 58(8):937–951

Wilkinson JJ, Stoffell B, Wilkinson CC, Jeffries TE, Appold MS (2009) Anomalously metal-rich fluids form hydrothermal ore deposits. Science 323(5915):764–767

Winckler G, Kipfer R, Aescbach-Hertig W, Botz R, Schmidt M, Schuler S, Bayer R (2000) Sub sea floor boiling of Red Sea Brines: new indication from noble gas data. Geochim Cosmochim Acta 64(9):1567–1575

Yardley BWD (2005) 100th anniversary special paper: metal concentrations in crustal fluids and their relationship to ore formation. Econ Geol 100(4):613–632

Yardley BWD, Banks D, Bottrell SH, Diamond LW (1993) Post-metamorphic gold-quartz veins from N.W. Italy: the composition and origin of the ore fluid. Mineral Mag 57:407–422

Yokochi R, Marty B, Pik R, Burnard P (2005) High $^{3}He/^{4}He$ ratios in peridotite xenoliths from SW Japan revisited: Evidence for cosmogenic ^{3}He released by vacuum crushing. Geochem Geophys Geosyst 6:12

Zaikowski A, Kosanke BJ, Hubbard N (1987) Noble gas composition of deep brines from the Palo Duro Basin, Texas. Geochim Cosmochim Acta 51:73–84

Zeng Z, Qin Y, Zhai S (2001) He, Ne and Ar isotope compositions of fluid inclusions in hydrothermal sulfides from the TAG hydrothermal field Mid-Atlantic Ridge. Sci China Ser D Earth Sci 44(3):221–228

Zherebtsova IK, Volkova NN (1966) Experimental study of behaviour of trace elements in the process of natural solar evaporation of Black Sea water and Lake Sasky-Sivash brine. Geochem Int 3:656–670

Zhou S, Ye X (2002) Noble gas isotopic compositions of deep carbonate rocks from the Tarim Basin. Chin Sci Bull 47(9):774–778

Ziegler JF (1980) Hanfbook of stopping cross-sections for energentic ions in all elements. Pergamon Press, New York

Zuber A, Weise SM, Osenbruck K, Matenko T (1997) Origin and age of saline waters in Busko Spa (Southern Poland) determined by isotope, noble gas and hydrochemical methods: evidence of interglacial and pre-quaternary warm climate recharges. Appl Geochem 12(5):643–660

Noble Gases as Tracers of Mantle Processes and Magmatic Degassing

M. A. Moreira and M. D. Kurz

Abstract

Noble gas geochemistry provides powerful tools for constraining mantle degassing through geological time. However, noble gas elemental and isotopic ratios are often disturbed by melting, magma degassing and atmospheric contamination. It is necessary to understand and quantify these shallow influences in order to obtain the noble gas elemental and isotopic ratios in the mantle. In this chapter, we present an overview of the key parameters that are necessary to derive mantle compositions. We discuss solubilities in silicate melts, crystal/melt partition coefficients during melting, and different models for vesiculation and degassing, along with the preferred method to correct for atmospheric contamination, using neon isotopic compositions. Using selected samples from mid-ocean ridge basalts (MORB) and ocean island basalts (OIB), we give the probable mantle contents and elemental and isotopic compositions of He, Ne, Ar and Xe in the depleted mantle and in the high ^{3}He source. These estimates cannot be reconciled with ancient depletion models for unradiogenic noble gas isotopic compositions, found in some oceanic island basalts, which are best explained by relatively undegassed sources deep in the mantle.

1 Introduction

Noble gases are excellent tracers of mantle processes. They form a single chemical family, the last column of the periodic table, which indicates that they are inert with respect to chemical reactions. Each noble gas element has both non radiogenic and radiogenic isotopes, which provide extremely useful time constraints on mantle processes. Because of their inert chemical nature, they accumulate in the atmosphere, and are unique indicators of the history

M. A. Moreira (✉)
Equipe de Géochimie et Cosmochimie, Institut de Physique du Globe de Paris, Sorbonne Paris Cité, CNRS (UMR 7154), 1 rue Jussieu, 75238 Paris Cedex, France
e-mail: moreira@ipgp.fr

M. D. Kurz
Department of Marine Chemistry and Geochemistry, Woods Hole Oceanographic Institution, Woods Hole, MA 02543, USA
e-mail: mkurz@whoi.edu

P. Burnard (ed.), *The Noble Gases as Geochemical Tracers*, Advances in Isotope Geochemistry,
DOI: 10.1007/978-3-642-28836-4_12,

of mantle degassing. Xenon isotopes are of particular interest, and ^{129}I–^{129}Xe systematics have demonstrated that the atmosphere was partly formed during the first hundred of million years by massive degassing of the mantle, perhaps from a magma ocean (Coltice et al. 2009; Kunz et al. 1998; Ozima et al. 1985; Staudacher and Allègre 1982; Yokochi and Marty 2006). However, degassing of the mantle is still continuing due to plate tectonics and mantle convection, as illustrated by the measured mantle ^{3}He flux. Pioneering research in the late 1960s demonstrated an association of ^{3}He excesses with mantle degassing (Clarke et al. 1969; Mamyrin et al. 1969), which stimulated decades of mantle helium studies. Flux estimates of global ^{3}He degassing rates range from 500 to 1,000 mol/year (Lupton and Craig 1975; Farley et al. 1995; Bianchi et al. 2010). This relatively well documented mantle degassing flux is unique among geochemical tracers and approximately balances the atmospheric ^{3}He loss rate to space. As discussed further below, the ^{3}He flux places important constraints on mantle noble gas concentrations.

Present-day mantle contains both primordial (e.g. ^{3}He, ^{20}Ne, ^{36}Ar, ^{130}Xe) and radiogenic isotopes (^{4}He, ^{40}Ar, ^{129}Xe, ^{136}Xe), but in different proportions depending on the geological context. Mid Oceanic Ridge Basalts (MORB) and Oceanic Island basalts (OIB) have different isotopic ratios of the noble gases. Early studies demonstrated that MORB glasses have a remarkably homogeneous helium isotopic ratio of $^{4}He/^{3}He \sim 90{,}000 \pm 10{,}000$ or $R/Ra = 8 \pm 1$ (where $R = {}^{3}He/{}^{4}He$ and Ra the atmospheric ratio) (Kurz and Jenkins 1981; Kurz et al. 1982b). More recent studies have documented slightly larger variability within normal MORB from different ocean basins (e.g. Georgen et al. 2003; Graham et al. 2001; Mahoney et al. 1989), but are still relatively homogeneous compared to OIBs, which have $^{4}He/^{3}He$ both lower and higher than MORB, varying between 18,000 and more than 200,000 (Allègre et al. 1995; Class et al. 2005; Graham et al. 1993; Hilton et al. 1999; Kurz et al. 1982a, 1983, 2004b; Moreira et al. 1999; Parai et al. 2009; Stuart et al. 2003). The classical interpretation of this dichotomy is that the OIB source reservoir contains variable amount of recycled material, with high $U/^{3}He$ ratio, which would yield higher $^{4}He/^{3}He$, as well as a relatively undegassed source, with a low $U/^{3}He$, which has a lower $^{4}He/^{3}He$ than MORB.

Much attention has been paid to the origin and location of the unradiogenic helium (low $^{4}He/^{3}He$) in an undegassed reservoir, which contains a higher proportion of primordial or primitive noble gases relative to radiogenic noble gases. The OIB source is generally enriched in trace elements such as U and Th compared to the MORB source. Therefore, to obtain lower $^{4}He/^{3}He$ in the OIB source, it must be enriched in ^{3}He. This classical model is known as the two-layer mantle model (Allègre 1987), which conflicts with whole mantle convection models, i.e. as suggested by tomographic images of slabs penetrating the lower mantle (Grand et al. 1997). Although it is still an open question, it has been shown by (Gonnermann and Mukhopadhyay 2009) that subduction of noble gas-depleted slabs into the lower mantle could lead to a decrease of noble gas concentration, by dilution, without a significant change in the isotopic ratios, depending on relative volumes. Moreover, subduction may not have continuously occurred since 4.5 Ga but may have started only $\sim$3 Ga ago, reinforcing the idea that the lower mantle could have preserved some primordial rare gas isotopic signatures.

Other hypotheses have been proposed to explain the presence of unradiogenic noble gas isotopic compositions in some OIBs, including noble gas storage within the core, within residual crystals from a basal ocean magma, or within the D″ layer (Coltice et al. 2011; Porcelli and Halliday 2001; Tolstikhin et al. 2006; Tolstikhin and Hofmann 2005). At present, these reservoirs can be considered as potential sources of primordial noble gases but rigorous evaluation will require the development of noble gas silicate/melt and silicate/iron partitioning at high pressures and temperatures. Because the partitioning behavior is not well known, these

alternative scenarios cannot yet be considered more viable than the lower mantle as the source of primordial noble gases.

Another controversy relates to the so-called helium paradox (Anderson 1998). Higher concentrations of primordial isotopes are expected in OIB glasses compared to MORB, which is not observed (Moreira and Sarda 2000). It has also been suggested that helium is more compatible than Th and U on silicate melting, resulting in a residue that has a lower (Th + U)/He than the parental mantle, which would then freeze the isotopic composition (Parman et al. 2005). In this model the unradiogenic $^4He/^3He$ values found in some OIBs would then reflect ancient depleted mantle reservoirs.

One goal of this chapter is to discuss these controversies in the context of melting and degassing processes. After briefly discussing the different mantle samples available to constrain concentrations, elemental and isotopic compositions and the technical aspects to obtain these results, we discuss the methodologies of calculating magmatic and ultimately mantle concentrations and isotopic compositions of the rare gases.

2 Samples Available for Probing the Mantle

Mantle derived noble gases can be found in volcanic gas emissions (e.g. fumaroles), ground water samples, CO_2 well gases, submarine glasses, ultramafic xenoliths, phenocrysts in basaltic lavas, and diamonds, which are phenocrysts or xenocrysts within kimberlite melts. Each of these sample types presents a unique set of assumptions and analytical challenges, particularly with respect to recovering mantle source information.

Gas and fluids from some thermal springs give access to the helium isotopic composition of active volcanoes through the hydrothermal alteration of bedrock and/or gas–water interaction in deep aquifers. It is generally necessary to measure neon to correct for atmospheric helium components, i.e. by assuming that all neon is atmospheric and exploiting the contrast in He/Ne ratios between the mantle ($\sim$3,000) and air (0.29). Helium is the only rare gas that has been extensively used to obtain mantle-derived components in thermal springs due to the dominance of atmospheric components for the heavy noble gases (Allard et al. 1997; Hennecke and Manuel 1975; Jean-Baptiste et al. 2009; Pedroni et al. 1999; van Soest et al. 1998).

CO_2 well gases, although rare in terms of geographical distribution, provide important constraints on mantle noble gas isotopic compositions. It has been shown that these CO_2 emanations contain mantle-derived gases (Ballentine 1997; Cafee et al. 1999; Gilfillan et al. 2008; Holland and Ballentine 2006; Staudacher 1987; Xu et al. 1995). Due to large quantities of analyzable gas, high accuracy and precision on isotopic compositions can be achieved. Significant results on well gas xenon and krypton isotopic ratios have been recently published that show that isotopic ratios of non-radiogenic krypton and xenon are different in the mantle and in the atmosphere (Cafee et al. 1999; Holland and Ballentine 2006; Holland et al. 2009). This observation has fundamental implications for the origin and evolution of the atmosphere. One uncertainty with respect to well gases is that they reside within the continental crust for millions of years, their emplacement timing and mechanisms are not well understood, and therefore may have been influenced by complex mixing and fractionation processes. Although the measurements are highly precise, some of the isotopic anomalies are quite small (Cafee et al. 1999; Holland and Ballentine 2006; Holland et al. 2009).

Olivine and pyroxene phenocrysts in basaltic melts contain melt and fluid inclusions that can potentially preserve mantle noble gases. In general helium has very low concentrations in phenocrysts (10^{-10}–10^{-8} ccSTP/gram) but reliably reflects the magmatic $^4He/^3He$ ratio (e.g. Kurz 1993; Kurz et al. 2004a). However, with only a few exceptions, measurement of noble gases heavier than helium have not yielded clear isotopic mantle unradiogenic isotopic excesses, compared to air (Dixon 2003; Dixon et al. 2000;

Hanyu et al. 2001; 2011; Kaneoka and Takaoka 1977; Kaneoka et al. 1986; Madureira et al. 2005; Marty et al. 1994; Parai et al. 2009; Staudacher and Allègre 1993; Staudacher et al. 1990). Several neon studies have documented mantle isotopic compositions in subaerial OIB lavas, but with very small concentrations and consequently large uncertainties in isotopic compositions (e.g. Dixon et al. 2000; Jackson et al. 2009; Madureira et al. 2005; Parai et al. 2009). The helium isotopic ratios are sometimes more radiogenic in pyroxene than in olivines. (Hilton et al. 1995; Marty et al. 1994 and Shaw et al. (2006), which could reflect either later crystallization or wall rock assimilation in magma chambers. In addition, there are some indications of grain size dependant helium isotopic variations in olivine phenocryst populations, which may reflect different phenocryst generations, or xenocrysts, within the same samples (Kurz et al. 2004a). For the moment, with the exception of helium, noble gas measurements in phenocrysts have not been widely used for mantle studies because of the important atmospheric contamination for the heaviest rare gases and the analytical challenges in measuring small abundances.

Peridotite and ultramafic cumulate xenoliths are sometimes more gas rich than basaltic phenocrysts, and some isotopic excesses of Ne, Ar and Xe, relative to air, have been observed (Burnard et al. 1998; Czuppon et al. 2009, 2010; Hopp et al. 2004, 2007; Kaneoka et al. 1977, 1986; Poreda and Farley 1992; Staudacher et al. 1986, 1990; Valbracht et al. 1996; Yamamoto et al. 2009a). However, xenoliths in alkaline lavas can derive from the mantle or lithosphere and have often been deformed pre- and syn-eruption, so interpretation of the noble gases is difficult in light of these complexities.

Diamonds should provide constraints on mantle isotopic compositions because their stability field places their origin at mantle depths greater than 150 km. However, the formation conditions are complex and may be related to subcontinental lithosphere and deep continental crust. In addition, diamonds are generally found in ancient kimberlites or in alluvial deposits, having resided in the continental crust for long periods, which means that nucleogenic and cosmogenic origins must be constrained (e.g. Kurz et al. 1987; Lal et al. 1987). Studies where the five noble gases were analyzed in the same samples are rare (Gautheron et al. 2005; Honda et al. 1987, 2004; Ozima and Zashu 1988, 1991; Wada and Matsuda 1998). All these studies suggest a present-day MORB or crustal composition for the rare gases in diamonds, which could be in agreement with a subcontinental lithospheric mantle origin. Noble gases have also been used to distinguish crustal and mantle diamond genesis (Honda et al. 2004, 2011). Data on noble gas diffusion in diamonds are also rare, but helium diffusion coefficients have been estimated to be between 3×10^{-17} (Zashu and Hiyagon 1995) and roughly 10^{-12} cm^2/s (Lal et al. 1987) at mantle temperature. Such low values suggest that diamond can preserve their noble gas contents for billions of years. It is therefore not clear why more primitive noble gas signatures have not been observed in diamonds.

The most commonly studied samples for the MORB mantle reservoir are glassy margins from pillow lavas. Basalts are the most common product of mantle melting, representing an average mantle composition after $\sim$10 % melting and therefore provide important mantle volatile samples. The thin layer of glassy basalt, at the interface with seawater, preserves mantle noble gases dissolved in the glass and within vesicles, due to high eruption depths (>2,000 m) and rapid quenching (Dymond and Hogan 1973; Fischer 1971; Kurz and Jenkins 1981; Marty et al. 1983; Ozima and Zashu 1983) compared to the crystallized interior of the pillow. The glass contains relatively high noble gas abundances and often preserve a mantle component. For example, helium contents in MORB glasses are typically 10^{-6}–10^{-4} cc STP/gram, or roughly 10^2–10^6 higher than phenocrysts. For this reason, many studies have focused on the glassy samples to obtain concentrations and isotopic compositions of heavy rare gases in the mantle (Bach and Niedermann 1998; Burnard et al. 2002, 2003, 2004; Furi et al. 2010; Hiyagon et al. 1992; Honda et al. 1993a; Kurz et al. 2005; Marty 1989; Marty

and Ozima 1986; Marty et al. 1983; Moreira and Allègre 2002; Moreira et al. 1995, 1996, 1998; Niedermann and Bach 1998; Niedermann et al. 1997; Nishio et al. 1999; Ozima and Zashu 1983; Poreda and Radicati di Brozolo 1984; Sarda et al. 1985, 1988, 2000; Staudacher and Allègre 1982; Staudacher et al. 1989; Stroncik et al. 2008). Despite the fact that submarine glasses are ideal for noble gas measurements due to rapid quenching and relatively high magmatic gas concentrations, they are still susceptible to atmospheric contamination. As discussed further below, this is illustrated by mixing relations in neon and argon isotopes, but the mechanisms whereby atmospheric noble gases are introduced into the glass are unknown and could relate to mantle source variations, magma chamber processes, seafloor eruption dynamics, or laboratory procedures (Ballentine and Barfod 2000; Sarda 2004).

Due to the ubiquitous processes of degassing, even at and below the ocean floor, it is often assumed that the most gas rich samples are the most representative of the mantle. For this reason, popping rocks have received considerable attention. Popping rocks are glassy submarine basalt glasses that contain so much gas, within CO_2 rich vesicles, that they explode (popping) when recovered above sea level. Although there have been several reported localities (Pineau et al. 1976) the most extensively studied samples come from the Mid Atlantic Ridge near 14 N° (Burnard et al. 1997; Cartigny et al. 2008; Moreira et al. 1998; Sarda and Graham 1990; Staudacher et al. 1989). These samples are important because they contain the highest abundance of mantle noble gases and are discussed further below.

Some oceanic hotspots also have submarine or subglacial (Iceland) eruptions that allow sampling of submarine glasses and heavy noble gas analyzes (Dixon et al. 2000; Furi et al. 2010; Harrisson et al. 1999; Honda and Woodhead 2005; Honda et al. 1991, 1993b; Kurz et al. 2009b; Moreira et al. 2001; Raquin and Moreira 2009; Staudacher and Allègre 1989; Staudacher et al. 1986; Trieloff et al. 2000). However, this is relatively rare and in most cases, noble gas analyses have been performed in minerals (xeno or phenocrysts) with the issues discussed above.

3 Technical Aspects

It is beyond the scope of this chapter to give a comprehensive discussion of analytical techniques. However, we give a brief overview of the analytical procedures most commonly used in the analyses of noble gases by mass spectrometry. Samples are typically cleaned in solvents to remove dust and hydrocarbon contamination (typically using ethanol, methanol, or acetone) followed by washing in distilled water and drying before placement into a crusher, furnace or laser ultra-high-vacuum chamber. The samples are typically pumped in ultra-high-vacuum and baked at 100–150 °C for 12–24 h before analysis, in order to obtain low blanks for heavy noble gases. The general assumption is that this procedure will remove any easily desorbed atmospheric component. Rock samples can then be crushed, heated under vacuum or ablated using UV laser in order to extract gases. Active gases that are produced during the extraction procedure, such as CO_2, H_2O, N_2, O_2 are removed by gettering, which involves exposure to hot titanium (800 °C) or Zr–Al, or Zr–V–Fe alloys (e.g. Ferrario 1996; Stout and Gibbons 1955). The rare gases are not affected by this purification sequence, and are then typically trapped onto a charcoal trap held at 10 K using a helium expansion cryogenic system. Sequential desorption of each noble gas into a static mass spectrometer is achieved by increasing temperature with precise temperature control (e.g. Lott and Jenkins 1984; Lott 2001; Reynolds et al. 1978). Noble gases are inlet successively into the mass spectrometer in order to obtain the best partial pressure for measurement, and also to avoid peak superposition (e.g. $^{40}Ar^{++}$ on $^{20}Ne^{+}$) and competition for electrons, which can influence sensitivity within the mass spectrometer. Depending on the mass resolution of the instrument, peak superposition must be corrected (e.g. HD^{+} on $^{3}He^{+}$; CO_2^{++} on $^{22}Ne^{+}$ or $^{40}Ar^{++}$ on $^{20}Ne^{+}$). Due to pressure dependence of

sensitivity in electron bombardment ion sources, it is also crucial to measure standards at the same partial pressure conditions as the samples (e.g. Burnard and Farley 2000).

Static magnetic-sector mass spectrometers are the most common instrumentation for noble gas measurements and are broadly similar to the pioneering designs of Nier (e.g. Nier 1947; Reynolds 1956), using electron bombardment in a magnetic field (called a Nier type source). Clarke and colleagues introduced an instrument with larger analyzer magnet, stronger source electromagnet (for higher sensitivity), and a split flight tube, specifically designed to resolve H_3 and HD from ^{3}He, and optimize the measurement of helium isotopes (Clarke et al. 1976), but are generally not used for heavier noble gases. Modern commercial instruments combine high sensitivity with the ability to resolve some of the interferences on neon (e.g. Marrocchi et al. 2009). Quadrupole mass spectrometers are now more commonly used for abundance measurements and have some advantages, such as rapid mass scanning and lower overall cost. When using ion counting system, dead time corrections can be applied for large signals. These isotopic ratios and abundances are then corrected for blanks and for mass discrimination using standards, which can be derived from an air standard or calibrated gas mixtures in a calibrated volume.

4 Correction for the Atmospheric Component in Mantle Samples

4.1 The Origin of Air Components in Mantle-Derived Samples

Noble gases with an atmospheric signature are often measured in mantle-derived samples (Ballentine and Barfod 2000; Burnard et al. 1994; Harrisson et al. 1999; Honda et al. 1991, 1993b; Moreira et al. 1998; Sarda et al. 1988, 2000; Staudacher and Allègre 1989; Staudacher et al. 1986, 1989, 1990). Although the air contamination mechanism for volcanic gases and/or water samples is obvious (e.g. most of the water is meteoric), the origin of the air-like signature in submarine basaltic glasses and phenocrysts is still unclear. Contamination in magma chambers by seawater circulation, during eruption, or during sample storage and preparation in the laboratory are often proposed as possible mechanisms (Ballentine and Barfod 2000; Burnard et al. 2003; Farley and Poreda 1993; Farley and Craig 1994; Harrisson et al. 2003; Patterson et al. 1990; Trieloff et al. 2003).

Laser extraction has been used to measure noble gases within individual vesicles, in highly vesicular MORB samples by Burnard (1999a) and Raquin et al. (2008), in order to constrain the residence sites of atmospheric rare gases, and to determine the mantle composition prior to air contamination. Raquin et al. (2008) obtained neon and argon isotopic compositions in single vesicles that were mantle-like and distinct from air. In contrast to step-crushing experiments on the same sample, which shows important quantities of atmospheric rare gases, the laser experiments on individual bubbles do not show this atmospheric component. It was concluded that the air component was located in cracks or vesicles equilibrated at atmospheric pressure, and therefore that the contamination probably occurs at the surface (Raquin et al. 2008).

Some authors, arguing that recycling of atmospheric rare gases into the mantle is possible, proposed a mantle origin for the atmospheric signature. Sarda et al. (1998), based on a $^{40}Ar/^{36}Ar$–$^{206}Pb/^{204}Pb$ correlation (in MORB glasses from the Mid-Atlantic Ridge) suggested that the air-like signature is derived from the pyroxenite recycled component in a marble cake mantle structure. In such a scenario, the pyroxenite reflects subducted oceanic crust, stirred by mantle convection. Burnard (1999b), on the contrary, suggested that this correlation reflects contamination after degassing and that the correlation is induced by the occurrence of high $^{206}Pb/^{204}Pb$ samples from topographic highs on the Mid-Atlantic Ridge, which favors degassing, vesiculation, and then air contamination, due to relatively shallow depths.

Holland and Ballentine (2006), based on the similarity between the seawater and the mantle

noble gas abundance patterns, and on the measurement of excess non-radiogenic xenon isotopes, compared to air, in CO2-well gases, suggest a massive recycling of atmospheric noble gases into the mantle (Holland and Ballentine 2006). However, such a model fails to explain the solar-like $^{20}Ne/^{22}Ne$ ratio and the ^{129}Xe excess observed on MORB samples (Moreira and Raquin 2007; Staudacher and Allègre 1988), as well as the elemental ratios of the OIB source, including the $^{3}He/^{130}Xe$ ratio (Mukhopadhyay 2011, 2012). Staudacher et al. (1988) originally suggested that subduction zones act as barriers to recycling noble gases into the mantle, because the gases are quantitatively removed by melting and degassing of the down going slab. Subduction of atmospheric noble gases into the mantle has not yet been demonstrated to be viable based on mass balances. The budgets of the noble gas abundances in sediments and altered oceanic crust are required but are not yet well known. In addition, the details of the melting, melt migration processes, and degassing processes during slab dehydration are not well constrained, and the subduction barrier hypothesis remains an important hypothesis to be tested.

In summary, most authors agree that air contamination occurs within the crust, during eruption or in the laboratory during storage of the samples. The exact location of this component within mantle glass samples is unclear, but appears to be linked to vesicularity, at least within submarine basalt glasses (Ballentine and Barfod 2000). Cracks or partially closed vesicles, that are difficult to pump overnight, could be the location of the air component.

4.2 Neon Isotope Systematics and the Atmospheric Correction

Neon isotopes are often used to correct for air contamination in terrestrial samples. Indeed, the $^{20}Ne/^{22}Ne$ isotopic ratios can be considered as a stable isotopic ratio in the mantle (Both ^{20}Ne and ^{22}Ne are produced by nucleogenic pathways, but they are sufficiently slow as to be negligible.). Numerous studies have shown that the mantle $^{20}Ne/^{22}Ne$ is higher than in the atmosphere (9.8), probably due to mass fractionating neon escape from the early terrestrial atmosphere when the atmosphere was hotter, the Earth less massive, or with no magnetic field. Mixing between a solar-like primary atmosphere and material having planetary neon (Neon A with $^{20}Ne/^{22}Ne \sim 8$) is also a possible scenario to produce the neon isotopic composition of the atmosphere (Marty 2012). The exact value of the mantle $^{20}Ne/^{22}Ne$ isotopic ratio is a matter of debate. Most high precision $^{20}Ne/^{22}Ne$ measurements in mantle-derived rocks show values less than 12.8, close to the so-called Ne–B component [$\sim$12.6 (Black 1972)], but lower than the solar value [13.8 (Grimberg et al. 2006)]. Implications of the mantle $^{20}Ne/^{22}Ne$ value are beyond the scope of the paper, but relate to the processes of noble gas acquisition by the early Earth, which include solar gas solubility in a magma ocean, or solar wind implantation in the parent body precursors. The Ne–Ar isotope systematics can be better explained by the scenario of solar wind implantation (Trieloff and Kunz 2005; Trieloff et al. 2002; Raquin and Moreira 2009), but this fails to explain Kr and Xe isotopic signatures of the Earth (in fact no scenario is able to explain the xenon isotopic signature). However, some samples have $^{20}Ne/^{22}Ne$ higher than the Ne–B value (e.g. a magnetite sample from Kola shows $^{20}Ne/^{22}Ne$ of 13.0 ± 0.4 at 2σ level), which could suggest that the mantle has a $^{20}Ne/^{22}Ne$ ratio higher than 12.8 (Yokochi and Marty 2004). Whatever the actual $^{20}Ne/^{22}Ne$ isotopic ratio in the mantle (e.g. solar or neon B), the linear trends commonly found in mantle sample suites (e.g. Sarda et al. 1988) can be used to correct the other isotopic ratios from atmospheric contamination. Assuming that each measurement is a mixture between the mantle component and the atmosphere, and considering that $^{20}Ne/^{22}Ne$ is homogeneous in the mantle, an air-corrected $^{21}Ne/^{22}Ne$ ratio can be derived for each sample using the linear arrays in the neon isotope diagram (e.g. Moreira and Allègre 1998). Determination of the other rare gas isotopic ratios (e.g. $^{40}Ar/^{36}Ar$, $^{129}Xe/^{130}Xe$)

requires the knowledge of the elemental ratios (e.g. $^{22}Ne/^{36}Ar$, $^{22}Ne/^{130}Xe$) in both components. These elemental ratios strongly depend on the degassing process of the magma, and are therefore difficult to estimate. A better approach is step crushing, which generally allows the determination of the hyperbolic mixing curve and of the air-corrected isotopic and elemental ratios. This approach has been applied to the popping rock and to Iceland subglacial glasses in order to estimate elemental ratios in the mantle (e.g. Moreira et al. 1998; Trieloff et al. 2000; Harrisson et al. 2003; Burnard et al. 2003).

5 Elemental Fractionation During Melting, Vesiculation and Degassing

Three relatively well-understood physical processes should be sufficient to explain mantle rare gas elemental ratios: melting, degassing and atmospheric contamination. The previous section described how to correct for atmospheric contamination assuming a solar-like (or neon B) ratio for neon isotopes. In this section we discuss the effect of melting on the elemental ratios and show that degassing is the dominant process that fractionates the elemental ratios in basaltic magma.

5.1 Partition Coefficients of Rare Gases Between Solid Silicates and Basaltic Melt

It has been known for decades that basaltic phenocrysts generally have significantly lower noble gas contents than submarine basaltic glasses, which has led to general recognition that noble gases are incompatible during melting, at least among those who make measurements in natural samples. Partition coefficients determined from laboratory experiments have yielded variable results, depending on the methodologies employed. The first attempts to determine partition coefficients involved natural samples or experiments where the coexisting crystals were directly compared to the host glasses. These early studies focused mainly on helium in olivine, including natural crystals (Kurz 1993; Marty and Lussiez 1993) and laboratory synthesized crystals (Hiyagon and Ozima 1986), but have also included natural plagioclase (Kurz et al. 1982b). The results of these studies showed that helium and argon are incompatible elements, but the crystal melt partition coefficients (Kd) are highly variable due to the difficulty of separating the crystals from the host glass, coupled with the presence of melt inclusions and bubbles within the crystals. Even tiny amounts of host glass can have an impact on the Kd estimates, so these early studies can be considered as upper limits.

Another experimental approach is to determine solubilities in crystals by equilibrating directly with controlled partial pressures of gas, thus avoiding the need to separate laboratory grown crystals from coexisting glass (Broadhurst et al. 1990, 1992). The partition coefficients can then theoretically be obtained by dividing the crystal solubility by the melt solubility (which are relatively well defined at low pressures). In order to enhance rapid equilibration with laboratory-produced gas atmospheres, Broadhurst et al. (1990, 1992) used fine grained (<10 microns) powders. However, this procedure can trap gas between grains due to sintering at high temperature, thus yielding high gas contents, apparently high solubilities, and high Kd. In order to avoid this problem Parman et al. (2005) used the same approach but equilibrated millimeter sized crystals of olivine for long time periods with helium. They used visual inspection to argue against the presence of defects or inclusions, but a significant fraction of the helium was released by crushing in vacuum, suggesting that defects or inclusions played some role in the results.

The lowest values for silicate/melt partition coefficients have been determined using crystals grown from melts, but using laser extraction methods for the noble gas measurements (Brooker et al. 2003; Heber et al. 2007). These studies avoid the problems of sintering and melt contamination using the small spot size of laser extraction, which allows selective ablation of specific zones within individual crystals. Heber et al. (2007) illustrated the effects of melt and

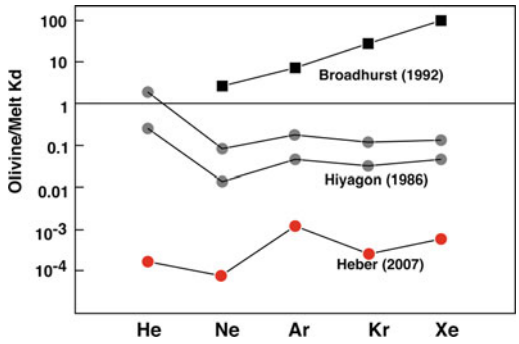

Fig. 1 Olivine/melt partitioning coefficients for noble gases. Data are derived from Broadhurst et al. (1992), Heber et al. (2007) and Hiyagon and Ozima (1986). The D values show that noble gases are highly incompatible elements. The most recent values (Heber et al. 2007) are considered the most reliable (see text)

bubble contamination using this method. The olivine/melt and clinopyroxene/melt noble gas Kd values were between 10^{-4} and 10^{-3}, lower by factors of 10^3–10^6 from the earlier experiments (see summary for olivine in Fig. 1). These recent studies do not show systematic differences in Kd with mass, which is predicted by the "zero charge" model of Brooker et al. (2003), i.e. implying that charge is the dominant factor controlling substitution into olivine and clinopyroxene at low pressure, and that all the noble gases should have similar partition coefficients. The experiments do show significant variability, and this is still an open question.

From the most recent studies, all the noble gases are highly incompatible and therefore are efficiently extracted from the mantle during melting. A notable exception is the study of Watson et al. (2007) who used Rutherford backscattering to measure laboratory based partition coefficients. They claim that argon is a compatible element, with olivine/melt partition coefficients between 1 and 10,000, depending on Ar fugacity. None of these values are consistent with other recent studies or with data from natural samples, and would pose a major problem for the K–Ar budget. For example, since ^{40}Ar in the atmosphere is produced from decay of ^{40}K, with a half live of $\sim$1 Ga, it would be extremely difficult to explain the present day atmospheric ^{40}Ar inventory unless the mantle had unrealistic amounts of K. For example, considering the ^{4}He flux at ridges ($\sim 10^8$ mol/year) and the ^{4}He/^{40}Ar ratio ($\sim$2) of MORB (Moreira et al. 1998), the ^{40}Ar flux is 5×10^7 mol/year. Crust formation rate is 5×10^{16} g/year. Therefore, there is $\sim 2 \times 10^{-5}$ cc/g of ^{40}Ar in the undegassed crust. Therefore, with D $\sim 10^3$, as suggested by (Watson et al. 2007), there should be ^{40}Ar $\sim 2 \times 10^{-2}$ cc/g in the mantle. To produce this concentration in 4.5 Ga of ^{40}K decay, the mantle should have a K content of 28 %, which is unrealistic by at least a factor of 1,000. It is unclear why the Watson et al. (2007) study differs from all others, but may relate to the methodology used, i.e. Rutherford backscattering as opposed to mass spectrometry.

Noble gas partitioning is generally discussed in terms of relative incompatibility with their parent elements such as K, U and Th. For example, it has been proposed that the low ^{4}He/^{3}He observed in OIB, relative to MORB, could be the result of ancient melting events, and the residual mantle would have a low (U + Th)/^{3}He, if helium is less incompatible than U and Th. Indeed, U and Th are sited within CPX that melts first whereas helium is probably homogeneously distributed due to its fast diffusivity. Melting could then lead to relative enrichment of helium. The same is then proposed for neon and argon. Such a hypothesis has been suggested by several authors (Albarède 2008; Anderson 1998; Coltice and Ricard 1999; Heber et al. 2007; Meibom et al. 2003; Parman et al. 2005). However, there are notable flaws in such a scenario. First, a residue of melting would have a depleted trace element pattern, which is not observed in OIB. Second, the mantle residue would have a helium content that is 10^{-3} of the mantle (with D = 10^{-4} and F = 10 %). Such a gas-poor residue could never be observed when mixed with normal MORB mantle or recycled material rich in U and Th (and ^{4}He*), and could not explain the observed ^{3}He flux. In fact, there are numerous examples of along-axis helium isotopic variability showing such mixing between MORB and high ^{3}He/^{4}He sources (e.g. Kurz et al. 2005; Moreira et al. 1995). Finally, using a simple closed-system evolution model

for neon isotopes (a closed system is inherent to ancient depletion scenarios), Kurz et al. demonstrated that if an ancient depletion event were to explain the Galapagos neon isotopes, it must have occurred at least 4.4 Ga ago (Kurz et al. 2009b). Therefore, at that point, the relative compatibility between noble gases and their parents has no consequences for the origin of the "primitive" signature of OIB. Clearly, ancient depletion models do not explain the observations, and the major effect that produces parent/daughter fractionation must be primordial degassing.

Based on the sparse literature data on mantle partitioning, it is not yet clear that the actual partition coefficients are known well enough to constrain the models. In addition, the exact residence sites of mantle noble gases are not known, i.e. it is not clear if they are located in minerals, and which minerals dominate at high pressure. They could be located within grain boundaries. Indeed, diffusion can occur within grains and therefore, at some point, noble gases reach grain boundaries where diffusion may be faster (Hiraga et al. 2007). Therefore, the question of partitioning between minerals and melt may be more complex than reflected in the laboratory experiments. One example of this complexity is reflected in the crushing experiments performed by Parman et al. (2005). They found that more than 30 % of the helium in their experimentally equilibrated defect-free olivine was released by crushing in vacuum. This suggests that helium is contained within defects or bubbles in the olivine, which may dominate the partitioning behavior in a non-equilibrium fashion. Another example is the recent study of deformed peridotites, some of which contain more helium than basalts (Kurz et al. 2009a).

5.2 Diffusive Fractionation During Melting

Kinetic He–Ar fractionation during mantle melting has been theoretically proposed by Burnard (2004), based on the fact that noble gases have different diffusivities. This fractionation mechanism was also proposed to explain the correlation between pre-degassing $^{4}He/^{40}Ar^{*}$ and $^{3}He/^{4}He$ in MORB from South East Indian Ridge (Burnard et al. 2004). Yamamoto et al. (2009b) proposed that low $^{4}He/^{40}Ar^{*}$ ratios (down to 0.1) measured in subcontinental xenoliths reflect kinetic fractionation during melting that produces these low $^{4}He/^{40}Ar^{*}$ (and $^{3}He/^{4}He$) in the residual mantle then sampled by mantle xenoliths. Moreira and Sarda (2000) have a different explanation of the low $^{4}He/^{40}Ar^{*}$ in mantle xenoliths. They suggested that this reflects magma percolation through lithosphere that leaves small vesicles behind magma, as observed in laboratory by Schiano et al. (2007). These small vesicles have low $^{4}He/^{40}Ar^{*}$ because argon is much more soluble in melts. However, for most of MORB and OIB, this possible kinetic effect during melting is masked by degassing.

5.3 Solubility and Partitioning Between Melt and Gas

Solubility is the key physical parameter that controls the equilibrium noble gas partitioning between melt and the gas phase. Noble gas solubilities in silicate melts decrease with ionic size, which is the opposite of noble gas solubilities in water (Jambon et al. 1986; Lux 1987; Shibata et al. 1998). Guillot and Sarda (2006) have modeled the noble gas solubilities in tholeite melts using the theory of hard spheres, and demonstrated that melt noble gas solubilities/concentrations vary linearly with pressure up to ~30 kbars (90 km). These theoretical values are in agreement with laboratory experiments of Schmidt and Keppler and Iacono-Marziano et al. (Carroll and Stolper 1993; Iacono-Marziano et al. 2010; Miyazaki et al. 2004; Schmidt and keppler 2002). Around 50 kbars, the relationship between concentrations in melt and pressure is no longer linear (Guillot and Sarda 2006). The deviation from Henry's law above 50 kbars may have some consequences for deep melting (>150 km), mainly for hot mantle plume melting under thick lithosphere.

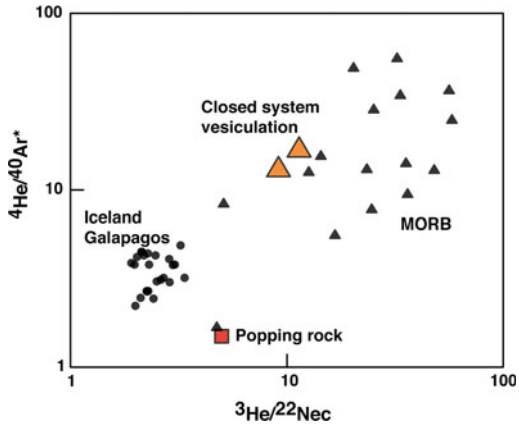

Fig. 2 $^4He/^{40}Ar^*$ vs. the $^3He/^{22}Ne$ corrected for air contamination assuming $^{20}Ne/^{22}Ne = 12.6$ in the mantle. Only samples with $^{20}Ne/^{22}Ne$ higher than 10.5 are reported here. MORB (*triangle*) and glass samples from Iceland and Galapagos (*dots*) are reported as well as the value of magma that has suffered a degassing after vesiculation in closed system (equilibrium vesiculation; *orange triangle*). The popping rock value (*square*) is derived from (Moreira et al. 1998). This figure shows that MORB probably suffers degassing in disequilibrium. There is a kinetic effect that increases the helium content in vesicles compared to the equilibrium vesiculation (see Aubaud et al. 2004). Note that OIB samples reported here are only samples with $^4He/^{40}Ar^*$ between 2 and 5, indicating they did not experience gas loss

5.4 Degassing Processes Constrained by Rare Gases

The classic vesiculation and degassing model assumes that in a closed system, noble gases are in equilibrium between the gas phase and the magma according to their solubility. When gas loss occurs, the residual melt has fractionated elemental ratios (e.g. $^4He/^{40}Ar \sim 15$–20 compared to a mantle value ~ 2 because the solubility ratio is ~ 10 (Jambon et al. 1986). Then a second vesicle generation is possible during eruption at the seafloor. This second generation of vesicles has fractionated elemental composition. Some gas-rich samples such as popping rocks apparently did not suffer gas loss and therefore have preserved the mantle compositions and are rich in gases. This model has been extensively discussed, and on first order, explains the observations (Burnard et al. 2002, 2003, 2004; Honda and Patterson 1999; Jambon et al. 1986; Macpherson et al. 2005; Marty and Zimmermann 1999; Moreira and Sarda 2000; Sarda and Moreira 2002; Yamamoto and Burnard 2005).

However, this model fails to explain high $^3He/^{22}Ne$ and $^4He/^{40}Ar$ ratios observed in some MORB (Fig. 2) and fails to provide a solution to the helium paradox (e.g. OIB have less gases than MORB) (Honda and Patterson 1999; Moreira and Sarda 2000). Moreira and Sarda (2000) proposed an apparent helium solubility higher by a factor of ~ 10 in order to explain these high $^3He/^{22}Ne$ and $^4He/^{40}Ar$ ratios. This high apparent solubility is probably linked to high diffusivity of helium as suggested by Aubaud et al. (2004). They propose that carbon isotope fractionation occurs during vesiculation as the carbon isotopes diffuse at different speeds. They extended this interpretation to the He/Ar ratio and such a model is able to reproduce some of the high He/Ar measured in MORB. A new generation of vesicle formation models are now proposed and best explain the observed elemental ratios He/Ar and He/CO_2 (Paonita and Martelli 2006, 2007).

Moreover, such a vesiculation model involving solubility and diffusivity can also explain the $^{38}Ar/^{36}Ar$ isotopic and $^{84}Kr/^{36}Ar$ elemental fractionations observed in pumices from explosive volcanoes (Ruzié and Moreira 2009) and provide constraints on the timing of vesiculation and magma fragmentation. The vesiculation model involving both solubility and diffusivity is the possible isotope fractionation of noble gases between vesicles and melt. This may be important for helium due to the large mass difference between ^3He and ^4He, but can be also important for neon. It is therefore important to underline that some elevated $^{20}Ne/^{22}Ne$ (>9.8) in some samples could result from such an isotopic fractionation.

Finally, degassing in a disequilibrium model offers a solution to the helium paradox. Gonnermann and Mukhopadhyay proposed that because the OIB source contains more CO_2, and OIB magmas will therefore be more degassed than MORB magmas (Gonnermann and Mukhopadhyay 2007). According to them, the OIB source does contain more helium than the MORB source.

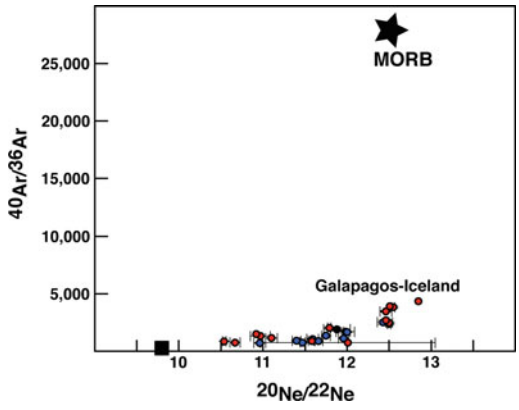

Fig. 3 $^{40}Ar/^{36}Ar$ vs. $^{20}Ne/^{22}Ne$ for Galapagos submarine samples and Iceland (subglacial) obtained by step crushing (Trieloff et al. 2000; Raquin and Moreira 2009) and with $^{4}He/^{40}Ar^{*}$ between 2 and 5. The MORB value is derived from (Moreira et al. 1998). The figure shows that for mantle $^{20}Ne/^{22}Ne$, the $^{40}Ar/^{36}Ar$ ratios of the Galapagos and Iceland sources are much lower than the one of the MORB source

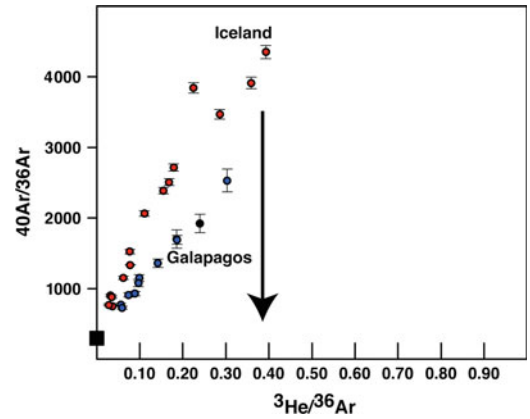

Fig. 4 Knowing the $^{40}Ar/^{36}Ar$ of the Iceland and Galapagos sources (from Fig. 3), one can derive the $^{3}He/^{36}Ar$ ratios in these sources

5.5 Concentration, Elemental and Isotopic Composition of Rare Gases in the Mantle

5.5.1 Elemental Ratios

The best way to obtain elemental ratios is to select mantle samples with $^{4}He/^{40}Ar^{*}$ close to the production ratio (2–5). Otherwise, although it is possible to correct elemental fractionation for degassing and atmospheric contamination, this method leads to uncertainties in the elemental ratios.

There are differences between OIB and MORB sources for noble gas elemental ratios (Figs. 3, 4, 5). Strong evidence for different $^{3}He/^{22}Ne$ ratio in the two reservoirs is provided by the observed correlation between $^{4}He/^{3}He$ and $^{21}Ne/^{22}Ne$ (corrected for air contamination). This correlation is observed for n-MORB, E-MORB, on ridge hotspot and off axis hotspots. It can be explained by a different $^{3}He/^{22}Ne$ ratio in MORB compared to OIB sources (Dixon 2003; Dixon et al. 2000; Furi et al. 2010; Hopp et al. 2004; Kurz et al. 2005, 2009b; Madureira et al. 2005; Moreira and Allègre 1998; Moreira et al. 1995, 2001; Sarda et al. 2000; Trieloff et al. 2000, 2002; Yokochi and Marty 2004; Hopp and Trieloff 2008). This is not a decoupling between helium and neon, but simply a mixture between two components with different $^{3}He/^{22}Ne$ ratios. Moreover, the measured and air-corrected (using solar neon or neon B) $^{3}He/^{22}Ne$ ratios for samples having close-to-production ratio $^{4}He/^{40}Ar^{*}$ also have $^{3}He/^{22}Ne$ lower than MORB ($^{3}He/^{22}Ne \sim 2$ for Galapagos versus ~ 6 for MORB (Moreira et al. 1998; Raquin and Moreira 2009). The origin of these distinct elemental ratios between MORB and OIB is not clear. Coltice et al. (2011) proposed that it reflects magma ocean crystallization and that helium and neon have different partitioning coefficient between melt and perovskite. Yokochi and Marty (2004) proposed that the higher $^{3}He/^{22}Ne$ ratio in the MORB source reflects an ancient degassing, i.e. due to different solubilities of He and Ne–helium being more soluble than neon in magma- which produces elemental fractionation (Yokochi and Marty 2004). Or it may reflect heterogeneous accretion of the earth, with the lower mantle having a different $^{3}He/^{22}Ne$ source material than the upper mantle (e.g. more solar-wind implanted material vs. solar gas solubilization).

The $^{3}He/^{36}Ar$ and $^{3}He/^{130}Xe$, corrected for air contamination, are also different for MORB and OIB (Fig. 4, 5 and Table 1) and similarly could be explained by different histories of the two sources.

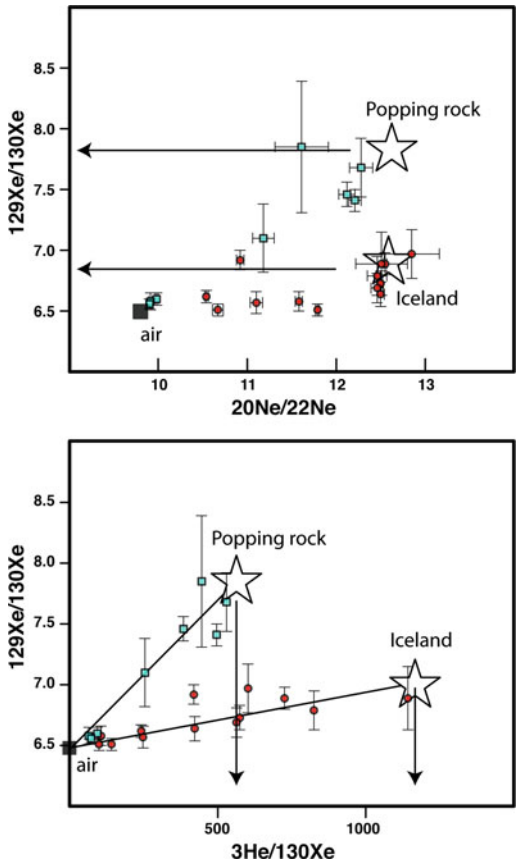

Fig. 5 The same approach as Figs. 3 and 4 can be done for xenon. Popping rock data are from (Moreira et al. 1998). Iceland data are from (Trieloff et al. 2000)

5.5.2 Noble Gas Concentrations in the MORB Source

Mantle concentration estimates are always complicated due to all the processes described above. Two methods have been used. Cartigny et al. (2008) use a CO_2/Nb of 530 and a mean MORB Nb content of 3.31 ppm. With a $CO_2/^3He$ of 2.7 10^9 for the MORB source derived from undegassed samples (Marty and Tolstikhin 1998; Moreira and Cartigny unpublished data on popping rock), one gets a ^3He content in the oceanic crust of $\sim 3 \times 10^{-10}$ cc/g. Another method uses the helium flux at ridges (Craig et al. 1975). The ^3He flux is estimated between 500 and 1,000 mol/year (Bianchi et al. 2010; Farley et al. 1995). Global oceanic crust production is 5×10^{16} g/year.

Table 1 Elemental and isotopic ratios in MORB and OIB sources. When given, uncertainties are standard deviation of the mean data

Reservoir	$^4He/^3He$	R/Ra	$^{20}Ne/^{22}Ne$	$^{21}Ne/^{22}Ne$	$^{40}Ar/^{36}Ar$	$^{129}Xe/^{130}Xe$	$^3He/^{22}Ne$	$^3He/^{36}Ar$	$^3He/^{130}Xe$	$^4He/^{40}Ar^*$
AIR	722,000	1	9.8	0.029	295.5	6,496	~0	~0	~0.002	Nd
MORB	90,000	8	12.6	0.060	~30,000	7.7	5.1	0.45	600	1.5
OIB (Galapagos)		23	12.6	0.033	~3,000	6.7[a]	2.3 ± 0.5	0.35	~1000[a]	4.3 ± 0.4
OIB (Iceland)		17.5	12.6	0.035	~5,000	6.8	2.5 ± 0.3	0.4	~1200	3.0 ± 0.6

[a] unpublished data of Moreira (xenon in Galapagos samples) MORB data are from (Moreira et al. 1998). Galapagos data are from Raquin and Moreira (2009); Iceland data are from Trieloff et al. (2000) and Furi et al. (2010)
Nd not determined

Table 2 Noble gas abundances in the mantle sources

Reservoir	^{3}He (10^{-10} cc/g)	^{22}Ne (10^{-12} cc/g)	^{36}Ar (10^{-12} cc/g)	^{130}Xe (10^{-14} cc/g)
MORB	2.2–4.5	43–88	490–1,000	37–75
OIB	>14	>580	>4,000	>127

Therefore, if crust is fully degassed, ^{3}He concentration in undegassed oceanic crust should be between 2.2 and 4.5 $\times$ 10^{-10} cc/g, close to the previous method. Moreira et al. (2001) have analyzed helium and neon in gabbros and observed ^{3}He concentrations that are lower than 2 $\times$ 10^{-12} ccSTP/g, confirming that crust is indeed degassed. For comparison, the ^{3}He in popping rock 2πD43 is $\sim 10^{-9}$ cc/g (Javoy and Pineau 1991; Moreira et al. 1998), 2–3 times the theoretical content in the crust, which could indicate this sample reflects a slightly gas-rich source, a low melting rate area, or that this reflects vesicle accumulation in a magma chamber.

Assuming a mean melting rate of 10 %, the ^{3}He content in the mantle is therefore $\sim 3 \pm 2 \times 10^{-11}$ cc/g and $\sim 3 \pm 2 \times 10^{-6}$ ccSTP/g of ^{4}He. Using elemental ratios, it is therefore possible to obtain the other mantle noble gas concentrations. Tables 1 and 2 give a summary of the noble gas content, elemental ratios and isotopic ratios in the MORB source mantle.

5.5.3 Noble Gas Concentrations in the OIB Source(s)

Direct estimate of the ^{3}He content of the OIB source is difficult. Galapagos samples with ^{4}He/^{40}Ar* close to the production ratio show helium contents of few 10^{-6} ccSTP/g (Raquin and Moreira 2009). Iceland subglacial glasses have similar helium concentrations (Trieloff et al. 2000). Therefore, for now, samples from OIB having primitive helium and neon and unfractionated He/Ar show much lower helium content than MORB. Based on their non-equilibrium degassing model, Gonnermann and Mukhopadhyday (2007) constrain the He content in the pre-degassed melt to be $\sim 10^{-4}$ cc/g, suggesting that more than 99 % of helium is lost without significant elemental fractionation during non equilibrium magmatic degassing.

The second approach to determine the helium abundance in the OIB source, and therefore the other noble gases, is to calculate the minimum helium that is necessary to preserve in a closed system, during 4.5 Ga, the ^{4}He/^{3}He ratio of OIB. Uranium and thorium are relatively well known in OIB. For example, Fernandina (Galapagos) samples have 0.5 ppm U and 1.5 ppm Th (Geist et al. 2006). Assuming 5 % melting, this gives 25 ppb U and 72 ppb Th in the Galapagos source. Starting helium isotopic composition is probably the solar wind value [^{4}He/^{3}He $\sim$ 2,500 (Wieler 2002)]. Fernandina samples have ^{4}He/^{3}He of $\sim$30,000; R/Ra $\sim$23 (Kurz et al. 2009b). With the classic equation of radiogenic helium production, we predict a minimum ^{3}He content of 1.4 $\times$ 10^{-9} ccSTP/g necessary for the ^{4}He/^{3}He to evolve from 2,500 to 30,000; which corresponds to present-day ^{4}He of 4.3 $\times$ 10^{-5} ccSTP/g. This content is $\sim$10 times the MORB source helium content.

Again, knowing the ^{3}He content and the noble gas elemental ratios, the other noble gas concentrations can be derived (Tables 1, 2). We note that there are very few OIB samples with measurements of all the noble gases, and even fewer with unfractionated He/Ar ratios, so the data in Tables 1 and 2 are estimates based on a very limited data set.

6 Conclusions

We have summarized the different shallow processes that modify the elemental and isotopic composition of the rare gases. Atmospheric contamination can be corrected using the ^{20}Ne/^{22}Ne ratio, if one assumes it has either a solar or a neon B value. Constraining the elemental ratios in pre-degassed magma requires the knowledge of the vesiculation process. This can be either in equilibrium or in disequilibrium

(e.g. kinetic). Existing MORB glass data suggest that it is indeed in disequilibrium, and that diffusion is an important aspect of the vesiculation process. Using samples with $^{4}He/^{40}Ar^{*}$ ratios close to the production ratio, along with the known ^{3}He flux, we can derive elemental and isotopic compositions in the different mantle sources. These estimates cannot be reconciled with ancient depletion models for unradiogenic noble gas isotopic compositions, and are best explained by relatively undegassed sources deep in the mantle.

In order to better constrain the evolution of the atmosphere/mantle system, it will be necessary to obtain precise and unambiguous elemental and isotopic ratios in archean rocks (e.g. crustal or komatiites) to constrain both the mantle and the atmosphere compositions at that time. This has been tested in few studies for helium, argon or xenon but there are often difficulties to interpret the value because of secondary nuclear reactions (Matsumoto et al. 2002; Moreira 2007; Moreira and Raquin 2007; Pinti 2001; Pujol et al. 2009, 2011; Richard et al. 1996).

Another important aspect of the noble gas evolution on Earth will be the determination of elemental fractionations (melt/crystal or silicate/iron) in a magma ocean at either low or high pressures (Coltice et al. 2011; Labrosse et al. 2007; Porcelli and Halliday 2001). However, due to sample size in these HPHT experiments, noble gas analyses are still a challenge.

Acknowledgments We thank Pete Burnard for his patience and his thoughtful review of the manuscript. MK wishes to thank Institut de Physique du Globe de Paris for support while this manuscript was completed. This is IPGP contribution N°3337.

References

Albarède F (2008) Rogue mantle helium and neon. Science 319:943–945

Allard P, Jean-Baptiste P, D'Alessandro W, Parello F, Parisi B, Flehoc C (1997) Mantle-derived helium and carbon in groundwaters and gases of Mount Etna, Italy. Earth Planet Sci Lett 149:501–516

Allègre CJ (1987) Isotope geodynamics. Earth Planet Sci Lett 86:175–203

Allègre CJ, Moreira M, Staudacher T (1995) 4He/3He dispersion and mantle convection. Geophys Res Lett 22(17):2325–2328

Anderson DL (1998) A model to explain the various paradoxes associated with mantle noble gas geochemistry. Proc Natl Acad Sci USA 95:9087–9092

Aubaud C, Pineau F, Jambon A, Javoy M (2004) Kinetic disequilibrium of C, He, Ar and carbon isotopes during degassing of mid-ocean ridge basalts. Earth Planet Sci Lett 222:391–406

Bach W, Niedermann S (1998) Atmospheric noble gases in volcanic glasses from the southern Lau basin: origin from the subducting slab? Earth Planet Sci Lett 160:298–309

Ballentine CJ (1997) Resolving the mantle He/Ne and crustal 21Ne/22Ne in well gases. Earth Planet Sci Lett 152(1–4):233–250

Ballentine C, Barfod D (2000) The origin of air-like noble gases in MORB and OIB. Earth Planet Sci Lett 180:39–48

Bianchi D, Sarmiento JL, Gnanadesikan A, Key RM, Schlosser P, Newton R (2010) Low helium flux from the mantle inferred from simulations of oceanic helium isotope data. Earth Planet Sci Lett 297: 379–386

Black DC (1972) On the origins of trapped helium, neon and argon isotopic variations in meteorites—I. Gas-rich meteorites, lunar soil and breccia. Geochim Cosmochim Acta 36(3):347–375

Broadhurst CL, Drake MJ, Hagee BE, Bernatowicz TJ (1990) Solubility and partitioning of Ar in anorthite, diopside, forsterite, spinel, and synthetic basaltic liquids. Geochim Cosmochim Acta 54:299–309

Broadhurst CL, Drake MJ, Hagee BE, Bernatowicz TJ (1992) Solubility and partitioning of Ne, Ar, Kr, and Xe in minerals and synthetic basaltic melts. Geochim Cosmochim Acta 56:709–723

Brooker RA, Zu Z, Blundy JD, Kelley SP, Allan NL, Wood BJ, Chamorro EM, Wartho JA, Purton JA (2003) The 'Zero charge' partitioning behaviour of noble gases during mantle melting. Nature 423: 738–741

Burnard P (1999a) The bubble-by-bubble volatile evolution of two mid-ocean ridge basalts. Earth Planet Sci Lett 174:199–211

Burnard PG (1999b) Origin of argon-lead isotopic correlation in basalts. Science 286:871

Burnard P (2004) Diffusive fractionation of noble gases and helium isotopes during mantle melting. Earth Planet Sci Lett 220(3–4):287–295

Burnard PG, Farley KA (2000) Calibration of pressure-dependent sensitivity and discrimination in nier-type noble gas ion sources, G-cube, 2000GC000038

Burnard PG, Stuart FM, Turner G, Oskarsson N (1994) Air contamination of basaltic magmas; implications for high 3 He/4He mantle Ar isotopic composition. J Geophys Res B, Solid Earth Planets, 99(9): 17, 709–717, 715

Burnard P, Graham D, Turner G (1997) Vesicle-specific noble gas analyses of «popping rock»: implications

for primordial noble gases in the earth. Science 276:568–571
Burnard PG, Farley KA, Turner G (1998) Multiple fluid pulses in a Samoan harzburgite. Chem Geol 147 (1–2):99–114
Burnard P, Graham DW, Farley KA (2002) Mechanisms of magmatic gas loss along the southeast Indian ridge and the Amsterdam—St. Paul Plateau. Earth Planet Sci Lett 203:131–148
Burnard P, Harrison D, Turner G, Nesbitt R (2003) Degassing and contamination of noble gases in mid-Atlantic ridge basalts. Geochem Geophys Geosyst 4
Burnard P, Graham DW, Farley KA (2004) Fractionation of noble gases (He, Ar) during MORB mantle melting: a case study on the southeast Indian ridge. Earth Planet Sci Lett 227:457–472
Cafee MW, Hudson GP, Velsko C, Huss GR, Alexander EC, Chivas R (1999) Primordial noble gases from earth's mantle: identification of primitive volatile component. Science 285:2115–2118
Carroll MR, Stolper E (1993) Noble gas solubilities in silica melts and glasses: new experimental results for argon and the relationship between solubility and ionic porosity. Geochem Cosmoch Acta 57: 5039–5051
Cartigny P, Pineau F, Aubaud C, Javoy M (2008) Towards a consistent mantle carbon flux estimate: Insights from volatile systematics (H_2O/Ce, δD, CO_2/Nb) in the North Atlantic mantle (14° N and 34° N). Earth Planet Sci Lett 265:672–685
Clarke WB, Beg MA, Craig H (1969) Excess 3He in the sea: evidence for terrestrial primordial helium. Earth Planet Sci Lett 6:213–220
Clarke WB, Jenkins WJ, Top Z (1976) Determination of tritium by mass spectrometric measurement of 3He. Int J Appl Radiat Isot 27:512–522
Class C, Goldstein S, Stute M, Kurz MD, Schlosser P (2005) Grand Comore island: a well-constrained "low 3He/4He" mantle plume. Earth Planet Sci Lett 233:391–409
Coltice N, Ricard Y (1999) Geochemical observations and one layer mantle convection. Earth Planet Sci Lett 174:125–137
Coltice N, Marty B, Yokochi R (2009) Xenon isotope constraints on the thermal evolution of the early earth. Chem Geol 266:4–9
Coltice N, Moreira M, Labrosse S, Hernlund JW (2011) Crystallization of a basal magma ocean recorded by helium and neon. Earth Planet Sci Lett 308:193–199
Craig H, Clarke WB, Beg MA (1975) Excess 3He in deep water on the east Pacific rise. Earth Planet Sci Lett 26:125–132
Czuppon G, Matsumoto T, Handler MR, Matsuda J-I (2009) Noble gases in spinel peridotite xenoliths from Mt Quincan, North Queensland, Australia: undisturbed MORB-type noble gases in the subcontinental lithospheric mantle. Chem Geol 266:19–25
Czuppon G, Matsumoto T, Matsuda J-I, Everard J, Sutherland L (2010) Noble gases in anhydrous mantle xenoliths from Tasmania in comparison with other localities from eastern Australia: implications for the tectonic evolution. Earth Planet Sci Lett 299:317–327
Dixon E (2003) Interpretation of helium and neon isotopic heterogeneity in Icelandic basalts. Earth Planet Sci Lett 206:83–99
Dixon E, Honda M, McDougall I, Campbell I, Sigurdsson I (2000) Preservation of near-solar isotopic ratios in Icelandic basalts. Earth Planet Sci Lett 180:309–324
Dymond J, Hogan L (1973) Noble gas abundance patterns in deap sea basalts—primordial gases from the mantle. Earth Planet Sci Lett 20:131
Farley KA, Craig H (1994) Atmospheric argon contamination of ocean island basalt olivine phenocrysts. Geochem Cosmoch Acta 58(11):2509–2517
Farley KA, Poreda RJ (1993) Mantle neon and atmospheric contamination. Earth Planet Sci Lett 114: 325–339
Farley KA, Maier-Reimer E, Schlosser P, Broecker WS (1995) Constraints on mantle 3He fluxes and deep-sea circulation from an oceanic general circulation model. J Geophys Res 100:3829–3839
Ferrario B (1996) Chemical pumping in vacuum technology. Vacuum 47:363–370
Fischer T (1971) Incorporation of Ar in east Pacific basalts. Earth Planet Sci Lett 12:321–324
Furi E, Hilton DR, Halldorsson SA, Barry P, Hahm D, Fischer T, Gronvold K (2010) Apparent decoupling of the He and Ne isotope systematics of the Icelandic mantle: the role of He depletion, melt mixing, degassing fractionation and air interaction. Geochem Cosmoch Acta 74:3307–3332
Gautheron C, Cartigny P, Moreira M, Harris JW, Allègre CJ (2005) Evidence for a mantle component shown by rares gases, C and N-isotopes in polycrystalline diamonds from Orapa (Botswana). Earth Planet Sci Lett 240:559–572
Geist D, Fornari D, Kurz MD, Harpp KS, Soule SA, Perfit MR, Koleszar AM (2006) Submarine Fernandina: magmatism at the leading edge of the Galapagos hot spot, G3, 7(12)
Georgen JE, Kurz M, Dick HJB, Lin J (2003) low 3He/4He ratios in basalt glasses from the western southwest Indian ridge (10–24°E). Earth Planet Sci Lett 206:509–528
Gilfillan S, Ballentine CJ, Holland G, Blagburn D, Lollar BS, Stevens S, Schoell M, Cassidy M (2008) The noble gas geochemistry of natural CO_2 gas reservoirs from the Colorado Plateau and Rocky Mountain provinces, USA. Geochem Cosmoch Acta 72: 1174–1198
Gonnermann HM, Mukhopadhyay S (2007) Non-equilibrium degassing and a primordial source for helium in ocean-island volcanism. Nature 449:1037–1040
Gonnermann HM, Mukhopadhyay S (2009) Preserving noble gases in a convecting mantle. Nature 459: 560–564
Graham DW, Humphris SE, Jenkins WJ, Kurz MD (1993) Helium isotope geochemistry of some volcanic rocks from Saint Helena. Earth Planet Sci Lett 110:121–131

Graham DW, Lupton JE, Spera FJ, Christie DM (2001) Upper-mantle dynamics revealed by helium isotope variations long the southeast Indian ridge. Nature 409:701–703

Grand SP, van der Hilst RD, Widiyantoro S (1997) Global seismic tomography; a snapshot of convection in the Earth. GSA Today 7(4):1–7

Grimberg A, Baur H, Bochsler P, Buhler F, Burnett DS, Hays CC, Heber VS, Jurewicz AJG, Wieler R (2006) Solar wind neon from genesis: implications for the lunar noble gas record. Science 314:1133–1135

Guillot B, Sarda P (2006) The effect of compression on noble gas solubility in silicate melts and consequences for degassing at mid-ocean ridges. Geochem Cosmoch Acta 70:1215–1230

Hanyu T, Dunai T, Davies G, Kaneoka I, Nohda S, Uto K (2001) Noble gas study of the Reunion hotspot: evidence for distinct less-degassed mantle sources. Earth Planet Sci Lett 193:83–98

Hanyu T, Tatsumi Y, Kimura J-I (2011) Constraints on the origin of the Himu reservoir from He-Ne-Ar isotope systematics. Earth Planet Sci Lett 307: 377–386

Harrisson D, Burnard P, Turner G (1999) Noble gas behaviour and composition in the mantle: constraints from the Iceland Plume. Earth Planet Sci Lett 171:199–207

Harrisson D, Burnard P, Trieloff M, Turner G (2003) Resolving atmospheric contaminants in mantle noble gas analyses. Geochem Geophys Geosyst 4

Heber VS, Brooker RA, Kelley SP, Wood BJ (2007) Crystal-melt partitioning of noble gases (helium, neon, argon, krypton, and xenon) for olivine and clinopyroxene. Geochim Cosmochim Acta 71: 1041–1061

Hennecke EW, Manuel OK (1975) Noble gases in CO_2 well gas, Harding County, New Mexico. Earth Planet Sci Lett 27:346–355

Hilton DR, Barling J, Wheller GE (1995) Effect of shallow-level contamination on the helium isotope systematics of ocean-island lavas. Nature 373: 330–333

Hilton DR, Grönvold K, Macpherson C, Castillo P (1999) Extreme 3He/4He ratios in northwest Iceland: constraining the common component in mantle plumes. Earth Planet Sci Lett 173:53–60

Hiraga T, Hirschmann MM, Kohlstedt DL (2007) Equilibrium interface segregation in the diopside–forsterite system II: applications of interface enrichment to mantle geochemistry. Geochem Cosmoch Acta 71:1281–1289

Hiyagon H, Ozima M (1986) Partition of gases between olivine and basalt melt. Geochim Cosmochim Acta 50:2045–2057

Hiyagon H, Ozima M, Marty B, Zashu S, Sakai H (1992) Noble gases in submarine glasses from mid-oceanic ridges and Loihi seamount: constraints on the early history of the Earth. Geochim Cosmochim Acta 56:1301–13016

Holland G, Ballentine CJ (2006) Seawater subduction controls the heavy noble gas composition of the mantle. Nature 441:186–191

Holland G, Cassidy M, Ballentine CJ (2009) Meteorite Kr in earth's mantle suggests a late accretionary source for the atmosphere. Science 326:1522–1525

Honda M, Patterson DB (1999) Systematic elemental fractionation of mantle-derived helium, neon, and argon in mid-oceanic ridge glasses. Geochim Cosmochim Acta 63:2863–2874

Honda M, Woodhead JD (2005) A primordial solar-neon enriched component in the source of EM-I-type ocean island basalts from the pitcairn seamounts, Polynesia. Earth Planet Sci Lett 236:597–612

Honda M, Reynolds JH, Roedder E, Epstein S (1987) Noble gases in diamonds: occurrences of solar like helium and neon. J Geophys Res 92(B12);12507–12521

Honda M, McDougall I, Patterson DB, Doulgeris A, Clague D (1991) Possible solar noble-gas component in Hawaiian basalts. Nature 349:149–151

Honda M, Patterson DB, McDougall I, Falloon (1993a) Noble gases in submarine pillow basalt glasses from the Lau Basin: detection of a solar component in backarc basin basalts. Earth Planet Sci Lett 120: 135–148

Honda M, McDougall I, Patterson DB, Doulgeris A, Clague D (1993b) Noble gases in submarine pillow basalt glasses from Loihi and Kilauea, Hawaii: a solar component in the earth. Geochim Cosmochim Acta 57:859–874

Honda M, Phillips D, Harris JW, Yatsevich I (2004) Unusual noble gas composition in polycrystalline diamonds: preliminary results from the Jwaneng kimberlite, Botswana. Chem Geol 203:347–358

Honda M, Phillips D, Harris JW, Matsumoto T (2011) He, Ne and Ar in peridotitic and eclogitic paragenesis diamonds from the Jwaneng kimberlite, Botswana—implications for mantle evolution and diamond formation ages. Earth Planet Sci Lett 301:43–51

Hopp J, Trieloff M (2008) Helium deficit in high 3He/4He parent magmas: predegassing fractionation, not a "helium paradox". G 3:9

Hopp J, Trieloff M, Altherr R (2004) Neon isotopes in mantle rocks from the Red Sea region reveal large-scale plume-lithosphere interaction. Earth Planet Sci Lett 219:61–76

Hopp J, Trieloff M, Buikin AI, Korochantseva EV, Scharz WH, Althaus T, Altherr R (2007) Heterogeneous mantle argon isotope composition in the subcontinental lithospheric mantle beneath the Red Sea region. Chem Geol 240:36–53

Iacono-Marziano G, Paonita A, Rizzo A, Scaillet B, Gaillard F (2010) Noble gas solubilities in silicate melts: new experimental results and a comprehensive model of the effects of liquid composition, temperature and pressure. Chem Geol 279:145–157

Jackson MG, Kurz MD, Hart SR (2009) Helium and neon isotopes in phenocrysts from Samoan lavas: evidence

for heterogeneity in the terrestrial high 3He/4He mantle. Earth Planet Sci Lett 287(3–4):519–528

Jambon A, Weber H, Braun O (1986) Solubility of He, Ne, Ar, Kr and Xe in a basalt melting in the range 1250–1600 °C. Geochemical implications. Geochim Cosmochim Acta 50:401–408

Javoy M, Pineau F (1991) The volatiles record of a «popping» rock from the mid-Atlantic ridge at 14° N: chemical and isotopic composition of gas trapped in the vesicles. Earth Planet Sci Lett 107:598–611

Jean-Baptiste P, Allard P, Coutinho R, Ferreira T, Fourre E, Queiroz G, Gaspar JL (2009) Helium isotopes in hydrothermal volcanic fluids of the Azores archipelago. Earth Planet Sci Lett 281:70–80

Kaneoka I, Takaoka N (1977) Excess 129Xe and high 3He/4He ratios in olivine phenocrysts of Kapuho lava and xenolithic dunites from Hawaii. Rock Magn Paleogeophysics 4:139–143

Kaneoka I, Takaoka N, Aoki K (1977) Rare gases in a phlogopite nodule and a phlogopite-bearing peridotite in South African kimberlites. Earth Planet Sci Lett 36(1):181–186

Kaneoka I, Takaoka N, Upton BGJ (1986) Noble gas systematics in basalts and a dunite nodule from Réunion and Grand Comore Islands, Indian Ocean. Chem Geol 59:35–42

Kunz J, Staudacher T, Allègre CJ (1998) Plutonium-fission xenon found in earth's mantle. Science 280:877–880

Kurz MD (1993) Mantle heterogeneity beneath oceanic islands: some inferences from isotopes. Philos Trans R Soc Lond A342:91–103

Kurz MD, Jenkins WJ (1981) The distribution of helium in oceanic basalt glasses. Earth Planet Sci Lett 53:41–54

Kurz MD, Jenkins WJ, Hart SR (1982a) Helium isotopic systematics of oceanic islands and mantle heterogeneity. Nature 297:43–47

Kurz MD, Jenkins WJ, Schilling J-G, Hart SR (1982b) Helium isotopic variation in the mantle beneath the central North Atlantic Ocean. Earth Planet Sci Lett 58:1–14

Kurz MD, Jenkins WJ, Hart SR, Clague D (1983) Helium isotopic variations in volcanic rocks from Loihi seamount and the island of Hawaii. Earth Planet Sci Lett 66:388–406

Kurz MD,Gurney JJ (1987) Helium isotopic variability within single diamonds from the Orapa kimberlite pipe. Earth Planet Sci Lett 86:57–68

Kurz MD, Curtice J, Lott DE III, Solow A (2004a) Rapid helium isotopic variability in Mauna Kea shield lavas from the Hawaian scientific drilling project. Geochem Geophys Geosyst 5(4):

Kurz MD, Fornari D, Geist D, Curtice J, Lott D (2004) Helium and neon from the deep earth: submarine Galapagos glasses and global correlations. In: Goldschmidt conference, Copenhagen, 5–11 June 2004

Kurz MD, Moreira M, Curtice J, Lott DE III, Mahoney JJ, Sinton JM (2005) Correlated helium, neon, and melt production on the super-fast spreading east Pacific rise near 17°S. Earth Planet Sci Lett 232:125–142

Kurz MD, Warren JM, Curtice J (2009a) Mantle deformation and noble gases: helium and neon in oceanic mylonites. Chem Geol 266:10–18

Kurz MD, Curtice J, Fornari D, Geist D, Moreira M (2009b) Primitive neon from the center of the Galapagos hotspot. Earth Planet Sci Lett 286:23–34

Labrosse S, Hernlund JW, Coltice N (2007) A crystallizing dense magma ocean at the base of earth's mantle. Nature (accepted)

Lal D, Nishiizumi K, Klein J, Middleton R, Craig H (1987) Cosmogenic 10Be in zaire alluvial diamonds: Implications for 3He contents of diamonds, Nature 328:139–141

Lott DEI (2001) Improvements in noble gas separation methodology: a nude cryogenic trap, G-cube, 2001GC000202

Lott DE, Jenkins WJ (1984) An automated cryogenic charcoal trap system for helium isotope mass spectrometry. Rev Sci Inst 55:1982–1988

Lupton JE, Craig H (1975) Excess 3He in oceanic basalts: evidence for terrestrial primordial helium. Earth Planet Sci Lett 26:133–139

Lux G (1987) The behavior of noble gases in silicate liquids: solution, diffusion, bubbles and surface effects, with application to natural samples. Geochim Cosmochim Acta 51:1549–1560

Macpherson CG, Hilton DR, Mertz DF, Dunai T (2005) Sourcesn degassing, and contamination of CO_2, H_2O, He, Ne and Ar in basaltic glasses from Kolbeinsey ridge, north Atlantic. Geochem Cosmoch Acta 69:5729–5746

Madureira P, Moreira M, Mata J, Allègre CJ (2005) Primitive helium and neon isotopes in Terceira island (Azores archipelago). Earth Planet Sci Lett 233: 429–440

Mahoney JJ, Natland JH, White WM, Poreda R, Bloomer SH, Flsher RL, Baxter AN (1989) Isotopic and geochemical provinces of the western Indian Ocean spreading centers. J Geophys Res 94(B4):4033–4052

Mamyrin BZ, Tolsthikin IN, Anufriyev GS, Kamenskii IL (1969) Isotopic analysis of terrestrial helium on a magnetic resonance mass spectrometer. Geochem Int 6:517–524

Marrocchi Y, Burnard P, Hamilton D, Colin A, Pujol M, Zimmermann L (2009) Neon isotopic measurements using high-resolution, multicollector noble gas mass spectrometer: HELIX-MC. Geochem Geophys Geosyst G3(10):1–8

Marty B (1989) Neon and xenon isotopes in MORB: implications for the earth-atmosphere evolution. Earth Planet Sci Lett 94:45–56

Marty B (2012) The origins and concentrations of water, carbon, nitrogen and noble gases on earth. Earth Planet Sci Lett 313–314:56–66

Marty B, Lussiez P (1993) Constraints on rare gas partition coefficients from analysis of olivine-glass from a picritic mid oceanic ridge basalt. Chem Geol 106:1–7

Marty B, Ozima M (1986) Noble gas distribution in oceanic basalts glasses. Geochim Cosmochim Acta 50:1093–1097

Marty B, Tolstikhin IN (1998) CO_2 fluxes from mid-ocean ridges, arcs and plumes. Chem Geol 145: 233–248

Marty B, Zimmermann L (1999) Volatiles (He, C, N, Ar) in mid ocean ridge basalts: assessment of shallow level fractionation and characterization of source composition. Geochem Cosmochem Acta 63: 3619–3633

Marty B, Zashu S, Ozima M (1983) Two noble gas components in a mid-Atlantic ridge basalt. Nature 302(5905):238–240

Marty B, Trull T, Lussiez P, Basile I, Tanguy JC (1994) He, Ar, O, Sr and Nd isotope constraints on the origin and evolution of Mount Etna magmatism. Earth Planet Sci Lett 126:23–39

Matsumoto T, Seta A, Matsuda JI, Takebe M, Chen Y, Arai S (2002) Helium in the archean komatiites revisited: significantly high 3He/4He ratios revealed by fractional crushing gas extraction. Earth Sci Rev 196:213–225

Meibom A, Anderson DL, Sleep NH, Frei R, Page Chamberlain C, Hren MT, Wooden JL (2003) Are high 3He/4He ratios in oceanic basalts an indicator of deep-mantle plume components? Earth Planet Sci Lett 208:197–204

Miyazaki A, Hiyagon H, Siugiura N, Hirose K, Takahashi E (2004) Solubilities of nitrogen and noble gases in silicate melts under various oxygen fugacities: implications for the origin and degassing history of nitrogen and noble gases in the earth. Geochem Cosmoch Acta 68:387–401

Moreira M (2007) Constraints on the origin of the 129Xe on earth using the tellurium double beta decay. Earth Planet Sci Lett 264

Moreira M, Allègre CJ (1998) Helium–neon systematics and the structure of the mantle. Chem Geol 147: 53–59

Moreira M, Allègre CJ (2002) Rare gas systematics on mid Atlantic ridge (37°–40°). Earth Planet Sci Lett 198:401–416

Moreira M, Raquin A (2007) Noble gas subduction in the mantle: the "subduction barrier" revisited. C R Geosci 339:937–945

Moreira M, Sarda P (2000) Noble gas constraints on degassing processes. Earth Planet Sci Lett 176: 375–386

Moreira M, Staudacher T, Sarda P, Schilling J-G, Allègre CJ (1995) A primitive plume neon component in MORB: the Shona ridge-anomaly, south Atlantic (51–52°S). Earth Planet Sci Lett 133:367–377

Moreira M, Valbracht P, Staudacher T, Allègre CJ (1996) Rare gas systematics in Red Sea ridge basalts. Geophys Res Lett 23:2453–2456

Moreira M, Kunz J, Allègre CJ (1998) Rare gas systematics on popping rock: estimates of isotopic and elemental compositions in the upper mantle. Science 279:1178–1181

Moreira M, Doucelance R, Dupré B, Kurz M, Allègre CJ (1999) Helium and lead isotope geochemistry in the Azores archipelago. Earth Planet Sci Lett 169: 189–205

Moreira M, Breddam K, Curtice J, Kurz M (2001) Solar neon in the Icelandic mantle: evidence for an undegassed lower mantle. Earth Planet Sci Lett 185:15–23

Mukhopadhyay S (2011) I-Pu-Xe in OIBs and the early separation of the plume source from the MORB source mantle. Mineral Mag 75

Mukhopadhyay S (2012) Early differentiation and volatile accretion recorded in deep mantle neon and xenon. Nature. doi:10.1038/nature11141

Niedermann S, Bach W (1998) Anomalously nucleogenic neon in North Chile ridge basalt glasses suggesting a previously degassed mantle source. Earth Planet Sci Lett 160:447–462

Niedermann S, Bach W, Erzinger J (1997) Noble gas evidence for a lower mantle component in MORB from the southern east Pacific rise: decoupling of helium and neon isotope systematics. Geochim Cosmochim Acta 61:2697–2715

Nier AO (1947) A mass spectrometer for isotope and gas analysis. Rev Sci Instrum 18:398–411

Nishio Y, Ishii T, Gamo T, Sano Y (1999) Volatile element isotopic systematics of the rodrigues triple junction Indian Ocean MORB: implications for mantle heterogeneity. Earth Planet Sci Lett 170:241–253

Ozima M, Zashu S (1983) Noble gases in submarine pillow-glasses. Earth Planet Sci Lett 62:24–40

Ozima M, Zashu S (1988) Solar-type Ne in zaire cubic diamonds. Geochim Cosmochim Acta 52:19–25

Ozima M, Zashu S (1991) Noble gas state of the ancient mantle as deduced from noble gases in coated diamonds. Earth Planet Sci Lett 105:13–27

Ozima M, Podozek FA, Igarashi G (1985) Terrestrial xenon isotope constraints on the early history of the earth. Nature 315:471–474

Paonita A, Martelli M (2006) Magma dynamics at mid-ocean ridges by noble gas kinetic fractionation: assessment of magmatic ascent rates. Earth Planet Sci Lett 241:138–158

Paonita A, Martelli M (2007) A new view of the He–Ar–CO2 degassing at mid-ocean ridges: homogeneous composition of magmas from the upper mantle. Geochem Cosmoch Acta 71:1747–1763

Parai R, Mukhopadhyay S, Lassiter JC (2009) New constraints on the HIMU mantle from neon and helium isotopic compositions of basalts from the Cook–Austral Islands. Earth Planet Sci Lett 277: 253–261

Parman SW, Kurz MD, Hart SR, Grove TL (2005) Helium solubility in olivine and implications for high $^3He/^4He$ in ocean island basalts. Nature 437: 1140–1143

Patterson DB, Honda M, McDougall I (1990) Atmospheric contamination: a possible source for heavy noble gases basalts from Loihi seamount, Hawaii. Geophys Res Lett 17:705–708

Pedroni A, Hammerschmidt K, Friedrichsen H (1999) He, Ne, Ar, and C isotope systematics of geothermal

emanations in the Lesser Antilles Islands arc. Geochem Cosmoch Acta 63:515–532

Pineau F, Javoy M, Bottinga Y (1976) $^{13}C/^{12}C$ ratios of rocks and inclusions in popping rocks of the mid Atlantic ridge and their bearing on the problem of isotopic composition of deep-seated carbon. Earth Planet Sci Lett 29:413–421

Pinti D (2001) Anomalous xenon in archean cherts from Pilbara Craton, Western Australia. Chem Geol 175:387–395

Porcelli D, Halliday A (2001) The core as a possible source of mantle helium. Earth Planet Sci Lett 192:45–56

Poreda RJ, Farley KA (1992) Rare gases in Samoan xenoliths. Earth Planet Sci Lett 113:129–144

Poreda R, Radicati di Brozolo F (1984) Neon isotope variations in mid-Atlantic ridge basalts. Earth Planet Sci Lett 69:277–289

Pujol M, Marty B, Burnard P, Philippot P (2009) Xenon in Archean barite: weak decay of 130Ba, mass-dependent isotopic fractionation and implication for barite formation. Geochem Cosmoch Acta 73: 6834–6846

Pujol M, Marty B, Burgess R (2011) Chondritic-like xenon trapped in Archean rocks: a possible signature of the ancient atmosphere. Earth Planet Sci Lett 308:298–306

Raquin A, Moreira M (2009) Air 38Ar/36Ar in the mantle: implication on the nature of the parent bodies of the earth. Earth Planet Sci Lett 287:551–558

Raquin A, Moreira M, Guillon F (2008) He, Ne and Ar systematics in single vesicles: mantle isotopic ratios and origin of the air component in basaltic glasses. Earth Planet Sci Lett 274:142–150

Reynolds JH (1956) High sensitivity mass spectrometer for noble gas analysis. Rev Sci Instrum 27:928–934

Reynolds JH, Jeffery PM, McCrory GA, Varga PM (1978) Improved charcoal trap for rare gas mass spectrometry. Rev Sci Instrum 49:547–548

Richard D, Marty B, Chaussidon M, Arndt N (1996) Helium isotopic evidence for a lower mantle component in depleted archean komatiite. Science 273: 93–95

Ruzié L, Moreira M (2009) Magma degassing process during plinian eruptions. J Volcanol Geoth Res (submitted)

Sarda P (2004) Surface noble gas recycling to the terrestrial mantle. Earth Planet Sci Lett 228:49–63

Sarda P, Graham DW (1990) Mid-ocean ridge popping rocks: implications for degassing at ridge crests. Earth Planet Sci Lett 97:268–289

Sarda P, Moreira M (2002) Vesiculation and vesicle loss in mid oceanic ridge basalt glasses: He, Ne, Ar elemental fractionation and pressure influence. Geochem Cosmoch Acta 66:1449–1458

Sarda P, Staudacher T, Allègre CJ (1985) 40Ar/36Ar in MORB glasses: constraints on atmosphere and mantle evolution. Earth Planet Sci Lett 72:357–375

Sarda P, Staudacher T, Allègre CJ (1988) Neon isotopes in submarine basalts. Earth Planet Sci Lett 91:73–88

Sarda P, Moreira M, Staudacher T (1998) Argon-lead isotopic correlation in mid-Atlantic ridge basalts. Science 283:666–668

Sarda P, Moreira M, Staudacher T, Schilling J-G, Allègre CJ (2000) Rare gas systematics on the southernmost mid-Atlantic ridge: constraints on the lower mantle and the dupal source. J Geophys Res 105:5973–5996

Schiano P, Provost A, Clocchiatti R, Faure F (2007) Transcrystalline melt migration and earth's mantle. Science 314:970–974

Schmidt BC, Keppler H (2002) Experimental evidence for high noble gas solubilities in silicate melts under mantle pressures. Earth Planet Sci Lett 195:277–290

Shaw AM, Hilton DR, Fisher TP, Walker JA, de Leew GAM (2006) Helium isotope variations in mineral separates from Costa Rica and Nicaragua: assessing crustal contributions, timescale variations and diffusion-related mechanisms. Chem Geol 230:124–139

Shibata T, Takahashi E, Matsuda J-I (1998) Solubility of neon, argon, krypton, and xenon in binary and ternary silicate systems: a new view on noble gas solubility. Geochem Cosmoch Acta 62:1241–1253

Staudacher T (1987) Upper mantle origin for Harding County well gases. Nature 325:605–607

Staudacher T, Allègre CJ (1982) Terrestrial xenology. Earth Planet Sci Lett 60:389–406

Staudacher T, Allègre CJ (1988) Recycling of oceanic crust and sediments: the noble gas subduction barrier. Earth Planet Sci Lett 89:173–183

Staudacher T, Allègre CJ (1989) Noble gases in glass samples from Tahiti: Teahitia, Rocard and Mehetia. Earth Planet Sci Lett 93:210–222

Staudacher T, Allègre CJ (1993) Age of the second caldera of Piton de la Fournaise volcano, Réunion Island, determined by cosmic ray produced ^{3}He and ^{21}Ne, Earth Planet Sci Lett (in the press)

Staudacher T, Kurz MD, Allègre CJ (1986) New noble-gas data on glass samples from Loihi seamount and Hualalai and on dunite samples from Loihi and Reunion Island. Chem Geol 56:193–205

Staudacher T, Sarda P, Richardson SH, Allègre CJ, Sagna I, Dmitriev LV (1989) Noble gases in basalt glasses from a mid-Atlantic ridge topographic high at 14°N: geodynamic consequences. Earth Planet Sci Lett 96:119–133

Staudacher T, Sarda P, Allègre CJ (1990) Noble gas systematics of Réunion Island, Indian Ocean. Chem Geol 89:1–17

Stout VL, Gibbons MD (1955) Gettering of gas by titanium. J Appl Phys 26(12):1488–1492

Stroncik NA, Niedermann S, Haase K (2008) Plume–ridge interaction revisited: evidence for melt mixing from He, Ne and Ar isotope and abundance systematics. Earth Planet Sci Lett 268:424–432

Stuart FM, Lass-Evans S, Fitton JG, Ellam RM (2003) High 3He/4He ratios in picritic basalts from Baffin Island and the role of a mixed reservoir in mantle plumes. Nature 424:57–59

Tolstikhin I, Hofmann AW (2005) Early crust on top of the earth's core. Phys Earth Planet Inter 148:109–130

Tolstikhin IN, Kramers JD, Hofmann AW (2006) A chemical earth model with whole mantle convection: the importance of a core–mantle boundary layer (D″) and its early formation. Chem Geol 226:79–99

Trieloff M, Kunz J (2005) Isotope systematics of noble gases in the earth's mantle: possible sources of primordial isotopes and implications for mantle structure. Phys Earth Planet Inter 148:13–38

Trieloff M, Kunz J, Clague DA, Harrison D, Allègre CJ (2000) The nature of pristine noble gases in mantle plumes. Science 288:1036–1038

Trieloff M, Kunz J, Allègre CJ (2002) Noble gas systematics of the reunion mantle plume source and the origin of primordial noble gases in earth's mantle. Earth Planet Sci Lett 200:297–313

Trieloff M, Falter M, Jessberger EK (2003) The distribution of mantle and atmospheric argon in oceanic basalt glasses. Geochem Cosmoch Acta 67: 1229–1245

Valbracht PJ, Honda M, Matsumoto T, Matielli N, Mc Dougall I, Ragettli R, Weis D (1996) Helium, neon and argon isotope systematics in kerguelen ultramafic xenoliths implications for mantle source signature. Earth Planet Sci Lett 138:29–38

van Soest MC, Hilton DR, Kreulen R (1998) Tracing crustal and slab contributions to arc magmatism in the Lesser Antilles island arc using helium and carbon relationships in geothermal fluids. Geochem Cosmoch Acta 62:3323–3335

Wada N, Matsuda J-I (1998) A noble gas study of cubic diamonds from zaire: constraints on their mantle source, Geochem Cosmoch Acta 62:2335–2345

Watson EB, Thomas JB, Cherniak DJ (2007) 40Ar retention in the terrestrial planets. Nature 449: 299–304

Wieler R (2002) Noble gases in the solar system, in noble gases in geochemistry and cosmochemistry. Rev Mineral Geochem 47:21–70

Xu S, Nakai S, Wakita H, Wang X (1995) Mantle-derived noble gases in natural gases from Songliao basin, China. Geochem Cosmoch Acta 59:4675–4683

Yamamoto JB, Burnard PG (2005) Solubility controlled noble gas fractionation during magmatic degassing: implications for noble gas compositions of primary melts of OIB and MORB. Geochem Cosmoch Acta 69:727–734

Yamamoto J, Hirano N, Abe N, Hanyu T (2009a) Noble gas isotopic compositions of mantle xenoliths from northwestern Pacific lithosphere. Chem Geol 268:313–323

Yamamoto J, Nishimura K, Sugimoto T, Takemura K, Takahata N, Sano Y (2009b) Diffusive fractionation of noble gases in mantle with magma channels: origin of low He/Ar in mantle-derived rocks. Earth Planet Sci Lett 280:167–174

Yokochi R, Marty B (2004) A determination of the neon isotopic composition of the deep mantle. Earth Planet Sci Lett 225:77–88

Yokochi R, Marty B (2006) Geochemical constraints on mantle dynamics in the hadeen. Earth Planet Sci Lett 238:17–30

Zashu S, Hiyagon H (1995) Degassing mechanisms of noble gases from carbonado diamonds. Geochim Cosmochim Acta 59:1321–1328